frontiers | Research Topics

Innovative strategies for enhancing plant resilience to phytopathogenic microbes

Edited by
Temoor Ahmed, Dirk Janssen and Yasser Nehela

Published in
Frontiers in Plant Science

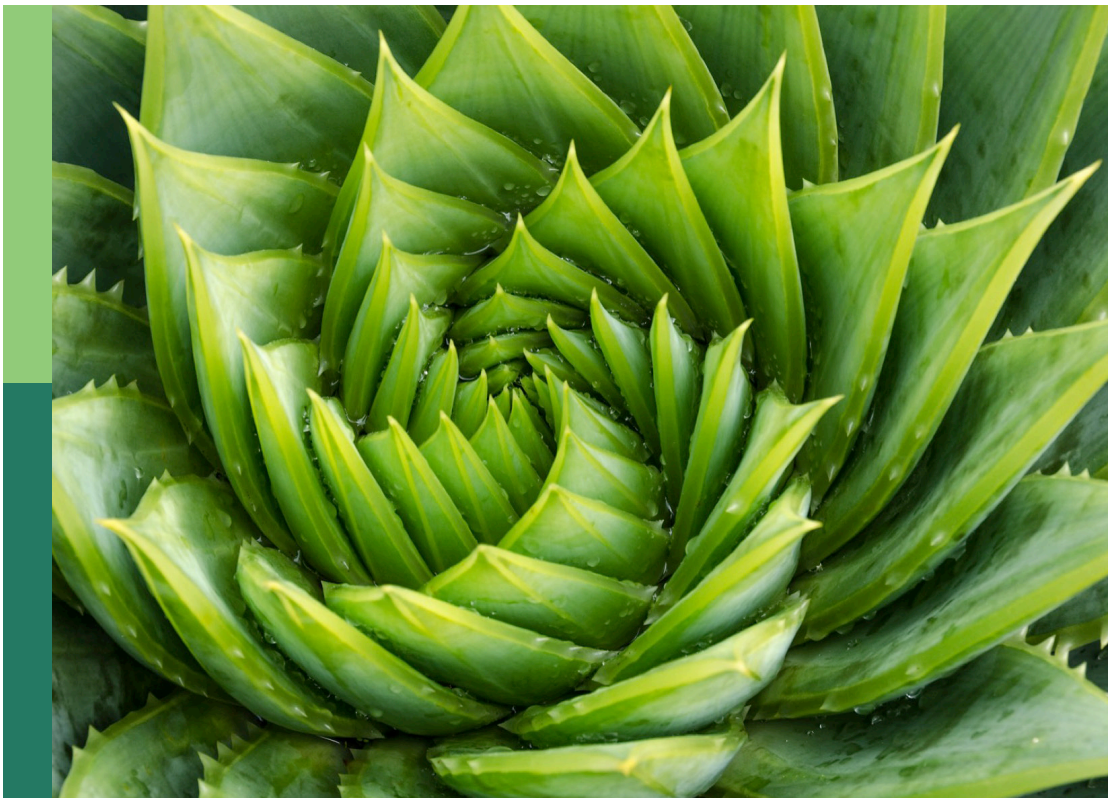

FRONTIERS EBOOK COPYRIGHT STATEMENT

The copyright in the text of individual articles in this ebook is the property of their respective authors or their respective institutions or funders. The copyright in graphics and images within each article may be subject to copyright of other parties. In both cases this is subject to a license granted to Frontiers.

The compilation of articles constituting this ebook is the property of Frontiers.

Each article within this ebook, and the ebook itself, are published under the most recent version of the Creative Commons CC-BY licence. The version current at the date of publication of this ebook is CC-BY 4.0. If the CC-BY licence is updated, the licence granted by Frontiers is automatically updated to the new version.

When exercising any right under the CC-BY licence, Frontiers must be attributed as the original publisher of the article or ebook, as applicable.

Authors have the responsibility of ensuring that any graphics or other materials which are the property of others may be included in the CC-BY licence, but this should be checked before relying on the CC-BY licence to reproduce those materials. Any copyright notices relating to those materials must be complied with.

Copyright and source acknowledgement notices may not be removed and must be displayed in any copy, derivative work or partial copy which includes the elements in question.

All copyright, and all rights therein, are protected by national and international copyright laws. The above represents a summary only. For further information please read Frontiers' Conditions for Website Use and Copyright Statement, and the applicable CC-BY licence.

ISSN 1664-8714
ISBN 978-2-8325-6490-5
DOI 10.3389/978-2-8325-6490-5

Generative AI statement
Any alternative text (Alt text) provided alongside figures in the articles in this ebook has been generated by Frontiers with the support of artificial intelligence and reasonable efforts have been made to ensure accuracy, including review by the authors wherever possible. If you identify any issues, please contact us.

About Frontiers

Frontiers is more than just an open access publisher of scholarly articles: it is a pioneering approach to the world of academia, radically improving the way scholarly research is managed. The grand vision of Frontiers is a world where all people have an equal opportunity to seek, share and generate knowledge. Frontiers provides immediate and permanent online open access to all its publications, but this alone is not enough to realize our grand goals.

Frontiers journal series

The Frontiers journal series is a multi-tier and interdisciplinary set of open-access, online journals, promising a paradigm shift from the current review, selection and dissemination processes in academic publishing. All Frontiers journals are driven by researchers for researchers; therefore, they constitute a service to the scholarly community. At the same time, the *Frontiers journal series* operates on a revolutionary invention, the tiered publishing system, initially addressing specific communities of scholars, and gradually climbing up to broader public understanding, thus serving the interests of the lay society, too.

Dedication to quality

Each Frontiers article is a landmark of the highest quality, thanks to genuinely collaborative interactions between authors and review editors, who include some of the world's best academicians. Research must be certified by peers before entering a stream of knowledge that may eventually reach the public - and shape society; therefore, Frontiers only applies the most rigorous and unbiased reviews. Frontiers revolutionizes research publishing by freely delivering the most outstanding research, evaluated with no bias from both the academic and social point of view. By applying the most advanced information technologies, Frontiers is catapulting scholarly publishing into a new generation.

What are Frontiers Research Topics?

Frontiers Research Topics are very popular trademarks of the *Frontiers journals series*: they are collections of at least ten articles, all centered on a particular subject. With their unique mix of varied contributions from Original Research to Review Articles, Frontiers Research Topics unify the most influential researchers, the latest key findings and historical advances in a hot research area.

Find out more on how to host your own Frontiers Research Topic or contribute to one as an author by contacting the Frontiers editorial office: frontiersin.org/about/contact

Innovative strategies for enhancing plant resilience to phytopathogenic microbes

Topic editors

Temoor Ahmed — Zhejiang University, China

Dirk Janssen — IFAPA Centro La Mojonera, Spain

Yasser Nehela — Tanta University, Egypt

Citation

Ahmed, T., Janssen, D., Nehela, Y., eds. (2025). *Innovative strategies for enhancing plant resilience to phytopathogenic microbes*. Lausanne: Frontiers Media SA.

doi: 10.3389/978-2-8325-6490-5

Table of contents

05 Editorial: Innovative strategies for enhancing plant resilience to phytopathogenic microbes
Temoor Ahmed, Dirk Janssen and Yasser Nehela

08 Recent advances in nano-enabled immunomodulation for enhancing plant resilience against phytopathogens
Hafiza Ayesha Masood, Yetong Qi, Muhammad Khubaib Zahid, Zhitao Li, Salman Ahmad, Ji-Min Lv, Muhammad Shafiq Shahid, Hamada E. Ali, Gabrijel Ondrasek and Xingjiang Qi

21 Exploring plant growth promoting traits and biocontrol potential of new isolated *Bacillus subtilis* BS-2301 strain in suppressing *Sclerotinia sclerotiorum* through various mechanisms
Muhammad Ayaz, Qurban Ali, Wei Zhao, Yuan-Kai Chi, Farman Ali, Khan Abdur Rashid, Shun Cao, Yan-qiu He, Abdul Aziz Bukero, Wen-Kun Huang and Ren-De Qi

38 Arbuscular mycorrhizal fungi improve the disease resistance of *Lycium barbarum* to root rot by activating phenylpropane metabolism
Nan Li, Wei Chen, Bin Wang, Chongqing Zhang, Yupeng Wang, Ruiyun Li, Yuke Yan and Jing He

51 A fungal endophyte induces local cell wall–mediated resistance in wheat roots against take-all disease
Tania Chancellor, Daniel P. Smith, Wanxin Chen, Suzanne J. Clark, Eudri Venter, Kirstie Halsey, Esther Carrera, Vanessa McMillan, Gail Canning, Victoria J. Armer, Kim E. Hammond-Kosack and Javier Palma-Guerrero

68 A protein elicitor PeVn1 from *Verticillium nonalfalfae* HW recognized as a MAMP triggers plant immunity response
Ziyu Zhang, Dong Wang, Baozhu Dong, Yu Wang, Jialu Xu, Jianxiu Hao and Hongyou Zhou

82 LAZARUS 1 functions as a positive regulator of plant immunity and systemic acquired resistance
Yue Chen, Yue Han, Weijie Huang, Yanjun Zhang, Xiaoli Chen, Dongyue Li, Yi Hong, Huhu Gao, Kewei Zhang, Yuelin Zhang and Tongjun Sun

93 Tetramycin ameliorates tebuconazole·azoxystrobin to control leaf spot and viral diseases of Taizishen
Bing Tian, Chenglin Tang, Jiaqi Liu, Boya Jin and Cheng Zhang

108 Evaluation the role of *Luteibacter pinisoli* DP2-30 in mitigating pine wilt disease caused by *Bursaphelenchus xylophilus* through modulation of host microbiome
Waqar Ahmed, Wenhua Ye, Jidong Pan, Songsong Liu, Wenxia Ji, Shun Zhou, Fusheng Wang, Zhiguang Li, Mohamed Mohany and Xinrong Wang

127 Development of a lytic Ralstonia phage cocktail and evaluation of its control efficacy against tobacco bacterial wilt
Haoxin He, Ke Yi, Lei Yang, Yongfeng Jing, Lifu Kang, Zhihao Gao, Dong Xiang, Ge Tan, Yunsheng Wang, Qian Liu, Lin Xie, Shiya Jiang, Tianbo Liu and Wu Chen

139 The role of foliar endophytes in modulating southern corn rust severity: implications for biocontrol strategies
Lujia Yang, Lili Li, Yingying Song, Yongsheng Zhang, Jie Yang, Hongying Cui, Wenxiu Guo, Suhong Lv and Xingyuan Men

frontiers | Frontiers in Plant Science

TYPE Editorial
PUBLISHED 10 June 2025
DOI 10.3389/fpls.2025.1632709

Check for updates

OPEN ACCESS

EDITED AND REVIEWED BY
Brigitte Mauch-Mani,
Retired, Fribourg, Switzerland

*CORRESPONDENCE
Yasser Nehela
yasser.nehela@agr.tanta.edu.eg

RECEIVED 21 May 2025
ACCEPTED 26 May 2025
PUBLISHED 10 June 2025

CITATION
Ahmed T, Janssen D and Nehela Y (2025) Editorial: Innovative strategies for enhancing plant resilience to phytopathogenic microbes. *Front. Plant Sci.* 16:1632709. doi: 10.3389/fpls.2025.1632709

COPYRIGHT
© 2025 Ahmed, Janssen and Nehela. This is an open-access article distributed under the terms of the Creative Commons Attribution License (CC BY). The use, distribution or reproduction in other forums is permitted, provided the original author(s) and the copyright owner(s) are credited and that the original publication in this journal is cited, in accordance with accepted academic practice. No use, distribution or reproduction is permitted which does not comply with these terms.

Editorial: Innovative strategies for enhancing plant resilience to phytopathogenic microbes

Temoor Ahmed[1], Dirk Janssen[2] and Yasser Nehela[3]*

[1]Xianghu Laboratory, Hangzhou, China, [2]Instituto Andaluz de Investigación y Formación Agraria (IFAPA) Centro La Mojonera, Almería, Spain, [3]Department of Agricultural Botany, Faculty of Agriculture, Tanta University, Tanta, Egypt

KEYWORDS

phytopathogens, plant resilience, disease management, host-pathogen interactions, genetic engineering, biocontrol agents, sustainable agriculture

Editorial on the Research Topic
Innovative strategies for enhancing plant resilience to phytopathogenic microbes

Plant diseases pose a significant threat to global food security, biodiversity, and economic stability. Plants face constant attack from a diverse array of pathogens including bacteria, fungi, viruses, and nematodes that collectively cause devastating agricultural losses (Ristaino et al., 2021; Wang et al., 2022). The financial impact is staggering, with annual crop yield losses from pathogens and pests estimated at $220 billion worldwide. These losses don't merely represent economic figures; they translate to real food shortages, compromised regional economies, and cascading socioeconomic challenges (Singh et al., 2023). The extensive use of traditional chemical pesticides and antibiotics involving toxic substances has become more challenging due to severe ecotoxicological challenges (Ahmed et al., 2023). Thus, there is an urgent need to develop effective and robust eco-friendly plant disease management approaches to overcome global food crisis.

A recent Research Topic of "Frontiers in Plant Science" explores groundbreaking research aimed to enhancing plant resilience to phytopathogenic microbes. The Research Topic features nine original research papers and one comprehensive review that collectively advances our understanding of sustainable agriculture through enhanced disease resistance. The featured research illuminates several critical areas: the molecular interactions between plants and pathogens, novel approaches to disease management, biotechnological innovations for improved resistance, and the complex interplay between climate change and disease dynamics. For example, Ayaz et al. showed that *Bacillus subtilis* BS-2301 exhibits strong antifungal activity against *Sclerotinia sclerotiorum* via ROS accumulation, OA reduction, and hyphal damage. It also promotes plant growth, enhances antioxidant defense, and upregulates disease-resistant genes. Overall, *Bacillus subtilis* BS-2301 is a promising biocontrol agent for sustainable agriculture with broad-spectrum antagonism and growth-promoting traits. In another study, Arbuscular mycorrhizal fungi (AMF) *Rhizophagus intraradices* enhance *Lycium barbarum* resistance to *Fusarium solani* by boosting phenylpropane metabolism, increasing lignin (141.65%) and flavonoids (44.61%), and elevating defense-related enzymes and hormones. AMF symbiosis improves plant

growth (24.83% height increase) and strengthens early pathogen response, offering a sustainable biocontrol strategy against root rot (Li et al.).

Chancellor et al. revealed that *Gaeumannomyces hyphopodioides* controls take-all disease by locally modifying wheat root gene expression, suppressing cell wall–related genes (*CESA*, *XTH*), and forming lipid-rich subepidermal vesicles (SEVs). These findings highlight a novel biocontrol mechanism, offering potential strategies for enhancing wheat resistance against *G. tritici* in the absence of resistant cultivars. Another study identifies PeVn1, a novel protein elicitor from *Verticillium nonalfalfae*, which triggers plant immune responses via NbBAK1/NbSOBIR1-dependent cell death, ROS burst, and defense activation. PeVn1 enhances resistance against multiple pathogens, offering potential for developing protein-based biocontrol agents in sustainable agriculture (Zhang et al.). Chen et al. demonstrated that LAZ1 and LAZ1H1 are evolutionarily conserved positive regulators of SAR, modulating *CBP60g* and *SARD1* expression and SA/NHP biosynthesis. Their overexpression enhances pathogen resistance, highlighting their potential as targets for improving plant immunity in crops.

The application of 0.3% tetramycin and reduced-dose tebuconazole·azoxystrobin synergistically controls Taizishen leaf diseases (90.03–90.46% efficacy), enhances physiological activity (electrical signals, photosynthesis, nutrient transport), improves growth/quality metrics, and reduces pesticide use, offering an efficient and sustainable disease management strategy (Tian et al.). Ahmed et al. demonstrated that *Luteibacter pinisoli* DP2–30 effectively combats pine wilt disease through potent nematicidal activity (>95% mortality), suppressed egg hatching (43-49%), and microbiome modulation—notably enriching Rhodanobacteraceae. Its dual-action mechanism (direct pathogen suppression and host microbiota restructuring) offers promising eco-friendly PWD control. Another recent study identified phage cocktails (BPC-1) with exceptional bacterial wilt control efficacy (99.25%), combining broad-host-range (YL1/YL4) and high-efficacy (YL2/YL3) phages. Structural analyses of tail fiber proteins reveal key amino acid determinants for host specificity, offering optimized phage-based solutions for sustainable bacterial wilt management (He et al.). Yang et al. revealed that *P. polysora* infection restructures maize endophytic communities, reducing diversity and network complexity while revealing key fungal associations (e.g., *Alternaria*-resistance correlation). Temperature-driven microbial assembly and differential regional resilience offer new insights for developing microbiome-based SCR management strategies. Last, a review published by Masood et al. demonstrated that nano-enabled immunomodulation offers a sustainable approach to enhance plant disease resistance through engineered nanomaterials that trigger immune responses, deliver bioactive compounds, and reshape microbiomes. Additionally, this review systematically examines current advances in nano-enabled immunomodulation approaches, explores their underlying mechanisms, and identifies key research directions to address current limitations for eco-friendly plant disease control. Together, these studies provide a foundation for developing more resilient agricultural systems capable of withstanding emerging pathogenic threats.

Author contributions

TA: Writing – review & editing, Writing – original draft, Data curation, Conceptualization, Validation, Investigation. DJ: Writing – original draft, Data curation, Investigation, Conceptualization, Supervision, Writing – review & editing. YN: Investigation, Supervision, Writing – review & editing, Conceptualization, Writing – original draft, Data curation.

Acknowledgments

The guest editors express profound appreciation to the authors, peer reviewers, and Frontiers publication team for their expert contributions, with particular thanks to Berna Ustun (content specialist) for her exceptional support.

Conflict of interest

The authors declare that the research was conducted in the absence of any commercial or financial relationships that could be construed as a potential conflict of interest.

Generative AI statement

The author(s) declare that Generative AI was used in thecreation of this manuscript. During the preparation of this work the author(s) used Grammarly and Claude tool to improve language and readability. After using this tool, the author(s) reviewed and edited the content as needed and take(s) full responsibility for the content of the publication.

Publisher's note

All claims expressed in this article are solely those of the authors and do not necessarily represent those of their affiliated organizations, or those of the publisher, the editors and the reviewers. Any product that may be evaluated in this article, or claim that may be made by its manufacturer, is not guaranteed or endorsed by the publisher.

References

Ahmed, T., Noman, M., Gardea-Torresdey, J. L., White, J. C., and Li, B. (2023). Dynamic interplay between nano-enabled agrochemicals and the plant-associated microbiome. *Trends Plant Sci.* 28, 1310–1325. doi: 10.1016/j.tplants.2023.06.001

Ristaino, J. B., Anderson, P. K., Bebber, D. P., Brauman, K. A., Cunniffe, N. J., Fedoroff, N. V., et al. (2021). The persistent threat of emerging plant disease pandemics to global food security. *Proc. Natl. Acad. Sci.* 118, e2022239118. doi: 10.1073/pnas.2022239118

Singh, B. K., Delgado-Baquerizo, M., Egidi, E., Guirado, E., Leach, J. E., Liu, H., et al. (2023). Climate change impacts on plant pathogens, food security and paths forward. *Nat. Rev. Microbiol.* 21, 640–656. doi: 10.1038/s41579-023-00900-7

Wang, Y., Pruitt, R. N., Nürnberger, T., and Wang, Y. (2022). Evasion of plant immunity by microbial pathogens. *Nat. Rev. Microbiol.* 20, 449–464. doi: 10.1038/s41579-022-00710-3

frontiers | Frontiers in Plant Science

TYPE Review
PUBLISHED 07 August 2024
DOI 10.3389/fpls.2024.1445786

Check for updates

OPEN ACCESS

EDITED BY
Yasser Nehela,
University of Florida, United States

REVIEWED BY
Fasih Ullah Haider,
Chinese Academy of Sciences (CAS), China
Amir Raza,
University of Arizona, United States
Irfan Manzoor,
Government College University, Faisalabad, Pakistan

*CORRESPONDENCE
Xingjiang Qi
qixj@zaas.ac.cn
Zhitao Li
lzt92616@sina.cn

†These authors have contributed equally to this work

RECEIVED 08 June 2024
ACCEPTED 22 July 2024
PUBLISHED 07 August 2024

CITATION
Masood HA, Qi Y, Zahid MK, Li Z, Ahmad S, Lv J-M, Shahid MS, Ali HE, Ondrasek G and Qi X (2024) Recent advances in nano-enabled immunomodulation for enhancing plant resilience against phytopathogens. *Front. Plant Sci.* 15:1445786. doi: 10.3389/fpls.2024.1445786

COPYRIGHT
© 2024 Masood, Qi, Zahid, Li, Ahmad, Lv, Shahid, Ali, Ondrasek and Qi. This is an open-access article distributed under the terms of the Creative Commons Attribution License (CC BY). The use, distribution or reproduction in other forums is permitted, provided the original author(s) and the copyright owner(s) are credited and that the original publication in this journal is cited, in accordance with accepted academic practice. No use, distribution or reproduction is permitted which does not comply with these terms.

Recent advances in nano-enabled immunomodulation for enhancing plant resilience against phytopathogens

Hafiza Ayesha Masood[1,2,3†], Yetong Qi[1†], Muhammad Khubaib Zahid[4], Zhitao Li[1*], Salman Ahmad[5], Ji-Min Lv[1], Muhammad Shafiq Shahid[6], Hamada E. Ali[7], Gabrijel Ondrasek[8] and Xingjiang Qi[1*]

[1]Xianghu Laboratory, Hangzhou, China, [2]MEU Research Unit, Middle East University, Amman, Jordan, [3]Department of Life Sciences, Western Caspian University, Baku, Azerbaijan, [4]Institute of Nuclear Agricultural Sciences, Zhejiang University, Hangzhou, China, [5]Department of Plant Pathology, Faculty of Agriculture, University of Sargodha, Sargodha, Pakistan, [6]Department of Plant Sciences, College of Agricultural and Marine Sciences, Sultan Qaboos University, Muscat, Oman, [7]Department of Biology, College of Science, Sultan Qaboos University, Muscat, Oman, [8]Faculty of Agriculture, University of Zagreb, Zagreb, Croatia

Plant diseases caused by microbial pathogens pose a severe threat to global food security. Although genetic modifications can improve plant resistance; however, environmentally sustainable strategies are needed to manage plant diseases. Nano-enabled immunomodulation involves using engineered nanomaterials (ENMs) to modulate the innate immune system of plants and enhance their resilience against pathogens. This emerging approach provides unique opportunities through the ability of ENMs to act as nanocarriers for delivering immunomodulatory agents, nanoprobes for monitoring plant immunity, and nanoparticles (NPs) that directly interact with plant cells to trigger immune responses. Recent studies revealed that the application of ENMs as nanoscale agrochemicals can strengthen plant immunity against biotic stress by enhancing systemic resistance pathways, modulating antioxidant defense systems, activating defense-related genetic pathways and reshaping the plant-associated microbiomes. However, key challenges remain in unraveling the complex mechanisms through which ENMs influence plant molecular networks, assessing their long-term environmental impacts, developing biodegradable formulations, and optimizing targeted delivery methods. This review provides a comprehensive investigation of the latest research on nano-enabled immunomodulation strategies, potential mechanisms of action, and highlights future perspectives to overcome existing challenges for sustainable plant disease management.

KEYWORDS

agriculture, nanomaterials, immunomodulation, phytopathogens, disease resistance

1 Introduction

Agriculture is the most important sector that plays a crucial role in providing food, supporting economic stability, and maintaining ecological balance worldwide (Hartmann and Six, 2023). Plant pathogens, including fungi, bacteria, viruses, and other pathogens, pose a severe threat to agricultural productivity and food security worldwide (Kim et al., 2023). In the last few decades, due to trade globalization, climate change, and other factors, new pathogens are constantly emerging, and existing diseases are also spreading, posing a serious threat to agricultural production (Singh et al., 2023). Moreover, since the Green Revolution the global population has dramatically raised by more than 5 billion people, and the shortage of typical agricultural methods has critically restrained our capability to conserve food safety (Conway, 1998). Traditional methods such as broad-spectrum antibiotics and chemical pesticides provide some support; however, they also pose adverse effects to the environment and human health and can also lead to drug resistance in plant pathogens (Ahmed et al., 2022). To address these issues, traditional breeding and modern biotechnology are expected to significantly improve plant resilience to various pathogens by improving crop resistance genes and immune signaling pathways (Conway, 1998; Munaweera et al., 2022).

Although genetic modifications of plants offer promising advantages, these require risk assessment and careful consideration to confirm their safety and sustainability (Anders et al., 2021). Therefore, it is important to find new strategies for environmentally friendly and sustainable plant disease management. Enhancing crop resilience to pathogens is one of the key strategies to control plant diseases and maintain agricultural sustainability, while minimizing the reliance on traditional pesticides (Hannan Parker et al., 2022; Ngou et al., 2022). Notably, the innate immune system of plants provides a strong defense against pathogen invasion (Ma et al., 2021), but how to effectively regulate and enhance plant immunity remains to be established. In recent years, the application of nanotechnologies in agriculture has attracted increasing attention, due to their unique nanoscale-specific properties such as high efficiency, large surface area, small size, targeted delivery, and controlled release (Beckers et al., 2021).

Nano-enabled immunomodulation involves the use of engineered nanomaterials (ENMs) as nanoscale agrochemicals to modulate the immune response of plants to improve disease resistance (Ahmed et al., 2024; Zhang et al., 2024). ENMs can be used as nanocarriers to efficiently and precisely deliver immune signaling molecules or genes to specific locations in cells, thereby regulating the plant immune system (Zhang et al., 2021b). Additionally, nanoprobe technology is also used to monitor key biomolecular changes in plant immunity, and biotic and abiotic stress responses in real-time (Son et al., 2023). Recent studies have demonstrated that ENMs application strengthens the plant immunity and tolerance against biotic stress by enhancing systemic acquired resistance (SAR) and induced systemic resistance (ISR), and modulating antioxidative defense systems. For example, the foliar application of silica nanoparticles (SiNPs) 100 mg L^{-1} improved the disease resistance in *Arabidopsis thaliana* plants against bacterial pathogen *Pseudomonas syringae* by inducing the SAR in a dose-dependent manner. SAR-inducing phytohormone such as SA successfully enhances stress tolerance by upregulating the expression of pathogenesis-related genes (El-Shetehy et al., 2021). In another recent study, Noman et al. (2024) reported that salicylic acid (SA) coated biogenic iron nanoparticles (bio-FeNPs) at 100 mg Kg^{-1} concentration significantly suppressed Fusarium wilt disease in watermelon (*Citrullus lanatus* L.) caused by a fungal pathogen *Fusarium oxysporum* f. sp. *niveum* by improving SAR response via triggering antioxidative defense systems and SA signaling pathway genes. These findings suggest that nano-enabled immunomodulation might be an alternative way for enhancing plant resilience against phytopathogens; however, mechanistic insights and translation of these approaches from laboratory to the field scale involves significant challenges.

The aim of this review is to provide a comprehensive overview of the latest research progress in nano-enabled immunomodulation for enhancing plant resilience against phytopathogens threats. We aim to elucidate the potential mechanisms by which ENMs can modulate plant immune responses, critically evaluate the latest research advances, and highlight future challenges and opportunities for translating these approaches into sustainable agricultural practices.

2 Dynamics of immunomodulation in plants against phytopathogens

The coevolution of plants and microbial pathogens has led to an intricate interplay of defense and attack mechanisms (Fields and Friman, 2022; Harris and Mou, 2024). Microbial pathogens have developed strategies for evading or suppressing plant immune systems; however, plants employ various sophisticated defense mechanisms in response (Sun and Zhang, 2021). Notably, effector-triggered immunity (ETI) and pattern-triggered immunity (PTI) are two primary defense mechanisms of innate plant immunity against phytopathogens. In plants, NOD-like receptors (NLRs) constitute sensor and helper NLRs, which are responsible for ETI (Laflamme et al., 2020; Nabi et al., 2024). For example, Wang et al. (2023) reported that *MPK3* and *MPK6* suppression in Arabidopsis can potentially reduce pre-PTI-mediated ETI suppression (PES) through inhibition of two protein phosphatases genes (*AP2C1* and *PP2C5*). Furthermore, recognition of conserved microbial features such as microbe-associated molecular patterns (MAMPs) through plant pattern recognition receptors (PRRs) can initiate PTI. However, phytopathogens can evade PTI by shielding or modifying MAMPs, inhibition of PRRs or downstream signaling components by secreting effectors (Lü et al., 2022; Loo et al., 2022; Totsline et al., 2023). Lee et al. (2024) reported that AVRblb2 pathogen effector forms a complex with calmodulin-like (CML) and calmodulin (CaM) proteins to interact with NbCNGC18 to disrupt PAMP-triggered immunity signaling. These mechanisms can potentially hijack plant defense systems,

driven by the coevolutionary relationship between plants and phytopathogens (Sood et al., 2021; Harris and Mou, 2024).

Pathogen effectors can also play a central role in modulating plant immunity (Dou and Zhou, 2012), which target various components of plant immune system, from early recognition events to downstream signaling and defense responses (Figure 1). Effectors can prevent release, binding, or perception of MAMPs, or inhibit key signaling hubs such as receptor-like cytoplasmic kinases, interfere with PRR complexes, MAPK cascades, and phytohormone signaling pathways (Ceulemans et al., 2021; Iswanto et al., 2022). In a recent study, Qiu et al. (2023b) reported that inhibition of *GmLHP1-2*/*GmPHD6* complex transcriptional activity in soybean due to suppressing effect of PsAvh110 nuclear effector from *Phytophthora sojae* can potentially evade plant immunity response. In another study, Shang et al. (2024) reported that CfEC12 (a fungal effector) from *Colletotrichum fructicola binds to* MdNIMIN2 and disrupting its interaction with MdNPR1 leading to suppression of salicylic acid defense pathway.

Pathogens create a favorable environment for infection by rewiring plant immune signaling networks. In addition to suppressing immune signaling pathways, pathogens also target and manipulate the downstream defense outputs of the plant immune system (Mishra et al., 2021; Singh et al., 2023). Effectors and secreted enzymes help pathogens overcome physical and chemical barriers in the plant, such as cell wall reinforcements, antimicrobial compounds, and hydrolytic enzymes. Some pathogens produce toxins or phytohormone mimics that further manipulate plant physiology and development to their advantage (Kaur et al., 2022; Wang et al., 2022). The dynamics of plant-pathogen interactions are further shaped by the spatiotemporal regulation of immunity and infection processes (König et al., 2021). Plants must balance the allocation of resources between growth and defense, while pathogens face the challenge of avoiding detection and preserving host viability. Therefore, timing and localization of immune responses and pathogen colonization are critical determinants of disease outcomes (Li et al., 2020; Monson et al., 2022). Taken together, the dynamics of plant immunomodulation against phytopathogens involve an intricate interplay of recognition mechanisms that detect PAMPs, DAMPs and effector molecules, subsequent signaling cascades that transmit this detection, and the activation of diverse defense responses. Furthermore, the application of ENMs to modulate plant immune responses has emerged as a promising

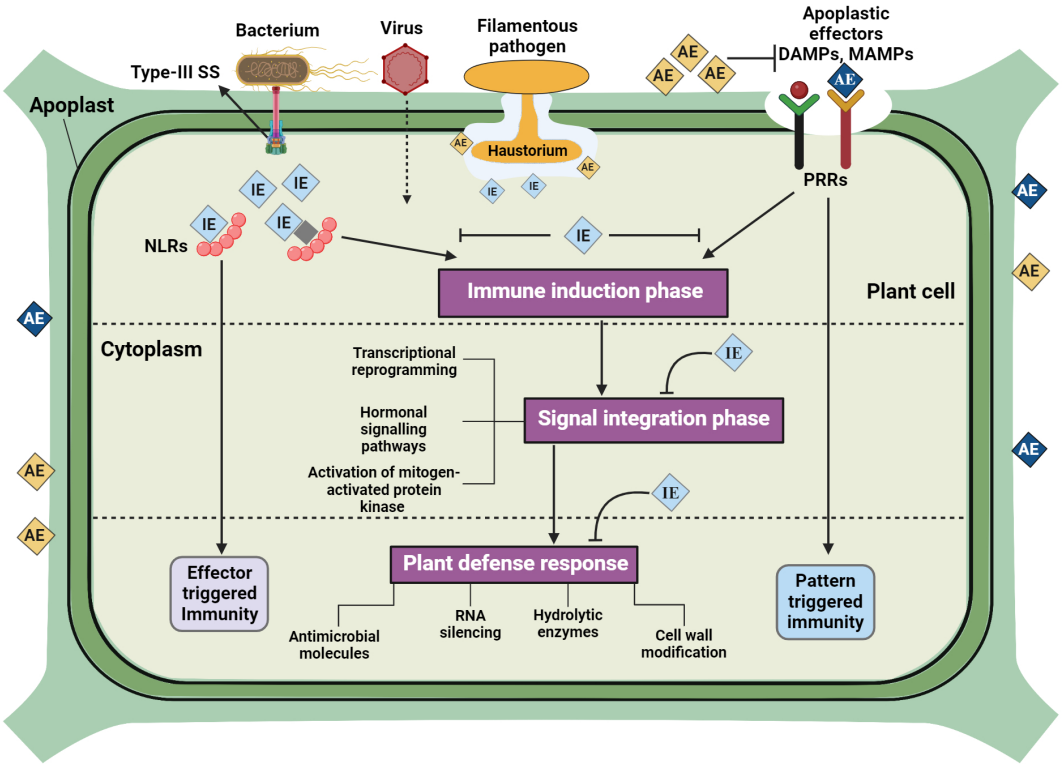

FIGURE 1
Schematic representation of plant immunomodulation against microbial pathogens. Microbial pathogens invasion initiates plant defense responses in three phases including immune recognition, signal integration, and defense response. Firstly, plants perceive pathogen-associated molecular patterns (PAMPs), damage-associated molecular patterns (DAMPs), and microbial effectors through intracellular and surface receptors. Secondly, various immune signaling events are activated, which involve the integration of immune signals from the recognition of diverse patterns and effectors. Finally, an effective and swift defense response is initiated in each cellular compartment of the plant cell, which leads to pattern-triggered immunity (PTI) and NLR-mediated pathways triggering the effector-triggered immunity (ETI) response. Host resistance is modulated by the cumulative action of effectors transmitted by microbial pathogens.

alternative strategy for enhancing plant disease resistance and management (Liu et al., 2024; Zhang et al., 2024).

3 Nano-enabled technologies for plant immunomodulation

The plant immune system is essential for maintaining plant health and responding to pathogen invasions. However, the traditional methods (conventional breeding, crop rotation chemical fertilizers and pesticides) for activating or regulating plant immunity have shortcomings such as low efficiency and poor targeting (Raymaekers et al., 2020; Ma et al., 2021). Nano-enabled agriculture provides a new idea for the precise regulation of plant immunity and reducing the dependence on chemical pesticides (Fiol et al., 2021). Nano-enabled immunomodulation mechanisms lies in the ability of ENMs to act as nanoscale delivery platform for immunomodulatory agents (Noman et al., 2023b). Notably, ENMs as nanoscale carrier can efficiently carry immune signaling molecules (such as protein, enzymes, hormones, and RNA, etc.) into plant cells and activate immune responses (Vega-Vásquez et al., 2021; Liu et al., 2024). ENMs can be divided into different groups (metal based or inorganic ENMs, carbonaceous ENMs, polymer ENMs and hybrid ENMs) based on their unique nanoscale properties including size, shape, crystalline structure, chemical composition (Figure 2) (Saleh, 2020). Metal-based or inorganic ENMs mainly including zinc (Zn), gold (Au), silver (Ag), copper (Cu), titanium (Ti) and silica, which shown great potential for enhancing plant immunity against pathogens and environmental stresses (Mitchell et al., 2021). These inorganic ENMs can be produced to desired properties, geometries, sizes, and with desired functionalization/coatings to optimize benefit. Ma et al. (2020) reported that nanoscale Cu (250 mg L^{-1}) amendments significantly suppressed soybean sudden death syndrome by activating plant immunity and enhancing the phytohormone contents, photosynthetic endpoints, antioxidant enzymes and nutritional status.

Carbon-based ENMs including carbon dots (CDs), carbon nanotubes (CNTs) and graphene NPs have been shown to promote plant growth and resilience against pathogens (Li et al., 2023). For example, Adeel et al. (2021) demonstrated that foliar exposure of CNTs at 200 mg L^{-1} significantly suppressed tobacco mosaic virus

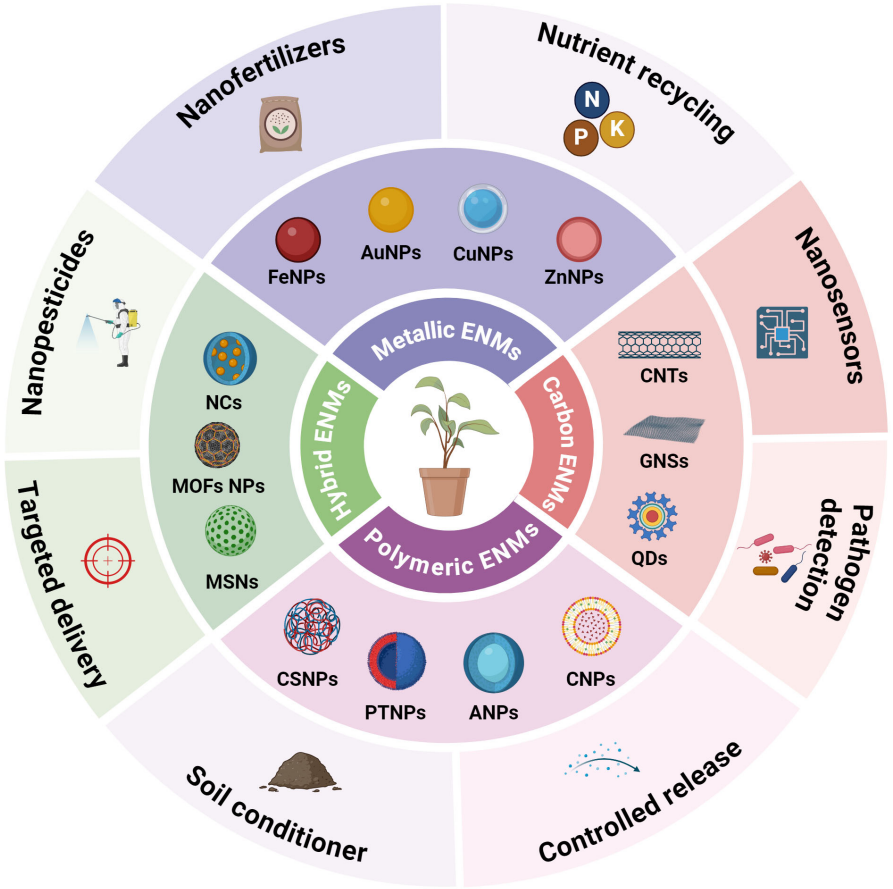

FIGURE 2
Schematic illustration of the current engineered nanomaterials (ENMs) toolbox to improve plant immunity against microbial pathogens. ENMs can be divided into different groups based on their unique physiochemical properties. nanoparticles (NPs), metal-organic framework (MOFs), nanocapsules (NCs), mesoporous silica nanoparticles (MSNs) chitosan (Cs), pectin (Pt), cellulose (Cl), alginate (A), quantum dots (QDs), graphene nanosheets (GNSs), carbon nanotubes (CNs), iron (Fe), copper (Cu), gold (Au) and zinc (Zn).

infection by activating of the defense system in tobacco (*Nicotiana benthamiana*) plants. Additionally, CNTs application enhanced the plant immunity by triggering defense-related phytohormones, antioxidant enzymes and improving photosynthetic performance. Polymeric ENMs such as polylactic acid, chitosan, pectin, carboxymethyl cellulose and alginate have attracted recent attention for controlled and sustained release of amicrobial agents and protect plants against pathogens (Shakiba et al., 2020; Vemula and Reddy, 2023). In a recent study, Hafeez et al. (2024) reveled that biologically produced chitosan NPs enhanced the rice blast disease resistance by improving antioxidant defense system (SOD, APX and CAT), nutrient uptake, photosynthesis efficiency and reducing the cellular oxidative stress (MDA and H_2O_2) in rice (*Oryza sativa* L.) plants. Nanohybrid, such as liposomes, nanocapsules (NCs), nanoemulsions and mesoporous silica nanoparticles (MSNs) can be engineered to carry pesticides, nutrients, enzymes and phytohormones for targeted delivery. Abdelrasoul et al. (2020) demonstrated that monoterpenes-based nanoemulsions at 100 mg L^{-1} concentration inhibited the *Pectobacterium carotovorum* and *Ralstonia solanacearum* pathogens growth and induced systemic resistance in potato (*Solanum tuberosum* L.) leaves by improving antioxidant enzymes activity. Overall, ENMs are able to modulate plant immune responses through multiple pathways, not only enhancing plant resistance to pathogens, but also promoting crop growth and increasing yields (Figure 2). However, there is still little understanding of the translocation, transformation, residue, and long-term environmental impact of ENMs in plants, and further research needs to be explored the potential mechanisms. In addition, the development of more environmentally friendly, efficient, and biodegradable ENMs formulations is also a key direction in future research.

4 Mechanisms of nano-enabled immunomodulation in plants

4.1 Nano-enabled activation of phytohormone signaling

Phytohormone signaling pathways are involved in inducing a variety of defense responses against biotic and abiotic stresses. Plant hormones such as jasmonic acid (JA), salicylic acid (SA), ethylene (ET) and abscisic acid (ABA) play an important role in the plant immune response against pathogens (Huang et al., 2020; Zhao et al., 2021). In recent years, nano-enabled activation of plant hormone signaling represents an innovative approach in plant disease management (Figure 3). ENMs can design too slowly release hormones in a controlled manner, thus activating signaling pathways and enhancing the plant resistance to microbial pathogens (Tripathi et al., 2022; Liu et al., 2024). For example, Noman et al. (2024) observed that soil-application with SA-doped FeNPs suppressed the Fusarium wilt disease in watermelon through inhibiting the fungal invasive growth and improving the antioxidative capacity, and primed a SAR response via activating the SA signaling genes (Figure 4B). In another study, lanthanum

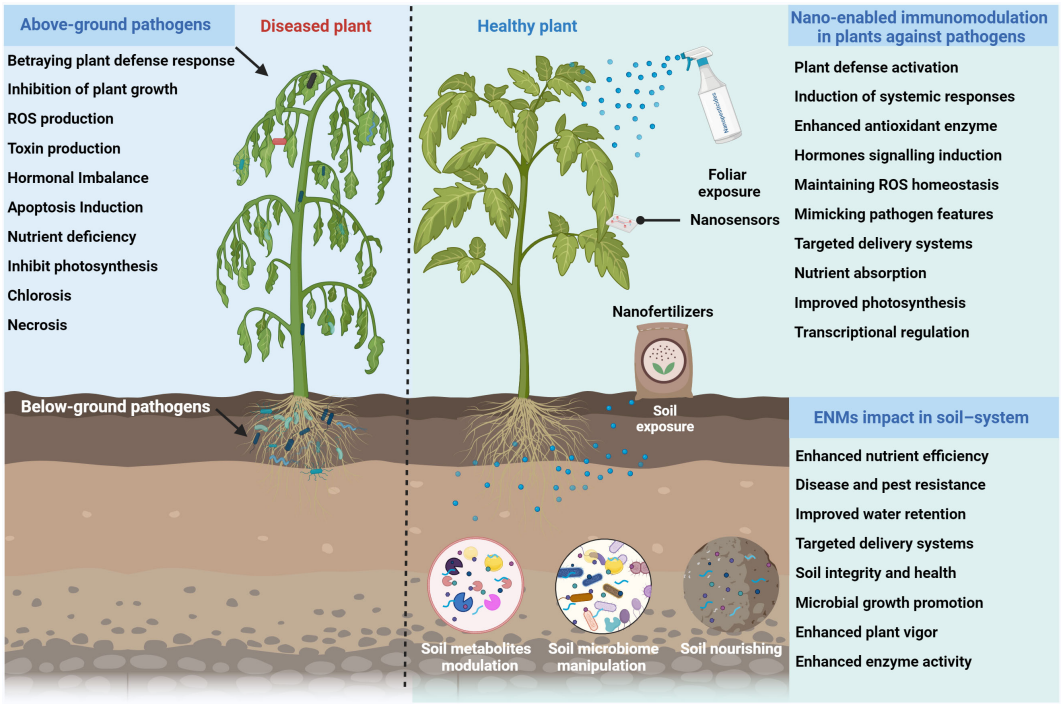

FIGURE 3
Schematic representation of nano-enabled immunomodulation to revolutionize plant health through several mechanisms. On the left, the diseased plant shows symptoms due to various pathogen-induced mechanisms, which inhibit plant growth. On the right, foliar and soil exposure to ENMs enhance plant growth by activating systemic responses, enhancing antioxidant enzyme activity, inducing hormone signaling, and maintaining ROS homeostasis.

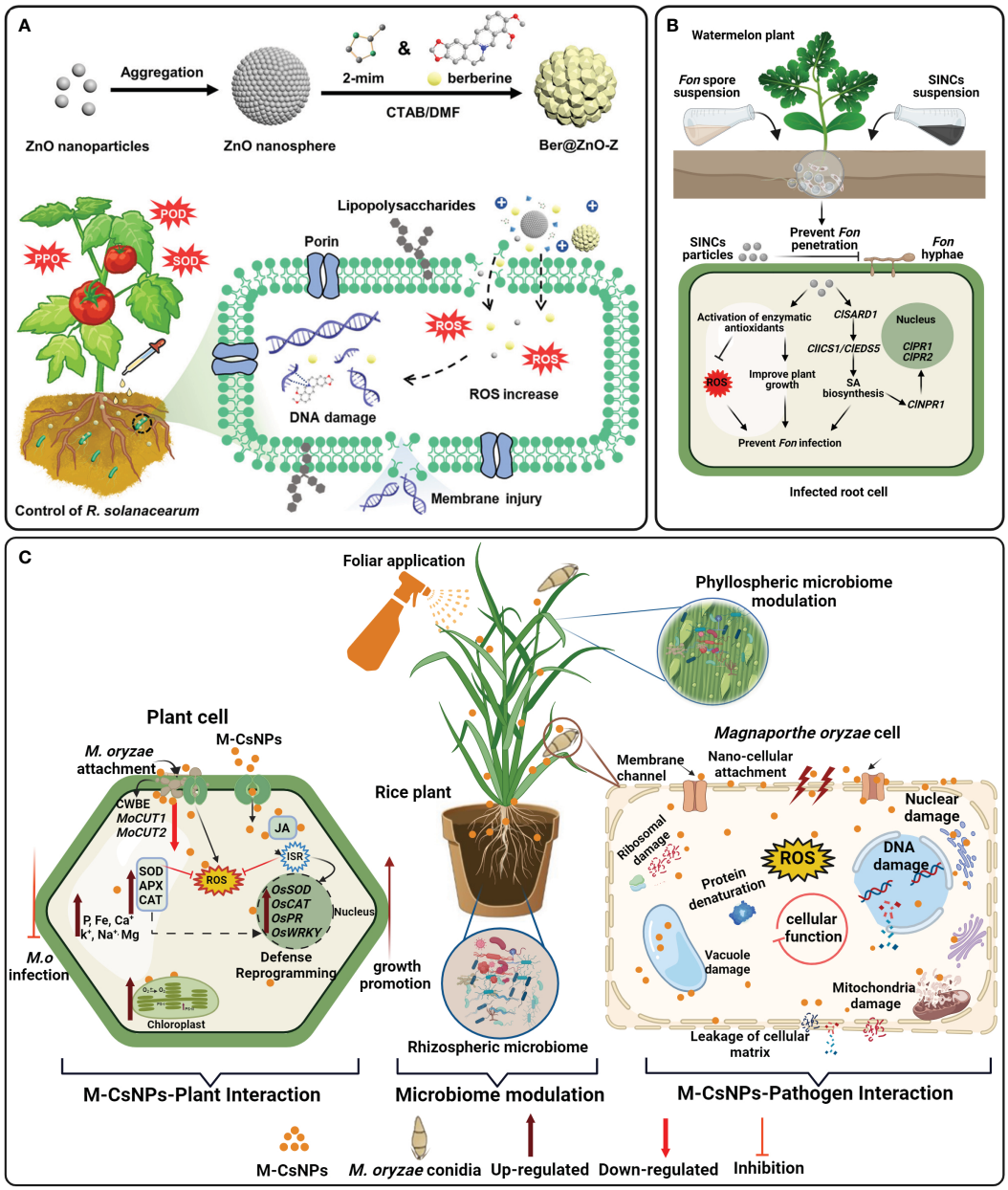

FIGURE 4
Examples of engineered nanomaterials (ENMs) used for plant disease management through immunomodulation. **(A)** The figure illustrates the synthesis of berberine-loaded ZnO-Z (Ber@ZnO-Z) nanosphere to synergistically control the bacterial wilt disease in tomato plants through direct pathogen inhibition and modulating antioxidant enzymes. Adapted with permission from reference (Liang et al., 2022). Copyright 2022 American Chemical Society. **(B)** Therapeutic delivery of salicylic acid-coated biogenic iron nanocomposites (BINCs) suppressed Fusarium wilt damages in watermelon plants by inducing systemic acquired resistance (SAR) and modulating antioxidative defense system. Adapted with permission from reference (Noman et al., 2024). Copyright 2024 Elsevier. **(C)** Schematic representation of the proposed mechanism of moringa chitosan nanoparticles (M-CsNPs) to control bacterial rice blast disease of rice. M-CsNPs act as nanofungicides that inhibit the pathogen *Magnaporthe oryzae* infection and improve defense responses by improving biochemical attributes and regulating transcriptional traits and modulating plant-associated microbiome. Adapted with permission from reference (Hafeez et al., 2024). Copyright 2024 Elsevier.

oxide NMs at 200 mg L^{-1} with different surface modifications significantly suppressed cucumber wilt disease by 12.50–52.11% by improving total amino acids, vitamin contents, and activating SA-dependent systemic acquired resistance (Cao et al., 2023a). Similarly, elemental sulfur NPs increase resistance against Fusarium wilt disease, caused by a fungal pathogen *Fusarium oxysporum* f. sp. *lycopersici*. Notably, sulfur NPs 30–100 mg L^{-1} suppressed pathogen infection by regulating the SA-dependent systemic acquired resistance pathway and modulating of the expression of antioxidase-related and pathogenesis-related genes.

Polymeric ENMs have also demonstrated excellent ability to regulate plant hormone signaling (Table 1). For example, Giri et al. (2023) reported that chitosan fabricated AgNPs control the bacterial leaf spot disease in tomato plants by inducing SAR

TABLE 1 Potential applications of engineered nanomaterials (ENMs) for improving immunomodulatory mechanisms and enhancing disease resilience in agricultural crops.

ENMs	ENMs concentrations	Target pathogens	Host plants	Mechanisms	References
Chitosan NPs	200 mg L^{-1}	*Magnaporthe oryzae*	Rice	Enhanced disease resistance by improving antioxidant enzymes, photosynthesis pigments and reshaping the rhizosphere microbiome	(Hafeez et al., 2024)
Chitosan-coated silica NPs	200 mg L^{-1}	*Fusarium virguliforme*	Soybeans	Reduced disease incidence by improving chlorophyll and micronutrient contents	(O'Keefe et al., 2024).
Chitosan coated zinc oxide NPs	200 µg mL^{-1}	*Pseudomonas syringae* pv. *tomato*	Tomato	Suppressed bacterial speck disease by improving photosynthesis parameters	(Esserti et al., 2024)
Chitosan coated iron NPs	250 mg L^{-1}	*Xanthomonas oryzae* pv. *oryzae*	Rice	Reduced disease incidence by inducing plant antioxidative defense mechanisms, and modulating microbiome	(Ahmed et al., 2022)
Copper chitosan NPs	0.16% w/v	*Curvularia lunata*	Maize	Enhanced defense responses by regulating antioxidant enzymes activity and photosynthesis profile	(Choudhary et al., 2017)
Copper oxide NPs	10-50 ppm	*Fusarium oxysporum*. f. sp. *ciceris*	Chickpea	Enhanced disease resistance by increasing photosynthetic rate, protein, tannin, phenolics, and flavonoid and enzyme contents	(Tiwari et al., 2024)
Copper NPs	31.25 mg L^{-1}	*Rhizoctonia solani*	Tomato	Suppressed disease progression by activating antioxidative defense response and improving chlorophyll contents	(Shen et al., 2020)
Copper NPs	100 µg mL^{-1}	*Acidovorax citrulli*	Watermelon	Activated antioxidant enzymes and stomatal immunity for disease suppression	(Noman et al., 2023c)
Zinc oxide NPs	–	*Fusarium oxysporum*	Tomato	Enhanced disease resistance by inducing plant defense responses	(Bouqellah et al., 2024)
Zinc oxide NPs	500 µg mL^{-1}	*Fusarium oxysporum*	Eggplant	Reduced disease incidence by activating plant biochemical defense mechanisms	(Abdelaziz et al., 2022)
Sulfur NPs	200 mg L^{-1}	*Fusarium oxysporum* f. sp. *Lycopersici*	Tomato	Preserved the enrichment of plant beneficial bacteria	(Steven et al., 2024).
Sulfur NPs	100 mg L^{-1}	*Fusarium oxysporum* f. sp. *Lycopersici*	Tomato	Reduced disease incidence by activating SA-mediated disease resistance mechanisms	(Cao et al., 2021)
Sulfur NPs	100 mg L^{-1}	*Pectobacterium carotovorum*	Lettuce	Decreased the disease occurrence by activating SA- and JA-dependent pathways	(Cao et al., 2023b)
Lanthanum silicate NPs	100 mg L^{-1}	*Rhizoctonia solani*	Rice	Enhanced disease resistance by regulating SAR immune responses	(Cao et al., 2023a)
Selenium	5 mg L^{-1}	*Rhizoctonia solani*	Rice	Suppressed disease by promoting flavonoid biosynthesis, antioxidative system and SA -dependent acquired disease resistance	(Chen et al., 2024)
SA-coated iron NPs	100 mg Kg L^{-1}	*Fusarium oxysporum* f. sp. *niveum*	Watermelon	Suppressed Fusarium wilt by inducing SAR response via activating antioxidative capacity and SA signaling pathway	(Noman et al., 2024)
Iron NPs	0.25 mM	*Fusarium oxysporum*	Cucumber	Reduced the disease incidence by improving morphological traits and photosynthetic pigments	(El-Batal et al., 2023)
Silver NPs	20 ppm	*Alternaria solani*	Tomato	Inhibited disease incidence by activating antioxidant enzymes and maintaining ROS homeostasis	(Narware et al., 2024)
Silver NPs	100 mg L^{-1}	*Xanthomonas oryzae* pv. *oryzae*	Rice	Decreased disease occurrence by regulating plant antioxidative defense system	(Ahmed et al., 2020)
Manganese NPs	100 µg mL^{-1}	*Fusarium oxysporum* f. sp. *niveum*	Watermelon	Suppressed disease progression by activating antioxidative defense response, phytohormones and modulating microbial community	(Noman et al., 2023a)
Manganese NPs	500 µg mL^{-1}	*Fusarium oxysporum* f. sp. *niveum*	Watermelon	Decreased disease occurrence by regulating the expression of defense-related genes	(Elmer et al., 2018)

(Continued)

TABLE 1 Continued

ENMs	ENMs concentrations	Target pathogens	Host plants	Mechanisms	References
Titanium dioxide NPs		*Ralstonia solanacearum*	Tomato	Increased disease resistance by regulating antioxidative immune responses	(Pan et al., 2023)
Quantum dots	50 mg L^{-1}	*Verticillium dahliae*	Cotton	Suppressed disease by maintaining ROS homeostasis	(Qiu et al., 2023a)
Silica NPs	25-1600 mg L^{-1}	*Pseudomonas syringae*	*Arabidopsis thaliana*	Increased disease resistance by inducing SAR immune responses	(El-Shetehy et al., 2021)
MOFs NPs	5-15 mg L^{-1}	*Phytophthora infestans*	Wheat	Controlled release of fungicide significantly inhibited the fungal pathogen and improved the plant growth	(Shan et al., 2020)
MOFs NPs	1 mg L^{-1}	*Rhizoctonia solani*	Rice	*In vitro* studies showed the antifungal activity of MOFs, while also enhancing plant growth	Huang et al., 2023)

mechanism through upregulating stress hormones responsive genes (*PR1*, *NHO1*, *NPR1*, *MYC2*, *JAR1*, *ERF1*). Taken together, these previous studies confirm that ENMs can precisely regulate plant immune responses by influencing hormone concentrations and regulating signaling pathways. However, the mechanism of action of different ENMs is different, and the specific effect may also vary depending on the plant species and the type of pathogen. In the future, it is necessary to study the interaction between ENMs and molecular networks in plants and explore new strategies to improve the specificity of immune mechanisms.

4.2 Nano-enabled stimulation of antioxidant defense system

Nano-enabled stimulation of the plant antioxidant defense system offers a promising approach to mitigating the deleterious effects of oxidative stress induced by pathogens (Pan et al., 2023). This system is designed to neutralize reactive oxygen species (ROS) generated during pathogen attacks or other stress conditions. ROS can cause oxidative damage to cellular components, including lipids, proteins, and DNA, ultimately leading to cell death and tissue dysfunction (Chen et al., 2023). The antioxidant defense enzymes (CAT, SOD, POD, APX, PPO) acts as a frontline defense, mitigating the detrimental effects of ROS and protecting plant cells from oxidative stress (Dvořák et al., 2021). ENMs with their unique physicochemical properties, have demonstrated the ability to modulate the plant antioxidant defense system. Notably, ENMs can interact with plant cells and trigger specific signaling pathways (Figure 3), leading to the upregulation of antioxidant enzymes and the biosynthesis of non-enzymatic antioxidants (Abdelrhim et al., 2021; Tiwari et al., 2024). For example, Noman et al. (2023c) investigated that foliar exposure of biogenic CuNPs at 100 µg mL^{-1} concentration substantially suppressed bacterial fruit blotch disease in watermelon plants by triggering antioxidants enzymes (CAT, SOD and POD), modulating stomatal immunity, and reducing the ROS activity.

In another study, biologically synthesized AgNPs improved early blight disease resistance by enhancing antioxidant enzymes (CAT, LPX, PO, SOD), and maintaining ROS (H_2O_2 and O^-_2) homeostasis in tomato plants (Narware et al., 2024). Similarly, FeO nanocomposites control the cucumber wilt disease caused by *Fusarium oxysporum* by stimulating morphological performances, total phenol, soluble protein contents, photosynthetic pigments and antioxidant enzymes (POD and PPO) (El-Batal et al., 2023). Liang et al. (2022) demonstrated that berberine loaded ZnO NMs at 100-1000 ug mL^{-1} significantly reduced the tomato bacterial wilt disease severity by 45.8% by improving the plant growth and antioxidant enzymes (SOD, PPO, PPO) (Figure 4A). Previous studies primarily focused on the mitigation of pathogen-induced oxidative stress by enhancing antioxidant activity (Table 1). However, ongoing research exploring biocompatible ENMs formulations and targeted delivery methods holds immense potential for sustainable agriculture and food security.

4.3 Nano-enabled regulation of photosynthesis and nutritional profile

Photosynthesis is an important process that drives plant growth and development, is often disrupted by pathogen infections (Yang and Luo, 2021). Phytopathogens can negatively impact photosynthesis by disrupting the structure and function of photosynthetic apparatus, reducing the efficiency of light harvesting, and impairing carbon fixation. Consequently, this can lead to reduced plant productivity, compromised nutrient acquisition, and an overall decline in plant health (Parveen and Siddiqui, 2021; Karpagam et al., 2023). In recent years, ENMs mediated regulation of photosynthesis and the nutritional profile of plants represents a promising strategy in sustainable agriculture, offering a multifaceted approach to mitigating the impacts of pathogens on crop productivity and quality (Figure 3). Importantly, ENMs can interact with plant cells and trigger specific signaling pathways, leading to the upregulation of photosynthetic enzymes, the biosynthesis of pigments, and the modulation of nutrient uptake and assimilation (Ahmed et al., 2022; Parveen and Siddiqui, 2022). For example, the foliar application of ZnONPs at 0.20 mL^{-1} concentrations significantly enhanced the plant growth and photosynthesis efficiency (Total chlorophyll and carotenoids contents) of tomato plants under

several bacterial and fungal pathogens infection (Parveen and Siddiqui, 2021).

In another recent study, Esserti et al. (2024) chitosan embedded ZnONPs effectively control the bacterial speck disease of tomato by improving the plant growth, photosynthetic pigments (Chlorophyll a, Chlorophyll b, carotenoids), and gas exchange parameters such as internal CO_2 concentration, net photosynthesis rate, transpiration rate and stomatal conductance. Notable, this study showed that bacterial speck disease significantly affected plant biomass and photosynthetic performance; however, NP applications mitigate the negative impact of phytopathogens. Likewise, Mogazy et al. (2022) reported that Ca and FeNPs at (100 and 200 ppm) positively regulate innate immune responses in strawberry (*Fragaria ananassa*) plants against gray mold disease caused by a fungal pathogen *Botrytis cinerea*. This study revealed that foliar exposure of NPs significantly increased the vitamin, phenolics, and flavonoids contents, and nutritional profile (Zn^{2+}, Mg^{2+}, Ca^{2+}, Fe, N, P, and K^{+}) in strawberry plants as compared to infected control. Likewise, chitosan coated mesoporous SiNPs treatment significantly reduced the sudden death syndrome by 30% and increased the micronutrient (Zn, Mn, Mg, K, B) content, and chlorophyll efficiency in soybean plants (O'Keefe et al., 2024). Taken together, previous studies demonstrated that nano-enabled regulation of nutritional profiles and photosynthesis shows great promise in mitigating pathogen impacts on crops (Table 1). However further research on ENMs toxicity, application methods, and biosafety is recommended for sustainable agricultural applications.

4.4 Nano-enabled modulation of microbiome and metabolites

The plant-associated microbiome (bacteria, fungi, viruses) plays a crucial role in plant health, growth, and resistance against pathogens (Trivedi et al., 2020; Steven et al., 2024). The plant-associated microbiome serves as a frontline defense against pathogens, conferring protection through various mechanisms, such as competitive exclusion, antimicrobial compound production, and the induction of systemic resistance pathways in plants (Fitzpatrick et al., 2020; Wang et al., 2022). Additionally, the intricate network of metabolites produced by plants and their associated microbiomes acts as a defensive arsenal against invading pathogens (Liu et al., 2020; Rangel and Bolton, 2022). However, microbial pathogens can disrupt the delicate balance of the plant microbiome, leading to dysbiosis and compromising plant health (Zhang et al., 2021a). Nano-enabled microbiome engineering has recently emerged as a powerful platform to enhance plant resilience against pathogenic threats (Ahmed et al., 2023; Hussain et al., 2023). In recent years, several studies have demonstrated the potential impact of ENMs plant-associated microbiome under biotic stress condition. The application of biogenic chitosan-Fe nanocomposite (BNCs) at 250 µg mL^{-1} concentration significantly reduced the bacterial leaf blight (BLB) disease incidence (67.1%) by enhancing the relative abundance of beneficial bacterial community such as *Allorhizobium*, *Ochrobactrum*, *Pseudolabrys*, *Sphingomonas*, *Devosia*, *Bradyrhizobium* and *Methylobacterium* in rice plants (Ahmed et al., 2022).

Additionally, BNCs amendments also enhanced the rice plant growth by modulating antioxidant enzymes, enhancing photosynthesis efficiency, and reducing ROS activity. Similarly, Noman et al. (2023a) revealed that soil application of biologically synthesized manganese (Mn) NPs control the Fusarium wilt disease in watermelon by enhancing SAR mechanism via triggering antioxidative defense machinery, SA signaling pathway, and modulating the soil bacterial community (*Sphingomonas*, *Gemmatimonadaceae*, *Nocardioides*, and *Burkholderiaceae*) and fungal community (*Penicillium*, *Botryotrichum*, *Conocybe*, and *Mortierella*). The foliar spray of nitrogen-doped CDs (10 mg L^{-1}) alleviated tomato bacterial wilt disease induced damage by 71.2% through indirect resistance activation (SAR activation) and ROS scavenging. Moreover, metabolomics profile revealed that nitrogen doped CDs significantly improved the fatty acid and tricarboxylic acid synthesis in tomato plants (Luo et al., 2021). Similarly, the application of sulfur NMs at 10–100 mg L^{-1} significantly decreased the occurrence of bacterial soft rot disease in lettuce (*Lactuca sativa* L.) plants by improving the chlorophyll contents, antioxidant enzymes and regulating the defense-related genes expression. In addition, metabolomics analysis showed that sulfur NMs enhanced the tricarboxylic acid cycle and also regulated SA and JA metabolite biosynthesis, thereby enhancing the bacterial soft rot disease resistance in lettuce (Cao et al., 2023b). Taken together, nano-enabled modulation of microbiome and metabolites profile to enhance plant disease resistance has the potential to serve as highly sustainable, efficient, sustainable, and non-toxic alternative for the management of plant diseases (Figure 3).

4.5 Nano-enabled activation of defense related genetic pathways

Plants have evolved intricate defense mechanisms to protect themselves against a wide range of microbial pathogens. These defense responses are governed by complex genetic pathways that involve the coordinated expression of numerous genes encoding various proteins, enzymes, and signaling molecules (Kaur et al., 2022). After pathogens attack, specific defense-related genes are activated, triggering a cascade of events that ultimately lead to the production of antimicrobial compounds, the reinforcement of physical barriers, and the activation of systemic resistance pathways (Nishad et al., 2020; Dodds et al., 2024). Nano-enabled activation of defense-related genetic pathways represents a promising strategy in sustainable agriculture, offering a targeted and efficient approach to enhancing plant resilience against pathogenic threats (Cao et al., 2023a). For example, selenium (Se) NMs application 5 mg L^{-1} decreased the disease severity (68.8%) by enhancing the organic Se content (44.8%), nutritional quality by (7.2%) and rice yield up to (31.1%). Additionally, metabolomic and transcriptomic analyses confirmed that SeNMs simultaneously boosted the SA and JA dependent acquired disease resistance pathways, flavonoid biosynthesis and antioxidative defense system. Notably, Importantly, SeNMs significantly upregulated

the expression of genes *LOX2*, *LOX3*, *LOX6*, *OPR1*, *PR1*, *PR3*, *AOC*, and *JAR* while reducing the expression level of genes *POD*, *CAT*, and *SOD2* in rice plants compared to the infected controls, indicating overall stimulation of SAR in SeNM-treated rice (Chen et al., 2024).

Similarly, Hafeez et al. (2024) revealed that foliar exposure of biogenic chitosan NPs at 200 mg L^{-1} significantly control the rice blast disease by triggering defense related genes expression such as (*OsNPP1*, *OsGRF9, WRKY71, OsAPX, OsSOD, OsCAT, OsNPR1, OsPR1, OsPR9*, and *MoCUT2*) in rice plants (Figure 4C). In another study, seed primed with AgNPs enhanced the rice blast disease resistant by triggering transcriptional and metabolic reprogramming in rice seeds. In this study, KEGG pathway of transcriptomics data demonstrated that AgNPs-priming activated stress signaling and defense related pathways, such as MAPK signaling pathway, flavonol biosynthesis, glutathione metabolism, plant hormone signal transduction, and plant–pathogen interaction (Yan et al., 2022). Similarly, the application of ROS-generating AgNPs as nano-stimulants significantly triggered plant immune/stress responses against rice blast disease. The disease resilience mechanisms showed that AgNPs mediated "stress memory" induced considerable transcriptional reprogramming in rice leaves by modulating the expression of defense genes, including pathogen-plant interaction genes, cell membrane lipid metabolism genes, specialized metabolite biosynthesis-related genes, and other genes related to biosynthesis. These studies have demonstrated the potential of nanotechnology-mediated activation of defense-related gene expression in enhancing crop resilience against pathogens. However, further research is needed to explore the molecular signaling pathways involved in the interactions between ENMs and plant pathogens, as well as their co-stimulating impact on plant defense against phytopathogens.

5 Concluding remarks and future outlook

The promising field of nano-enabled immunomodulation has demonstrated exceptional opportunities to enhance plant resilience against a multitude of phytopathogenic threats (Zhang et al., 2024). The unique physicochemical properties of ENMs, coupled with their ability to interact with and modulate intricate plant defense mechanisms, have positioned them as promising tools in sustainable disease management strategies (Singh et al., 2024). However, as this domain continues to evolve, several critical considerations and future research directions must be addressed to harness the full potential of these innovative approaches. Firstly, while significant progress has been made in elucidating the underlying mechanisms through which ENMs influence plant immune responses, a comprehensive understanding of the complex interplay between ENMs and the intricate molecular networks governing plant defense remains elusive (Zhang et al., 2020; Kumar et al., 2024). Future endeavors should focus on unraveling the intricate signaling cascades, transcriptional regulation by ENMs, enabling the development of more targeted and efficient immunomodulatory strategies (Ma et al., 2023b; Zhang et al., 2024).

Additionally, the transformation of nano-enabled immunomodulation from laboratory-scale studies to field applications necessitates rigorous investigations into the environmental fate, behavior, and potential risks associated with the use of ENMs in agricultural settings (Ahmed et al., 2023; Ma et al., 2023a). Comprehensive assessments of the long-term impacts on soil health, nutrient cycling, and ecosystem dynamics are imperative to ensure the responsible and sustainable integration of these technologies into agricultural practices (Ijaz et al., 2023). Furthermore, the development of environmentally friendly, biodegradable, and biocompatible ENM formulations should be a priority, minimizing potential adverse effects on non-target organisms and ensuring compatibility with diverse plant species and environmental conditions (Balusamy et al., 2023; Wahab et al., 2024). Interdisciplinary collaborations between material scientists, plant biologists, and ecotoxicologists could facilitate the design and synthesis of tailored nanomaterials that balance efficacy, sustainability, and biosafety considerations (Shelar et al., 2023; Zain et al., 2023).

Another crucial aspect that warrants attention is the optimization of ENM delivery methods and application techniques. Developing efficient and targeted delivery systems, such as nanocarriers or nanoemulsions, could enhance the bioavailability and site-specific delivery of immunomodulatory agents, minimizing potential off-target effects and maximizing the desired immune responses (Ma et al., 2023c; Jeon et al., 2024). By addressing these critical considerations and leveraging the transformative potential of nanotechnology, researchers and agricultural stakeholders can revolutionize plant disease management practices, contributing to a more resilient, sustainable, and secure global food system.

Author contributions

HM: Investigation, Resources, Software, Validation, Visualization, Writing – original draft. YQ: Data curation, Investigation, Resources, Software, Visualization, Writing – original draft, Writing – review & editing. MZ: Conceptualization, Resources, Software, Validation, Visualization, Writing – original draft, Writing – review & editing. ZL: Formal analysis, Funding acquisition, Investigation, Software, Supervision, Validation, Writing – review & editing. SA: Conceptualization, Data curation, Investigation, Validation, Writing – review & editing. J-ML: Data curation, Formal analysis, Investigation, Software, Validation, Writing – review & editing. MS: Data curation, Formal analysis, Investigation, Validation, Writing – review & editing. HA: Conceptualization, Resources, Validation, Visualization, Writing – review & editing. GO: Data curation, Funding acquisition, Software, Validation, Visualization, Writing – review & editing. XQ: Conceptualization, Data curation, Funding acquisition, Investigation, Software, Supervision, Visualization, Writing – original draft, Writing – review & editing.

Funding

The author(s) declare financial support was received for the research, authorship, and/or publication of this article. This research was supported by the Project of Xianghu Laboratory under Grant No. 2023C02031 and 2023C1S02002, and the Scientific Research Foundation of Xianghu Laboratory. This study has been partly conducted under the IP-2022-10-7906 funded by the Croatian Science Foundation, and WAST2GROW project (NPOO.C3.2.R3-I1.04.0143) founded by the Ministry of Science and Education, R. of Croatia.

Acknowledgments

During the preparation of this work the author(s) used BioRender to make figures and used Claude tool to improve language and readability. After using this tool, the author(s) reviewed and edited the content as needed and take(s) full responsibility for the content of the publication.

Conflict of interest

The authors declare that the research was conducted in the absence of any commercial or financial relationships that could be construed as a potential conflict of interest.

Publisher's note

All claims expressed in this article are solely those of the authors and do not necessarily represent those of their affiliated organizations, or those of the publisher, the editors and the reviewers. Any product that may be evaluated in this article, or claim that may be made by its manufacturer, is not guaranteed or endorsed by the publisher.

References

Abdelaziz, A. M., Salem, S. S., Khalil, A. M., El-Wakil, D. A., Fouda, H. M., and Hashem, A. H. (2022). Potential of biosynthesized zinc oxide nanoparticles to control Fusarium wilt disease in eggplant (Solanum melongena) and promote plant growth. *BioMetals* 35, 601–616. doi: 10.1007/s10534-022-00391-8

Abdelrasoul, M. A., Eid, A. R., and Badawy, M. E. (2020). Preparation, characterizations and antibacterial activity of different nanoemulsions incorporating monoterpenes: in *vitro* and in *vivo* studies. *Arch. Phytopathol. Plant Prot.* 53, 310–334. doi: 10.1080/03235408.2020.1744977

Abdelrhim, A. S., Mazrou, Y. S., Nehela, Y., Atallah, O. O., El-Ashmony, R. M., and Dawood, M. F. (2021). Silicon dioxide nanoparticles induce innate immune responses and activate antioxidant machinery in wheat against Rhizoctonia solani. *Plants* 10, 2758. doi: 10.3390/plants10122758

Adeel, M., Farooq, T., White, J. C., Hao, Y., He, Z., and Rui, Y. (2021). Carbon-based nanomaterials suppress tobacco mosaic virus (TMV) infection and induce resistance in Nicotiana benthamiana. *J. Hazard. Mater.* 404, 124167. doi: 10.1016/j.jhazmat.2020.124167

Ahmed, T., Noman, M., Gardea-Torresdey, J. L., White, J. C., and Li, B. (2023). Dynamic interplay between nano-enabled agrochemicals and the plant-associated microbiome. *Trends Plant Sci.* 28, 1310–1325. doi: 10.1016/j.tplants.2023.06.001

Ahmed, T., Noman, M., Jiang, H., Shahid, M., Ma, C., Wu, Z., et al. (2022). Bioengineered chitosan-iron nanocomposite controls bacterial leaf blight disease by modulating plant defense response and nutritional status of rice (Oryza sativa L.). *Nano Today* 45, 101547. doi: 10.1016/j.nantod.2022.101547

Ahmed, T., Noman, M., White, J. C., Ma, C., Wang, Q., and Li, B. (2024). Quantum dots: next shift to combat plant diseases. *Trends Plant Sci*. doi: 10.1016/j.tplants.2024.02.006

Ahmed, T., Shahid, M., Noman, M., Niazi, M. B. K., Mahmood, F., Manzoor, I., et al. (2020). Silver nanoparticles synthesized by using Bacillus cereus SZT1 ameliorated the damage of bacterial leaf blight pathogen in rice. *Pathogens* 9, 160. doi: 10.3390/pathogens9030160

Anders, S., Cowling, W., Pareek, A., Gupta, K. J., Singla-Pareek, S. L., and Foyer, C. H. (2021). Gaining acceptance of novel plant breeding technologies. *Trends Plant Sci.* 26, 575–587. doi: 10.1016/j.tplants.2021.03.004

Balusamy, S. R., Joshi, A. S., Perumalsamy, H., Mijakovic, I., and Singh, P. (2023). Advancing sustainable agriculture: a critical review of smart and eco-friendly nanomaterial applications. *J. Nanobiotechnol.* 21, 372. doi: 10.1186/s12951-023-02135-3

Beckers, S. J., Staal, A. H., Rosenauer, C., Srinivas, M., Landfester, K., and Wurm, F. R. (2021). Targeted drug delivery for sustainable crop protection: transport and stability of polymeric nanocarriers in plants. *Adv. Sci.* 8, 2100067. doi: 10.1002/advs.202100067

Bouqellah, N. A., El-Sayyad, G. S., and Attia, M. S. (2024). Induction of tomato plant biochemical immune responses by the synthesized zinc oxide nanoparticles against wilt-induced Fusarium oxysporum. *Int. Microbiol.* 27, 435–448. doi: 10.1007/s10123-023-00404-7

Cao, X., Chen, X., Liu, Y., Wang, C., Yue, L., Elmer, W. H., et al. (2023a). Lanthanum silicate nanomaterials enhance sheath blight resistance in rice: mechanisms of action and soil health evaluation. *ACS Nano.* 17, 15821–15835. doi: 10.1021/acsnano.3c03701

Cao, X., Liu, Y., Luo, X., Wang, C., Yue, L., Elmer, W., et al. (2023b). Mechanistic investigation of enhanced bacterial soft rot resistance in lettuce (Lactuca sativa L.) with elemental sulfur nanomaterials. *Sci. Total Environ.* 884, 163793. doi: 10.1016/j.scitotenv.2023.163793

Cao, X., Wang, C., Luo, X., Yue, L., White, J. C., Elmer, W., et al. (2021). Elemental sulfur nanoparticles enhance disease resistance in tomatoes. *ACS Nano.* 15, 11817–11827. doi: 10.1021/acsnano.1c02917

Ceulemans, E., Ibrahim, H. M., De Coninck, B., and Goossens, A. (2021). Pathogen effectors: exploiting the promiscuity of plant signaling hubs. *Trends Plant Sci.* 26, 780–795. doi: 10.1016/j.tplants.2021.01.005

Chen, S., Guo, X., Zhang, B., Nie, D., Rao, W., Zhang, D., et al. (2023). Mesoporous silica nanoparticles induce intracellular peroxidation damage of Phytophthora infestans: A new type of green fungicide for late blight control. *Environ. Sci. Technol.* 57, 3980–3989. doi: 10.1021/acs.est.2c07182

Chen, X., Jiang, Y., Wang, C., Yue, L., Li, X., Cao, X., et al. (2024). Selenium nanomaterials enhance sheath blight resistance and nutritional quality of rice: mechanisms of action and human health benefit. *ACS Nano*. doi: 10.1021/acsnano.4c01835

Choudhary, R. C., Kumaraswamy, R., Kumari, S., Sharma, S., Pal, A., Raliya, R., et al. (2017). Cu-chitosan nanoparticle boost defense responses and plant growth in maize (Zea mays L.). *Sci. Rep.* 7, 9754. doi: 10.1038/s41598-017-08571-0

Conway, G. (1998). *The doubly green revolution: food for all in the twenty-first century* (Ithaca, New York: Cornell University Press). doi: 10.7591/9781501722660

Dodds, P. N., Chen, J., and Outram, M. A. (2024). Pathogen perception and signalling in plant immunity. *Plant Cell.*, koae020. doi: 10.1093/plcell/koae020

Dou, D., and Zhou, J.-M. (2012). Phytopathogen effectors subverting host immunity: different foes, similar battleground. *Cell Host Microbe* 12, 484–495. doi: 10.1016/j.chom.2012.09.003

Dvořák, P., Krasylenko, Y., Zeiner, A., Šamaj, J., and Takáč, T. (2021). Signaling toward reactive oxygen species-scavenging enzymes in plants. *Front. Plant Sci.* 11, 618835. doi: 10.3389/fpls.2020.618835

El-Batal, A. I., El-Sayyad, G. S., Al-Shammari, B. M., Abdelaziz, A. M., Nofel, M. M., Gobara, M., et al. (2023). Protective role of iron oxide nanocomposites on disease index, and biochemical resistance indicators against Fusarium oxysporum induced-cucumber wilt disease: *In vitro*, and in *vivo* studies. *Microb. Pathog.* 180, 106131. doi: 10.1016/j.micpath.2023.106131

Elmer, W., de la Torre-Roche, R., Pagano, L., Majumdar, S., Zuverza-Mena, N., Dimkpa, C., et al. (2018). Effect of metalloid and metal oxide nanoparticles on Fusarium wilt of watermelon. *Plant Dis.* 102, 1394–1401. doi: 10.1094/PDIS-10-17-1621-RE

El-Shetehy, M., Moradi, A., Maceroni, M., Reinhardt, D., Petri-Fink, A., Rothen-Rutishauser, B., et al. (2021). Silica nanoparticles enhance disease resistance in Arabidopsis plants. *Nat. Nanotechnol.* 16, 344–353. doi: 10.1038/s41565-020-00812-0

Esserti, S., Billah, R. E. K., Venisse, J.-S., Smaili, A., Dich, J., Es-sahm, I., et al. (2024). Chitosan embedded with ZnO nanoparticles and hydroxyapatite: synthesis, antiphytopathogenic activity and effect on tomato grown under high density. *Sci. Hortic.* 326, 112778. doi: 10.1016/j.scienta.2023.112778

Fields, B., and Friman, V.-P. (2022). Microbial eco-evolutionary dynamics in the plant rhizosphere. *Curr. Opin. Microbiol.* 68, 102153. doi: 10.1016/j.mib.2022.102153

Fiol, D. F., Terrile, M. C., Frik, J., Mesas, F. A., Álvarez, V. A., and Casalongué, C. A. (2021). Nanotechnology in plants: recent advances and challenges. *J. Chem. Technol. Biotechnol.* 96, 2095–2108. doi: 10.1002/jctb.6741

Fitzpatrick, C. R., Salas-González, I., Conway, J. M., Finkel, O. M., Gilbert, S., Russ, D., et al. (2020). The plant microbiome: from ecology to reductionism and beyond. *Annu. Rev. Microbiol.* 74, 81–100. doi: 10.1146/annurev-micro-022620-014327

Giri, V. P., Pandey, S., Srivastava, S., Shukla, P., Kumar, N., Kumari, M., et al. (2023). Chitosan fabricated biogenic silver nanoparticles (Ch@BSNP) protectively modulate the defense mechanism of tomato during bacterial leaf spot (BLS) disease. *Plant Physiol. Biochem.* 197, 107637. doi: 10.1016/j.plaphy.2023.03.014

Hafeez, R., Guo, J., Ahmed, T., Jiang, H., Raza, M., Shahid, M., et al. (2024). Bio-formulated chitosan nanoparticles enhance disease resistance against rice blast by physiomorphic, transcriptional, and microbiome modulation of rice (Oryza sativa L.). *Carbohydr. Polym.* 334, 122023. doi: 10.1016/j.carbpol.2024.122023

Hannan Parker, A., Wilkinson, S. W., and Ton, J. (2022). Epigenetics: a catalyst of plant immunity against pathogens. *New Phytol.* 233, 66–83. doi: 10.1111/nph.17699

Harris, F. M., and Mou, Z. (2024). Damage-associated molecular patterns and systemic signaling. *Phytopathology* 114, 308–327. doi: 10.1094/PHYTO-03-23-0104-RVW

Hartmann, M., and Six, J. (2023). Soil structure and microbiome functions in agroecosystems. *Nat. Rev. Earth Environ.* 4, 4–18. doi: 10.1038/s43017-022-00366-w

Huang, W., Wang, M., Hu, Z., Yang, T., Pei, H., and Zhang, F. (2023). Multifunctional metal-organic framework with pH-response for co-delivery of prochloraz and siRNA to synergistic control pathogenic fungi. *Colloids Surf. A: Physicochem. Eng. Aspects* 670, 131563.

Huang, S., Zhang, X., and Fernando, W. D. (2020). Directing trophic divergence in plant-pathogen interactions: antagonistic phytohormones with NO doubt? *Front. Plant Sci.* 11, 600063. doi: 10.3389/fpls.2020.600063

Hussain, M., Shakoor, N., Adeel, M., Ahmad, M. A., Zhou, H., Zhang, Z., et al. (2023). Nano-enabled plant microbiome engineering for disease resistance. *Nano Today* 48, 101752. doi: 10.1016/j.nantod.2023.101752

Ijaz, M., Khan, F., Ahmed, T., Noman, M., Zulfiqar, F., Rizwan, M., et al. (2023). Nanobiotechnology to advance stress resilience in plants: Current opportunities and challenges. *Mater. Today Bio.* 9, 10075. doi: 10.1016/j.mtbio.2023.100759

Iswanto, A. B. B., Vu, M. H., Pike, S., Lee, J., Kang, H., Son, G. H., et al. (2022). Pathogen effectors: What do they do at plasmodesmata? *Mol. Plant Pathol.* 23, 795–804. doi: 10.1111/mpp.13142

Jeon, S. J., Zhang, Y., Castillo, C., Nava, V., Ristroph, K., Therrien, B., et al. (2024). Targeted delivery of sucrose-coated nanocarriers with chemical cargoes to the plant vasculature enhances long-distance translocation. *Small* 20, 2304588. doi: 10.1002/smll.202304588

Karpagam, T., Shanmugapriya, A., Suganya, V., Varalakshmi, B., and Firdous, J. (2023). "Advanced study of plant-microbe interactions in photosynthesis," in *Plant-Microbe Interaction-Recent Advances in Molecular and Biochemical Approaches* (Elsevier), 205–228. doi: 10.1016/B978-0-323-91875-6.00011-6

Kaur, S., Samota, M. K., Choudhary, M., Choudhary, M., Pandey, A. K., Sharma, A., et al. (2022). How do plants defend themselves against pathogens-Biochemical mechanisms and genetic interventions. *Physiol. Mol. Biol. Plants.* 28, 485–504. doi: 10.1007/s12298-022-01146-y

Kim, D.-Y., Patel, S. K., Rasool, K., Lone, N., Bhatia, S. K., Seth, C. S., et al. (2023). Bioinspired silver nanoparticle-based nanocomposites for effective control of plant pathogens: A review. *Sci. Total Environ.*, 168318.

König, A., Müller, R., Mogavero, S., and Hube, B. (2021). Fungal factors involved in host immune evasion, modulation and exploitation during infection. *Cell. Microbiol.* 23, e13272. doi: 10.1111/cmi.13272

Kumar, D., Singh, R., Upadhyay, S. K., Verma, K. K., Tripathi, R. M., Liu, H., et al. (2024). Review on interactions between nanomaterials and phytohormones: Novel perspectives and opportunities for mitigating environmental challenges. *Plant Sci.* 340, 111964. doi: 10.1016/j.plantsci.2023.111964

Laflamme, B., Dillon, M. M., Martel, A., Almeida, R. N., Desveaux, D., and Guttman, D. S. (2020). The pan-genome effector-triggered immunity landscape of a host-pathogen interaction. *Science* 367, 763–768. doi: 10.1126/science.aax4079

Lee, S., Lee, H. Y., Kang, H. J., Seo, Y. E., Lee, J. H., and Choi, D. (2024). Oomycete effector AVRblb2 targets cyclic nucleotide-gated channels through calcium sensors to suppress pattern-triggered immunity. *New Phytol.* 241, 1277–1291. doi: 10.1111/nph.19430

Li, P., Lu, Y.-J., Chen, H., and Day, B. (2020). The lifecycle of the plant immune system. *Crit. Rev. Plant Sci.* 39, 72–100. doi: 10.1080/07352689.2020.1757829

Li, K., Tan, H., Li, J., Li, Z., Qin, F., Luo, H., et al. (2023). Unveiling the effects of carbon-based nanomaterials on crop growth: from benefits to detriments. *J. Agric. Food Chem.* 71, 11860–11874. doi: 10.1021/acs.jafc.3c02768

Liang, W., Cheng, J., Zhang, J., Xiong, Q., Jin, M., and Zhao, J. (2022). pH-Responsive on-demand alkaloids release from core–shell ZnO@ ZIF-8 nanosphere for synergistic control of bacterial wilt disease. *ACS Nano.* 16, 2762–2773. doi: 10.1021/acsnano.1c09724

Liu, H., Brettell, L. E., Qiu, Z., and Singh, B. K. (2020). Microbiome-mediated stress resistance in plants. *Trends Plant Sci.* 25, 733–743. doi: 10.1016/j.tplants.2020.03.014

Liu, Z., Wen, F., Cheng, X., and Wu, Z. (2024). Nano-controlled release of phytohormones will broaden its application on plant protection. *Adv. Agrochem.* 3, 39–42. doi: 10.1016/j.aac.2023.11.004

Loo, E. P.-I., Tajima, Y., Yamada, K., Kido, S., Hirase, T., Ariga, H., et al. (2022). Recognition of microbe-and damage-associated molecular patterns by leucine-rich repeat pattern recognition receptor kinases confers salt tolerance in plants. *Mol. Plant-Microbe Interact.* 35, 554–566. doi: 10.1094/MPMI-07-21-0185-FI

Lü, P., Liu, Y., Yu, X., Shi, C.-L., and Liu, X. (2022). The right microbe-associated molecular patterns for effective recognition by plants. *Front. Microbiol.* 13, 1019069. doi: 10.3389/fmicb.2022.1019069

Luo, X., Cao, X., Wang, C., Yue, L., Chen, X., Yang, H., et al. (2021). Nitrogen-doped carbon dots alleviate the damage from tomato bacterial wilt syndrome: systemic acquired resistance activation and reactive oxygen species scavenging. *Environ. Sci.: Nano.* 8, 3806–3819.

Ma, C., Borgatta, J., Hudson, B. G., Tamijani, A. A., de la Torre-Roche, R., Zuverza-Mena, N., et al. (2020). Advanced material modulation of nutritional and phytohormone status alleviates damage from soybean sudden death syndrome. *Nat. Nanotechnol.* 15, 1033–1042. doi: 10.1038/s41565-020-00776-1

Ma, C., Han, L., Shang, H., Hao, Y., Xu, X., White, J. C., et al. (2023a). Nanomaterials in agricultural soils: Ecotoxicity and application. *Curr. Opin. Environ. Sci. Health* 31, 100432. doi: 10.1016/j.coesh.2022.100432

Ma, K.-W., Niu, Y., Jia, Y., Ordon, J., Copeland, C., Emonet, A., et al. (2021). Coordination of microbe–host homeostasis by crosstalk with plant innate immunity. *Nat. Plants.* 7, 814–825. doi: 10.1038/s41477-021-00920-2

Ma, Y., Wang, Y., Zhao, R., Wang, Z., Li, S., Yu, M., et al. (2023c). pH-responsive ZIF-8 film-coated mesoporous silica nanoparticles for clean, targeted delivery of fungicide and environmental hazard reduction. *J. Environ. Chem. Eng.* 11, 111513. doi: 10.1016/j.jece.2023.111513

Ma, N. L., Zhang, N., Yong, W. T. L., Misbah, S., Hashim, F., Soon, C. F., et al. (2023b). Use, exposure and omics characterisation of potential hazard in nanomaterials. *Mater. Today Adv.* 17, 100341. doi: 10.1016/j.mtadv.2023.100341

Mishra, B., Kumar, N., and Mukhtar, M. S. (2021). Network biology to uncover functional and structural properties of the plant immune system. *Curr. Opin. Plant Biol.* 62, 102057. doi: 10.1016/j.pbi.2021.102057

Mitchell, M. J., Billingsley, M. M., Haley, R. M., Wechsler, M. E., Peppas, N. A., and Langer, R. (2021). Engineering precision nanoparticles for drug delivery. *Nat. Rev. Drug Discovery* 20, 101–124. doi: 10.1038/s41573-020-0090-8

Mogazy, A. M., Mohamed, H. I., and El-Mahdy, O. M. (2022). Calcium and iron nanoparticles: A positive modulator of innate immune responses in strawberry against Botrytis cinerea. *Process Biochem.* 115, 128–145. doi: 10.1016/j.procbio.2022.02.014

Monson, R. K., Trowbridge, A. M., Lindroth, R. L., and Lerdau, M. T. (2022). Coordinated resource allocation to plant growth–defense tradeoffs. *New Phytol.* 233, 1051–1066. doi: 10.1111/nph.17773

Munaweera, T., Jayawardana, N., Rajaratnam, R., and Dissanayake, N. (2022). Modern plant biotechnology as a strategy in addressing climate change and attaining food security. *Agric. Food Secur.* 11, 1–28. doi: 10.1186/s40066-022-00369-2

Nabi, Z., Manzoor, S., Nabi, S. U., Wani, T. A., Gulzar, H., Farooq, M., et al. (2024). Pattern-Triggered Immunity and Effector-Triggered Immunity: crosstalk and cooperation of PRR and NLR-mediated plant defense pathways during host–pathogen interactions. *Physiol. Mol. Biol. Plants.*, 1–18. doi: 10.1007/s12298-024-01452-7

Narware, J., Singh, S. P., Ranjan, P., Behera, L., Das, P., Manzar, N., et al. (2024). Enhancing tomato growth and early blight disease resistance through green-synthesized silver nanoparticles: Insights into plant physiology. *S. Afr. J. Bot.* 166, 676–689. doi: 10.1016/j.sajb.2024.01.059

Ngou, B. P. M., Jones, J. D., and Ding, P. (2022). Plant immune networks. *Trends Plant Sci.* 27, 255–273. doi: 10.1016/j.tplants.2021.08.012

Nishad, R., Ahmed, T., Rahman, V. J., and Kareem, A. (2020). Modulation of plant defense system in response to microbial interactions. *Front. Microbiol.* 11, 514909. doi: 10.3389/fmicb.2020.01298

Noman, M., Ahmed, T., Ijaz, U., Shahid, M., Nazir, M. M., Azizullah,, et al. (2023a). Bio-functionalized manganese nanoparticles suppress Fusarium wilt in watermelon (Citrullus lanatus L.) by infection disruption, host defense response potentiation, and soil microbial community modulation. *Small* 19, 2205687. doi: 10.1002/smll.202205687

Noman, M., Ahmed, T., Shahid, M., Nazir, M. M., Li, D., and Song, F. (2024). Salicylic acid-doped iron nano-biostimulants potentiate defense responses and suppress Fusarium wilt in watermelon. *J. Adv. Res.* 59, 19–33. doi: 10.1016/j.jare.2023.06.011

Noman, M., Ahmed, T., Wang, J., Ijaz, M., Shahid, M., Islam, M. S., et al. (2023b). Nano-enabled crop resilience against pathogens: potential, mechanisms and strategies. *Crop Health* 1, 15. doi: 10.1007/s44297-023-00015-8

Noman, M., Ahmed, T., White, J. C., Nazir, M. M., Azizullah,, Li, D., et al. (2023c). Bacillus altitudinis-Stabilized Multifarious Copper Nanoparticles Prevent Bacterial Fruit Blotch in Watermelon (Citrullus lanatus L.): Direct Pathogen Inhibition, In Planta Particles Accumulation, and Host Stomatal Immunity Modulation. *Small* 19, 2207136. doi: 10.1002/smll.202207136

O'Keefe, T. L., Deng, C., Wang, Y., Mohamud, S., Torres-Gómez, A., Tuga, B., et al. (2024). Chitosan-Coated Mesoporous Silica Nanoparticles for Suppression of Fusarium virguliforme in Soybeans (Glycine max). *ACS Agric. Sci. Technol.*

Pan, X., Nie, D., Guo, X., Xu, S., Zhang, D., Cao, F., et al. (2023). Effective control of the tomato wilt pathogen using TiO 2 nanoparticles as a green nanopesticide. *Environ. Sci.: Nano.* 10, 1441–1452.

Parveen, A., and Siddiqui, Z. A. (2021). Zinc oxide nanoparticles affect growth, photosynthetic pigments, proline content and bacterial and fungal diseases of tomato. *Arch. Phytopathol. Plant Prot.* 54, 1519–1538. doi: 10.1080/03235408.2021.1917952

Parveen, A., and Siddiqui, Z. A. (2022). Impact of silicon dioxide nanoparticles on growth, photosynthetic pigments, proline, activities of defense enzymes and some bacterial and fungal pathogens of tomato. *Vegetos* 35, 83–93. doi: 10.1007/s42535-021-00280-4

Qiu, X., Kong, L., Chen, H., Lin, Y., Tu, S., Wang, L., et al. (2023b). The Phytophthora sojae nuclear effector PsAvh110 targets a host transcriptional complex to modulate plant immunity. *Plant Cell* 35, 574–597. doi: 10.1093/plcell/koac300

Qiu, P., Li, J., Zhang, L., Chen, K., Shao, J., Zheng, B., et al. (2023a). Polyethyleneimine-coated MXene quantum dots improve cotton tolerance to Verticillium dahliae by maintaining ROS homeostasis. *Nat. Commun.* 14, 7392. doi: 10.1038/s41467-023-43192-4

Rangel, L. I., and Bolton, M. D. (2022). The unsung roles of microbial secondary metabolite effectors in the plant disease cacophony. *Curr. Opin. Plant Biol.* 68, 102233. doi: 10.1016/j.pbi.2022.102233

Raymaekers, K., Ponet, L., Holtappels, D., Berckmans, B., and Cammue, B. P. (2020). Screening for novel biocontrol agents applicable in plant disease management–a review. *Biol. Control* 144, 104240. doi: 10.1016/j.biocontrol.2020.104240

Saleh, T. A. (2020). Nanomaterials: Classification, properties, and environmental toxicities. *Environ. Technol. Innov.* 20, 101067. doi: 10.1016/j.eti.2020.101067

Shakiba, S., Astete, C. E., Paudel, S., Sabliov, C. M., Rodrigues, D. F., and Louie, S. M. (2020). Emerging investigator series: polymeric nanocarriers for agricultural applications: synthesis, characterization, and environmental and biological interactions. *Environ. Sci.: Nano.* 7, 37–67. doi: 10.1039/C9EN01127G

Shan, Y., Cao, L., Muhammad, B., Xu, B., Zhao, P., Cao, C., et al. (2020). Iron-based porous metal–organic frameworks with crop nutritional function as carriers for controlled fungicide release. *J. colloid Interface Sci.* 566, 383–393. doi: 10.1016/j.jcis.2020.01.112

Shang, S., Liu, G., Zhang, S., Liang, X., Zhang, R., and Sun, G. (2024). A fungal CFEM-containing effector targets NPR1 regulator NIMIN2 to suppress plant immunity. *Plant Biotechnol. J.* 22, 82–97. doi: 10.1111/pbi.14166

Shelar, A., Nile, S. H., Singh, A. V., Rothenstein, D., Bill, J., Xiao, J., et al. (2023). Recent advances in nano-enabled seed treatment strategies for sustainable agriculture: challenges, risk assessment, and future perspectives. *Nano-Micro Lett.* 15, 54. doi: 10.1007/s40820-023-01025-5

Shen, Y., Borgatta, J., Ma, C., Elmer, W., Hamers, R. J., and White, J. C. (2020). Copper nanomaterial morphology and composition control foliar transfer through the cuticle and mediate resistance to root fungal disease in tomato (Solanum lycopersicum). *J. Agric. Food Chem.* 68, 11327–11338. doi: 10.1021/acs.jafc.0c04546

Singh, R., Choudhary, P., Kumar, S., and Daima, H. K. (2024). Mechanistic approaches for crosstalk between nanomaterials and plants: plant immunomodulation, defense mechanisms, stress resilience, toxicity, and perspectives. *Environ. Sci.: Nano*.

Singh, B. K., Delgado-Baquerizo, M., Egidi, E., Guirado, E., Leach, J. E., Liu, H., et al. (2023). Climate change impacts on plant pathogens, food security and paths forward. *Nat. Rev. Microbiol.* 21, 640–656. doi: 10.1038/s41579-023-00900-7

Son, W. K., Choi, Y. S., Han, Y. W., Shin, D. W., Min, K., Shin, J., et al. (2023). *In vivo* surface-enhanced Raman scattering nanosensor for the real-time monitoring of multiple stress signalling molecules in plants. *Nat. Nanotechnol.* 18, 205–216. doi: 10.1038/s41565-022-01274-2

Sood, M., Kapoor, D., Kumar, V., Kalia, N., Bhardwaj, R., Sidhu, G. P., et al. (2021). Mechanisms of plant defense under pathogen stress: A review. *Curr. Protein Pept. Sci.* 22, 376–395. doi: 10.2174/1389203722666210125122827

Steven, B., Hassani, M. A., LaReau, J. C., Wang, Y., and White, J. C. (2024). Nanoscale sulfur alters the bacterial and eukaryotic communities of the tomato rhizosphere and their interactions with a fungal pathogen. *NanoImpact* 33, 100495. doi: 10.1016/j.impact.2024.100495

Sun, T., and Zhang, Y. (2021). Short-and long-distance signaling in plant defense. *Plant J.* 105, 505–517. doi: 10.1111/tpj.15068

Tiwari, V., Bambharoliya, K. S., Bhatt, M. D., Nath, M., Arora, S., Dobriyal, A. K., et al. (2024). Application of green synthesized copper oxide nanoparticles for effective mitigation of Fusarium wilt disease in roots of Cicer arietinum. *Physiol. Mol. Plant Pathol.*, 102244. doi: 10.1016/j.pmpp.2024.102244

Totsline, N., Kniel, K. E., and Bais, H. P. (2023). Microgravity and evasion of plant innate immunity by human bacterial pathogens. *NPJ Microgravity.* 9, 71. doi: 10.1038/s41526-023-00323-x

Tripathi, D., Singh, M., and Pandey-Rai, S. (2022). Crosstalk of nanoparticles and phytohormones regulate plant growth and metabolism under abiotic and biotic stress. *Plant Stress.* 6, 100107. doi: 10.1016/j.stress.2022.100107

Trivedi, P., Leach, J. E., Tringe, S. G., Sa, T., and Singh, B. K. (2020). Plant–microbiome interactions: from community assembly to plant health. *Nat. Rev. Microbiol.* 18, 607–621. doi: 10.1038/s41579-020-0412-1

Vega-Vásquez, P., Mosier, N. S., and Irudayaraj, J. (2021). Nanovaccine for plants from organic waste: D-limonene-loaded chitosan nanocarriers protect plants against Botrytis cinerea. *ACS Sustain. Chem. Eng.* 9, 9903–9914.

Vemula, M., and Reddy, A. V. B. (2023). Polymeric nanoparticles as effective delivery systems in agriculture sustainability. *Nanotechnol. Environ. Eng.* 8, 805–814. doi: 10.1007/s41204-023-00319-8

Wahab, A., Muhammad, M., Ullah, S., Abdi, G., Shah, G. M., Zaman, W., et al. (2024). Agriculture and environmental management through nanotechnology: Eco-friendly nanomaterial synthesis for soil-plant systems, food safety, and sustainability. *Sci. Total Environ.*, 171862.

Wang, Y., Pruitt, R. N., Nuernberger, T., and Wang, Y. (2022). Evasion of plant immunity by microbial pathogens. *Nat. Rev. Microbiol.* 20, 449–464. doi: 10.1038/s41579-022-00710-3

Wang, D., Wei, L., Liu, T., Ma, J., Huang, K., Guo, H., et al. (2023). Suppression of ETI by PTI priming to balance plant growth and defense through an MPK3/MPK6-WRKYs-PP2Cs module. *Mol. Plant* 16, 903–918. doi: 10.1016/j.molp.2023.04.004

Yan, X., Chen, S., Pan, Z., Zhao, W., Rui, Y., and Zhao, L. (2022). AgNPs-triggered seed metabolic and transcriptional reprogramming enhanced rice salt tolerance and blast resistance. *ACS Nano.* 17, 492–504. doi: 10.1021/acsnano.2c09181

Yang, H., and Luo, P. (2021). Changes in photosynthesis could provide important insight into the interaction between wheat and fungal pathogens. *Int. J. Mol. Sci.* 22, 8865. doi: 10.3390/ijms22168865

Zain, M., Ma, H., Chaudhary, S., Nuruzaman, M., Azeem, I., Mehmood, F., et al. (2023). Nanotechnology in precision agriculture: Advancing towards sustainable crop production. *Plant Physiol. Biochem.*, 108244. doi: 10.2139/ssrn.4663507

Zhang, J., Cook, J., Nearing, J. T., Zhang, J., Raudonis, R., Glick, B. R., et al. (2021a). Harnessing the plant microbiome to promote the growth of agricultural crops. *Microbiol. Res.* 245, 126690. doi: 10.1016/j.micres.2020.126690

Zhang, P., Guo, Z., Ullah, S., Melagraki, G., Afantitis, A., and Lynch, I. (2021b). Nanotechnology and artificial intelligence to enable sustainable and precision agriculture. *Nat. Plants.* 7, 864–876. doi: 10.1038/s41477-021-00946-6

Zhang, P., Guo, Z., Zhang, Z., Fu, H., White, J. C., and Lynch, I. (2020). Nanomaterial transformation in the soil–plant system: implications for food safety and application in agriculture. *Small* 16, 2000705. doi: 10.1002/smll.202000705

Zhang, P., Jiang, Y., Schwab, F., Monikh, F. A., Grillo, R., White, J. C., et al. (2024). Strategies for enhancing plant immunity and resilience using nanomaterials for sustainable agriculture. *Environ. Sci. Technol.* doi: 10.1021/acs.est.4c03522

Zhao, B., Liu, Q., Wang, B., and Yuan, F. (2021). Roles of phytohormones and their signaling pathways in leaf development and stress responses. *J. Agric. Food Chem.* 69, 3566–3584. doi: 10.1021/acs.jafc.0c07908

frontiers | Frontiers in Plant Science

TYPE Original Research
PUBLISHED 22 August 2024
DOI 10.3389/fpls.2024.1444328

Check for updates

OPEN ACCESS

EDITED BY
Temoor Ahmed,
Zhejiang University, China

REVIEWED BY
Arshad Ali,
Universiti Malaysia Sabah, Malaysia
Mahesh Adhikari,
University of Florida, United States
Yuyu Li,
Institute of Grassland Research, China

*CORRESPONDENCE
Wen-Kun Huang
wkhuang2002@163.com
Ren-De Qi
rende7@126.com

RECEIVED 05 June 2024
ACCEPTED 30 July 2024
PUBLISHED 22 August 2024

CITATION
Ayaz M, Ali Q, Zhao W, Chi Y-K, Ali F, Rashid KA, Cao S, He Y-q, Bukero AA, Huang W-K and Qi R-D (2024) Exploring plant growth promoting traits and biocontrol potential of new isolated *Bacillus subtilis* BS-2301 strain in suppressing *Sclerotinia sclerotiorum* through various mechanisms. *Front. Plant Sci.* 15:1444328. doi: 10.3389/fpls.2024.1444328

COPYRIGHT
© 2024 Ayaz, Ali, Zhao, Chi, Ali, Rashid, Cao, He, Bukero, Huang and Qi. This is an open-access article distributed under the terms of the Creative Commons Attribution License (CC BY). The use, distribution or reproduction in other forums is permitted, provided the original author(s) and the copyright owner(s) are credited and that the original publication in this journal is cited, in accordance with accepted academic practice. No use, distribution or reproduction is permitted which does not comply with these terms.

Exploring plant growth promoting traits and biocontrol potential of new isolated *Bacillus subtilis* BS-2301 strain in suppressing *Sclerotinia sclerotiorum* through various mechanisms

Muhammad Ayaz[1,2], Qurban Ali[3], Wei Zhao[1], Yuan-Kai Chi[1], Farman Ali[4], Khan Abdur Rashid[5], Shun Cao[1], Yan-qiu He[1], Abdul Aziz Bukero[6], Wen-Kun Huang[2*] and Ren-De Qi[1*]

[1]Institute of Plant Protection and Agro-Products Safety, Anhui Academy of Agricultural Sciences, Hefei, China, [2]State Key Laboratory for Biology of Plant Diseases and Insect Pests, Institute of Plant Protection, Chinese Academy of Agricultural Sciences, Beijing, China, [3]Department of Biology, College of Science, United Arab Emirates University, Al-Ain, Abu-Dhabi, United Arab Emirates, [4]Department of Entomology, Abdul Wali Khan University, Mardan, Pakistan, [5]Department of Plant Pathology, Key Laboratory of Monitoring and Management of Crop Diseases and Pest Insects, College of Plant Protection, Ministry of Education, Nanjing Agricultural University, Nanjing, China, [6]MARA-CABI Joint Laboratory for Bio-safety, Institute of Plant Protection, Chinese Academy of Agricultural Science, Beijing, China

Sclerotinia sclerotiorum (Lib.) de Bary is the causative agent of stem white mold disease which severely reduces major crop productivity including soybean and rapeseed worldwide. The current study aimed to explore plant growth-promoting traits and biocontrol of new isolated *Bacillus subtilis* BS-2301 to suppress *S. sclerotiorum* through various mechanisms. The results indicated that the BS-2301 exhibited strong biocontrol potential against *S. sclerotiorum* up to 74% both in dual culture and partition plate experiments. The BS-2301 and its crude extract significantly suppressed *S. sclerotiorum* growth involving excessive reactive oxygen species (ROS) production in mycelia for rapid death. Furthermore, the treated hyphae produced low oxalic acid (OA), a crucial pathogenicity factor of *S. sclerotiorum*. The SEM and TEM microscopy of *S. sclerotiorum* showed severe damage in terms of cell wall, cell membrane breakage, cytoplasm displacement, and organelles disintegration compared to control. The pathogenicity of *S. sclerotiorum* exposed to BS-2301 had less disease progression potential on soybean leaves in the detached leaf assay experiment. Remarkably, the strain also demonstrated broad-range antagonistic activity with 70%, and 68% inhibition rates against *Phytophthora sojae* and *Fusarium oxysporum*, respectively. Furthermore, the strain exhibits multiple plant growth-promoting and disease-prevention traits, including the production of indole-3-acetic acid (IAA), siderophores, amylases, cellulases and proteases as well as harboring calcium phosphate decomposition activity. In comparison to the control, the BS-2301 also showed great potential for enhancing soybean seedlings growth for different parameters, including shoot

length 31.23%, root length 29.87%, total fresh weight 33.45%, and total dry weight 27.56%. The antioxidant enzymes like CAT, POD, SOD and APX under BS-2301 treatment were up-regulated in *S. sclerotiorum* infected plants along with the positive regulation of defense-related genes (*PR1-2*, *PR10*, *PAL1*, *AOS*, *CHS*, and *PDF1.2)*. These findings demonstrate that the BS-2301 strain possesses a notable broad-spectrum biocontrol potential against different phytopathogens and provides new insight in suppressing *S. sclerotiorum* through various mechanisms. Therefore, BS-2301 will be helpful in the development of biofertilizers for sustainable agricultural practices.

KEYWORDS

***Bacillus subtilis*, stem white mold, growth promotion, ROS, oxalic acid**

1 Introduction

White stem mold, caused by the devastating fungus *Sclerotinia sclerotiorum*, globally affects major crop productivity. The pathogen is highly notorious, affecting nearly 500 plant species, including rapeseed, sunflower, cabbage, soybean, beans, and carrot. Studies on *S. sclerotiorum*-infected plants show reduced growth, leaf lesions, and wilting, which can lead to plant death (Massawe et al., 2018; Farzand et al., 2019a). The development of sclerotia and mycelial growth has been identified as pathogenicity factors in *S. sclerotiorum*, but oxalic acid (OA) is mainly considered a major influencer of pathogenicity in plants (Massawe et al., 2018; Farzand et al., 2019a). Polygalacturonases, pectinolytic cell wall-degrading enzymes (CWDE), have also been identified as important pathogenicity factors (Smolińska and Kowalska, 2018; Farzand et al., 2019a). These enzymes become active when the OA establishes a low pH environment (pH 3-4). A mutant of *S. sclerotiorum* lacking OA exhibits less pathogenicity against susceptible plants, based on previous studies (Liang et al., 2015; Massawe et al., 2018). *S. sclerotiorum* produces sclerotia to survive in harsh environments for long time, but under favorable conditions, it germinate to form apothecia containing ascospores and spread the disease (Foley et al., 2016; Taylor et al., 2018).

Many control strategies, such as breeding resistant crops, moisture monitoring, and crop rotation are considered less effective for managing *S. sclerotiorum* due to sclerotia formation in the soil and its potential to infect multiple crops. Applying synthetic fungicides is the most effective control strategy (Jones et al., 2014; Zhai et al., 2023). However, the use of excessive chemicals has raised serious issues regarding environmental pollution and human health. Recently, researchers have shown more interest in biological control as a successful strategy to manage plant diseases without negatively impacting the environment (Ayaz et al., 2021). It has been shown that biological control agents (BCAs), particularly *Bacillus* endophytes, can protect plants from multiple phytopathogens such as fungi, bacteria, and nematodes (Fira et al., 2018; Ayaz et al., 2023). Many plant-associated microorganisms have been screened for their ability to suppress phytopathogens both *in vitro* and *in plant* experiments, providing direction for novel BCAs identification. To date, the well-known antagonistic bacteria identified from the rhizosphere of various plants are *Pseudomonas* and *Bacillus* species (Chen et al., 2009; Wang et al., 2018).

Bacillus spp. produces a wide range of compounds that promote plant growth, promotion, and control diseases. They can regulate phytohormones and defense-related genes during biotic stress (Wu et al., 2019; Gu et al., 2022). *Bacillus* spp. suppress pathogens by regulating plant antioxidant enzymes, such as superoxide dismutase (SOD), catalases (CAT), peroxidase (POD), phenylalanine ammonia-lyase (PAL), ascorbate peroxidase (APX) and polyphenol oxidase (PPO) (Xu et al., 2008; Rais et al., 2017). Studies have shown positive regulation of defense-related genes, such as *PR1-2*, *PR10*, *CHS*, *PAL1*, and *PDF1.2* in soybean plants infected with pathogens under plant growth promoting rhizobacteria treatment (Xu et al., 2012; Zhai et al., 2023). *Bacillus* spp. can also stimulate plant growth by solubilizing soil nutrients and nitrogen fixation. For example, *B. velezensis* FZB42 enhances tomato growth by regulating phytohormone production, nutrient absorption, and root development under biotic stress (Borriss, 2011; Wu et al., 2014). It was also observed that *Bacillus* spp. in the rhizosphere effectively colonizes roots for biofilm formation to control *Ralstonia solanacearum* (Chen et al., 2013). *Bacillus* spp. can produce resistant endospores and a wide range of antimicrobial compounds. Introducing novel *Bacillus* strains in biocontrol strategies could reduce the need for chemical fertilizers and support sustainable agriculture (Xu et al., 2008; Wang et al., 2018).

The agriculture industry could greatly benefit from the discovery of novel BCAs. The objective of the current study is to examine the plant growth-promoting traits and biocontrol potential of the newly isolated *B. Subtilis* BS-2301 in soybean plants, with a focus on its ability to suppress *S. sclerotiorum* through various mechanisms. The BS-2301 exhibited broad-spectrum antagonistic activity and effectively suppressed *S. sclerotiorum* by reducing sclerotia formation,

decreasing oxalic acid production, inducing excessive ROS production, and causing structural deformities in the pathogen hyphae. Additionally, the strain was found to regulate antioxidant enzymes, plant growth, and defense-related genes in infected soybean plants. The present work provides new insights related to the biocontrol potential of the BS-2301 strain using various mechanisms to combat *S. sclerotiorum*. These findings suggest that BS-2301, with its strong biocontrol potential against *S. sclerotiorum*, could be utilized in different formulations to develop biopesticides for sustainably managing white mold disease in agriculture sector.

2 Material and methods

2.1 Strain identification, plant pathogens, and growth conditions

The BS-2301, isolated from the rhizosphere of a soybean plant was provided by Dr. Zhao Wei in the Institute of Plant Protection and Agro-product Safety, Anhui Academy of Agricultural Sciences, Hefei (31° 50' 54.2328" N and 117° 16' 20.5032" E) China. All fungal and oomycetes plant pathogens, such as *S. sclerotiorum, Fusarium oxysporum*, and *Phytophthora sojae*, were supplied by Prof. Dr. Rende Qi from the same institute. The strain BS-2301 and DH5α were grown in Luria Bertani (LB) broth overnight at 25°C and stored in a 60% (v/v) glycerol solution at -80°C for future use (Ayaz et al., 2022). The fungal pathogens were maintained on PDA, while the Oomycetes phytopathogens were grown in V8 juice at 25°C for 5-7 days to obtain fresh cultures (Farzand et al., 2019a; Yu et al., 2023). The BS-2301 strain was identified as a *B. subtilis* based on 16S rRNA sequencing. Universal primers 27F (5'-AGAGTTTGATCMTGGCTCAG-3′) and 1492R (5'-TACGGYTACCTTGTTACGACTT-3′) were used to amplify the 16S rRNA of BS-2301 (Jo et al., 2020). A Basic Local Alignment Tool (BLAST) for the 16S rRNA sequence was performed to determine its similarity with closely related bacterial strains (Ki et al., 2009). Subsequently, the strain was sent to "Novogene, Beijing, China" for whole genome sequencing. The local cultivar of soybean (Zheng 1307) seed was surface serialized for 3-5 minutes with 5% sodium hypochlorite and 70% ethanol solutions, respectively, then rinsed with ddH_2O thrice. The seeds were air-dried on a clean bench before being used for *in vitro* and *in planta* experiments (Zubair et al., 2019).

2.2 Plant growth promoting traits

The newly isolated BS-2301 was evaluated for plant growth-promoting traits, including IAA production, phosphate solubilization, siderophore production, and biofilm formation described below.

2.2.1 Indole acetic acid production

Briefly, the Salkowski method was used to detect IAA production by BS-2301. After inoculating 5 µL of a fresh overnight culture of BS-2301 into 5 mL of LB medium supplemented with 2.5 mg/mL of tryptophan, the mixture was cultured for 7 days at 28°C. Subsequently, 2 mL of the supernatant was collected and mixed with 4 mL of Salkowski reagent (12 g/L of $FeCl_3$ and 8 M H_2SO_4) and incubated for 30 minutes at room temperature in the dark. The presence of pink color in the BS-2301 sample indicated IAA production (Khan et al., 2023).

2.2.2 Siderophores production

The BS-2301 strain was used for siderophore production on chromeazurol-S (CAS) agar medium. The first 5 µL of fresh overnight BS-2301 culture was spotted on the CAS agar plate for siderophore production. After 7 days of incubation at 28°C, the appearance of an orange translucent zone indicated positive activity in siderophore formation by the strain (Xu et al., 2019).

2.2.3 Biofilm formation

The strain was also analyzed for its potential to form a stable biofilm following a previous protocol (Zhai et al., 2023). The bacterial cells from overnight culture 1×10^8 CFU mL^{-1} were collected and washed thrice with sterilized water. Subsequently, 1 mL of fresh LB medium and 100 µL of the bacterial culture were added to a 24-well polystyrene plate (Jiang et al., 2013). As a control, a bacteria-free sterilized LB medium was used. The plate was then incubated for 12, 24, 48, 72, 96, and 120 hours at 28°C. After incubation the developed biofilm was stained for 20 minutes using a 0.1% crystal violet aqueous solution. It was then rinsed three times with sterile distilled water and instantly decolorized for 20 minutes using a 1 mL solution of 95% ethanol. The crystal violet absorbance was measured at OD_{570} to evaluate the biofilm formation by BS-2301 (Peeters et al., 2008). Additionally, 2 mL of fresh LB medium was added to a polystyrene 6-well plate with sterile 1 cm cover glasses. Afterward, 20 µL (1×10^8 CFU mL^{-1}) of BS-2301 bacterial suspension was added to the LB medium and then stained with crystal violet. The cover glass was rinsed off the unbound dye solution and left to air dry. The biofilm developed on the glass cover was examined under an optical microscope with 10x and 40x magnifications at various time intervals. The experiment was performed thrice with at least five replicates (Zhai et al., 2023).

2.2.4 Phosphate solubilization assay

The phosphate solubilization activity was screened for BS-2301 on LB media supplemented with Ca3(PO4)2 (Pi medium) following the previous protocol (Chen and Liu, 2019). The BS-2301 capacity to solubilize phosphate was determined by the formation of clear zones surrounding the colony.

2.3 Extracellular enzymes production

The strain was also screened for extracellular enzymes such as proteases, cellulases, and amylases using previously published protocols.

2.3.1 Proteases activity

Briefly, to assess the protease activity, the BS-2301 was incubated at 28°C for 4 days on Nutrient Agar (NA) enriched medium with 1% skim milk. The presence of transparent, white-background zones surrounding the colony indicated proteolytic activity (Artha et al., 2019).

2.3.2 Amylase activity

For amylase activity, the BS-2301 strain was grown on an NA medium supplemented with 1% starch and incubated at 28°C for 4 days. After that, Lugol's iodine solution (1%) was added to Petri plates, and the development of clear zones around the colony demonstrated the presence of amylase activity (Artha et al., 2019).

2.3.3 Cellulases activity

The medium supplemented with CMC was used for the cellulase enzyme production activity assay. The BS-2301 strain was inoculated on a CMC-enriched NA medium. To detect cellulolytic activity, the Petri plates were covered with congo red solution. Clear zones from pink to yellow around the BS-3201 colony, indicated the presence of cellulase enzyme activity (Artha et al., 2019).

2.4 Dual culture and partition petri plates antagonistic assay

A dual-culture and partition plate assays were carried out to observe the inhibition potential of BS-2301 against fungal and oomycete pathogens directly or indirectly (Massawe et al., 2018; Farzand et al., 2019a). In brief, for the direct antagonistic assay, small plugs (0.5 cm) of the selected pathogens (*S. Sclerotiorum*, *F. oxysporum*, and *P. sojae*) were placed in the center of each petri plate filled with PDA or V8 media. Subsequently, on a sterilized filter paper disc, 3 cm away from the pathogen plug, 5 µL of BS-2301 overnight culture (10^6 CFU mL^{-1}) and its crude extract (15µL) were inoculated. After sealing the Petri plates with parafilm, they were incubated for 4-6 days at 28°C (Farzand et al., 2019a). Using the partition plate approach, the antifungal efficacy of BS-2301 was investigated to prevent direct contact with the tested pathogens (Massawe et al., 2018). Briefly, 0.5 cm paper discs were impregnated with 5 µL of the overnight BS-2301 culture (10^6 CFU mL^{-1}) on one side of the partition plate containing LB media. Subsequently, a 0.5 cm diameter plug of each pathogen was placed on the other side with PDA or V8 media required for fungal and oomycetes pathogens respectively. The parafilm-sealed plates were incubated at 28°C for up to 6 days. The pathogen's mycelium growth inhibition (%) was calculated using the formula below:

$$Rate\ of\ Inhibition\ (\%) = [(C - T)/C] \times 100$$

where C and T represent the mycelial growth length of each pathogen in the control (without BS-2301) and treatment (inoculated with BS-2301) from the center to the edges of the plate, respectively. The experiments were conducted four times, with at least five replicates for each treatment.

2.5 The impact of BS-2301 on sclerotia amount, development, and viability

The sclerotia assay was conducted using the dual-culture method. Briefly, *S. sclerotiorum* mycelial plugs (0.5 cm) from a fresh culture were sliced and placed on a PDA in the middle of a plate. The BS-2301 overnight culture (10^6 CFU mL^{-1}) or its crude extract (15 µL) was impregnated on a paper disc 3 cm away from the fungal plugs. The plates were then tightly sealed with parafilm and incubated at 25°C. The number, mean weight, texture, and interior color of the sclerotia were visually examined at 14 days post-inoculation (dpi) under different treatments (Massawe et al., 2018).

2.6 Assessment of reactive oxygen species

Excessive production of ROS in the hyphae causes severe damage to the fungus, leading to rapid death. ROS accumulation was evaluated in *S. sclerotiorum* mycelia treated with BS-2301 using fluorescence microscopy and the probe dichloro-dihydro-fluorescein diacetate (DCFH-DA) (Ayaz et al., 2021). Untreated hyphae were used as a control. Briefly, *S. sclerotiorum* was cultured at 25°C for 96 hours and exposed to BS-2301 and its crude extract. The treated mycelia were collected and transferred to 10 mM sodium phosphate buffer (pH 7.4) into Eppendorf tubes (1.5 mL). Subsequently, 10 µL of DCFH-DA (Solarbio® CAT No: D6470) was added to the samples for staining and incubated at 25°C in the dark for 30 minutes. The DCHF-DA stained damaged mycelia produced green fluorescence were examined using an image-pro express software (6.2) Olympus 1 x 71 microscope (Olympus, Tokyo, Japan).

2.7 Morphological and ultrastructural changes in *S. sclerotiorum* mycelia

The damage in *S. sclerotiorum* mycelia was observed using scanning electron microscopy (SEM) and transmission electron microscopy (TEM) under different treatments compared with control. The collected mycelia were washed three times in a 100 mM phosphate buffer after being treated with 2.5% glutaraldehyde to prepare them for SEM. Subsequently, the samples were dehydrated using an ethanol gradient and post-fixed for three hours in an osmium tetroxide (1%) solution. After that, the samples were coated on gold particles and analyzed at a 5 kV voltage using a Hitachi S-3000 N SEM (Hitachi). The prefixed samples were divided into pieces with an ultra-microtome, placed inside an Epon 812 for TEM analysis, and observed under a Hitachi H-600 TEM (Farzand et al., 2019a; Ali et al., 2023).

2.8 Oxalic acid production assay in BS-2301 treated *S. sclerotiorum* mycelia

S. sclerotiorum was assessed for its oxalic acid production in PDA media supplemented with bromophenol, an indicator of oxalic acid production. To study the impact of BS-2301 and its crude extract on oxalic acid production of *S. sclerotiorum* during the antagonistic assay, fungal plugs (0.6 cm) were sliced from the edge of the inhibitory zone and placed on the bromophenol blue-modified PDA plates (Massawe et al., 2018). These plates were then incubated at 25°C for 96 hours. The width of the yellow acidification zone, indicating OA production, was measured at 24-

hour intervals following a previously established protocol (Massawe et al., 2018; Farzand et al., 2019a). The experiment was repeated five times, with three replicates for each treatment.

2.9 Biocontrol efficacy of BS-2301 against *S. sclerotiorum* on detached leaves

To evaluate the biocontrol efficacy of BS-2301 against *Sclerotinia* stem rot on detached leaves, a local soybean cultivar (Zheng 1307) susceptible to the disease was used. Leaves from 30-day-old rapeseed and soybean plants were surface sterilized using 75% ethanol for 3 minutes, rinsed three times in sterile distilled water, and air-dried on sterile filter paper. *S. sclerotiorum* mycelial plugs (0.6 cm) from the edge of the inhibition zones were excised and inoculated on detached leaves. Untreated *S. sclerotiorum* served as the control (not exposed to BS-2301) (Cao et al., 2023). Additionally, in partition plates, detached leaves with healthy fungal plugs (0.6 cm) were exposed to BS-2301 volatiles grown in the second compartment on the LB medium. The sealed parafilm plates were kept at 25°C, 85% RH an 8-h light and 16-h dark photoperiod for 5 days. Lesion sizes were measured to assess the biocontrol efficacy of different BS-2301 treatments against *S. sclerotiorum* on detached leaves (Massawe et al., 2018). The experiment was repeated five times, with three replicates of each treatment.

2.10 Plant defense enzymes and malondialdehyde analysis

Soybean seedlings (V2 stage) were inoculated with BS-2301 overnight fresh culture (10^8 CFU mL^{-1}), with H_2O used as a control (Zhai et al., 2023). After 72 h of inoculation, *S. sclerotiorum* mycelial plugs (0.6 cm) were placed on the stem of each plant, which had been previously wounded with a sterilized razor. Leaves samples were collected at 4 dpi for analysis of defense enzymes. The activity of four key antioxidant enzymes such as ascorbate peroxidase (APX), superoxide dismutase (SOD), catalase (CAT), and peroxidase (POD) was determined using kits (Nanjing Jiancheng Bioengineering Institute) protocols (Yong et al., 2008). Briefly, frozen leaf samples (0.3 g) were crushed in a phosphate buffer solution (pH 7.8) containing 1 mM EDTA over an ice bath. The resulting mixture was centrifuged at 1200 × g for 30 minutes at 4 °C, and the supernatant was collected as the final enzyme extract. The absorbance activity of SOD, APX, CAT, and POD was measured at 450, 290, 405, and 420 nm respectively, with ddH_2O serving as a reference. The malondialdehyde (MDA) was determined following the protocol previously reported (Ali et al., 2023).

2.11 Growth promotion and induction of systemic resistance in soybean plants by BS-2301

In vitro experiments were conducted to observe the direct and indirect effects of the BS-2301 on soybean seedling growth (Ali et al., 2023; Khan et al., 2023). Briefly, surface sterilization for 5 minutes of soybean seeds was carried out with sterilized sodium hypochlorite (5%) followed by ethanol (70%) solutions, then washed 4 times with sterilized water (ddH_2O) and placed in an overnight culture of BS-2301 (10^8 CFU mL^{-1}) for 15 minutes. After air drying on a clean bench, the seeds were transferred to sterilized 9 cm Petri plates containing 0.8% MS medium. For the indirect effect, the partition plates approach was utilized to observe the impact of BS-2301-VOCs on soybean growth promotion. The partition plate was set up with three soybean seeds on one side and LB agar medium having BS-2301 on opposite side were kept for 12 days at 25°C under 16 h light/8 h dark photoperiod in a growth chamber.

A Pot experiment was conducted to validate the *in vitro* findings, demonstrating BS-2301 role in enhancing plant growth and disease suppression. Soybean seeds were surface sterilized with 70% ethanol and 5% sodium hypochlorite solutions, followed by rinsing with ddH_2O. The effectiveness of the sterilization process was confirmed by incubating LB plates with the wash water at 37°C for 4 days which showed no bacterial growth. Three soybean seeds were grown in plastic glasses (6 x 3 cm) containing sterilized soil and at the V2 stage the plants were inoculated with an overnight culture of BS-2301 (10^8 CFU mL^{-1}). After 72 h, *S. sclerotiorum* plugs were placed on the soybean stems, which were previously wounded and wrapped with parafilm. Disease severity was assessed at 10 dpi by measuring lesion size compared to the control (Farzand et al., 2019a; Zhai et al., 2023). The experiment was repeated thrice with at least four replicates for each treatment.

2.12 Expression profiling of defense-related genes

The expression profiling of defense-linked genes (*PR1-2*, *PR10*, *PAL1*, *AOS*, *CHS*, and *PDF1.2*) in soybean plants was evaluated in a pot experiment. The experiment included four treatments (i) soybean plants treated with water (CK), (i) soybean plants treated with BS-2301 only, (ii) soybean plants inoculated with *S. sclerotiorum* (S.s), and (iii) soybean plants containing both BS-2301 and *S. sclerotiorum* (S.s+BS-2301) following a previously reported protocol (Zhai et al., 2023). Leaves from different treatments were collected 96 h after *S. sclerotiorum* inoculation. Leaf samples were used for total RNA extraction using the Trelief™ RNAprep pure Plant kit (Lot Number: TSP411, China) and cDNA synthesis was performed using the Goldenstar™ RT6 cDNA synthesis Kit ver.2 (Beijing TsingKe Biotech Co., Ltd). Gene sequences (Supplementary Table S1) were obtained from NCBI on January 15, 2024, and primers were designed using the Primer Quest online application (https://sg.idtdna.com/PrimerQuest/Home/Index). The housekeeping actin-3 (Gene ID=100798052) was used as a reference. The selected gene expression was determined using a Bio-RAD thermal cycler (CFX96TM Real-time system, USA) with the following PCR program: 30 seconds of initial denaturation at 95°C, 40 cycles at 95°C for 5 seconds, and 34 s at 60°C. Finally, $2^{-\Delta\Delta Ct}$ C comparative was exploited for relative quantification (Zubair et al., 2019).

2.13 Statistical analysis

Each experiment was carried out with a completely randomized design. Standard deviations (SD) were used to express the results based on at least four replications (n = 4). An analysis of variance (ANOVA) was performed, followed by the Tukey Honestly Significant Difference (HSD) to determine significant differences at $p \leq 0.05$. The experimental data were analyzed using Statistix 8.1 software, and the graphics were generated using Origin's graphics and analysis program (Version 2022, Origin Lab Corporation).

3 Results

3.1 BS-2301 genetic features and plant growth promoting traits

Based on 16S rRNA and whole-genome sequencing data, the newly isolated strain belongs to *B. subtilis*. The 16S rRNA sequence of BS-2301 closely matched with *B. subtilis* (Figure 1B) using NCBI blast analysis. The 16S rRNA of BS-2301 is submitted to GenBank (Accession: PQ013083). The strain was further sequenced using PacBio Sequel II and Illumina NovaSeq PE150 platforms, resulting in a 4.21 Mb circular chromosome with 43.51% GC content. The total genome contains 4,674 predicted genes grouped into different categories. Anti-smash software analysis revealed 14 secondary metabolite clusters (Figure 1A) including surfactin, fengycin, plipastatin, bacillaene, sactipeptide, ranthipeptide, bacilysin and bacillibactin. BS-2301 exhibits various plant growth-promoting traits, involving the production of IAA for plant growth promotion. The strain also produces extracellular enzymes, such as cellulase, protease, amylase, and siderophore that mostly play an important role in the biocontrol of phytopathogens and plant growth promotion. Inoculation of BS-2301 on the agar medium showed positive halos for siderophore, cellulase, protease, and amylase production. Additionally, BS-2301 exhibited phosphate solubilization ability, as indicated by a clear halo zone on Pikovskaya (PVK) agar medium (Figure 2).

3.2 Broad spectrum biocontrol potential against different phytopathogens

The broad-spectrum biocontrol potential of BS-2301 against various phytopathogens, including *S. sclerotium*, *P. sojae*, and *F. oxysporum* were observed in the present work. The results indicated that BS-2301 and its crude extract showed significant antagonistic activity against *S. sclerotium*, followed by *P. sojae* and *F. oxysporum*, with growth inhibition rates of 74%, 70%, and 68%, respectively. The antagonistic effect of BS-2301 varied among the selected phytopathogens, ranging from 68% to 75%, with the highest inhibition observed against *S. sclerotiorum* (Figures 3A, C).

Furthermore BS-2301-VOCs, demonstrated strong broad-spectrum antagonistic activity against the selected pathogens in partition Petri plate experiments compared to DH5α and the control. BS-2301-VOCs were most effective against *S. sclerotium*,

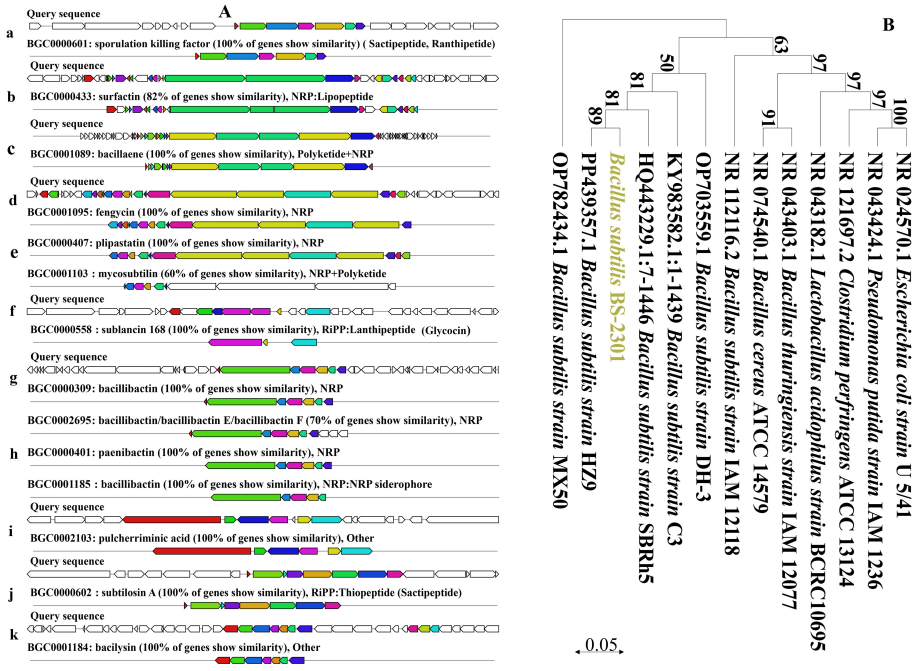

FIGURE 1
Detail of various gene clusters prediction resposible for antimicrobial compounds synthesis in BS-2301 genome and phylogenetic analysis of BS-2301 based on 16S rRNA **(A)** Prediction of gene clusters for diffeent antimicrobial compounds synthesis **(a-k)** in BS-2301 genome through antiSMASH bacterial version online tool **(B)** Phylogenetic tree conntructed from 16S rRNA using neighbour joining method comaparison with closely related Bacterail strains. The phylogentic tree is made through MEGA 11 software and the bootstrap value are mentioned at each node point.

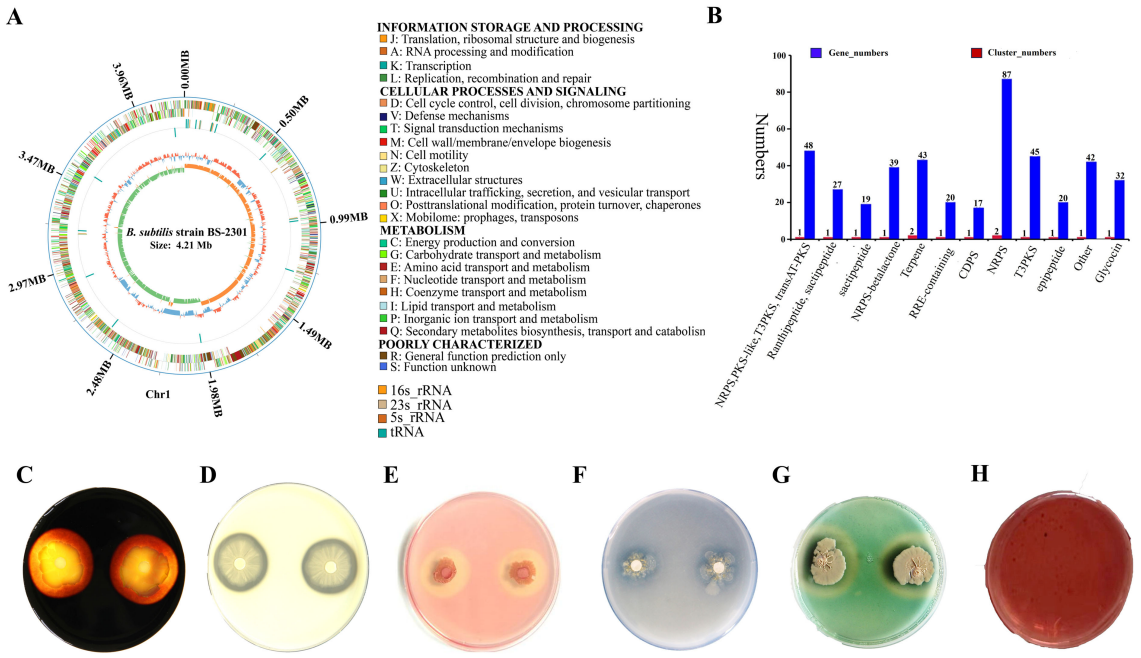

FIGURE 2
Genetic features and plant growth-promoting traits of *B. subtilis* strain BS-2301. **(A)** BS-2301 circular chromosome map in GC view and COG function classification **(B)** Secondary metabolites gene clusters **(C)** amylase **(D)** protease **(E)** cellulase **(F)** phosphate solubilization **(G)** siderophore production and **(H)** Indole Acetic Acid (IAA) assay. Each experiment was repeated thrice with five replicates.

followed by *P. sojae* and *F. oxysporum*, with growth inhibition rates of 72%, 67%, and 65%, respectively (Figures 3B, D). Overall, the findings suggest that BS-2301 possesses strong broad-spectrum biocontrol potential, with the highest inhibitory effect observed against *S. sclerotiorum* in both dual culture and partition plate experiments.

3.3 Evaluation of oxidative damage in *S. sclerotiurum* mycelia

S. sclerotiorum hyphae exposed to BS-3201, crude extract, and BS-2301-VOCs accumulated ROS that led to oxidative stress and rapid cell death. The results indicated that BS-2301 and crude extract significantly induced oxidative damage in the treated mycelia compared to BS-2301-VOCs (Figure 4). The untreated control plates showed no damage to hyphae under green and white light fluorescence. Overall, the findings demonstrated that BS-2301 in the dual culture method significantly increased oxidative stress in *S. sclerotiorum*, followed by the crude extract and BS-2301-VOCs.

3.4 Reduction in *S. sclerotiorum* disease progression on soybean detached leaves

The efficacy of BS-2301 in controlling *S. sclerotiorum* was evaluated using a soybean detached leaf assay. Results showed a significant decrease in disease severity on soybean leaves treated with BS-2301 and crude extract compared to control. The lesion diameter on leaves treated with BS-2301 and crude extract was notably smaller than on control leaves inoculated with healthy fungal plugs. The control group exhibited more severe symptoms, with an average lesion diameter of 3.2 cm, while BS-2301 and crude extract groups had diameters of 1.6 cm and 1.9 cm, respectively (Figure 5A). Furthermore, the indirect impact of BS-2301-VOCs on S. *sclerotiorum* progression indicated a significant reduction in disease progression on soybean leaves compared to DH5α and the control (Figure 5B). Overall BS-2301, crude extract, and BS-2301-VOCs effectively inhibited *S. sclerotiorum* disease progression on soybean leaves compared to the control and DH5α.

3.5 *S. sclerotiorum* oxalic acid production, sclerotia number, and mycelia morphology

Various experiments, including the OA production assay, sclerotia number assessment, and examination of mycelial morphological and ultrastructural changes, were conducted to evaluate the detrimental effects of BS-2301 and its crude extract on *S. sclerotiorum*. The results of the bromophenol blue acidification assay showed that BS-3201 and the crude extract significantly reduced OA production of *S. sclerotiorum* compared to the control (untreated fungal plugs). Healthy untreated fungal plugs exhibited yellow coloration at 48 and 72 hpi and grew faster than those treated with BS-2301 and the crude extract. Treated fungal plugs failed to acidify the medium at 72 hpi, indicated by the retention of blue color compared to the control. Some slight

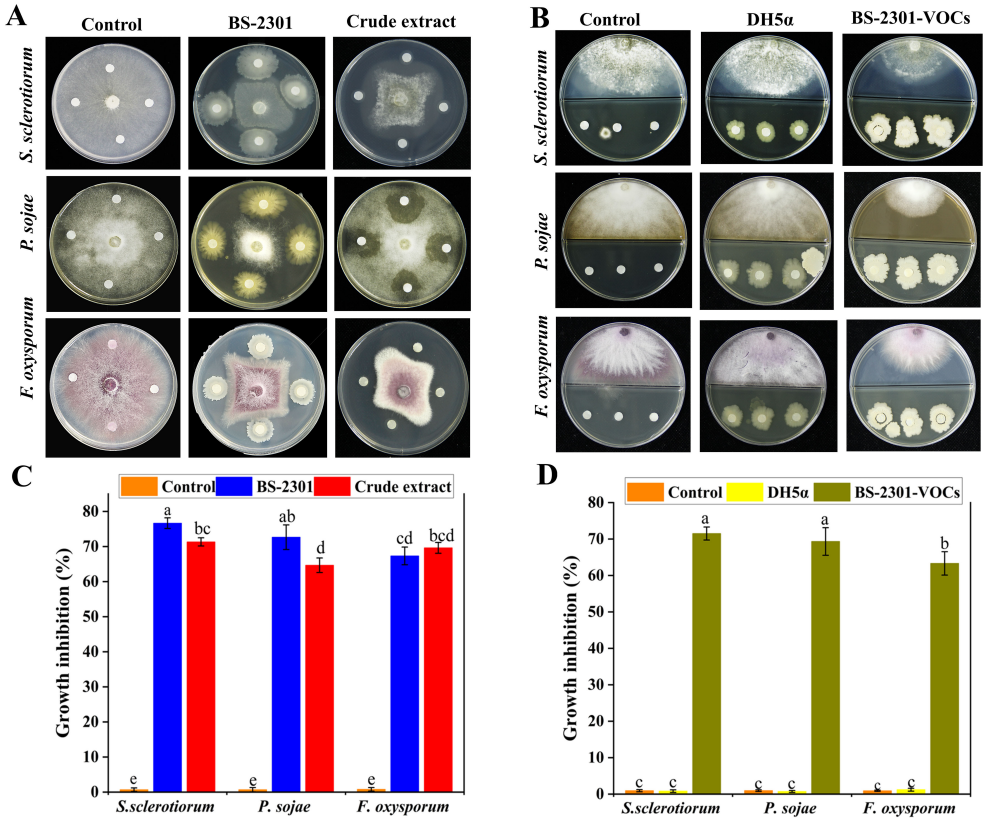

FIGURE 3
Broad spectrum antagonistic potential of BS-2301 against *S. sclerotiorum*, *P. sojae*, and *F. oxysporum*. **(A)** Dual culture method was used to study the direct effect of BS-2301 and crude extract on the selected pathogens compared to the control **(B)** Partition Petri plate experiment showing the indirect inhibitory effect of BS-2301-VOCs on above-mentioned phytopathogens compared to DH5α and control **(C)** Graphical representation of BS-2301 direct effect on growth inhibition of selected pathogens **(D)** Graphical display of BS-2301-VOCs antagonistic effect on above pathogens. Each experiment was repeated thrice with five replicates. The lowercase letters on the columns show significant differences among the treatments using Tukey's HSD test.

acidification was observed in BS-2301 and crude extract-treated fungal plates at 72 hpi, along with reduced mycelial growth (Figure 6A).

Following the observed inhibition of *S. sclerotiorum* mycelial growth, the impact of BS-3201 and the crude extract on sclerotia production and viability was investigated. The results revealed a significant decrease in sclerotia formation in treated *S. sclerotiorum* compared to the control. The number and weight of sclerotia were reduced by up to 50% in both BS-2301 and crude extract-treated fungal plates, with smaller and softer sclerotia formed in the treated groups (Figures 6B, D, E).

Morphological and ultrastructural changes in *S. sclerotiorum* mycelia were examined using SEM and TEM. Control hyphae appeared long, dense, and cylindrical under SEM, while BS2301 and crude extract-treated fungal hyphae displayed deformities, such as plasmolysis, curling, shrinkage, pore formation, and distortion. TEM analysis breakdown of the cell wall and membrane, loss of cellular integrity, cell shrinkage, membrane damage, uneven cell thickness, displacement of cellular contents, and leakage of cytoplasmic material in BS-2301 and crude extract-treated *S. sclerotiorum*, contrasting with the intact structure of untreated fungal mycelia. (Figure 6C).

3.6 Biofilm formation by BS-2301

The ability of BS-2301 to produce biofilm was determined under different time intervals using an optical microscope (Figures 7A–F). The results showed that BS-2301 cells were dispersed and had low adhesion before 24 h. After 48 h, some cells began to cluster and form distinctive biofilm structures. Over time, the number of bacteria adhering to the cover glass increased significantly, and reached at peak after 120 hours. Biofilm formation was quantified using an ultraviolet spectrophotometer at OD_{570} (Figure 7G), showed a steady increase in biofilm production over time, with the highest levels observed after 120 h

3.7 *In vitro* plant growth promotion in soybean seedlings by BS-2301

Soybean seeds inoculated with BS-2301 exhibited higher germination rates and increased seedling growth compared to DH5α and the control (Figure 8A). The findings demonstrated that both direct application of BS-2301 and indirect exposure to

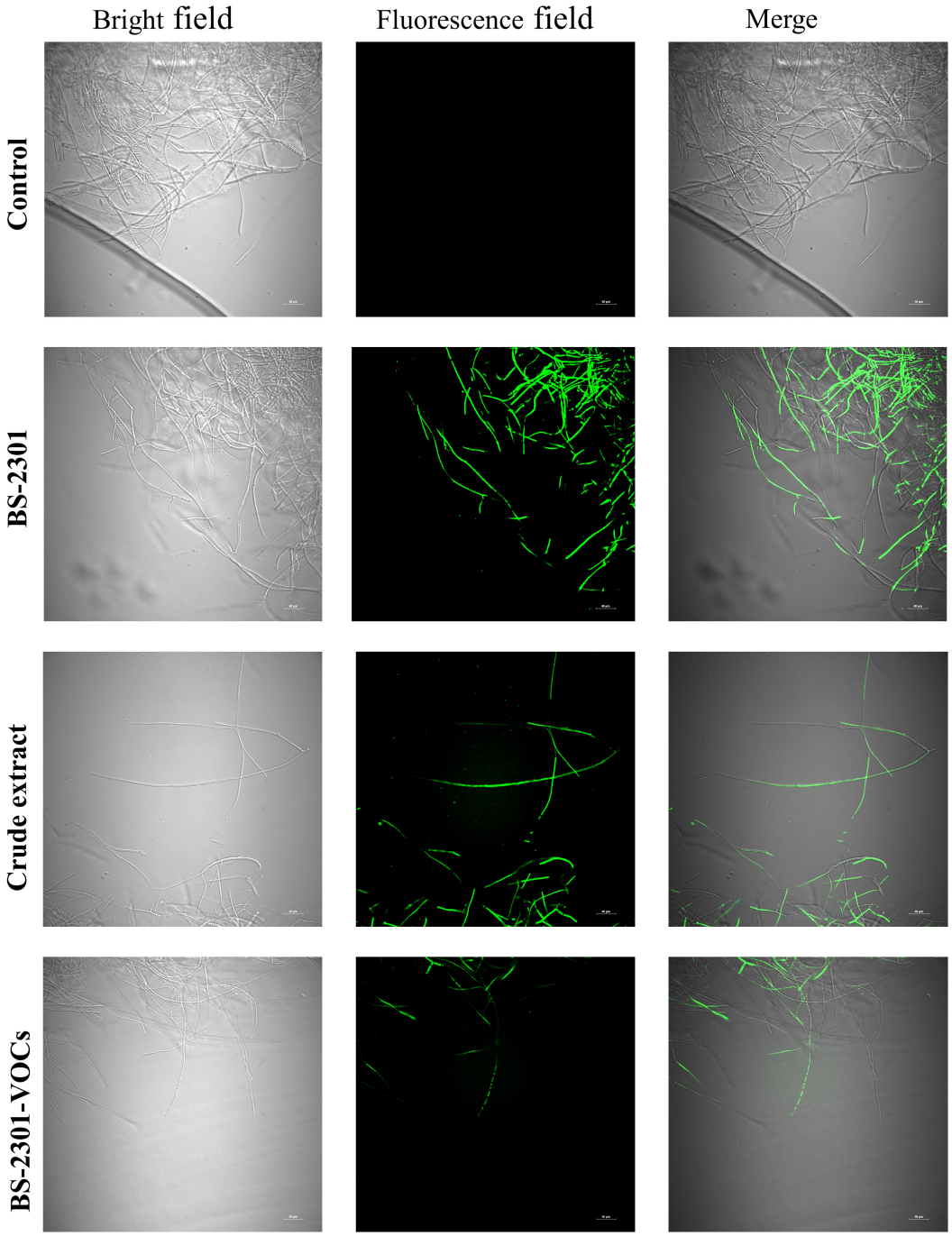

FIGURE 4
Formation of Reactive oxygen species (ROS) using bright and green field microscopy in *S. sclerotiorum* mycelia treated with BS-2301, crude extract, and BS-2301-VOCs. Using DCFH-DA staining, ROS in the mycelia after different treatments was observed. The scale bar represents 40 µm.

BS-2301-VOCs enhanced soybean seedling growth leading to increased shoot length (up to 35%), root length (up to 29%), total fresh weight (up to 33%) and total dry weight (up to 28%). Additionally, it was observed that the direct impact of BS-2301 on soybean seedling growth was slightly greater than the indirect effect of BS-2301-VOCs (Figure 8B).

3.8 *In planta* biocontrol efficacy of BS-2301 against *S. sclerotiorum* in soybean plants

Pot experiment showed that BS-2301 significantly enhanced soybean growth and reduced disease severity caused by

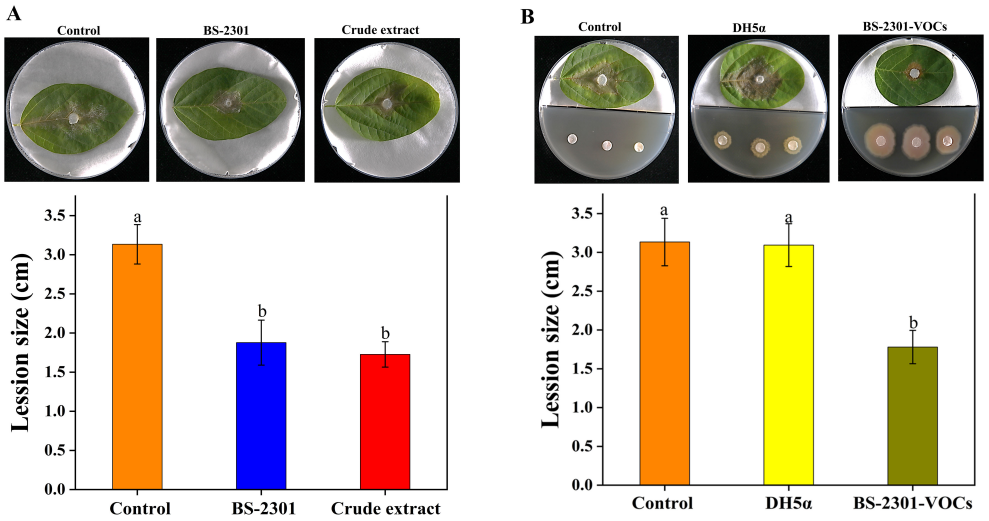

FIGURE 5
Detached leaf assay for analyzing the biocontrol efficacy of BS-2301, crude extract, and BS-2301-VOCs against *S. sclerotiorum* disease on soybean leaves. **(A)** Reduction in *S.sclerotiorum* disease progression treated with BS-2301 and crude extract compared to control (healthy fungal plugs) on soybean leaves **(B)** The indirect effect of BS-2301-VOCs on *S. sclerotiorum* disease progression on soybean leaves compared to DH5α and control. The experiment was repeated three times with five replicates for each treatment. The lowercase letters above the columns indicate significant differences among the treatments, following Tukey's HSD test.

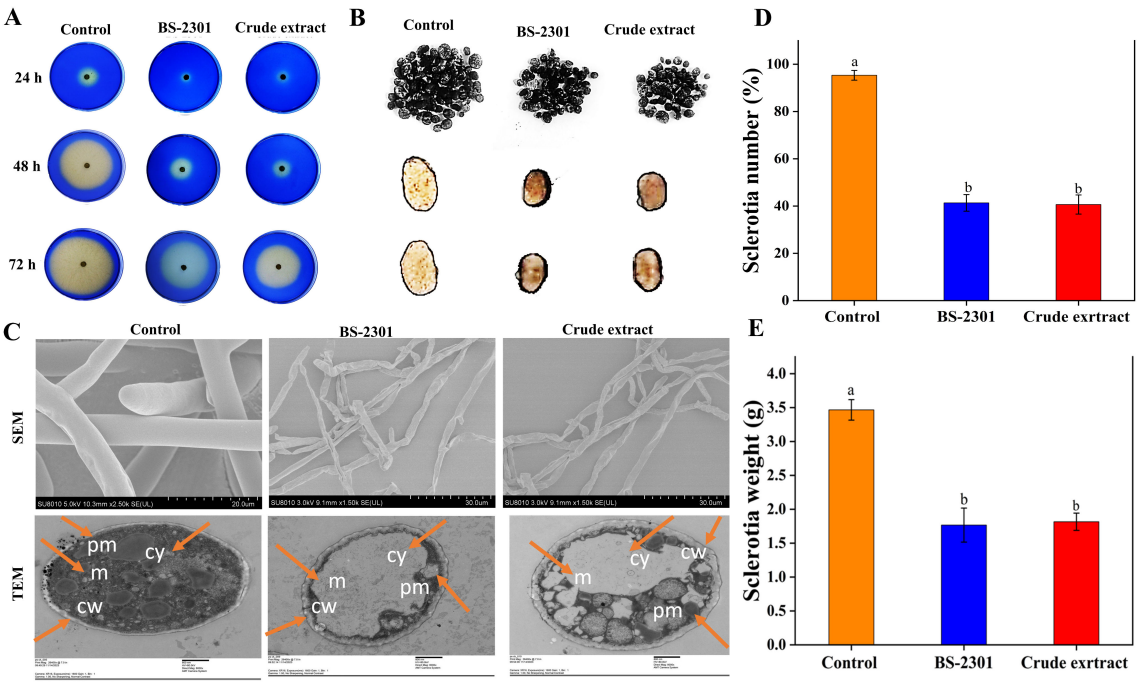

FIGURE 6
The effect of BS-2301 and crude extract on *S. sclerotiorum* oxalic acid production, sclerotia formation, and mycelial morphology **(A)** Illustration of the bromophenol blue acidification assay for oxalic acid production in treated and untreated *S. sclerotiorum* **(B)** Illustration of sclerotia formation in *S. sclerotiorum* under BS-2301 and crude extract treatments **(C)** Examination of treated *S. sclerotium* under SEM and TEM microscopy (cy, cytoplasm, pm, plama membrane, cw, cell wall and m, mitochondria) **(D)** Graph showing the number of sclerotia **(E)** Graph showing the weight of sclerotia. The experiment was repeated three times with five replicates for each treatment. The lowercase letters above the columns indicate significant differences among the treatments, following Tukey's HSD test.

10.3389/fpls.2024.1444328

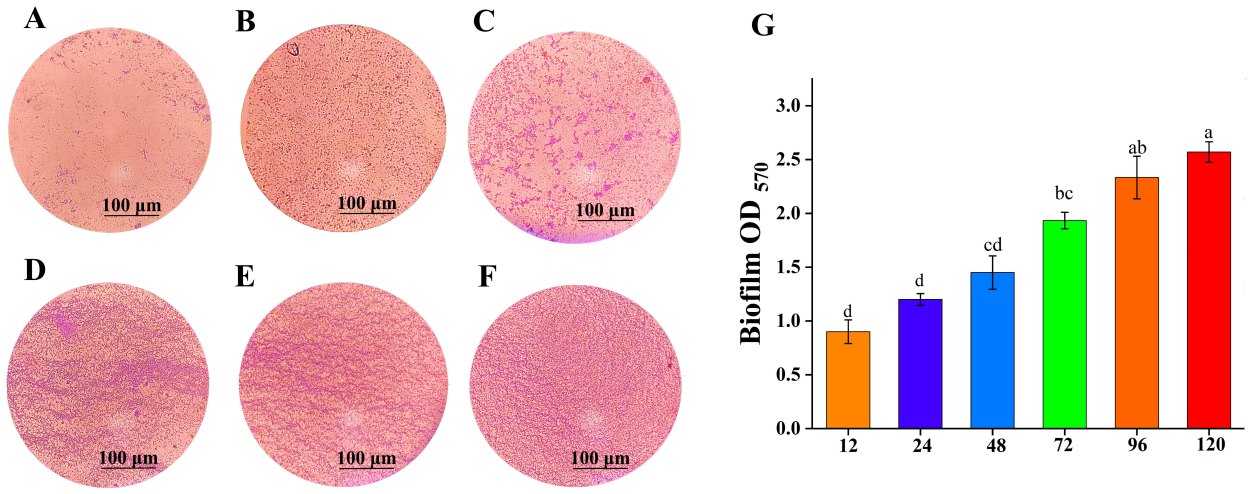

FIGURE 7
Biofilm formation ability of BS-2301 at various time intervals. **(A–F)** shows biofilm formation stained with crystal violet dye at 12, 24, 48, 72, 96, and 120 hours, respectively. **(G)** Biofilm formation optical density at OD_{570} at different time intervals. The lowercase letters above the columns indicate significant differences among the treatments based on Tukey's HSD test.

S. sclerotiorum in soybean plants. Soybean plants inoculated with BS-2301 exhibited maximum growth compared to the control group (Figure 9A). BS-2301 treatment led to increased shoot length, root length, total fresh weight, and total dry weight in soybean plants, including those with *S. sclerotiorum* plugs on the stem (S.s + BS-2301) (Figure 9A). The growth promotion rate under BS-2301 treatment were 37% for shoot length, 30% for root length, 33% for total fresh weight, and 28% for total dry weight. The results indicated significant growth promotion in healthy soybean plants treated with BS-2301, followed by those with *S. sclerotiorum* (S.s + BS-2301) as shown in Figure 9A. Plants with *S. sclerotiorum* plugs on the stem without BS-2301 treatment (S.s) exhibited larger lesion

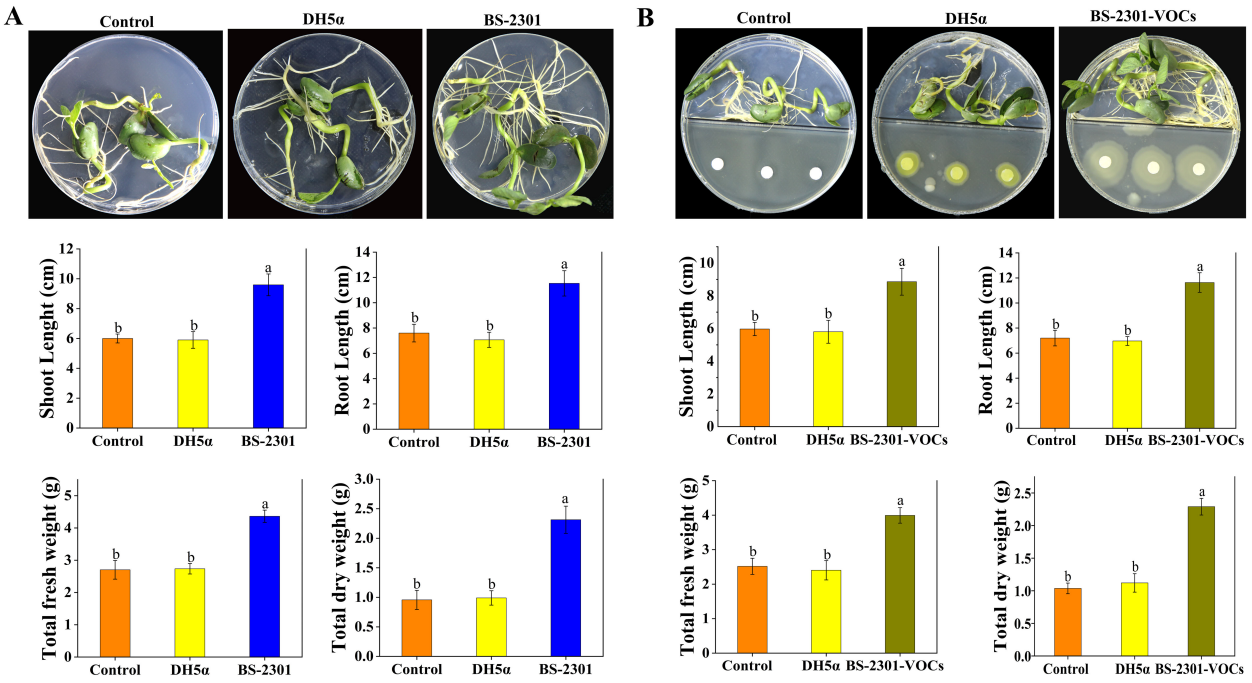

FIGURE 8
In vitro Petri plates experiments showing the direct and indirect effect of BS-2301 and BS-2301-VOCs on soybean seedling growth. **(A)** Comparison of soybean seedling growth directly influenced by BS-2301, DH5α, and control. **(B)** Visual presentation of the impact of BS-2301-VOCs on soybean seedlings' growth compared to DH5α and the control. The graphs show the measurements of shoot length, root length, total fresh weight, and total dry weight for both direct and indirect experiments. The lowercase letters above the columns represent significant differences among the treatments based on Tukey's HSD test at $P \leq 0.05$.

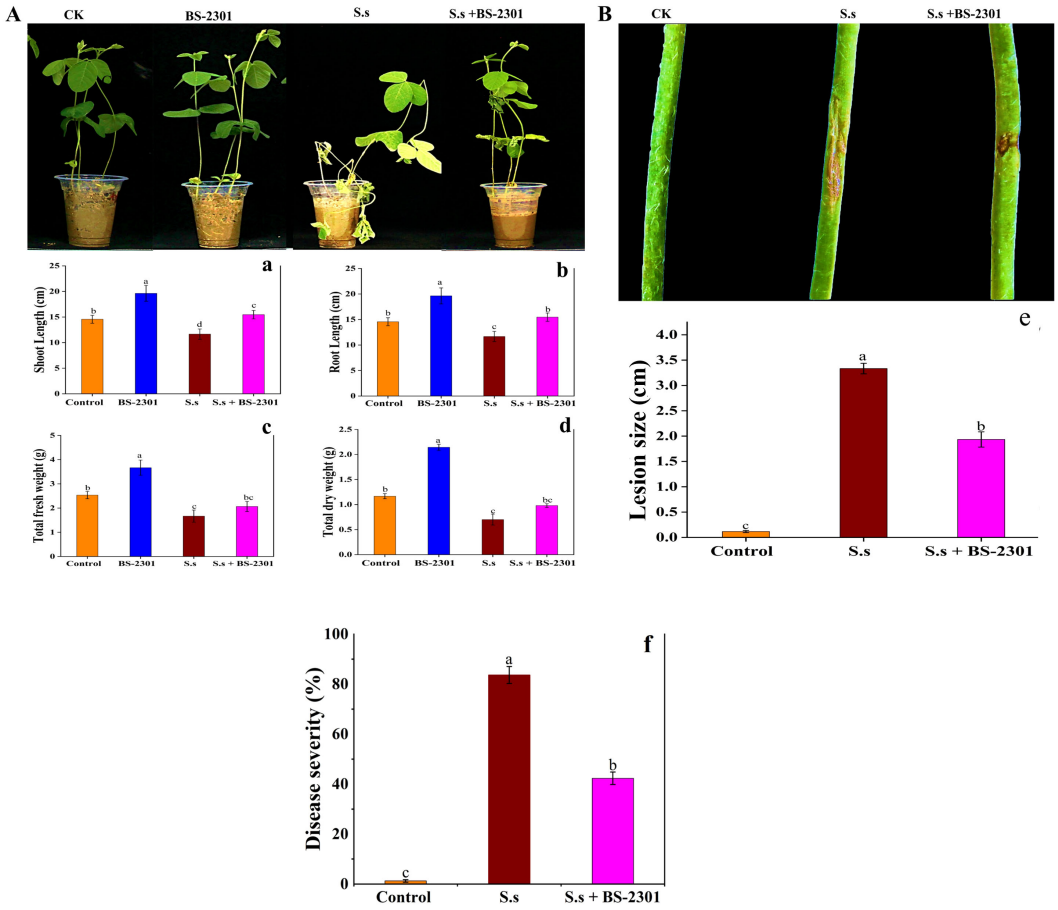

FIGURE 9
Effect of BS-2301 on soybean growth promotion and reduction of *S. sclerotiorum* disease. **(A)** Illustration of BS-2301 soybean growth promotion under different treatments **(B)** visual representation of reduction in *S. sclerotiorum* lesions on soybean under BS-2301 treatment. Graphical representation of shoot length (a), root length (b), total fresh weight (c), and total dry weight (d), graph showing *S. sclerotiorum* lesion size on soybean stems under different treatments (e), disease severity (f). The lowercase letters on the columns show significant differences among treatments, following Tukey's HSD test at $P \leq 0.05$.

sizes and high disease severity while BS-2301-treated soybean plants (S.s + BS-2301) exhibited reduced disesse severity and small lesion szie on stem (Figure 9B). These findings demonstrate the strong biocontrol efficacy of BS-2301 against *S. sclerotiorum* disease progression in soybean plants.

3.9 Defence enzymes regulation by BS-2301

Compared to plants infected with *S. sclerotiorum* alone, soybean plants treated with BS-2301 showed a significant increase in the activity of plant defense enzymes. Specifically, SOD activity increased by 34%, CAT by 30%, POD by 27%, and APX by 25% (Figures 10A–D). These findings suggest that BS-2301 may regulate defense enzymes in soybean plants to reduce the excessive oxidative stress caused by *S. sclerotiorum* infection. The results also showed a significant reduction (35%) in MDA levels in infected plants treated with BS-2301 (S.s + BS-2301), indicating a reduction in oxidative stress (Figure 10E). Overall, the findings demonstrate that BS-2301 plays a crucial role in regulating soybean defense enzymes to mitigate oxidative stress in *S. sclerotiorum*-infected plants.

3.10 Profiling of defense-related genes in soybean plants

Soybean disease resistance could be associated with six genes: *PR10*, *PR1-2*, *PDF1.2*, *CHS*, *AOS*, and *PAL1*. The results revealed a 3-5 fold up-regulation of these genes in soybean plants treated with BS-2301 under *S. sclerotiorum* infection (S.s + BS-2301) compared to infected plants without BS-2301 (S.s) (Figure 11). The relative expression data indicated a significant upregulation of defense genes in infected soybeans plants under BS-2301 (S.s + BS-2301) compared to the S.s group. These results suggest that *B. subtilis* BS-2301 can enhance soybean resistance to *S. sclerotiorum* by triggering signaling pathways associated with PR proteins, plant defensins, and secondary metabolites.

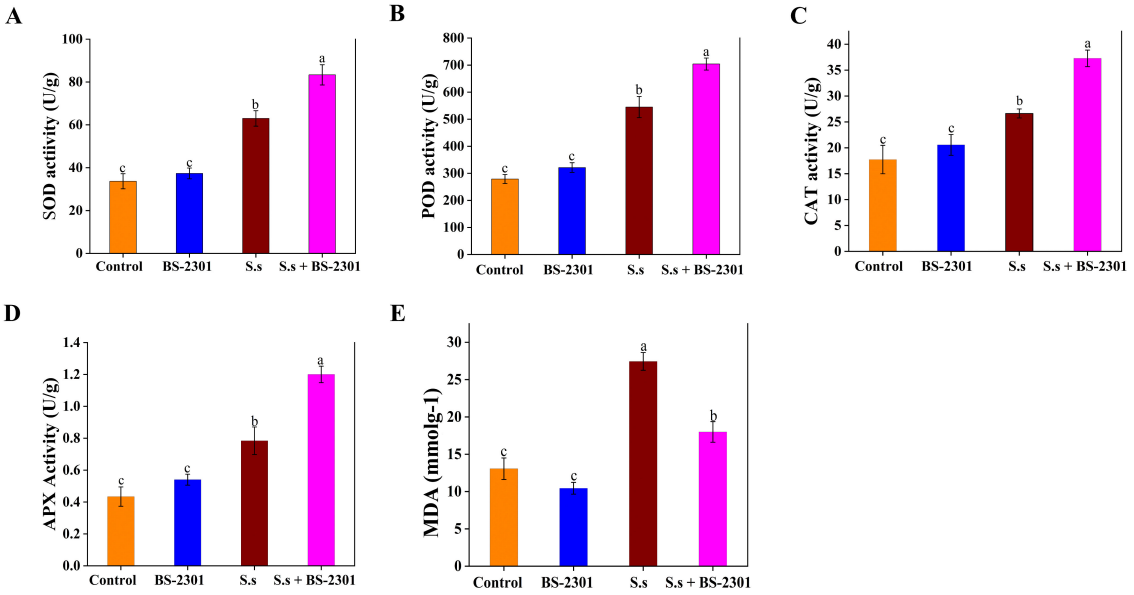

FIGURE 10
Regulation of defense enzymes and MDA levels in soybean under BS-2310 treatment. **(A)** Catalaze (CAT), **(B)** Superoxidase dismutase (SOD), **(C)**, Peroxidase (POD), **(D)** Ascorbate peroxidase (APX), and **(E)** Malondialdehyde (MDA). The significant difference among treatments was indicated by lowercase letters above the columns through Tuckey's HSD test at $P \leq 0.05$.

4 Discussion

The safe and eco-friendly nature of biocontrol for plant diseases has sparked interest among researchers in studying beneficial microbes from various regions. *Bacillus* species are considered highly effective biocontrol agents of various phytopathogens (Farzand et al., 2019b; Ayaz et al., 2022). *Bacillus* strains exhibit numerous plant growth-promoting traits and suppress plant pathogens through various mechanisms. Previous research has identified several biocontrol agents for managing white stem mold disease in rapeseed plants (Chen et al., 2014; Ribeiro et al., 2021). The current study aimed to explore plant growth-promoting traits and biocontrol potential of the newly isolated strain BS-2301 against *S. sclerotiorum* in

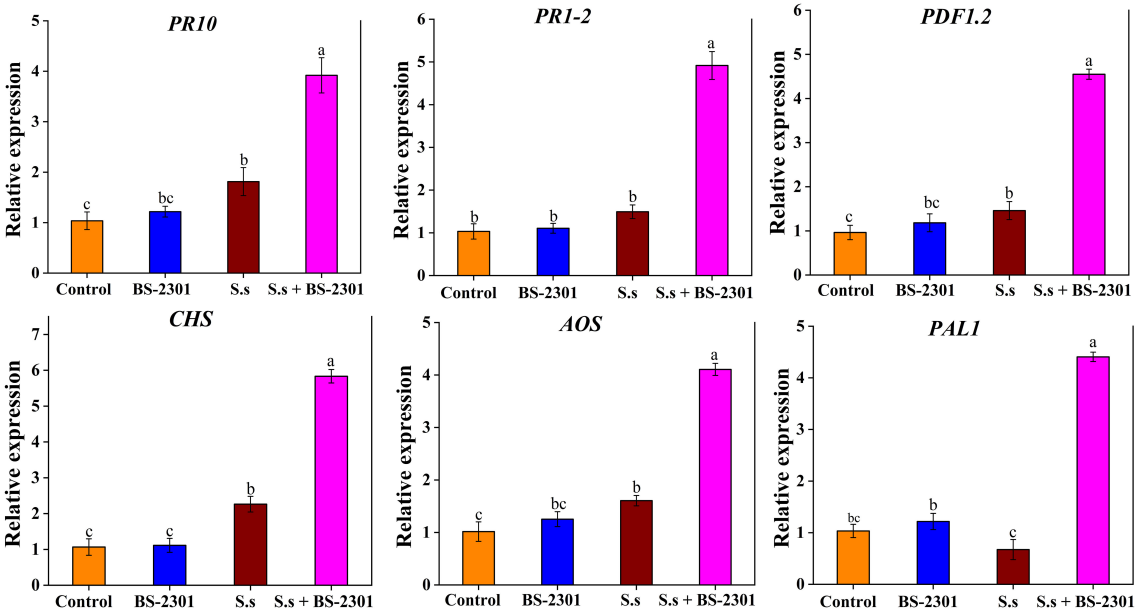

FIGURE 11
Expression profiling of six defense-related genes (*PR1-2*, *PR10*, *CHS*, *AOS*, *PAL1*, and *PDF1.2*) in soybean under different treatments. The significant difference among treatments was indicated by lowercase letters above the columns through Tuckey's HSD test at $P \leq 0.05$.

soybean plants. BS-2301 was identified as a *B. subtilis* strain based on 16S rRNA and whole genome sequencing. Previous studies have shown that *B. subtilis* inhibits a wide range of phytopathogens under laboratory conditions (Zhu et al., 2020). In the current study, BS-2301 exhibited broad-spectrum biocontrol efficacy against *S. sclerotiorum* (75%), *P. sojae* (72%), and *F. oxysporum* (70%) in dual culture and partition plate experiments. The direct inhibitory effect of BS-2301 and its crude extract was strongest against *S. sclerotiorum*, followed by *P. sojae* and *F. oxysporum*. Additionally, BS-2301 volatiles showed an indirect suppressive effect on the pathogens in partition plate experiments. Overall, BS-2301 exhibited strong biocontrol potential against *S. sclerotiorum* with a maximum growth inhibition rate of up to 74% compared to the control.

This study provides new insight into suppressing *S. sclerotiorum* through various mechanisms under BS-2301 treatments. The *S. sclerotiorum* hyphae were challenged with severe oxidative stress by exposure to BS-2301 or crude extract in direct contact or indirectly through BS-2301-VOCs. The results align with previous studies showing high ROS production in fungal mycelia exposed to biocontrol agents (Massawe et al., 2018; Ali et al., 2023). Our findings are consistent with (Massawe et al., 2018) who established a link between severe oxidative stress with negative effects on fungal cellular components, including DNA. BS-2301 induced severe oxidative stress in *S. sclerotiorum* like extreme temperatures, heavy metal stress, and UV radiation, leading to ROS accumulation surpassing the organism's antioxidant defense capacity. The morphological and ultrastructural changes in treated *S. sclerotiorum* observed under TEM and SEM microscopy match the findings from previous studies, including breakdown of cell membranes, cell breakage, plasmolysis, cytoplasm displacement, and organelle disintegration (Giorgio et al., 2015; Ntalli et al., 2017). Oxalic acid (OA) production is a key factor in *S. sclerotiorum* pathogenicity, facilitating the creation of a conducive environment for hydrolytic enzymes (Massawe et al., 2018; Farzand et al., 2019a). Our study hypothesized that BS-2301 could affect OA production in *S. sclerotiorum*. The bromophenol blue assay showed reduced acidification, indicating lower OA production in *S. sclerotiorum* challenged with BS-2301 and crude extract than in the control. The *Bacillus* VOCs have been demonstrated to modify *S. sclerotiorum* OA in reduced pathogenicity, suggesting that decreased production of OA may weaken the host-pathogen interaction (Massawe et al., 2018; Zhu et al., 2022). Furthermore, BS-2301 markedly reduced sclerotia development, which is a resilient structure that can survive harsh conditions for years before germinating into infective hyphae (Hegedus and Rimmer, 2005; Ordóñez-Valencia et al., 2015). The interference of BS-2301 with fungal mycelia likely contributed to the reduction in sclerotia formation. The studies by (Kai et al., 2009) and (Massawe et al., 2018) have shown that *Bacillus* species VOCs can inhibit sclerotia germination. Our findings suggest that BS-2301 and its crude extract may disrupt sclerotia melanin synthesis by interacting with tyrosin oxidation products and dehydroxyphenol compounds, the key components of melanin found in sclerotia.

The PGPR has been shown to support plant growth in harsh conditions through extracellular enzymes, siderophores and IAA production (Zubair et al., 2021; Ali et al., 2022). *Bacillus* spp. produce enzymes like chitinase, protease, β-1,3-glucanase, and cellulase (Ajuna et al., 2023). Researchers have extensively studied *Bacillus* due to its remarkable characteristics (Patel et al., 2023). For example, *B. cereus* YN917 produces various enzymes and exhibits mineral phosphate decomposition activity (Zhou et al., 2021). *Bacillus velezensis* NKG-2 has been shown to produce cellulase, β-glucanase, chitinase, IAA, and siderophore (Myo et al., 2019). The *B. subtilis* BS-2301 in the present study produced extracellular enzymes such as amylase, cellulases, and proteases and exhibited PGP traits such as siderophores production, IAA synthesis, and phosphorus-solubilizing activity. These traits may help soybean plants survive infections with *S. sclerotiorum*. Additionally, different gene clusters in BS-2301 genome were predicted for important antimicrobial compounds like bacilysin, fengycin, and surfactant. Previous studies have demonstrated the remarkable potential of fengycin produced from *B. amyloliquefaciens* FZB42 in managing *S. sclerotiorum*. It was found that fengycin triggered ISR in infected tomato plants and downregulated the pathogenicity genes in *S. sclerotiorum* (Farzand et al., 2019a). Surfactin is an important antimicrobial lipopeptide with antifungal activities against multiple plant pathogenic fungi and might have potential uses in agriculture. The surfactin isolated from *Brevibacillus brevis* KN8(2) has been evaluated for its antifungal activity against *F. moniliforme*. The study suggested that surfactin might be an effective bio-fungicide for controlling plant diseases (Krishnan et al., 2019). Previous studies showed bacilysin an effective biocontrol agent for *Xanthomonas* disease suppression in rice plant. The expression of genes related to *Xanthomonas* pathogenicity, cell division and cell wall synthesis was downregulated under bacilysin treatment (Wu et al., 2015). In present study, the BS-2301 genome was also found to possessed surfactin, fengycin and bacilysin gene clusters that might suppress *S. sclerotiorum* through various mechanisms.

The scientific community has shown considerable interest in identifying novel beneficial microbes to control phytopathogens and improve plant health (Ayaz et al., 2023). The study by (Khan et al., 2020) reported *B. subtills* KSU-110 reduced *Fusarium* wilt disease of tomato in greenhouse experiments. In present studies, BS-2301 was found to make soybean resistant to *S. sclerotiorum* under pot experiment. Our study revealed that soybean leaves in BS-2301 treated plants exhibited enhanced activity of POD, SOD, CAT, and APX compared to the control. It was previously reported that PGPR in host plants regulates antioxidant enzymes like POD, SOD, and CAT which help in removing excessive ROS and preventing pathogen invasion (Ali et al., 2023; Zhai et al., 2023). Our results showed up-regulation of antioxidant enzymes in infected soybean plants, possibly involved in reducing excessive ROS production after *S. sclerotiorum* infection. The active antioxidant enzyme system plays a crucial role in maintaining normal plant cell growth. Pathogen and abiotic stressors can damage plant cells, leading to MDA production, and indicating cell death or degeneration (Liu et al., 2021). Soybean treated with

the BS-2301 strain had lower MDA content compared to *S. sclerotiorum*-infected soybeans, suggesting reduced cellular damage in treated plants. This indicates that BS-2301 can trigger defense-related enzyme activities in soybeans, reducing *S. sclerotiorum* infection. our findings support previous research showing up-regulation of antioxidant enzymes and reduced MDA content in rice infected with *Xanthomonas oryzae* and *Ralstonia solani* under *Bacillus* VOCs treatment (Ali et al., 2023). Moreover, PGPR may trigger ISR by interacting with plant defense genes and signaling pathways to minimize plant pathogen infection (Salwan et al., 2023). Gene expression profiling revealed increased expression of defense-related genes (*PR1-2, PR10, PDF1.2, CHS, PAL1*, and *AOS*) in soybean plants treated with BS-2301, indicating significant up-regulation of plant defense genes. Our results align with previous research showing that *Klebsiella variicola* FH-1 strain activated ISR against *S. sclerotiorum* in soybeans by positively regulating defense-related genes (Zhai et al., 2023). In conclusion, our study demonstrates that the newly isolated *B. subtilis* BS-2301 exhibits a plethora of plant growth-promoting traits and biocontrol potential to suppress different plant pathogens, trigger ISR, reduce stem lesions, enhance antioxidant enzymes, and regulate plant defense genes to control *S. sclerotiorum* disease in soybean plants.

5 Conclusion

The present study identified a newly isolated *B. subtilis* BS-2301 with potent broad-spectrum biocontrol potential against *S. sclerotiorum*, *P. sojae*, and *F. oxysporum*. The findings shed light on BS-2301 biocontrol mechanism against *S. sclerotiorum* involving excessive ROS production leading to pathogen cell death. The BS-2301 induced morphological and ultrastructural changes in *S. sclerotiorum* mycelia, including cell wall and membrane breakage, cytoplasmic displacement, and organelle disintegration. Treatment with BS-2301 resulted in reduced oxalic acid production and sclerotia formation which are considered key pathogenicity factors in *S. sclerotiorum* infection. Additionally, BS-2301 promoted soybean plant growth and inhibited *S. sclerotiorum* disease progression on soybean leaves and stem in both *in vitro* and pot experiments. The plant-growth-promoting and biocontrol efficacy of BS-2301 may be attributed to extracellular enzymes, secondary metabolites, VOCs, IAA synthesis, and stable biofilm formation. BS-2301 induced systemic resistance in soybean plants by regulating antioxidant enzymes and defense-related genes during *S. sclerotiorum* infection. Overall, *B. subtilis* BS-2301 exhibited plant growth-promoting potential and effectively suppressed *S. sclerotiorum* through various mechanisms. This study lays the foundation for managing *S. sclerotiorum* disease in soybean plants, with further research need to evaluate BS-2301 efficacy in field trials.

Data availability statement

The original contributions presented in the study are included in the article/Supplementary Material. Further inquiries can be directed to the corresponding authors.

Author contributions

MA: Conceptualization, Data curation, Formal Analysis, Methodology, Software, Visualization, Writing – original draft, Writing – review & editing. QA: Formal Analysis, Methodology, Software, Visualization, Writing – review & editing. WZ: Data curation, Formal Analysis, Methodology, Software, Visualization, Writing – review & editing. YC: Data curation, Formal Analysis, Methodology, Software, Validation, Visualization, Writing – review & editing. FA: Data curation, Formal Analysis, Methodology, Software, Writing – review & editing. KR: Data curation, Formal Analysis, Software, Visualization, Writing – review & editing. SC: Formal Analysis, Methodology, Visualization, Writing – review & editing. YH: Formal Analysis, Methodology, Writing – review & editing. AB: Data curation, Formal Analysis, Visualization, Writing – review & editing. WH: Investigation, Methodology, Project administration, Resources, Software, Supervision, Validation, Visualization, Writing – review & editing, Conceptualization, Data curation, Formal Analysis, Funding acquisition. RQ: Conceptualization, Data curation, Formal Analysis, Funding acquisition, Investigation, Methodology, Project administration, Resources, Software, Supervision, Validation, Visualization, Writing – review & editing.

Funding

The authors declare financial support were received for the research, authorship, and/or publication of this article. This work is supported by the National Key Research and Development Program of China (grant no. 2021YFC2600404, 2023YFD1401000) and Natural Science Foundation of China (grant no. 32172382).

Conflict of interest

The authors declare that the research was conducted in the absence of any commercial or financial relationships that could be construed as a potential conflict of interest.

Publisher's note

All claims expressed in this article are solely those of the authors and do not necessarily represent those of their affiliated organizations, or those of the publisher, the editors and the reviewers. Any product that may be evaluated in this article, or claim that may be made by its manufacturer, is not guaranteed or endorsed by the publisher.

Supplementary material

The Supplementary Material for this article can be found online at: https://www.frontiersin.org/articles/10.3389/fpls.2024.1444328/full#supplementary-material

References

Ajuna, H. B., Lim, H. I., Moon, J. H., Won, S. J., Choub, V., Choi, S. I., et al. (2023). The prospect of hydrolytic enzymes from *bacillus* species in the biological control of pests and diseases in forest and fruit tree production. *Int. J. Mol. Sci.* 24, 16889. doi: 10.3390/ijms242316889

Ali, Q., Ayaz, M., Mu, G., Hussain, A., Yuanyuan, Q., Yu, C., et al. (2022). Revealing plant growth-promoting mechanisms of *Bacillus* strains in elevating rice growth and its interaction with salt stress. *Front. Plant Sci.* 13. doi: 10.3389/fpls.2022.994902

Ali, Q., Khan, A. R., Tao, S., Rajer, F. U., Ayaz, M., Abro, M. A., et al. (2023). Broad-spectrum antagonistic potential of Bacillus spp. volatiles against *Rhizoctonia solani* and *Xanthomonas oryzae* pv. oryzae. *Physiol. Plant* 175, 1–16. doi: 10.1111/ppl.14087

Artha, O. A., Sudarno,, Pramono, H., and Sari, L. A. (2019). Identification of extracellular enzyme-producing bacteria (proteolytic, cellulolytic, and amylolytic) in the sediment of extensive ponds in Tanggulrejo, Gresik. *IOP Conf. Ser. Earth Environ. Sci.* 236. doi: 10.1088/1755-1315/236/1/012003

Ayaz, M., Ali, Q., Farzand, A., Khan, A. R., Ling, H., and Gao, X. (2021). Nematicidal volatiles from *Bacillus atrophaeus* GBSC56 promote growth and stimulate induced systemic resistance in tomato against. *Meloidogyne incognita. Int. J. Mol. Sci.* 22, 5049. doi: 10.3390/ijms22095049

Ayaz, M., Ali, Q., Jiang, Q., Wang, R., Wang, Z., Mu, G., et al. (2022). Salt tolerant *bacillus* strains improve plant growth traits and regulation of phytohormones in wheat under salinity stress. *Plants* 11, 2769. doi: 10.3390/plants11202769

Ayaz, M., Li, C.-H., Ali, Q., Zhao, W., Chi, Y.-K., Shafiq, M., et al. (2023). Bacterial and fungal biocontrol agents for plant disease protection: Journey from lab to field, current status, challenges, and global perspectives. *Molecules* 28, 6735. doi: 10.3390/molecules28186735

Borriss, R. (2011). "Use of plant-associated *bacillus* strains as biofertilizers and biocontrol agents in agriculture," in Dinesh, K. Maheshwari Dept. of Botany Microbiology, Gurukul Kangri University, Haridwar (Uttarakhand), 249404, India. eds. *Bacteria in Agrobiology: Plant Growth Responses*, (Berlin, Heidelberg: Springer), 41–76. doi: 10.1007/978-3-642-20332-9_3

Cao, S., Jiang, B., Yang, G., Pan, G., Pan, Y., Chen, F., et al. (2023). Isolation and evaluation of *Bacillus subtilis* RSS-1 as a potential biocontrol agent against *Sclerotinia sclerotiorum* on oilseed rape. *Eur. J. Plant Pathol.* 166, 9–25. doi: 10.1007/s10658-023-02642-x

Chen, X. H., Koumoutsi, A., Scholz, R., Schneider, K., Vater, J., Süssmuth, R., et al. (2009). Genome analysis of *Bacillus amyloliquefaciens* FZB42 reveals its potential for biocontrol of plant pathogens. *J. Biotechnol.* 140, 27–37. doi: 10.1016/j.jbiotec.2008.10.011

Chen, Y., Gao, X., Chen, Y., Qin, H., Huang, L., and Han, Q. (2014). Inhibitory efficacy of endophytic *Bacillus subtilis* EDR4 against *Sclerotinia sclerotiorum* on rapeseed. *Biol. Control* 78, 67–76. doi: 10.1016/j.biocontrol.2014.07.012

Chen, Y., Yan, F., Chai, Y., Liu, H., Kolter, R., Losick, R., et al. (2013). Biocontrol of tomato wilt disease by *Bacillus subtilis* isolates from natural environments depends on conserved genes mediating biofilm formation. *Environ. Microbiol.* 15, 848–864. doi: 10.1111/j.1462-2920.2012.02860.x

Chen, Q., and Liu, S.. (2019). Identification and Characterization of the Phosphate-Solubilizing Bacterium Pantoea sp. S32 in Reclamation Soil in Shanxi, China. *Front. Microbiol.* 10, 1–12. doi: 10.3389/fmicb.2019.02171

Farzand, A., Moosa, A., Zubair, M., Khan, A. R., Massawe, V. C., Tahir, H. A. S., et al. (2019a). Suppression of *Sclerotinia sclerotiorum* by the Induction of Systemic Resistance and Regulation of Antioxidant Pathways in Tomato Using Fengycin Produced by *Bacillus amyloliquefaciens* FZB42. *Biomolecules* 9, 613. doi: 10.3390/biom9100613

Farzand, A., Moosa, A., Zubair, M., Rashid Khan, A., Hanif, A., Tahir, H. A. S., et al. (2019b). Marker assisted detection and LC-MS analysis of antimicrobial compounds in different *Bacillus* strains and their antifungal effect on *Sclerotinia sclerotiorum*. *Biol. Control* 133, 91–102. doi: 10.1016/j.biocontrol.2019.03.014

Fira, D., Dimkić, I., Berić, T., Lozo, J., and Stanković, S. (2018). Biological control of plant pathogens by *Bacillus* species. *J. Biotechnol.* 285, 44–55. doi: 10.1016/j.jbiotec.2018.07.044

Foley, M. E., Doğramacı, M., West, M., and Underwood, W. R. (2016). Environmental factors for germination of *Sclerotinia sclerotiorum* sclerotia. *J. Plant Pathol. Microbiol.* 7, 379–383. doi: 10.4172/2157-7471

Giorgio, A., De Stradis, A., Lo Cantore, P., and Iacobellis, N. S. (2015). Biocide effects of volatile organic compounds produced by potential biocontrol rhizobacteria on *Sclerotinia sclerotiorum*. *Front. Microbiol.* 6, 1056. doi: 10.3389/fmicb.2015.01056

Gu, Y., Zheng, R., Sun, C., and Wu, S. (2022). Isolation, identification and characterization of two kinds of deep-sea bacterial lipopeptides against food borne pathogens. *Frontier in Microbiology* 13, 1–11. doi: 10.3389/fmicb.2022.792755

Hegedus, D. D., and Rimmer, S. R. (2005). *Sclerotinia sclerotiorum:* when "to be or not to be" a pathogen? *FEMS Microbiol. Lett.* 251, 177–184. doi: 10.1016/j.femsle.2005.07.040

Jiang, W., Wang, K., Wu, Q., Dong, S., Liu, P., and Zhang, J. (2013). Effects of narrow plant spacing on root distribution and physiological nitrogen use efficiency in summer maize. *Crop J.* 1, 77–83. doi: 10.1016/j.cj.2013.07.011

Jo, H. W., Tagele, S. B., Pham, H. Q., Kim, M. C., Choi, S. D., Kim, M. J., et al. (2020). Response of soil bacterial community and pepper plant growth to application of *Bacillus thuringiensis* KNU-07. *Agronomy* 10, 551. doi: 10.3390/agronomy10040551

Jones, E. E., Rabeendran, N., and Stewart, A. (2014). Biocontrol of *Sclerotinia sclerotiorum* infection of cabbage by *Coniothyrium minitans* and *Trichoderma* spp. *Biocontrol Sci. Technol.* 24, 1363–1382. doi: 10.1080/09583157.2014.940847

Kai, M., Haustein, M., Molina, F., Petri, A., Scholz, B., and Piechulla, B. (2009). Bacterial volatiles and their action potential. *Appl. Microbiol. Biotechnol.* 81, 1001–1012. doi: 10.1007/s00253-008-1760-3

Khan, A. R., Ali, Q., Ayaz, M., Bilal, M. S., Sheikh, T. M. M., Gu, Q., et al. (2023). Plant–microbes interaction: exploring the impact of cold-tolerant *bacillus* strains RJGP41 and GBAC46 volatiles on tomato growth promotion through different mechanisms. *Biol. (Basel).* 12, 940. doi: 10.3390/biology12070940

Khan, A. R., El-Komy, M. H., Ibrahim, Y. E., Hamad, Y. K., Molan, Y. Y., and Saleh, A. A. (2020). Organic management of tomato *Fusarium* wilt using a native *Bacillus subtilis* strain and compost combination in Saudi Arabia. 23, 1003–1012. doi: 10.17957/IJAB/15.1379

Ki, J. S., Zhang, W., and Qian, P. Y. (2009). Discovery of marine *Bacillus* species by 16S rRNA and rpoB comparisons and their usefulness for species identification. *J. Microbiol. Methods* 77, 48–57. doi: 10.1016/j.mimet.2009.01.003

Krishnan, N., Velramar, B., and Velu, R. K. (2019). Investigation of antifungal activity of surfactin against mycotoxigenic phytopathogenic fungus *Fusarium moniliforme* and its impact in seed germination and mycotoxicosis. *Pestic. Biochem. Physiol.* 155, 101–107. doi: 10.1016/j.pestbp.2019.01.010

Liang, X., Liberti, D., Li, M., Kim, Y., Hutchens, A., Wilson, R. O. N., et al. (2015). Oxaloacetate acetylhydrolase gene mutants of *Sclerotinia sclerotiorum* do not accumulate oxalic acid, but do produce limited lesions on host plants. *Mol. Plant Pathol.* 16, 559–571. doi: 10.1111/mpp.12211

Liu, Y., Li, Y., Bi, Y., Jiang, Q., Mao, R., Liu, Z., et al. (2021). Induction of defense response against *Alternaria* rot in Zaosu pear fruit by exogenous L-lysine through regulating ROS metabolism and activating defense-related proteins. *Postharvest Biol. Technol.* 179, 111567. doi: 10.1016/j.postharvbio.2021.111567

Massawe, V. C., Hanif, A., Farzand, A., Mburu, D. K., Ochola, S. O., Wu, L., et al. (2018). Volatile compounds of endophytic Bacillus spp. have biocontrol activity against *Sclerotinia sclerotiorum*. *Phytopathology* 108, 1373–1385. doi: 10.1094/PHYTO-04-18-0118-R

Myo, E. M., Liu, B., Ma, J., Shi, L., Jiang, M., Zhang, K., et al. (2019). Evaluation of *Bacillus velezensis* NKG-2 for bio-control activities against fungal diseases and potential plant growth promotion. *Biol. Control* 134, 23–31. doi: 10.1016/j.biocontrol.2019.03.017

Ntalli, N., Ratajczak, M., Oplos, C., Menkissoglu-Spiroudi, U., and Adamski, Z. (2017). Acetic acid, 2-undecanone, and (E)-2-decenal ultrastructural malformations on. *J. Nematol.* 48, 248–260. doi: 10.21307/jofnem-2017-033

Ordóñez-Valencia, C., Ferrera-Cerrato, R., Quintanar-Zúñiga, R. E., Flores-Ortiz, C. M., Guzmán, G. J. M., Alarcón, A., et al. (2015). Morphological development of sclerotia by *Sclerotinia sclerotiorum:* a view from light and scanning electron microscopy. *Ann. Microbiol.* 65, 765–770. doi: 10.1007/s13213-014-0916-x

Patel, M., Islam, S., Husain, F. M., Yadav, V. K., Park, H. K., Yadav, K. K., et al. (2023). *Bacillus subtilis* ER-08, a multifunctional plant growth-promoting rhizobacterium, promotes the growth of fenugreek (*Trigonella foenum-graecum* L.) plants under salt and drought stress. *Front. Microbiol.* 14. doi: 10.3389/fmicb.2023.1208743

Peeters, E., Nelis, H. J., and Coenye, T. (2008). Comparison of multiple methods for quantification of microbial biofilms grown in microtiter plates. *J. Microbiol. Methods* 72, 157–165. doi: 10.1016/j.mimet.2007.11.010

Rais, A., Jabeen, Z., Shair, F., Hafeez, F. Y., and Hassan, M. N. (2017). *Bacillus* spp., a bio-control agent enhances the activity of antioxidant defense enzymes in rice against *Pyricularia oryzae*. *PLoS One* 12, e0187412. doi: 10.1371/journal.pone.0187412

Ribeiro, I. D. A., Bach, E., da Silva Moreira, F., Müller, A. R., Rangel, C. P., Wilhelm, C. M., et al. (2021). Antifungal potential against *Sclerotinia sclerotiorum* (Lib.) de Bary and plant growth promoting abilities of *Bacillus* isolates from canola (*Brassica napus* L.) roots. *Microbiol. Res.* 248, 126754. doi: 10.1016/j.micres.2021.126754

Salwan, R., Sharma, M., Sharma, A., and Sharma, V. (2023). Insights into plant beneficial microorganism-triggered induced systemic resistance. *Plant Stress* 7, 100140. doi: 10.1016/j.stress.2023.100140

Smolińska, U., and Kowalska, B. (2018). Biological control of the soil-borne fungal pathogen *Sclerotinia sclerotiorum*—-a review. *J. Plant Pathol.* 100, 1–12. doi: 10.1007/s42161-018-0023-0

Taylor, A., Coventry, E., Handy, C., West, J. S., Young, C. S., and Clarkson, J. P. (2018). Inoculum potential of *Sclerotinia sclerotiorum* sclerotia depends on isolate and host plant. *Plant Pathol.* 67, 1286–1295. doi: 10.1111/ppa.12843

Wang, X. Q., Zhao, D. L., Shen, L. L., Jing, C. L., and Zhang, C. S. (2018). "Application and mechanisms of *Bacillus subtilis* in biological control of plant disease," in Meena, V. S., ICAR-Vivekananda Institute of Hill Agriculture, Almora, Uttarakhand, India. eds. *Role rhizospheric microbes soil Vol. 1 Stress Manag. Agric. Sustain.* (Singapore: Springer), 225–250. doi: 10.1007/978-981-10-8402-7_9

Wu, H., Gu, Q., Xie, Y., Lou, Z., Xue, P., Fang, L., et al. (2019). Cold-adapted *Bacilli* isolated from the Qinghai–Tibetan Plateau are able to promote plant growth in extreme environments. *Environ. Microbiol.* 21, 3505–3526. doi: 10.1111/1462-2920.14722

Wu, L., Wu, H., Chen, L., Xie, S., Zang, H., Borriss, R., et al. (2014). Bacilysin from *Bacillus amyloliquefaciens* FZB42 has specific bactericidal activity against harmful algal bloom species. *Appl. Environ. Microbiol.* 80, 7512–7520. doi: 10.1128/AEM.02605-14

Wu, L., Wu, H., Chen, L., Yu, X., Borriss, R., and Gao, X. (2015). Difficidin and bacilysin from *Bacillus amyloliquefaciens* FZB42 have antibacterial activity against *Xanthomonas oryzae* rice pathogens. *Sci. Rep.* 5, 12975. doi: 10.1038/srep12975

Xu, P., Wu, J., Xue, A., LI, W., Chen, W., Lai, W. E. I., et al. (2012). Differentially expressed genes of soybean during infection by *Phytophthora sojae*. *J. Integr. Agric.* 11, 368–377. doi: 10.1016/S2095-3119(12)60021-5

Xu, W., Wang, F., Zhang, M., Ou, T., Wang, R., Strobel, G., et al. (2019). Diversity of cultivable endophytic bacteria in mulberry and their potential for antimicrobial and plant growth-promoting activities. *Microbiol. Res.* 229, 126328. doi: 10.1016/j.micres.2019.126328

Xu, X., Qin, G., and Tian, S. (2008). Effect of microbial biocontrol agents on alleviating oxidative damage of peach fruit subjected to fungal pathogen. *Int. J. Food Microbiol.* 126, 153–158. doi: 10.1016/j.ijfoodmicro.2008.05.019

Yong, Z., Hao-Ru, T., and Ya, L. (2008). Variation in antioxidant enzyme activities of two strawberry cultivars with short-term low temperature stress. *World J. Agric. Sci.* 4, 458–462.

Yu, C., Chen, H., Zhu, L., Song, Y., Jiang, Q., Zhang, Y., et al. (2023). Profiling of antimicrobial metabolites synthesized by the endophytic and genetically amenable biocontrol strain *bacillus velezensis* DMW1. *Microbiol. Spectr.* 11, e00038–e00023. doi: 10.1128/spectrum.00038-23

Zhai, Q., Pan, Z., Zhang, C., Yu, H., Zhang, M., Gu, X., et al. (2023). Colonization by *Klebsiella variicola* FH-1 stimulates soybean growth and alleviates the stress of Sclerotinia sclerotiorum. *J. Integr. Agric.* 22, 2729–2745. doi: 10.1016/j.jia.2023.01.007

Zhou, H., Ren, Z., Zu, X., Yu, X., Zhu, H., Li, X., et al. (2021). Efficacy of plant growth-promoting bacteria *Bacillus cereus* YN917 for biocontrol of rice blast. *Front. Microbiol.* 12, 684888. doi: 10.3389/fmicb.2021.684888

Zhu, G. Y., Shi, X. C., Wang, S. Y., Wang, B., and Laborda, P. (2022). Antifungal mechanism and efficacy of kojic acid for the control of *sclerotinia sclerotiorum* in soybean. *Front. Plant Sci.* 13. doi: 10.3389/fpls.2022.845698

Zhu, J., Tan, T., Shen, A., Yang, X., Yu, Y., Gao, C., et al. (2020). Biocontrol potential of *Bacillus subtilis* IBFCBF-4 against *Fusarium* wilt of watermelon. *J. Plant Pathol.* 102, 433–441. doi: 10.1007/s42161-019-00457-6

Zubair, M., Farzand, A., Mumtaz, F., Khan, A. R., Sheikh, T. M. M., Haider, M. S., et al. (2021). Novel genetic dysregulations and oxidative damage in *Fusarium graminearum* induced by plant defense eliciting psychrophilic *Bacillus atrophaeus* TS1. *Int. J. Mol. Sci.* 22, 12094. doi: 10.3390/ijms222212094

Zubair, M., Hanif, A., Farzand, A., Sheikh, T. M. M., Khan, A. R., Suleman, M., et al. (2019). Genetic screening and expression analysis of psychrophilic Bacillus spp. Reveal their potential to alleviate cold stress and modulate phytohormones in wheat. *Microorganisms* 7, 337. doi: 10.3390/microorganisms7090337

frontiers | Frontiers in Plant Science

TYPE Original Research
PUBLISHED 04 September 2024
DOI 10.3389/fpls.2024.1459651

Check for updates

OPEN ACCESS

EDITED BY
Yasser Nehela,
University of Florida, United States

REVIEWED BY
Pradeep Singh,
Eternal University, India
Ashwin Revanna,
Centre for Natural Biological Resources and Community Development (CNBRCD), India

*CORRESPONDENCE
Jing He
hejing268@aliyun.com

RECEIVED 04 July 2024
ACCEPTED 16 August 2024
PUBLISHED 04 September 2024

CITATION
Li N, Chen W, Wang B, Zhang C, Wang Y, Li R, Yan Y and He J (2024) Arbuscular mycorrhizal fungi improve the disease resistance of *Lycium barbarum* to root rot by activating phenylpropane metabolism.
Front. Plant Sci. 15:1459651.
doi: 10.3389/fpls.2024.1459651

COPYRIGHT
© 2024 Li, Chen, Wang, Zhang, Wang, Li, Yan and He. This is an open-access article distributed under the terms of the Creative Commons Attribution License (CC BY). The use, distribution or reproduction in other forums is permitted, provided the original author(s) and the copyright owner(s) are credited and that the original publication in this journal is cited, in accordance with accepted academic practice. No use, distribution or reproduction is permitted which does not comply with these terms.

Arbuscular mycorrhizal fungi improve the disease resistance of *Lycium barbarum* to root rot by activating phenylpropane metabolism

Nan Li[1], Wei Chen[1], Bin Wang[1], Chongqing Zhang[1], Yupeng Wang[1], Ruiyun Li[1], Yuke Yan[1] and Jing He[1,2]*

[1]College of Forestry, Gansu Agricultural University, Lanzhou, China, [2]Wolfberry Harmless Cultivation Engineering Research Center of Gansu Province, Lanzhou, China

Root rot is one of the common diseases of *Lycium barbarum*. Pathogens can cause devastating disasters to plants after infecting host plants. This study investigated the effect of arbuscular mycorrhizal fungi (AMF) *Rhizophagus intraradices* inoculation on phenylpropane metabolism in *L. barbarum* and evaluated its resistance to root rot. The experiment was set up with AMF inoculation treatments (inoculated or not) and root rot pathogen-*Fusarium solani* inoculation treatments (inoculated or not). The results showed that AMF was able to form a symbiosis with the root system of *L. barbarum*, thereby promoting plant growth significantly and increasing plants' resistance to disease stress. The plant height of AMF-colonized *L. barbarum* increased by 24.83% compared to non-inoculated diseased plants. After inoculation with AMF, the plant defense response induced by pathogen infection was stronger. When the enzyme activity of the leaves reached the maximum after the onset of mycorrhizal *L. barbarum*, phenylalanine ammonia-lyase, cinnamic acid-4-hydroxylase, and 4-coumaric acid-CoA ligase increased by 3.67%, 31.47%, and 13.61%, respectively, compared with the non-inoculated diseased plants. The products related to the lignin pathway and flavonoid pathway downstream of phenylpropane metabolism such as lignin and flavonoids were also significantly increased by 141.65% and 44.61% compared to nonmycorrhizal diseased plants. The activities of chitinase and β-1,3-glucanase increased by 36.00% and 57.96%, respectively. The contents of salicylic acid and jasmonic acid were also 17.7% and 31.63% higher than those of nonmycorrhizal plants in the early stage of plant growth, respectively. The results indicated that AMF significantly promoted plant growth and enhanced disease resistance by increasing enzyme activities and the production of lignin and flavonoids.

KEYWORDS

root rot of *Lycium barbarum*, *Rhizophagus intraradices*, phenylpropane metabolism, pathogenesis-related protein, disease resistance

1 Introduction

Lycium barbarum L. is a deciduous shrub belonging to the genus *Lycium* of the Solanaceae family. It is mainly distributed in the arid and semi-arid environments in northwest and north China, as well as Eurasia, Africa, and North and South America (Gong et al., 2022). It has a wide range of cultivation scales in China, mainly concentrated in Nei Monggol, Gansu, Ningxia, Shaanxi, and Qinghai provinces (Zhang et al., 2018). As an excellent shrub for soil and water conservation, *L. barbarum* has significant ecological value, including drought resistance, windbreak and sand fixation capabilities, and soil improvement properties. Its roots, stems and leaves are used as medicine, and its fruits are rich in bioactive substances (polysaccharides, minerals, carotenoids, and polyphenols), making them excellent functional food and natural medicine (Gao et al., 2017; Wang et al., 2018; Yu et al., 2023).

With the continuous expansion of the cultivation scale of *L. barbarum*, the occurrence of *L. barbarum* diseases is becoming more and more serious. Root rot is one of the common diseases in *L. barbarum*, mainly caused by *Fusarium solani*. Pathogenic fungi can bring devastating disasters to plants after infecting host plants, which not only seriously affects the quality of *L. barbarum*, but also poses a huge threat to local economic development. In the early stages of the disease, the roots swell, and the swelling intensifies in the middle stage with a small amount of defoliation. In the later stage, the roots completely rot and show reddish brown, and the plants shed a large amount of leaves until they wither and die (He et al., 2023; Zhang et al., 2023a). In the main cultivation areas of *L. barbarum*, the incidence of root rot can reach 50%, resulting in serious yield and income reduction, drastically hindering the development of the *L. barbarum* industry (Zhu et al., 2023). So far, chemical control remains the most important method for managing this disease. However, long-term use of chemical agents can lead to increased resistance in pathogenic fungi and environmental pollution. Biological control has attracted more and more attention because of its safety, environmental protection, no residue, and other advantages that chemical control can't surpass. At present, the use of biocontrol microorganisms instead of synthetic fungicides has become a hot topic for many scholars, progressive farmers, cultivators, and even end users.

Arbuscular Mycorrhizal Fungi (AMF) are a group of widely distributed soil fungi that typically form symbiotic relationships with about 85% of terrestrial plants (Khaliq et al., 2022). In forestry production and ecological restoration and protection, AMF, as a ubiquitous symbiotic microorganism with plants, has a high application value and potential production and development prospects (Qu et al., 2022b). Studies have shown that AMF can respond to biotic stresses such as diseases (Devi et al., 2022) and pests (Wang et al., 2023b), and abiotic stresses such as drought (Zou et al., 2021), waterlogging (Xu et al., 2024), low temperature (Li et al., 2020) and salinity (Li et al., 2024) by changing root morphological structure, competing with pathogens for photosynthetic products and living space, activating disease-related defense enzyme systems, and regulating the formation of secondary metabolites of host plants. Aseel et al. (2019) found that after inoculation with AMF, the gene expression level of the phenylpropane synthesis pathway in diseased tomatoes was up-regulated, which reduced the severity of tomato mosaic disease. Pre-inoculation with *Glomus versiformme* significantly alleviated *Fusarium* wilt caused by *Fusarium oxysporum* (Pu et al., 2022). Wang et al. (2022) studied the differentially expressed genes of apple plants inoculated with AMF at the transcriptional level after infection with *F. solani* compared with non-inoculated plants, and found that *MdWRKY40* played an important role in the resistance of mycorrhizal apple seedlings to pathogen infection. At the same time, it was also found that inoculation of AMF significantly increased the resistance of apples to *Neonectria ditissima* (Despina et al., 2018). Therefore, in the context of sustainability of ecosystem health, the application of AMF is expected to be a promising biocontrol method due to their ability to promote plant growth and enhance disease resistance (George and Ray, 2023).

The phenylpropane pathway (PPP) is one of the important defense pathways in plants (Despina et al., 2018). A large number of studies have shown that the activity of key enzymes in the PPP, the content of phenylpropanoid compounds, and their derivatives are closely related to the strength of plant disease resistance (Dong and Lin, 2021). At the same time, PPP is also involved in the synthesis of plant disease-resistant hormones. For example, the accumulation of salicylic acid (SA) can activate plant disease-resistant immune signaling pathways and comprehensively regulate plant disease-resistant immune systems (Vlot et al., 2009). Wei et al. (2017) found that hot air treatment induced resistance to *Alternaria alternata* and *Botrytis cinerea* by activating the PPP in cherry tomato fruits. Ge et al. (2018) confirmed that ε-poly-L-lysine treatment enhanced the resistance of apple fruits to *Penicillium expansum* by activating reactive oxygen species (ROS) metabolism and PPP. Qu et al. (2022) found that melatonin enhances the postharvest resistance of blueberry fruits to *Valsa* canker by mediating the jasmonic acid (JA) signaling pathway and PPP (Qu et al., 2022a). At present, the research on *L. barbarum* root rot mainly focuses on the pathogenesis (Gao et al., 2022), antagonistic fungi screening and so on (Wang et al., 2023a). Our previous study found that *Rhizophagus intraradices* can form a good symbiotic system with *L. barbarum* and enhance the resistance to root rot (Li et al., 2022). However, how *R. intraradices* influences the PPP of *L. barbarum* and thereby induces it to improve disease resistance has not been reported. Therefore, this study mainly focused on the PPP, growth parameter measurements, PPP pathway-related enzyme activities, pathogenesis-related proteins, related enzyme activities in signal substances, and key substance contents of *L. barbarum*, to reveal the mechanism of AMF-induced *L. barbarum* resistance to root rot from the perspective of PPP, and provide a theoretical basis for the biological control of *L. barbarum* root rot.

2 Materials and methods

2.1 Materials

The tested AMF agent was *Rhizophagus intraradices* BGC-BG09, which was provided by the Institute of Plant Nutrition and Resources of Beijing Academy of Agriculture and Forestry

Sciences. Maize was used as the host for propagation, and the propagated substrate was used as inoculum which contained spores, hyphae, and fine root segments. Subsequently, we isolated and screened the spores using wet sieving and sucrose centrifugation, stained them following the method described by Kumar et al. (2008), and then observed and counted them under a somatic microscope to determine the number of viable spores present in the inoculum.

F. solani was isolated from the diseased plants of typical *L. barbarum* root rot, and preserved in the forest protection laboratory of Forestry College of Gansu Agricultural University after a pathogenicity test. Before inoculation, the isolated fungus was activated by sub-culturing on a PDA plate and stored at 4°C. 10 mL of sterile water and two drops of Tween-80 was added to the purified *F. solani* after multiple cultures and gently shook it to ensure the conidia were completely dislodged. The spore count was then performed using a hemocytometer. When using the hemocytometer, the number of spores in each small square was first measured and then converted to the number of spores per milliliter of the fungal suspension. Based on the counting results, the suspension was diluted to 1×10^7 spores/mL for later use.

2.2 Experimental design

The pot experiment was carried out in the economic forest teaching and scientific research practice base of Forestry College of Gansu Agricultural University from March 2023 to September 2023. To avoid the presence of native AMF, sterilized soil was used in all the treatments. The one-year-old seedlings of *L. barbarum* of the same size were selected and transplanted into a 35 cm × 24 cm pot (disinfected with 0.5% sodium hypochlorite) for treatment. In the inoculation group, 10 g of *R. intraradices* inoculum (approximately 100 viable spores per gram) was evenly spread in the pot at the base of root contact before *L. barbarum* transplantation ensuring full contact with the roots. In the non-inoculation group, the same amount of inactivated *R. intraradices* inoculum (autoclaved at 121°C for 2 h) was added following the method used for inoculated pots. and 10 mL microbial filtrate (0.2 μm microporous membrane) of the *R. intraradices* inoculum was added to ensure the consistency of microbial flora. After transplantation, normal watering and fertilizer management were performed. *L. barbarum* seedlings were allowed to grow for 30 d of disease-free stress period to establish a good symbiotic relationship with *R. intraradices*. Later *F. solani* was inoculated after determining the formation of mycorrhiza. The pathogen was inoculated by the root-injury method. 100 mL of *F. solani* spore suspension with a concentration of 10^7 CFU·mL^{-1} was directly injected into the root, and the same amount of sterile water was added into the control group (CK). The environmental conditions during seedling growth were as follows: temperature range of 20-26°C, relative humidity of 65% -90%, and natural light. Maintain a regular supply of water during seedling growth.

A total of 4 treatments were set up: T1 control: neither *R. intraradices* nor *F. solani* inoculation (-R.i-F.s); T2: inoculated with only *R. intraradices* (+R.i-F.s); T3: inoculated with only *F. solani* (-R.i+F.s); T4: double inoculation with *R. intraradices* and *F. solani* (+R.i+F.s), and replicated 24 pots per treatment totaling to 96 pots. During the experiment, normal watering and fertilizer management of each plant was maintained. The plant growth indices (including leaf number, plant height, stem diameter, etc.) were observed and recorded at 15 d (leaf expansion period), 30 d (flowering period), 60 d (initial fruit period), 90 d (full fruit period) and 120 d (final fruit period) after *F. solani* inoculation. Leaves were collected at different growth stages to determine physiological and biochemical indexes such as disease resistance-related enzyme activity, JA, and SA.

2.3 Determination of mycorrhizal colonization rate

Staining was carried out using the Trypan Blue staining method (Eke et al., 2020). Root samples of different periods were collected and cut into root segments of about 1 cm. The root segments were placed in a centrifuge tube, and 3 mL of 0.5% KOH (immersed root segments) was added and kept in a water bath at 90°C for 15 mins. The root samples were dispersed by gently shaking. Later, the root samples were washed with water 3-5 times until the water flow remained no longer yellow. The cleaned root samples were soaked in 1% HCl for 2 min and removed. To the acidified roots in the centrifuge tube, 0.05% Trypan Blue staining solution (distilled water: glycerol: lactic acid=1:1:3) was added to soak and kept in a water bath at 90°C for 30 min, Later the roots in the tubes were soaked again with 1:1 lactic acid glycerol solution for 12 h (to remove excess stain in roots) and mycorrhizal colonization in roots was observed for mycorrhizal colonization under microscope and estimated according to below equation by.

$$\text{Root colonization rate} = \frac{\text{number of infected root segments}}{\text{number of detected root segments}} \times 100\,\%$$

2.4 Determination of morbidity, disease index, and growth parameters

After the inoculation of *F. solani*, a real-time investigation of *L. barbarum* plants was carried out. After *L. barbarum* shows symptoms of disease, the number of diseased *L. barbarum* leaves was investigated at different growth periods, respectively. The number of diseased leaves was recorded, and the incidence and disease index were calculated according to the corresponding grading standards (Gu et al., 2009).

The plant height and basal diameter of seedlings were measured by tape and vernier caliper, respectively. After the leaves were picked,

fresh weight was weighed, dried to constant weight at 65°C in the oven and dry weight was weighed.

$$\text{morbidity} = \frac{\text{Number of diseased plants}}{\text{Investigate the number of plants}} \times 100\,\%$$

$$\textit{disease index} = \sum \frac{\text{Number of diseased plants at all levels} \times \text{The disease grade value}}{\text{Total number of survey plants} \times \text{The highest level value}} \times 100$$

$$\text{control effect}(\%) = \frac{\text{Control disease index} - \text{treatment disease index}}{\text{Control disease index}} \times 100$$

The determination of chlorophyll content referred to the method of Ronen and Galun (1984). 0.2 g fresh leaves were quickly frozen in liquid nitrogen and ground into powder. Dimethyl sulfoxide (analytical purity) was used to extract the powder in a constant temperature water bath at 60°C for 1 h in the dark. The supernatant was collected and the absorbance of chlorophyll a and b was determined at 663 and 645 nm.

2.5 Determination of SA and JA

The content of SA and JA was determined using the corresponding enzyme-linked immunosorbent assay (ELISA) kits. The corresponding item numbers are YX-22154P and YX-21810P. The kits were all from Shanghai Youyou Biotechnology Co., Ltd.

2.6 Determination of pathogenesis-related protein in *L. barbarum* leaves

The extraction method of enzyme solution was referred to as 2.5.1. Chitinase activity was measured using the corresponding ELISA kit. The corresponding item number of the kit is YX-E22624P, which was obtained from Sino Best Biological Technology Co., Ltd. The extraction of β-1,3-glucanase was determined according to the method of Zhang et al. (2013). The amount of enzyme required for the reaction system to change the absorbance value at 540 nm by 0.01 per hour was an enzyme activity unit (U). The polygalacturonase (PG) was determined according to the method of Cao et al. (2007). The mass of polygalacturonic acid hydrolyzed into galacturonic acid ($mg{\cdot}h^{-1}{\cdot}g^{-1}$) was expressed as per gram of plant tissue sample (fresh weight) per hour at 37°C. Determination of pectin methylgalacturonase (PMG) was based on the method of Cao et al. (2007), expressed as the mass per gram of plant tissue sample per hour at 37°C catalyzed substrate hydrolysis to produce galacturonic acid ($mg{\cdot}h^{-1}{\cdot}g^{-1}$).

2.7 Determination of enzyme activities and products related to PPP in *L. barbarum* leaves

Phenylalanine ammonia-lyase (PAL) activity was determined according to the method of Khumalo et al. (2017). The amount of enzyme required to change the absorbance value at 290 nm by 0.01 per minute of the reaction system was used as an enzyme activity unit (U). The activity of cinnamic acid-4-hydroxylase (C4H) was determined according to the method of Ackah et al. (2022), the method of enzyme solution extraction was referred to as 2.5.1, and the amount of enzyme required to change the absorbance value at 340 nm by 0.01 per minute of the reaction system was taken as an enzyme activity unit (U). Determination of 4-coumaric acid-CoA ligase (4CL) activity according to the method of Ackah et al. (2022), the amount of enzyme required to change the absorbance value at 333 nm by 0.01 per minute of the reaction system was taken as an enzyme activity unit (U). Determination of chalcone isomerase (CHI) activity according to the method of Latunde-Dada et al. (1987), the amount of enzyme required to change the absorbance value at 290 nm by 0.01 per minute of the reaction system was used as an enzyme activity unit (U). The activities of chalcone synthase (CHS), flavanone hydroxylase (F3H), hydroxycinnamic acid transferase (HCT), cinnamoyl-CoA reductase (CCR), and cinnamyl alcohol dehydrogenase (CAD) were determined using the corresponding ELISA kits. The corresponding item numbers of the kits are YX-E21833P, YX-E22631P, YX-E22626P, YX-E22625P, and YX-E21912P. All of the above kits were derived from Sino Best Biological Technology Co., Ltd. Lignin content was determined by A280 nm·mg protein according to the method of Bonawitz et al. (2014). Contents of flavonoids and total phenols were determined according to the method of Cao et al. (2007). The flavonoid content was expressed as OD_{325} nm/g, and the total phenol content was expressed as the absorbance value of fresh weight per gram plant tissue at 280 nm, and calculated by gallic acid standard curve, expressed as mg g^{-1}.

2.8 Data processing and analysis

SPSS 26.0 was used to test the homogeneity of variance on the original data. When the Sig value was > 0.05, the variance was considered to be homogeneous, and then one-way ANOVA analysis of variance was performed. Duncan's method was used for specific *post-hoc* tests, and the significance level was set as $\alpha = 0.05$. The data were expressed as mean ± standard error (SE). Origin 2021 was used for plotting.

3 Results and analysis

3.1 *R. intraradices* colonization and infection in *L. barbarum* roots

The colonization rate gradually increased with the change in the plant growth period. The colonization rate of mycorrhizal diseased plants in the middle and late stages was lower than that of plants inoculated with only *R. intraradices*, indicating that the presence of *F. solani* had a negative effect on the colonization of *R. intraradices* (Figure 1A). The colonization structure of *R. intraradices*, such as hyphae, arbuscular and vesicles, could be observed after *R. intraradices* inoculation (Figures 1B–D). In contrast, no

10.3389/fpls.2024.1459651

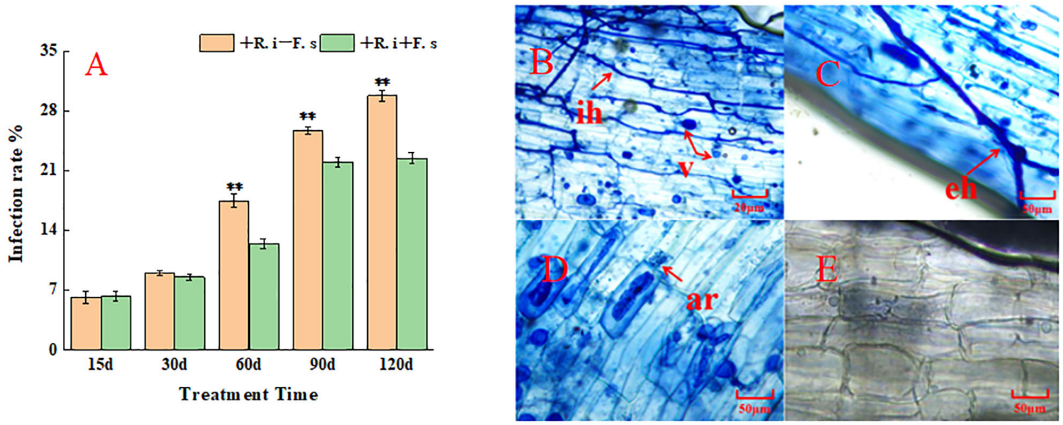

FIGURE 1
Mycorrhizal colonization rate and infection structure of *L. barbarum* roots at different growth stages. **(A)** Mycorrhizal infection rate; **(B–E)** *R. intraradices* infection structure: ih, intraradical hyphae; eh, exogenous hyphae; v, vesicles; ar, arbuscule.

R. intraradices colonization was observed in the non-inoculated treatment (Figure 1E), the colonization rate of control plants was 0.

3.2 Effect of *R. intraradices* on growth parameters, incidence, and disease index of *L. barbarum* under different inoculation treatments

Whether inoculated with *R. intraradices* or not, the *L. barbarum* plants inoculated with *F. solani* would develop disease in the later growth stages. However, the colonization of *R. intraradices* could significantly reduce the incidence and disease index of *L. barbarum*, indicating that the inoculation of *R. intraradices* to the roots of *L. barbarum* plants could significantly enhance the resistance of plants and reduce the occurrence of root rot (Table 1).

With the change in the growth potential of *L. barbarum* plants, there was a significant difference between the *L. barbarum* plants colonized by *R. intraradices* and the *L. barbarum* plants in the control group. At the same time, due to the presence of *R. intraradices*, the height of mycorrhizal plants was significantly higher than that of plants only inoculated with *F. solani* at the later stage (Figure 2).

3.3 Effects of *R. intraradices* on PPP metabolic pathway in *L. barbarum* leaves under different inoculation treatments

3.3.1 Enzyme activities related to the PPP

The two treatments of only inoculation with *R. intraradices* and only inoculation with *F. solani* could induce the increase of PAL activity in leaves (appeared in different periods). After pre-inoculation with *R. intraradices*, PAL activity could be enhanced under *F. solani* stress to alleviate the damage caused by *F. solani*. The treatment of inoculated *F. solani* showed a trend of increasing first and then decreasing, reaching the maximum at 60 days. The enzyme activity of mycorrhizal diseased plants was 3.67% higher than that of non-mycorrhizal diseased plants (Figure 3A).

Mycorrhizal *L. barbarum* significantly increased C4H activity by 22.64%, 17.64%, 26.61% and 31.47% under *F. solani* stress. The C4H activity of mycorrhizal plants increased gradually in five periods and reached the maximum at 120 d, which was 41.4% and 33.0% higher than that of non-mycorrhizal diseased plants and mycorrhizal diseased plants, respectively. Because of the inoculation of *F. solani*, the mycorrhizal plants had the opposite trend with the treatment of *R. intraradices* alone in the later stage, which was consistent with the trend of single inoculation of *F. solani* (Figure 3B). Under the condition of inoculation with *F. solani*, the 4CL activity of mycorrhizal plants was 3.44%, 24.34%, 15.97% and 13.61% higher than that of non-mycorrhizal plants within 15-90 days (Figure 3C).

With the increase in treatment time, the activity of CHS inoculated with *F. solani* showed a decreasing trend. After inoculation with *R. intraradices*, the trend of *F. solani* inoculation treatment was opposite to that of non-*F. solani* inoculation treatment in the later stage, which was consistent with the trend of single *F. solani* inoculation treatment. The enzyme activity of mycorrhizal plants in the mid to late stage (60-120 d) was significantly higher than that of single inoculation of *F. solani* by 11.03%, 17.83% and 12.21%. It can be seen that *R. intraradices* can play a better role in improving CHS activity under disease stress (Figure 3D). After inoculation with *F. solani*, the CHI activity of mycorrhizal and non-mycorrhizal seedlings showed a gradual downward trend. Under disease stress, compared with non-inoculated *R. intraradices*, the enzyme activity of AMF-inoculated leaves increased significantly by 19.7%, 19.2%, 33.2%, 20.1% and 15.5% in five periods (Figure 3E). The enzyme activity of the treatment only inoculated with *R. intraradices* showed a trend of increasing first and then decreasing, reaching the maximum at 60 d (Figure 3E). The F3H activity of the four treatments showed a trend of increasing first and then decreasing as a whole. Under the treatment of *F. solani* inoculation, the difference between *R. intraradices* inoculation and non-AMF inoculation was not

10.3389/fpls.2024.1459651

TABLE 1 Effects of different inoculation treatments on growth parameters of *L. barbarum*.

Days(d)	Treatment	-R. i-F. s	-R. i+F. s	+R. i-F. s	+R. i+F. s
leaf expansion period	stem thickness/mm	7.93 ± 0.57b	7.07 ± 0.46c	11.77 ± 0.81a	12.35 ± 0.57a
	plant height/cm	60.42 ± 14.63b	59.37 ± 17.37b	80.62 ± 11.63a	85.73 ± 14.63a
	number of leaves	121.53 ± 17.53b	119.33 ± 23.64b	169.78 ± 29.83a	179.63 ± 27.47a
	leaf aspect ratio	3.03 ± 0.71b	3.56 ± 1.85a	3.07 ± 0.54b	3.56 ± 0.47b
	leaf area/cm^2	6.53 ± 1.39bc	5.19 ± 1.49c	8.13 ± 1.74ab	8.04 ± 1.32a
	leaf blade girth/cm	13.19 ± 1.96bc	12.49 ± 1.22c	15.62 ± 1.93ab	16.26 ± 0.68a
	leaf index	0.15 ± 0.01a	0.13 ± 0.01a	0.13 ± 0.06a	0.12 ± 0.01a
	leaf water content	0.82 ± 0.01a	0.78 ± 0.02a	0.82 ± 0.05a	0.83 ± 0.02a
	Morbidity	0	8.33%	0	4.17%
	disease index	0	8.33	0	4.17
	control effect %	/	/	/	50
flowering period	stem thickness/mm	9.1 ± 1.39b	7.07 ± 1.02b	13.17 ± 1.99a	15.15 ± 1.83a
	plant height/cm	74.42 ± 16.67bc	69.67 ± 21.13c	87.83 ± 15.75ab	91.92 ± 14.63a
	number of leaves	183.92 ± 21.1b	167.33 ± 29.77b	219.58 ± 29.83a	222.42 ± 45.93a
	leaf aspect ratio	3.42 ± 0.71b	4.54 ± 1.85a	3.56 ± 0.54b	3.66 ± 0.47b
	leaf area/cm^2	7.14 ± 1.59bc	6.1 ± 1.48c	8.23 ± 2.1ab	8.96 ± 1.41a
	leaf blade girth/cm	13.97 ± 1.52bc	13.12 ± 1.36c	15.07 ± 1.81ab	16.14 ± 0.91a
	leaf index	0.14 ± 0.01a	0.14 ± 0.01a	0.15 ± 0.06a	0.14 ± 0.01a
	leaf water content	0.81 ± 0.01a	0.81 ± 0.02a	0.81 ± 0.05a	0.82 ± 0.02a
	Morbidity	4.17%	16.67%	0	8.33%
	disease index	4.17	10.42	0	8.33
	control effect %	/	/	/	20
initial fruit period	stem thickness/mm	9.19 ± 0.81c	7.25 ± 0.82d	14.57 ± 1.01a	12.67 ± 1.58b
	plant height/cm	105.7 ± 17.74ab	93.8 ± 24.01b	118.2 ± 27.96a	104.4 ± 26.13ab
	number of leaves	147.1 ± 34.08b	104.3 ± 30.77c	191.3 ± 23.00a	176.8 ± 40.93ab
	leaf aspect ratio	3.65 ± 0.51a	4.06 ± 0.74a	3.68 ± 0.44a	3.71 ± 0.31a
	leaf area/cm^2	8.25 ± 292.10b	7.12 ± 238.91b	9.06 ± 203.81ab	10.85 ± 215.98a
	leaf blade girth/cm	14.92 ± 26.37b	14.44 ± 19.96b	15.78 ± 15.36b	17.48 ± 18.4a
	leaf index	0.15 ± 0.01a	0.13 ± 0.02c	0.14 ± 0.01ab	0.14 ± 0.01ab
	leaf water content	0.82 ± 0.01a	0.81 ± 0.05a	0.82 ± 0.04a	0.83 ± 0.04a
	Morbidity	8.00%	29.17%	0	16.67%
	disease index	8.33	20.83	0	16.67
	control effect %	/	/	/	20
full fruit period	stem thickness/mm	11.1 ± 1.72ab	9.93 ± 0.56b	12.59 ± 1.23a	12.52 ± 2.26a
	plant height/cm	107.00 ± 19.52ab	96.00 ± 21.89b	131.33 ± 20.47a	102.17 ± 27.71b
	number of leaves	169.33 ± 18.79a	107.67 ± 37.58b	187.17 ± 29.92a	169.00 ± 15.31a
	leaf aspect ratio	3.93 ± 0.45a	4.02 ± 0.97a	3.72 ± 0.53a	3.84 ± 0.71a
	leaf area/cm^2	7.48 ± 0.81b	6.09 ± 1.28b	10.25 ± 0.75a	9.54 ± 2.97a
	leaf blade girth/cm	14.9 ± 1.07bc	13.65 ± 1.35c	16.96 ± 0.75ab	16.44 ± 2.14a

(Continued)

10.3389/fpls.2024.1459651

TABLE 1 Continued

Days(d)	Treatment	-R. i-F. s	-R. i+F. s	+R. i-F. s	+R. i+F. s
	leaf index	0.14 ± 0.01a	0.13 ± 0.02a	0.14 ± 0.01a	0.14 ± 0.01a
	leaf water content	0.77 ± 0.01b	0.8 ± 0.01ab	0.81 ± 0.03ab	0.85 ± 0.1a
	Morbidity	8.33%	45.83%	4.17%	20.83%
	disease index	8.33	23.61	4.17	12.5
	control effect %	/	/	/	47
final fruit stage	stem thickness/mm	10.75 ± 1.21ab	9.75 ± 0.43b	12.73 ± 1.41a	12.48 ± 2.25a
	plant height/cm	113.00 ± 17.74a	102.00 ± 21.89b	127.33 ± 20.26a	110.17 ± 24.41a
	number of leaves	153.31 ± 18.79a	89.37 ± 37.58b	169.27 ± 17.94a	154.00 ± 14.91a
	leaf aspect ratio	4.24 ± 0.14a	4.3 ± 0.26a	3.74 ± 0.57ab	3.46 ± 0.08b
	leaf area/cm^2	5.24 ± 1.17bc	3.98 ± 0.61c	7.76 ± 1.58a	7.12 ± 0.5ab
	leaf blade girth/cm	12.55 ± 1.25bc	11.07 ± 0.71c	14.32 ± 0.77a	13.8 ± 0.47ab
	leaf index	0.13 ± 0.00ab	0.13 ± 0.01b	0.15 ± 0.02a	0.15 ± 0.00a
	leaf water content	0.79 ± 0.04a	0.72 ± 0.08a	0.72 ± 0.08a	0.77 ± 0.02a
	Morbidity	12.50%	54.17%	4.17%	29.17%
	disease index	12.5	29.17	4.17	16.67
	control effect %	/	/	/	43

The values are mean ± standard error (SE); Different lowercase letters represent significant differences between data in the same column (P<0.05),-R. i-F. s: neither inoculated with R. intraradices nor F. solani; +R. i-F. s: inoculated R. intraradices but not with F. solani; -R. i+F. s: not inoculated with R. intraradices but with F. solani; +R. i+F. s: Double inoculation with R. intraradices and F. solani.

significant in the early stages and was significant in the middle and late stages, which was in line with the trend of CHS. *R. intraradices* increased F3H activity as a whole, higher than the other three treatments (Figure 3F).

After *R. intraradices* inoculation, HCT activity showed a gradual downward trend regardless of whether the *F. solani* was inoculated or not (Figure 3G). Regardless of *R. intraradices* inoculation status, both treatments inoculated with *F. solani* showed a trend of increasing first and then decreasing. Under the stress of disease, the activity of *L. barbarum* inoculated with *R. intraradices* was significantly increased by 20.24%, 5.58%, 11.20%, 13.63% and 11.47% compared with that without *R. intraradices* inoculation (Figure 3G). CAD activity was significantly increased by 5.92%, 31.56%, 7.46%, 11.32%, and 26.88% (Figure 3I). CCR activity showed a decreasing and then increasing trend in all three treatments except the control (Figure 3H). Under disease stress, compared with non-AMF inoculation, the CAD activity of AMF-inoculated plants was significantly increased by 45.76%, 37.00%, 47.67%, 54.20%, and 58.65%.

3.3.2 Products related to the PPP

The flavonoid content showed a trend of increasing first and then decreasing as a whole. In the first three periods, compared with non-inoculated *R. intraradices*, the flavonoid content in *L. barbarum* leaves inoculated *R. intraradices* under disease stress was significantly increased by 64.59%, 141.65%, and 30.81% (Figure 4A). In contrast, in the first three periods, there was no significant difference in lignin content between mycorrhizal and non-mycorrhizal plants, and increased significantly by 34.13% and 44.61% only in the latter two periods (Figure 4B). The total phenol content of the *F. solani* inoculation treatment showed a gradual downward trend, while the content in mycorrhizal plants showed a trend of increasing first and then decreasing due to the infection of *F. solani*. At 15 d, there was no significant difference between the two treatments inoculated with *F. solani*. The total phenol content of mycorrhizal plants was significantly higher than that of non-mycorrhizal plants by 35.79%, 27.01%, and 18.97% (Figure 4C).

3.4 Effects of *R. intraradices* on the content of plant signaling substances in leaves of *L. barbarum* under different inoculation treatments

With the prolongation of treatment time, the SA content of each treatment showed a gradual downward trend. The SA content of mycorrhizal plants in the early stage (15 d, 30 d) was 11.7% and 17.7% higher than that of only inoculated *F. solani* treatment (Figure 5A). The JA content of all treatments, except for the treatments double inoculated with *R. intraradices* and *F. solani*, showed a general trend of decreasing and then increasing (Figure 5B).

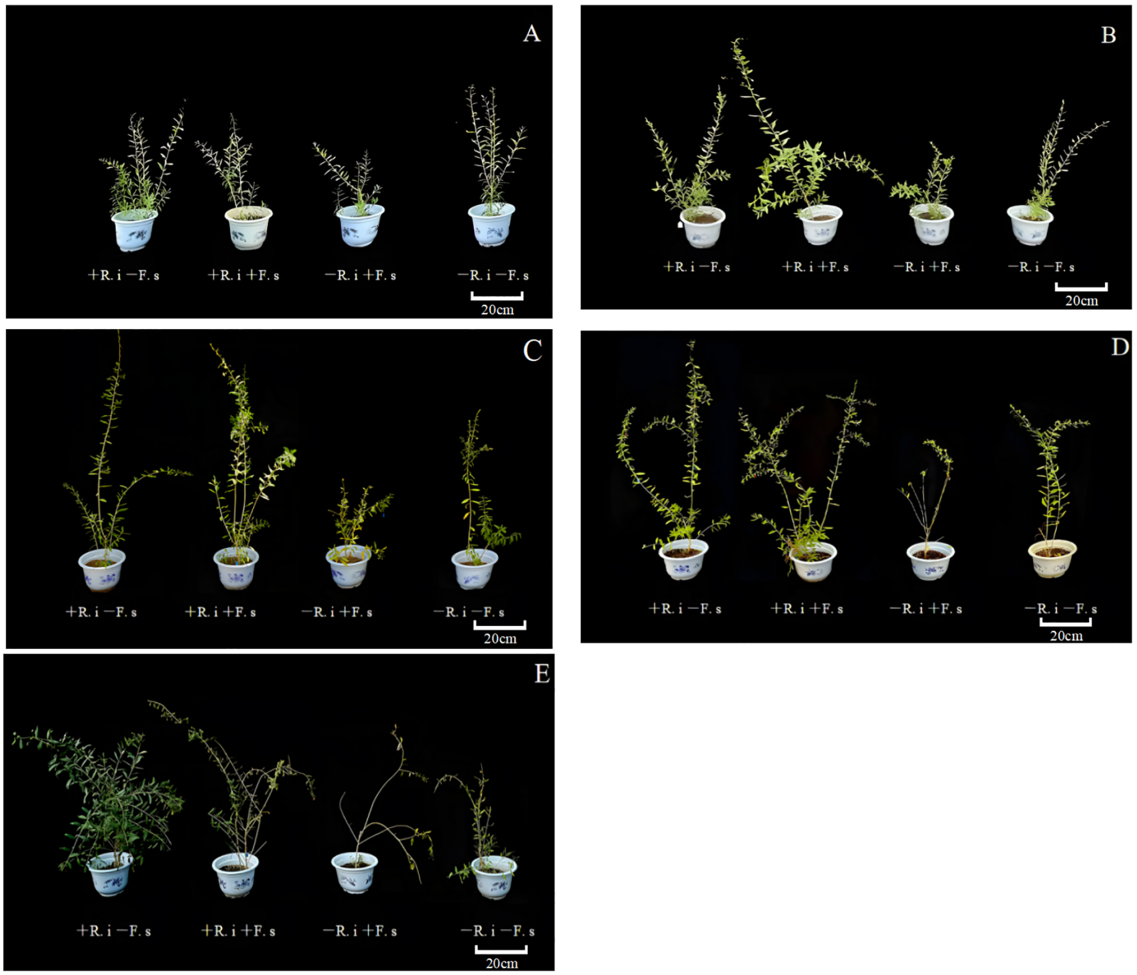

FIGURE 2
Growth status of *L. barbarum* in different periods. **(A)** 15 d (leaf expansion period); **(B)** 30 d (flowering period); **(C)** 60 d (first fruit stage); **(D)** 90 d (full fruit stage); **(E)** 120 d (final fruit stage).

3.5 Effects of *R. intraradices* on pathogenesis-related proteins of *L. barbarum* leaves under different inoculation treatments

In general, chitinase showed a decreasing trend. Under disease stress, compared with non-inoculated treatment, the chitinase activity of mycorrhizal *L. barbarum* increased significantly by 13.0% and 36.0% in the first two periods, and there was no significant difference in the middle and late periods. However, the mycorrhizal *L. barbarum* plants were treated at a high enzyme activity level in five periods, which was higher than that of the mycorrhizal plants treated with pathogenic fungi by 26.74%, 2.31%, 10.39%, 13.67% and 8.73%, respectively (Figure 6A).

At the same time, the β-1,3-glucanase activity of the *F. solani* treatment showed a gradual downward trend. After inoculation with *R. intraradices*, the β-1,3-glucanase activity showed a trend of increasing first and then decreasing with or without inoculation with *F. solani*. The enzyme activity of the five periods was higher than that of the treatment inoculated with *F. solani* (Figure 6B). The activity of pectin methylgalacturonic acid enzyme in different treatments showed a gradual downward trend. The enzyme activity of mycorrhizal diseased plants in the early stage was higher than that of the other three treatments, while the enzyme activity of mycorrhizal plants without *F. solani* inoculation increased in the later stage (Figure 6D). *R. intraradices* inoculation significantly increased the activity of polygalacturonase, *R. intraradices* inoculation significantly increased the activity of polygalacturonase, and the enzyme activity of *R. intraradices* and pathogen inoculation treatment was higher than that of pathogen inoculation treatment (Figure 6C) in five periods.

4 Discussion

In this study, pot experiments were conducted to investigate the effects of *R. intraradices* on the growth, related physiological changes and root rot resistance of *L. barbarum*. The results showed that the colonization rate of mycorrhizal plants increased gradually with the change of treatment time, but the presence of *F. solani* showed a negative effect on the colonization of *R. intraradices*. The reason may be that there was a direct

10.3389/fpls.2024.1459651

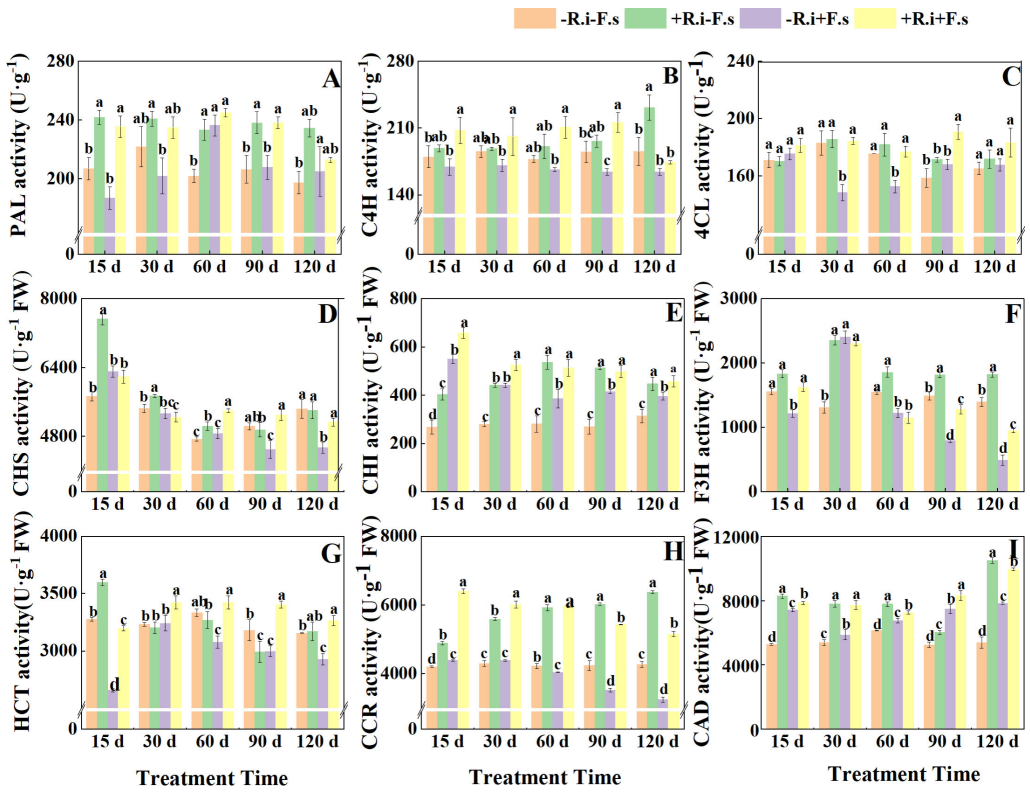

FIGURE 3
Effects of *R. intraradices* on the activities of PAL **(A)**, C4H **(B)**, 4CL **(C)**, CHS **(D)**, CHI **(E)**, F3H **(F)**, HCT **(G)**, CCR **(H)**, CAD **(I)** in *L. barbarum* leaves under different inoculation treatments. Different lowercase letters indicated significant differences between the control and treatments ($p < 0.05$).

interaction between the two, or the infection of *F. solani* caused poor growth of *L. barbarum* plants and reduced the nutrient supply to *R. intraradices*, which slowed down the growth of *R. intraradices*, thus resulting in a decrease in mycorrhizal infection rate. In addition, the biomass and chlorophyll content of mycorrhizal *L. barbarum* increased at different degrees, indicating that *R. intraradices* promoted the growth of plants by facilitating the uptake of water and nutrients from the soil, which was consistent with the results with other reports showing that *R. intraradices* increasing the absorption of nutrients by host plants through mycelium, thereby promoting the growth of *Ambrosia artemisiifolia* and colonization in the roots of *Cinnamomum migao* seedlings and promoting their growth and thereby reducing the incidence and disease index of root rot, and indirectly enhance the resistance of *L. barbarum* to root rot (Liao et al., 2021; Kong et al. 2021).

Phenylalanine is one of the final products of the shikimic acid pathway. Phenylpropanoid metabolism produces more than 8000 aromatic compounds. The reaction of the PPP is catalyzed by PAL, C4H, and 4CL. The three-step catalytic reaction is considered to be the core reaction of the entire metabolic pathway and directly determines whether the PPP can proceed smoothly

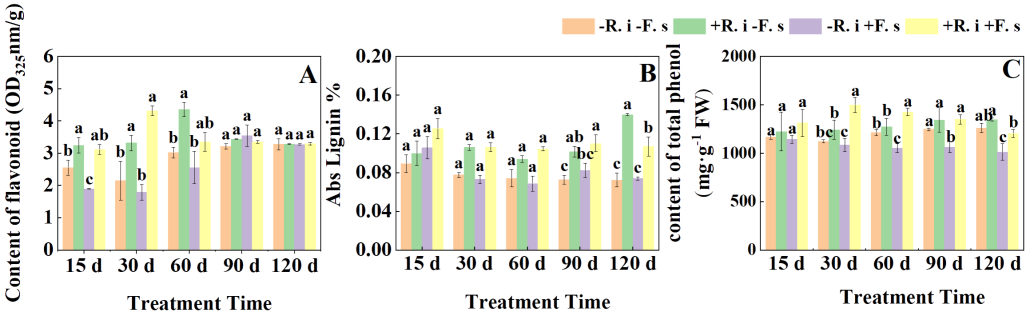

FIGURE 4
Effects of *R. intraradices* on the content of flavonoid **(A)**, Abs Lignin **(B)**, total phenol **(C)** in *L. barbarum* leaves under different inoculation treatments. Different lowercase letters indicated significant differences between the control and treatments ($p < 0.05$).

10.3389/fpls.2024.1459651

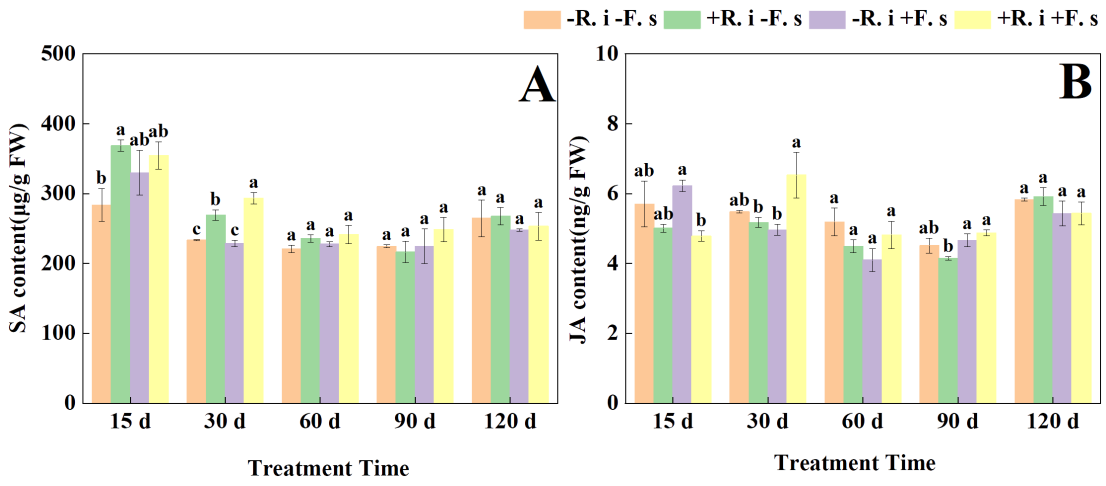

FIGURE 5
Effects of *R. intraradices* on the content of SA **(A)**, JA **(B)** in *L. barbarum* leaves under different inoculation treatments. Different lowercase letters indicated significant differences between the control and treatments ($p < 0.05$).

(Fraser et al., 2011). There are many downstream branches of the PPP, among which the lignin and flavonoid metabolic pathways are the two main branches studied in this paper. PAL is a key enzyme and rate-limiting enzyme in phenylpropanoid metabolism, which plays an important role in plant growth and development, disease resistance and stress resistance (Zhang et al., 2023b). C4H catalyzed the hydroxylation of cinnamic acid to p-coumaric acid. Then p-coumarate coenzyme A was formed under the catalysis of 4-coumarate-CoA ligase. These compounds were transformed into various phenylpropanoids as substrates for the next reaction. Our study found that the PAL, 4CL and C4H of mycorrhizal diseased plants were significantly higher than those of non-mycorrhizal diseased plants, indicating that *R. intraradices* inoculation could activate the PAL, 4CL and C4H activities in *L. barbarum* root rot plants, thus accelerating the process of PPP. This was consistent with the results of AMF inoculation increased PAL activity in pepper leaves and mechanically damaged tomato leaves (Song et al., 2018; Oliveira et al., 2022).

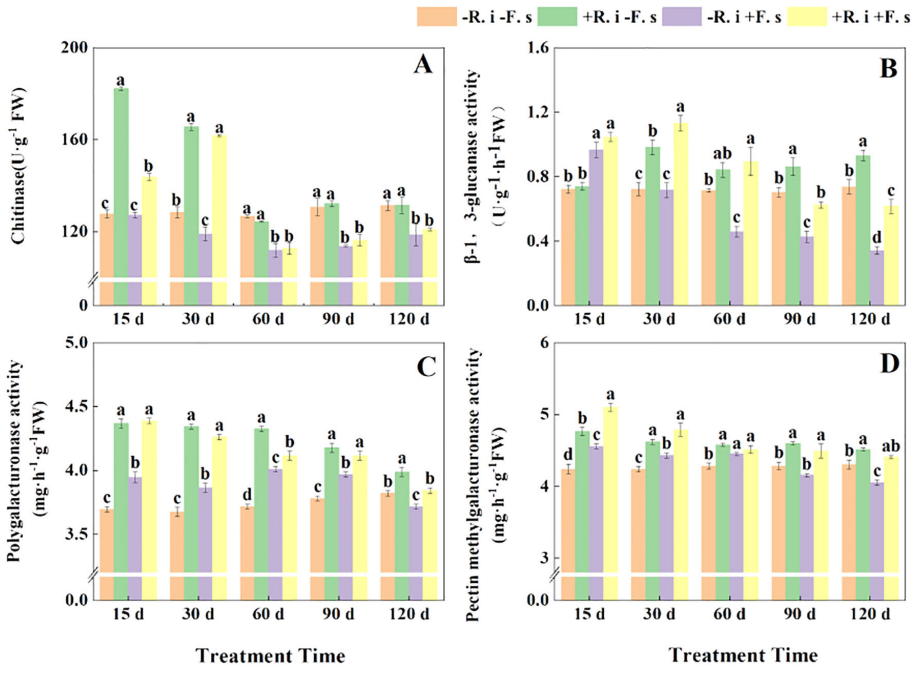

FIGURE 6
Effects of *R. intraradices* on the activities of chitinase **(A)**, β-1,3-glucanase **(B)**, polygalacturonase **(C)**, pectin methylgalacturonic **(D)** in *L. barbarum* leaves under different inoculation treatments. Different lowercase letters indicated significant differences between the control and treatments ($p < 0.05$).

Other catalytic enzymes in the PPP of plants, such as HCT, are considered to be a key factor in controlling the direction of downstream metabolism of monophenolic compounds, and CHI and CHS serve as key enzymes in the downstream branching flavonoid metabolic pathway. Our study found that the activities of HCT, CHI and CHS in *L. barbarum* plants inoculated with *R. intraradices* were significantly higher than those of non-inoculated plants. Studies have found that C4H, CHI, 4CL, and PAL activities and *PtPAL1* and *Pt4CL* expressions were induced by *Funneliformis mosseae* under water stress (Liu et al., 2022), which was similar to the results of this study. At the same time, the plant PPP generally participates in disease resistance immunity through two aspects. On the one hand, synthesizing lignin promotes the degree of cell lignification and forms a physical barrier to prevent the invasion of pathogenic fungi. On the other hand, it produces a variety of metabolites such as phenols and flavonoids to inhibit the growth of pathogenic fungi (Shang et al., 2022).

The products after the above reaction are used as precursors to produce total phenols, flavonoids and lignin under the catalysis of enzymes. Our study found that *R. intraradices* inoculation increased the content of lignin, total phenols and flavonoids in *L. barbarum* within a certain treatment time range, and enhanced its disease resistance. However, the lignin content in the leaves was not significantly different in the early stage. It was speculated that it may be related to the infection of *F. solani* and the fact that the disease site of the plant is in the root, which has little effect on the above-ground part. In the later stage, the accumulation of lignin inhibited the reproduction of *F. solani*. The increase in flavonoid content is of great significance to improve the disease resistance of *L. barbarum*. Phenolic substances can further oxidize polyphenols into quinones that are highly toxic to pathogens and have a certain inhibitory effect on pathogen production (Hua et al., 2017). This was consistent with the results of *Pichia guilliermondii* promoting the accumulation of total phenols, total flavonoids and main monomeric phenolic compounds by increasing the enzyme activity and gene expression level of phenylalanine ammonia-lyase and 4-coumaric acid-CoA ligase, and inducing the resistance of peach fruit soft rot caused by *Rhizopus stolonifer* (Li et al., 2023).

Phytohormones play an important role in plant immunity and defense mechanisms. SA, as a phenolic plant hormone, initiates the expression of disease-related genes and participates in the synthesis of defensive compounds involving local resistance and systemic acquired resistance. It can regulate a variety of plant growth and development phenotypes, including seed germination, fruit ripening, senescence, and defense responses to biotic and abiotic stresses (Wani et al., 2017). This study showed that the SA level of *L. barbarum* plants increased. When infected by *F. solani*, the SA level of mycorrhizal *L. barbarum* plants was significantly higher than that of non-mycorrhizal plants, indicating that the content of endogenous hormones was significantly affected after *F. solani* infected plants. However, the presence of *R. intraradices* can increase the content of plant hormones, and is more effective in controlling soil-borne pathogens. The trend of JA content in the later stage was slightly different from that of SA, probably because as an important signal molecule in plant defense response, SA and JA-mediated pathways were relatively independent and antagonistic at some sites. However, SA and JA are not opposite, and there are still intersections in the process of regulating plant disease resistance. Ambarwati et al. (2022) found that mycorrhiza enhanced the resistance of tropical pepper to *Ralstonia solanacearum* by increasing the relative gene expression levels of JA and SA. Fujita et al. (2024) showed that mycorrhizal colonization activated the tomato immune system, resulting in higher expression levels of SA and JA-related defense genes, which were similar to our study.

In the plant-activated defense system, in addition to activating the defense enzyme protection system, it also includes the induction of pathogenesis-related proteins. Chitinase is a pathogenesis-related protein, and its hydrolysate chitin oligosaccharides can be used as an elicitor to induce defense responses in plants, thereby inhibiting the growth of pathogens (Chen et al., 2022). Pathogenic fungal infection can induce the rapid accumulation of β-1,3-glucanase in plants, which is one of the main defense responses of plants. When plants are invaded by pathogens, the secreted chitinase and β-1,3-glucanase can decompose chitin and β-1,3-glucan exposed to the tips of fungal hyphae, thus directly participating in the process of plant disease resistance (Li et al., 2004). The production of polygalacturonase and pectin methylgalacturonase can not only form complexes with pectin, an important component of the cell wall but also specifically recognize cell wall degrading enzymes of pathogens, thereby eliminating pathogens and reducing the damage of pathogens to plants (Davidsson et al., 2017). In this study, when the pathogen invaded the plant, the activities of chitinase and β-1,3-glucanase in mycorrhizal *L. barbarum* were significantly higher than those in diseased plants, which was consistent with the results of Pu et al. (2022) and Wang et al. (2021). At the same time, the activities of pectin methylgalacturonase and polygalacturonase were also significantly different. Zhang and Tang (2021) showed that inoculation with AMF could increase the activity of polygalacturonase in *P. cathayana* to inhibit the growth of mycelia, reduce the damage of pathogens to *P. cathayana*, and improve the disease resistance of *P. cathayana*, which was similar to this study.

The mechanisms by which AMF improve plant disease resistance include competing with pathogens for nutrients, regulating host endogenous hormones, and activating host defense systems (increasing host defense enzyme activity, inducing the synthesis of pathogenesis-related proteins and secondary metabolites). In this paper, through the determination of the above indicators, it is helpful to better understand the growth-promoting effect and disease resistance mechanism of *R. intraradices* as a biocontrol microorganism on *L. barbarum* plants and to evaluate the role and value of *R. intraradices* to a certain extent. ln summary, mycorrhizal colonization can enhance the ability of *L. barbarum* to resist root rot by inducing the activation of the phenylpropane metabolic pathway and increasing the content of pathogenesis-related proteins and plant signaling substances. It is suggested that *R. intraradices* plays a beneficial role in sustainable agriculture by symbiotically associating with *L. barbarum*. However, the internal molecular mechanism of how *R. intraradices* induces and activates the PPP in *L. barbarum* plants is still unclear. The differential gene expression of *L. barbarum* plants treated with *R. intraradices* can be further studied by

transcriptomics technology, to analyze the roles of key differential genes and key pathways, find the relationship between key differential genes, and verify the mechanism of *R. intraradices* treatment to improve the resistance of *L. barbarum* plants to root rot at the molecular level.

5 Conclusion

R. intraradices could establish a stable symbiotic relationship with the roots of *L. barbarum*, promote the accumulation of biomass, increase the chlorophyll content, reduce the incidence and disease index of root rot, and enhance the activity of phenylpropanoid metabolism-related enzymes, the content of pathogenesis-related proteins and the content of plant signal substances in the leaves of *L. barbarum*. The results showed that *R. intraradices* inoculation treatment increased the activity of phenylpropanoid metabolism-related enzymes and the content of resistant substances in *L. barbarum* plants, thereby enhancing the resistance of *L. barbarum* plants to root rot.

Data availability statement

The original contributions presented in the study are included in the article/supplementary material. Further inquiries can be directed to the corresponding author.

Author contributions

NL: Writing – original draft, Investigation, Data curation. WC: Writing – review & editing, Supervision. BW: Writing – review & editing, Supervision. CZ: Writing – review & editing, Data curation. YW: Writing – review & editing, Methodology. RL: Writing – review & editing, Methodology. YY: Writing – review & editing, Investigation. JH: Visualization, Supervision, Writing – review & editing, Funding acquisition.

Funding

The author(s) declare financial support was received for the research, authorship, and/or publication of this article. Natural Science Foundation of Gansu Province, Award Number: 20JR10RA508.

Acknowledgments

The author would like to thank the facilities, support and encouragement provided by the Engineering Research Center of Harmless Cultivation of *L. barbarum* in Gansu Province.

Conflict of interest

The authors declare that the research was conducted in the absence of any commercial or financial relationships that could be construed as a potential conflict of interest.

Publisher's note

All claims expressed in this article are solely those of the authors and do not necessarily represent those of their affiliated organizations, or those of the publisher, the editors and the reviewers. Any product that may be evaluated in this article, or claim that may be made by its manufacturer, is not guaranteed or endorsed by the publisher.

References

Ackah, S., Xue, S. L., Osei, R., Kweku-Amagloh, F., Zong, Y. Y., Prusky, D., et al. (2022). Chitosan treatment promotes wound healing of apple by eliciting phenylpropanoid pathway and enzymatic browning of wounds. *Front. Microbiol.* 13. doi: 10.3389/fmicb.2022.828914

Ambarwati, E., Arwiyanto., T., Widada, J., Alam, T., Andika, L. P., and Taryono, (2022). The genes associated with jasmonic acid and salicylic acid are induced in tropical chili pepper against Ralstonia solanacearum by applying arbuscular mycorrhizal fungi. *Horticulturae* 8, 876. doi: 10.3390/horticulturae8100876

Aseel, D. G., Rashad, Y. M., and Hammad, S. M. (2019). Arbuscular mycorrhizal fungi trigger transcriptional expression of flavonoid and chlorogenic acid biosynthetic pathways genes in tomato against tomato mosaic virus. *Sci. Rep.* 09, 9692. doi: 10.1038/s41598-019-46281-x

Bonawitz, N. D., Kim, J. I., Tobimatsu, Y., Ciesielski, P. N., Anderson, N. A., Ximenes, E., et al. (2014). Disruption of mediator rescues the stunted growth of a lignin-deficient *Arabidopsis* mutant. *Nature* 509, 376–380. doi: 10.1038/nature13084

Cao, J. K., Jiang, W. B., and Zhao, Y. M. (2007). *Guidance of postharvest physiological and biochemical experiments of fruits and vegetables* (Beijing: China Light Industry Press).

Chen, Y. L., Cen, G. L., Sun, T. T., You, C. H., Que, Y. X., and Su, Y. C. (2022). Progress on plant Chitinase and β-1, 3-glucanase and their synergistic function in disease resistance. *J. Agric. Biotechnol.* 30, 1394–1411. doi: 10.3969/j.issn.1674-7968.2022.07.016

Davidsson, P., Brogerg, M., Kariola, T., Sipari, N., Pirhonen, M., and Palva, E. T. (2017). Short oligogalacturonides induce pathogen resistance-associated gene expression in *Arabidopsis thaliana*. *BMC Plant Biol.* 17, 19. doi: 10.1186/s12870-016-0959-1

Despina, B., Cotton, T. E. A., Daniell, T. J., Bidartondo, M. I., Cameron, D. D., and Evans, K. L. (2018). The effects of arbuscular mycorrhizal fungal colonisation on nutrient status, growth, productivity, and canker resistance of apple (*Malus pumila*). *Front. Microbiol.* 9. doi: 10.3389/fmicb.2018.01461

Devi, N. O., Tombisana Devi, R. K., Debbarma, M., Hajong, M., and Thokchom, S. (2022). Effect of endophytic *Bacillus* and arbuscular mycorrhiza fungi (AMF) against *Fusarium* wilt of tomato caused by *Fusarium oxysporum* f. sp. *lycopersici*. *Egypt J. Biol. Pest Co.* 32, 1. doi: 10.1186/s41938-021-00499-y

Dong, N. Q., and Lin, H. X. (2021). Contribution of phenylpropanoid metabolism to plant development and plant-environment interactions. *J. Integr. Plant Biol.* 63, 180–209. doi: 10.1111/jipb.13054

Eke, P., Adamou, S., Fokom, R., Nya, V. D., Fokou, P. V. T., Wakam, L. N., et al. (2020). Arbuscular mycorrhizal fungi alter antifungal potential of lemongrass essential oil against *Fusarium solani*, causing root rot in common bean (*Phaseolus vulgaris L.*). *Heliyon* 6, e05737. doi: 10.1016/j.heliyon.2020.e05737

Fraser, C. M., and Chapple, C. (2011). The phenylpropanoid pathway in *Arabidopsis*. *Arabidopsis Book.* 9, e0152. doi: 10.1199/tab.0152

Fujita, M., Kusajima, M., Fukagawa, M., Okumura, Y., Nakajima, M., Akiyama, K., et al. (2024). Response of tomatoes primed by mycorrhizal colonization to virulent and avirulent bacterial pathogens. *Sci. Rep.* 12–4686. doi: 10.1038/s41598-022-08395-7

Gao, H. H., Jia, C. B., Han, Q., Su, J. Y., and Xu, C. Y. (2022). Microbiological mechanism of root rot of *Lycium barbarum* Ningqi-7. *Biotechnol. Bullet.* 38, 244–251. doi: 10.13560/j.cnki.biotech.bull.1985.2022-0363

Gao, Y., Wei, Y., Wang, Y., Gao, F., and Chen, Z. (2017). *Lycium barbarum*, a traditional Chinese herb and promising anti-aging agent. *Aging Dis.* 8, 778–791. doi: 10.14336/AD.2017.0725

Ge, Y. H., Wei, M. L., Li, C. Y., Chen, Y. R., Lv, J. Y., Meng, K., et al. (2018). Reactive oxygen species metabolism and phenylpropanoid pathway involved in disease resistance against *Penicillium expansum* in apple fruit induced by ε-poly-l-lysine. *J. Sci. Food Agric.* 13, 5082–5088. doi: 10.1002/jsfa.9046

George, N. P., and Ray, J. ,. G. (2023). The inevitability of arbuscular mycorrhiza for sustainability in organic agriculture-A critical review. *Front. Sustain. Food Syst.* 7, 1124688. doi: 10.3389/fsufs.2023.1124688

Gong, H., Rehman, F., Ma, Y., Biao, A., Zeng, S. H., Yang, T. S., et al. (2022). Germplasm resources and strategy for genetic breeding of *Lycium* species: A review. *Front. Plant Sci.* 13. doi: 10.3389/fpls.2022.802936

Gu, L. J., Xu, B. L., Liang, Q. L., and Xue, Y. Y. (2009). Occurrence of *Pythium* root rot in turf grass and identification of the pathogen. *Acta Pratacult. Sinica.* 18, 175–180. doi: 10.11686/cyxb20090425

He, J., Zhang, X. Y., Wang, Q. H., Li, N., Ding, D. D., and Wang, B. (2023). Optimization of the fermentation conditions of *Metarhizium robertsii* and its biological control of wolfberry root rot disease. *Microorganisms* 11, 2380. doi: 10.3390/microorganisms11102380

Hua, X. Y., Tao, S., Sun, S. N., Guo, N., Yan, X. F., and Lin, J. X. (2017). Research progress on phenolic compounds of plant secondary metabolites. *Biotechnol. Bull.* 33, 22–29. doi: 10.13560/j.cnki.biotech.bull.1985.2017-0546

Khaliq, A., Perveen, S., Alamer, K. H., Haq, M. Z. U., Rafique, Z., M. Alsudays, I., et al. (2022). Arbuscular mycorrhizal fungi symbiosis to enhance plant-soil interaction. *Sustainability* 14, 7840. doi: 10.3390/su14137840

Khumalo, K. N., Tinyane, P., Soundy, P., Romanazzi, G., Glowacz, M., and Sivakumar, D. (2017). Effect of thyme oil vapour exposure on the brown rot infection, phenylalanine ammonia-lyase (PAL) activity, phenolic content and antioxidant activity in red and yellow skin peach cultivars. *Sci. Hortic.* 214, 195–199. doi: 10.1016/j.scienta.2016.11.044

Kong, L. J., Chen, X., Yerger, E. H., Li, Q., Chen, F. X., Xu, H. Y., et al. (2021). Arbuscular mycorrhizal fungi enhance the growth of the exotic species *Ambrosia artemisiifolia*. *J. Plant Ecol.* 03), 3. doi: 10.1093/jpe/rtab087

Kumar, T., Majumdar, A., Das, P., Sarafis, V., and Ghose, M. (2008). Trypan blue as a fluorochrome for confocal laser scanning microscopy of arbuscular mycorrhizae in three mangroves. *Biotech. Histochem.* 83, 153–159. doi: 10.1080/10520290802336161

Latunde-Dada, A. O., Dixon, R. A., and Lucas, J. A. (1987). Induction of phytoalexin biosynthetic enzymes in resistant and susceptible lucerne callus lines infected with *Verticillium albo-atrum*. *Physiol. Mol. Plant Pathol.* 31, 15–23. doi: 10.1016/0885-5765(87)90003-8

Li, B. L., Ding, D. D., He, J., Li, Y. X., Zhao, J. T., Hou, C. X., et al. (2022). Effects of arbuscular mycorrhizal on the growth of *Lycium barbarum* and its resistance to root rot. *J. Yunnan Agric. Univ. (Nat. Sci).* 37, 547–552. doi: 10.12101/j.issn.1004-390X(n).202111047

Li, Y. F., Ji, N. N., Zuo, X. X., Hou, Y. Y., Zhang, J. L., Zou, Y. Y., et al. (2023). PpMYB308 is involved in *Pichia guilliermondii*-induced disease resistance against *Rhizopus* rot by activating the phenylpropanoid pathway in peach fruit. *Postharvest Biol. Technol.* 195, 112115. doi: 10.1016/j.postharvbio.2022.112115

Li, C. J., Shan, S. H., Xu, T. T., and Guan, Q. X. (2004). Research development of chitinase and -1,3-glucanase genes. *Lett. Biotechnol.* 15, 4. doi: 10.3969/j.issn.1009-0002.2004.05.023

Li, A., Wu, C. X., Zheng, X., Nie, R. N., Tang, J. L., Ji, X. Y., et al. (2024). Physiological and biochemical responses of arbuscular mycorrhizal fungi in symbiosis with *Juglans nigra* L. seedlings to alleviate salt stress. *Rhizosphere* 31, 100928. doi: 10.1016/j.rhisph.2024.100928

Li, S. X., Yang, W. Y., Guo, J. H., Li, X. N., Lin, J. X., and Zhu, X. C. (2020). Changes in photosynthesis and respiratory metabolism of maize seedlings growing under low temperature stress may be regulated by arbuscular mycorrhizal fungi. *Plant Physiol. Biochem.* 154, 1–10. doi: 10.1016/j.plaphy.2020.05.025

Liao, X., Chen, J., Guan, R., Liu, J. M., and Sun, Q. W. (2021). Two arbuscular mycorrhizal fungi alleviates drought stress and improves plant growth in *Cinnamomum migao* seedlings. *Mycobiology* 49, 396–405. doi: 10.1080/12298093.2021.1938803

Liu, X. Q., Cheng, S., Aroca, R., Zou, Y. N., and Wu, Q. S. (2022). Arbuscular mycorrhizal fungi induce flavonoid synthesis for mitigating oxidative damage of trifoliate orange under water stress. *Environ. Exp. Bot.* 204, 105089. doi: 10.1016/j.envexpbot.2022.105089

Oliveira, J. S. D., Ramos, N. P., Júnior, J. L., Xavier, L. P., Andrade, E. H., Mello, A. H., et al. (2022). Secondary metabolism and plant growth of *Piper divaricatum* (Piperaceae) inoculated with arbuscular mycorrhizal fungi and phosphorus supplementation. *Agronomy* 12, 596. doi: 10.3390/agronomy12030596

Pu, C. Y., Ge, Y., Yang, G., Zheng, H., Guan, W., Chao, Z., et al. (2022). Arbuscular mycorrhizal fungi enhance disease resistance of *Salvia miltiorrhiza* to *Fusarium* wilt. *Front. Plant Sci.* 13. doi: 10.3389/fpls.2022.975558

Qu, G. F., Wu, W. N., Ba, L. J., Ma, C., Ji, N., and Cao, S. (2022a). Melatonin enhances the postharvest disease resistance of blueberries fruit by modulating the jasmonic acid signaling pathway and phenylpropanoid metabolites. *Front. Chem.* 10. doi: 10.3389/fchem.2022.957581

Qu, S. L., Wu, Y. F., Liu, Z. K., Wang, G. L., Chen, Y. J., and Rong, Y. P. (2022b). Research progress for effects of arbuscular mycorrhizal fungi on growth and development of alfalfa. *Acta Agrestia Sinica.* 30, 2529–2534. doi: 10.11733/j.issn.1007-0435.2022.10.001

Ronen, R., and Galun, M. (1984). Pigment extraction from lichens with dimethyl sulfoxide (DMSO) and estimation of chlorophyll degradation. *Environ. Exp. Bot.* 3, 239–245. doi: 10.1016/0098-8472(84)90004-2

Shang, J., Wu, W. Z., and Ma, Y. G. (2022). Phenylpropanoid metabolism pathway in plants. *CJBMB* 38, 1467–1476. doi: 10.13865/j.cnki.cjbmb.2022.03.1604

Song, Y. Y., Xia, M., Lin, Y. B., Lin, X. H., Ding, C. H., Wang, J., et al. (2018). Colonization with arbuscular mycorrhizal fungus *Funneliformis mosseae* enhanced the responses of tomato plants to mechanical wounding. *J. Appl. Ecol.* 29, 3811–3818. doi: 10.13287/j.1001-9332.201811.035

Vlot, A. C., Dempsey, D. A., and Klessig, D. F. (2009). Salicylic acid, a multifaceted hormone to combat disease. *Annu. Rev. Phytopathol.* 47, 177–206. doi: 10.1146/annurev.phyto.050908.135202

Wang, G. Q., Du, X. Q., Ma, C., Zhu, T. T., Zhen, R., and Yue, S. J. (2023a). Identification of the pathogen causing root rot of *Lycium barbarum* and screening of antagonists. *Agric. Res. Arid. Areas.* 06), 251–259. doi: 10.7606/j.issn.1000-7601.2023.06.26

Wang, Y. J., Li, Y., and Duan, T. (2023b). Arbuscular mycorrhizal fungus changes alfalfa response to pathogen infection activated by pea aphid infestation. *Front. Microbiol.* 13. doi: 10.3389/fmicb.2022.1074592

Wang, M., Tang, W., Xiang, L., Chen, X. S., Shen, X., Yin, C. M., et al. (2022). Involvement of MdWRKY40 in the defense of mycorrhizal apple against *Fusarium solani*. *BMC Plant Biol.* 22, 385. doi: 10.1186/s12870-022-03753-z

Wang, Q., Zeng, S. H., Wu, X. Y., LeI, H. H., Wang, Y., and Tang, H. R. (2018). Interspecies developmental differences in metabonomic phenotypes of *Lycium ruthenicum* and L. barbarum fruits. *J. Proteome Res.* 9, 3223–3236. doi: 10.1021/acs.jproteome.8b00349

Wang, M., Zhang, R., Zhao, L., Wang, H. Y., Chen, X. S., Mao, Z. Q., et al. (2021). Indigenous arbuscular mycorrhizal fungi enhance resistance of apple rootstock 'M9T337' to apple replant disease. *Physiol. Mol. Plant Pathol.* 116, 101717. doi: 10.1016/j.pmpp.2021.101717

Wani, A. B., Chadar, H., Wani, A. H., Singh, S., and Upadhyay, N. (2017). Salicylic acid to decrease plant stress. Environ. *Chem. Lett.* 15, 101–123. doi: 10.1007/s10311-016-0584-0

Wei, Y. Y., Zhou, D. D., Peng, J., Pan, L. Q., and Tu, K. (2017). Hot air treatment induces disease resistance through activating the phenylpropanoid metabolism in cherry tomato fruit. *J. Agr. Food Chem.* 65, 8003–8010. doi: 10.1021/acs.jafc.7b02599

Xu, Y., Tu, Y., Feng, J., Peng, Z., Peng, Y., and Huang, J. (2024). Arbuscular mycorrhizal fungi mediate the acclimation of rice to submergence. *Plants* 13, 1908. doi: 10.3390/plants13141908

Yu, J., Yan, Y., Zhang, L., Mi, J., Yu, L. M., Zhang, F. F., et al. (2023). A comprehensive review of goji berry processing and utilization. *Food Sci. Nutr.* 11, 7445–7457. doi: 10.1002/fsn3.3677

Zhang, C. Q., Ding, D. D., Wang, B., Wang, Y. P., Li, N., Li, R. Y., et al. (2023a). Effect of potato glycoside alkaloids on energy metabolism of *Fusarium solani*. *J. Fungi.* 9, 777. doi: 10.3390/jof9070777

Zhang, Y., and Tang, M. (2021). Effects of arbuscular mycorrhizal fungi on biomass and disease-resistance enzyme activities of *Cathay poplar* against canker. *Mycosystema* 40, 1110–1122. doi: 10.13346/j.mycosystema.200308

Zhang, D., Xia, T., Dang, S., Fan, G., and Wang, Z. (2018). Investigation of Chinese wolfberry (*Lycium* spp.) germplasm by restriction site-associated DNA sequencing (RAD-seq). *Biochem. Genet.* 56, 575–585. doi: 10.1007/s10528-018-9861-x

Zhang, D. D., Yun, X. F., Bao, Y. Y., Qian, C., and Gao, X. M. (2013). Effect of extracts celery fresh root and rhizosphere area on the Chitinase and bata1.3-glucan engymes activity of cucumber leaf. *J. Inn. Mong. Agric. Univ. (Nat. Sci. Ed.).* 34, 21–27. doi: 10.1186/s12870-023-04472-9

Zhang, H. Y., Zhang, X. H., Zhao, H. X., Hu, J., Wang, Z. Y., Yang, G. S., et al. (2023b). Genome-wide identification and expression analysis of *phenylalanine ammonia-lyase* (PAL) family in rapeseed (*Brassica napus* L.). *BMC Plant Biol.* 23, 481. doi: 10.1186/s12870-023-04472-9

Zhu, J., Cheng, L., Yao, Q., Li, Q. R., Chen, H. Y., and Guo, Q. Y. (2023). Isolation and identification of pathogenic fungi and antagonistic bacteria from *Lycium barbarum* root rot. *Acta Agricult. Boreali-occidentalis Sinica.* 32, 1120–1130. doi: 10.7606/j.issn.1004-1389.2023.07.016

Zou, Y. N., Wu, Q. S., and Kuca, K. (2021). Unravelling the role of arbuscular mycorrhizal fungi in mitigating the oxidative burst of plants under drought stress. *Plant Biol.* 23, 50–57. doi: 10.1111/plb.13161

frontiers | Frontiers in Plant Science

TYPE Original Research
PUBLISHED 18 September 2024
DOI 10.3389/fpls.2024.1444271

Check for updates

OPEN ACCESS

EDITED BY
Yasser Nehela,
University of Florida, United States

REVIEWED BY
Ruchi Agarrwal,
National Research Center on Pomegranate (ICAR), India
Tariq Mukhtar,
Pir Mehr Ali Shah Arid Agriculture University, Pakistan
Neeraj Pal,
Meril Life Sciences Pvt. Ltd., India

*CORRESPONDENCE
Kim E. Hammond-Kosack
kim.hammond-kosack@rothamsted.ac.uk

†PRESENT ADDRESSES
Tania Chancellor,
Crop Science Centre, Department of Plant Sciences, University of Cambridge, Cambridge, United Kingdom
Daniel P. Smith,
John Innes Centre, Department of Computational and Systems Biology, Norwich John Innes Centre, Norwich, United Kingdom
Eudri Venter,
JEOL (UK) Ltd., Welwyn Garden City, Hertfordshire, United Kingdom
Vanessa McMillan,
National Institute of Agricultural Botany (NIAB), Cambridge, United Kingdom
Javier Palma-Guerrero,
Department of Crop Sciences, Research Institute of Organic Agriculture (FIBL), Frick, Switzerland

RECEIVED 05 June 2024
ACCEPTED 06 August 2024
PUBLISHED 18 September 2024

CITATION
Chancellor T, Smith DP, Chen W, Clark SJ, Venter E, Halsey K, Carrera E, McMillan V, Canning G, Armer VJ, Hammond-Kosack KE and Palma-Guerrero J (2024) A fungal endophyte induces local cell wall–mediated resistance in wheat roots against take-all disease.
Front. Plant Sci. 15:1444271.
doi: 10.3389/fpls.2024.1444271

A fungal endophyte induces local cell wall–mediated resistance in wheat roots against take-all disease

Tania Chancellor[1†], Daniel P. Smith[1†], Wanxin Chen[1], Suzanne J. Clark[1], Eudri Venter[1†], Kirstie Halsey[1], Esther Carrera[2], Vanessa McMillan[1†], Gail Canning[1], Victoria J. Armer[1], Kim E. Hammond-Kosack[1*] and Javier Palma-Guerrero[1†]

[1]Rothamsted Research, Strategic Areas: Protecting Crops and the Environment, Intelligent Data Ecosystems, Plant Sciences for the Bioeconomy, Harpenden, United Kingdom, [2]Institute for Plant Molecular and Cell Biology, University of Valencia, Valencia, Spain

Take-all disease, caused by the Ascomycete fungus *Gaeumannomyces tritici*, is one of the most important root diseases of wheat worldwide. The fungus invades the roots and destroys the vascular tissue, hindering the uptake of water and nutrients. Closely related non-pathogenic species in the *Magnaporthaceae* family, such as *Gaeumannomyces hyphopodioides*, occur naturally in arable and grassland soils and have previously been reported to reduce take-all disease in field studies. However, the mechanism of take-all protection has remained unknown. Here, we demonstrate that take-all control is achieved via local but not systemic host changes in response to prior *G. hyphopodioides* root colonisation. A time-course wheat RNA sequencing analysis revealed extensive transcriptional reprogramming in *G. hyphopodioides*–colonised tissues, characterised by a striking downregulation of key cell wall–related genes, including genes encoding cellulose synthases (CESA), and xyloglucan endotransglucosylase/hydrolases (XTH). In addition, we characterise the root infection biologies of *G. tritici* and *G. hyphopodioides* in wheat. We investigate the ultrastructure of previously described "subepidermal vesicles" (SEVs), dark swollen fungal cells produced in wheat roots by non-pathogenic *G. hyphopodioides*, but not by pathogenic *G. tritici*. We show that *G. hyphopodioides* SEVs share key characteristics of fungal resting structures, containing a greater number of putative lipid bodies and a significantly thickened cell wall compared to infection hyphae. We hypothesise that SEVs are fungal resting structures formed due to halted hyphal growth in the root cortex, perhaps as a stress response to locally induced wheat defence responses. In the absence of take-all resistant wheat cultivars or non-virulent *G. tritici* strains, studying closely related non-pathogenic *G. hyphopodioides* provides a much needed avenue to elucidate take-all resistance mechanisms in wheat.

KEYWORDS

wheat root transcriptome, root endophyte, root pathogen, wheat defences, cell-wall modifications, fungal biocontrol

1 Introduction

Wheat (*Triticum aestivum*) is one of the most important cereal crops worldwide, providing around 20% of human caloric intake globally. Sustaining excellent root health is critical for the acquisition of water and essential nutrients. As global temperatures continue to rise, root health is predicted to face increasing threats from various soil-borne fungal pathogens (Delgado-Baquerizo et al., 2020). The necrotrophic fungal pathogen *Gaeumannomyces tritici*, belonging to the *Magnaporthaceae* family, is responsible for take-all disease, one of the most important root problems of wheat crops worldwide (Freeman and Ward, 2004; Palma-Guerrero et al., 2021). The disease drastically diminishes grain yields during heavy infection episodes. However, due to the genetic intractability of *G. tritici*, both the pathogen and the cereal-pathosystem remain understudied by the molecular plant–microbe interaction community. Root-confined vascular infection by *G. tritici* results in the development of characteristic necrotic lesions originating from the stele, which severely disrupt root functions, causing premature crop ripening and reduced grain yield/quality (Asher and Shipton, 1981; Huang et al., 2001). Take-all fungal inoculum builds up in the soil following consecutive wheat crops, and, although recent surveys of take-all disease levels are lacking, yield losses of up to 60% have been reported in the UK (McMillan et al., 2011). At present, take-all resistant wheat cultivars are not commercially available, and current fungicide seed treatments do not provide complete protection (Freeman et al., 2005). For a comprehensive review on our current understanding of the *G. tritici*–wheat pathogen system, including detailed spatial and temporal descriptions of the *G. tritici* life cycle and infection process, please see the work of Palma-Guerrero et al. (2021).

Understanding root immunity is essential for the development of take-all resistant cultivars. However, the classical model of immunity, characterised by the concerted effect of pathogen-associated molecular pattern (PAMP)–triggered immune responses and effector-triggered immune responses, is predominantly based on foliar pathogens (Boller and Felix, 2009; Jones and Dangl, 2006; Pok et al., 2022). Roots must constantly interact with a diverse soil microbiome and distinguish pathogenic microbes from, sometimes closely related, non-pathogenic endophytes or beneficial symbionts (Thoms et al., 2021). How plants engage with beneficial microorganisms while restricting damaging pathogens is regarded as one of the top 10 unanswered questions by the molecular plant–microbe interaction (MPMI) research community (Harris et al., 2020). The selective response of plants to microbes with different lifestyles can be partly explained by the compartmentalisation of localised immune responses in roots (Zhou et al., 2020), and the recognition of microbe-associated molecular patterns (MAMPs), damage-associated molecular patterns (DAMPs), and PAMPs by multiple receptors (Thoms et al., 2021). However, further comparative studies into endophytic and pathogenic plant infecting microbes are sorely needed.

Several members of the *Magnaporthaceae* family are classified within the *Gaeumannomyces-Phialophora* complex (Hernández-Restrepo et al., 2016). *Phialophora* species, such as *Gaeumannomyces hyphopodioides*, occur naturally in grasslands and arable field sites although do not cause disease symptoms in arable crops (Deacon, 1973; Ulrich et al., 2000; Ward and Bateman, 1999). For this reason, such species have been described as "non-pathogenic." Wheat root colonisation by non-pathogenic *Magnaporthaceae* species can be easily distinguished from wheat root infection by pathogenic *G. tritici* due to the inability of non-pathogenic species to infect the vascular tissues and due to the production of dark swollen fungal cells by non-pathogenic species in the root cortex. The swollen cells measure between 12 µm and 30 µm in diameter, depending on the fungal species, and may be formed following growth cessation of a hyphal apex (Deacon, 1976a). These enigmatic structures have been previously described as pigmented cells (Holden, 1976), growth cessation structures (Deacon, 1976a), or subepidermal vesicles (SEVs) (Osborne et al., 2018). The closely related rice leaf blast pathogen *Magnaporthe oryzae* is also reported to form SEV-like structures in cereal roots. *M. oryzae* can infect rice root tissues, producing brown spherical structures resembling SEVs in epidermal and cortical cells (Dufresne and Osbourn, 2001; Marcel et al., 2010). SEV-like structures are also common among dark septate endophytes (DSEs), a diverse group of root colonising ascomycete fungi with elusive functions, often found inhabiting stressful environments. The DSEs are morphologically characterised by the production of highly melanised septate hyphae which grow intraradically, producing structures referred to as "microsclerotia," but which bear striking similarities to the SEVs of the *Magnaporthaceae* species (Ban et al., 2012; Knapp et al., 2018). The function of these "microsclerotia" in the fungal life cycle of the DSE remains unknown, and their ultrastructure has yet to be investigated. Thus, SEVs appear to be specific to root colonising/infecting fungi, although little is known about SEV formation, SEV ultrastructure, or the involvement of SEVs in root infection processes.

Prior colonisation by certain non-pathogenic *Magnaporthaceae* species is reported to provide protection against take-all disease in field studies (Wong et al., 1996). Furthermore, Osborne et al. (2018) demonstrated that certain elite winter wheat varieties have an improved ability to promote *G. hyphopodioides* populations in field soils, suggesting that careful cultivar choice during wheat rotations could provide a natural level of biocontrol. However, as far as we are aware, disease protection by non-pathogenic *Magnaporthaceae* species has not been reported in any recent publications, and the mechanisms underlying disease control remain unknown.

Root endophytes can provide protection against plant pathogens directly or indirectly. Direct antagonism may be achieved by mycoparasitism, antibiosis, or competition for nutrients, whereas indirect antagonism can be achieved via host-mediated defence responses. Importantly, the exact mechanisms underpinning host-mediated defence can differ between the endophyte species and the host plant in question. The two most well characterised forms of induced resistance, induced systemic resistance (ISR) and systemic acquired resistance (SAR), can be distinguished by the type of elicitors involved and the signalling pathways that are induced (Pieterse et al., 2014). SAR can be triggered by plant detection of both MAMPs and DAMPs and is dependent on salicylic acid (SA) signalling. Conversely, ISR is generally induced via the plant detection of MAMPs and results in the priming of jasmonic acid (JA)/ethylene (ET)–responsive genes, resulting in a faster and stronger defence response against subsequent

pathogen attacks (Choudhary et al., 2007). However, induced resistance mechanisms are not restricted to SAR and ISR. Non-pathogenic strains in the *Fusarium oxysporum* species complex are known to provide protection against Fusarium wilt disease, a major disease caused by pathogenic *F. oxysporum* strains (de Lamo and Takken, 2020). This phenomenon, termed by the authors as endophyte-mediated resistance (EMR), is reportedly independent of JA, ET, and SA signalling, although little else is known about the mechanisms responsible for EMR (Constantin et al., 2019). *Serendipita indica* (= *Pirisformospora indica*), an endophyte with a diverse host range, is known to provide disease resistance against a large number of fungal pathogens via multiple defence pathways (Qiang et al., 2012). In wheat, pre-treatment with *S. indica* provided effective protection against root rot disease caused by *Fusarium graminearum* (Li et al., 2022). Although the mechanism of protection is likely to be complex, transcriptomic analyses suggested that the activation of mitogen-activated protein kinase (MAPK) cascades involved in immunity, and the upregulation of phenylpropanoid biosynthesis genes may play a role in the observed disease resistance (Li et al., 2022). In summary, EMR mechanisms are species-specific and highly complex. Detailed *in vitro*, *in planta*, and transcriptomic analyses are needed to determine the mode(s) of EMR in specific plant species.

In this study, we set out to elucidate the mechanism of take-all disease control by *G. hyphopodioides* in wheat using *in vitro* and *in planta* assays combined with detailed host transcriptome profiling. In addition, we aimed to better characterise the infection/colonisation processes of *G. tritici* and *G. hyphopodioides*. Finally, we aimed to study the ultrastructure of fungal SEVs produced by *G. hyphopodioides*. We provide the first comparative analysis of wheat transcriptional responses to *G. tritici* and *G. hyphopodioides* across key stages of early fungal infection. We characterise the different fungal structures produced and some of the wheat cell-wall changes occurring during root infection. Our findings shed light on the distinct plant responses to these two closely related root infecting fungi with contrasting lifestyles and help to pinpoint localised mechanisms for the control of take-all disease by *G. hyphopodioides*. Together, our findings contribute to an improved understanding of wheat root resistance against take-all disease.

2 Materials and methods

2.1 Fungal isolation and culture

G. hyphopodioides (taxon id: 1940676) and *G. tritici* (taxon id: 36779) strains were isolated from field soils at Rothamsted Farm using the soil baiting method (McMillan et al., 2011; Osborne et al., 2018). Fungal isolates (see Table 1) were maintained on potato dextrose agar (PDA) plates at 21°C in the dark.

2.2 Seedling infection pot assays

For seedling pot experiments, plastic pots (7.5-cm wide × 11-cm tall) were filled with damp horticultural sand, and 10 untreated wheat seeds cv. Hereward were sown on the surface. Hereward was chosen due to its strong susceptibility to take-all disease and its ability to build high levels of take-all inoculum (McMillan et al., 2011). Seeds were covered with a thin layer of grit and pots were placed in a controlled environment growth room for 2 weeks (16-h day, light intensity of 250 µmols, 15°C day, 10°C night). *G. tritici* (isolate 16.NZ.1d) and *G. hyphopodioides* (isolate NZ.129.2C.17) inocula were prepared by placing 10 fungal plugs (7-mm diameter) taken from the leading edge of each colony into a 1-L flask containing 400 mL of potato dextrose broth. Flasks were placed in an orbital incubator for 7 days at 25°C, 120 revolutions per minute (RPM). Liquid cultures were homogenised by passing through a 2.8-mm sterile sieve. Homogenised cultures were diluted with sterile distilled water in a 2:3 ratio. The first inoculum treatment was added into the pots after 2 weeks of plant growth. Inoculum (50 mL) was poured directly onto the root system using a funnel inserted into the sand. All seedlings were harvested 3 weeks after the final inoculum addition to allow take-all disease symptoms to develop (see Supplementary Figure S1A). Five replicates were prepared per treatment, and the experiment was repeated twice. An additional experiment using wheat cv. Chinese Spring was also carried out due to the availability of an annotated genome (IWGSC RefSeq v2.1) (Zhu et al., 2021).

For split-root experiments, roots from 2-week-old wheat seedlings (cv. Chinese Spring) were split across two pots (pot A and pot B) joined at one side. Pots were filled with sand and covered with grit. Roots in pot A received *G. hyphopodioides* liquid inoculum (isolate NZ.129.2C.17), using the method described above. Plants were left to grow for one week before inoculating with *G. tritici* liquid inoculum (isolate 17LH(4)19d1). To investigate whether *G. hyphopodiodes* provides local control against take-all disease, *G. tritici* inoculum was added to *G. hyphopodioides*–colonised roots in pot A. To investigate whether *G. hyphopodiodes* provides systemic control against take-all disease, *G. tritici* inoculum was added to uninoculated roots in pot B (see Supplementary Figure S1B). Plants were harvested 3 weeks later. Five replicates were prepared per treatment, and the experiment was repeated three times.

2.3 Disease quantifications

Visual disease assessments were carried out as previously described (McMillan et al., 2011), and qPCR quantification of *G. tritici* fungal biomass was performed by targeting a 105-bp partial DNA sequence of the translation elongation factor 1-alpha (*EF1-α*) gene, using primers GtEFF1 (5′-CCCTGCAAGCTCTTCCTCTTAG-3′) and GtEFR1 (5′-GCATGCGAGGTCCCAAAA-3′) with the TaqMan probe (5′-6FAM-ACTGCACAGACCATC-MGB-3′) (Thermo Scientific™, USA) (Keenan et al., 2015).

2.4 Plant growth, inoculation, and root sampling for RNA sequencing and bioimaging

A precision inoculation method was developed to enable the investigation of local plant responses to fungal infection (see

TABLE 1 Full list of fungal isolates used in the present study.

Isolate name	Year isolated	Rothamsted research field	ITS species identification	Experiment
NZ.129.2C.17	2016	New Zealand	*G. hyphopodioides*	Seedling pot infection assays, split-root experiment, and fungal confrontation assay
63B-1	2018	Delafield	*G. hyphopodioides*	Fungal confrontation assay
NZ.24.2A.15	2015	New Zealand	*G. hyphopodioides*	Fungal confrontation assay
S.03.13	2013	Summerdells I	*G. hyphopodioides*	Fungal confrontation assay
P.09.13	2013	Pastures	*G. hyphopodioides*	Fungal confrontation assay
105C-1	2018	Delafield	*G. hyphopodioides*	Fungal confrontation assay
P.10.13	2013	Pastures	*G. hyphopodioides*	Fungal confrontation assay
16.NZ.1d	2016	New Zealand	*G. tritici*	Seedling pot infection assays, Split-root experiment, and fungal confrontation assay
17LH(4)19d1	2017	Long Hoos	*G. tritici*	Seedling pot infection assays, split-root experiment, and fungal confrontation assay
17LH(4)8d	2017	Long Hoos	*G. tritici*	Fungal confrontation assay
17LH(4)9d2	2017	Long Hoos	*G. tritici*	Fungal confrontation assay
17LH(4)23d	2017	Long Hoos	*G. tritici*	Fungal confrontation assay
17LH(4)4e	2017	Long Hoos	*G. tritici*	Fungal confrontation assay

Supplementary Figure S2). Wheat seeds cv. Chinese Spring were surface sterilised with 5% (v/v) sodium hypochlorite for 5 min and pre-germinated in a controlled environment growth chamber cabinet (20°C day, 16°C night, 16-h light cycle) for 2 days. Three pre-germinated seeds were transplanted onto a square petri dish plate (12 cm × 12 cm) containing 1.5% (w/v) water agar. Five replicates were prepared for each treatment. Plates were placed vertically in the growth cabinet. After 4 days, one root from each plant was inoculated with a fungal plug (4 cm × 0.5 cm) cut from the leading edge of a 2-week-old fungal colony growing on 1.5% water agar. Inoculated roots were sampled daily from 2 to 6 days postinoculation (dpi). Briefly, two 1-cm root samples were harvested from the inoculated area on each root and snap-frozen in liquid nitrogen for RNA extraction. To determine the stage of fungal colonisation in these harvested samples, 2 cm × 0.5 cm root pieces were sampled from the areas directly above and below each sample. Root pieces were stored in 50% ethanol for subsequent assessment by confocal microscopy.

2.5 Fluorescent staining and confocal microscopy analyses

To assess colonisation in whole root pieces, samples were cleared in 10% w/v potassium hydroxide for 5 min at 70°C, before staining with propidium iodide (PI) (10 µg/mL) and wheat germ agglutinin (WGA), Alexa Fluor™ 488 Conjugate (WGA) (10 µg/mL). To visualise vascular infection by *G. tritici*, transversal root sections were cut by hand using a fine edged razor blade under a dissecting microscope. Confocal microscopy was performed using a ZEISS 780 Confocal Laser Scanning Microscope (ZEISS, Germany). WGA fluorescence was excited at 495 nm and detected at 519 nm. PI fluorescence was excited at 535 nm and detected at 617 nm.

2.6 RNA extraction

Following confocal assessment (see above), root pieces (1 cm each) at the same stage of fungal colonisation were pooled together to create a single sample for RNA extraction. Total RNA was extracted from frozen root material using the E.Z.N.A.® Plant RNA Kit with the associated RNase-free DNase I Set (Omega-Biotek, USA), following the standard protocol provided. RNA quality was assessed based on the RNA integrity number (RIN), measured using the Bioanalyser 2100 with the corresponding RNA 6000 Nano Kit (Agilent, USA), as per manufacturer's instructions.

2.7 Library preparation and sequencing

mRNA library preparation was carried out by Novogene (China) using the Novogene RNA Library Prep Set (PT042) for polyA enrichment. Libraries were sequenced by Illumina NovaSeq to generate 150-bp paired-end reads, with a target of 40 million paired-end reads per sample.

2.8 Transcriptome annotation and analysis

Quality control of reads was performed using MultiQC (https://multiqc.info/). Sequence trimming of recognised adaptors was

performed using Trimmomatic where appropriate (Bolger et al., 2014). Reads were mapped to the Chinese Spring (IWGSC RefSeq v2.1) (Zhu et al., 2021) using HiSat2 (Kim et al., 2019). To ensure that fungal biomass was consistent among replicates of the same treatment, reads were also mapped to the *G. tritici* genome (Okagaki et al., 2015). Three samples were identified as outliers based on standardised residuals of the percentage of reads mapped to *G. tritici*. Outliers were subsequently excluded from further analyses (Supplementary Table S10). All treatments contained at least four biological replicates, with the majority containing five biological replicates. Reads were not aligned to *G. hyphopodioides* due to the lack of a high-quality genome. Count determination was performed using FeatureCounts (Liao et al., 2014) on the R Bioconductor platform (https://bioconductor.org/).

Library normalisation and differential expression (DE) calling was carried out using the Bioconductor package DESeq2 (Love et al., 2014) in R studio. Gene expression levels were compared between *G. tritici*–infected and *G. hyphopodioides*–colonised samples and the uninoculated control samples for each time point individually. DE genes were identified by applying a log2 fold change filter of ≥1 or ≤−1. The DESeq2 implementation of Benjamini–Hochberg (Benjamini and Hochberg, 1995) was used to control for multiple testing ($q < 0.05$). Gene Ontology (GO) enrichment analysis was performed for significantly up- and downregulated wheat genes separately via http://www.geneontology.org, using the Panther classification system.

2.9 Statistical analyses

Statistical analyses were done using Genstat 20th Edition (VSN International Ltd, Hemel Hempstead, UK). Percentage disease data were analysed using a Generalised Linear Regression Model (GLM) with a binomial distribution and LOGIT link function. Analyses were adjusted for over-dispersion and treatment effects tested using deviance ratios (F-statistics) when the residual mean deviance was greater than 1. Data were back-transformed from the LOGIT scale [using the equation $\exp(x)/(1+\exp(x))$] for graphical presentation. For continuous outcome variables, namely fungal colony diameter, plant biomass, *G. tritici* fungal biomass and phytohormone concentration, data were analysed by analysis of variance (ANOVA). Prior to analysis, data were checked for normality by assessing histograms of residuals. *G. tritici* fungal biomass data were square root transformed prior to ANOVA testing, and data were back-transformed for graphical presentation. Tukey's multiple comparisons test was carried out when more than one interaction was of interest.

3 Results

3.1 Hyphal interactions between *G. hyphopodioides* and *G. tritici*

To investigate the role of direct hyphal interaction in take-all control, a series of fungal confrontation assays were conducted on PDA plates. Prior to hyphal contact, the individual growth rates of *G. tritici* and *G. hyphopodioides* colonies did not significantly differ from the dual colony controls (Supplementary Table S1). The same was true when the two species were grown in a "sandwich" plate set-up (Figure 1A, Supplementary Table S2), suggesting that, prior to hyphal contact, *G. hyphopodioides* does not produce diffusible antifungal compounds or volatile organic compounds capable of inhibiting *G. tritici*. When hyphae of the two fungal species interacted in confrontation assays, a dark barrage was observed in the interaction zone (Figure 1A). The observed barrage formed 1–2 days following hyphal interaction, perhaps suggesting that direct interaction causes hyphal stress in at least one of the interacting species. A dark barrage was not observed when isolates of the same species were confronted (Supplementary Figure S3). Despite *in vitro* barrage formation, fungal antibiosis is unlikely to be the mechanism responsible for take-all control.

3.2 Pre-treatment with *G. hyphopodioides* provides local control against take-all disease

To investigate the hypothesis that non-pathogenic *G. hyphopodioides* provides protection against take-all disease by inducing wheat resistance, seedling co-inoculation experiments were carried out under controlled environment conditions. *G. hyphopodioides* inoculum was added to wheat seedlings (cv. Hereward) growing in pots 1 week prior, 2 weeks prior, at the same time as, and 2 weeks after inoculation with pathogenic *G. tritici*. Characteristic black necrotic root lesions were observed in *G. tritici*–infected control plants. SEVs were observed in plants co-inoculated with *G. hyphopodioides* (Figure 1B). The data revealed a significant reduction in both take-all disease levels and *G. tritici* fungal biomass in plants pre-treated with *G. hyphopodioides* 2 weeks prior or 1 week prior to *G. tritici* inoculation (Figures 1C, D). Hence, even very early colonisation by *G. hyphopodioides* is sufficient for take-all control. These findings were consistent with additional experiments involving a different *G. tritici* isolate (Gt 17LH(4)19d1) and wheat cultivar (cv. Chinese Spring) (Supplementary Figure S4).

Seedlings co-inoculated with *G. hyphopodioides* and *G. tritici* at the same time had no effect on take-all disease levels or *G. tritici* fungal biomass. Importantly, adding *G. hyphopodioides* after *G. tritici* resulted in increased levels of take-all disease and *G. tritici* fungal biomass (Figures 1C, D). Furthermore, the shoot and root dry biomass of plants in this latter treatment were significantly reduced, indicating that seedling health is negatively affected when *G. hyphopodioides* infections occur in addition to *G. tritici* infection (Figures 1E, F). These findings suggest that the earlier *G. tritici* infections somehow lead to the suppression of critical local defence responses, and this now permits *G. hyphopodioides* to colonise throughout the wheat root system. These findings should be taken into careful consideration when evaluating the potential of *G. hyphopodioides* as a biocontrol agent.

Split-root experiments were carried out to determine whether *G. hyphopodioides* provides local or systemic protection against

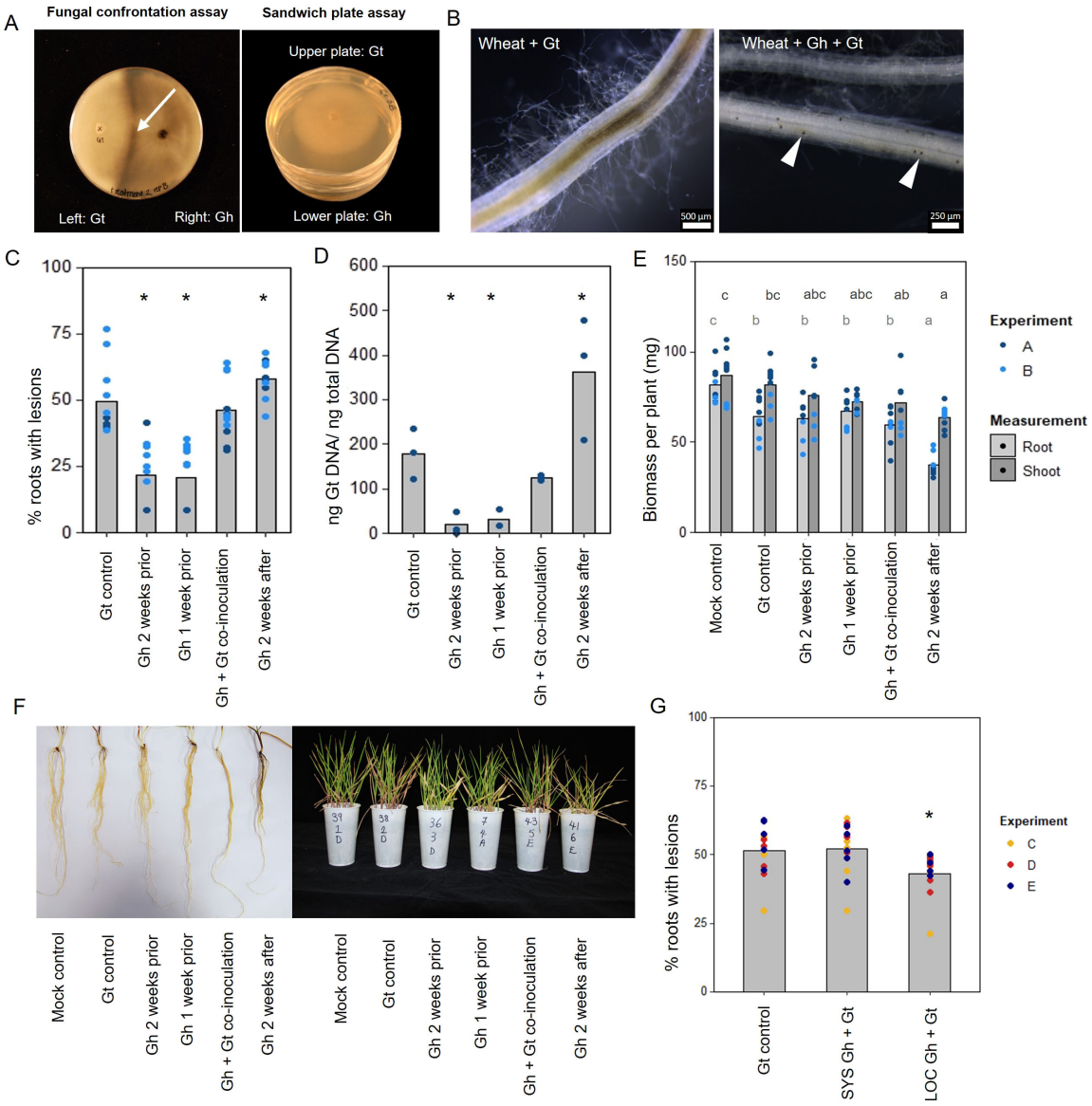

FIGURE 1
In vitro and *in planta* interaction studies involving endophytic *G. hyphopodioides* and pathogenic *G. tritici*. **(A)** *In vitro* fungal interaction assays on PDA plates. Fungal confrontation assays imaged 2 days following hyphal interaction, and colonies in sandwich plate assays imaged 6 days after establishment. Arrow indicates a dark barrage in the interaction zone. **(B)** Stereomicroscope images of wheat roots infected with *G. tritici* only or co-inoculated with *G. hyphopodioides*. Arrowheads indicate *G. hyphopodioides* sub-epidermal vesicles (SEVs). **(C)** Percentage of wheat roots (cv. Hereward) with take-all root lesions in co-inoculation experiments with *G. hyphopodioides* (GLM: $F = 25.99$, d.f. 4, 49, $p < 0.001$). **(D)** *G. tritici* fungal biomass (ng *G. tritici* DNA/ng total DNA) in co-inoculation experiments with *G. hyphopodioides*, as quantified by qPCR ($F = 61.10$, d.f. 4, 38, $p < 0.001$). **(E)** Shoot and root dry biomass (mg) in *G. tritici* co-inoculation experiments with *G. hyphopodioides* ($F = 6.49$, d.f. 5, 36, $p < 0.001$; $F = 4.50$, d.f. 5, 36, $p < 0.01$, respectively). **(F)** Representative images of wheat roots (left) and shoots (right) in co-inoculation experiments. **(G)** The percentage of wheat roots (cv. Chinese Spring) with take-all lesions in split root co-inoculation experiments with *G. hyphopodioides* ($F = 29.44$, d.f. 2, 36, $p = 0.007$). Asterisks indicate a significant difference to the *G. tritici* control as calculated by Dunnett's *post-hoc* test ($p < 0.05$). Letters indicate significant differences as calculated by Tukey's multiple comparisons test ($p < 0.05$). Gt, *G. tritici*; Gh, *G. hyphopodioides*; SYS, systemic; LOC, local.

take-all disease. Significant disease reduction was achieved only in roots which had been directly inoculated with *G. hyphopodioides* (LOC) and not in systemic roots (SYS), which had not been directly inoculated with *G. hyphopodioides* (Figure 1G). Taken together, we demonstrate that local induced wheat resistance plays a crucial role in the control of take-all disease by *G. hyphopodioides*, and this response is consistent across both winter and spring wheat types.

3.3 The differing infection biologies *of G. hyphopodioides* and *G. tritici* in wheat roots

To study fungal infection processes during early root colonisation, wheat seedlings (cv. Chinese Spring) were root inoculated with either *G. hyphopodioides* (NZ.129.2C.17) or *G.*

tritici (Gt 17LH(4)19d1) in an agar plate system. Plants were harvested at 2, 4, and 5 dpi to capture key stages of fungal infection for later RNA-seq analysis. At 2 dpi, very few hyaline runner hyphae were detected on the root surface of plants inoculated with either *G. tritici* or *G. hyphopodioides*, and hyphae had not yet penetrated the epidermal cells in either interaction (Figures 2A, B). By 4 dpi, hyaline runner hyphae covered a greater area of the root surface (Supplementary Figure S5) and hyphae were detected in epidermal and cortical cells of both *G. tritici*– and *G. hyphopodioides*–inoculated roots (Figures 2A, B). At 5 dpi, hyaline runner hyphae were detected across a large area of the root surface (Supplementary Figure S5) in both fungal treatments. *G. tritici* hyphae infected the stele, whereas *G. hyphopodioides* hyphal growth was arrested in the cortex (Figure 2B). *G. hyphopodioides* hyphae were detected in cortical cells, from which SEVs were formed (Figure 2A).

Although the role of fungal SEVs in the infection process of *G. hyphopodioides* is unknown, the presence of these characteristic structures serves as visual confirmation of *G. hyphopodioides* colonisation in the root cortex (Osborne et al., 2018). Newly formed SEVs could be visualised by WGA staining, whereas mature SEVs, which were darker in colour, could not be visualised by WGA staining (Supplementary Figure S6). *G. tritici* did not produce SEVs in wheat roots at any time point, and *G. hyphopodioides* hyphae were not observed in the stele at any time point (Supplementary Figure S5). To investigate the structure of mature SEVs, wheat plants (cv. Hereward) were inoculated with *G. hyphopodioides* (NZ.129.2C.17) in a seedling pot infection assay. Colonised plants were harvested at 5 weeks postinoculation and imaged by transmission electron microscopy (TEM). Comparative analysis of intraradical fungal hyphae and SEVs revealed that SEVs contain a greater number of putative lipid bodies and a significantly thickened cell wall, comprising two to three layers of differing densities (Figures 3A, B). Multiple SEVs were often observed in a single plant cell (Figure 3C) and SEVs were often found appressed to the plant cell wall (Figures 3D, E).

3.4 Wheat transcriptional remodelling during fungal infection

The data discussed in this publication have been deposited in NCBI's Gene Expression Omnibus and are accessible through GEO Series accession number GSE242417 (https://www.ncbi.nlm.nih.gov/geo/query/acc.cgi?acc=GSE242417). Three time points (2, 4, and 5 dpi) were selected for RNA-seq analysis based on the stage of fungal infection (Supplementary Figure S7). Principal component analysis (PCA) of sample distances demonstrated a good level of clustering between biological replicates, although *G. tritici*–infected samples exhibited comparatively higher levels of variation (Figure 4A). Gene expression levels were compared between *G. tritici*–infected or *G. hyphopodioides*–colonised plants and the uninoculated control plants at each time point individually. Full lists of the differentially expressed genes (DEGs) can be found in Supplementary Table S3. As expected, the number of wheat DEGs between the uninoculated control and *G. tritici*–infected or *G. hyphopodioides*–colonised plants was low at 2 dpi (77 and 62, respectively). By 4 dpi, *G. tritici* infection and *G. hyphopodioides* colonisation resulted in the DE of 1,061 and 1,635 wheat genes,

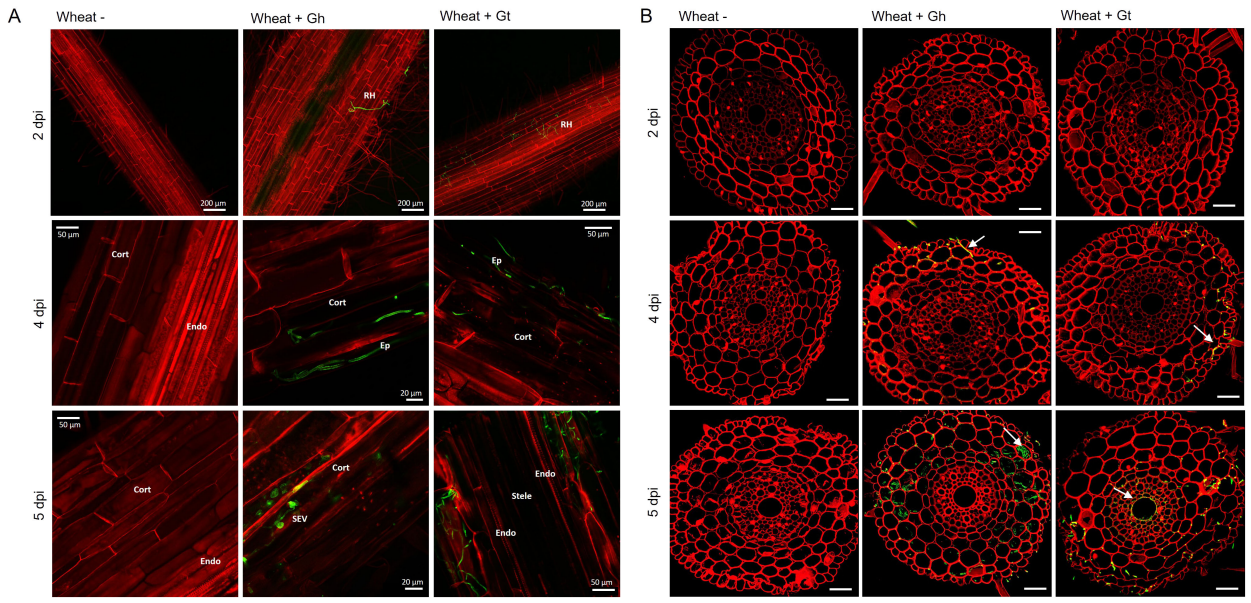

FIGURE 2
Fluorescence images obtained by confocal microscopy of mock inoculated, *G. hyphopodioides*–colonised, or *G. tritici*–infected wheat roots. **(A)** Confocal micrographs of whole root pieces highlighting fungal infection structures. **(B)** Z-stack images of transversal sections showing colonisation of different root cell layers across time points. Gt, *G. tritici*; Gh, *G. hyphopodioides*; RH, runner hyphae; Ep, epidermal cell; Cort, cortical cell; SEV, subepidermal vesicle; Endo, endodermal barrier. Fungal hyphae (green) are stained with WGA-AF488, and plant cell walls (red) are stained with propidium iodide. White arrows in panel **(B)** indicate fungal hyphae. Scale bars in panel **(B)** represent 50 µm.

respectively. At 5 dpi, a striking number of wheat genes were DE in response to *G. hyphopodioides* colonisation (7,532), whereas the number of DEGs in response to *G. tritici* infection (1,074) showed little change compared to 4 dpi (Figure 4B).

To investigate wheat transcriptional changes during the infection progression of *G. hyphopodioides* compared to *G. tritici*, GO enrichment analyses were carried out on the sets of DEGs described above. At 2 dpi, genes involved in the diterpenoid biosynthetic process/metabolic process and gibberellin biosynthesis process were upregulated in *G. tritici*–inoculated roots. A large number of broad-spectrum phytoalexins in wheat are diterpenoids, requiring the biosynthesis of gibberellins (GAs) (Polturak et al., 2022). Thus, early responses to *G. tritici* may involve the production of antimicrobial compounds. Meanwhile, genes involved in the biosynthetic process/metabolic process were downregulated in *G. hyphopodioides*–inoculated roots (Supplementary Figures S8A, B). At 4 dpi, genes involved in the cinnamic acid biosynthetic/metabolic process and the L-phenylalanine metabolic/catabolic process were upregulated in *G. hyphopodioides*–colonised wheat roots, suggesting that lignin biosynthesis is important at this time point. However, these GO terms were not significantly enriched until 5 dpi in *G. tritici*–infected roots, suggesting that lignin biosynthesis is also involved in the defence response to *G. tritici*, although at a later stage than *G. hyphopodioides*. Other enriched terms in *G. hyphopodioides*–colonised plants at 5 dpi included response to wounding, regulation of defence responses and regulation of the JA signalling pathway. Downregulated terms included gene expression and RNA metabolic process, suggesting fine-tuning of wheat expression patterns in response to *G. hyphopodioides*. In addition, plant-type cell-wall organisation or biogenesis was downregulated, suggesting that the cell wall may play a role in the local wheat response to *G. hyphopodioides* (Supplementary Figures S8A, B).

Next, we compared the unique and shared wheat transcriptional responses to the two fungal species. At 5 dpi, 97% of the genes which were DE in response to *G. tritici* infection were also DE in response to *G. hyphopodioides* colonisation (Figure 4C). Within this core set of genes at 5 dpi, highly enriched GO biological process terms included plant response to biotic stimulus and isoprenoid biosynthetic/metabolic process (Figure 4D). The plant response to biotic stimulus term comprised 42 DE genes, 14 of which encoded proteins containing small cysteine-rich protein domains, often associated with pathogenesis-related proteins. Six genes encoded chitinases, two encoded wound-induced proteins (WIN) and a further four encoded protein kinase domain-containing proteins, thus indicating a clear defence response to both fungi (Supplementary Table S4). Enriched biological process GO terms among shared downregulated genes included response to nitrate, nitrate transmembrane transport, and nitrate assimilation (Figure 4D). Highly enriched molecular function GO terms among upregulated genes included manganese ion binding,

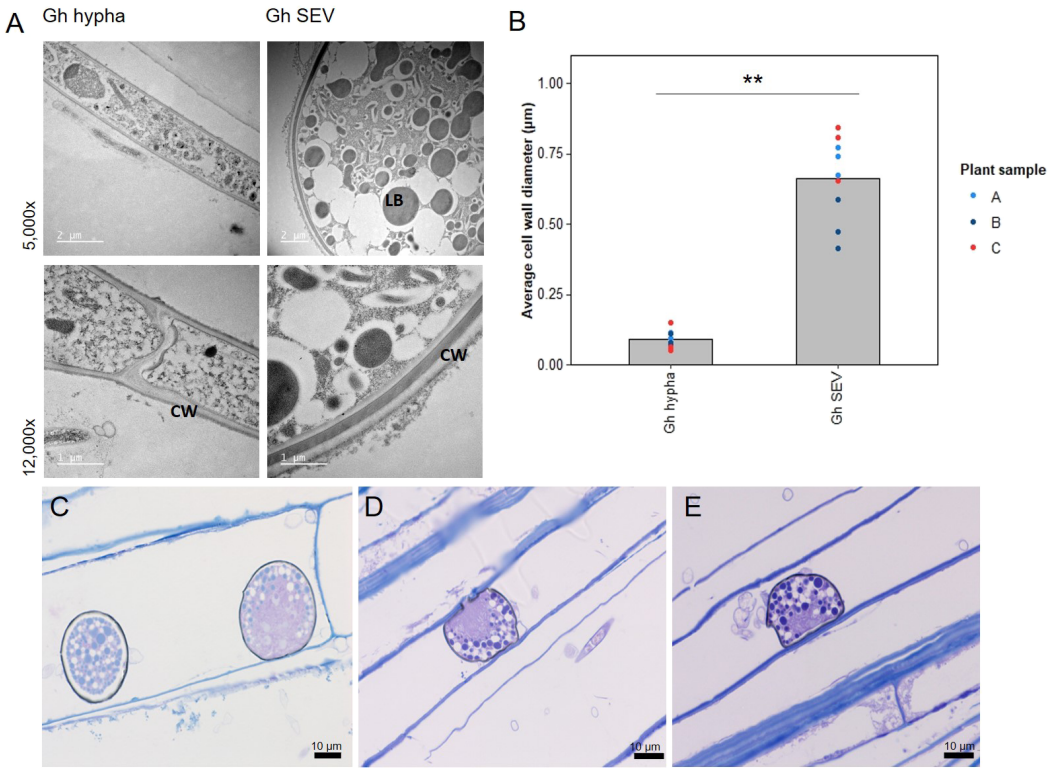

FIGURE 3
Subepidermal vesicles (SEVs) produced by *G. hyphopodioides* (Gh) in wheat roots. **(A)** Transmission electron micrographs (TEM) of *Gh* hyphae (left) and SEVs (right). **(B)** Average cell wall diameter (µm) of *Gh* fungal structures ($F = 8.3$, d.f. 2, 12, $p < 0.01$). **(C–E)** Light micrographs of *Gh* SEVs in semi-thin sections, stained with toluidine blue. CW, plant cell wall; LB, putative lipid body. **=p<0.01.

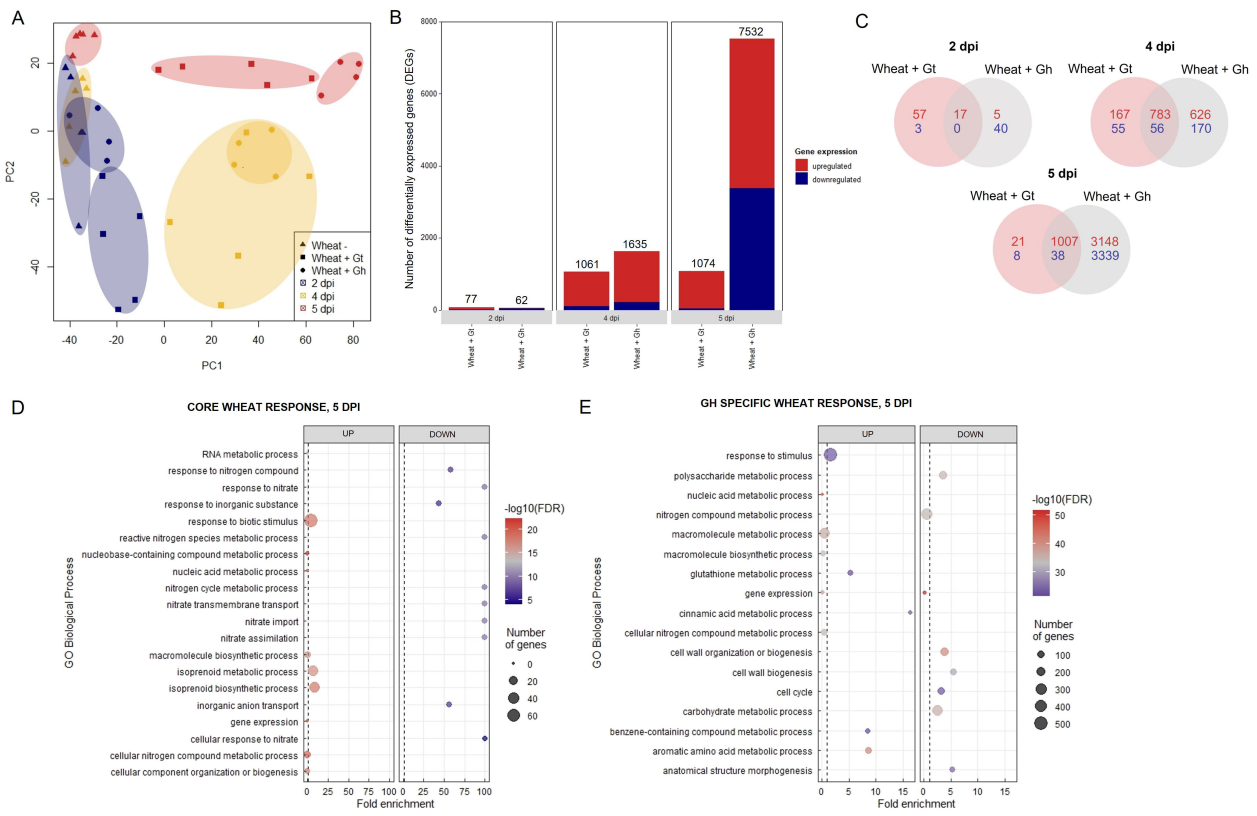

FIGURE 4
Transcriptional profiling of *G. hyphopodioides*–colonised or *G. tritici*–infected wheat roots. **(A)** Principal component analysis (PCA) plot of sample distances based on transformed (variance stabilising transformation) gene count data. Data points have been categorised by shape and colour to denote treatment and time point, respectively. **(B)** The number of differentially expressed genes (DEGs) in wheat colonised by *G. hyphopodioides* or *G. tritici* compared to uninoculated control samples. **(C)** Venn diagram highlighting the number of unique and shared wheat DEGs in *G. tritici*–infected or *G. hyphopodioides*–colonised samples compared to the uninoculated control samples. **(D)** Top 10 enriched biological process GO terms among DEGs in the shared wheat response to both *G. tritici* and *G. hyphopodioides* at 5 dpi. **(E)** Top 10 enriched biological process GO terms unique to the wheat response to *G. hyphopodioides* colonisation at 5 dpi. The top 10 GO terms were determined by false discovery rate (FDR).

oxidoreductase activity, and heme binding. Highly enriched molecular function GO terms among downregulated genes included nitrate transmembrane transporter activity and oxygen binding (Supplementary Table S5A). Highly enriched cellular component GO terms among upregulated genes included extracellular region (Supplementary Table S5B).

GO enrichment analysis was repeated on the subset of genes that were DE in response to *G. hyphopodioides*, but not *G. tritici*, at 5 dpi. Genes in this subset were of particular interest due to their potential role in *G. hypophodioides*–mediated take-all control. Cinnamic acid metabolic process and glutathione metabolic process were among the top 10 upregulated biological process GO terms. Phenolic compounds such as cinnamic acid are known to have antifungal properties and increased production of cinnamic acid can inhibit pathogen growth (Shalaby and Horwitz, 2015). Furthermore, glutathione plays diverse roles in plant immunity, both acting as an antioxidant and as a modulator of signalling processes associated with disease resistance (Zechmann, 2020). Further investigation is required to assess the role of plant phenolics and glutathione in the *G. hyphopodioides*–wheat interaction. Cell-wall organisation or biogenesis, cell cycle, and anatomical structure morphogenesis were among the top 10 downregulated biological process GO terms (Figure 4E). Highly enriched molecular function GO terms among upregulated genes included phenylalanine ammonia lyase (PAL) activity, glutathione transferase activity, and ion binding. In contrast, structural constituents of chromatin, tubulin binding and nucleosome binding were highly enriched among the downregulated genes (Supplementary Table S6A). Highly enriched cellular component function GO terms among downregulated genes included microtubule cytoskeleton, nucleosome, and protein–DNA complex (Supplementary Table S6B). The plant cytoskeleton plays a crucial and dynamic role in plant–microbe interactions (Wang et al., 2022). In addition, histone modification and chromatin remodelling are known to contribute to plant disease resistance (Kang et al., 2022). Indeed, there is evidence that pathogen modulated microtubule dynamics can be regulated by histone modifications (Hu et al., 2014). Thus, it is tempting to suggest

that similar mechanisms could be at play in the *G. hyphopodioides*–wheat interaction.

3.5 Wheat phytohormone response to *G. hyphopodioides* colonisation and *G. tritici* infection

Regulation of the JA signalling pathway was identified as a newly upregulated GO term at 5 dpi in *G. hyphopodioides*–colonised roots (see above). The GO term comprised 26 DEGs (out of a total of 77 known genes in wheat), all of which encoded TIFY transcriptions factors (TIFY TFs). In contrast, just three genes encoding TIFY TFs (TIFY10C-like_TraesCS5D02G219300, TIFY10C-like _TraesCS5B02G211000, and TIFY11E-like_ TraesCS7D02G204700) were DE in *G. tritici*–infected plants compared to the control. Although not identified by GO enrichment analysis, we also investigated the expression of JA biosynthesis genes. In total, 23 JA biosynthesis–related genes were DE (17 up/6 down) in response to *G. hyphopodioides* at 5 dpi. The list included lipoxygenase (*LOX*), allene oxide synthase (*AOS*) and *AOS-like*, 12-oxophytodienoate reductase (*OPR*) and *OPR-like*, and 3-ketoacyl-CoA thiolase (*KAT-like*) genes. Of these genes, only one (LOX8_TraesCS7B02G145200) was differentially expressed in response to *G. tritici* at 5 dpi (Figure 5A, Supplementary Table S7).

The JA and ET signalling are often closely linked. Therefore, we investigated genes involved in ET biosynthesis and signalling. Five ACC-oxidase (*ACO-like*) genes were upregulated in response to *G. hyphopodioides* at 5 dpi. In addition, 22 ET-responsive transcription factor-like (*ERF-like*) genes, key integrators of downstream ET and JA signal transduction pathways (Lorenzo et al., 2003), were DE (19 up/3 down) in response to *G. hyphopodioides* by 5 dpi. In contrast, four *ERF-like* genes (TraesCS4A02G001300, TraesCS5B02G565400, TraesCS1A02G231200, and TraesCS1B02G231500) were upregulated at 4 dpi and two (TraesCS5B02G565400 and TraesCS1A02G231200) were upregulated at 5 dpi in *G. tritici*–infected roots compared to the control (Figure 5B, Supplementary Table S7). SA is another key phytohormone involved in the plant response to pathogen invasion. SA signalling was not identified as a significantly enriched GO term in response to *G. hyphopodioides* or *G. tritici* at any time point.

To investigate whether the local transcriptional changes described above resulted in altered hormone levels, hormone quantifications of JA and SA were carried out in *G. hyphopodioides*–colonised, *G. tritici*–infected, and uninoculated

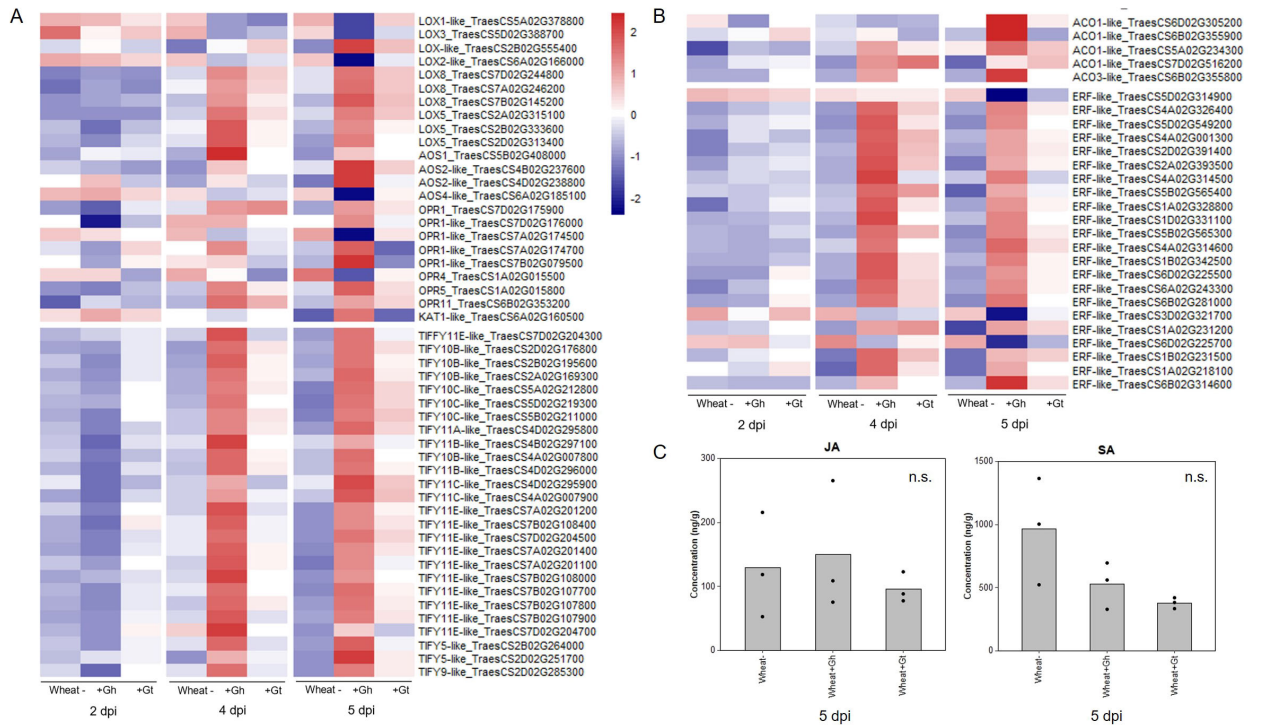

FIGURE 5
Wheat phytohormone-associated gene responses and JA quantification in response to *G. hyphopodioides* (Gh) colonisation or *G. tritici* (Gt) infection. **(A)** Expression of genes involved in the biosynthesis of JA and the regulation of the JA-mediated signalling pathway. **(B)** Expression of genes involved in ET biosynthesis and downstream ET signalling pathways. Heatmap data represent LOG transformed normalised genes counts. **(C)** Phytohormone quantification of JA and SA in roots harvested at 5 dpi ($F = 0.30$, d.f. 2, 6, $p = 0.75$; $F = 4.19$, d.f. 2, 6, $p = 0.07$, respectively). n.s., not significant. Data have been back-transformed from a square root scale. *ACO*, 1-aminocyclopropane-1-carboxylic acid oxidase; *AOC*, allene oxide cyclase; *AOS*, allene oxide synthase; *ERF*, ethylene responsive transcription factor; *KAT*, 3-ketoacyl-CoA thiolase; *LOX*, lipoxygenase; *OPR*, 12-oxophytodienoate reductase; *TIFY*, TIFY-domain containing transcription factor.

10.3389/fpls.2024.1444271

control roots at 5 dpi. We found no significant difference in the levels of JA or SA between any treatments (Figure 5C).

3.6 *G. hyphopodioides* colonisation results in the early induction of lignin biosynthesis genes

PAL activity, essential for the lignin biosynthesis pathway, was identified as a significantly enriched molecular function GO term in the unique wheat response to *G. hyphopodioides* at 5 dpi (see Supplementary Table S6A). To investigate root lignification in response to *G. hyphopodioides* and *G. tritici*, we explored the expression of key genes involved in the lignin biosynthesis pathway in wheat (Figure 6A). *G. hyphopodioides* colonisation resulted in the earlier upregulation of lignin biosynthesis genes compared to *G. tritici*, with key genes such as arogenate dehydratase (*ADT*), phenylalanine ammonia-lyase (*PAL*), cinnamate 4-hydroxylase (*4CL*), and cinnamoyl-CoAreductase (*CCR*) significantly upregulated at 4 dpi (Figure 6B). However, two of eight caffeic acid *O*-methyltransferase (*COMT*) genes detected were already significantly upregulated in response to *G. tritici* at 2 dpi (TraesCS5D02G488800 and TraesCS5D02G488900). Interestingly, the remaining *COMT* genes (TraesCS2B02G066100, TraesCSU02G024300, TraesCS3B02G612000, TraesCS7D02G539100, TraesCS6D02G008200, and TraesCS7D02G538900) were strongly downregulated in response to *G. hyphopodioides* by 5 dpi, suggesting a decrease in the proportion of syringyl (S)-lignin. Most striking, however, was the significant upregulation of 37 *PAL* genes in response to *G. hyphopodioides*, compared to the upregulation of just 12 *PAL* genes in response to *G. tritici* at 5 dpi (Figure 6B, Supplementary Table S8).

To visualise lignification of infected root tissues, potassium permanganate staining was performed on transverse sections of samples harvested at 5 dpi (Figure 6C). The percentage of total cell-wall area with dark potassium permanganate staining (measured in ImageJ) was used to quantify relative cell-wall lignification. Based on these measurements, *G. tritici*–infected roots exhibited the highest levels of cell-wall lignification, although both *G.*

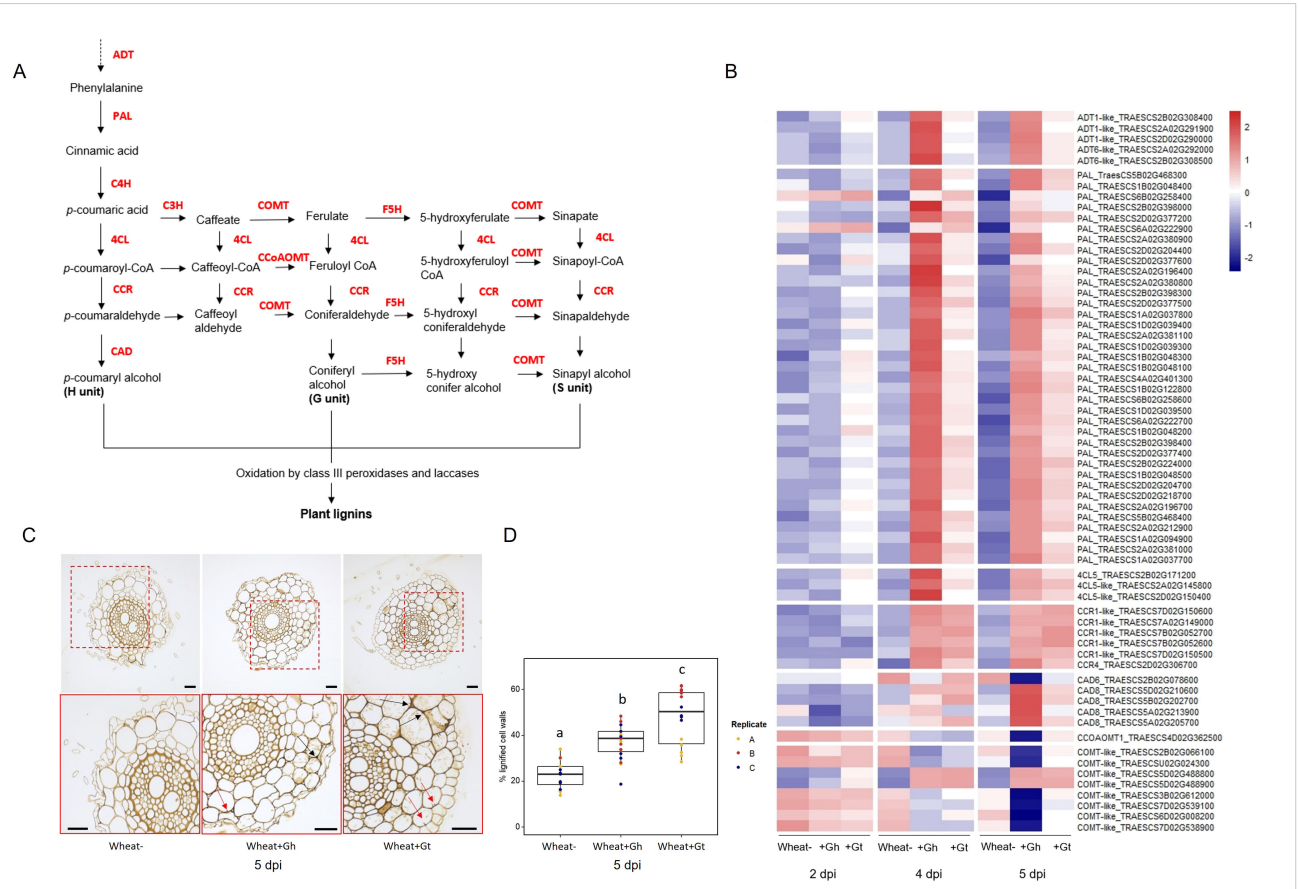

FIGURE 6
Lignin biosynthesis pathway and the lignin responses to *G. hyphopodioides* colonisation or *G tritici* infection. **(A)** Schematic of the lignin biosynthesis pathway in plants [adapted from Nguyen et al. (2016)]. **(B)** Expression of key genes involved in the lignin biosynthesis pathway, based on LOG transformed normalised gene counts. **(C)** Micrographs of transversal root sections stained with potassium permanganate for the visualisation of cell wall lignification in response to fungal infection at 5 dpi. Black arrows indicate lignified cell wall thickenings, and red arrows indicate plant lignitubers. Scale bars represent 50 µm. **(D)** Mean percentage of total cell wall area stained within dark parameters, indicating relative cell wall lignification ($F = 34.61$, d.f. 2, 50, $p < 0.001$). Lowercase letters indicate Tukey *post-hoc* groupings. *ADT*, arogenate dehydratase; *PAL*, phenylalanine ammonia-lyase; *C4H*, cinnamate 4-hydroxylase; *4CL*, 4-coumarate CoA ligase; *HCT*, quinateshikimate *p*-hydroxycinnamoyltransferase; C3H, *p*-coumaroylshikimate 3′-hydroxylase; *CCoAOMT*, caffeoyl-CoA *O*-methyltransferase; *CCR*, cinnamoyl-CoAreductase; *F5H*, ferulate 5-hydroxylase; *CAD*, cinnamyl alcohol dehydrogenase; *COMT*, caffeic acid *O*-methyltransferase.

hyphopodioides and *G. tritici* infection resulted in increased cell-wall lignin levels compared to uninoculated control roots at 5 dpi (Figure 6D). Plant lignitubers, lignified callose deposits surrounding hyphal tips (Bradshaw et al., 2020; Huang et al., 2001; Park et al., 2022), were often detected in cells containing fungal hyphae, although these structures were more common in *G. tritici*–infected samples.

3.7 *G. hyphopodioides* colonisation results in local downregulation of cell-wall organisation and biogenesis genes

As mentioned previously, biological process GO term "cell-wall organisation and biogenesis" was identified as being unique to the wheat response to *G. hyphopodioides* at 5 dpi (see Figure 4E). In total, 124 genes involved in cell-wall organisation and biogenesis (out of 1,122 total known genes involved in cell-wall organisation and biogenesis in wheat) were downregulated in response to *G. hyphopodioides* at 5 dpi (Supplementary Table S9). In contrast, *G. tritici* infection did not lead to the DE of any genes within the cell-wall organisation and biogenesis GO term. Focusing on the top 30 DE genes within this GO term in *G. hyphopodioides*–colonised plants at 5 dpi, we identified six xyloglucan endotransglycosylases/hydrolases (*XTH*) genes, three cellulose synthase CESA–like A-like (*CSLA*) genes, one CESA-like F (*CSLF*) gene, and three fasciclin-like arabinogalactan (*FLA*) genes (Figure 7A). Although just one *CESA-like* gene was present in the list of top 30 DEGs, a total of 10 *CESA* genes were downregulated at 5 dpi (Supplementary Table S9). To validate gene expression in the RNA-seq dataset, we identified key cell wall–related genes where all three wheat homoeologs were downregulated in *G. hyphopodioides*–colonised plant roots relative to the mock-inoculated controls (Figure 7B). RT-qPCR analyses of the selected targets revealed that, as expected, cell wall–related genes *CESA7-like*, *COBL-5D*, and *FLA11* were significantly downregulated in *G. hyphopodioides*–colonised plants compared to the mock-inoculated controls (Figure 7C).

Collectively, a wide and diverse range of transcriptional changes occurs in wheat roots in response to *G. hyphopodioides* colonisation, creating a mutually antagonistic structural, physiological, and chemical environment that limits *G. tritici* hyphal progress into the deeper root tissues. There is a possibility that *G. hyphopodioides* downregulates the wheat genes involved in cell-wall organisation and biogenesis in an attempt to maintain hyphal access to locally

A

Gene ID	Gene name	Log2FC	padj
TraesCS5A02G548500	XTH	-5.66	4.27E-22
TraesCS7A02G363000	XTH	-4.52	1.51E-17
TraesCS7D02G360100	XTH	-5.10	2.71E-10
TraesCS7D02G294300	CSLF6	-3.49	4.39E-10
TraesCS4B02G383000	XTH	-3.39	4.97E-10
TraesCS4D02G358700	XTH	-3.81	5.00E-10
TraesCS7B02G265000	XTH	-6.31	5.28E-10
TraesCS6A02G169200	CSLA1-like	-4.05	6.71E-09
TraesCS6B02G197200	CSLA1-like	-3.61	7.97E-09
TraesCS3B02G376800	EXPA2	-3.43	1.03E-08
TraesCS3B02G120700	FLA11	-4.06	1.13E-08
TraesCS2A02G082500	IRX9	-4.36	1.35E-08
TraesCS6D02G158600	CSLA1	-3.57	5.19E-08
TraesCS2D02G091400	Unknown	-4.14	7.54E-08
TraesCS5D02G137300	GT3	-3.10	1.77E-07
TraesCS3D02G105500	FLA11	-3.80	2.79E-07
TraesCS2D02G080400	IRX9	-4.33	3.13E-07
TraesCS2A02G153000	PAE	-2.86	3.45E-07
TraesCS5A02G143800	GAUT7	-3.65	4.99E-07
TraesCS1D02G404700	FLA6	-3.28	1.03E-06
TraesCS6A02G131900	IRX15-like	-5.26	1.27E-06
TraesCS2D02G099900	PME	-8.49	1.48E-06
TraesCS4A02G227100	GXM-like	-7.37	1.62E-06
TraesCS5D02G107900	COBL-5B	-3.33	2.20E-06
TraesCS5D02G280400	CTL1	-2.22	2.68E-06
TraesCS6D02G121700	IRX15-like	-4.45	3.22E-06
TraesCS5A02G129800	GT3	-2.80	5.03E-06
TraesCS1D02G111600	FLA11	-7.80	7.85E-06
TraesCS4D02G086700	GXM1-like	-4.24	8.06E-06
TraesCS1B02G167200	CESA7-like	-3.04	9.85E-06

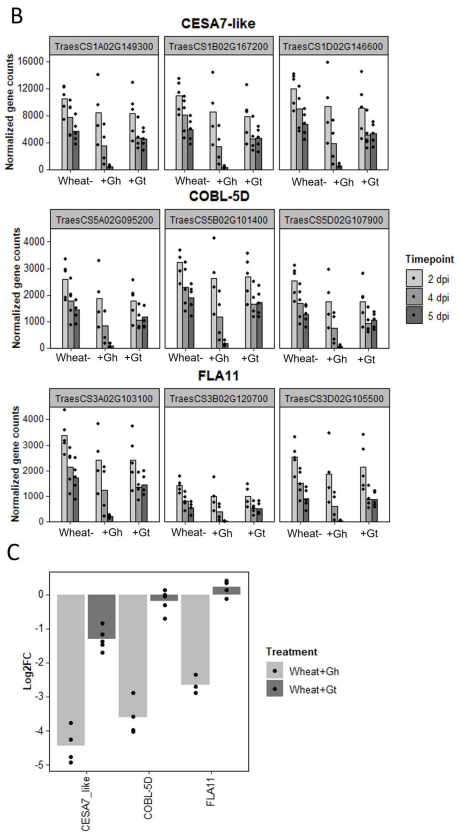

FIGURE 7
Colonisation by *G. hyphopodioides* results in local downregulation of cell wall–related genes. **(A)** The top 30 most differentially expressed genes relating to cell wall organisation and biogenesis in *G. hyphopodioides*–colonised plants at 5 dpi. Ordered by significance (padj). **(B)** Gene counts of selected genes across time points. **(C)** qPCR expression analysis of *CESA7-like, COBL-5D* and *FLA11* in *G. hyphopodioides*–colonised or *G. tritici*–infected plants at 5 dpi (Log2FC relative to the mock-inoculated control).

available water and nutrient sources, but, where these changes fail to occur, hyphal growth rates slow and these abiotic stresses trigger SEV formation.

4 Discussion

Although transcriptional studies into the *G. tritici*–wheat interaction have been carried out previously for both host (Kang et al., 2019a; Yang et al., 2015; Zhang et al., 2020) and pathogen (Gazengel et al., 2020; Kang et al., 2019b), this is not the case for the *G. hyphopodioides*–wheat interaction. To investigate early wheat responses to *G. tritici* infection and uncover the local wheat defence mechanisms responsible for *G. hyphopodiodes*–induced disease control, we performed comparative transcriptome profiling of *G. hyphopodioides*–colonised and *G. tritici*–infected wheat using a precision inoculation method. Through detailed screening of infected root material by confocal microscopy, we were able to characterise infection progression across several time points. In support of early studies into non-pathogenic *Magnaporthaceae* species (Holden, 1976; Speakman and Lewis, 1978), we observed that, whereas pathogenic *G. tritici* grew into the vascular tissues of wheat at 5 dpi, growth of endophytic *G. hyphopodioides* was always limited to the inner cortex. In addition, we observed the formation of *G. hyphopodioides* SEVs in cortical cells at 5 dpi, whereas SEVs were not observed in *G. tritici*–infected roots at any time point. Interestingly, the formation of *G. hyphopodioides* SEVs at 5 dpi was concomitant with a dramatic increase in the number of wheat DEGs. In contrast, the number of wheat DEGs in *G. tritici*–infected roots showed minimal increase between 4 dpi and 5 dpi.

TEM analysis of mature *G. hyphopodioides* SEVs revealed that SEVs share key similarities with fungal resting structures such as chlamydospores, both being characterised by a significantly thickened, multi-layered cell wall and an increased number of putative lipid bodies (Francisco et al., 2019). Therefore, we hypothesise that *G. hyphopodioides* SEVs are fungal resting structures where growth has ceased and SEVs may be produced as a stress response to locally induced host defences, as indicated by extensive transcriptional reprogramming at 5 dpi. Further investigations are required to test this hypothesis and to determine what function, if any, SEVs may play in fungal root infection. In contrast, *G. tritici* infections resulted in far fewer DEGs at 5 dpi (1,074), the majority of which were upregulated. Interestingly, almost all DEGs identified in response to *G. tritici* infection were also shared with the wheat response to *G. hyphopodioides* colonisation. Despite triggering a significant wheat defence response, *G. tritici* successfully causes disease, suggesting an ability to either suppress or overcome the local wheat defences triggered. Therefore, future studies should focus on the elucidation of *G. tritici* effectors, enzymes, and secondary metabolites, which no doubt contribute to *G. tritici* pathogenicity. One such effector, the ortholog of the barley powdery mildew effector gene BEC1019, has already been associated with *G. tritici* virulence in wheat (Zhang et al., 2019).

Strikingly, 11% of all known cell-wall organisation/biogenesis related genes in wheat were downregulated in *G. hyphopodioides*–colonised plants at 5 dpi, whereas none were significantly downregulated in response to *G. tritici*. Impairment of cell-wall integrity (CWI) by pathogen invasion triggers the release of antimicrobial compounds and DAMPs, the latter inducing plant innate immune responses upon recognition by plant pattern recognition receptors (Miedes et al., 2014). In this study, *G. hyphopodioides* colonisation triggered the downregulation of 13 *FLA* genes and 18 *XTH* genes. FLA proteins contain a putative cell adhesion domain, which may link the cell membrane and the cell wall. *FLA* mutants in Arabidopsis exhibit a range of phenotypes including reduced cellulose content, altered secondary cell-wall deposition, and reduced tensile strength (Ashagre et al., 2021). *XTH* genes are also involved in the maintenance of CWI; these genes encode xyloglucan modifying enzymes that cleave xyloglucan chains to enable cell-wall expansion or alter cell-wall strength (Cosgrove, 2005). In addition, we detected the downregulation of 10 *CESA* genes. Although the exact mechanism is not yet known, a number of studies in Arabidopsis indicate a link between *CESA* expression, CWI, and disease resistance. Mutations in the *CESA4*, *CESA7*, and *CESA8* genes, required for secondary cell-wall formation in Arabidopsis, confer enhanced resistance to the necrotrophic fungus *Plectrosphaerella cucumerina* and the biotrophic bacterium *Ralstonia solanacearum* (Hernández-Blanco et al., 2007). In addition, pathogenic *Fusarium oxysporum* root infection of Arabidopsis results in the downregulation of various *CESAs*, causing an alteration in primary cell-wall cellulose and contributing to disease resistance (Menna et al., 2021). Furthermore, mutations in *CESA* genes in Arabidopsis trigger the activation of defence responses and the biosynthesis of lignin, regulated at least in part, by the JA and ET signalling pathways (Caño-Delgado et al., 2003). A link between JA/ET signalling and reduced cellulose levels has also previously been reported by Ellis et al. (2002). Thus, our finding that *G. hyphopodioides* colonisation results in the upregulation of lignin biosynthesis genes and JA/ET signalling genes is pertinent.

Lignin polymers are a major component of the secondary cell wall of vascular plants, and lignin biosynthesis is known to be upregulated in response to pathogen attack by functioning as a physical barrier. Increased lignification is well-known to cause a physical barrier to microbial invasion (Miedes et al., 2014). Increased levels of lignin are present in cell-wall appositions such as papillae, which form one of the first layers of plant immunity, and in lignitubers, which surround invading hyphae. Both responses slow pathogen growth (Łaźniewska et al., 2012). Increased lignification has been documented in response to colonisation by beneficial fungi such as Trichoderma species, potentially playing a role in induced resistance against plant pathogens (Basińska-Barczak et al., 2020). Indeed, previous studies have reported higher levels of cell-wall lignification in response to colonisation by several non-pathogenic *Magnaporthaceae* species (Huang et al., 2001; Speakman and Lewis, 1978). In the present study, we detected earlier and higher expression of lignin biosynthesis genes in *G. hyphopodioides*–colonised tissues compared to *G. tritici*–infected tissues. In contrast, local cell-wall lignification (as determined by potassium permanganate staining) was more prominent in *G. tritici*–infected roots at 5 dpi. However, the downregulation of

several *COMT* genes in response to *G. hyphopodioides* is noteworthy. *COMT* genes are involved in the synthesis of the S unit of lignin, and downregulation of these genes has a minimal effect on total lignin content (Nguyen et al., 2016). Such changes in lignin composition can drastically alter the outcome of plant-pathogen interactions (Höch et al., 2021; Ma et al., 2018; Quentin et al., 2009). Therefore, despite contrasting results, cell-wall lignification could play an important role in *G. hyphopodioides*–mediated take-all control.

In our dataset, 26 genes encoding TIFY TFs, involved in the cross-talk between JA and other phytohormones (Singh and Mukhopadhyay, 2021) were upregulated in response to *G. hyphopodioides* at 5 dpi. Just three *TIFY* TFs were significantly upregulated in response to *G. tritici*. In addition, *G. hyphopodioides* colonisation resulted in the upregulation of a greater number of *ERF-like* genes, known to integrate ET and JA signal transduction pathways (Lorenzo et al., 2003). Phytohormone quantifications using ultrahigh-performance liquid chromatography yielded highly variable results, and we were unable to detect significant differences in JA or SA levels between treatments. Although a somewhat surprising finding, this finding could potentially be explained by the early stage of infection captured, at which point take-all root lesions had not yet developed. The high levels of variability may also be a result of the transient nature of phytohormone signalling, particularly in the case of JA (Ruan et al., 2019). Future studies should probably quantify phytohormone levels across different time points, from early infection through to disease symptom development. Thus, unlike in EMR by non-pathogenic *Fusarium* species, *G. hyphopodioides*–induced resistance is potentially mediated, at least to some extent, by the JA/ET signalling pathway. Further investigation is required to determine whether the disruption of CWI mechanisms is directly responsible for the activation of JA/ET-mediated defence pathway and the lignin biosynthesis pathway. In addition, future studies should investigate plant and fungal gene expression during *G. tritici* infection of roots already colonised by *G. hyphopodioides*.

The biocontrol potential of several non-pathogenic *Magnaporthaceae* species has been reported since the 1970s (Deacon, 1973, 1976b; Wong and Southwell, 1980). However, the precise mechanisms of control and the molecular pathways underpinning these interactions have remained underexplored. In this study, we show that induced wheat resistance mechanisms play a key role in *G. hyphopodioides*–mediated disease reduction. Furthermore, we demonstrate that these resistance mechanisms operate at a local scale, with effective disease protection conferred in roots pre-treated with *G. hyphopodioides*. However, adding *G. hyphopodioides* after *G. tritici* resulted in increased take-all disease levels; hence, the application of *G. hyphopodioides* to wheat fields already harbouring significant levels of *G. tritici* inoculum is unlikely to provide disease control. Such a strategy may even be detrimental to disease control efforts. Therefore, the potential for *G. hyphopodioides* to become pathogenic in wheat and/or other cereal crops requires careful investigation. Future studies should also investigate the potential cost of *G. hyphopodioides*–mediated resistance on plant health and yield. Though *G. hyphopodioides*–mediated resistance operates at a local scale, the induction of diverse defence pathways may create a trade-off with plant growth (He et al., 2022). In addition, cell-wall reinforcement with lignins may limit root growth, potentially having downstream effects on soil anchorage and water/nutrient uptake pathways. Nevertheless, farmers may carefully exploit the disease suppression ability of *G. hyphopodioides* by growing wheat cultivars known to support natural *G. hyphopodioides* populations, particularly when placed early in wheat rotations prior to the buildup of *G. tritici* inoculum (Osborne et al., 2018).

In summary, we demonstrate rapid and extensive transcriptional reprogramming in *G. hyphopodioides*–colonised wheat roots, characterised by the strong local induction of diverse plant defence mechanisms. We propose that the collective effects of these local defence mechanisms, particularly relating to cell wall–related resistance, are responsible for *G. hyphopodioides*–mediated take-all control. Due to the lack of high-quality annotated *G. tritici* and *G. hyphopodioides* genomes, comparative analysis of fungal gene expression during *G. hyphopodioides* colonisation and *G. tritici* infection was not possible in this study. When combined with the RNA-seq dataset presented here, future genome sequencing projects will no doubt facilitate the investigation of novel *G. tritici* pathogenicity factors. In addition, further analysis of non-pathogenic and pathogenic fungi within the diverse *Magnaporthaceae* family may help to address wider questions relating to pathogen organ specificity, conserved fungal root infection strategies, and the determinants of fungal pathogenicity.

Data availability statement

The datasets presented in this study can be found in online repositories. The names of the repository/repositories and accession number(s) can be found in the article/Supplementary Material.

Author contributions

TC: Writing – review & editing, Writing – original draft, Visualization, Validation, Resources, Project administration, Methodology, Investigation, Formal analysis, Data curation, Conceptualization. DS: Writing – review & editing, Writing – original draft, Methodology, Formal analysis, Data curation. WC: Writing – review & editing, Investigation, Formal analysis. SC: Writing – review & editing, Methodology, Formal analysis. EV: Writing – review & editing, Methodology, Investigation. KH: Writing – review & editing, Methodology, Investigation. EC: Writing – review & editing, Methodology, Investigation. VM: Writing – review & editing, Supervision, Methodology, Funding acquisition, Conceptualization. GC: Writing – review & editing, Methodology, Investigation. VA: Writing – review & editing, Methodology, Investigation. KH-K: Writing – review & editing, Writing – original draft, Supervision, Resources, Methodology, Funding acquisition, Conceptualization. JP-G: Writing – review & editing, Writing – original draft, Supervision, Resources, Project administration, Methodology, Investigation, Funding acquisition, Conceptualization.

Funding

The author(s) declare financial support was received for the research, authorship, and/or publication of this article. TC was supported by the Biotechnology and Biological Sciences Research Council (BBSRC) funded University of Nottingham Doctoral Training Programme (BB/M008770/1). JP-G, DS, and KH-K were supported by the BBSRC Institute Strategic Programme (ISP) Grant, Designing Future Wheat (BBS/E/C/000I0250). In addition, DS is supported by the BBSRC ISP Grant (BB/CCG2280/1) and KH-K by the BBSRC ISP Grant, Delivering Sustainable Wheat (BB/X011003/1 and BBS/E/RH/230001B). GC is supported by the DEFRA funded Wheat Genetic Improvement Network, WGIN (CH0109) and the BBSRC ISP Growing Health (BBS/E/RH/230003A). VA is supported by the BBSRC funded South West Biosciences Doctoral Training Partnership (BB/T008741/1).

Acknowledgments

We thank Smita Kurup and Hannah Walpole (Plant Sciences for the Bioeconomy, Rothamsted Research) for advice and assistance with fluorescent staining and confocal microscopy of wheat roots; Jess Hammond (Protecting Crops and the Environment, Rothamsted Research) for help with fungal isolations and plant care; and Matthew Dickinson (University of Nottingham) for his feedback on the project.

Conflict of interest

The authors declare that the research was conducted in the absence of any commercial or financial relationships that could be construed as a potential conflict of interest.

Publisher's note

All claims expressed in this article are solely those of the authors and do not necessarily represent those of their affiliated organizations, or those of the publisher, the editors and the reviewers. Any product that may be evaluated in this article, or claim that may be made by its manufacturer, is not guaranteed or endorsed by the publisher.

Supplementary material

The Supplementary Material for this article can be found online at: https://www.frontiersin.org/articles/10.3389/fpls.2024.1444271/full#supplementary-material

References

Ashagre, H., Zaltzman, D., Idan-Molakandov, A., Romano, H., Tzfadia, O., and Harpaz-Saad, S. (2021). FASCICLIN-LIKE 18 is a new player regulating root elongation in *Arabidopsis thaliana*. *Front. Plant Sci.* 12. doi: 10.3389/FPLS.2021.645286/BIBTEX

Asher, M. J. C., and Shipton, P. J. (1981). *Biology and control of take-all*. Academic Press, London, United Kingdom.

Ban, Y., Tang, M., Chen, H., Xu, Z., Zhang, H., and Yang, Y. (2012). The response of dark septate endophytes (DSE) to heavy metals in pure culture. *PLoS ONE* 7 (10), e47968. doi: 10.1371/journal.pone.0047968

Basińska-Barczak, A., Błaszczyk, L., and Szentner, K. (2020). Plant cell wall changes in common wheat roots as a result of their interaction with beneficial fungi of *Trichoderma*. *Cells* 9 (10), 2319. doi: 10.3390/cells9102319

Benjamini, Y., and Hochberg, Y. (1995). Controlling the false discovery rate: A practical and powerful approach to multiple testing. *J. R. Stat. Society: Ser. B (Methodological)* 57 (10), 289–300. doi: 10.1111/J.2517-6161.1995.TB02031.X

Bolger, A. M., Lohse, M., and Usadel, B. (2014). Trimmomatic: A flexible trimmer for Illumina sequence data. *Bioinformatics* 30, 2114–2120. doi: 10.1093/bioinformatics/btu170

Boller, T., and Felix, G. (2009). A renaissance of elicitors: perception of microbe-associated molecular patterns and danger signals by pattern-recognition receptors. *Annu. Rev. Plant Biol.* 60, 379–406. doi: 10.1146/annurev.arplant.57.032905.105346

Bradshaw, R. E., Bellgard, S. E., Black, A., Burns, B. R., Gerth, M. L., McDougal, R. L., et al. (2020). *Phytophthora agathidicida*: research progress, cultural perspectives and knowledge gaps in the control and management of kauri dieback in New Zealand. *Plant Pathol.* 69, 3–16. doi: 10.1111/ppa.13104

Caño-Delgado, A., Penfield, S., Smith, C., Catley, M., and Bevan, M. (2003). Reduced cellulose synthesis invokes lignification and defense responses in *Arabidopsis thaliana*. *Plant J.* 34, 351–362. doi: 10.1046/j.1365-313X.2003.01729.x

Choudhary, D. K., Prakash, A., and Johri, B. N. (2007). Induced systemic resistance (ISR) in plants: Mechanism of action. *Indian J. Microbiol.* 47, 289–297. doi: 10.1007/s12088-007-0054-2

Constantin, M. E., de Lamo, F. J., Vlieger, B. V., Rep, M., and Takken, F. L. W. (2019). Endophyte-mediated resistance in tomato to fusarium oxysporum is independent of ET, JA, and SA. *Front Plant Sci.* 10, 1–14. doi: 10.3389/fpls.2019.00979

Cosgrove, D. J. (2005). Growth of the plant cell wall. *Nat. Rev. Mol. Cell Biol.* 6, 850–861. doi: 10.1038/nrm1746

Deacon, J. W. (1973). *Phialophora radicicola* and *Gaeumannomyces graminis* on roots of grasses and cereals. *Trans. Br. Mycological Soc.* 61, 471–485. doi: 10.1016/s0007-1536(73)80117-2

Deacon, J. W. (1976a). Biology of the *Gaeumannomyces graminis* Arx & Olivier/*Phialophora radicicola* Cain Complex on Roots of the *Gramineae*. *EPPO Bull.* 6, 349–363. doi: 10.1111/j.1365-2338.1976.tb02033.x

Deacon, J. W. (1976b). Biological control of the take-all fungus, *Gaeumannomyces graminis*, by *Phialophora radicicola* and similar fungi. *Soil Biol. Biochem.* 8, 275–283. doi: 10.1016/0038-0717(76)90057-2

de Lamo, F. J., and Takken, F. L. W. (2020). Biocontrol by *Fusarium oxysporum* using endophyte-mediated resistance. *Front. Plant Sci.* 11. doi: 10.3389/FPLS.2020.00037/BIBTEX

Delgado-Baquerizo, M., Guerra, C. A., Cano-Díaz, C., Egidi, E., Wang, J. T., Eisenhauer, N., et al. (2020). The proportion of soil-borne pathogens increases with warming at the global scale. *Nat. Climate Change* 10, 550–554. doi: 10.1038/s41558-020-0759-3

Dufresne, M., and Osbourn, A. E. (2001). Definition of tissue-specific and general requirements for plant infection in a phytopathogenic fungus. *Mol. Plant-Microbe Interact.* 14, 300–307. doi: 10.1094/MPMI.2001.14.3.300

Ellis, C., Karafyllidis, I., and Turner, J. G. (2002). Constitutive activation of jasmonate signaling in an Arabidopsis mutant correlates with enhanced resistance to *Erysiphe cichoracearum*, *Pseudomonas syringae*, and *Myzus persicae*. *Mol. Plant-Microbe Interact.* 15, 1025–1030. doi: 10.1094/MPMI.2002.15.10.1025

Francisco, C. S., Ma, X., Zwyssig, M. M., McDonald, B. A., and Palma-Guerrero, J. (2019). Morphological changes in response to environmental stresses in the fungal plant pathogen *Zymoseptoria tritici*. *Sci. Rep.* 9, 1–18. doi: 10.1038/s41598-019-45994-3

Freeman, J., and Ward, E. (2004). *Gaeumannomyces graminis*, the take-all fungus and its relatives. *Mol. Plant Pathol.* 5, 235–252. doi: 10.1111/j.1364-3703.2004.00226.x

Freeman, J., Ward, E., Gutteridge, R. J., and Bateman, G. L. (2005). Methods for studying population structure, including sensitivity to the fungicide silthiofam, of the cereal take-all fungus, *Gaeumannomyces graminis* var. *tritici*. *Plant Pathol.* 54, 686–698. doi: 10.1111/j.1365-3059.2005.01252.x

Gazengel, K., Lebreton, L., Lapalu, N., Amselem, J., Guillerm-Erckelboudt, A. Y., Tagu, D., et al. (2020). pH effect on strain-specific transcriptomes of the take-all fungus. *PloS One* 15 (7), e0236429. doi: 10.1371/journal.pone.0236429

Harris, J. M., Balint-Kurti, P., Bede, J. C., Day, B., Gold, S., Goss, E. M., et al. (2020). What are the top 10 unanswered questions in molecular plant-microbe interactions? *Mol. Plant-Microbe Interact.* 33, 1354–1365. doi: 10.1094/MPMI-08-20-0229-CR

He, Z., Webster, S., and He, S. Y. (2022). Growth–defense trade-offs in plants. *Curr. Biol.* 32, 634–639. doi: 10.1016/j.cub.2022.04.070

Hernández-Blanco, C., Feng, D. X., Hu, J., Sánchez-Vallet, A., Deslandes, L., Llorente, F., et al. (2007). Impairment of cellulose synthases required for Arabidopsis secondary cell wall formation enhances disease resistance. *Plant Cell* 19, 890–903. doi: 10.1105/tpc.106.048058

Hernández-Restrepo, M., Groenewald, J. Z., Elliott, M. L., Canning, G., McMillan, V. E., and Crous, P. W. (2016). Take-all or nothing. *Stud. Mycology* 83, 19–48. doi: 10.1016/j.simyco.2016.06.002

Höch, K., Koopmann, B., and von Tiedemann, A. (2021). Lignin composition and timing of cell wall lignification are involved in Brassica napus resistance to stem rot caused by Sclerotinia sclerotiorum. *Phytopathology* 111 (8), 1438–1448. doi: 10.1094/PHYTO-09-20-0425-R

Holden, J. (1976). Infection of wheat seminal roots by varieties of *Phialophora radicicola* and *Gaeumannomyces graminis*. *Soil Biol. Biochem.* 8, 109–119. doi: 10.1016/0038-0717(76)90074-2

Hu, M., Pei, B. L., Zhang, L. F., and Li, Y. Z. (2014). Histone H2B monoubiquitination is involved in regulating the dynamics of microtubules during the defense response to *Verticillium dahliae* toxins in arabidopsis. *Plant Physiol.* 164, 1857–1865. doi: 10.1104/pp.113.234567

Huang, L., Kang, Z., and Buchenauer, H. (2001). Comparison of infection of wheat roots by *Phialophora graminicola* and *Gaeumannomyces graminis* var. *tritici* by ultrastructural and cytochemical studies. *J. Plant Dis. Prot.* 108, 593–607.

Jones, J. D. G., and Dangl, J. L. (2006). The plant immune system. *Nature* 444, 323–329. doi: 10.1038/nature05286

Kang, H., Fan, T., Wu, J., Zhu, Y., and Shen, W. H. (2022). Histone modification and chromatin remodeling in plant response to pathogens. *Front. Plant Sci.* 13. doi: 10.3389/fpls.2022.986940

Kang, X., Guo, Y., Leng, S., Xiao, L., Wang, L., Xue, Y., et al. (2019a). Comparative Transcriptome Profiling of *Gaeumannomyces graminis* var. *tritici* in Wheat Roots in the Absence and Presence of Biocontrol *Bacillus velezensis* CC09. *Front. Microbiol.* 10. doi: 10.3389/fmicb.2019.01474

Kang, X., Wang, L., Guo, Y., Zain Ul Arifeen, M., Cai, X., Xue, Y., et al. (2019b). A Comparative Transcriptomic and Proteomic Analysis of Hexaploid Wheat's Responses to Colonization by *Bacillus velezensis* and *Gaeumannomyces graminis*, Both Separately and Combined. *Mol. Plant-Microbe Interact.* 32. doi: 10.1094/MPMI-03-19-0066-R

Keenan, S., Cromey, M. G., Harrow, S. A., Bithell, S. L., Butler, R. C., Beard, S. S., et al. (2015). Quantitative PCR to detect *Gaeumannomyces graminis* var. *tritici* in symptomatic and non-symptomatic wheat roots. *Australas. Plant Pathol.* 44, 591–597. doi: 10.1007/s13313-015-0379-y

Kim, D., Paggi, J. M., Park, C., Bennett, C., and Salzberg, S. L. (2019). Graph-based genome alignment and genotyping with HISAT2 and HISAT-genotype. *Nat. Biotechnol.* 37, 907–915. doi: 10.1038/s41587-019-0201-4

Knapp, D. G., Németh, J. B., Barry, K., Hainaut, M., Henrissat, B., Johnson, J., et al. (2018). Comparative genomics provides insights into the lifestyle and reveals functional heterogeneity of dark septate endophytic fungi. *Sci. Rep.* 8, 1–13. doi: 10.1038/s41598-018-24686-4

Łaźniewska, J., Macioszek, V. K., and Kononowicz, A. K. (2012). Plant-fungus interface: The role of surface structures in plant resistance and susceptibility to pathogenic fungi. *Physiol. Mol. Plant Pathol.* 78, 24–30. doi: 10.1016/j.pmpp.2012.01.004

Li, L., Guo, N., Feng, Y., Duan, M., and Li, C. (2022). Effect of Piriformospora indica-Induced Systemic Resistance and Basal Immunity Against *Rhizoctonia cerealis* and *Fusarium graminearum* in Wheat. *Front. Plant Sci.* 13. doi: 10.3389/fpls.2022.836940

Liao, Y., Smyth, G. K., and & Shi, W. (2014). FeatureCounts: An efficient general purpose program for assigning sequence reads to genomic features. *Bioinformatics* 30, 923–930. doi: 10.1093/bioinformatics/btt656

Lorenzo, O., Piqueras, R., Sánchez-Serrano, J. J., and Solano, R. (2003). ETHYLENE RESPONSE FACTOR1 integrates signals from ethylene and jasmonate pathways in plant defense. *Plant Cell* 15, 165–178. doi: 10.1105/TPC.007468

Love, M. I., Huber, W., and Anders, S. (2014). Moderated estimation of fold change and dispersion for RNA-seq data with DESeq2. *Genome Biol.* 15, 550. doi: 10.1186/s13059-014-0550-8

Marcel, S., Paszkowski, U., Sawers, R., Oakeley, E., and Angliker, H. (2010). Tissue-adapted invasion strategies of the rice blast fungus *Magnaporthe oryzae*. *Plant Cell* 22, 3177–3187. doi: 10.1105/tpc.110.078048

Ma, Q. H., Zhu, H. H., and Qiao, M. Y. (2018). Contribution of both lignin content and sinapyl monomer to disease resistance in tobacco. *Plant Pathology* 67 (3), 642–650. doi: 10.1111/PPA.12767

McMillan, V. E., Hammond-Kosack, K. E., and Gutteridge, R. J. (2011). Evidence that wheat cultivars differ in their ability to build up inoculum of the take-all fungus, *Gaeumannomyces graminis* var. *tritici*, under a first wheat crop. *Plant Pathol.* 60, 200–206. doi: 10.1111/j.1365-3059.2010.02375.x

Menna, A., Dora, S., Sancho-Andrés, G., Kashyap, A., Meena, M. K., Sklodowski, K., et al. (2021). A primary cell wall cellulose-dependent defense mechanism against vascular pathogens revealed by time-resolved dual transcriptomics. *BMC Biol.* 19, 1–20. doi: 10.1186/s12915-021-01100-6

Miedes, E., Vanholme, R., Boerjan, W., and Molina, A. (2014). The role of the secondary cell wall in plant resistance to pathogens. *Front. Plant Sci.* 5. doi: 10.3389/fpls.2014.00358

Nguyen, T. N., Son, S. H., Jordan, M. C., Levin, D. B., and Ayele, B. T. (2016). Lignin biosynthesis in wheat (*Triticum aestivum* L.): Its response to waterlogging and association with hormonal levels. *BMC Plant Biol.* 16. doi: 10.1186/s12870-016-0717-4

Okagaki, L. H., Nunes, C. C., Sailsbery, J., Clay, B., Brown, D., John, T., et al. (2015). Genome sequences of three phytopathogenic species of the magnaporthaceae family of fungi. *Genes, Genomes, Genetics* 5. doi: 10.1534/g3.115.020057

Osborne, S. J., McMillan, V. E., White, R., and Hammond-Kosack, K. E. (2018). Elite UK winter wheat cultivars differ in their ability to support the colonization of beneficial root-infecting fungi. *J. Exp. Bot.* 69, 3103–3115. doi: 10.1093/jxb/ery136

Palma-Guerrero, J., Chancellor, T., Spong, J., Canning, G., Hammond, J., McMillan, V. E., et al. (2021). Take-all disease: new insights into an important wheat root pathogen. *Trends Plant Sci.* 26, 836–848. doi: 10.1016/j.tplants.2021.02.009

Park, J. R., Kim, E. G., Jang, Y. H., Yun, B. J., and Kim, K. M. (2022). Selection strategy for damping-off resistance gene by biotechnology in rice plant. *Plant Soil* 474, 277–296. doi: 10.1007/s11104-022-05334-3

Pieterse, C. M. J., Zamioudis, C., Berendsen, R. L., Weller, D. M., Van Wees, S. C. M., and Bakker, P. A. H. M. (2014). Induced systemic resistance by beneficial microbes. *Annu. Rev. Phytopathol.* 52, 347–375. doi: 10.1146/annurev-phyto-082712-102340

Pok, B., Ngou, M., Ding, P., and Jones, J. D. G. (2022). Thirty years of resistance: Zig-zag through the plant immune system. *Plant Cell* 34, 1447–1478. doi: 10.1093/PLCELL/KOAC041

Polturak, G., Dippe, M., Stephenson, M. J., Misra, R. C., Owen, C., Ramirez-Gonzalez, R. H., et al. (2022). Pathogen-induced biosynthetic pathways encode defense-related molecules in bread wheat. *PNAS* 119 (116), e2123299119. doi: 10.1073/pnas.2123299119

Qiang, X., Weiss, M., Kogel, K.-H., and Schäfer, P. (2012). *Piriformospora indica*-a mutualistic basidiomycete with an exceptionally large plant host range: mutualistic root symbiosis. *Mol. Plant Pathol.* 13, 508–518. doi: 10.1111/j.1364-3703.2011.00764.x

Quentin, M., Allasia, V., Pegard, A., Allais, F., Ducrot, P. H., Favery, B., et al. (2009). Imbalanced lignin biosynthesis promotes the sexual reproduction of homothallic oomycete pathogens. *PLoS Pathogens* 5 (1), 1–9. doi: 10.1371/journal.ppat.1000264

Ruan, J., Zhou, Y., Zhou, M., Yan, J., Khurshid, M., Weng, W., et al. (2019). Jasmonic acid signaling pathway in plants. *Int. J. Mol. Sci.* 20, 2479. doi: 10.3390/ijms20102479

Shalaby, S., and Horwitz, B. A. (2015). Plant phenolic compounds and oxidative stress: integrated signals in fungal–plant interactions. *Curr. Genet.* 61, 347–357. doi: 10.1007/s00294-014-0458-6

Singh, P., and Mukhopadhyay, K. (2021). Comprehensive molecular dissection of TIFY Transcription factors reveal their dynamic responses to biotic and abiotic stress in wheat (*Triticum aestivum* L.). *Sci. Rep.* 11, 1–17. doi: 10.1038/s41598-021-87722-w

Speakman, J. B., and Lewis, B. G. (1978). Limitation of *Gaeumannomyces graminis* by wheat root responses to *Phialophora radicicola*. *New Phytol.* 80, 373–380. doi: 10.1111/j.1469-8137.1978.tb01571.x

Thoms, D., Liang, Y., and Haney, C. H. (2021). Maintaining symbiotic homeostasis: How do plants engage with beneficial microorganisms while at the same time restricting pathogens? *Mol. Plant-Microbe Interact.* 34, 462–469. doi: 10.1094/MPMI-11-20-0318-FI

Ulrich, K., Augustin, C., and Werner, A. (2000). Identification and characterization of a new group of root-colonizing fungi within the *Gaeumannomyces-Phialophora* complex. *New Phytol.* 145, 127–135. doi: 10.1046/j.1469-8137.2000.00553.x

Wang, J., Lian, N., Zhang, Y., Man, Y., Chen, L., Yang, H., et al. (2022). The cytoskeleton in plant immunity: dynamics, regulation, and function. *Int. J. Mol. Sci.* 23, 15553. doi: 10.3390/ijms232415553

Ward, E., and Bateman, G. L. (1999). Comparison of *Gaeumannomyces*- and *Phialophora*-like fungal pathogens from maize and other plants using DNA methods. *New Phytol.* 141, 323–331. doi: 10.1046/j.1469-8137.1999.00346.x

Wong, P. T. W., Mead, J. A., and Holley, M. P. (1996). Enhanced field control of wheat take-all using cold tolerant isolates of *Gaeumannomyces graminis* var. *graminis* and Phialophora sp. (lobed hyphopodia). *Plant Pathol.* 45, 285–293. doi: 10.1046/j.1365-3059.1996.d01-132.x

Wong, P. T. W., and Southwell, R. J. (1980). Field control of take-all of wheat by avirulent fungi. *Ann. Appl. Biol.* 94, 41–49. doi: 10.1111/j.1744-7348.1980.tb03894.x

Yang, L., Xie, L., Xue, B., Goodwin, P. H., Quan, X., Zheng, C., et al. (2015). Comparative Transcriptome Profiling of the Early Infection of Wheat Roots by *Gaeumannomyces graminis* var. *tritici*. *PloS One* 10, e0120691. doi: 10.1371/journal.pone.0120691

Zechmann, B. (2020). Subcellular roles of glutathione in mediating plant defense during biotic stress. *Plants* 9, 1–21. doi: 10.3390/plants9091067

Zhang, Y., Xu, K., Yu, D., Liu, Z., Peng, C., Li, X., et al. (2019). The highly conserved barley powdery mildew effector BEC1019 confers susceptibility to biotrophic and necrotrophic pathogens in wheat. *Int. J. Mol. Sci.* 20, 1–16. doi: 10.3390/ijms20184376

Zhang, J., Yan, H., Xia, M., Han, X., Xie, L., Goodwin, P. H., et al. (2020). Wheat root transcriptional responses against *Gaeumannomyces graminis* var. *tritici*. *Phytopathol. Res.* 2. doi: 10.1186/s42483-020-00066-7

Zhou, F., Emonet, A., Dénervaud Tendon, V., Marhavy, P., Wu, D., Lahaye, T., et al. (2020). Co-incidence of damage and microbial patterns controls localized immune responses in roots. *Cell* 180, 440–453. doi: 10.1016/j.cell.2020.01.013

Zhu, T., Wang, L., Rimbert, H., Rodriguez, J. C., Deal, K. R., De Oliveira, R., et al. (2021). Optical maps refine the bread wheat *Triticum aestivum* cv. Chinese Spring genome assembly. *Plant J.* 107, 303–314. doi: 10.1111/TPJ.15289

COPYRIGHT

© 2024 Chancellor, Smith, Chen, Clark, Venter, Halsey, Carrera, McMillan, Canning, Armer, Hammond-Kosack and Palma-Guerrero. This is an open-access article distributed under the terms of the Creative Commons Attribution License (CC BY). The use, distribution or reproduction in other forums is permitted, provided the original author(s) and the copyright owner(s) are credited and that the original publication in this journal is cited, in accordance with accepted academic practice. No use, distribution or reproduction is permitted which does not comply with these terms.

frontiers | Frontiers in Plant Science

TYPE Original Research
PUBLISHED 10 October 2024
DOI 10.3389/fpls.2024.1468437

Check for updates

OPEN ACCESS

EDITED BY
Yasser Nehela,
University of Florida, United States

REVIEWED BY
Xiaofeng Su,
Chinese Academy of Agricultural Sciences, China
Jingyi Zhang,
Oklahoma State University, United States
Luigi Fiorentino,
Wageningen University and Research, Netherlands

*CORRESPONDENCE
Jianxiu Hao
haojianxiu1003@163.com
Hongyou Zhou
hongyouzhou2002@aliyun.com

RECEIVED 22 July 2024
ACCEPTED 23 September 2024
PUBLISHED 10 October 2024

CITATION
Zhang Z, Wang D, Dong B, Wang Y, Xu J, Hao J and Zhou H (2024) A protein elicitor PeVn1 from *Verticillium nonalfalfae* HW recognized as a MAMP triggers plant immunity response.
Front. Plant Sci. 15:1468437.
doi: 10.3389/fpls.2024.1468437

COPYRIGHT
© 2024 Zhang, Wang, Dong, Wang, Xu, Hao and Zhou. This is an open-access article distributed under the terms of the Creative Commons Attribution License (CC BY). The use, distribution or reproduction in other forums is permitted, provided the original author(s) and the copyright owner(s) are credited and that the original publication in this journal is cited, in accordance with accepted academic practice. No use, distribution or reproduction is permitted which does not comply with these terms.

A protein elicitor PeVn1 from *Verticillium nonalfalfae* HW recognized as a MAMP triggers plant immunity response

Ziyu Zhang, Dong Wang, Baozhu Dong, Yu Wang, Jialu Xu, Jianxiu Hao* and Hongyou Zhou*

College of Horticulture and Plant Protection, Inner Mongolia Agricultural University, Key Laboratory of Biopesticide Creation and Resource Utilization for Autonomous Region Higher Education Institutions, Hohhot, China

Protein elicitors can induce plant systemic resistance to pathogens. The recognition of a potential elicitor activates intracellular signaling events, leading to plant resistance against pathogens. In this study, a novel protein elicitor was isolated from the culture filtrate of *Verticillium nonalfalfae* and named PeVn1, which can induce cell death in several plant species. The PeVn1 gene was then cloned and expressed in *Escherichia coli*. The recombinant protein PeVn1 triggers cell death in *Nicotiana benthamiana* in *NbBAK1* and *NbSOBIR1* dependent manner. Through bioassay analysis showed that the recombinant PeVn1 induced early defense induction events, such as reactive oxygen species burst, callose deposition and the activation of defense hormone signaling pathways and defense enzyme activities. Moreover, PeVn1 significantly enhanced resistance of *Nicotiana benthamiana* to *Sclerotinia sclerotiorum*, *Botrytis cinerea* and *N. benthamiana* mosaic virus and tomato to *Pseudomonas syringae* pv. *Tomato* DC3000. In conclusion, our study reveals that PeVn1 protein as a microbe-associated molecular pattern can induce plant immune responses, which provides a theoretical basis for the development of novel protein-induced disease resistance agents.

KEYWORDS

elicitors, *Verticillium nonalfalfae*, PeVn1, resistance, microbe-associated molecular pattern

1 Introduction

Plant immune system is divided into two main layers, the first basic immune response is triggered mainly by pattern recognition receptors (PRRs) located on the surface of plant cells that recognize highly conserved Microbe-Associated Molecular Patterns (MAMPs) from pathogenic or non-pathogenic bacteria (Boller and He, 2009)), which are essential for microbial growth or lifestyles (Zipfel and Felix, 2005; Jones and Dangl, 2006). Thus the defense response induced by PRRs mediated perception of MAMP is also known as Pattern-

Triggered Immunity (PTI) or Microbe-Associated Molecular Patterns-Triggered Immunity MAMP-Triggered Immunity (MTI) (Liu et al., 2014). This response is accompanied by disease-fighting responses such as rapid changes in intracellular ion levels, bursts of reactive oxygen species (ROS), calcium-dependent protein kinases (CDPK), activation of Mitogen-Activated Protein Kinases (MAPK) cascades, activation of the expression of a number of related immune genes, and callosal deposition that can effectively inhibit the invasion of the vast majority of pathogenic bacteria in the environment (Boudsocq and Sheen, 2013; Ranf et al., 2015). Many PRRs rely on BRASSINOSTEROID INSENSITIVE 1-ASSOCIATED RECEPTOR KINASE 1 (BAK1) family proteins as well as SUPPRESSOR OF BIR1-1 (SOBIR1) to trigger defense responses (Liebrand et al., 2014). ROS are believed to be a signaling molecule for plant defense and interact with other signaling networks in plants (Miller et al., 2008). ROS accumulation is controlled by enzymes that detoxify ROS, such as superoxide dismutase (SOD), catalase (CAT), ascorbate peroxidase (POD), and glutathione reductase (Apel and Hirt, 2004).

To date, a large number of MAMP/PAMP have been reported in plant pathogenic viruses, bacteria, fungi and oomycetes, and these MAMP can be categorized according to the type of substances: proteins, organic glycoconjugates, lipids or lipopeptides (Zipfel and Felix, 2005; Boudsocq and Sheen, 2013). In bacteria flagellin is one of the most studied MAMPs, and the Arabidopsis receptor FLS2, which recognizes bacterial flagellin, belongs to the LRR-RLK. A conserved 22-amino-acid sequence at the N-terminus of bacterial flagellin (flg22) is sufficient for FLS2 recognition (Zipfel and Felix, 2005). In fungi chitin is one of the most studied MAMPs. Chitin is recognized by the phytochitin receptor (CERK1) and lysine motif receptor kinase 5 (LYK5), mediating downstream immune responses (Langner and Göhre, 2016). In addition, proteins secreted by pathogenic bacteria, also known as MAMPs, are inducing an immune response and enhancing plant resistance by referring to classes of MAMPs as elicitor, which can be categorized as proteins, glycans, peptides, lipids, and others (Boutrot and Zipfel, 2017).

Elicitors induced defense responses are currently receiving a great deal of attention in the study of plant induced resistance responses (Czobor et al., 2017). The protein elicitor PeBL1 was previously screened from *Brevibacillus laterosporus* strain A60 (Wang et al., 2015). This elicitor stimulates typical defense responses, such as allergic responses, ROS bursts, extracellular alkalinization, and lignin accumulation in *N. benthamiana* leaves and increases *N. benthamiana* resistance to tobacco mosaic virus (TMV)-GFP and systemic resistance to *Pseudomonas syringae* pv. *tabaci*. PevD1 from *Verticillium dahliae* induces the accumulation of phenolics, callose, and lignin and enhances resistance to TMV and *V. dahliae* infection in *N. benthamiana* (Wang et al., 2012; Liang et al., 2018). The protein elicitor PeSy1 isolated from strain *Sclerotinia yanglingensis* Hhs.015 induced resistance to *N. benthamiana* and acted as a Microbial-Associated Molecular Patterns (MAMP) to induce an immune response in the plant, which enhanced resistance to *S. sclerotiorum*, *Phytophthora capsica* and other pathogenic bacteria (Wang et al., 2023). Although numerous elicitors have been identified, our comprehension of how these agents initiate plant defense responses remains incomplete (Pršić and Ongena, 2020).

Verticillium nonalfalfae is another pathogenic species that has a more limited host range than *V. dahliae* (Inderbitzin et al., 2011). However, it is a causal agent of *Verticillium* wilt, which results in the death of several important crops (Inderbitzin and Subbarao, 2014). The infestation of hops (Humulus lupulus L.) by *V. nonalfalfae* has been reported with the occurrence of strains of different virulence. Pathogenic strains can lead to a reduction in hops production. By analyzing the whole genome sequencing of *V. nonalfalfae*, a large number of secreted proteins have been obtained, among which key proteins have been identified as virulence factors (Marton et al., 2018). The endoglucanase VdEG-1 (Novo et al., 2006) and the specific secreted protein VdSSP1 (Liu et al., 2013) are further potential carbohydrate-degrading enzymes important for *V. dahliae* pathogenicity. VnaPRX1.1277 and VnaSSP4.2 are required virulence factors to promote colonization of hop plants by *V. dahliae* (Flajsman et al., 2016). The secreted Aspf2-like protein VDAL in *V. dahliae* is responsible for the wilting of plant leaves. Overexpression of VDAL in *Arabidopsis thaliana* and cotton resulted in enhanced resistance of the overexpressed plants to *V. dahliae*, while not affecting normal plant growth and development (Jiang et al., 2022). Ave1 is a secreted protein that is specific to the *V. dahliae* race 1. It is capable of triggering immunity by recognizing the Ve1 tomato resistance receptor (Jonge et al., 2012). Consequently, elicitors that activate plant immunity can be used to enhance plant disease resistance.

Nevertheless, many *V. nonalfalfae* secreted proteins regulating plant immunity remain to be characterized. In this study, a novel secreted MAMP, named PeVn1, was isolated and characterized from *V. nonalfalfae*. PeVn1 stimulates disease resistance and induces immune responses in *N. benthamiana*. Moreover, it is dependent on *BAK1* and *SOBIR1* to induce plant cell death, further elucidating the mechanisms by which PeVn1 induces plant immunity. Our findings provide a potential strategy for the biological control of agricultural diseases.

2 Results

2.1 Isolation and identification of the *V. nonalfalfae* HW protein MAMP

This study showed that the supernatant from the culture filtrate broth of *V. nonalfalfae* HW induced cell death in *N. benthamiana* leaves. Crude proteins were extracted from the culture filtrate supernatant at a saturated concentration of 75% ammonium sulfate and dialyzed to induce cell death in the *N. benthamiana* leaves (Supplementary Figures 1). The active fractions were purified using a Superdex 200 increase 10/300 GL, yielding three peaks (Figure 1A).The fraction corresponding to peak A3 induced cell death activity in tobacco (Figure 1B). As shown in SDS-PAGE, a single band was identified from A3 with a size of about 15 kDa. To determine the identity of the protein present in A3, a single SDS-PAGE band was cut and identified by mass spectrometry (Figure 1C). Based on liquid chromatography tandem mass spectrometry, reliable sequences were obtained for six peptides: (a) SMAVASTTWTIENTR, (b) QIVWPAYTDKQLAK, (c) AVVVKPNQNYPVQALP, (d)

10.3389/fpls.2024.1468437

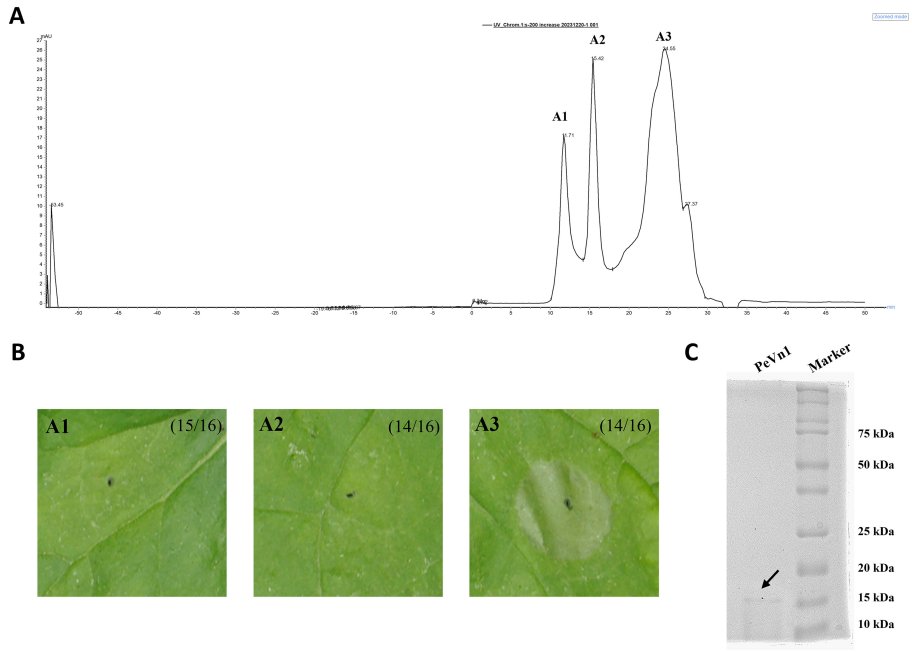

FIGURE 1
Separation and purification of MAMP with potential cell death activity from *V. nonalfalfae* HW. **(A)** Chromatogram by Superdex 200 increase 10/300 GL gel column. **(B)** Cell death activity was determined by pairwise fractionation of fractions 1, 2 and 3 obtained from fractions 1, 2 and 3. **(C)** Detection of fraction 3 by Thomas blue staining, SDS-PAGE running gel. black arrows represent the target proteins of fraction 3.

QLAKAVVVKPNQNYPVQALP, (e) SSKQIVWPAYTDK and (f) ANDCTWTFSVNTGSSNTPCTFHTK. The peptides showed high similarity to the putative protein from *V. nonalfalfae* VnAa140/NRRL 66861 by sequence comparison using BLASTp (XP. 028497723.1). Based on these results, the coding sequence of the protein secreted from *V. nonalfalfae* HW was determined. The coding sequence was cloned into a *pET* vector (with a His tag) with the signal peptide region removed and expressed in *E. coli* BL21 cells. The recombinant protein was purified using HisPur Ni-NTA resin. Its molecular weight was approximately 15 kDa according to SDS-PAGE (Supplementary Figures 2A). Cell death was detected by infiltrated *N. benthamiana* leaves in the recombinant protein. The results demonstrated that the recombinant protein could induce cell death after 3 days (Supplementary Figures 2B). Leaf cell death was observed by trypan blue staining. We hypothesized that PeVn1 is a MAMP secreted by *V. nonalfalfae* HW.

2.2 PeVn1 characterization

The SMART analysis indicates that PeVn1 is a putative protein with no significant structural matches, with the exception of the signal peptide (Figure 2A). To further verify whether PeVn1 is a secreted protein, The PeVn1 signal peptide was tested using an invertase enzyme to examine its function for secretion in yeast (Jacobs et al., 1997). The signal peptide was inserted into the *pSUC2* vector, which was transformed into the YTK12 yeast strain. All transformants containing the positive control Avr1b signal peptide or the test PeVn1 grew well on the CMD−W and YPRAA plates, indicating that the PeVn1 signal peptide had a secretion function. In addition, the enzyme activity of the secreted invertase from the transformants was detected *in vivo*. 2,3,5-triphenyl tetrazolium chloride was converted into the insoluble red-colored 1,3,5-triphenyl formazan after adding yeast containing Avr1b or $PeVn1^{SP}$, indicating that invertase was secreted from the yeast in the presence of the PeVn1 signal peptide (Supplementary Figure 3). PeVn1 consists of 146 amino acid residues, of which the first 19 are N-terminal signal peptides with a molecular weight of 15 kDa and a PI of 9.42. A phylogenetic tree was constructed using fifteen sequences with high homology to PeVn1 obtained from the NCBI database (Figure 2B). Multiple sequence comparisons based on homologous sequences showed that PeVn1 belongs to *Verticillium* spp., but its protein sequence was 66.32% similar (Figure 2C) and conserved in *Verticillium* sp., with 49.57% similarity (Figure 2D). The protein structure was predicted by SWISS-MODEL and the structural confidence of the best-matched structure of PeVn1 was 95.14% with only 10 β-folding (Figure 2E). These results suggested that PeVn1 is a secreted protein that is conserved in *V. nonalfalfae*.

2.3 Protein PeVn1 induces cell death in plants

The cell death activity of recombinant PeVn1 in tobacco was further analyzed. Necrotic areas appeared in *N. benthamiana* leaf

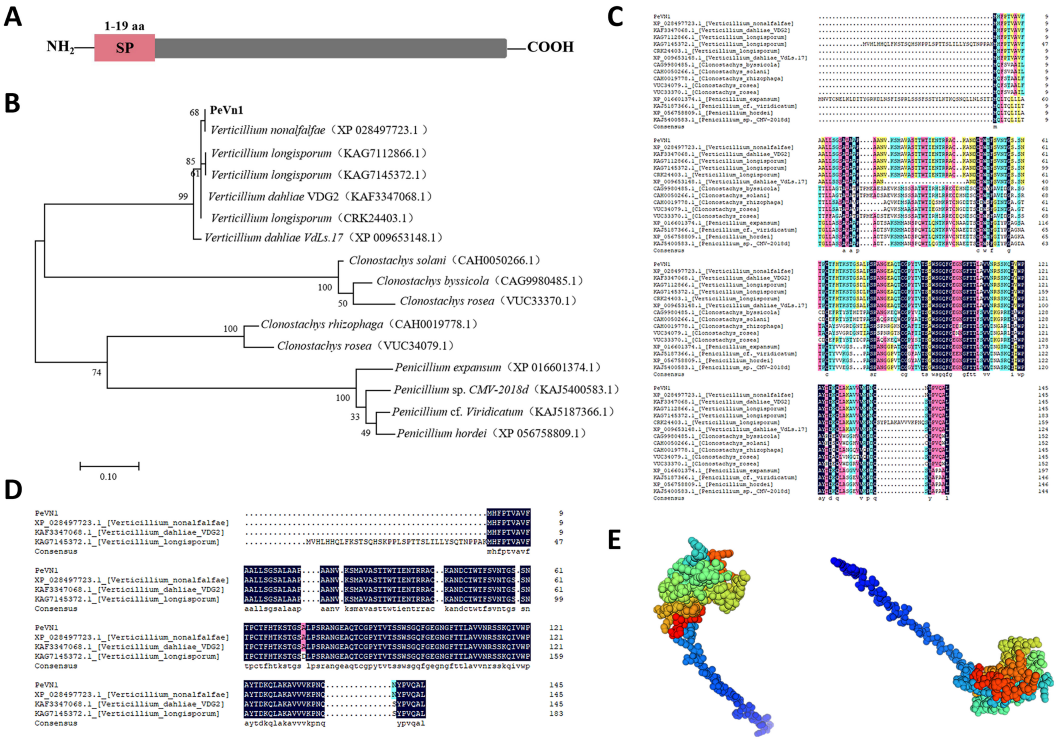

FIGURE 2
Bioinformatics analysis of PeVn1. **(A)** Signal peptide prediction of PeVn1,N-terminal 1-19 aa is the signal peptide region. **(B)** Construction of a phylogenetic tree of PeVn1 based on amino acid sequences. **(C, D)** Conserved region analysis of PeVn1. Colored boxes represent conserved amino acid. **(E)** Prediction of the tertiary structure of PeVn1.

blades after infiltrated in different concentrations of PeVn1, 3 days after treatment (Figure 3A). Cell death increased with increasing concentration, and the recombinant protein did not induce cell death at 100°C in the thermal stability test. These findings suggest that PeVn1 exhibits hypersensitive response activity in *N. benthamiana* (Figure 3B). In addition, we conducted cell death assays in different crops and found that PeVn1 induced cell death in potato and oat plants, while no necrotic response was observed in tomato plants, suggesting that the necrotic response induced by PeVn1 was species specific (Figure 3C).

2.4 Analysis of PeVn1 subcellular localization and signal peptide function

To clarify the specific locations at which PeVn1 functions, its subcellular localization was analyzed. Using *N. benthamiana* leaf cells, PeVn1 was found to be localized in the plasma membrane and nucleus, as was PeVn1$^{\Delta SP}$, suggesting that the signal peptide of PeVn1 may have secretory activity (Figure 4A). To verify whether the inhibitory activity of PeVn1 is dependent on the signal peptide, PeVn1$^{\Delta SP}$ was constructed into an expression vector for transient expression in tobacco. The results showed that PeVn1 without the signal peptide still induced cell death in *N. benthamiana* leaves, so the stimulation of immune responses by PeVn1 may not be dependent on the signal peptide (Figure 4B).

2.5 PeVn1 triggers defense responses in *N. benthamiana*

The burst of ROS is a hallmark of plant defense response signaling during plant-microbe interactions. HR is accompanied by early plant defense responses such as ROS bursts, callus deposition and defense gene expression (Schwessinger and Ronald, 2012; Han and Hwang, 2017). To investigate whether PeVn1-induced HR is associated with plant immune responses, we injected 5 μM of the recombinant protein PeVn1 and assessed ROS accumulation using 3,3'-diaminobenzidine staining and pale green fluorescence of callose deposition in leaf cells under UV excitation after aniline blue staining (Figures 5A, B). The MAPK pathway has an important role in cell signaling and participates in plant immune responses (Li et al., 2022). By detecting MAPK phosphorylation, as in leaves treated with flg22, PeVn1 was able to induce MAPK activation in tobacco leaves, and the degree of activation increased with time (Figure 5C). To determine whether PeVn1 activates plant defense responses, genes related to PTI and defense responses in *N. benthamiana* were selected for RT-qPCR analysis. These results indicated a significant increase in the relative expression of defense response and PTI-related genes. Among these, *NbPR1* and *NbPR2* are marker genes for SA, *NbPR4* and *NbERF1* are marker genes for JA/ET, and *NbCYP71D20* and *NbAcre31* are PTI-related marker genes. Thus, PeVn1 may function as a protein exciter and MAMP that induces plant defense responses mediated by SA and JA/ET dependent signaling pathways and responds to PTI related pathway genes (Figure 5D).

10.3389/fpls.2024.1468437

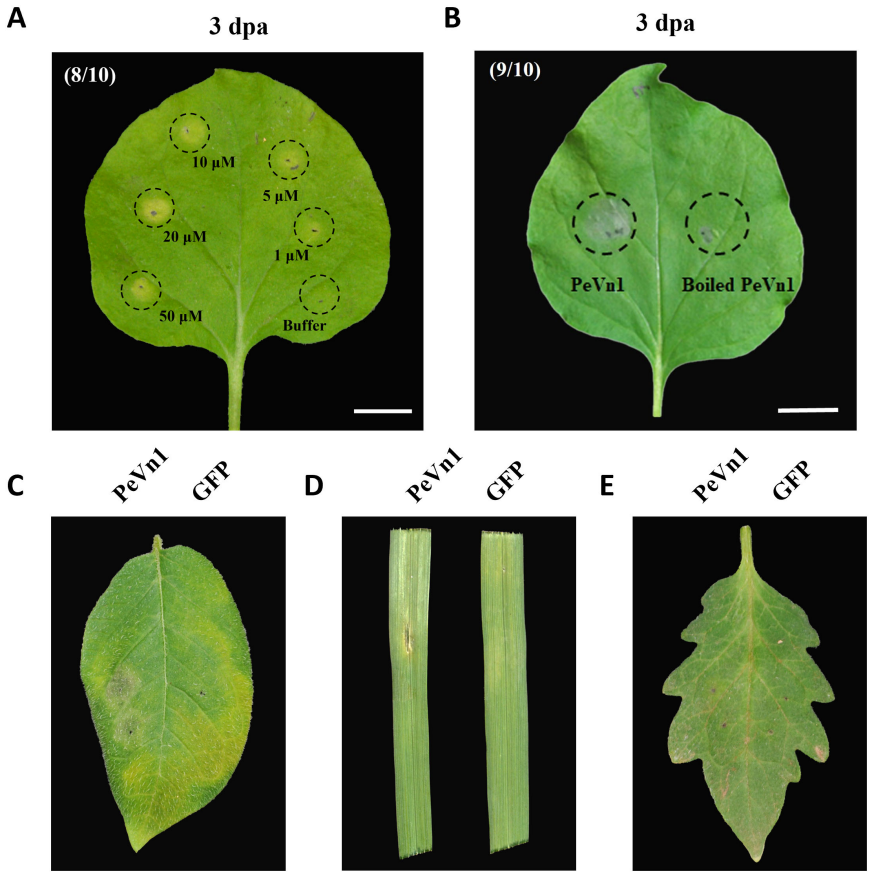

FIGURE 3
Cell death activity of PeVn1 induced in *N. benthamiana* and other plants. **(A)** Recombinant protein PeVn1 was divided into 1-50 μM and immersed into *N. benthamiana* and the HR response was observed and photographed after 3 d. **(B)** The thermal stability of PeVn1 was determined by immersing 5 μM of the recombinant protein PeVn1 in *N. benthamiana* leaves at 100°C for 15 min. **(C–E)** The detection of cell death responses induced by 5 μm PeVn1 on potato **(C)**, oat **(D)** and tomato **(E)**, 20 mM Tris-HCl as control.

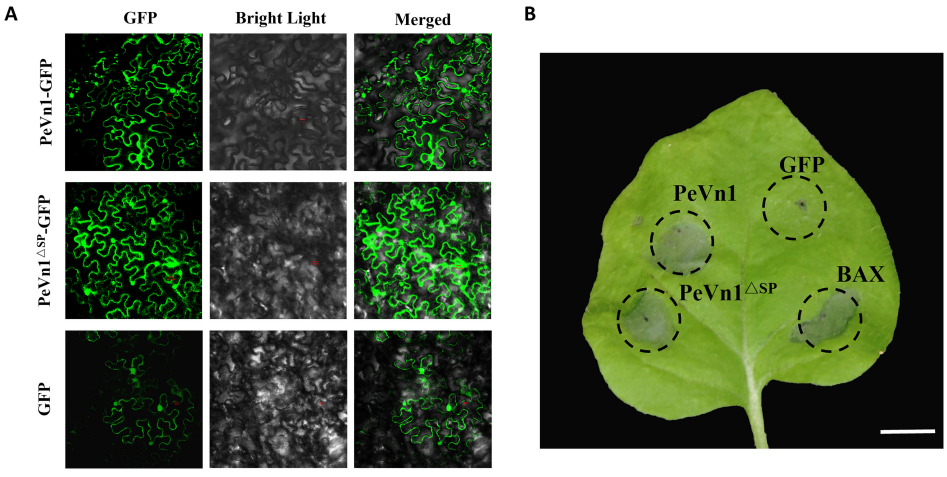

FIGURE 4
Subcellular localization and signaling peptides for PeVn1-primed immunity. **(A)** Subcellular localization of PeVn1 in *N. benthamiana* leaves. **(B)** Photographs of *N. benthamiana* leaves were taken at 4 days post infiltration. Bars are 20 μm.

10.3389/fpls.2024.1468437

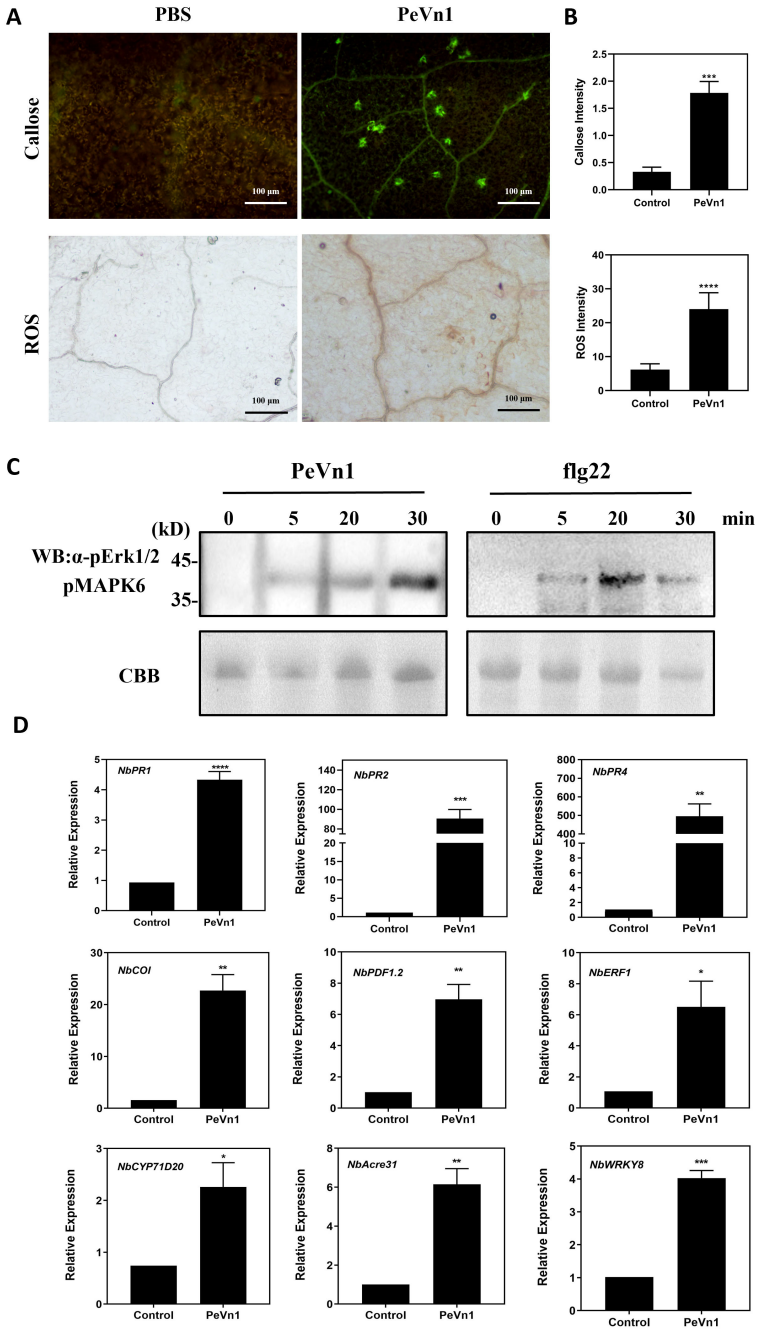

FIGURE 5
PeVn1 induces early immune responses in *N. benthamiana*. **(A)** *N. benthamiana* leaf blades were treated with 5 μM PeVn1 or buffer control for 24h, Reactive oxygen species (ROS) were observed as brick red staining after 3,3' - diaminobenzidine (DAB) reaction (bars are 1 cm) and callose was observed as pale green fluorescence under UV light after aniline blue reaction (bars are 100 μm).**(B)** ROS and callus deposition in *N. benthamiana* leaves were quantified by the software ImageJ. Mean ± SE. **(C)** PeVn1 and flg22 induced MAPK activation in *N. benthamiana*. The leaves were infiltrated with 5 μM PeVn1 or flg22, and total proteins were extracted for immunoblotting with an anti-pERK1/2 antibody. Protein loading is indicated by Coomassie brilliant blue (CBB) staining. **(D)** *N. benthamiana* leaves were treated with 5μM recombinant protein PeVn1 and the expression of defense and PTI related genes measured after 48h. *NbEF1α* was used as an internal control gene for normalization. Mean and SE were calculated from three biological replicates. The statistical analyses were performed with Student's t test. Bars indicate ± SE. *p < 0.1, **p < 0.01, ***p < 0.001, ****p < 0.0001.

2.6 PeVn1 defense-related enzyme activities

The accumulation of ROS is regulated by enzymes that detoxify ROS, including superoxide dismutase (SOD), peroxidase (POD), catalase (CAT), and phenylalanine ammonia-lyase (PAL) (Apel and Hirt, 2004). Enzyme activities related to defense showed a different pattern after PeVn1 treatment compared to those in the control group. Following treatment with the PeVn1 protein solution, the activities of POD, SOD, CAT and PAL gradually increased, peaking

after 5 days. In general, the enzyme activity in the treated group was higher than that in the control group. The SOD activity in the treated group exhibited an initial increase on day 2, reaching a peak on day 5 with an enzyme activity of 79 U, which was 23 U higher than that in the control group. Nevertheless, this discrepancy was not statistically significant (Figure 6A). The peak enzyme activity of POD in the treated group was 4.25 times higher than that in the control group. Similarly, the peak CAT activity was 70 U, which was 3.4 times higher than that in the control group (Figures 6B, C). The peak enzyme activity of PAL was 1,747 U, which was 2.1 times higher than that of the control group (Figure 6D).

2.7 Immune responses stimulated by PeVn1 are dependent on *NbBAK1* and *NbSOBIR1*

It has been shown that *NbBAK1* and *NbSOBIR1* receptor kinases are involved in a variety of plant immune responses in plant immunity. Therefore, to test whether *NbBAK1* and *NbSOBIR1* mediate PeVn1 induced cell death in *N. benthamiana*, we used VIGS to silence *NbBAK1* and *NbSOBIR1* in *N. benthamiana* leaf blades, using TRV-GFP as the empty control and *TRV-INF1* as the positive control. PeVn1 did not induce cell death in the silenced *NbBAK1* and *NbSOBIR1* plants (Figure 7A). Other silenced leaves were extracted for a RT-qPCR silencing efficiency assay when albino symptoms appeared, and the silencing efficiencies of *NbBAK1* and *NbSOBIR1* were found to be between 52% and 64% (Figure 7B). The results showed that PeVn1 did not induce cell death in *NbBAK1* and *NbSOBIR1* silenced plants. Western blotting showed that PeVn1 was expressed in the leaves of both *NbBAK1* and *NbSOBIR1* silenced plants (Figure 7C). These results suggest that PeVn1 may be a MAMP whose induction of plant cell death is dependent on *NbBAK1* and *NbSOBIR1*.

2.8 PeVn1 enhances plant disease resistance

To verify whether PeVn1 can induce plant disease resistance, we inoculated *N. benthamiana* leaves with the plant pathogenic fungi *S. sclerotiorum* and *B. cinerea* and *N. benthamiana* mosaic virus green fluorescent protein (TMV-GFP). PeVn1 at a concentration of 5 μM was immersed into the leaves separately and inoculated with the pathogenic fungi 24 h later. The results showed that the lesion areas of *S. sclerotiorum* and *B. cinerea* were reduced by 53.5% and 69%, respectively, at 48 h after inoculation (Figures 8A, B). Similarly, the number of TMV-GFP lesions was reduced in PeVn1-treated plants compared to the control (Figures 8C, D), indicating that PeVn1 can inhibit the growth of plant pathogens and induce disease resistance in plants. In addition to plant leaves, tomato plants have also been used to study the resistance of PeVn1 to bacterial pathogens. Tomato leaves were sprayed with recombinant protein of PeVn1 at a concentration of 5 μM, and 24 h later, *Pst* DC3000 was inoculated into tomato plants. The results showed that the density of pathogens and spots in PeVn1-treated tomato plants were significantly reduced compared to the control (Figures 8E–G).The results showed that PeVn1 could inhibit the proliferation of fungi and viruses in tobacco and in bacteria in tomato.

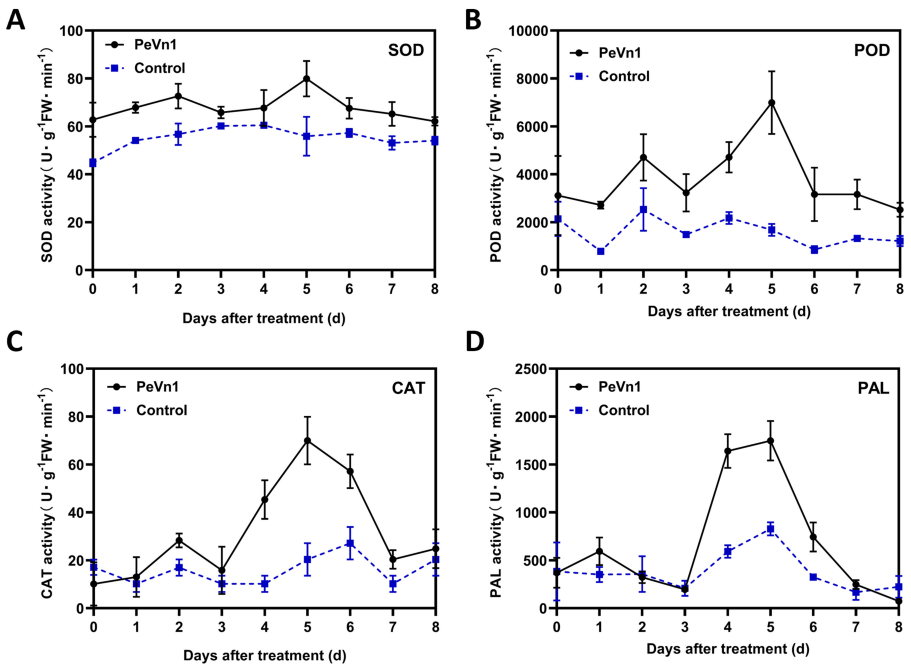

FIGURE 6
Changes in SOD **(A)**, POD **(B)**, CAT **(C)** and PAL **(D)** defense enzyme activities in PeVn1-His-treated *N. benthamiana* leaves. *N. benthamiana* leaves were treated with 5 μM PeVn1 or buffer control for 0-8 dat. Error bars indicate standard deviation among triplicates.

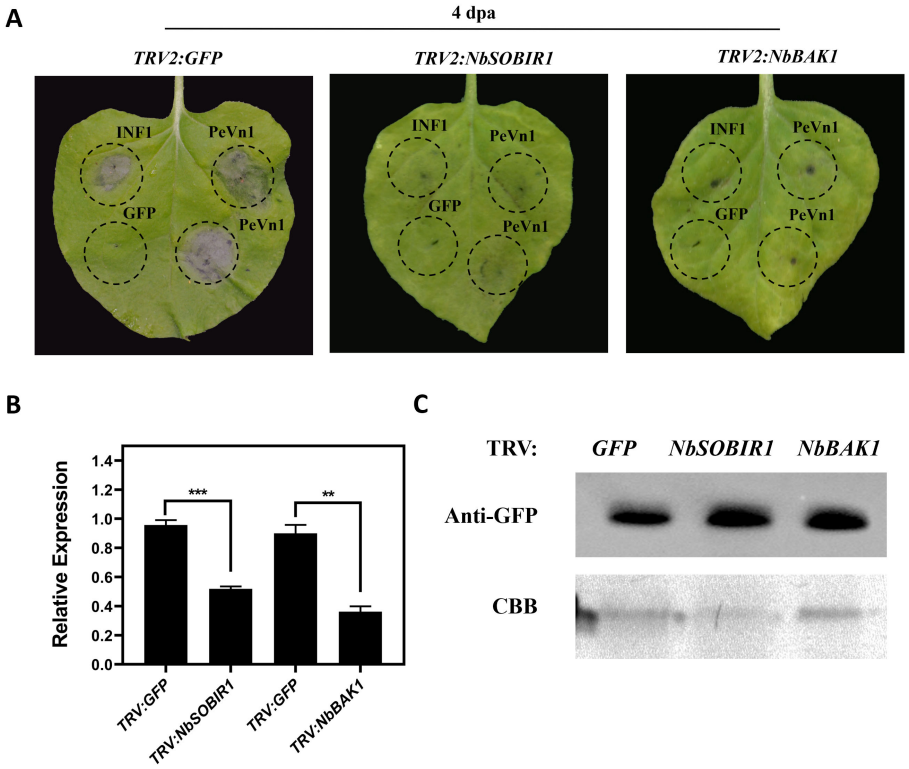

FIGURE 7
Required for PeVn1-induced cell death are *NbBAK1* and *NbSOBIR1*. **(A)** The *TRV2* construct of *Agrobacterium tumefaciens* was infiltrated into the gene-silenced plants. Photographs were taken 4 days post-infiltration (dpa), and GFP-silenced plants were used as controls. **(B)** Expression levels of *NbBAK1* and *NbSOBIR1* after VIGS treatment as assessed by quantitative reverse transcription PCR. *NbEF1α* was used as an internal reference gene. **(C)** Western blotting analysis of transiently expressed PeVn1 in *NbBAK1* and *NbSOBIR1* silenced *N. benthamiana* leaves. Protein loading is indicated by Coomassie brilliant blue (CBB) staining. *p < 0.1, **p < 0.01, ***p < 0.001.

3 Discussion

The investigation and development of plant immune priming mechanisms have provided novel methodologies and perspectives for plant protection. Protein elicitors not only induce the ability of plants to resist pathogenic invasion but also exhibit stress resistance and growth promoting functions. In this study, a novel protein elicitor PeVn1, was isolated and identified from the culture filtrate of *V. nonalfalfae*. The recombinant PeVn1 purified induces cell death in *N. benthamiana*. The cell death activity was enhanced with increasing concentration. In addition, PeVn1 does not cause cell death after incubation at 100°C for 15 min. Cell death can also be induced by PeVn1 in other plant species such as potato and oat (Midgley et al., 2022).The recognition of MAMP by plants induces early plant defense responses, including ROS bursts and callose deposition (Sun and Zhang, 2020). Research has shown that PeVn1 induces ROS bursts, callus deposition, and activation of the MAPK signaling pathway. In addition, PeVn1 resulted in significant upregulated of the expression of two PTI genes (*NbCYP71D20* and *NbAcre31*), and these results suggest that PeVn1 acts as a MAMP to trigger an immune response in *N. benthamiana*.

Proteins secreted by cells are typically characterized by low molecular weight and high cysteine residue content. These characteristics play a pivotal role in the cells' crucial defense functions (Templeton et al., 1994). As an example, VmE02 comprising 146 amino acids and ten cysteine residues, initiates plant immune responses and enhances *N. benthamiana* resistance against *S. sclerotiorum* and *P. capsici* (Nie et al., 2019). The SCRP protein SsSSVP1$^{\Delta SP}$ identified in *S. sclerotiorum* can interact with the conserved cytochrome b-c1 complex subunit QCR8 in plants, thereby eliciting an immune response (Lyu et al., 2016). In our study, PeVn1 possessing a molecular weight of 14.6 kDa and four cysteine residues, shared amino acid sequence identity with the uncharacterized protein, D7B24_002174, although without an identified domain. Signal peptide prediction revealed that PeVn1 contains 19 N-terminal signal peptide residues, classifying it as a canonical secretory protein (Figure 2A).

The plant plastid exosome space is an important site for pathogen invasion, and plants and pathogens have a close relationship (Orozco-Cárdenas et al., 2001; Garcia-Brugger et al., 2006). To clarify the specific location where PeVn1 exerts its function, transient expression and subcellular localization of PeVn1 were analyzed. We found that PeVn1 induced cell death with or without SP (Figure 4). The subcellular localization of PeVn1 is localized to the plasma membrane and nucleus, suggesting that it has multiple pathways of action. Plants use PRRs on cell membranes to recognize PAMPs (polysaccharide substances of

10.3389/fpls.2024.1468437

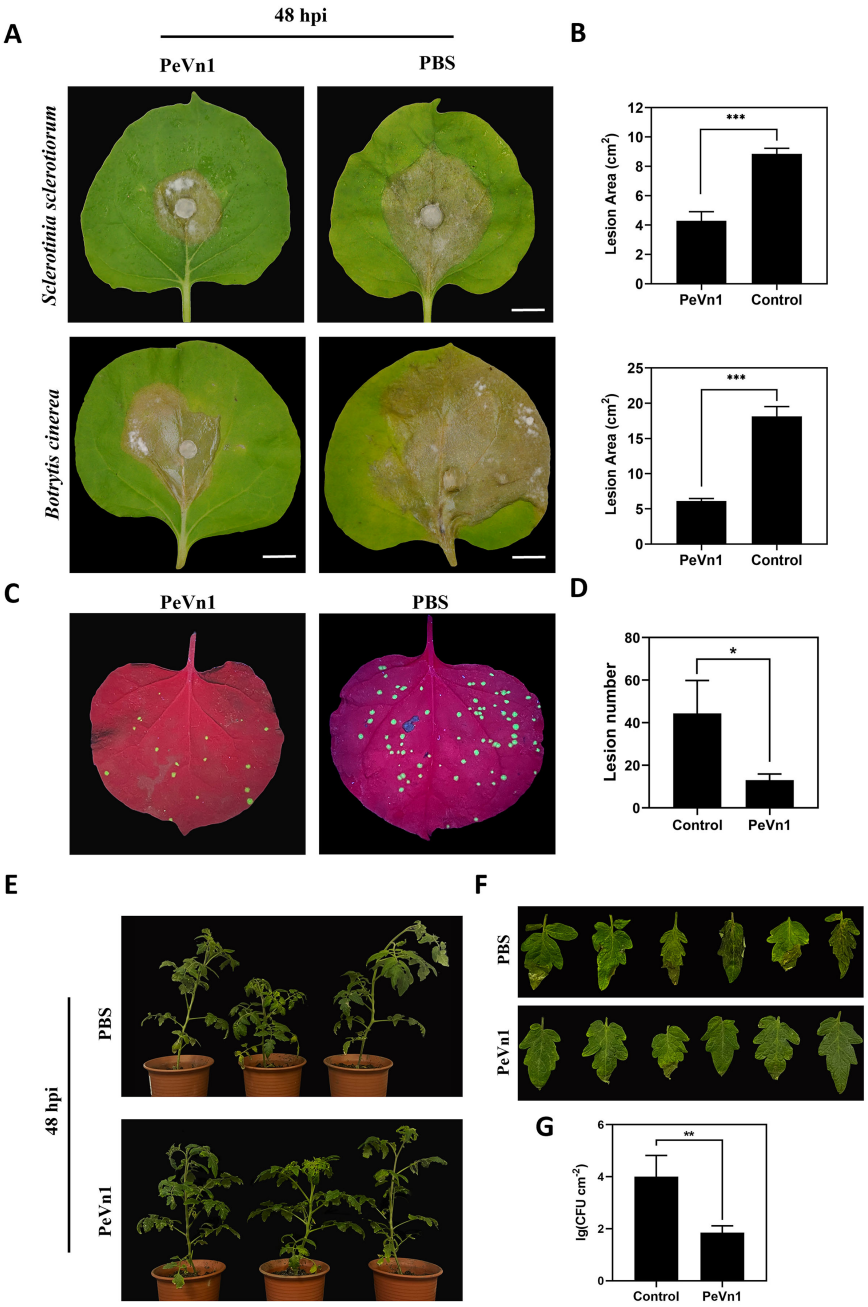

FIGURE 8
Analysis of PeVn1-induced disease resistance. **(A, B)** Representative leaves showing *Sclerotinia sclerotiorum* and *Botrytis cinerea* infection after treatment with 5 μM PeVn1 or phosphate-buffered saline (PBS) control. *N. benthamiana* leaves were inoculated with *S. sclerotiorum* and *B. cinerea* after PeVn1 treatment for 24 h. **(C)** 5 μM recombinant protein PeVn1 was immersed into *N. benthamiana* leaf blades and 24 h later, TMV-GFP supernatant was frictionally inoculated into *N. benthamiana* leaf blades and 4 d later, the photos were taken under the UV lamp. **(D)** Calculation of TMV in *N. benthamiana* leaf blades. *N. benthamiana* leaves; the number of TMV-GFP spots decreased significantly after PeVn1 treatment **(E–G)** Recombinant protein 5 μM PeVn1 was sprayed and inoculated onto tomato leaves and after 3 d of moist incubation, *Pst* DC3000 bacterial suspension was sprayed and inoculated onto tomato leaves and after 3 d of incubation, tomato leaves were photographed, and the number of colonies was counted. The number of colonies in tomato leaves was significantly reduced after PeVn1 treatment. The control group was PBS buffer. The experiment was conducted three times with similar results. Bars are 1 cm. Bars indicate ± SE. *p < 0.1, **p < 0.01, ***p < 0.001.

fungi, bacterial flagellin, and Harpin proteins) to elicit PTIs, which are widely distributed and conserved in plant pathogenic bacteria. Plants contain two types of PRRs, including Receptor-Like Proteins (RLPs), which contain only a segment of intracellular structural domains with no kinase activity, and Receptor-Like Kinases (RLKs), which usually consist of kinase, transmembrane, and ligand structural domain (Gui et al., 2017). *BAK1* and *SOBIR1* are two conserved RLKs with short leucine-rich repeat sequences in their extracellular domains. These domains act as coreceptors for various MAMP-induced immune responses (Burgh et al., 2019). The results

showed that PeVn1-induced cell death was dependent on *BAK1* and *SOBIR1*, further confirming that PeVn1 is a MAMP. Nonetheless, further studies are needed to identify the receptors that can recognize PeVn1 (Figure 7).

The most widely utilized signaling pathways in plants are the SA and JA/ET (van Wees et al., 2000; Nomoto et al., 2021; Zhu et al., 2021). Some evidence suggests that depending on the specific pathogen, the SA, JA, and ET pathways can interact with each other and modulate plant defense responses (Koornneef and Pieterse, 2008). In the present study, PeVn1 significantly upregulated the SA and JA/ET genes in *N. benthamiana* (Figure 5C), indicating that PeVn1 induced the expression of genes related to SA synthesis in *N. benthamiana* (*NbPR1* and *NbPR2*). The significant upregulation of JA-responsive genes (*NbPR4*, *NbCOI*, and *NbPDF1*.2) and ET-responsive gene *NbERF1* suggest that PeVn1 induces JA gene expression and ET synthesis in tobacco. The process of ROS accumulation is regulated by a series of enzymes that function to detoxify ROS, including SOD, CAT, POD and glutathione reductase (Apel and Hirt, 2004). These results suggest the potential activation of multiple signaling pathways in PeVn1 triggered resistance, enhancing plant resistance to pathogens under PeVn1 treatment. It was found that PeVn1 induced activities of PAL, CAT, POD and SOD (Figure 6). To determine whether the PeVn1 mediated defense response of *N. benthamiana* is resistant to various phytopathogens, we selected *S. sclerotiorum*, *B. cinerea* and TMV-GFP. The results showed that the treatment of PeVn1 resulted in a significant reduction in lesion area and relative biomass. In addition, recombinant protein PeVn1 treatment also induced resistance in plants against a variety of pathogenic fungi and bacteria.

Overall, our study reports a novel protein elicitor PeVn1 from *V. nonalfalfae* HW that induces *N. benthamiana* HR and acts as a MAMP to induce plant immune responses, and PeVn1 induces *BAK1* and *SOBIR1* dependent cell death and activates defense related events in *N. benthamiana* and enhanced plant resistance to *S. sclerotiorum*, *B. cinerea*, TMV-GFP and *Pst* DC3000. These findings further elucidate the biological functions of PeVn1 and the molecular mechanisms underlying the regulation of plant defense mechanisms, thereby establishing a foundation for future research.

4 Materials and methods

4.1 Strain culture and plant growing conditions

Verticillium nonalfalfae HW was cultured in PDA medium at 25°C for 2 weeks, and then mycelium at the edge of the colony was picked and inoculated with the Czapek medium and cultured in the dark at 25°C for 14 days at 150 rpm, *S. sclerotiorum* and *Botrytis cinerea* were cultured in PDA medium at 25°C for 3 days, *Pseudomonas syringae* pv. *tomato* (Pst) DC3000 was cultured in KB medium at 28°C with 150 rpm shaking overnight, *E. coli* DH5α and BL21 (DE3) were incubated in LB medium at 37°C, 180 rpm on a shaker. *A. tumefaciens* GV3101 25 μg/mL rifampicin was incubated in LB medium containing *A. tumefaciens* GV3101 25 μg/mL rifampicin. 28°C, 220 rpm, 18 h.

Nicotiana benthamiana and tomato plants were cultivated at 25°C with a photoperiod of 16 h and an 8 h dark period. All strains and seeds were provided by the Plant Pathology Laboratory of the College of Horticulture and Plant Protection, Inner Mongolia Agricultural University. Tomato seeds were purchased from the Meng Miao Seed Company (Hohhot, China).

4.2 Extraction, isolation and identification of proteins secreted from strain HW

Strain HW was incubated for 7 days, before collecting the supernatant. The supernatant was then collected by centrifugation at 13,000 rpm for 30 min at 4°C. Subsequent to centrifugation at 13,000 rpm for 30 min at 4°C, the supernatant was filtered twice with a 0.45 μm filter (Millipore, Suzhou, China) until no organisms were present. Proteins were precipitated overnight at 4°C by the addition of a 75% ammonium sulfate solution. Following centrifugation, the precipitate was dissolved in 20 mM Tris-HCl and dialyzed for a period of two days. The dialyzed proteins were further purified using the gel filtration-preloaded columns of the AKTA protein purification system (Superdex 200 Increase 10/300 GL; Cytiva, MA, USA). The purified proteins were tested for cell death activity in *N. benthamiana* leaves, and the fractions with cell death activity were separated by sodium dodecyl sulfate polyacrylamide gel electrophoresis. A single band was cut and identified by liquid chromatography/mass spectrometry.

4.3 Purification and expression of PeVn1 in prokaryotic systems

The PeVn1 sequence, which does not contain a signal peptide, was inserted between the *Bam*HI and *Xho*I sites of the *pET* vector to construct the plasmid. Supplementary Table 1 lists all the primers used. The plasmids were then expressed in *E. coli* BL21 (DE3), and the expression of the target proteins was induced by adding 1 mM IPTG to the induced culture at 16°C, 80 rpm for 12 h. The expression of the target proteins was then induced by adding 1 mM IPTG to the induced culture at 16°C, 80 rpm. After centrifugation, the organisms were collected, washed thrice in phosphate-buffered saline (PBS) (20 mM Na_2HPO_4, 300 mM NaCl, pH 8.0), and lysed by ultrasonication to obtain a crude extract of the recombinant protein. Purification of the filtrate was achieved through affinity chromatography, employing HisPur Ni-NTA agarose (Cytiva), and the concentration of PeVn1 was quantified by BCA protein assay. When the purified protein concentration exceeded 0.1 mg/mL, it was dialyzed with PBS for subsequent experiments.

4.4 Protein expression in *N. benthamiana*

For cell death assays, *A. tumefaciens* GV3101 constructed with *PVX-PeVn1-GFP*, *PVX-eGFP* or *PVX-Bax* in the potato virus X (PVX) vector was washed three times with 10 mM $MgCl_2$ and diluted to an OD_{600} of 0.8. The corresponding infusate was injected into the dorsal part of the leaf using a 1 mL syringe. To clarify the exact location of PeVn1 function, *pCAMBIA1300-PeVn1-GFP* and *pCAMBIA1300-PeVn1$^{\Delta SP}$-GFP* were transformed into *A. tumefaciens* and the suspension with OD_{600} = 0.8 was injected into 4 week *N. benthamiana* leaf blades in a glass greenhouse at 22°C. At 48 hpi, the suspension was incubated in a glass greenhouse for 2 h and washed thrice with 10 mM $MgCl_2$. greenhouse at 22°C. At 48 h post infection (hpi), the leaf epidermis was treated and observed under a confocal microscope.

4.5 Bioinformatic analysis of PeVn1

To conduct protein structure analysis of PeVn1, its signal peptide was predicted using the SignaIP website (http://www.cbs.dtu.dk/services/SignalP/), and the protein transmembrane helix was predicted using the TMHMM website (http://www.cbs.dtu.dk/services/TMHMM/). The primary protein structural information, such as molecular weight and isoelectric point of PeVn1, was analyzed using ProParam (http://web.expasy.org/cgi-bin/protparam/protparam) (Kumar et al., 2018). The tertiary structure was predicted using SWISS-MODEL software (https://www.swissmodel.expasy.org/) (Waterhouse et al., 2018). The amino acid sequences were obtained from the UniProt database (https://www.uniprot.org/). Homologous sequences from the NCBI database were compared using BLASTp and 15 sequences with high similarity were selected. Sequence conservation was analyzed using DNAMAN software. Phylogenetic dendrograms were constructed using MEGA 6.0 and the neighbor-joining method. PeVn1 data were submitted to the NCBI database under the GenBank number XP 028497723.1.

4.6 Transient expression of proteins in yeast

The signal peptide sequence was cloned into the *pSUC2* vector, which carries the sucrose invertase gene SUC2 without the initiation ATG codon and the signal peptide sequence and was transformed into yeast YTK12 (Jacobs et al., 1997). The transformant strains were then screened on CMD−W plates (0.67% yeast nitrogen base, 2% sucrose, 0.1% glucose, 2% agar, 0.075% tryptophan dropout supplement) and selective YPRAA plates (1% yeast extract, 2% peptone, 2% raffinose, 2 μg/ml antimycin A, 2% agar). YTK12 strains with empty *pSUC* vector or *pSUC2-Avr1b* were used as negative and positive controls, respectively. The enzymatic activity was tested by reducing 2,3,5-triphenyl tetrazolium chloride to red 1,3,5-triphenyl formazan.

4.7 Determination of the cell death response of recombinant proteins to different crops

To test the necrotic activity of the recombinant protein against different plants, 5 μm of the recombinant protein was infiltrated into the leaves of *N. benthamiana* and also into the leaves of potato (*Solanum tuberosum* L.), oat (*Avena* L.), and tomato (*Solum lycopicum*). Photographs were taken three days after infiltration. The experiment was repeated with at least three biological replicates. *N. benthamiana* leaves were immersed in 1 mg/mL trypan blue dye solution and boiled for 2 min. After standing to return to room temperature, the leaves were rinsed 3-4 times with sterile water and decolorized by adding 2.5 g/mL chloral hydrate.

4.8 Physicochemical properties and induction of early plant responses by PeVn1

Determination of the lowest excitation concentration of recombinant protein PeVn1, the recombinant protein PeVn1 was injected into *N. benthamiana* leaves at concentrations of 1, 5, 10, 20 and 50 μM. The thermal stability of the recombinant protein PeVn1 was determined. The recombinant protein PeVn1 was injected into *N. benthamiana* at an appropriate concentration later, the leaves were incubated at 100°C for 15 min. The PeVn1 pure protein of appropriate concentration was injected into *N. benthamiana* to observe its immune response. Leaves at 24 h posttreatment were cut into small pieces, 1 × 1 cm. H_2O_2 was detected by DAB staining and callose was detected by aniline blue staining as described previously (Niu et al., 2011). ROS burst was identified via light microscopy, while callus deposition was observed using a fluorescence microscope (Nikon, Japan).

4.9 MAPK assay

Leaves of *N. benthamiana* were treated with 5 μM PeVn1, and samples were taken at 0, 5, 20, and 30 min to extract total plant proteins with RIPA buffer (50 mmol/L Tris pH7.5, 150 mmol/L NaCl, 1% Triton X-100, 1% deoxycholate, 1% SDS, 0.5 mmol/L EDTA, 1×PMSF, 1×protease inhibitor cocktail) to extract total plant protein. Western blot was performed using pERK1/2 antibody.

4.10 Bioassay for PeVn1-induced disease resistance in plants

The leaves were treated with 5 μM PeVn1 and PBS (Control) for 24 h. After 24 h, cultured *S. sclerotiorum* and *B. cinerea* were inoculated onto the leaves and incubated in the greenhouse at 25°C for 24 to 72 h to observe the onset of disease. Photographs were taken and the lesions' size was calculated using ImageJ software at

48 hpi. An equal volume of 5 μM PeVn1 and PBS was sprayed on 5-6 week old tomato leaves, which were incubated at 24°C under humid conditions for 3 days. After centrifugation of the cultured *Pst* DC3000 sap, the bacterial body was collected and suspended using 10 mM $MgCl_2$ with OD_{600} = 0.1, before uniformly spraying on the leaves. After 3 days, three leaves were taken from each treatment and ground into a powder. The powder was diluted to 10^{-6} concentration using sterile water, coated on King's B medium containing 50 μg/mL rifampicin at 37°C, and the number of colonies was determined after 2 days. The number of colonies was determined by the *Pst* DC3000 method. The experiment was repeated at least thrice. *N. benthamiana* leaves were treated with 5 μM PeVn1 and PBS (Control). After 24 h, the leaves were inoculated with *TMV-GFP*. For *TMV-GFP* inoculum preparation, leaves previously infected with *TMV-GFP* were ground, homogenized in PBS buffer, and centrifuged at 3500 g for 10 min. The supernatant was collected and inoculated onto leaves using the rubbing method. After inoculation and incubation for 4 days, the number of spots was counted under a UV lamp. Three replicates were performed for each treatment group. Viral suppression was calculated as follows: suppression (%) = (Nc-NT)/Nc × 100, where Nc and NT represent the number of lesions on the control and PeVn1-treated leaves, respectively.

4.11 Determination of defense-related enzyme activities after PeVn1 treatment of tobacco

The activities of SOD, POD, CAT and PAL were determined in PeVn1 (5 μM) treated *N. benthamiana* leaves at different intervals (0-8 days). Samples of treated *N. benthamiana* leaves (0.1 g) were collected at different intervals (0-8 days) and immediately frozen in liquid nitrogen. At least three samples were used to determine enzyme activity. Frozen tissue samples were treated as previously described (Zhang et al., 2015). First, the samples with 3 mL of PBS (20 mM Na_2HPO_4, 300 mM NaCl, pH 8.0) with 1.33 mM ethylenediaminetetraacetic acid and 1% (w/v) polyvinyl-pyrrolidone were ground at 4°C. The homogenate was centrifuged at 8000 g for 20 min, and then the obtained extract was 150 and subjected to enzyme assay for SOD, POD, CAT, and PAL. The activities of these enzymes were determined using assay kits (Sinobestbio, Shanghai, China) according to the manufacturer's instructions.

4.12 RNA extraction and RT-qPCR analysis

Total RNA was extracted from *N. benthamiana* leaf blades using a Plant RNA Extraction Kit (TAKARA). cDNA was reverse transcribed using PrimeScript™ RT Master Mix (TAKARA). Quantitative PCR was performed using the LightCycler 96 System (Roche) and TB Green® Premix Ex Taq™ II (TAKARA) to determine gene expression. All experiments consisted of three biological and three technical replicates, and the *EF1α* gene in *N. benthamiana* was used as a reference control for normalization. The relative expression of each gene was calculated using the $2^{-\Delta\Delta Ct}$ comparison method (Livak and Schmittgen, 2001). Supplementary Table 1 lists all the primers used for RT-qPCR.

4.13 VIGS in *N. benthamiana*

To silence *NbBAK1* and *NbSOBIR1*, the target genes were cloned into the *pTRV2* vector, with *pTRV2:PDS* and *pTRV2:GFP* used as positive and negative controls, respectively. The vectors were *de novo* synthesized in *A. tumefaciens* GV3101. Bacterial fluids Infiltrated into *N. benthamiana* leaf blades at an OD_{600} of 0.8 After a 2 weeks period, the silencing efficiency of *BAK1* and *SOBIR1* was determined by RT-qPCR at the location of the treated leaves. The albino phenotype due to PDS gene silencing was used as a reference.

4.14 Statistical analysis

All the data presented are the mean values of three biological repetitions and were statistically analyzed via one-way ANOVA and Tukey's test ($p < 0.05$) using GraphPad Prism 8.0 software.

Data availability statement

The datasets presented in this study can be found in online repositories. The names of the repository/repositories and accession number(s) can be found below: https://www.ncbi.nlm.nih.gov/genbank/, XP 028497723.1.

Author contributions

ZZ: Conceptualization, Validation, Writing – original draft, Writing – review & editing. DW: Funding acquisition, Resources, Writing – review & editing. BD: Methodology, Project administration, Writing – review & editing. YW: Supervision, Validation, Writing – review & editing. JX: Investigation, Validation, Writing – review & editing. JH: Data curation, Funding acquisition, Methodology, Project administration, Resources, Supervision, Writing – review & editing. HZ: Funding acquisition, Project administration, Resources, Supervision, Writing – review & editing.

Funding

The author(s) declare that financial support was received for the research, authorship, and/or publication of this article. This study was supported by the "Biopesticide Creation and Utilization Team" project of Inner Mongolia Agricultural University (BR22-13-11), the Local Fund Project of the National Natural Science Foundation of China (20222QN03001), the Scientific Research Start-up Fund

for High-level Talents of Inner Mongolia Agricultural University (NDYB2020-15), the Project Fund for the "Research and Development of Novel Plant Micro-ecological Agents and Their Industrialization" of the Department of Education of the Inner Mongolia Autonomous Region (Rz2300003665), and the Project of the Basic Scientific Research Funds for Colleges and Universities Directly Under the Direct Subsidiarity of the Inner Mongolia Autonomous Region (BR22-11-14).

Conflict of interest

The authors declare that the research was conducted in the absence of any commercial or financial relationships that could be construed as a potential conflict of interest.

Publisher's note

All claims expressed in this article are solely those of the authors and do not necessarily represent those of their affiliated organizations, or those of the publisher, the editors and the reviewers. Any product that may be evaluated in this article, or claim that may be made by its manufacturer, is not guaranteed or endorsed by the publisher.

Supplementary material

The Supplementary Material for this article can be found online at: https://www.frontiersin.org/articles/10.3389/fpls.2024.1468437/full#supplementary-material

References

Apel, K., and Hirt, H. (2004). Reactive oxygen species: metabolism, oxidative stress, and signal transduction. *Annu Rev Plant Biol*. 55, 373–399. doi: 10.1146/annurev.arplant.55.031903.141701

Boller, T., and He, S. Y. (2009). Innate immunity in plants: an arms race between pattern recognition receptors in plants and effectors in microbial pathogens. *Science*. 324, 742–744. doi: 10.1126/science.1171647

Boudsocq, M., and Sheen, J. (2013). CDPKs in immune and stress signaling. *Trends Plant Sci*. 18, 30–40. doi: 10.1016/j.tplants.2012.08.008

Boutrot, F., and Zipfel, C. (2017). Function, discovery, and exploitation of plant pattern recognition receptors for broad-spectrum disease resistance. *Annu. Rev. Phytopathol*. 55, 257–286. doi: 10.1146/annurev-phyto-080614-120106

Burgh, A. M. V. D., Postma, J., Robatzek, S., and Joosten, M. H. A. J. (2019). Kinase activity of SOBIR1 and BAK1 is required for immune signalling, 3. *Mol Plant Pathol*. 20 (3), 410–422. doi: 10.1111/mpp.12767

Czobor, Á., Hajdinák, P., and Szarka, A. (2017). Rapid ascorbate response to bacterial elicitor treatment in Arabidopsis thaliana cells. *Acta Physiologiae Plantarum*. 39 (2), 62. doi: 10.1007/s11738-017-2365-1

Flajsman, M., Mandelc, S., Radisek, S., Stajner, N., Jakse, J., Kosmelj, K., et al. (2016). Identification of novel virulence-associated proteins secreted to xylem by verticillium nonalfalfae during colonization of hop plants. *Mol. Plant Microbe Interact*. 29, 362–373. doi: 10.1094/mpmi-01-16-0016-r

Garcia-Brugger, A., Lamotte, O., Vandelle, E., Bourque, S., Lecourieux, D., Poinssot, B., et al. (2006). Early signaling events induced by elicitors of plant defenses. *Mol. Plant. Microbe Interact*. 19, 711–724. doi: 10.1094/MPMI-19-0711

Gui, Y., Zhang, W., Zhang, D., Zhou, L., Short, D. P. G., Wang, J., et al. (2017). A verticillium dahliae extracellular cutinase modulates plant immune responses. *Mol. Plant Microbe Interact*. doi: 10.1094/MPMI-06-17-0136-R

Han, S. W., and Hwang, B. K. (2017). Molecular functions of Xanthomonas type III effector AvrBsT and its plant interactors in cell death and defense signaling. *Planta*. 245, 237–253. doi: 10.1007/s00425-016-2628-x

Inderbitzin, P., Bostock, R. M., Davis, R. M., Usami, T., Platt, H. W., and Subbarao, K. V. (2011). Phylogenetics and taxonomy of the fungal vascular wilt pathogen Verticillium, with the descriptions of five new species. *PloS One*. 6, e28341. doi: 10.1371/journal.pone.0028341

Inderbitzin, P., and Subbarao, K. V. (2014). Verticillium systematics and evolution: how confusion impedes Verticillium wilt management and how to resolve it. *Phytopathology*. 104, 564–574. doi: 10.1094/phyto-11-13-0315-ia

Jacobs, K. A., Collins-Racie, L. A., Colbert, M., Duckett, M., Golden-Fleet, M., Kelleher, K., et al. (1997). A genetic selection for isolating cDNAs encoding secreted proteins. *Gene*. 198 (1-2), 289–296. doi: 10.1016/S0378-1119(97)00330-2

Jiang, S., Zheng, W., Li, Z., Tan, J., Wu, M., Li, X., et al. (2022). Enhanced Resistance to Sclerotinia sclerotiorum in Brassica rapa by Activating Host Immunity through Exogenous Verticillium dahliae Aspf2-like Protein (VDAL) Treatment. *Int. J. Mol. Sci*. 23, 13958. doi: 10.3390/ijms232213958

Jones, J. D., and Dangl, J. L. (2006). The plant immune system. *Nature*. 444, 323–329. doi: 10.1038/nature05286

Jonge, R. D., Esse, H. P. V., Maruthachalam, K., Bolton, M. D., Santhanam, P., Saber, M. K., et al. (2012). Tomato immune receptor Ve1 recognizes effector of multiple fungal pathogens uncovered by genome and RNA sequencing. *Proc Natl Acad Sci U. S. A*. 109 (13), 5110–5115. doi: 10.1073/pnas.1119623109

Koornneef, A., and Pieterse, C. M. (2008). Cross talk in defense signaling. *Plant Physiol*. 146, 839–844. doi: 10.1104/pp.107.112029

Kumar, S., Stecher, G., Li, M., Knyaz, C., and Tamura, K. (2018). MEGA X: Molecular Evolutionary Genetics Analysis across computing platforms. *Mol. Biol. Evol*. 35 (6), 1547–1549. doi: 10.1093/molbev/msy096

Langner, T., and Göhre, V. (2016). Fungal chitinases: function, regulation, and potential roles in plant/pathogen interactions. *Curr. Genet*. 62, 243–254. doi: 10.1007/s00294-015-0530-x

Li, L., Zhu, X.-M., Zhang, Y.-R., Cai, Y.-Y., Wang, J.-Y., Liu, M.-Y., et al. (2022). Research on the molecular interaction mechanism between plants and pathogenic fungi. *Int J Mol Sci*. 23 (9), 4658. doi: 10.3390/ijms23094658

Liang, Y., Cui, S., Tang, X., Zhang, Y., Qiu, D., Zeng, H., et al. (2018). An Asparagine-Rich Protein Nbnrp1 Modulate Verticillium dahliae Protein PevD1-Induced Cell Death and Disease Resistance in *Nicotiana benthamiana*. *Front. Plant Sci*. 9. doi: 10.3389/fpls.2018.00303

Liebrand, T. W., van den Burg, H. A., and Joosten, M. H. (2014). Two for all: receptor-associated kinases SOBIR1 and BAK1. *Trends Plant Sci*. 19, 123–132. doi: 10.1016/j.tplants.2013.10.003

Liu, S. Y., Chen, J. Y., Wang, J. L., Li, L., Xiao, H. L., Adam, S. M., et al. (2013). Molecular characterization and functional analysis of a specific secreted protein from highly virulent defoliating Verticillium dahliae. *Gene*. 529, 307–316. doi: 10.1016/j.gene.2013.06.089

Liu, W., Liu, J., Triplett, L., Leach, J. E., and Wang, G. L. (2014). Novel insights into rice innate immunity against bacterial and fungal pathogens. *Annu. Rev. Phytopathol*. 52, 213–241. doi: 10.1146/annurev-phyto-102313-045926

Livak, K. J., and Schmittgen, T. D. (2001). Analysis of relative gene expression data using real-time quantitative PCR and the 2(-Delta Delta C(T)) Method. *Methods*. 25, 402–408. doi: 10.1006/meth.2001.1262

Lyu, X., Shen, C., Fu, Y., Xie, J., Jiang, D., Li, G., et al. (2016). A small secreted virulence-related protein is essential for the necrotrophic interactions of sclerotinia sclerotiorum with its host plants. *PloS Pathog*. 12, e1005435. doi: 10.1371/journal.ppat.1005435

Marton, K., Flajšman, M., Radišek, S., Košmelj, K., Jakše, J., Javornik, B., et al. (2018). Comprehensive analysis of Verticillium nonalfalfae in silico secretome uncovers putative effector proteins expressed during hop invasion. *PloS One*. 13, e0198971. doi: 10.1371/journal.pone.0198971

Midgley, K. A., van den Berg, N., and Swart, V. (2022). Unraveling plant cell death during phytophthora infection. *Microorganisms*. 10, 1139. doi: 10.3390/microorganisms10061139

Miller, G., Shulaev, V., and Mittler, R. (2008). Reactive oxygen signaling and abiotic stress. *Physiol. Plant*. 133, 481–489. doi: 10.1111/j.1399-3054.2008.01090.x

Nie, J., Yin, Z., Li, Z., Wu, Y., and Huang, L. (2019). A small cysteine-rich protein from two kingdoms of microbes is recognized as a novel pathogen-associated molecular pattern. *New Phytol*. 222, 995–1011. doi: 10.1111/nph.15631

Niu, D. D., Liu, H. X., Jiang, C. H., Wang, Y. P., Wang, Q. Y., Jin, H. L., et al. (2011). The plant growth-promoting rhizobacterium Bacillus cereus AR156 induces systemic resistance in Arabidopsis thaliana by simultaneously activating salicylate- and

jasmonate/ethylene-dependent signaling pathways. *Mol. Plant Microbe Interact.* 24, 533–542. doi: 10.1094/mpmi-09-10-0213

Nomoto, M., Skelly, M. J., Itaya, T., Mori, T., Suzuki, T., Matsushita, T., et al. (2021). Suppression of MYC transcription activators by the immune cofactor NPR1 fine-tunes plant immune responses. *Cell Rep.* 37, 110125. doi: 10.1016/j.celrep.2021.110125

Novo, M., Pomar, F., Gayoso, C., and Merino, F. (2006). Cellulase activity in isolates of verticillium dahliae differing in aggressiveness. *Plant Dis.* 90, 155–160. doi: 10.1094/pd-90-0155

Orozco-Cárdenas, M. L., Narváez-Vásquez, J., and Ryan, C. A. (2001). Hydrogen peroxide acts as a second messenger for the induction of defense genes in tomato plants in response to wounding, systemin, and methyl jasmonate. *Plant Cell.* 13, 179–191. doi: 10.1105/tpc.13.1.179

Pršić, J., and Ongena, M. (2020). Elicitors of plant immunity triggered by beneficial bacteria. *Front. Plant Sci.* 11. doi: 10.3389/fpls.2020.594530

Ranf, S., Gisch, N., Schäffer, M., Illig, T., Westphal, L., Knirel, Y. A., et al. (2015). A lectin S-domain receptor kinase mediates lipopolysaccharide sensing in Arabidopsis thaliana. *Nat. Immunol.* 16, 426–433. doi: 10.1038/ni.3124

Schwessinger, B., and Ronald, P. C. (2012). Plant innate immunity: perception of conserved microbial signatures. *Annu. Rev. Plant Biol.* 63, 451–482. doi: 10.1146/annurev-arplant-042811-105518

Sun, L., and Zhang, J. (2020). Regulatory role of receptor-like cytoplasmic kinases in early immune signaling events in plants. *FEMS Microbiol. Rev.* 44, 845–856. doi: 10.1093/femsre/fuaa035

Templeton, M. D., Rikkerink, E., and Beever, R. E. (1994). Small, cysteine-rich proteins and recognition in fungal-plant interactions. *Mol. Plant-Microbe Interact.* 7 (3), 320. doi: 10.1094/MPMI-7-0320

van Wees, S. C., de Swart, E. A., van Pelt, J. A., van Loon, L. C., and Pieterse, C. M. (2000). Enhancement of induced disease resistance by simultaneous activation of salicylate- and jasmonate-dependent defense pathways in Arabidopsis thaliana. *Proc. Natl. Acad. Sci. U.S.A.* 97, 8711–8716. doi: 10.1073/pnas.130425197

Wang, J., Liu, S., Ren, P., Jia, F., Kang, F., Wang, R., et al. (2023). A novel protein elicitor (PeSy1) from Saccharothrix yanglingensis induces plant resistance and interacts with a receptor-like cytoplasmic kinase in *Nicotiana benthamiana*. *Mol. Plant Pathol.* 24, 436–451. doi: 10.1111/mpp.13312

Wang, H., Yang, X., Guo, L., Zeng, H., and Qiu, D. (2015). PeBL1, a novel protein elicitor from Brevibacillus laterosporus strain A60, activates defense responses and systemic resistance in *Nicotiana benthamiana*. *Appl. Environ. Microbiol.* 81, 2706–2716. doi: 10.1128/aem.03586-14

Wang, B., Yang, X., Zeng, H., Liu, H., Zhou, T., Tan, B., et al. (2012). The purification and characterization of a novel hypersensitive-like response-inducing elicitor from Verticillium dahliae that induces resistance responses in tobacco. *Appl. Microbiol. Biotechnol.* 93, 191–201. doi: 10.1007/s00253-011-3405-1

Waterhouse, A., Bertoni, M., Bienert, S., Studer, G., Tauriello, G., Gumienny, R., et al. (2018). SWISS-MODEL: homology modelling of protein structures and complexes. *Nucleic Acids Res.* 46, W296–w303. doi: 10.1093/nar/gky427

Zhang, M., Li, Q., Liu, T., Liu, L., Shen, D., Zhu, Y., et al. (2015). Two cytoplasmic effectors of Phytophthora sojae regulate plant cell death via interactions with plant catalases. *Plant Physiol.* 167 (1), 164–175. doi: 10.1104/pp.114.252437

Zhu, D., Zhang, X., Zhou, J., Wu, Y., Zhang, X., Feng, Z., et al. (2021). Genome-wide analysis of ribosomal protein GhRPS6 and its role in cotton verticillium wilt resistance. *Int. J. Mol. Sci.* 22, 1795. doi: 10.3390/ijms22041795

Zipfel, C., and Felix, G. (2005). Plants and animals: a different taste for microbes? *Curr. Opin. Plant Biol.* 8, 353–360. doi: 10.1016/j.pbi.2005.05.004

frontiers | Frontiers in Plant Science

TYPE Original Research
PUBLISHED 20 November 2024
DOI 10.3389/fpls.2024.1490466

Check for updates

OPEN ACCESS

EDITED BY
Yasser Nehela,
University of Florida, United States

REVIEWED BY
Aswin Nair,
Umeå University, Sweden
Toshik Iarley Da Silva,
Federal University of the Recôncavo of Bahia, Brazil
Qi Zheng,
Shandong University, China

*CORRESPONDENCE
Tongjun Sun
suntongjun@caas.cn

RECEIVED 03 September 2024
ACCEPTED 30 October 2024
PUBLISHED 20 November 2024

CITATION
Chen Y, Han Y, Huang W, Zhang Y, Chen X, Li D, Hong Y, Gao H, Zhang K, Zhang Y and Sun T (2024) LAZARUS 1 functions as a positive regulator of plant immunity and systemic acquired resistance.
Front. Plant Sci. 15:1490466.
doi: 10.3389/fpls.2024.1490466

COPYRIGHT
© 2024 Chen, Han, Huang, Zhang, Chen, Li, Hong, Gao, Zhang, Zhang and Sun. This is an open-access article distributed under the terms of the Creative Commons Attribution License (CC BY). The use, distribution or reproduction in other forums is permitted, provided the original author(s) and the copyright owner(s) are credited and that the original publication in this journal is cited, in accordance with accepted academic practice. No use, distribution or reproduction is permitted which does not comply with these terms.

LAZARUS 1 functions as a positive regulator of plant immunity and systemic acquired resistance

Yue Chen[1,2], Yue Han[1,2], Weijie Huang[3], Yanjun Zhang[4], Xiaoli Chen[1,2], Dongyue Li[1,2], Yi Hong[1,2], Huhu Gao[1,2], Kewei Zhang[4], Yuelin Zhang[5] and Tongjun Sun[1,2]*

[1]Shenzhen Branch, Guangdong Laboratory of Lingnan Modern Agriculture, Agricultural Genomics Institute at Shenzhen, Chinese Academy of Agricultural Sciences, Shenzhen, China, [2]Genome Analysis Laboratory of the Ministry of Agriculture and Rural Affairs, Agricultural Genomics Institute at Shenzhen, Chinese Academy of Agricultural Sciences, Shenzhen, China, [3]Department of Botany, University of British Columbia, Vancouver, BC, Canada, [4]Zhejiang Provincial Key Laboratory of Biotechnology on Specialty Economic Plants, College of Life Sciences, Zhejiang Normal University, Jinhua, Zhejiang, China, [5]Key Laboratory of Bio-resource and Eco-environment of Ministry of Education, College of Life Sciences, Sichuan University, Chengdu, China

Systemic acquired resistance (SAR) is activated by local infection and confers enhanced resistance against subsequent pathogen invasion. Salicylic acid (SA) and N-hydroxypipecolic acid (NHP) are two key signaling molecules in SAR and their levels accumulate during SAR activation. Two members of plant-specific Calmodulin-Binding Protein 60 (CBP60) transcription factor family, CBP60g and SARD1, regulate the expression of biosynthetic genes of SA and NHP. CBP60g and SARD1 function as master regulators of plant immunity and their expression levels are tightly controlled. Although there are numerous reports on regulation of their expression, the specific mechanisms by which SARD1 and CBP60g respond to pathogen infection are not yet fully understood. This study identifies and characterizes the role of the LAZARUS 1 (LAZ1) and its homolog LAZ1H1 in plant immunity. A forward genetic screen was conducted in the *sard1-1* mutant background to identify mutants with enhanced SAR-deficient phenotypes (*sard* mutants), leading to the discovery of *sard6-1*, which maps to the *LAZ1* gene. LAZ1 and its homolog LAZ1H1 were found to be positive regulators of SAR through regulating the expression of *CBP60g* and *SARD1* as well as biosynthetic genes of SA and NHP. Furthermore, Overexpression of *LAZ1*, *LAZ1H1* and its homologs from *Nicotiana benthamiana* and potato enhanced resistance in *N. benthamiana* against *Phytophthora* pathogens. These findings indicate that LAZ1 and LAZ1H1 are evolutionarily conserved proteins that play critical roles in plant immunity.

KEYWORDS

salicylic acid, N-hydroxypipecolic acid, CBP60g, SARD1, LAZ1

Introduction

Plant immunity relies on two major classes of immune receptors, located on the cell surface or intracellularly, which recognize a wide range of pathogens, including viruses, bacteria, fungi, oomycetes, insects, and nematodes, and activation of the plant's immune system for self-defense (Jones et al., 2024; Man et al., 2022). The cell surface immune receptors, referred to as Pattern-Recognition Receptors (PRRs) detect pathogen-associated molecular patterns (PAMPs), activating pattern-triggered immunity (PTI), which restricts pathogen invasion (Jones and Dangl, 2006; Zhou and Zhang, 2020). Pathogens secrete effectors into host cells to suppress PTI and disrupt normal physiological processes, facilitating invasion (Jones and Dangl, 2006; Zhou and Zhang, 2020). Intracellular immune receptors, mainly a group of proteins with nucleotide-binding sites and leucine-rich repeat domains (NLRs), recognize effectors secreted by pathogens, activating effector-triggered immunity (ETI) (Jones and Dangl, 2006; Man et al., 2022; Zhou and Zhang, 2020). As a result, both PTI and ETI responses lead to the accumulation of defense signaling molecules, such as salicylic acid (SA) and N-hydroxypipecolic acid (NHP), and trigger secondary immune responses in distant tissues, known as systemic acquired resistance (SAR), which confer enhanced resistance against subsequent pathogen invasion (Chen et al., 2018; Fu and Dong, 2013; Hartmann and Zeier, 2019; Sun and Zhang, 2021).

SA and NHP are two plant defense signaling molecules involved in PTI, ETI and SAR (Hartmann and Zeier, 2019; Peng et al., 2021). Upon pathogen invasion, SA and NHP levels escalate in both local and systemic plant tissues (Hartmann and Zeier, 2019). Application of exogenous SA or NHP on plants enhances their disease resistance (Chen et al., 2018; Hartmann et al., 2018; Peng et al., 2021). In *Arabidopsis*, the perception of SA predominantly depends on the Non-expressor of *PR* genes 1 (NPR1) and its homologs, NPR1-LIKE proteins 3 and 4 (NPR3/4), leading to upregulating the expression of genes associated with immune responses (Ding et al., 2018; Fu et al., 2012; Wu et al., 2012). Although perception of SA by NPR1 and NPR3/NPR4 is required for NHP-induced resistance in *Arabidopsis*, NPR proteins fail to bind to NHP (Liu et al., 2020), implying that SA and NHP signaling might occur via distinct pathways.

Biosynthesis processes of both SA and NHP are well illustrated. SA biosynthesis in plants is mediated by the isochorismate synthase (ICS) and phenylalanine (Phe) ammonia-lyase (PAL) pathways (Peng et al., 2021). In *Arabidopsis thaliana*, the ICS pathway contributes predominantly to SA levels. The ICS pathway include ICS1, the MATE transporter EDS5 and the aminotransferase PBS3 (Rekhter et al., 2019; Torrens-Spence et al., 2019). ICS1 is the rate limiting enzyme of the ICS pathway and its expression level is tightly regulated by various transcription factors (Huang et al., 2020; Wildermuth et al., 2001). The NHP biosynthetic process involves three enzymatic steps performed by the aminotransferase ALD1, the reductase SARD4 and the monooxygenase FMO1, catalyzing the conversion of lysine into NHP (Chen S. et al., 2021; Ding et al., 2016; Navarova et al., 2012). Expression of these NHP biosynthetic genes is also dynamically controlled during plant defense (Huang et al., 2020).

Two members of plant-specific Calmodulin-Binding Protein 60 (CBP60) transcription factor family, CBP60g and SARD1, regulate expression of biosynthesis genes of both SA and NHP upon pathogen infection (Sun et al., 2015; Wang et al., 2009; Zhang et al., 2010). Despite their common ancestry within the same protein family, CBP60g and SARD1 operate through separate pathways. The loss of either SARD1 or CBP60g results in a significant reduction in the levels of *ICS1* and SA, while in the *sard1-1 cbp60g-1* double mutant, the induction of *ICS1* expression and the biosynthesis of SA are both blocked, suggesting that SARD1 and CBP60g regulate *ICS1* expression through two parallel pathways (Wang et al., 2011; Zhang et al., 2010). Expression of *SARD1* and *CBP60g* is also tightly regulated by various transcription factors, including positive regulators such as TGA1/4, NPR1, CBP60b, WRKY54/79 and GBPL3, as well as negative ones, including CAMTA1/2/3, NPR3/4 and HDA6 (Chen et al., 2021; Ding et al., 2018; Huang et al., 2021; Kim et al., 2022; Li et al., 2021; Sun et al., 2018, 2020; Wu et al., 2021). CBP60g is also regulated post-translationally. CALMODULIN (CAM) TOUCH3 and its homologs CAM1/4/6 cooperate with calcium-dependent protein kinases (CPK4/5/6/11) to phosphorylate and activate CBP60g (Sun et al., 2022). Although significant advances as mentioned above have been made, the specific mechanisms by which SARD1 and CBP60g respond to pathogen infection are not yet fully understood.

In pursuit of a deeper comprehension of CBP60g's role in modulating plant immune responses, we conducted a forward genetic screen in *sard1-1* mutant background to look for mutants with enhanced *SAR-deficient* (*sard*) phenotype using the SAR assay developed by our group (Zhang et al., 2010). After two rounds of SAR screen, about 80 mutants show inheritable enhanced *sard* phenotype. The candidate mutants are further narrowed down to about 40 through direct sequencing known SAR genes, including *CBP60g*, *ICS1*, *EDS5*, *PBS3*, *ALD1* and *FMO1 etc*. In this study, we characterized and identified one of *sard1-1* enhancer mutants, namely *sard1-1 sard6-1*, using bulked-segregant analysis sequencing (BSA-Seq) and genetic complementation, confirming that *SARD6* encodes LAZARUS1 (LAZ1, AT4G38360). LAZ1 encodes a protein with a domain of unknown function (DUF300) and has been previously shown to modulate brassinosteroid and programmed cell death signaling pathways (Liu et al., 2018; Malinovsky et al., 2010). Here, we show that LAZ1 and its homolog LAZ1 HOMOLOG1 (LAZ1H1, AT1G77220) are positive regulators of plant immunity and SAR. In addition, LAZ1 and LAZ1H1 are conserved proteins and overexpression of their homologs from *Nicotiana benthamiana* (*Nb*) and *Solanum tuberosum* in *Nb* leaf showed enhanced resistance against *Phytophthora* pthogens. These results suggest that LAZ1 and LAZ1H1 are evolutionarily conserved and play a positive role in immunity.

Materials and methods

Plant material and growth environment

Arabidopsis plants were grown in soil at 23°C/21 °C day/night under 16/8-h light/dark cycles in a growth chamber with 40%

relative humidity (RH) (Bi et al., 2010). The *N. benthamiana* plants were sowed and grown in a controlled environment room (CER) at 22 °C and 45–65% humidity with a 16/8-h light/dark cycles (Lin et al., 2023). Four-week-old plants were used for assay. The potato plants were grown in an artificial climate chamber at 25 ± 2 °C and 58–67% relative humidity under a 16/8-h light/dark photoperiod (Yang et al., 2023).

Mapping-by-sequencing

Mapping-by-sequencing involves combining next-generation sequencing with classical genetic mapping to identify candidate mutations associated with a phenotype was carried out as previously described (Sun et al., 2020). The mutant phenotype of the selected F_2 lines were confirmed by examining the self-fertilized F_3 progeny. Leaves were collected from the F_3 progeny of 30 F_2 lines with confirmed mutant-like phenotype. Genomic DNA was extracted from the mixed tissue and sent for WGS. WGS reads were aligned with the TAIR10 reference genome. SNPs were identified and the ratios of SNPs were plotted and used for linkage analysis. Genes containing nonsynonymous mutations in the linkage region were selected as candidate genes for knockout analysis.

Mutant generation

The *laz1* mutations were generated by targeting *AT4G38360* in *sard1-1* and Col using the egg cell- specific promoter-controlled CRISPR/Cas9 system (Wang et al., 2015). The *laz1h1* mutations were generated by targeting *AT1G77220* in *sard1-1* and Col, respectively, using the same CRISPR/Cas9 system. The *sard1-1 sard6-2* F_2 mutant was obtained by crossing *sard1-1* with SALK_023954C (*laz1-7*). The *sard1-1*mutant was reported (Zhang et al., 2010). Refer to Supplementary Table S1 for a comprehensive list of all primers utilized in this process.

Quantitative PCR

Total RNA was extracted from various tissues using TRIzol reagent (Invitrogen). Complementary DNAs (cDNAs) were synthesized using a ReverTra Ace kit (Toyobo) and served as templates for quantitative reverse transcription polymerase chain reaction (qRT-PCR), which was conducted with a SYBR Premix ExTaq kit (Takara) on a Bio-Rad iQ2 system. The procedure was as follows: initial polymerase activation for 30 s at 95°C followed by 40 cycles of 95°C for 5 s and 60°C for 20 s (Chen Y. et al., 2021). Each sample underwent three biological replicates and three technical replicates. The expression levels of the target genes were normalized to those of the actin gene. Primers used for qPCR can be found in Supplementary Table S1.

Pathogen infection assays

The obligate pathogen *Hyaloperonospora arabidopsidis* (*Hpa*) Noco2 spore suspension in water was weekly propagated on Col seedlings at 18 °C and 60-80% humidity with a 12/12-h light/dark cycles (Zhang et al., 2010; Bi et al., 2010). The *Phytophthora infestans* (*P. infestans*) strain 1306 were cultured on Rye A agar medium at 18°C in the dark. The *Phytophthora capsici* (*P. capsici*) strain BYA5 was cultured on Rye A agar medium at 24°C in the dark (Abrahamian et al., 2016; Wang et al., 2019). The bacterial pathogen *Pseudomonas syringae pv maculicola* (*Psm*) ES4326 was cultured on King's B medium Agar plate supplemented with 50 μg/mL streptomycin at 28°C incubator (Zhang et al., 2010).

For infection with *Psm* ES4326 (diluted in 10 mM $MgCl_2$ to OD_{600} as indicated below) or 10 mM $MgCl_2$, leaves of 3-week-old plants were infiltrated with the bacteria at a dose of OD_{600} = 0.0025-0.005 for SAR and OD_{600} = 0.001 for gene expression. For SAR assay (Zhang et al., 2010), the *Hpa* Noco2 infection assay was carried out on 3-week-old soil-grown seedlings two days after infection with *Psm* ES4326, by spraying plants with *Hpa* Noco2 spore suspension at a concentration of 5 x 10^4 spores/mL. Inoculated plants were covered with a clean dome and grown at 18 °C under 12/12-h light/dark cycles in a growth chamber and growth of *Hpa* Noco2 was quantified seven days later. For genes expression, infected leaves were collected at two days after inoculation, two or three infected leaves of different plants were collected as one sample, and three samples were used for each genotype (Bi et al., 2010; Lan et al., 2023).

For inoculation assay with *P. infestans* strain 1306 (Abrahamian et al., 2016) and *P. capsici* strain BYA5 (Wang et al., 2019) on *Nb* leaves, Agrobacterium tumefaciens cultures were resuspended in infiltration buffer (10 mM $MgCl_2$, 10 mM MES [pH 5.6], and 150 μM acetosyringone) at a final concentration of OD_{600} = 0.6 and infiltrated into leaves for transient expression of interested genes in planta. The leaves were detached 48h after agroinfiltration, then inoculated with *P. capsici* BYA5 mycelium (r = 2.5 mm) or 10 μL of the *P. infestans* 1306 zoospore suspension (200 zoospores/μL). The lesion areas (cm^2) of *P. capsici*-inoculated leaves were measured under UV light at 48 h after inoculation. The *P. infestans*-inoculated leaves were incubated in a growth chamber at 18°C, and lesion areas were scored 3-4 days after infection.

Determination of SA concentrations

The total SA was extracted following a modified method previously described for extraction of phenolic compounds (Zhang et al., 2012). About 100 mg of leaf tissue from 3- or 4-week-old plants 2 days after inoculation with *Psm* ES4326 (OD_{600} = 0.001) was collected, in four biological replicates from independent plants for each genotype. The rosette leaves were ground in liquid nitrogen. Around 100mg powders were added into 1ml 80% MeOH in a 2ml eppendorf tube. Then the eppendorf tube was agitated for 2hr at 4°C, and then centrifuged at 13,000g at 4°C for 10 min. The supernatant was transferred into a new eppendorf tube, and the sediment was re-

extracted with 500µl 100% MeOH. Both extracts were combined and blow-dryed by nitrogen gas, then was resolved by 500µl sodium acetate (0.1M, pH 5.5). The resuspension was added with 10 µl β-glucosidase (1Uµl-1) and hydrolyzed at 37°C for 2hr in the water bath. After the hydrolysate was heated in boiling water for 5 min and centrifuged at 13,000g at 4°C for 10 min, the supernatant was used for analyzing total SA by HPLC as mentioned previously (Zhang et al., 2012). SA was detected at 296-nm excitation and 410-nm emission by using fluorescence detector. According to the standard curve, the concentration of SA is calculated by the HPLC peak area.

Results

Identification of *sard1-1 sard6-1* mutants

As shown in Figures 1A, B, wild-type (Col) plants were susceptible to the virulent isolate of *Hyaloperonospora arabidopsidis* (*Hpa*) Noco2. After treatment with the bacterial pathogen *Pseudomonas syringae pv maculicola* (*Psm*) ES4326, Col plants became resistant against *Hpa* Noco2, suggesting an robust SAR response induced by *Psm* infection. The *sard1-1* plants showed a mild SAR-compromised phenotype, while the *sard1-1 sard6-1* double mutant exhibited an exacerbated SAR-deficient phenotype. We examined *Psm*-induced expression of the defense marker genes *PR1* and *PR2* in those lines and found that induction of both genes in *sard1-1 sard6-1* double mutant by *Psm* treatment was significantly reduced compared to that in *sard1-1* mutant (Figures 1C, D). We also detected a further compromised induction of critical genes involved in SA biosynthesis *CBP60g* and *ICS1* in the *sard1-1 sard6-1* mutant compared to *sard1-1* mutant (Figures 1E, F). Next, we quantified SA levels in Col, *sard1-1* and the *sard1-1 sard6-1* mutant plants. Following treatment with *Psm*, the total SA levels in the *sard1-1 sard6-1* mutant was significantly reduced compared to those in the Col or *sard1-1* plants (Figure 1G). These findings indicate that the systemic resistance in the *sard1-1 sard6-1* mutant may be impeded due to the impact on the induction of *CBP60g* and SA biosynthesis.

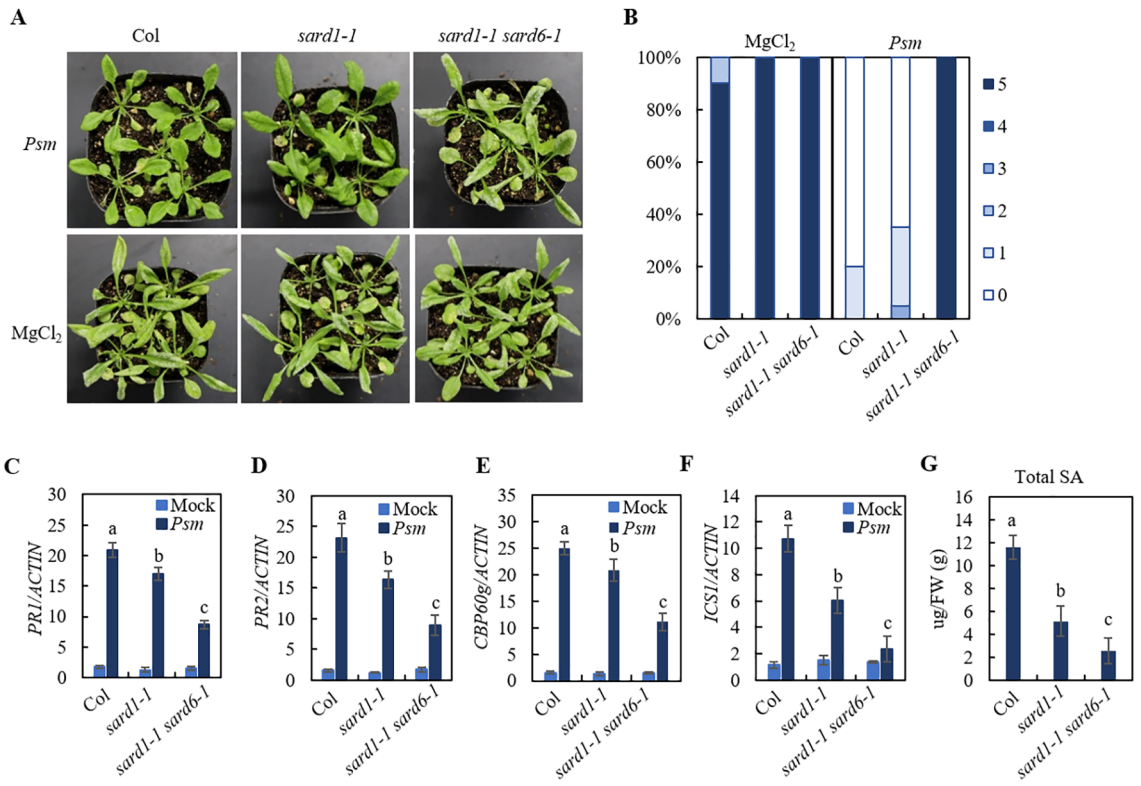

FIGURE 1
Identification of *sard1-1 sard6-1* mutant lines of Arabidopsis. **(A)** Growth of *Hpa* Noco2 on the distal leaves of wild-type Col, *sard1-1* and *sard1-1 sard6-1* plants in a SAR assay. Two primary leaves of 3-week-old plants were infiltrated with *Psm* ES4326 (OD_{600} = 0.0025) or 10 mM $MgCl_2$ (mock) 2 d before the plants were sprayed with *Hpa* Noco2 spore suspension (50,000 spores/mL in water). **(B)** SAR phenotypic statistics of wild-type Col, *sard1-1* and *sard1-1 sard6-1* plants. Disease ratings are as follows: 0, no conidiophores on plants; 1, one leaf is infected with no more than five conidiophores; 2, one leaf is infected with more than five conidiophores; 3, two leaves are infected but with no more than five conidiophores on each infected leaf; 4, two leaves are infected with more than five conidiophores on each infected leaf; 5, more than two leaves are infected with more than five conidiophores. The experiment was repeated three times with independently grown plants, yielding similar results. **(C–F)** Expression of *PR1, PR2 CBP60g* and *ICS1*. Total RNA was extracted from the leaves of 3-week-old plants 2 d after infiltration with *Psm* ES4326 (OD_{600} = 0.001) or 10 mM $MgCl_2$ (mock). Data were normalized relative to the expression of the *AtActin* gene. Error bars means ± SD of 3 biological replicates. Significant differences indicated by different letters were calculated using the Duncan's new multiple range test. **(G)** total SA levels in leaves of Col, *sard1-1* and *sard1-1 sard6-1* 2 days after inoculation with *Psm* ES4326 (OD_{600} = 0.001). Bars represent means ± SD (n = 3). Statistically significant differences among the samples are labelled with different letters (one-way ANOVA with Tukey's multiple comparisons test, P< 0.05).

SARD6 encodes LAZARUS1

To identify *sard6*, we performed combining next-generation sequencing with classical genetic mapping to identify candidate mutations associated with a phenotype on *sard1-1 sard6-1* mutant. The *sard1-1 sard6-1* mutant was backcrossed with the *sard1-1* line and resulting F_1 plants exhibit *sard1*-like *sard* phenotype (Figure 2A; Supplementary Figure S1A), suggesting *sard6-1* is a recessive mutant. In the F_2 generation, lines with *sard1-1 sard6-1*-like and *sard1*-like *sard* phenotype were kept and validated in the F3 progeny, respectively. Pooled genomic DNA from each segregant population (30 confirmed lines) was subjected to whole-genome next-generation sequencing (WGS). Analysis of the single nucleotide polymorphism (SNP) frequency distribution across the genome unveiled a linked genetic region on chromosome 4 (Supplementary Figure S1B). Within this chromosomal segment, three genes, *AT4G30790*, *AT4G30990* and *AT4G38360*, using linkage analysis, we detected G to A transitions that resulted in missense mutations (Figure 2B). To ascertain the gene correlating with the *sard1-1 sard6-1* phenotype, we generated deletion mutant for each gene in *sard1-1* background using CRISPR/Cas9 technology (Figure 2C). Upon subsequent SAR analysis of the homozygous lines for the three candidate genes, only *sard1-1 AT4G38360*-cr double mutant phenocopied *sard1-1 sard6-1*, indicating that *AT4G38360*, alias *LAZARUS1* (*LAZ1*) (Malinovsky et al., 2010), is the gene of interest (Figure 2D).

To further ascertain the association of the mutation in *AT4G38360* with the *sard1-1 sard6-1* phenotype, we identified the *sard1-1 sard6-2* double mutant from F_2 progeny of a cross between *sard1-1* and *sard6*-2, a T-DNA mutant SALK_023954C targeting the *At4G38360* locus and silencing the gene (Supplementary Figures S2A, S2C), and confirmed DNA fragment deletion in *sard1-1 AT4G38360*-cr double mutant (reassigned as *sard1-1 sard6*-3) using Sanger sequencing (Supplementary Figure S2B). Subsequent SAR verification revealed that both *sard1-1 sard6-2* and the *sard1-1 sard6-3* lines exhibited *sard1-1 sard6-1*-like *sard* phenotype (Figure 2E). Additionally, we performed genetic complementation by agrobacteria mediated transformation of a 4.3 kb fragment containing LAZ1 coding region into the *sard1-1 sard6-1* mutant. Three independent lines with LAZ1 expression were chosen and tested for SAR phenotype (Supplementary Figure S2D). As shown in Figure 2F, these three lines exhibited *sard1*-like *sard* phenotype, indicating that expressing LAZ1 revert the enhanced *sard* phenotype of *sard1-1 sard6-1*. These findings support that the *SARD6* locus corresponds to *AT4G38360*/*LAZ1*, encoding a protein with a DUF300 domain. This protein is implicated in vacuolar transport and appears to modulate brassinosteroid signaling pathways (Malinovsky et al., 2010). For simplicity and consistency, *sard6-1*, *sard6-2* and *sard6-3* is reassigned to *laz1-6*, *laz1-7 and laz1-8*, respectively (Supplementary Figure S2A).

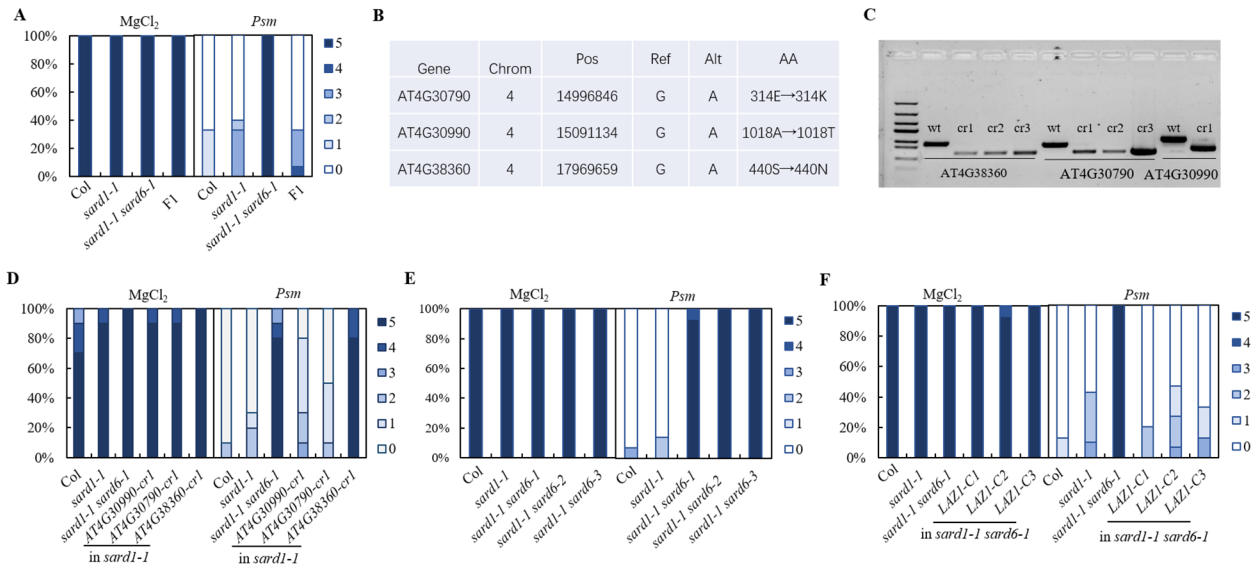

Gene	Chrom	Pos	Ref	Alt	AA
AT4G30790	4	14996846	G	A	314E→314K
AT4G30990	4	15091134	G	A	1018A→1018T
AT4G38360	4	17969659	G	A	440S→440N

FIGURE 2
Positional cloning and gene verification of *sard6*. **(A)** SAR phenotypic statistics of wild-type Col, *sard1-1*, *sard1-1 sard6-1* double mutants and the F_1 progeny of *sard1-1* crossed with *sard1-1 sard6-1* plants. **(B)** Compilation of candidate genes with annotations including Chromosome (Chrom), Position (Pos), Reference allele (Ref), Alternate allele (Alt), and Amino acid (AA) changes. **(C)** Electropherograms depicting the wild-type and knockout genotypes for the candidate genes. The wild-type (WT) lanes are aligned alongside those representing the respective deletion mutants generated using CRISPR/Cas9 system. cr1 lines are in *sard1-1* background and used in Figure 1D. **(D)** SAR phenotypic statistics comparing the wild-type Col, *sard1-1*, *sard1-1 sard6-1* double mutants, and deletion lines in *sard1-1* background: *AT4G30990-cr1* (deletion mutation in *AT4G30990*), *AT4G30790-cr1* (deletion in *AT4G30790*), and *AT4G38360-cr1* (deletion in *AT4G38360*). **(E)** SAR phenotypic statistics of wild-type Col, *sard1-1*, *sard1-1 sard6-1* and *sard1-1 sard6-2*, *sard1-1 sard6-3* plants. *sard6-2* and *sard6-3* are T-DNA allele and deletion allele for *AT4G38360*, respectively; see details in Supplementary Figures S2A, B. **(F)** SAR phenotypic statistics of wild-type Col, *sard1-1*, *sard1-1 sard6-1* and *sard1-1 laz1-C* plants. *sard1-1 laz1-C*: complementation lines of AT4G38360 in *sard1-1 sard6-1*.

LAZ1 HOMOLOGO1 positively regulates SAR

In Arabidopsis, LAZ1 has a close homolog, LAZ1 Homolog 1 (LAZ1H1, AT1G77220). Quantitative PCR analysis of the expression of *LAZ1* and *LAZ1H1* showed that both genes were induced after *Psm* ES4326 treatment (Supplementary Figures S3A, B), indicating that, like *LAZ1*, *LAZ1H1* may also play a role in plant immunity. To check whether LAZ1H1 contributes to SAR, we employed CRISPR/Cas9 technology to generate knockout mutants for *LAZ1H1* in both the Col and *sard1-1* backgrounds. Utilizing PCR amplification and sanger sequencing, we identified three homozygous deletion lines in the *sard1-1* background and three deletion lines in Col, designated as *sard1-1 laz1h1-1*, *sard1-1 laz1h1-2*, *sard1-1 laz1h1-3*, *laz1h1-4*, *laz1h1-5* and *laz1h1-6*, respectively (Supplementary Figure S3C). Upon verification of SAR response in the *sard1-1 laz1h1* lines, we observed that they exhibited the same phenotype as the *sard1-1 laz1-8* double knockout, while *laz1h1* mutants showed minimal *sard* phenotype (Supplementary Figure S3D), suggesting that LAZ1H1 also positively regulates SAR.

LAZ1 and LAZ1H1 play overlapping roles in plant immunity

To investigate the roles of *LAZ1* and *LAZ1H1* in SAR, we employed CRISPR/Cas9 technology to generate knockout mutants for *laz1* in Col background. Utilizing PCR amplification and sanger sequencing, we identified two homozygous deletion lines in Col, designated as *laz1-9*, *laz1-10* respectively (Supplementary Figure S2B), and generated *laz1-7 laz1h1-5* double mutant from F_3 progeny of a cross between *laz1-7* and *laz1h1-5*. *Psm*-induced SAR in Col, *laz1-7*, *laz1-9*, *laz1-10*, *laz1h1-5*, *laz1-7 laz1h1-5* plants were performed. Compared to Col, the mutants *laz1-7*, *laz1-9* and *laz1-10*, *laz1h1-5* exhibited a weak *sard* phenotype, *laz1-7 laz1h1-5* exhibited a stronger *sard* phenotype (Figure 3A).

We examined *Psm*-induced expression of *SARD1 and CBP60g* as well as biosynthetic genes of SA and NHP in Col, *laz1-7*, *laz1h1-5* and *laz1-7 laz1h1-5* lines and found that induction of these genes in three mutants were significantly reduced compared to that in Col, and the expression levels of *ICS1*, *EDS5*, *PBS3*, *ALD1*, *SARD4* and *FMO1* were lower in *laz1-7 laz1h1-5* (Figures 3B–D). The results showed that *laz1* and *laz1h1* play overlapping roles in plant immunity.

LAZ1 is not required for NHP-induced immunity

Given that NHP acts as the mobile signal for SAR (Chen et al., 2018; Hartmann et al., 2018) and that the LAZ1/LAZ1H1 are putative channel proteins, we investigated whether LAZ1/LAZ1H1 is necessary for NHP-induced immune responses. Col, along with the *laz1-7*, *laz1-9*, *laz1-10*, *laz1h1-4*, *laz1h1-5*, *laz1h1-6* and *laz1-7 laz1h1-5* mutants were utilized as experimental materials

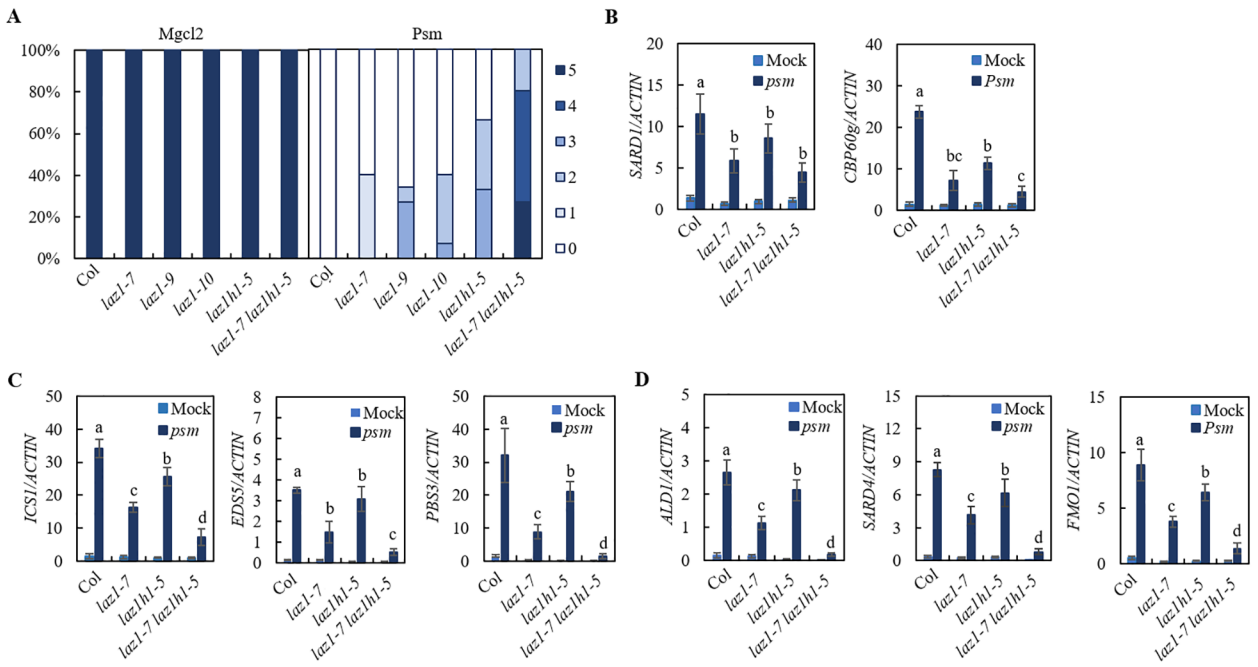

FIGURE 3
SAR phenotype in *laz1* and *laz1h1* mutants. **(A)** SAR phenotypic statistics in Col, *laz1-7*, *laz1-9*, *laz1-10*, *laz1h1-5* and *laz1-7 laz1h1-5* plants. **(B–D)** Expression of *SARD1*, *CBP60g*, *ICS1*, *EDS5*, *PBS3*, *ALD1*, *SARD4* and *FMO1*. Total RNA was extracted from the leaves of 3-week-old plants 2d after infiltration with *Psm* ES4326 (OD_{600} = 0.001) or 10 mM $MgCl_2$ (mock). Data were normalized relative to the expression of the *AtActin* gene. Error bars means ± SD of 3 biological replicates. Significant differences indicated by different letters were calculated using the Duncan's new multiple range test.

for verification. Initially, we infiltrated the primary leaves with 1 mM or 0.3 mM NHP and subsequently spray-inoculated the entire plants with a spore suspension of *Hpa* Noco2, separately. As depicted in Supplementary Figure S4, minimal pathogen growth was observed on Col pretreated with NHP, indicating that NHP confers robust resistance against *Hpa* Noco2. Similar outcomes were observed in the NHP-pretreated seven mutant lines. These results suggest that *laz1* and *laz1h1* are not involved in the regulation of NHP-induced immunity.

Overexpression of *LAZ1* and *LAZ1H1* enhances the resistance of *N. benthamiana* to *Phytophthora*

The results mentioned above suggest that LAZ1 and LAZ1H1 positively regulate immunity against the obligate oomycete *Hpa* Noco2. To determine if LAZ1 and LAZ1H1 could augment resistance against different *Phytophthora* pathogens, we individually inserted the genomic sequences of *LAZ1* and *LAZ1H1*, including 35S promoters, coding regions, and terminators, into the pCAMBIA1300 vector. These constructs were transformed into agrobacterium and used for agrobacterium-mediated transient overexpression of the respective proteins in *Nicotiana benthamiana* (*Nb*) leaves. After 48 hours post-infiltration of agrobacterium strain carrying 35S-*LAZ1*, 35S-*LAZ1H1* or empty vector, the *Nb* leaves were inoculated with spores of *P.infestans* strain 1306 or mycelium of *P.capsici* strain BYA5. The resulting lesion areas were evaluated 3-4 days following infection. In Figure 4A, *Nb* leaf areas overexpressing *LAZ1* exhibited significantly reduced lesion sizes compared to those with an empty-vector (EV) control after inoculation with *P.infestans* strain 1306, with statistically significant differences in lesion sizes observed (Figure 4B). Overexpression of *LAZ1H1* yielded analogous results (Figures 4C, D).

Similarly, overexpression of *LAZ1* or *LAZ1H1* lead to reduced lesion sizes compared to the EV control, following infection with *P.capsici* strain BYA5 (Figures 4E–H). These findings indicate that overexpression of *LAZ1* or *LAZ1H1* in *Nb* leaves can enhance resistance to *P.infestans* and *P.capsici*.

Overexpression of homologous genes of *LAZ1* enhances the resistance of *N. benthamiana* to *P.infestans*

Homologs of *LAZ1* were found in various plants. To understand whether homologs of the *LAZ1* gene in *N.benthamiana* and

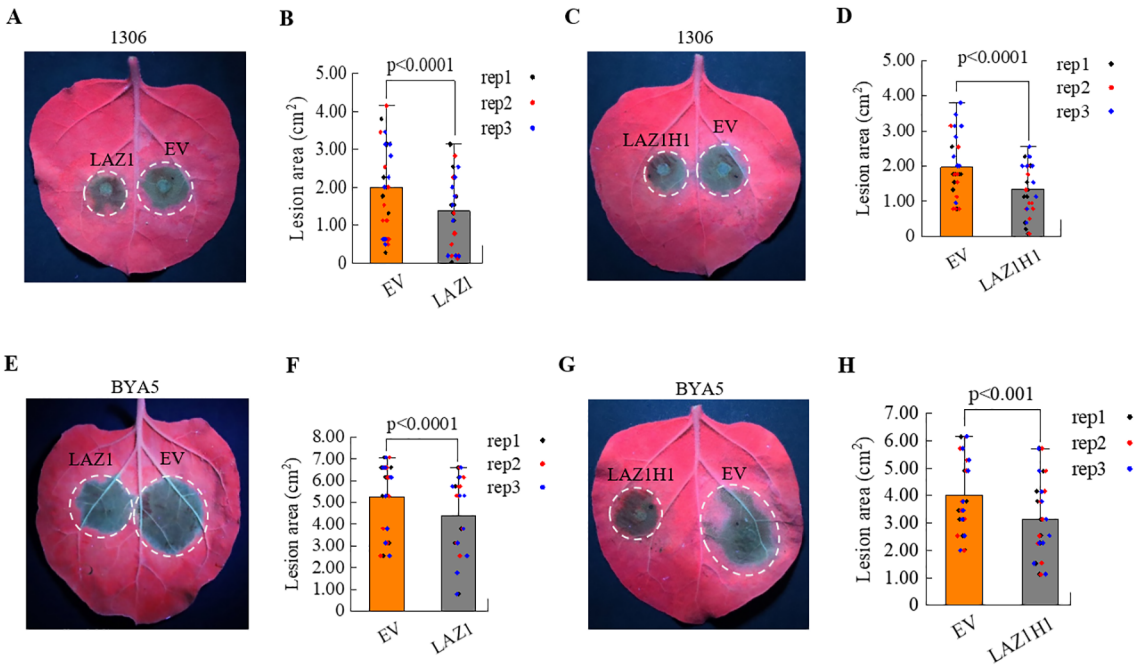

FIGURE 4
Impact of *LAZ1* and *LAZ1H1* on *N. benthamiana*. **(A)** Infection assays on *N. benthamiana* (*Nb*) leaves transient expression of LAZ1 or EV with *P. infestans* strain 1306. Two days after infiltration with Agrobacterium carrying *35S-LAZ1* or empty vector (EV), leaf areas were inoculated with *P. infestans* 1306 zoospore suspension. Detached leaves were incubated in a growth chamber at 18°C, and lesion areas were scored under UV light 3–4 days after infection. **(B)** Statistical analyses on lesion sizes of *Nb* leaves in Figure 4A (n=10-15 from three replicates). **(C)** Infection assays on *Nb* leaves transient expression of LAZ1H1 or EV with *P. infestans* strain 1306, following the same procedure as in Figure 4A. **(D)** Statistical analyses on lesion sizes of *Nb* leaves in Figure 4C (n=10-15 from three replicates). **(E–H)** Infection assays on *Nb* leaves transient expression of LAZ1, LAZ1H1 or EV with *P. capsici* strain BYA5. Two days after infiltration with Agrobacterium carrying *35S-LAZ1* **(E)**, *35S-LAZ1H1* **(G)** or empty vector (EV), leaf areas were inoculated with *P. capsici* BYA5 mycelium. Detached leaves were incubated in a growth chamber at 25°C, and lesion areas were measured under UV light 36 h after inoculation. Statistical analyses on lesion sizes were shown in **(F)** (n=10-15 from three replicates) and **(H)** (n=10-15 from three replicates), respectively. In **(B, D, F, H)** data were normally distributed and were shown as means ± SD. Outliers were identifed and removed using Grubbs test. Statistical significance was determined by Student's *t* test.

Solanum tuberosum (potato) can enhance resistance to *Phytophthora*, we identified sequences with high homology to *LAZ1* from the *N.benthamiana* genome database (https://nbenthamiana.jp/nbrowser/anno) (Kurotani et al., 2023) and the genome database of the diploid potato inbreeding line A157 (Zhang et al., 2021). The protein sequences of Nbe.v1.s00130g02480 (NB00130g02480) and Nbe.v1.s00150g07560 (NB00150g07560) in *N.benthamiana* and the protein sequences of A157_07G018790 and A157_12G022720 in A157 showed the highest homology to LAZ1 protein (Figure 5A). Phylogenetic analysis grouped these four genes into a single cluster, suggesting a close evolutionary relationship, and LAZ1 is closely related to these four proteins (Supplementary Figure S5A). The coding sequences (CDS) of these four homologs gene were amplified and individually inserted into the binary pCAMBIA1300 vector under the 35S promoter. Transient expression in *Nb* leaves followed by inoculation with *P.infestans* strain 1306 revealed that the lesion areas at sites of overexpression of these four genes were significantly reduced compared to the empty-vector (EV) control (Figure 5B), with statistically significant differences observed (Figure 5C). Validation through western blot analysis confirmed the presence of protein products encoded by these genes in *Nb* leaves (Supplementary Figure S5B). These

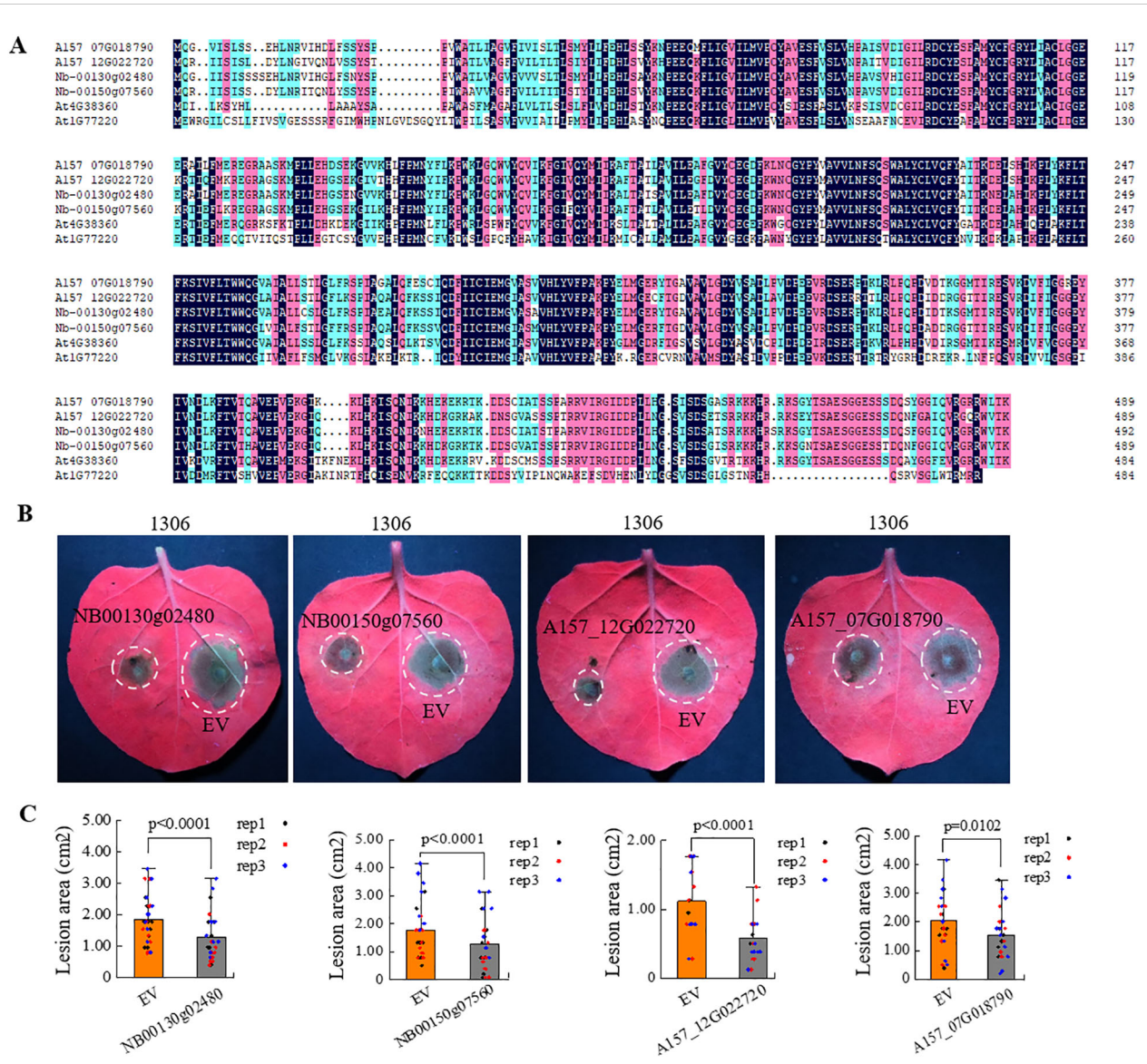

FIGURE 5
Influence of *LAZ1* homologous genes from *N. benthamiana* and potato on *N. benthamiana* immunity. **(A)** Protein sequence alignment with the highest homology of LAZ1 in *N. benthamiana* and potato. **(B)** Infection assays were performed on *Nb* leaves overexpressing the *LAZ1* homologous genes from *N. benthamiana* (*NB00130g02480* and *NB00150g07560*) and potato (*A157_12G022720* and *A157_07G018790*), challenged with *P. infestans* strain 1306. **(C)**, Data processing and statistical analysis of lesion sizes in **(B)**. Data were normally distributed and were shown as means ± SD (n=10-15 from three replicates). Outliers were identified and removed using Grubbs test. Statistical significance was determined by Student's *t* test.

findings indicate that overexpression of these *LAZ1* homologs significantly enhances the resistance of *N. benthamiana* to *P.infestans*.

Discussion

LAZ1/LAZ1H1 are positive regulators of SAR

LAZ1 and LAZ1H1 belong to the evolutionarily conserved DUF300 family of transmembrane proteins in eukaryotes. LAZ1 serves as a regulatory factor for certain Hypersensitive Response (HR) cell deaths conditioned by the TIR-NB-LRR protein RPS4 and by the CC-NB-LRR protein RPM1 (Malinovsky et al., 2010). LAZ1 and LAZ1H1 have been shown to play a pivotal role in maintaining vacuole membrane integrity, which is crucial for proper Brassinosteroid (BR) signaling (Liu et al., 2018). Despite these insights, the roles of LAZ1 and LAZ1H1 in the systemic acquired resistance (SAR) pathway remain unexplored. In this report, we show that LAZ1 and LAZ1H1 are positive regulators of SAR.

Employing a forward genetic strategy, we isolated the *sard1-1 sard6-1* mutant as one of *sard* enhancers of *sard1-1*. This *sard1-1 sard6-1* mutant exhibited severely impaired systemic resistance (Figures 1A, B). Through mapping-by-sequence and gene complementation, we identified that *SARD6* encodes LAZ1 (Figure 2). We also found that loss-of-function of *LAZ1H1* leads to enhanced SAR deficiency in *sard1-1* background (Supplementary Figure S3). Furthermore, we showed that the *laz1 laz1h1* double mutant exhibited stronger *sard* phenotype compared to *laz1* and *laz1h1* single mutants (Figure 3A), indicating a functional redundancy between LAZ1 and LAZ1H1 in regulation of SAR.

In this study, we have used *Psm* ES4326, a virulent pathogen which does not trigger HR, to induce SAR and found that *Laz1* and *laz1h1* mutants are compromised in SAR, suggesting that LAZ1/LAZ1H1 play an HR-independent role in SAR.

LAZ1/LAZ1H1 regulate SAR by affecting expression of biosynthesis genes of SA and NHP

SA and NHP are two key signaling molecules in SAR and expression levels of their biosynthetic genes are tightly controlled during plant immunity (Hartmann and Zeier, 2019; Peng et al., 2021). SARD1 and CBP60g are master transcriptional regulators in plant defense and positively regulate biosynthetic genes of SA and NHP (Sun et al., 2020). *Psm*-induced expression of *CBP60g* and *ICS1* in *sard1-1 sard6-1* was further diminished compared to that in *sard1-1* (Figures 1E, F) and total SA levels was lower in *sard1-1 sard6-1* than that in *sard1-1* (Figure 1G), indicating that the involvement of LAZ1 in SAR may be attributed to its regulatory effects on the expression of *CBP60g* and *ICS1*, as well as the accumulation of SA.

laz1 and *laz1h1* single mutants showed minor *sard* phenotype while *laz1 laz1h1* double mutant exhibited stronger *sard* phenotype (Figure 3A). Accordingly, *Psm*-induced expression of biosynthesis genes of SA and NHP in *laz1* and *laz1h1* single mutants was reduced compared to that in Col, and further diminished in *laz1 laz1h1* double mutant (Figures 3C, D), suggesting that LAZ1 and LAZ1H1 have an overlapping function in SAR and that they positively regulate SAR by modulating the expression of biosynthetic genes of SA and NHP. Since *Psm*-induced expression of *SARD1* and *CBP60g* was diminished in *laz1 laz1h1* double mutant (Figure 3B), it is possible that LAZ1 and LAZ1H1 modulate the expression of biosynthetic genes of SA and NHP through regulating expression of *SARD1* and *CBP60g*. In addition, we showed that NHP-induced resistance against *Hpa* Noco2 was not significantly affected in *laz1*, *laz1h1 or laz1 laz1h1* double mutant (Supplementary Figure S4). These results suggest that LAZ1 and LAZ1H1 regulate SAR mainly through affecting the expression of biosynthesis genes of SA and NHP. However, the underlying mechanism necessitates further investigation.

Recently, LAZ1 homologs in maize, ZmLAZ1-4 and ZmLAZ1-8, were predicted to bind metal ions including Zn^{2+}, Mg^{2+}, or Ca^{2+} and ZmLAZ1-4 protein was shown to act as a Zinc transporter that modulate Zinc homeostasis on plasma and vacuolar membrane (Liu et al., 2022), it will be interesting to test whether LAZ1 and LAZ1H1 combine Ca^{2+} and regulate the expression of defense genes through modulating calcium homeostasis during plant immunity.

LAZ1 and LAZ1H1 are evolutionarily conserved

LAZ1 and LAZ1H1 are conserved proteins with their homologs found in various plants. We showed overexpression of *LAZ1* and *LAZ1H1* as well as their close homologs from *N.benthamiana* and potato in *Nb* leaves leads to enhanced resistance to *Phytophthora* species (Figures 4, 5), suggesting that LAZ1 and LAZ1H1 are evolutionarily conserved in positive regulation of plant defense, thereby emphasizing the significance and utility of these genes in investigating plant-pathogen interactions. Presently, in potato, the cultivation of disease-resistant varieties is mainly to isolate disease resistance genes from wild species and introduce them into cultivated varieties through genetic transformation. The homologs of LAZ1 in potato were found to similarly bolster the plants' resistance to Phytophthora (Figures 5B, C). This study provides an important genetic resource for potato disease resistance breeding.

Data availability statement

The original contributions presented in the study are included in the article/Supplementary Material. Further inquiries can be directed to the corresponding author.

Author contributions

YC: Funding acquisition, Investigation, Writing – original draft, Data curation, Formal analysis, Visualization, Writing – review & editing. YHa: Data curation, Validation, Resources, Writing – review

& editing. WH: Data curation, Methodology, Writing – review & editing. YaZ: Data curation, Methodology, Writing – review & editing. XC: Resources, Validation, Writing – review & editing. DL: Methodology, Writing – review & editing. YHo: Methodology, Writing – review & editing. HG: Methodology, Writing – review & editing. KZ: Supervision, Writing – review & editing. YuZ: Supervision, Writing – review & editing, Conceptualization. TS: Conceptualization, Funding acquisition, Supervision, Writing – original draft, Writing – review & editing.

Funding

The author(s) declare financial support was received for the research, authorship, and/or publication of this article. This work was supported by the Guangdong Basic and Applied Basic Research Foundation (2023A1515110409 to YC) and by Science, Technology and Innovation Commission of Shenzhen Municipality, China (to TS).

Acknowledgments

We sincerely thank Jinmei Ding and Dr. Qing Kong (National Institute of Biological Sciences, Beijing) for assistance with the *sard1-1* suppressor screen, Dr. Qijun Chen (China Agricultural University) for sharing the pHEE401E constructs, Dr. Suomeng Dong (Nanjing Agricultural University) for *Phytophthora infestans* strain 1306 and Dr. Xili Liu (Northwest Agriculture & Forestry University) for *Phytophthora capsici* strain BYA5.

Conflict of interest

The authors declare that the research was conducted in the absence of any commercial or financial relationships that could be construed as a potential conflict of interest.

Publisher's note

All claims expressed in this article are solely those of the authors and do not necessarily represent those of their affiliated organizations, or those of the publisher, the editors and the reviewers. Any product that may be evaluated in this article, or claim that may be made by its manufacturer, is not guaranteed or endorsed by the publisher.

Supplementary material

The Supplementary Material for this article can be found online at: https://www.frontiersin.org/articles/10.3389/fpls.2024.1490466/full#supplementary-material

References

Abrahamian, M., Ah-Fong., A. M. V., Davis., C., Andreeva., K., and Judelson., H. S. (2016). Gene expression and silencing studies in *phytophthora infestans* reveal infection-specific nutrient transporters and a role for the nitrate reductase pathway in plant pathogenesis. *PloS Pathog.* 12, e1006097. doi: 10.1371/journal.ppat.1006097

Bi, D., Cheng, Y. T., Li, X., and Zhang, Y. (2010). Activation of plant immune re sponses by a gain-of-function mutation in an atypical receptor-like kinase. *Plant Physiol.* 153, 1771–1779. doi: 10.1104/pp.110.158501

Chen, S., Ding, Y., Tian, H., Wang, S., and Zhang, Y. (2021). WRKY54 and WRKY70 positively regulate SARD1 and CBP60g expression in plant immunity. *Plant Signal Behav.* 16, 1932142. doi: 10.1080/15592324.2021.1932142

Chen, Y. C., Holmes, E. C., Rajniak, J., Kim, J. G., Tang, S., Fischer, C. R., et al. (2018). N-Hydroxy-pipecolic acid is a mobile metabolite that induces systemic disease resistance in Ara bidopsis. *Proc. Natl. Acad. Sci. U.S.A.* 115, E4920–E4929. doi: 10.1073/pnas.1805291115

Chen, Y., Zhong, D., Yang, X., Zhao, Y., Dai, L., Zeng, D., et al. (2021). *ZmFdC2* encoding a ferredoxin protein with C-terminus extension is indispensable for maize growth. *Front. Plant Sci.* 12, 646359. doi: 10.3389/fpls.2021.646359

Ding, P., Rekhter, D., Ding, Y., Feussner, K., Busta, L., Haroth, S., et al. (2016). Characterization of a pipecolic acid biosynthesis pathway required for systemic acquired resistance. *Plant Cell* 28, 2603–2615. doi: 10.1105/tpc.16.00486

Ding, Y., Sun, T., Ao, K., Peng, Y., Zhang, Y., Li, X., et al. (2018). Opposite roles of salicylic acid receptors NPR1 and NPR3/NPR4 in tran scriptional regulation of plant immunity. *Cell* 6, 1454–1467. doi: 10.1016/j.cell.2018.03.044

Fu, Z. Q., and Dong, X. (2013). Systemic acquired resistance: turning local infection into global defense. *Annu. Rev. Plant Biol.* 64, 839–863. doi: 10.1146/annurev-arplant-042811-105606

Fu, Z. Q., Yan, S., Saleh, A., Wang, W., Ruble, J., Oka, N., et al. (2012). NPR3 and NPR4 are receptors for the immune signal salicylic acid in plants. *Nature* 486, 228–236. doi: 10.1038/nature11162

Hartmann, M., and Zeier, J. (2019). N-hydroxypipecolic acid and salicylic acid: a metabolic duo for systemic acquired resistance. *Curr. Opin. Plant Biol.* 50, 44–57. doi: 10.1016/j.pbi.2019.02.006

Hartmann, M., Zeier, T., Bernsdorff, F., Reichel-Deland, V., Kim, D., Hohmann, M., et al. (2018). Flavin monooxygenase-generated N-hydroxypipecolic acid is a critical element of plant systemic immunity. *Cell* 173, 456–469. doi: 10.1016/j.cell.2018.02.049

Huang, W., Wang, Y., Li, X., and Zhang, Y. (2020). Biosynthesis and regulation of salicylic acid and N-hydroxypipecolic acid in plant. *Mol. Plant* 13, 31–41. doi: 10.1016/j.molp.2019.12.008

Huang, W., Wu, Z., Tian, H., Li, X., and Zhang, Y. (2021). Arabidopsis CALMODULIN-BINDING PROTEIN 60b plays dual roles in plant immunity. *Plant Commun.* 2, 100213. doi: 10.1016/j.xplc.2021.100213

Jones, J. D. G., and Dangl, J. L. (2006). The plant immune system. *Nature* 444, 323–329. doi: 10.1038/nature05286

Jones, J. D. G., Staskawicz, B. J., and Dangl, J. L. (2024). The plant immune system: From discovery to deployment. *Cell* 187, 2095–2116. doi: 10.1016/j.cell.2024.03.045

Kim, J. H., Castroverde, C. D. M., Huang, S., Li, C., Hilleary, R., Seroka, A., et al. (2022). Increasing the resilience of plant immunity to a warming climate. *Nature* 607, 339–344. doi: 10.1038/s41586-022-04902-y

Kurotani, K.I., Hirakawa, H., Shirasawa, K., Tanizawa, Y., Nakamura, Y., Isobe, S., et al. (2023). Genome sequence and analysis of nicotiana benthamiana, the model plant for interactions between organisms. *Plant Cell Physiol.* 64, 248–257. doi: 10.1093/pcp/pcac168

Lan, J., Chen, Y., Pico, J., Ao, K., Xia, S., Wang, C., et al. (2023). Epigenetic regulation of N-hydroxypipecolic acid biosynthesis by the AIPP3-PHD2-CPL2 complex. *J. Integr. Plant Biol.* 65, 2660–2671. doi: 10.1111/jipb.v65.12

Li, L. S., Ying, J., Li, E., Ma, T., Li, M., Gong, L. M., et al. (2021). Arabidopsis CBP60b is a central transcriptional activator of immunity. *Plant Physiol.* 186, 1645–1659. doi: 10.1093/plphys/kiab164

Lin, X., Jia, Y., Heal, R., Prokchorchik, M., Sindalovskaya, M., Olave-Achury, A., et al. (2023). Solanum americanum genome-assisted discovery of immune receptors that detect potato late blight pathogen effectors. *Nat. Genet.* 55, 1579–1588. doi: 10.1038/s41588-023-01486-9

Liu, Y., Sun, T., and Sun, Y. (2020). Diverse roles of the salicylic acid receptors NPR1 and NPR3/NPR4 in plant immunity. *Plant Cell* 32, 4002–4016. doi: 10.1105/tpc.20.00499

Liu, Q., Vain, T., Viotti, C., Doyle, S. M., and Hofius, D. (2018). Vacuole integrity maintained by DUF300 proteins is required for brassinosteroid signaling regulation. *Mol. Plant* 11, 553–567. doi: 10.1016/j.molp.2017.12.015

Liu, B., Yu, H, Yang, Q., Ding, L., Sun, F., Qu, J., et al. (2022). Zinc transporter zmLAZ1-4 modulates zinc homeostasis on plasma and vacuolar membrane in maize. *Front. Plant Sci.* 13, 1–12. doi: 10.3389/fpls.2022.881055

Malinovsky, F. G., Peter, B., Katrine, F. B., Vig, M. K. L., Stephan, T., Martina, B., et al. (2010). Lazarus1, a DUF300 protein, contributes to programmed cell death associated with arabidopsis acd11 and the hypersensitive response. *PloS One* 5, e12586. doi: 10.1371/journal.pone.0012586

Man, N. B. P., Pingtao, D., and Jones, J. D. G. (2022). Thirty years of resistance: Zig-zag through the plant immune system. *Plant Cell* 34, 1447–1478. doi: 10.1093/plcell/koac041

Navarova, H., Bernsdorff, F., Doring, A. C., and Zeier, J. (2012). Pipecolic acid, an endogenous mediator of defense amplification and priming, is a critical regulator of inducible plant immunity. *Plant Cell* 24, 5123–5141. doi: 10.1105/tpc.112.103564

Peng, Y., Yang, J., Li, X., and Zhang, Y. (2021). Salicylic acid: biosynthesis and signaling. *Annu. Rev. Plant Biol.* 72, 761–791. doi: 10.1146/annurev-arplant-081320-092855

Rekhter, D., Lüdke, D., Ding, Y., Feussner, K., Zienkiewicz, K., Lipka, V., et al. (2019). Isochorismate-derived biosynthesis of the plant stress hormone salicylic acid. *Science* 365, 498–502. doi: 10.1126/science.aaw1720

Sun, T., Busta, L., Zhang, Q., Ding, P., Jetter, R., and Zhang, Y. (2018). TGACG-BINDING FACTOR 1 (TGA1) and TGA4 regulate salicylic acid and pipecolic acid biosynthesis by modulating the expression of SYSTEMIC ACQUIRED RESISTANCE DEFICIENT 1 (SARD1) and CALMODULIN-BINDING PROTEIN 60g (CBP60g). *New Phytol.* 217, 344–354. doi: 10.1111/nph.2018.217.issue-1

Sun, T., Huang, J., Xu, Y., Verma, V., Jing, B., Sun, Y., et al. (2020). Redundant CAMTA transcription factors negatively regulate the biosynthesis of salicylic acid and N -hydroxypipecolic acid by modulating the expression of SARD1 and CBP60g. *Mol. Plant* 13, 144–156. doi: 10.1016/j.molp.2019.10.016

Sun, L., Qin, J., Wu, X., Zhang, J., and Zhang, J. (2022). TOUCH 3 and CALMODULIN 1/4/6 cooperate with calcium-dependent protein kinases to trigger calcium-dependent activation of CAM-BINDING PROTEIN 60-LIKE G and regulate fungal resistance in plants. *Plant Cell* 34, 4088–4104. doi: 10.1093/plcell/koac209

Sun, T., and Zhang, Y. (2021). Short-and long-distance signaling in plant defense. *Plant J.* 105, 505–517. doi: 10.1111/tpj.v105.2

Sun, T., Zhang, Y., Li, Y., Zhang, Q., Ding, Y., and Zhang, Y. (2015). ChIP-seq reveals broad roles of SARD1 and CBP60g in regulating plant immunity. *Nat. Commun.* 6, 10159. doi: 10.1038/ncomms10159

Torrens-Spence, M. P., Bobokalonova, A., Carballo, V., Glinkerman, C. M., Pluskal, T., Shen, A., et al. (2019). PBS3 and EPS1 complete salicylic acid biosynthesis from isochorismate in arabidopsis. *Mol. Plant* 12, 1577–1586. doi: 10.1016/j.molp.2019.11.005

Wang, L., Tsuda, K., Sato, M., Cohen, J. D., Katagiri, F., and Glazebrook, J. (2009). Arabidopsis CaM Binding Protein CBP60g Contributes to MAMP-Induced SA Accumulation and Is Involved in Disease Resistance against Pseudomonas syringae. *PloS Pathog.* 5, e1000301. doi: 10.1371/journal.ppat.1000301

Wang, L., Tsuda, K., Truman, W., Sato, M., Nguyen, L. V., Katagiri, F., et al. (2011). CBP60g and SARD1 play partially redundant critical roles in salicylic acid signaling. *Plant J.* 67, 1029–1041. doi: 10.1111/j.1365-313X.2011.04655.x

Wang, Z. P., Xing, H. L., Dong, L., Zhang, H. Y., Han, C. Y., Wang, X. C., et al. (2015). Egg cell-specific promoter-controlled CRISPR/Cas9 efficiently generates homozygous mutants for multiple target genes in Arabidopsis in a single generation. *Genome Biol.* 16, 144. doi: 10.1186/s13059-015-0715-0

Wang, W. Z., Xue, Z. L., Miao, Q. J., Cai, M., Zhang, C., Li, J. T., et al. (2019). *PcMuORP1*, an oxathiapiprolin-resistance gene, functions as a novel selection marker for *phytophthora* transformation and CRISPR/cas9 mediated genome editing. *Front. Microbiol.* 10, 2402. doi: 10.3389/fmicb.2019.02402

Wildermuth, M. C., Dewdney, J., Wu, G., and Ausubel, F. M. (2001). Isochoris mate synthase is required to synthesize salicylic acid for plant defence. *Nature* 414, 562–565. doi: 10.1038/35107108

Wu, Z., He, L., Jin, Y., Chen, J., Shi, H., Wang, Y., et al. (2021). HISTONE DEACETYLASE 6 suppresses salicylic acid biosynthesis to repress autoimmunity1. *Plant Physiol.* 187, 2592–2607. doi: 10.1093/plphys/kiab408

Wu, Y., Zhang, D., Chu, J. Y., Boyle, P., Wang, Y., Brindle, I. D., et al. (2012). The Arabidopsis NPR1 protein is a receptor for the plant defense hormone salicylic acid. *Cell Rep.* 1, 639–647. doi: 10.1016/j.celrep.2012.05.008

Yang, W., Liu., C., Fu., Q., Jia., X., Deng., L., Feng., C., et al. (2023). Knockout of SlbZIP68 reduces late blight resistance in tomato. *Plant Sci.* 336, 111861. doi: 10.1016/j.plantsci.2023.111861

Zhang, K., Bhuiya, M. W., Pazo, J. R., Miao, Y., Kim, H., Ralph, J., et al. (2012). An engineered monolignol 4-o-methyltransferase depresses lignin biosynthesis and confers novel metabolic capability in Arabidopsis. *Plant Cell* 24, 3135–3152. doi: 10.1105/tpc.112.101287

Zhang, Y., Xu, S., Ding, P., Wang, D., Cheng, Y., Jing, H., et al. (2010). Control of salicylic acid synthesis and systemic acquired resistance by two members of a plant-specific family of transcription factors. *Proc. Natl. Acad. Sci. U.S.A.* 107, 18220–18225. doi: 10.1073/pnas.1005225107

Zhang, C., Yang, Z., Tang, D., Zhu, Y., and Huang, S. (2021). Genome design of hybrid potato. *Cell* 184, 3873–3883. doi: 10.1016/j.cell.2021.06.006

Zhou, J., and Zhang, Y. (2020). Plant immunity: danger perception and sig naling. *Cell* 5, 978–989. doi: 10.1016/j.cell.2020.04.028

frontiers | Frontiers in Plant Science

TYPE Original Research
PUBLISHED 04 February 2025
DOI 10.3389/fpls.2025.1543462

Check for updates

OPEN ACCESS

EDITED BY
Yasser Nehela,
Tanta University, Egypt

REVIEWED BY
Chaofeng Wang,
University of Nebraska-Lincoln, United States
Changwei Gong,
Sichuan Agricultural University, China

*CORRESPONDENCE
Cheng Zhang
chengz76@aliyun.com

†These authors have contributed equally to this work

RECEIVED 11 December 2024
ACCEPTED 16 January 2025
PUBLISHED 04 February 2025

CITATION
Tian B, Tang C, Liu J, Jin B and Zhang C (2025) Tetramycin ameliorates tebuconazole·azoxystrobin to control leaf spot and viral diseases of Taizishen. *Front. Plant Sci.* 16:1543462. doi: 10.3389/fpls.2025.1543462

COPYRIGHT
© 2025 Tian, Tang, Liu, Jin and Zhang. This is an open-access article distributed under the terms of the Creative Commons Attribution License (CC BY). The use, distribution or reproduction in other forums is permitted, provided the original author(s) and the copyright owner(s) are credited and that the original publication in this journal is cited, in accordance with accepted academic practice. No use, distribution or reproduction is permitted which does not comply with these terms.

Tetramycin ameliorates tebuconazole·azoxystrobin to control leaf spot and viral diseases of Taizishen

Bing Tian[1,2†], Chenglin Tang[3†], Jiaqi Liu[1], Boya Jin[1] and Cheng Zhang[1*]

[1]Key Laboratory of Environmental Pollution Monitoring and Disease of Ministry of Education, School of Public Health, Guizhou Medical University, Guiyang, Guizhou, China, [2]Guizhou Agricultural Ecology and Resource Protection Station, Agriculture and Rural Affairs Department of Guizhou Province, Guiyang, Guizhou, China, [3]Guizhou Crop Technology Extension Station, Agriculture and Rural Affairs Department of Guizhou Province, Guiyang, Guizhou, China

Leaf spot and viral diseases are the most frequently occurring leaf problems in Taizishen production. In this study, we examined the controlling role played by the co-application of tetramycin and low dose tebuconazole·azoxystrobin against leaf spot and viral diseases in Taizishen, investigating its resistance, electrophysiological information, growth and quality. Among them, electrophysiological information indicators include electrical signals [intrinsic capacitance (IC), resistance (IR), impedance (IZ), capacitive reactance (IXc), and inductive reactance (IXL)], intracellular water metabolism, nutrient transport, and plant metabolic activity. The results indicate that 0.3% tetramycin 1000-time + 75% tebuconazole·azoxystrobin 2000-time diluent controlled leaf spot and viral diseases the best, with protection effects of 90.03%~90.46% and 71.67%~73.08% at 15~30 days after the last fungicide application, respectively. These values are obviously higher than those treated with high doses of tetramycin or tebuconazole·azoxystrobin alone. Concurrently, their combined application could notably enhance total soluble flavonoids, total soluble phenols, protective enzyme activity, IC, intracellular water metabolism, nutrient transport, and metabolic activity, while reducing its MDA, IR, IZ, IXc, and IXL. Moreover, their co-application also could obviously ameliorate photosynthesis, biomass, agronomic trait, and root growth and quality, as well as actually reduce tebuconazole·azoxystrobin input. Additionally, the control effects of leaf spot and viral diseases in Taizishen treated by their combined application exhibited significant correlations with its disease resistance, electrophysiology, photosynthesis, growth, and quality parameters. This study highlights the combined application of low-dosage tebuconazole·azoxystrobin and tetramycin as a practicable measure for controlling leaf spot and viral diseases in Taizishen, promoting its resistance, growth, and quality, as well as reducing chemical pesticide application.

KEYWORDS

agricultural antibiotic, electrophysiological information, leaf spot and disease, viral disease, growth and quality, *Pseudostellaria heterophylla*

1 Introduction

Pseudostellaria heterophylla, also known by its Chinese name, Taizishen, is an edible, medicinal, and ornamental plant. It has a long history in traditional Chinese food and medicine for its multiple pharmacological functions, such as enhancing immunity, improving blood quality, moistening the lungs, inhibiting tumor cells, protecting myocardial function, invigorating the spleen–stomach, and preventing and curing COVID-19 (Choi et al., 2017; Shi et al., 2020; Wang et al., 2013; Zhang et al., 2016, 2021). Meanwhile, its roots, which are rich in polysaccharides, saponins, amino acids, flavonoids, and minerals, have high nutritious, medicinal, and economical value (Liao et al., 2018; Ma et al., 2022; Xu et al., 2023; Zhang et al., 2021). It is predominantly produced in China, the Korean Peninsula, the far east of Russia, and Japan (Liao et al., 2018). Recently, it has been popularly cultivated in the provinces of Guizhou, Fujian, Zhejiang, Sichuan, and Anhui in China, especially in Guizhou, where the cultivating area of over 20, 000 hm^2 ranks first in the country (Wu et al., 2016). Nevertheless, leaf spot disease caused by various pathogens, such as *Alteraria tenuissima*, *Arcopilus versabilis*, *Phyllosticta commonsii*, etc., and viral disease caused by *Turnip mosaic virus*, *Broad bean wilt virus*, *Tobacco mosaic virus*, *Cucumber mosaic virus*, etc., are most frequently occurring leaf diseases during Taizishen growth (He et al., 2021; Long et al., 2013; Li et al., 2018; Liang et al., 2022; Yang et al., 2023a, 2023). Leaf spot and viral diseases often occur from March to May, seriously restricting plant growth, root growth and quality, and the industry's development, as well as causing consistent economic losses of over 50% (Yang et al., 2023a). Thus, there is an urgent need to exploit a variety of potential practicable and environmentally friendly control strategies for leaf spot and viral diseases in Taizishen.

Generally, chemical fungicides are very effective and frequently adopted approaches for controlling plant diseases due to their low toxicity and high efficiency (Wang et al., 2022). Some chemical fungicides have been screened by scholars and applied for controlling Taizishen diseases, such as difenoconazole, pyraclostrobin, azoxystrobin, flusilazole, and tebuconazole (He et al., 2021; Long et al., 2013; Li et al., 2013, 2018; Shao et al., 2016; Yang et al., 2023a). For example, Shao et al. (2016) showed that 50% azoxystrobin water dispersible granule (WDG) exerted a controlling effect of 74.50%~76.61% on leaf spot disease in Taizishen. He et al. (2021) reported that a 35% triflumizole·tebuconazole suspension concentrate exhibited good antifungal activity on *A. tenuissima* with an EC_{50} value 36.10 μg ml^{-1}. Tebuconazole, a triazole fungicide that is extensively applied for controlling numerous plant fungi diseases, can inhibit the sterol biosynthesis of pathogens (Fustinoni et al., 2014; Paul et al., 2008; Liu et al., 2015). And azoxystrobin is a mitochondrial respiration inhibitor fungicide which has broad-spectrum systemic activity against many fungal pathogens (Adetutu et al., 2010; Rodrigues et al., 2013; Wang et al., 2016). However, it is widely known that pesticide residues are common after chemical fungicide application; these, in turn, pose potential risks to the environment, organisms, and humans (Wang et al., 2022). Accordingly, there has been a decline in the use of chemical pesticides that has been welcomed by the public. Notably, our two most recent works suggested that chitosan could enhance low-dosage difenoconazole in controlling Taizishen leaf spot disease and that oligochitosan as a potential synergist to promote the effects of pyraclostrobin on Taizishen leaf spot; these two measures have also helped in effectively reducing chemical pesticide application (Zhang et al., 2023, 2024). In seeking more options for preventing and controlling Taizishen leaf spot and viral diseases, a long-term concern consists in finding natural products that can enhance pesticides, reduce their application, and alleviate the pathogen resistance caused by long-term single-pesticide application.

Tetramycin, a novel natural, medical, and agricultural antibiotic metabolized by *Streptomyces hygrospinosus* var. Beijingensis, has two active compositions: tetramycin A and tetramycin B (Bo et al., 2012; Ren et al., 2014). Many studies have demonstrated that tetramycin could be widely applied for preventing and controlling various plant diseases infected by fungal and bacterial, including *Alternaria tenuissima*, *Botrytis cinerea*, *Pyricularia oryzae*, *Alternaria alternata*, *Colletotrichum scovillei*, *Phytophthora capsici*, *Pseudomonas syringae* pv. *Pseudomonas fulva*, and *Agrobacterium tumefaciens* etc (Chen et al., 2017; Gao et al., 2018; Song et al., 2016; Li et al., 2023; Ma et al., 2017, 2018; Wang et al., 2021a; Zhao et al., 2010). In China, tetramycin has also been found to control crop, fruit, and vegetable diseases, and is increasingly becoming a preferred adjuvant or alternative to chemical pesticides or conventional antibiotics (Li et al., 2014; Wang et al., 2021a). Recently, Wang et al. (2021a) found that tetramycin exhibited good antimicrobial activity against kiwifruit pathogens including *Pseudomonas syringae* pv. *Botryosphaeria dothidea*, *Pseudomonas fulva*, *Alternaria tenuissima*, etc. Subsequently, they found that chitosan could augment tetramycin's effect on soft rot disease in kiwifruit, including its effects on growth and quality (Wang et al., 2021b). Moreover, our recent works indicated that the joint application of tetramycin and chitosan or matrine could effectively control leaf spot or soft rot diseases by enhancing kiwifruit resistance, photosynthesis, and quality (Zhang et al., 2022a, 2022b). In this way, further research is needed to determine whether tetramycin can improve the controlling effect of tebuconazole·azoxystrobin against leaf spot and viral diseases in Taizishen, as well as whether their joint application could become another effective means of controlling disease and reducing the use of pesticides.

In the work, we first evaluated the field control efficacy of tebuconazole·azoxystrobin and tetramycin, as well as their formulas, in leaf spot and viral diseases in Taizishen. We simultaneously investigated the plant's disease resistance, electrophysiological information, leaf photosynthesis, and growth. Subsequently, its root growth and quality were also determined. This work provides another green, efficient, and environmentally friendly measure for controlling leaf spot and viral diseases in Taizishen.

2 Materials and methods

2.1 Tebuconazole·azoxystrobin and tetramycin

75% Tebuconazole·azoxystrobin (TA) water dispersible granule (WDG) was obtained from Sipcam Chemical Trading (Shanghai) Co. Ltd. (Shanghai, China), it contains 50% tebuconazole and 25% azoxystrobin. 0.3% tetramycin (TE) aqueous solutions (AS) was produced by Liaoning Microke Biological Engineering Co. Ltd. (Liaoning, China).

2.2 Field Taizishen orchard

Field experimental orchard of Taizishen with 'Guisheng 1' of the planting cultivar was located in Shibing County, China (27°16′ N, 107°97′ E). In the last two years, the leaf spot and virus diseases of Taizishen in this orchard were serious, and the natural incidence rates were about 40%~50% and 10%~20%, respectively. According to the reports of our cooperative research group, *Alternaria tenuissima* was the main pathogen of Taizishen leaf spot disease in this region, and *Turnip mosaic virus* and *Broad bean wilt virus* were the main pathogens of Taizishen virus disease (He et al., 2021; Liang et al., 2022). In the year of field experiment, the leaf spot and virus diseases were natural occurrence. Riding planting of Taizishen seed roots in this orchard, the plot area is 6.0 m^2 (2.0 m of length, 3.0 m of width, 0.2 m in between), and the seed cultivating density was 30 kg per 667 m^2. Moreover, its soil fertility are shown in Table 1.

2.3 Field control experiment

A completely randomized method was applied for delineating plots and leaf spraying method was applied for spraying fungicide.

TABLE 1 The soil fertility of Taizishen orchard.

Fertility	Content (g kg^{-1})	Fertility	Content (mg kg^{-1})
Organic matter	37.13	Available phosphorus	57.02
Total nitrogen	1.57	Available potassium	131.35
Total phosphorus	1.72	Available iron	8.33
Total potassium	1.23	Exchangeable magnesium	291.65
pH	4.96	Available zinc	2.01
Exchangeable calcium	21.04 cmol kg^{-1}	Available manganese	18.33
Alkali hydrolyzed nitrogen	115.63 mg kg^{-1}	Available boron	0.22

Six treatments were designed: (1) 75% tebuconazole·azoxystrobin WDG 2000-time + 0.3% tetramycin AS 1000-time diluent (TA 2000 +TE 1000), (2) 75% tebuconazole·azoxystrobin WDG 1500-time diluent (TA 1500), (3) 75% tebuconazole·azoxystrobin WDG 2000-time diluent (TA 2000), (4) 0.3% tetramycin AS 500-time diluent (TE 500), (5) 0.3% tetramycin AS 1000-time diluent (TE 1000), and (6) clear water with non-fungicide (Control). Meanwhile, each treatment contained three replicate plots, and fungicide diluent was sprayed on Taizishen aboveground parts by an electrostatic atomizer. The spraying dates were March 28, April 8, and April 18, respectively, and the application diluent amount each time was 60 L per 667 m^2.

2.4 Investigation methods

2.4.1 Control effect determination

Leaf spot and virus diseases of Taizishen were natural infections in the test area, and they were identified via symptom recognition method referred to He et al. (2021) and Liang et al. (2022). Leaf spot disease: In the early stage of leaf spot infection, the affected area of the leaves showed yellow spots with white center, light yellow edges, and water stained; As the infection time prolongs, the disease spot gradually expands to form a yellow brown withered spot; In the later stage of infection, the spots showed a circular pattern with black smalldots (conidia), and the whole leaves died under severe cases. Viral disease: When the disease was mild, the leaf veins became lighter and yellowish, often formed flower leaves with alternating shades of light and dark; When the disease was severe, the leaves were wrinkled and showed spots, the leaf edges were often curled, and large necrotic spots appeared on the infected leaves.

The disease index of leaf spot disease and incidence rate of viral disease were investigated on May 3 (15 days after the last spraying fungicide) and May 18 (30 days after the last spraying fungicide). One hundred plants were chosen from the east, south, west, north, central parts in every plot, and their diseased leaf and plant number of leaf spot and viral diseases were counted. The classification of diseased leaf rank for leaf spot disease:

0 rank: no spot;
1 rank: the spot extent was lower than 5% of total leaf extent;
3 rank: the spot extent was 6% to 10% of total leaf extent;
5 rank: the spot extent was 11% to 20% of total leaf extent;
7 rank: the spot extent was 21% to 50% of total leaf extent;
9 rank: the spot extent was more than 51% of total leaf extent.

Then, the disease index and control effect for leaf spot disease were determined as:

$$\text{Disease index} = 100 \times \sum (\text{Leaf number of each rank} \times \text{Rank value}) / (\text{Highest rank value} \times \text{Leaf total number}) \quad (1)$$

$$\text{Control effect (\%) of leaf spot disease} = 100 \times (1 - \text{Disease index of fungicide treatment} / \text{Disease index of non-fungicide treatment}) \quad (2)$$

Simultaneously, the incidence rate and control effect for viral disease was calculated as:

$$\text{Incidence rate of viral disease (\%)} = 100 \times (\text{Number of infected plants} / \text{total number of checked plants}) \quad (3)$$

$$\text{Control effect (\%) of viral disease} = 100 \times (1 - \text{Incidence rate of fungicide treatment} / \text{Incidence rate of non-fungicide treatment}) \quad (4)$$

2.4.2 Leaf resistance determination

Five Taizishen leaves were randomly sampled from the east, south, west, north, central parts in each plots on May 18 and brought their back to the laboratory for checking disease resistance levels according to Zhang et al. (2022c). Accordingly, thiobarbituric acid, rutin standard curve, and gallic acid standard curve methods were used for measuring malonaldehyde (MDA), total soluble flavonoids, and total soluble phenols conments, respectively. For MDA determination, 1.00 g sample was added into 5 mL 10% trichloroacetic acid ice bath to grind into homogenate, centrifuged; 2 mL supernatant was added into 2 mL 0.6% thiobarbituric acid solution, boiled at water bath (15 min), cooled and centrifugated, measured at $OD_{450\ nm}$ and $OD_{532\ nm}$, and 10% trichloroacetic acid as control. For total soluble flavonoids and total soluble phenols determination, 2.00 g sample was added into 20 mL 1% HCl-methyl alcohol (v/v) for extracting 1 h without light and centrifuged, then the supernatant was checked at $OD_{325\ nm}$ and $OD_{280\ nm}$, rutin and gallic acid as control, respectively. Moreover, their superoxide dismutase (SOD), phenylalaninammo nialyase (PAL), peroxidase (POD), and polyphenoloxidase (PPO) activities were analyzed by nitrogen blue tetrazole, trans-cinnamic acid, guaiacol, and catechol methods, respectively. Briefly, the appropriate amount sample was extracted by corresponding reagents and centrifuged, the supernatant was measured at $OD_{560\ nm}$, $OD_{290\ nm}$, $OD_{470\ nm}$, and $OD_{398\ nm}$ for checking SOD, PAL, POD, and PPO activities, respectively.

2.4.3 Electrophysiological information determination

Five Taizishen plants on the east, south, west, north, central parts in every plot were randomly selected for monitoring their electrophysiological information on May 18 according to the methods of Zhang et al. (2020, 2021a, 2021b) and Tian et al. (2024). In our previous studies, the theoretically intrinsic relationships between the clamping force and leaf R, Z, Xc or XL were revealed as R, Z, Xc or XL =y+k e^(-bF) based on the Nernst equation (Zhang et al., 2020, 2021a, 2021b). When the clamping force is 0 (F=0), then the intrinsic R, Z, Xc and XL of plant leaves could be monitored as IR, IZ, IXc or IXL =y+k, and intrinsic capacitance (IC) was calculated according to formula:

$$IC = \frac{1}{2\pi f IXc} \quad (5)$$

where π=3.1416, f= frequency.

Moreover, the intracellular water-holding capacity (IWHC), intracellular water-holding time (IWHT), water or nutrient transfer rate (WTR or NTR), nutrient flux per unit area (UNF), nutrient transport capacity (NTC), the active transport flow of nutrient (NAF), nutrient active transport capacity (NAC), metabolic flow (MF), metabolic rate (MR), and metabolic activity (MA) were calculated as (Tian et al., 2024):

$$IWHC = \sqrt{(IC)^3} \quad (6)$$

$$IWHT = IC \times IZ \quad (7)$$

$$WTR \text{ or } NTR = \frac{IWHC}{IWHT} \quad (8)$$

$$UNF = \frac{IR}{IXc} + \frac{IR}{IXL} \quad (9)$$

$$NTC = UNF \times NTR \quad (10)$$

$$UAF = \frac{IXc}{IXL} \quad (11)$$

$$NAC = UAF \times NTR \quad (12)$$

$$MF = \frac{1}{IR \times IZ \times IXc \times IXL} \quad (13)$$

$$MR = NTR \times NAC \quad (14)$$

$$MA = \sqrt[6]{MF \times MR} \quad (15)$$

2.4.4 Photosynthetic capability determination

Meanwhile, the chlorophyll content of the leaves aforementioned brought back to the laboratory (2.4.2) was extracted with ethanol/acetone (v/v, 2:1) and measured by ultraviolet spectrophotometry method (Zhang et al., 2022c). Additionally, ten fresh plants in same parts in each plot were selected on May 18 for monitoring their fully-expanded leaves' capability at 8:00~10:00 a.m by LI-6400XT photosynthesis measurement system (LI-COR Inc., Lincoln, NE, USA) (Chen et al., 2023).

2.4.5 Agronomic trait determination

Moreover, the total plant length, leaf width and length, and stem diameter ten of aforementioned Taizishen plants in each plot were monitored by ruler on May 18, and its leaf area could calculate as:

$$\text{Leaf area} = 0.666 \times \text{leaf width} \times \text{leaf length} \quad (16)$$

After the investigation of agronomic traits, these plants were sampled as a whole and brought back to the laboratory for

measuring their biomass. Total biomass, underground and above-ground biomass of Taizishen were weighed by electronic balance after drying at low temperature (Zhang et al., 2024).

2.4.6 Root growth and quality determination

On July 18, the tuberous roots of Taizishen were sampled for determining growth and medicinal quality. A vernier scale was used for surveying the length and diameter of 100 tuberous roots in each plot, and the gravimetric and oven-drying methods were applied for determining these tuberous roots' fresh and dry weight. Moreover, the medicinal quality of tuberous roots including extractum, ash, polysaccharide, and total saponins were analyzed as according to the detailed detection methods of Chinese Pharmacopoeia 2020 (2019).

2.5 Statistical analyses

The mean ± standard deviation (SD) of three replicates was indicated as data. The significance analysis of the difference between the mean values of the three replicates of every treatments was performed by a one-way analysis of variance (ANOVA) with Duncan's test, and the normality of the data was performed by the quantile–quantile (Q–Q) plot test. SPSS 18.0 software (SPSS Inc., Chicago, IL, USA) was used for analyzing variance and normality of data. Pearson's correlation analysis was used for creating a correlation matrix between the disease control efficacy and other parameters. Origin 10.0 was used for drawing figures.

3 Results

3.1 Influences of tebuconazole·azoxystrobin and tetramycin against leaf spot disease in Taizishen

The controlling effects of tebuconazole·azoxystrobin and tetramycin on leaf spot disease are displayed in Table 2. TA 2000 +TE 1000, TA 1500, TA 2000, TE 500, and TE 1000 significant ($P < 0.05$) decreased disease index compared with the control. Regarding leaf spot disease, tebuconazole·azoxystrobin displayed an excellent controlling ability; the controlling effects of TA 1500 and TA 2000 could reach 78.45%~76.17% and 67.74%~66.15% at 15 days and 30 days after the final fungicide application, respectively. Meanwhile, tetramycin also showed promising potential in controlling leaf spot disease; the controlling effects of TE 500 and TE 1000 were 75.41% ~80.55% and 74.81%~80.26% at 15 days and 30 days after the final fungicide application, respectively. Synergistically, TA 2000+TE 1000 displayed the best control of leaf spot disease, with an effect of 90.03% ~90.46% at 15~30 days after the final fungicide application, which is significant ($P < 0.05$) greater than those of TA 1500, TA 2000, TE 500, and TE 1000. These results indicate that low-dosage and persistent tetramycin, combined with quick-acting, persistent, and low-dosage tebuconazole·azoxystrobin, could more efficiently control leaf spot disease in Taizishen compared with high-dosage tebuconazole·azoxystrobin and tetramycin. Moreover, the effective ingredient dosages of fungicide per 667 m^2 for TA 2000+TE 1000, TA 1500, TA 2000, TE 500, and TE 1000 were 68.04 g, 90 g, 67.5 g, 1.08 g, and 0.54 g, respectively, indicating that the co-application of tebuconazole·azoxystrobin and tetramycin effectively reduced application dosage.

3.2 Influences of tebuconazole·azoxystrobin and tetramycin against viral disease in Taizishen

The controlling effects of tebuconazole·azoxystrobin and tetramycin on viral disease are shown in Table 3. Similarly, TA 2000 +TE 1000, TA 1500, TA 2000, TE 500, and TE 1000 obviously ($P < 0.05$) declined the incidence rate of viral disease compared with the control. The incidence rate of viral disease with TA 2000+TE 1000 treatment at 15 days after the final fungicide application was significant ($P < 0.05$) lower than that of TA 2000, TE 500, and TE 1000; that treated with TA 2000+TE 1000 at 30 days after the final fungicide

TABLE 2 The control effects of tebuconazole·azoxystrobin and tetramycin on leaf spot disease of Taizishen (*P. heterophylla*) at 15 and 30 days post-treatment under greenhouse conditions.

Treatments	15 days after applying fungicide		30 days after applying fungicide	
	Disease Index	Control effect (%)	Disease Index	Control effect (%)
Control	5.46 ± 0.14 ^{a}		6.23 ± 0.20 ^{a}	
TE 500	1.06 ± 0.10 ^{c}	80.55 ± 2.24 ^{c}	1.23 ± 0.07 ^{c}	80.26 ± 0.97 ^{c}
TE 1000	1.34 ± 0.11 ^{b}	75.41 ± 2.69 ^{d}	1.57 ± 0.08 ^{b}	74.81 ± 0.62 ^{d}
TA 1500	0.73 ± 0.08 ^{d}	86.60 ± 1.61 ^{b}	0.88 ± 0.10 ^{d}	85.87 ± 1.58 ^{b}
TA 2000	0.98 ± 0.10 ^{c}	82.02 ± 2.10 ^{c}	1.16 ± 0.04 ^{c}	81.36 ± 1.21 ^{c}
TA 2000+TE 1000	0.52 ± 0.08 ^{e}	90.46 ± 1.55 ^{a}	0.62 ± 0.04 ^{e}	90.03 ± 1.01 ^{a}
F values	992.065	22.321	1258.831	79.671
P values	<0.001	<0.001	<0.001	<0.001

Different lower-case letters represent statistically significant differences among treatments based on Duncan's test ($P < 0.05$). Control: water without fungicide. TE 500 and TE 1000: 0.3% tetramycin AS 500-time diluent or 1000-time diluent, respectively. TA 1500 and TA 2000: 75% tebuconazole·azoxystrobin WDG 1500-time diluent or 2000-time diluent, respectively. TA 2000 +TE 1000: 75% tebuconazole·azoxystrobin WDG 2000-time + 0.3% tetramycin AS 1000-time diluent.

application was significant ($P < 0.05$) lower than that of TA 1500, TA 2000, TE 500, and TE 1000. The controlling effect of viral disease under TA 2000+TE 1000 treatment at 15~30 days after the final fungicide application was 71.67%~73.08%, which was significant ($P < 0.05$) higher than that of TA 2000 and TE 1000, but only slightly higher than that of TA 1500 and TE 500. These findings suggest that the co-application of low-dosage tetramycin and tebuconazole·azoxystrobin also could more efficiently control viral disease in Taizishen compared with high-dosage tebuconazole·azoxystrobin and tetramycin, as well as reliably decreasing tebuconazole·azoxystrobin use dosage.

3.3 Influences of tebuconazole·azoxystrobin and tetramycin on MDA, total soluble flavonoids, total soluble phenols, and protective enzyme activity in Taizishen

The effects of tebuconazole·azoxystrobin and tetramycin on the MDA, total soluble flavonoids and total soluble phenols conments of Taizishen are depicted in Figure 1. TA 2000+TE 1000, TA 1500, and TE 500 significant ($P < 0.05$) increased the soluble protein content of Taizishen leaves at 30 days post-treatment compared with the control, while TA 2000 and TE 1000 had a slight effect on the soluble protein in leaves. Meanwhile, TA 2000+TE 1000, TA 1500, TA 2000, TE 500, and TE 1000 significant ($P < 0.05$) decreased the leaf MDA content at 30 days post-treatment and improved the leaf total soluble flavonoids content compared with control. Moreover, TA 2000+TE 1000 significant ($P < 0.05$) increased the leaf total soluble phenols content at 30 days post-treatment compared with both the control and TA 2000. Furthermore, the MDA content of leaves treated with TA 2000 +TE 1000 at 30 days post-treatment was significant ($P < 0.05$) lower than that of TA 2000 and TE 1000 and slightly lower than that of TA 1500 and TE 500; their total soluble flavonoids content was significant ($P < 0.05$) higher than that of TA 1500, TA 2000, and TE 1000 and slightly higher than that of TE 500; and their total soluble phenols content was significant ($P < 0.05$) greater than that of TA 2000 and slightly higher than that of TA 1500, TE 500, and TE 1000. These results highlight how the combined application of low-dosage tetramycin and tebuconazole·azoxystrobin could more effectively promote the total soluble flavonoids and total soluble phenols of Taizishen than their high-dosage alone application.

The effects of tebuconazole·azoxystrobin and tetramycin on the SOD, PAL, POD, and PPO activities of Taizishen are displayed in Figure 1. Compared with the control, TA 2000+TE 1000, TA 1500, TA 2000, TE 500, and TE 1000 could significant ($P < 0.05$) enhance the SOD and POD activities of Taizishen leaves at 30 days post-treatment, TA 2000+TE 1000, TA 1500, and TE 500 could significant ($P < 0.05$) improve their PAL activity, and A 2000+TE 1000 and TE 500 could significant ($P < 0.05$) promote their PPO activity. Furthermore, under TA 2000+TE 1000 treatment at 30 days post-treatment, the leaf SOD, PAL, and POD activities were significant ($P < 0.05$) higher than those of TA 1500, TA 2000, TE 500, and TE 1000. Under TA 2000+TE 1000 treatment at 30 days post-treatment, the PPO activity was significant ($P < 0.05$) higher than that of TA 2000 and slightly higher than that of TA 1500, TE 500, and TE 1000. Additionally, under TA 1500 or TE 500 treatment at 30 days post-treatment, leaf SOD, PAL, POD, and PPO activities were, respectively, slightly higher than those of TA 2000 or TE 1000; under TA 1500, TA 2000, TE 500, and TE 1000 treatments, these functions showed no significant ($P < 0.05$) differences. These results further suggest that tetramycin combined with tebuconazole·azoxystrobin could also obviously enhance the promoting roles of tetramycin or tebuconazole·azoxystrobin alone in the protective enzyme activities of Taizishen at 30 days post-treatment.

3.4 Influences of tebuconazole·azoxystrobin and tetramycin on the electrical signals, intracellular water metabolism, nutrient transport, and plant metabolic activity of Taizishen

The influences of tebuconazole·azoxystrobin and tetramycin on the IC, IR, IZ, IXL, and IXc of Taizishen are displayed in Table 4. Compared with the control, TA 2000+TE 1000, TA 1500, TA 2000,

TABLE 3 The control effects of tebuconazole·azoxystrobin and tetramycin on viral disease of Taizishen (*P. heterophylla*) at 15 and 30 days post-treatment under greenhouse conditions.

Treatments	15 days after applying fungicide		30 days after applying fungicide	
	Incidence rate (%)	Control effect (%)	Incidence rate (%)	Control effect (%)
Control	12.67 ± 0.58 ^{a}		15.33 ± 0.58 ^{a}	
TE 500	4.00 ± 0.00 ^{b}	67.52 ± 1.48 ^{ab}	5.00 ± 0.00 ^{b}	67.36 ± 1.20 ^{ab}
TE 1000	4.33 ± 0.58 ^{b}	64.74 ± 5.70 ^{b}	5.33 ± 0.58 ^{b}	65.14 ± 4.57 ^{b}
TA 1500	3.67 ± 0.58 ^{c}	70.30 ± 4.27 ^{ab}	5.00 ± 1.00 ^{b}	67.36 ± 1.20 ^{ab}
TA 2000	4.33 ± 0.58 ^{b}	64.74 ± 5.70 ^{b}	5.67 ± 0.58 ^{b}	63.06 ± 3.37 ^{b}
TA 2000+TE 1000	3.33 ± 0.58 ^{c}	73.08 ± 3.33 ^{a}	4.33 ± 0.58 ^{c}	71.67 ± 4.41 ^{a}
F values	99.145	3.771	220.029	2.955
P values	<0.001	0.040	<0.001	0.045

Different lower-case letters represent statistically significant differences among treatments based on Duncan's test ($P < 0.05$). Control: water without fungicide. TE 500 and TE 1000: 0.3% tetramycin AS 500-time diluent or 1000-time diluent, respectively. TA 1500 and TA 2000: 75% tebuconazole·azoxystrobin WDG 1500-time diluent or 2000-time diluent, respectively. TA 2000 +TE 1000: 75% tebuconazole·azoxystrobin WDG 2000-time + 0.3% tetramycin AS 1000-time diluent.

10.3389/fpls.2025.1543462

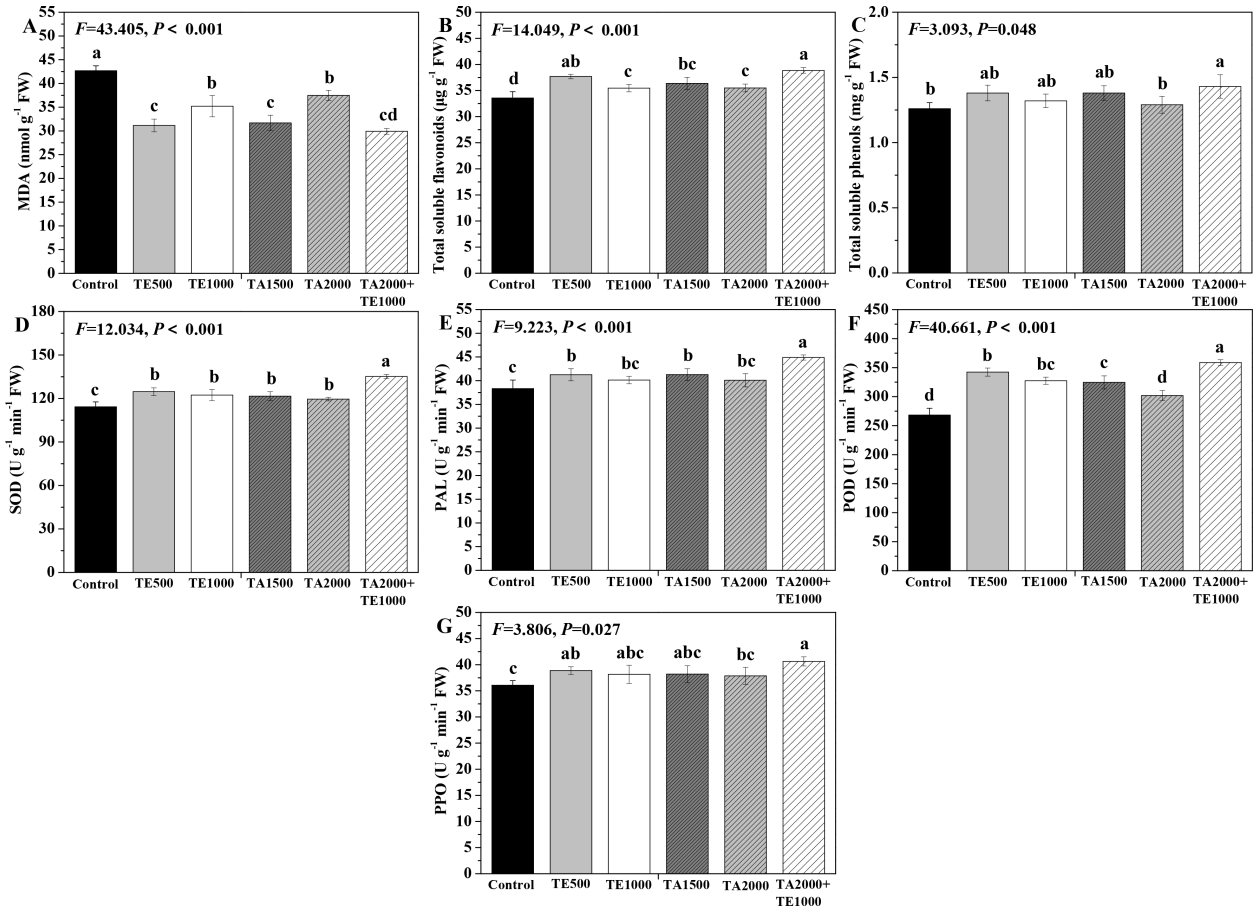

FIGURE 1
The effect of tebuconazole·azoxystrobin and tetramycin on the malondialdehyde (MDA) and some non-enzymatic and enzymatic antioxidants of Taizishen (*P. heterophylla*) leaves infected with leaf spot and viral diseases at 30 days post-treatment under greenhouse conditions. **(A)** MDA content (nmol g^{-1} FW), **(B)** Total soluble flavonoids content (μg g^{-1} FW), **(C)** total soluble phenolics content (mg g^{-1} FW), **(D)** Superoxide dismutase (SOD) activity (U g^{-1} min^{-1} FW), **(E)** phenylalanine ammonia-lyase (PAL) activity (U g^{-1} min^{-1} FW), **(F)** Peroxidase (POD) activity (UNITS), **(G)** polyphenol oxidase (PPO) activity (U g^{-1} min^{-1} FW). Bars denote the mean of three biological replicates (n=3), whereas error bars show the standard deviation. Different lower-case letters represent statistically significant differences among treatments based on Duncan's test ($P < 0.05$). Control: water without fungicide. TE 500 and TE 1000: 0.3% tetramycin AS 500-time diluent or 1000-time diluent, respectively. TA 1500 and TA 2000: 75% tebuconazole·azoxystrobin WDG 1000-time diluent or 2000-time diluent, respectively. TA 2000+TE 1000: 75% tebuconazole·azoxystrobin WDG 2000-time + 0.3% tetramycin AS 1000-time diluent.

TE 500, and TE 1000 significant ($P < 0.05$) increased the IC of Taizishen leaves at 30 days post-treatment, effectively decreased their IR, and significantly ($P < 0.05$) decreased their IXL. In addition, TA 2000+TE 1000, TA 1500, and TA 2000 significant ($P < 0.05$) decreased their IZ and IXc at 30 days post-treatment, both of which TE 500 and TE 1000 slightly decreased. Furthermore, under TA 2000+TE 1000 treatment at 30 days post-treatment, leaf IC was significant ($P < 0.05$) greater than that of TA 1500, TA 2000, TE 500, and TE 1000; under TA 2000+TE 1000 treatment, the IR was lower than that of TA 2000, TE 500, and TE 1000. Additionally, under TA 2000+TE 1000 treatment at 30 days post-treatment, IZ and IXc were significant ($P < 0.05$) lower than those of TE 500 and TE 1000, with no significant ($P < 0.05$) differences between TA 1500 and TA 2000. Moreover, under TA 1500 or TE 500 treatment at 30 days post-treatment, leaf IC was, respectively, higher than that of TA 2000 or TE 1000, and IR, IZ, IXL, and IXc were, respectively, lower than those of TA 2000 or TE 1000. These results show that the combined application of low-dosage tetramycin and tebuconazole·azoxystrobin could more effectively promote the IC of Taizishen, decreasing its IR, IZ, IXL, and IXc compared to their high-dosage, singular use and more effectively promoting its growth.

The influences of tebuconazole·azoxystrobin and tetramycin on the intracellular water metabolism, nutrient transport, and metabolic activity of Taizishen are displayed in Figure 2. In terms of intracellular water metabolism, TA 2000+TE 1000, TA 1500, TA 2000, TE 500, and TE 1000 significant ($P < 0.05$) enhanced IWHC at 30 days post-treatment compared with the control and TA 2000 +TE 1000, TA 1500, and TA 2000 significant ($P < 0.05$) increased WTR or NTR. Although these treatments could also improve IWHT, there were no differences between them. Moreover, the IWHC of Taizishen treated with TA 2000+TE 1000 at 30 days post-treatment was significant ($P < 0.05$) higher than that of TA 1500, TA 2000, TE 500, and TE 1000; the WTR or NTR treated with TA 2000+TE 1000 was also significant ($P < 0.05$) higher than that of TA 2000, TE 500, and TE 1000. For the nutrient transport status of

TABLE 4 The influences of tebuconazole·azoxystrobin and tetramycin on the IC, IR, IZ, IXL, and IXc of Taizishen (*P. heterophylla*) leaves infected with leaf spot and viral diseases at 30 days post-treatment under greenhouse conditions.

Treatments	IC (pF)	IR (MΩ)	IZ (MΩ)	IXL (MΩ)	IXc (MΩ)
Control	161.39 ± 19.06 ^{d}	0.65 ± 0.37 ^{a}	0.27 ± 0.07 ^{a}	0.33 ± 0.04 ^{a}	0.85 ± 0.37 ^{a}
TE 500	216.51 ± 23.57 ^{d}	0.63 ± 0.44 ^{a}	0.22 ± 0.03 ^{a}	0.25 ± 0.03 ^{b}	0.76 ± 0.33 ^{a}
TE 1000	191.67 ± 23.81 ^{d}	0.85 ± 0.39 ^{a}	0.25 ± 0.07 ^{a}	0.28 ± 0.04 ^{b}	1.02 ± 0.39 ^{a}
TA 1500	385.89 ± 66.31 ^{b}	0.29 ± 0.12 ^{b}	0.12 ± 0.03 ^{b}	0.14 ± 0.02 ^{cd}	0.36 ± 0.13 ^{b}
TA 2000	313.73 ± 14.45 ^{c}	0.37 ± 0.22 ^{ab}	0.14 ± 0.03 ^{b}	0.17 ± 0.01 ^{c}	0.46 ± 0.12 ^{b}
TA 2000+TE 1000	482.07 ± 16.41 ^{a}	0.33 ± 0.18 ^{ab}	0.10 ± 0.01 ^{b}	0.11 ± 0.00 ^{d}	0.36 ± 0.13 ^{b}
F values	44.280	0.958	8.230	37.035	1.512
P values	<0.001	0.044	0.001	<0.001	0.046

Different lower-case letters represent statistically significant differences among treatments based on Duncan's test ($P < 0.05$). Control: water without fungicide. TE 500 and TE 1000: 0.3% tetramycin AS 500-time diluent or 1000-time diluent, respectively. TA 1500 and TA 2000: 75% tebuconazole·azoxystrobin WDG 1500-time diluent or 2000-time diluent, respectively. TA 2000 +TE 1000: 75% tebuconazole·azoxystrobin WDG 2000-time + 0.3% tetramycin AS 1000-time diluent.

Taizishen at 30 days post-treatment, TA 2000+TE 1000 significant ($P < 0.05$) enhanced UNF compared with the control, and TA 2000 +TE 1000, TA 1500, TA 2000, TE 500, and TE 1000 significant ($P < 0.05$) improved NTC; in addition, TA 2000+TE 1000, TA 1500, and TA 2000 significant ($P < 0.05$) promoted NAC. Meanwhile, the UNF of Taizishen treated with TA 2000+TE 1000 at 30 days post-treatment was significant ($P < 0.05$) higher than that of TA 1500 and obviously higher than that of TA 2000, TE 500, and TE 1000; the NTC treated with TA 2000+TE 1000 at 30 days post-treatment was significant ($P < 0.05$) higher than that of TA 1500, TA 2000, TE 500, and TE 1000, and the NAC treated with TA 2000+TE 1000 at 30 days post-treatment was significant ($P < 0.05$) greater than that of TA 2000, TE 500, and TE 1000 and slight higher than that of TA 1500. Regarding the metabolic activity of Taizishen at 30 days post-treatment, TA 2000+TE 1000, TA 1500, and TA 2000 significant ($P < 0.05$) improved the MF, MR, and MA compared with the control, and TE 500 and TE 1000 also slightly promoted these properties. Nevertheless, the MF and MR of Taizishen treated with TA 2000+TE 1000 at 30 days post-treatment were significant ($P < 0.05$) higher than those of TA 2000, TE 500, and TE 1000 and slightly higher than those of TA 1500; the MA treated with TA 2000+TE 1000 was significant ($P < 0.05$) higher than that of TE 500 and TE 1000 and slightly higher than that of TA 1500 and TA 2000. These findings demonstrate that low-dosage tetramycin and tebuconazole·azoxystrobin effectively enhance the intracellular water metabolism, nutrient transport, and plant metabolic activity of Taizishen, improving its healthy growth. Furthermore, their low-dosage co-application was even more effective.

3.5 Influences of tebuconazole·azoxystrobin and tetramycin on the photosynthetic capability and agronomic traits of Taizishen

The influences of tebuconazole·azoxystrobin and tetramycin on the photosynthetic capability of Taizishen are depicted in Figure 3. Compared with the control, TA 2000+TE 1000 and TA 1500 significant ($P < 0.05$) enhanced the chlorophyll content of Taizishen at 30 days post-treatment and decreased its WUE. TA 2000+TE 1000, TA 1500, TA 2000, TE 500, and TE 1000 significant ($P < 0.05$) improved Pn and Tr, and TA 2000+TE 1000, TA 1500, and TE 500 significant ($P < 0.05$) increased Ci; furthermore, TA 2000+TE 1000, TA 1500, TE 500, and TE 1000 significant ($P < 0.05$) promoted Gs. Additionally, the leaf chlorophyll, Pn, Tr, Ci, and Gs of Taizishen treated by TA 2000+TE 1000 at 30 days post-treatment were significant ($P < 0.05$) higher: 1.01, 1.05, 1.04, and 1.07 times; 1.06, 1.08, 1.07, and 1.10 times; 1.06, 1.17, 1.12, and 1.15 times; 1.05, 1.09, 1.06, and 1.10 times; and 1.05, 1.02, 1.02, and 1.06 times compared with TA 1500, TA 2000, TE 500, and TE 1000, respectively. Meanwhile, the leaf chlorophyll, Pn, Tr, Ci, and Gs of Taizishen treated with TA 1500 or TE 500 at 30 days post-treatment were higher than those of TA 2000 or TE 1000, respectively. These results show that the combined application of low-dosage tetramycin and tebuconazole·azoxystrobin could more effectively improve the photosynthetic capacity of Taizishen than their high-dosage application alone. In addition, this combination could more reliably ameliorate growth.

The influences of tebuconazole·azoxystrobin and tetramycin on the biomass and agronomic traits of Taizishen are depicted in Figure 4. Compared with the control, TA 2000+TE 1000 and TE 500 significant ($P < 0.05$) enhanced the total biomass of Taizishen at 30 days post-treatment; TA 2000+TE 1000, TA 1500, and TE 500 significant ($P < 0.05$) increased its above- and underground biomass and stem diameter at 30 days post-treatment; TA 2000+TE 1000, TA 1500, TA 2000, TE 500, and TE 1000 significant ($P < 0.05$) increased its plant length at 30 days post-treatment; and TA 2000 +TE 1000 also significant ($P < 0.05$) increased its leaf area at 30 days post-treatment. Meanwhile, the above- and underground biomass, plant length, and stem diameter of Taizishen treated with TA 2000 +TE 1000 at 30 days post-treatment were significant ($P < 0.05$) higher than those of TA 1500, TA 2000, TE 500, and TE 1000. The findings demonstrate that low-dosage tetramycin, when used together with low-dosage tebuconazole·azoxystrobin, could more effectively promote the biomass, agronomic traits, and growth of Taizishen than their high-dosage application alone.

10.3389/fpls.2025.1543462

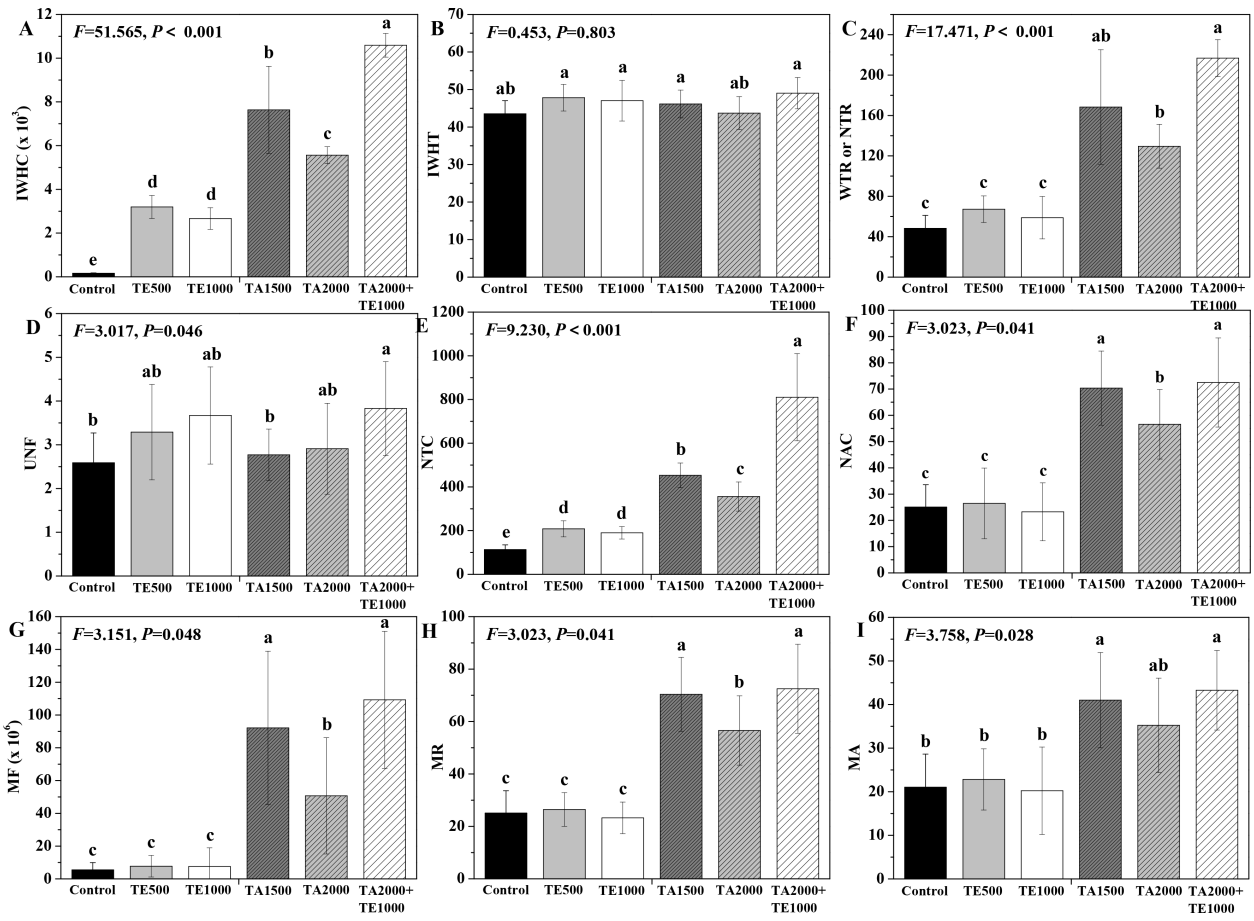

FIGURE 2
The effects of tebuconazole·azoxystrobin and tetramycin on the intracellular water metabolism, nutrient transport, and metabolic activity of Taizishen (*P. heterophylla*) leaves infected with leaf spot and viral diseases at 30 days post-treatment under greenhouse conditions. **(A)** Intracellular water-holding capacity (IWHC), **(B)** Intracellular water-holding time (IWHT), **(C)** Water or nutrient transfer rate (WTR or NTR), **(D)** Nutrient flux per unit area (UNF), **(E)** Nutrient transport capacity (NTC), **(F)** Nutrient active transport capacity (NAC), **(G)** Metabolic flow (MF), **(H)** Metabolic rate (MR), and **(I)** Metabolic activity (MA). Bars denote the mean of three biological replicates (n=3), whereas error bars show the standard deviation. Different lower-case letters represent statistically significant differences among treatments based on Duncan's test ($P < 0.05$). Control: water without fungicide. TE 500 and TE 1000: 0.3% tetramycin AS 500-time diluent or 1000-time diluent, respectively. TA 1500 and TA 2000: 75% tebuconazole·azoxystrobin WDG 1000-time diluent or 2000-time diluent, respectively. TA 2000+TE 1000: 75% tebuconazole·azoxystrobin WDG 2000-time + 0.3% tetramycin AS 1000-time diluent.

3.6 Influences of tebuconazole·azoxystrobin and tetramycin on yield and quality of Taizishen

The influences of tebuconazole·azoxystrobin and tetramycin on the fresh and dry weights, as well as the root length and diameter, are depicted in Figure 5. Compared with control, TA 2000+TE 1000, TA 1500, TA 2000, and TE 500 significant ($P < 0.05$) increased the fresh and dry weights and root length and diameter of Taizishen roots at 90 days post-treatment, while TE 1000 also significant ($P < 0.05$) enhanced their fresh weight and root length. Moreover, the fresh weight of Taizishen treated with TA 2000+TE 1000 at 90 days post-treatment was significant ($P < 0.05$) higher than that of TA 2000, TE 500, and TE 1000, and its dry weight and root length under TA 2000+TE 1000 treatment at 90 days post-treatment were significant ($P < 0.05$) higher than those of TA 1500, TA 2000, TE 500, and TE 1000. Furthermore, under TA 2000+TE 1000 treatment at 90 days post-treatment, the root diameter was significant ($P < 0.05$) higher than that of TA 2000 and TE 1000 alone. These results reveal that the ameliorating effects of the combination of low-dosage tebuconazole·azoxystrobin and tetramycin on Taizishen root growth and weight were better than those of singular, high doses.

The influences of tebuconazole·azoxystrobin and tetramycin on the medicinal quality of Taizishen roots are depicted in Figure 5. Compared with the control, TA 2000+TE 1000, TA 1500, and TE 500 significant ($P < 0.05$) improved the extractum, ash, polysaccharide, and total saponins of Taizishen roots at 90 days post-treatment, and TA 2000 and TE 1000 also significant ($P < 0.05$) increased their total saponins. Simultaneously, the extractum and total saponins of Taizishen roots under TA 2000+TE 1000 treatment at 90 days post-treatment were significant ($P < 0.05$) higher than those of TA 1500, TA 2000, TE 500, and TE 1000; under TA 2000+TE 1000 treatment at 90 days post-treatment, the ash content was significant ($P < 0.05$) higher than that of TA 2000 and TE 1000; and, under TA 2000+TE 1000 treatment at 90 days post-

10.3389/fpls.2025.1543462

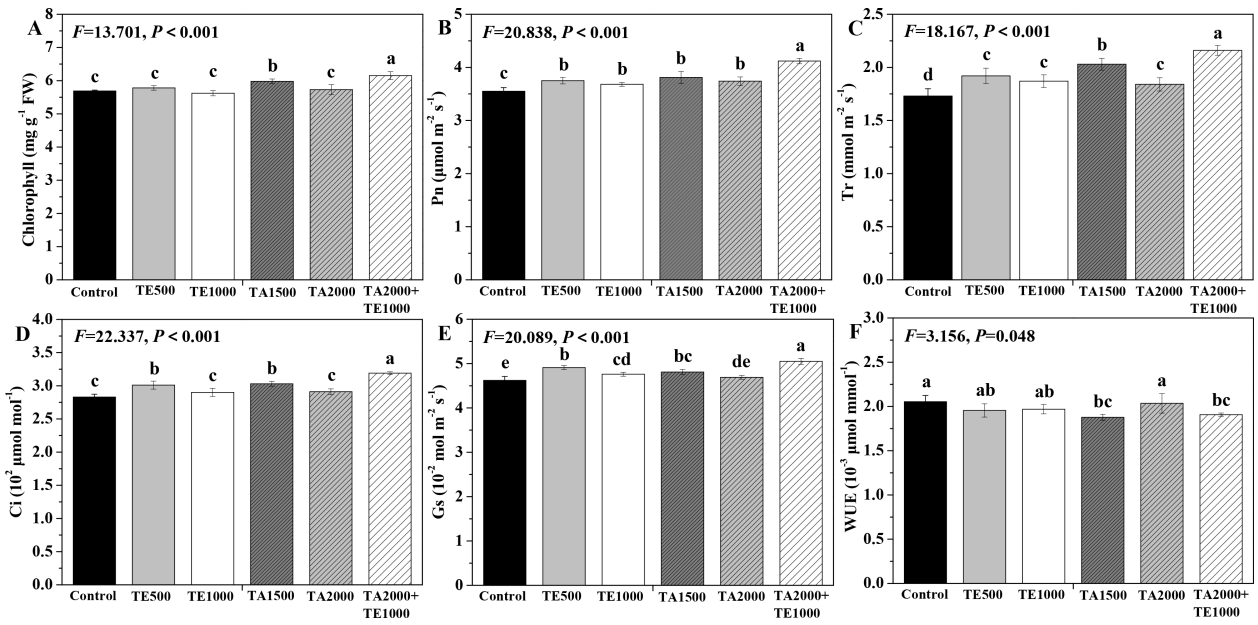

FIGURE 3
The effects of tebuconazole·azoxystrobin and tetramycin on the photosynthetic capability of Taizishen (*P. heterophylla*) leaves infected with leaf spot and viral diseases at 30 days post-treatment under greenhouse conditions. **(A)** chlorophyll content (mg g^{-1} FW), **(B)** photosynthetic rate (Pn) (μmol m^{-2} s^{-1}), **(C)** transpiration rate (Tr) (mmol m^{-2} s^{-1}), **(D)** intercellular carbon dioxide concentration (Ci) (μmol mol^{-1}), **(E)** stomatal conductance (Gs) (10^{-2} mol m^{-2} s^{-1}), and **(F)** water use efficiency (WUE) (10^{-3} μmol $mmol^{-1}$). Different lower-case letters represent statistically significant differences among treatments based on Duncan's test ($P < 0.05$). Control: water without fungicide. TE 500 and TE 1000: 0.3% tetramycin AS 500-time diluent or 1000-time diluent, respectively. TA 1500 and TA 2000: 75% tebuconazole·azoxystrobin WDG 1000-time diluent or 2000-time diluent, respectively. TA 2000+TE 1000: 75% tebuconazole·azoxystrobin WDG 2000-time + 0.3% tetramycin AS 1000-time diluent.

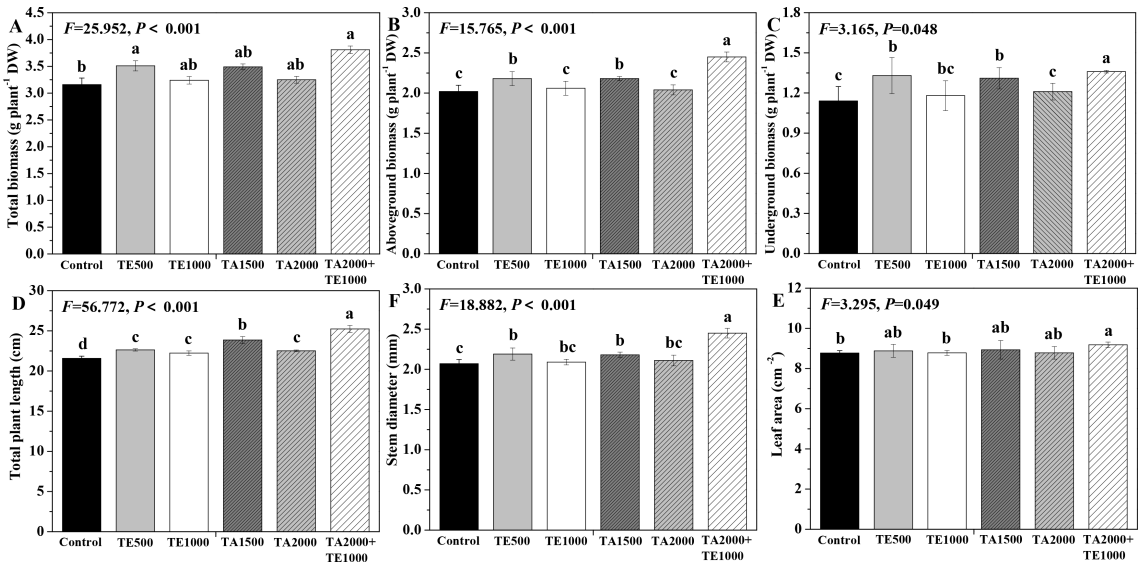

FIGURE 4
The effects of tebuconazole·azoxystrobin and tetramycin on the agronomic traits of Taizishen (*P. heterophylla*) plants infected with leaf spot and viral diseases at 30 days post-treatment under greenhouse conditions. **(A)** total biomass (g $plant^{-1}$ DW), **(B)** aboveground biomass (g $plant^{-1}$ DW), **(C)** underground biomass (g $plant^{-1}$ DW), **(D)** plant length (cm), **(E)** leaf area (cm^2), and **(F)** stem diameter (cm). Different lower-case letters represent statistically significant differences among treatments based on Duncan's test ($P < 0.05$). Control: water without fungicide. TE 500 and TE 1000: 0.3% tetramycin AS 500-time diluent or 1000-time diluent, respectively. TA 1500 and TA 2000: 75% tebuconazole·azoxystrobin WDG 1000-time diluent or 2000-time diluent, respectively. TA 2000+TE 1000: 75% tebuconazole·azoxystrobin WDG 2000-time + 0.3% tetramycin AS 1000-time diluent.

10.3389/fpls.2025.1543462

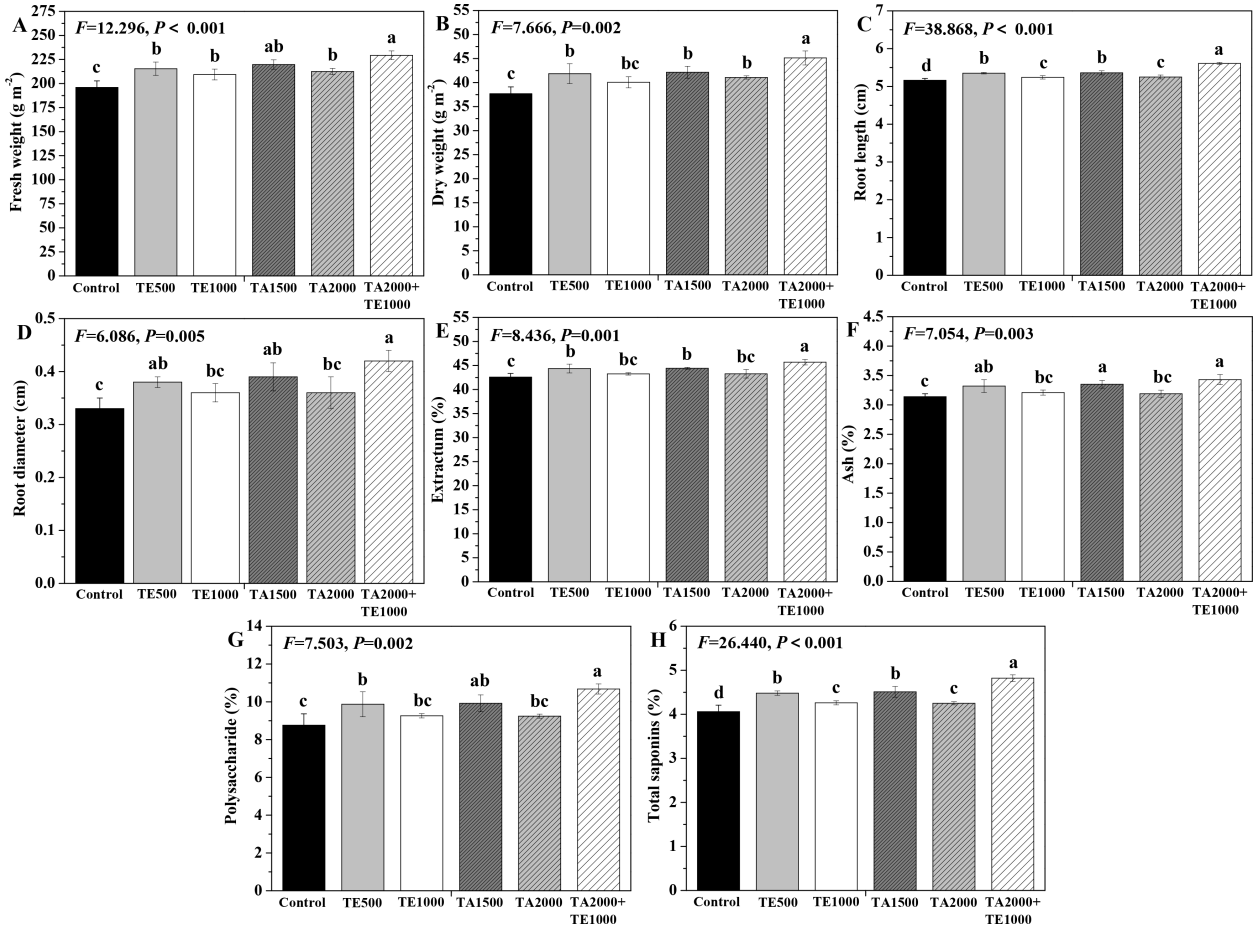

FIGURE 5
The effects of tebuconazole·azoxystrobin and tetramycin on the yield and quality of Taizishen (*P. heterophylla*) plants infected with leaf spot and viral diseases at 90 days post-treatment under greenhouse conditions. **(A)** fresh weight (g m^{-2}), **(B)** dry weight (g m^{-2}), **(C)** root length (cm), **(D)** root diameter (cm), **(E)** extractum (%), **(F)** ash (%), **(G)** polysaccharide (%), and **(H)** total saponins (%). Different lower-case letters represent statistically significant differences among treatments based on Duncan's test ($P < 0.05$). Control: water without fungicide. TE 500 and TE 1000: 0.3% tetramycin AS 500-time diluent or 1000-time diluent, respectively. TA 1500 and TA 2000: 75% tebuconazole·azoxystrobin WDG 1000-time diluent or 2000-time diluent, respectively. TA 2000+TE 1000: 75% tebuconazole·azoxystrobin WDG 2000-time + 0.3% tetramycin AS 1000-time diluent.

treatment, its polysaccharide content was also significant ($P < 0.05$) greater than that of TA 2000, TE 500, and TE 1000. Moreover, their extractum, ash, polysaccharide, and total saponin contents under TA 2000 or TE 500 treatment at 90 days post-treatment were apparently greater than those of TA 1500 or TE 1000. These results demonstrate that the medicinal quality of Taizishen root was better enhanced by tebuconazole·azoxystrobin + tetramycin than by tebuconazole·azoxystrobin or tetramycin alone.

3.7 Correlation analysis

Pearson's correlation analysis was used for creating a correlation matrix between the disease control efficacy and the resistance, electrophysiology, photosynthesis, growth, and quality parameters of Taizishen. As shown in Figure 6, the control effect of leaf spot disease in Taizishen is significant ($P < 0.05$) positive correlated with its MA, UAC, MR, MF, IWHC, WTR, NTC, Pn, plant length, fresh weight, dry weight, underground biomass, and root diameter, and significantly ($P < 0.01$) positive correlated with its IC and chlorophyll, as well as significant ($P < 0.05$) negative correlated with its IXc, IZ, and IXL. Meanwhile, the control effect of viral disease in Taizishen is significant ($P < 0.05$) positive correlated with its POD, SOD, PPO, PAL, total soluble flavonoids, Tr, fresh weight, dry weight and root length, and significantly ($P < 0.01$) positive correlated with its soluble protein, total soluble phenols, Gs, aboveground biomass, and ash, as well as significant ($P < 0.05$) negative correlated with its MDA. These results demonstrate that the control effect of leaf spot disease in Taizishen treated by the combination of low-dosage tebuconazole·azoxystrobin and tetramycin exhibited good correlations with its electrophysiology, photosynthesis, and growth parameters, and the control effect of viral disease in Taizishen treated by the combination of low-dosage tebuconazole·azoxystrobin and tetramycin exhibited good correlations with its disease resistance, photosynthesis, growth, and quality parameters.

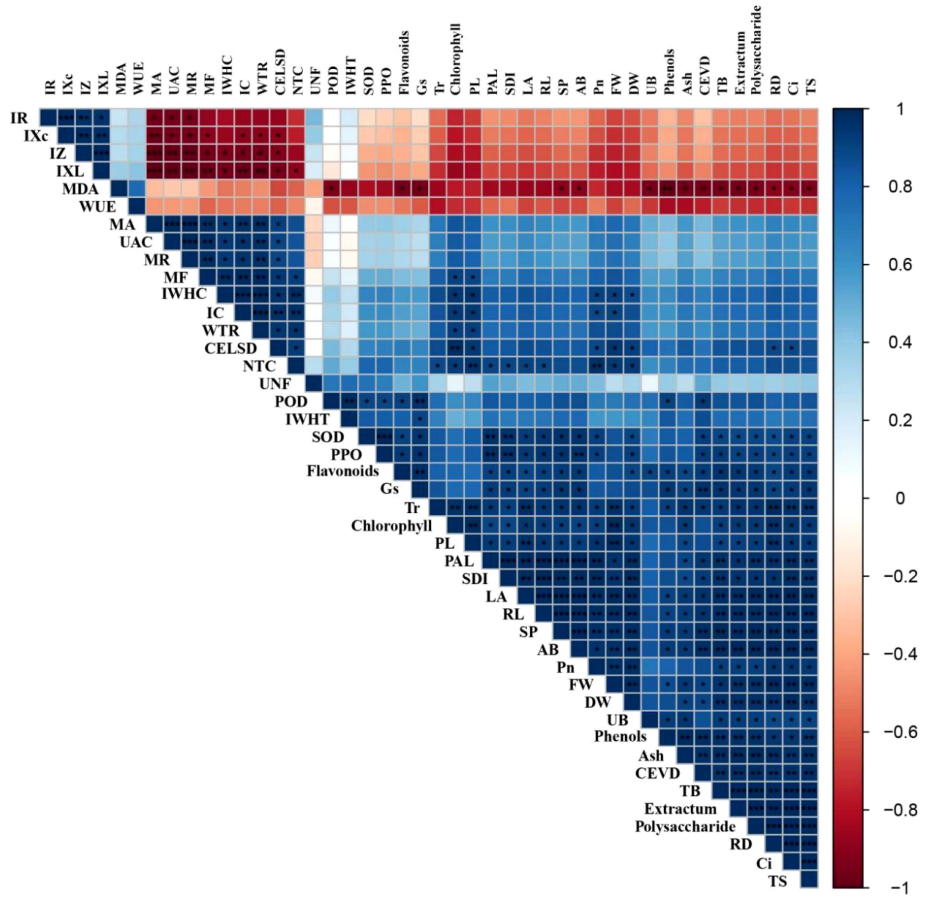

FIGURE 6
Correlation analysis between control efficacy and resistance, electrophysiology, photosynthesis, growth, and quality parameters. CELSD, control effect of leaf spot disease; CEVD, control effect of viral disease; SP, soluble protein; TB, total biomass; AB, aboveground biomass, UB, underground biomass; PL, plant length; LA, leaf area; SDI, stem diameter; FW, fresh weight; DW, dry weight; RL, root length; RD, root diameter; TS, total saponins. *, **, and *** represent significant correlations at 0.05 ($P < 0.05$), 0.01 ($P < 0.01$), and 0.001 ($P < 0.001$) levels, respectively.

4 Discussion

The leaf spot pathogens of Taizishen are *Alteraria tenuissima*, *Arcopilus versabilis*, *Phyllosticta commonsii*, etc., and those of viral disease are *Turnip mosaic virus*, *Broad bean wilt virus*, and *Tobacco mosaic virus* (He et al., 2021; Long et al., 2013; Li et al., 2018; Liang et al., 2022; Yang et al., 2023a, 2023). Tebuconazole can inhibit the sterol biosynthesis of numerous pathogenic fungi (Fustinoni et al., 2014; Paul et al., 2008; Liu et al., 2015), and azoxystrobin exerts broad-spectrum systemic activity on several pathogens (Adetutu et al., 2010; Rodrigue et al., 2013; Wang et al., 2016). Additionally, tetramycin can be widely applied for preventing and controlling various plant diseases caused by fungal, bacterial, and viral pathogens (Chen et al., 2017; Gao et al., 2018; Song et al., 2016; Li et al., 2023; Ma et al., 2017, 2018; Zhao et al., 2010). Wang et al. (2021a) reported that tetramycin exhibited superior antifungal activity against *Alternaria tenuissima*, a kiwifruit brown-spot pathogen with an EC_{50} value of 0.16 mg kg^{-1}. Moreover, our previous research findings showed that tetramycin, when combined with chitosan or matrine, could reliably control leaf spot or soft rot diseases in kiwifruit, improving its resistance, photosynthesis, and quality (Wang et al., 2021b; Zhang et al., 2022a, 2022b). In this study, TA 2000+TE 1000 displayed the best performance in controlling leaf spot and viral diseases, with effects of 90.03%~90.46% and 71.67%~73.08% at 15~30 days after the final fungicide application, respectively; these values are obviously higher than those of TA 1500, TA 2000, TE 500, and TE 1000. These results demonstrate that low-dosage tetramycin, combined with low-dosage tebuconazole·azoxystrobin, could more efficiently control leaf spot and viral diseases compared with high-dosage tebuconazole·azoxystrobin or tetramycin alone, as well as effectively reduce tebuconazole·azoxystrobin application. The superior antimicrobial activity of tetramycin, and the systemic, protective, and therapeutic characteristics of tebuconazole or azoxystrobin, effectively drove the synergistic effect of low-dosage tetramycin and tebuconazole·azoxystrobin in leaf spot and viral diseases.

Inducing disease resistance is considered a feasible method for controlling plant diseases. MDA, flavonoids, phenols, SOD, PAL, POD, and PPO activities, are actively involved in disease-resistance processes in plants (Vlot et al., 2021; Zhang et al., 2022a). For instance, flavonoids and phenols can enhance host cells'

ligninization by participating in lignin biosynthesis, SOD and POD can alleviate reactive oxygen species damage, and PAL and PPO can participate in lignin or phytoalexins biosynthesis (Vlot et al., 2021). Wang et al. (2021a) found that tetramycin could significant ($P < 0.01$) enhance the phenolic and flavonoid contents, as well as the SOD and PPO activities of kiwifruit, and notably increase fruit disease resistance. In this study, TA 2000+TE 1000 significant ($P < 0.05$) increased the total soluble flavonoids and total soluble phenols contents, SOD, PAL, POD, and PPO activities of Taizishen at 30 days post-treatment, while decreasing its MDA content. Meanwhile, the promoting or inhibitory effects of TA 1500, TA 2000, TE 500, and TE 1000 on these resistance parameters were weaker than those of TA 2000+TE 1000. These results show how the combined application of low-dosage tetramycin and tebuconazole·azoxystrobin could more promote the resistance substance contents and resistance enzyme activities of Taizishen than their high-dosage application alone. In this way, this treatment has promising potential for ameliorating disease resistance in Taizishen.

A plant's electrophysiological activities run throughout almost all of its life processes; these activities are considered the fastest responses to environmental stresses (Sukhov, 2016; Szechyńska-Hebda et al., 2017; Xing et al., 2022). Abiotic or biotic stress, such as diseases, insect pests, drought, and so on, can directly or indirectly causes dramatic changes in their electrophysiological activities (Sukhov, 2016; Szechyńska-Hebda et al., 2017; Xing et al., 2022; Tian et al., 2024; Zhang et al., 2020, 2021a, 2021b). Previously, it has been shown that C, R, Z, Xc, and XL are the most common electrical signals used to evaluate various plants' physiological status (Zhang et al., 2015; Xing et al., 2021; Zhang et al., 2020, 2021a, 2021b; Tian et al., 2024). In this work, the co-application of low-dosage tetramycin and tebuconazole·azoxystrobin could more effectively enhance the IC, intracellular water metabolism, nutrient transport, and plant metabolic activity of Taizishen and decline its IR, IZ, IXL, and IXc than their high-dosage, singular application. These results emphasize that the co-application of low-dosage tetramycin and tebuconazole·azoxystrobin could effectively promote healthy growth in Taizishen. This plant's electrophysiological information can effectively aid in characterizing its physiological activities, thus supporting the research conclusions of the above disease control roles following photosynthesis, biomass, and agronomic traits.

The physiological basis of plant growth and development is photosynthesis, and good growth facilities high biomass and quality. Wang et al. (2021b) reported that tetramycin, when used together with chitosan, could enhance the photosynthesis, growth, and quality of kiwifruit. Similarly, our previous research findings showed that tetramycin combined with matrine could also reliably enhance kiwifruit's photosynthesis, quality, and amino acid levels (Wang et al., 2021b; Zhang et al., 2022a, 2022b). In this study, compared with high-dosage tetramycin and tebuconazole·azoxystrobin, the combined application of low doses could more promote the chlorophyll, Pn, Tr, Ci, and Gs of Taizishen; more reliably increase its total, above-, and underground biomass, as well as its plant length, leaf area, and stem diameter; and more notably ameliorate its root weight, length, and diameter, as well as more obviously enhance its roots' extractum, ash, polysaccharide, and total saponin contents. Moreover, the control effect of leaf spot disease in Taizishen treated by the combination of low-dosage tebuconazole·azoxystrobin and tetramycin exhibited significant correlations with its electrophysiology, photosynthesis, and growth parameters, and the control effect of viral disease in Taizishen treated by the combination of low-dosage tebuconazole·azoxystrobin and tetramycin exhibited significant correlations with its MDA, total soluble flavonoids, total soluble phenols, protective enzyme activity, photosynthesis, growth, and quality parameters. These positive results underscore how the co-application of low-dosage tetramycin and tebuconazole·azoxystrobin can effectively control leaf spot and viral diseases in Taizishen, thereby facilitating good growth, high biomass, and an excellent medicinal quality.

In general, reducing the use of chemical pesticides and exploiting alternative technologies are two approaches that will always be favored by the public and the government. Meanwhile, high-efficacy and low-toxicity natural products for use as synergists in managing plant diseases and decreasing chemical pesticide use are being increasingly welcomed (Wang et al., 2022). In this study, the combined application of low-dosage tetramycin and tebuconazole·azoxystrobin could more control leaf spot and viral diseases in Taizishen compared with high-dosage tebuconazole·azoxystrobin or tetramycin alone. This treatment combination could enhance its disease resistance, intracellular water metabolism, nutrient transport, plant metabolic activity, photosynthesis, growth, yield, and quality, and reliably decrease tebuconazole·azoxystrobin application. Furthermore, the safe interval period is very long at over 60 days, and tetramycin is a natural, environmentally friendly, and low-toxicity antibiotic with wide applications in medical, agricultural, and other fields. Thus, the food safety risk with this combined treatment is minuscule to nonexistent. All in all, this work highlights how 75% tebuconazole·azoxystrobin WDG 2000-time + 0.3% tetramycin AS diluted 1000 times is a practicable formula for controlling leaf spot and viral diseases in Taizishen.

5 Conclusions

In summary, tetramycin could effectively assist low-dosage tebuconazole·azoxystrobin in protecting against leaf spot and viral diseases in Taizishen. Moreover, the co-application of low-dosage tetramycin and tebuconazole·azoxystrobin could more effectively improve the resistance-related substance contents and resistance enzyme activities of Taizishen than their high-dosage, singular application. Meanwhile, their combined application could more effectively ameliorate the plant's IC, intracellular water metabolism, nutrient transport, and plant metabolic activity, and decrease its IR, IZ, IXL, and IXc. Additionally, their combined application could also more effectively enhance the plant's photosynthesis, biomass, agronomic traits, and root growth and quality. This study highlights that the combined application of low-dosage tetramycin and tebuconazole·azoxystrobin can be recommended as a novel and practicable measure for controlling leaf spot and viral diseases in Taizishen.

Data availability statement

The original contributions presented in the study are included in the article/supplementary material. Further inquiries can be directed to the corresponding author/s.

Author contributions

BT: Data curation, Investigation, Methodology, Writing – original draft. CT: Investigation, Methodology, Resources, Software, Writing – original draft. JL: Data curation, Formal analysis, Investigation, Methodology, Writing – original draft. BJ: Data curation, Formal analysis, Investigation, Methodology, Software, Writing – original draft. CZ: Conceptualization, Funding acquisition, Project administration, Resources, Supervision, Writing – review & editing.

Funding

The author(s) declare financial support was received for the research, authorship, and/or publication of this article. This work was supported by the National Natural Science Foundation of China (No. 32360023), the Science-Technology Support Program of Guizhou Province (No. QKHZC(2023)Yiban074), the Earmarked Fund for Guizhou Modern Agriculture Research System (No. GZRNCYJSTX2025), the Humanities and Social Science Research Project of Guizhou Provincial University (No. 2024RW87), the Guizhou Provincial Foundation for Excellent Scholars Program (GCC(2023)076), the Youth Science and Technology Talent Growth Project of Guizhou Medical University (No. 22QNRC15).

Conflict of interest

The authors declare that the research was conducted in the absence of any commercial or financial relationships that could be construed as a potential conflict of interest.

Generative AI statement

The authors declare that no Generative AI was used in the creation of this manuscript.

Publisher's note

All claims expressed in this article are solely those of the authors and do not necessarily represent those of their affiliated organizations, or those of the publisher, the editors and the reviewers. Any product that may be evaluated in this article, or claim that may be made by its manufacturer, is not guaranteed or endorsed by the publisher.

References

Adetutu, E. M., Ball, A. S., and Osborn, A. M. (2010). Azoxystrobin and soil interactions: degradation and impact on soil bacterial and fungal communities. *J. Appl. Microbiol.* 105, 1777–1790. doi: 10.1111/j.1365-2672.2008.03948.x

Bo, C., Fen, Y., Zheng, X., Cui, D., Shao, Y., and Zhu, C. (2012). Genome mining of the biosynthetic gene cluster of the polyene macrolide antibiotic tetramycin and characterization of a P450 monooxygenase involved in the hydroxylation of the tetramycin B polyol segment. *Chembiochem* 13, 34–42. doi: 10.1002/cbic.201200402

Chen, F., Li, Q., Su, Y., Lei, Y., and Zhang, C. (2023). Chitosan spraying enhances the growth, photosynthesis, and resistance of continuous *Pinellia ternata* and promotes its yield and quality. *Molecules* 28, 2053. doi: 10.3390/molecules28052053

Chen, L. L., Guo, B. B., Li, B. X., Mu, W., and Liu, F. (2017). Toxicity and Control Efficacy of Tetramycin against *Passalora fulva*. *Chin. J. Pestic. Sci.* 19, 324–330. doi: 10.16801/j.issn.1008-7303.2017.0042

Chinese Pharmacopoeia Commission (2019). *General Principles of Four Parts of Chinese Pharmacopoeia 2020* (Beijing: China Medical Science and Technology Press).

Choi, Y., Kim, M., Ahn, K., Um, J., Lee, S., and Yang, W. (2017). Immunomodulatory effects of *Pseudostellaria heterophylla* (Miquel) pax on regulation of th1/th2 levels in mice with atopic dermatitis. *Mol. Med. Rep.* 15, 649. doi: 10.3892/mmr.2016.6093

Fustinoni, S., Mercadante, R., Polledri, E., Rubino, F. M., Mandic-Rajcevic, S., Vianello, G., et al. (2014). Biological monitoring of exposure to tebuconazole in winegrowers. *J. Expo Sci. Environ. Epidemiol.* 24, 643–649. doi: 10.1038/jes.2014.14

Gao, Y., He, L., Li, X., Lin, J., Mu, W., and Liu, F. (2018). Toxicity and biochemical action of the antibiotic fungicide tetramycin on *Colletotrichum scovillei*. *Pestic. Biochem. Physiol.* 147, 51–58. doi: 10.1016/j.pestbp.2018.02.012

He, J., Liang, S., Zhang, G., Zhao,, Zhi,, and Li, Z. (2021). Pathogen Identification and Screening of Fungicides against *Pseudostellaria heterophylla* (Miq.) Pax Leaf Spot. *J. South. Agr* 52, 2124–2132. doi: 10.3969/j.issn.2095-1191.2021.08.010

Li, H., Liu, J. B., Wang, T. J., Jiang, H., Zhang, R. B., and Guan, W. J. (2014). Research progress of ATP-binding cassette transporters in polyene antibiotic biosynthesis gene cluster. *Microbio. China* 41, 950–958. doi: 10.13344/j.microbiol.China.130407

Li, W., Long, Y., Yin, X., Wang, W., Zhang, R., Mo, F., et al. (2023). Antifungal Activity and Mechanism of Tetramycin against *Alternaria alternata*, the Soft Rot Causing Fungi in Kiwifruit. *Pestic Biochem. Physiol.* 192, 105409. doi: 10.1016/j.pestbp.2023.105409

Li, Z., Zhang, L., and Zhao, Z. (2013). Screening of leaf spot control agents of *Pseudostellaria heterophylla*. *Culture Planting* 01, 21–23. doi: 10.13605/j.cnki.52-1065/s.2013.01.006

Li, S., Zhou, X., and Yang, Y. (2018). Pathogen identification of leaf spot on *Pseudostellaria heterophylla* and screening of fungicides for its control. *Plant Prot.* 44, 182–185. doi: 10.16688/j.zwbh.2017284

Liang, S., Chen, X., Liu, Y., Feng, W., Li, C., Chen, X., et al. (2022). Rapid detection of *Broad bean wilt virus* 2 and *Turnip mosaic virus* in *Pseudostellaria heterophylla* by reverse transcription loop-mediated isothermal amplification assay. *J. Phytopathol.* 170, 535–545. doi: 10.1111/jph.13103

Liao, X., He, X., Xu, G., Wang, Z., Li, J., Guan, H., et al. (2018). Two Nitrogen-containing compounds from *Pseudostellaria heterophylla*. *Nat. Prod Commun.* 13, 343–346. doi: 10.1177/1934578X1801300318

Liu, N., Dong, F., Xu, J., Liu, X., Chen, Z., Tao, Y., et al. (2015). Stereoselective determination of tebuconazole in water and zebrafish by supercritical fluid chromatography tandem mass spectrometry. *J. Agric. Food Chem.* 63, 6297–6303. doi: 10.1021/acs.jafc.5b02450

Long, G., Ma, D., Xia, Z., and Shao, C. (2013). *Pseudostellaria heterophylla* main disease occurrence regulation and control counter measure in shibing county. *Culture Planting* 2), 46. doi: 10.13605/j.cnki.52-1065/s.2013.02.010

Ma, J., Sun, M., Qiu, L., Xie, Y., Ma, Y., and Liang, W. (2022). The 5-aminolevulinic acid (5-ALA) supplement enhances PSII photochemical activity and antioxidant activity in the late growth promotion of *Pseudostellaria heterophylla*. *Plants* 11, 3035. doi: 10.3390/plants11223035

Ma, D. C., Zhu, J. M., He, L., Cui, K., Mu, W., and Liu, F. (2017). Baseline Sensitivity and Control Efficacy of Tetramycin against *Phytophthora capsici* Isolates in China. *Plant Dis.* 102, 863–868. doi: 10.1094/pdis-09-17-1396-re

Ma, D. C., Zhu, J. M., Jiang, J. G., Zhao, Y. H., Li, B. X., Mu, W., et al. (2018). Evaluation of Bioactivity and Control Efficacy of Tetramycin against *Corynespora cassiicola*. *Pestic. Biochem. Physiol.* 152, 106–113. doi: 10.1016/j.pestbp.2018.09.009

Paul, P. A., Lipps, P. E., Hershman, D. E., McMullen, M. P., Draper, M. A., and Madden, L. V. (2008). Efficacy of triazole-based fungicides for fusarium head blight and deoxynivalenol control in wheat: a multivariate metaAnalysis. *Phytopathology* 98, 999–1011. doi: 10.1094/PHYTO-98-9-0999

Ren, J., Cui, Y., Zhang, F., Cui, H., Ni, X., Chen, F., et al. (2014). Enhancement of Nystatin Production by Redirecting Precursor Fluxes after Disruption of the Tetramycin Gene from *Streptomyces ahygroscopicus*. *Microbiol. Res.* 169, 602–608. doi: 10.1016/j.micres.2013.09.017

Rodrigues, E. T., Lopes, I., and Pardal, M. N. (2013). Occurrence, fate and effects of azoxystrobin in aquatic ecosystems: a review. *Environ. Int.* 53, 18–28. doi: 10.1016/j.envint.2012.12.005

Shao, C., Li, D., and Ma, D. (2016). Preliminary study on screening pesticide of prevention and control of *Pseudostellaria heterophylla* leaf spot. *Tillage Cultivation* 4), 29–30. doi: 10.13605/j.cnki.52-1065/s.2016.04.012

Shi, Y., Huang, Y., Wang, W., Yang, L., Zhou, H., and Sang, Z. (2020). Analysis on the current quality standards of chinese materia medica used in COVID-19 prevention and treatment. *Pharmacol. Res.* 160, 105074. doi: 10.1016/j.phrs.2020.105074

Song, Y., He, L., Chen, L., Ren, Y., Lu, H., Geng, S., et al. (2016). Baseline Sensitivity and Control Efficacy of Antibiosis Fungicide Tetramycin against *Botrytis cinerea*. *Eur. J. Plant Pathol.* 146, 337–347. doi: 10.1007/s10658-016-0920-z

Sukhov, V. (2016). Electrical signals as mechanism of photosynthesis regulation in plants. *Photosynth Res.* 130, 373–387. doi: 10.1007/s11120-016-0270

Szechyńska-Hebda, M., Lewandowska, M., and Karpiński, S. (2017). Electrical signaling, photosynthesis and systemic acquired acclimation. *Front. Physiol.* 8. doi: 10.3389/fphys.2017.00684

Tian, B., Tang, C., Liu, J., Wang, Q., Feng, W., Su, Y., et al. (2024). Impacts of epihomobrassinolide and thiamethoxam·Flutolanil·Azoxystrobin on the continuous cropping stress of pinellia ternata. *Horticulturae* 10, 696. doi: 10.3390/horticulturae10070696

Vlot, A. C., Sales, J. H., Lenk, M., Bauer, K., Brambilla, A., Sommer, A., et al. (2021). Systemic propagation of immunity in plants. *New Phytol.* 229, 1234–1250. doi: 10.1111/nph.16953

Wang, H., Huang, Y., Wang, J., Chen, X., Wei, K., Wang, M., et al. (2016). Activities of Azoxystrobin and Difenoconazole against *Alternaria alternata* and Their Control Efficacy. *Crop Prot* 90, 54–58. doi: 10.1016/j.cropro.2016.08.022

Wang, Q., Li, H., Lei, Y., Su, Y., and Long, Y. (2022). Chitosan as an adjuvant to improve isopyrazam azoxystrobin against leaf spot disease of kiwifruit and enhance its photosynthesis, quality, and amino acids. *Agriculture* 12, 373. doi: 10.3390/agriculture12030373

Wang, Z., Liao, S., He, Y., Li, J., Zhong, R., He, X., et al. (2013). Protective Effects of Fractions from *Pseudostellaria heterophylla* against Cobalt Chloride Induced Hypoxic Injury in H9c2 cell. *J. Ethnopharmacol* 147, 540–545. doi: 10.1016/j.jep.2013.03.053

Wang, Q., Zhang, C., Long, Y., Wu, X., Su, Y., Lei, Y., et al. (2021a). Bioactivity and control efficacy of the novel antibiotic tetramycin against various kiwifruit diseases. *Antibiotics* 10, 289. doi: 10.3390/antibiotics10030289

Wang, Q., Zhang, C., Wu, X., Long, Y., and Su, Y. (2021b). Chitosan augments tetramycin against soft rot in kiwifruit and enhances its improvement for kiwifruit growth, quality and aroma. *Biomolecules* 11, 1257. doi: 10.3390/biom11091257

Wu, L., Chen, J., Wu, H., Qin, X., Wang, J., Wu, Y., et al. (2016). Insights into the Regulation of Rhizosphere Bacterial Communities by Application of Bio-organic Fertilizer in *Pseudostellaria heterophylla* Monoculture Regime. *Front. Microbiol.* 7. doi: 10.3389/fmicb.2016.01788

Xing, D., Chen, X., Wu, Y., and Zwiazek, J. (2021). Leaf physiological impedance and elasticity modulus in *Orychophragmus violaceus* seedlings subjected to repeated osmotic stress. *Sci. Hortic.* 276, 109763. doi: 10.1016/j.scienta.2020.109763

Xing, D., Mao, R., Li, Z., Wu, Y., Qin, X., and Fu, W. (2022). Leaf intracellular water transport rate based on physiological impedance: A possible role of leaf internal retained water in photosynthesis and growth of tomatoes. *Front. Plant Sci.* 13. doi: 10.3389/fpls.2022.845628

Xu, L., Li, P., Su, J., Wang, D., Kuang, Y., Ye, Z., et al. (2023). EST-SSR development and genetic diversity in the medicinal plant *Pseudostellaria heterophylla* (Miq.) pax. *J. Appl. Res. Med. Aroma* 33, 100450. doi: 10.1016/j.jarmap.2022.100450

Yang, X., Su, Z., Chen, Q., Ai, Q., Yang, L., Zang, L., et al. (2023b). Study on the application of different biological agents in the production of *radix Pseudostellariae*. *Tillage Cultivation* 43, 89–91. doi: 10.13605/j.cnki.52-1065/s.2023.02.031

Yang, C., Yang, Y., Guo, L., Zhang, X., Pei, G., Zhang, H., et al. (2023a). Common diseases and drug use of *Pseudostellaria heterophylla*. *China J. Chin. Materia Med.* 48, 3281–3286. doi: 10.19540/j.cnki.cjcmm.20230214.102

Zhang, C., Dai, Y., Liu, J., Su, Y., and Zhang, Q. (2023). Chitosan enhances low-dosage difenoconazole to efficiently control leaf spot disease in *Pseudostellaria heterophylla* (Miq.) pax. *Molecules* 28, 6170. doi: 10.3390/molecules28166170

Zhang, L., Guo, Z., Gao, H., Pen, X., Li, Y., Sun, S., et al. (2016). Interaction of *pseudostellaria heterophylla* with quorum sensing and quorum quenching bacteria mediated by root exudates in a consecutive monoculture system. *J. Microbiol. Biotechnol.* 26, 2159. doi: 10.4014/jmb.1607.07073

Zhang, C., Li, W., Long, Y., Su, Y., and Zhang, Q. (2022b). Co-application of tetramycin and matrine improves resistance of kiwifruit against soft rot disease and enhances its quality and amino acids. *Antibiotics* 11, 671. doi: 10.3390/antibiotics11050671

Zhang, C., Li, J., Su, Y., and Wu, X. (2022c). Association of physcion and chitosan can efficiently control powdery mildew in *rosa roxburghi*i. *Antibiotics* 11, 1661. doi: 10.3390/antibiotics11111661

Zhang, C., Li, H., Wu, X., Su, Y., and Long, Y. (2022a). Co-application of tetramycin and chitosan in controlling leaf spot disease of kiwifruit and enhancing its resistance, photosynthesis, quality and amino acids. *Biomolecules* 12, 500. doi: 10.3390/biom12040500

Zhang, C., Su, Y., Wu, Y., Li, H., Zhou, Y., and Xing, D. (2021a). Comparison on the Nutrient Plunder Capacity of *Orychophragmus violaceus* and *Brassica napus* L. Based on Electrophysiological Information. *Horticulturae* 7, 206. doi: 10.3390/horticulturae7080206

Zhang, C., Tang, C., Wang, Q., Su, Y., and Zhang, Q. (2024). Synergistic effects of oligochitosan and pyraclostrobin in controlling leaf spot disease in *Pseudostellaria heterophylla*. *Antibiotics* 13, 128. doi: 10.3390/antibiotics13020128

Zhang, C., Wu, Y., Su, Y., Li, H., Fang, L., and Xing, D. (2021b). Plant's electrophysiological information manifests the composition and nutrient transport characteristics of membrane proteins. *Plant Signal Behav.* 16, 1918867. doi: 10.1080/15592324.2021.1918867

Zhang, C., Wu, Y., Su, Y., Xing, D., Dai, Y., Wu, Y., et al. (2020). A plant's electrical parameters indicate its physiological state: A study of intracellular water metabolism. *Plants* 9, 1256. doi: 10.3390/plants9101256

Zhang, M., Wu, Y., Xing, D., Zhao, K., and Yu, R. (2015). Rapid measurement of drought resistance in plants based on electrophysiological properties. *Trans. ASABE* 58, 1441–1446. doi: 10.13031/trans.58.11022

Zhang, J., Zhou, T., Zhang, C., Zheng, W., Li, J., Jiang, W., et al. (2021). Gibberellin disturbs the balance of endogenesis hormones and inhibits adventitious root development of *Pseudostellaria heterophylla* through regulating gene expression related to hormone synthesis. *Saudi J. Biol. Sci.* 28, 135–147. doi: 10.1016/j.sjbs.2020.09.022

Zhao, X., Zhong, L., Zhang, Q., Xu, C., Zhu, H., Lu, Z., et al. (2010). Effect of tetramycin on mycelia growth and spore germination of rice blast pathogen. *J. Microbiol.* 2, 43–45. doi: 10.3969/j.issn.1005-7021.2010.02.009

frontiers | Frontiers in Plant Science

TYPE Original Research
PUBLISHED 05 March 2025
DOI 10.3389/fpls.2025.1515506

Check for updates

OPEN ACCESS

EDITED BY
Temoor Ahmed,
Zhejiang University, China

REVIEWED BY
Muzammil Hussain,
Shenzhen University, China
Lukman Ahamad,
Guizhou University, China
Qurban Ali,
United Arab Emirates University,
United Arab Emirates

*CORRESPONDENCE
Xinrong Wang
xinrongw@scau.edu.cn

RECEIVED 23 October 2024
ACCEPTED 17 February 2025
PUBLISHED 05 March 2025

CITATION
Ahmed W, Ye W, Pan J, Liu S, Ji W, Zhou S, Wang F, Li Z, Mohany M and Wang X (2025) Evaluation the role of *Luteibacter pinisoli* DP2-30 in mitigating pine wilt disease caused by *Bursaphelenchus xylophilus* through modulation of host microbiome.
Front. Plant Sci. 16:1515506.
doi: 10.3389/fpls.2025.1515506

COPYRIGHT
© 2025 Ahmed, Ye, Pan, Liu, Ji, Zhou, Wang, Li, Mohany and Wang. This is an open-access article distributed under the terms of the Creative Commons Attribution License (CC BY). The use, distribution or reproduction in other forums is permitted, provided the original author(s) and the copyright owner(s) are credited and that the original publication in this journal is cited, in accordance with accepted academic practice. No use, distribution or reproduction is permitted which does not comply with these terms.

Evaluation the role of *Luteibacter pinisoli* DP2-30 in mitigating pine wilt disease caused by *Bursaphelenchus xylophilus* through modulation of host microbiome

Waqar Ahmed[1], Wenhua Ye[1], Jidong Pan[1], Songsong Liu[1], Wenxia Ji[1], Shun Zhou[1], Fusheng Wang[1], Zhiguang Li[1], Mohamed Mohany[2] and Xinrong Wang[1]*

[1]Guangdong Province Key Laboratory of Microbial Signals and Disease Control, College of Plant Protection, South China Agricultural University, Guangzhou, Guangdong, China, [2]Department of Pharmacology and Toxicology, College of Pharmacy, King Saud University, Riyadh, Saudi Arabia

Background and aim: Pine wilt disease (PWD), caused by the pine wood nematode (PWN) *Bursaphelenchus xylophilus*, poses a significant threat to pine forests worldwide. This study aimed to isolate bacterial strains from the rhizosphere of healthy *Pinus massoniana* and elucidate their biocontrol potential in mitigating PWD through direct nematicidal activity and manipulation of host microbiome.

Results: We successfully isolated the rhizobacterium strain DP2-30 from rhizosphere of healthy pine plants, which was identified as *Luteibacter pinisoli* on the basis of morphological, biochemical, and molecular analyses. The fermentation filtrates of strain DP2-30 displayed direct nematicidal activity of >95% (corrected mortality rate) on PWN after 48 hours of treatment. The fermentation broth and filtrates of strain DP2-30 significantly inhibited PWN egg hatching by 49.38% and 43.05%, respectively. Additionally, root drenching of strain DP2-30 fermentation broth significantly reduced PWD severity in pine seedlings (2 years old), with a control effect of 62.50%. Microbiome analyses revealed significant variations in the diversity, structure, and relative abundance of bacterial and fungal communities of pine plants combined treated with DP2-30 and PWN (T2), solely treated with PWN (T1), and control (treated with water). Bacterial phyla, Proteobacteria, Actinobacteriota, Chloroflexi, Acidobacteriota, and Armatimonadota and fungal phyla Ascomycota, Basidiomycota and Mortierellomycota were dominant in the all root and stem samples. The application of *L. pinisoli* DP2-30 significantly increased the relative abundance of the family Rhodanobacteraceae in the roots and stems of pine seedlings. Additionally, intra-kingdom co-occurrence network analysis revealed reduced complexity in the bacterial networks but increased complexity in the fungal networks of treated plants, suggesting enhanced functional redundancy and ecosystem stability.

Conclusions: Overall, this study highlights the potential of *L. pinisoli* DP2-30 as an effective biocontrol agent against PWD by directly killing PWN and manipulating the host microbiota.

KEYWORDS

***Bursaphelenchus xylophilus*, *Luteibacter pinisoli* DP2-30, biocontrol, host microbiome manipulation, forest health**

1 Introduction

Plant-parasitic nematodes (PPNs) are economically significant pests that negatively impact crop yield (Ayaz et al., 2021). To date, ~4100 species of PPNs have been documented in the literature, resulting in annually economic losses exceeding $150 billion (USD), globally (Diyapoglu et al., 2022). *Bursaphelenchus xylophilus*, the pine wood nematode (PWN), is a highly destructive pathogen responsible for causing pine wilt disease (PWD), which poses a substantial threat to pine forests worldwide (Kamaruzzaman et al., 2024) and ranks as the sixth most economically important PPN (Jones et al., 2013). PWN is originally native to North America, however it has been subsequently spread to numerous regions of Asia and Europe, resulting in significant ecological and economic losses (Dou and Yan, 2022). Insect vectors, usually longhorn beetles of the genus *Monochamus*, transmit and introduce the PWN into healthy pine trees from infected pine trees during oviposition or feeding (Akbulut and Stamps, 2012). Upon entering the susceptible host, the PWN undergoes fast reproduction and dissemination throughout the tree's vascular system, resulting in symptoms of wilting and eventually leading to the death of the whole tree (Modesto et al., 2022). Disease development is particularly severe in vulnerable pine species under favorable climatic conditions such as drought stress (Estorninho et al., 2022) and elevated temperatures (Pimentel and Ayres, 2018). Considering the far-reaching importance of pine forests for biodiversity preservation, ecological services, and timber supply the management of PWD and the mitigation of PWN effects on forest ecosystems have become the main objectives of researchers worldwide.

Currently, PWD management strategies focus on a combination of monitoring, early detection, and rapid response approaches (Chen et al., 2023). Integrated pest management (IPM) approaches such as cultural practices (improving tree health by appropriate watering, mulching, and pruning), biological control approaches, and chemical applications (insecticides and nematicides) are widely adopted to mitigate PWD incidence (Kim et al., 2020a). Efforts are being made in certain regions to decrease the population of pine sawyer beetles (*Monochamus* spp.), which serve as carriers for the PWN (He et al., 2020; Kim et al., 2020b). Additionally, there is an increasing focus on utilizing pine species (*Pinus pinea* and *P. radiata*) having resistant to PWN for reforestation and landscaping to mitigate incidence of PWD more effectively (Kamata, 2008). In heavily impacted regions, more extreme IPM approaches, such as removal, burning, and fumigation of trees and aerial spray and trunk injection of nematicides and insecticides have been undertaken to control the spread of the disease (Takai et al., 2003; Kwon et al., 2005; Bonifácio et al., 2014). Although, these approaches are effective to some extent, they also negatively impact the forest ecosystems. For example, excessive use of nematicides influences the diversity of other organism because of their nonselective nature, causes environmental hazards, and increases the risk of forest fires (Dou and Yan, 2022). Therefore, it is imperative to establish ecologically friendly methods to reduce the prevalence of PWD.

Biocontrol approaches using biocontrol agents (BCAs) have emerged as sustainable and environmentally friendly viable substitutes for chemical control for the management of PWD and mitigation of PWN impact (Sun et al., 2022; Kamaruzzaman et al., 2024). These strategies provide multiple advantages, such as a smaller ecological footprint, the possibility for long-lasting efficacy, and the ability to target specific pathogens (Dou and Yan, 2022). BCAs (bacteria and fungi) have shown great potential in mitigating PWD through different mechanisms, such as directly killing PWN (Liu et al., 2019b; Yin et al., 2020), producing specific nematicidal and volatile organic compounds (Li et al., 2018; Kang et al., 2021; Kamaruzzaman et al., 2024), and triggering host resistance (Chu et al., 2019; Kim et al., 2019). For example, *Esteya vermicola*, a nematophagous fungus that preys on PWN, has shown promising results in reducing populations of PWN and decreasing the incidence of PWD by killing and parasitizing PWN (Wang et al., 2018; Pires et al., 2022). Similarly, *Beauveria bassiana* and *Metarhizium anisopliae* possess the potential to kill PWN, hence reducing their numbers and halting the spread of PWD (Maehara et al., 2007; Kim et al., 2020b). Members of bacterial genera such as *Bacillus*, *Pseudomonas*, *Curtobacterium*, and *Stenotrophomonas* demonstrated strong nematicidal activities against PWN, mitigate PWD incidence and enhanced the plant growth by producing certain metabolites and volatile organic compounds (VOCs) that are toxic to PWN and by stimulating host immunity (Nascimento et al., 2013; Li et al., 2018; Dou and Yan, 2022). These BCAs can directly be directly applied to diseased trees and provide a viable solution, as they target various stages of the PWN life cycle, hence mitigates PWD in the pine forests. The biocontrol of PWN using fungi as BCAs is more prevalent than that of bacteria, and 100 strains from 51 fungal genera were reported as BCAs compared to bacteria (28 strains of 13 genera) (Dou and Yan, 2022). Thus, the biocontrol of PWD via bacterial BCAs has not yet been fully developed and needs further study.

The plant rhizosphere is recognized as one of the most complex ecosystems on Earth and serves as a hotspot for diverse microbes (Raaijmakers, 2014). The rhizosphere microbiome acts as a first line of defense for plants by establishing a complex community of beneficial microorganisms that can inhibit pathogen invasion (Li et al., 2021). Recently, the host microbiome has gained much attention for improving plant health and disease resistance against pathogens (Trivedi et al., 2020; Ahmed et al., 2022a). Beneficial microorganisms can colonize the host plant, improve nutrient absorption ability, secrete antimicrobial compounds, and stimulate host resistance against many plant pathogens, including PPNs (Ali et al., 2023; Dai et al., 2023). Many previous studies have demonstrated that introducing BCAs significantly mitigates disease incidence by manipulating the host microbiome and increasing the abundance of native microbial communities (Ahmed et al., 2022b; Li et al., 2023b). The microbiome of pine trees consists of diverse of bacterial and fungal communities that play vital roles in disease suppression, nutrient cycling, and plant growth promotion. Previous studies directly explained the biocontrol potential of BCAs (bacteria and fungi) against PWN by extraction of nematicidal compounds, specific secondary metabolites, and VOCs. However, no research has explored the potential of beneficial bacteria as BCAs in mitigating PWD by manipulating the host microbiome. In the present study, we screened a strain of rhizosphere bacteria with strong nematicidal activity against PWN from the rhizosphere soil of a healthy pine (*Pinus massoniana*) plant, and its biocontrol potential was studied against PWD through reshaping the host microbiome via amplicon sequencing. We assume that understanding and harnessing the potential of the host microbiome offers new avenues for developing innovative biocontrol strategies against PWN and improving the overall resilience of pine forests to PWD.

2 Materials and methods

2.1 Cultivation of pine wood nematode

The pine wood nematode (PWN) *Bursaphelenchus xylophilus* (Steiner and Buhrer, 1934) Nickle 1970 isolate was previously isolated and stored in our laboratory, Guangdong Province Key Laboratory of Microbial Signals and Disease Control, South China Agricultural University, China (Kamaruzzaman et al., 2024). PWN was grown on the mycelium of *Botrytis cinerea* (7-days old culture) cultured at 25°C for one week in the dark on potato dextrose agar. The Baermann funnel method was employed to harvest the PWN from the culture medium (Mannaa and Seo, 2023). The harvested nematodes were thoroughly washed with sterilized distilled water (sdH_2O) to remove most contaminants from the cuticle and stored at 4°C for future use.

2.2 Isolation and purification of bacterial strains

Soil samples were collected from roots of the of healthy *Pinus massoniana* free from PWN infestation, on the campus of South China Agricultural University, Guangzhou, China. Three soil samples were collected from *P. massoniana* and mixed together to create a composite sample. Bacterial strains were isolated from the collected soil sample using a serial dilution method described by Ahmed (Ahmed et al., 2022c). For the isolation of bacterial strains, one gram of soil was thoroughly mixed in 9 mL of sdH_2O and incubated at 28°C and 180 rpm for 30 minutes. The mixture was subsequently serially diluted (10-folds), and 100 µL of the diluted solution was spread on nutrient agar (NA) media supplemented with 50 mg/L Nystatin (to inhibit fungi growth) with a sterile spreader and incubated at 28°C for two days. On the basis of colony morphology (shape and color), a single colony was picked and streaked on NA medium for purification and 63 rhizobacterial strains were collected. After five rounds of streaking and purification, the purified strains were stored in 50% glycerol stock solution (v/v) at −20°C for future use (strains identification and nematode mortality assays).

2.3 Nematicidal potential of isolated bacterial strains against PWN

The isolated bacterial strains were reactivated on NA media at 28°C for 48 hours to determine their nematocidal potential against PWN. The nematicidal activity of the isolated strains was assessed against PWN via the preparation of fermentation filtrates (FFs) according to the methodology of Puttawong et al. (2024). The seeds solutions of the isolated bacterial strains were prepared by adding a single colony from each strain into 50 mL of nutrient broth (NB) and incubating at 28°C for 15 hours. For the preparation of FFs, 100 mL of NB was inoculated with 1% seed solution and incubated on a shaker for 72 hours at 28°C and 180 rpm. The fermentation mixture was subsequently centrifuged at 4°C and 10,000 rpm for 10 minutes, which was repeated twice. The supernatant was collected and subsequently filtered using a 0.22 µm bacterial filter to obtain FFs and then stored at 4°C for later use. We used the immersion method to evaluate the nematicidal activity of FFs of each bacterial strain against PWN (Moo-Koh et al., 2022). A mixture of 10 µL of nematodes suspension (~100 PWN) and 90 µL of FFs was added to a 48-well cell culture plate (each well) and incubated in the dark at 28°C for 48 hours, whereas sdH_2O was used as a control. Nematodes morphology was observed every 24 hours using a stereomicroscope (Nikon SMZ 745; Nikon, Tokyo, Japan) to calculate the corrected mortality rate (C-M-R). Nematodes were determined to be dead when their bodies were stiff and unresponsive to stimulation by a dissecting needle (Ali et al., 2023). The C-M-R was calculated via the following formula (Ayaz et al., 2021): $CM\ (\%) = (T - CK)/(1 - CK) \times 100$. Where T represents the mortality rate in the treatment group and CK represents the mortality rate in the control group. The assay was repeated three times, with minimum three replicates per treatment. From the isolated bacterial strains, strain DP2-30 exhibited strong nematicidal activity against PWN and was selected for subsequent analyses.

2.4 Identification and characterization of potent biocontrol strain

The potential biocontrol strain DP2-30 was identified on the basis of morphological (colony shape, color, cell size, and Gram

staining) and molecular (PCR amplification and phylogenetic analysis) characteristics. Morphological identification of strain DP2-30 was performed by growing it on NA media at 28°C for 48 hours. Gram staining of strain DP2-30 was performed using a Gram Stain Kit, Solarbio Life Sciences & Technology Co., Ltd. (Beijing, China). The cell morphology and size were observed by Scanning Electron Microscope (SEM; (LEO 1450 VP SEM, Germany) (Taheri et al., 2023). Molecular identification of strain DP2-30 was performed by PCR amplification of 16S *rRNA* gene via primer pair 27F-(5-AGAGTTTGATCCTGGCTCAG-3) and 1492R (5-GGTTACCTTGTTACGACTT-3) (Zhang et al., 2022b). The PCR products were observed using a 1% agarose gel electrophoresis in a gel documentation system (Tanon 2500) and sent to Guangzhou Aiji Biotechnology Co., Ltd. (Guangdong, China) for sequencing. The obtained sequencing results were analyzed by the BLASTN tool in the NCBI database. Mega 11 was used to edit, build, Clustal W, and alignment of sequences, and a phylogenetic tree was constructed with the neighbor-joining method (bootstrap analysis with 1000 replicates) by taking *Bacillus* sp. as an outgroup (Tamura et al., 2021).

2.5 Optimizing culture medium conditions to enhance *Luteibacter pinisoli* DP2-30 nematicidal activity against PWN

The effects of different culture medium conditions, such as incubation time (days), temperature (°C), shaking speed (rpm/min), and culture medium pH on the nematicidal activity of the *L. pinisoli* DP2-30 against PWN were assessed to optimize the fermentation conditions to maximize the nematicidal activity (Kamaruzzaman et al., 2024). The seed solution of strain DP2-30 was prepared as described above (Section 2.3), and 1% of the seed solution was used for subsequent analyses. The impact of incubation time on the nematicidal activity of strain DP2-30 was examined by growing strain DP2-30 in 100 mL of NB for 1, 2, 3, 4, 5, 6, and 7 days and the nematicidal activity was checked every 24 hours. To study how the pH of the culture medium influences the nematicidal activity of DP2-30 against PWN, the pH of the culture medium was adjusted to 4.0, 5.0, 6.0, 7.0, 8.0, 9.0, and 10.0. Subsequently, 100 mL of culture mediums (NB) with different pH values were inoculated with strain DP2-30 seed solution and incubated at 180 rpm/min and 28°C for 72 hours. To assess the effect of incubation temperature (°C), 100 mL of culture medium (NB) containing DP2-30 seed solution was cultured at 180 rpm/min and different temperatures 22, 25, 28, 31, 34, and 37°C for 72 hours. Finally, the impact of shaking speed (rpm/min) on the nematicidal activity of strain DP2-30 was determined by culturing 100 mL of NB at 120, 140, 160, 180, 200 and 220 rpm/min and 28°C for 72 hours. The FFs of strain DP2-30 for each assay were collected via centrifugation as mentioned in section 2.3, and their nematicidal activity was assessed as described above (Section 2.3). All the assays were performed three times, with at least three replications per treatment for each assay.

2.6 Effect of the *Luteibacter pinisoli* DP2-30 on the success hatching of PWN eggs

The effects of different conditions (FFs, fermentation broth (FB), and bacterial suspension) of strain DP2-30 on PWN eggs hatching were studied as described by Sun et al. (2022). The PWN eggs were collected following the methodology of Liu and colleagues (Liu et al., 2019a) and adjusted to a concentration of 100 eggs per 10 µL via a microscope (Nikon SMZ 745; Nikon, Tokyo, Japan). A 10 µL of egg suspension (contained ~100 PWN eggs) was added to a 48-well cell culture plate containing 90 µL of FFs, FB, and bacterial suspension (OD_{600} = 0.5) and incubated in the dark at 28°C for 36 h, while sdH_2O was used as a control. The PWN (L2 stage) number was counted under a stereomicroscope (Nikon SMZ 745; Nikon, Tokyo, Japan). The PWN egg hatching rate (HR: %) and relative inhibition rate (IR: %) were calculated using the following formulas: HR (%) = L2 × 100/eggs + L2 and IR (%) = (HR of control – HR of treatment) × 100/HR of control. The experiment was performed three times, with three replication per treatment.

2.7 Determining the plant growth-promoting ability of *Luteibacter pinisoli* DP2-30

The growth-promoting potential of strain DP2-30 was assessed on a model plant (tobacco; *Nicotiana benthamiana*). For the growth promotion assay, the FB and FFs of strain DP2-30 were obtained by growing it in NB media at 28°C and 180 rpm/min for 72 hours. Tobacco seeds were first surface sterilized with 10% sodium hypochlorite solution for 5 min, followed by 4 times washing with sdH_2O (Shoyeb et al., 2020). After surface sterilization, the tobacco seeds (30) were soaked in 2 mL of FFs and FB for 12 hours, while NB and sdH_2O were used as controls. The seeds (30 seeds per dish, 3 dishes per treatment) were then placed in Petri dishes containing MS media (0.8% agar, 1.5% sucrose, and pH 5.7) and placed in a light incubator at 25°C (12 h light and 12 h dark) under controlled conditions (Sheikh et al., 2023). The assay was performed three times with three dishes per treatment as replicates and each dish contained ten seeds. After 14 days, the seed germination rate, fresh weight, root length, and stem length were recorded and calculated (Sheikh et al., 2023).

2.8 *In planta* assay for determining the biocontrol efficacy of *Luteibacter pinisoli* DP2-30 against pine wilt disease and samples collection

The biocontrol potential of strain DP2-30 against PWD was investigated in a greenhouse pot experiment on 2-year-old pine seedlings (*P. massoniana*) artificially inoculated with PWN. Before the experiment, strain DP2-30 was grown in NB medium at 28°C and 180 rpm/min for 72 hours to prepare FB. The experiment was

executed following a completely randomized design under three conditions: T1 (inoculation of ~3000 PWN per mL/plant), T2 (combined application of DP2-30 FB and ~3000 PWN per mL/plant), and CK (application of sdH_2O as blank control). We used sdH_2O as control to establish a baseline for comparison, which allows us to assess the effects of DP2-30 without any confounding variables that might arise from other treatments. Strain DP2-30 FB (30 mL/plant) was inoculated via the root drenching method around the base of pine plant by disturbing the above 1 cm layer, and the PWN suspension was artificially inoculated into the main stem 5 cm below the top with superficial longitudinal incisions in a well-sealed premade parafilm funnel and kept moist (Rodrigues et al., 2021). Disease development was observed at 9 days of post-inoculation with PWN to 45 days with an interval of 9 days. The disease severity index (%) was calculated for each treatment using a 5-point disease grading scale (0: asymptomatic plants, 1: 1–25% wilting of pine needles, 2: 26–50% wilting of pine needles, 3: 51–75% wilting of pine needles, and 4: 76–100% wilting of pine needles or death of plant). The disease severity index (%) and control effect (%) were calculated using formulas as previously described by Kamaruzzaman et al. (2024). The experiment was repeated three times and 8 pine seedlings were inoculated per treatment as replicates for each individual assay. To study, the impact of strain DP2-30 on the host microbiome, particularly in the context of its potential role in managing PWN infestations through modulation of host microbiome. Root and stem samples were collected from the pine seedlings under different treatments from the *in-planta* biocontrol assay. A total of 36 samples (18 roots and 18 stems; 6 samples per treatment) were collected under different treatments (CK, T1, and T2), placed in liquid nitrogen, and stored at −80°C for host-microbiome analysis. The samples collected from each treatment were labelled according to sample type: CK-R, T1-R, and T2-R (roots) and CK-S, T1-S, and T2-S (stem).

2.9 DNA extraction, Illumina MiSeq sequencing, and data processing

The total genomic DNA from the plant samples were extracted as previously described in our study (Ahmed et al., 2022a), using a Plant DNA Extraction Kit (Zymo Research, USA). The quality of the extracted DNA was assessed at an $OD_{A260/A280}$ ratio of≥1.8 using an ND2000 nanodrop spectrophotometer (Thermo Scientific, USA). For microbiome analysis, the V5-V7 region of bacterial 16S rRNA gene and fungal ITS1 region were amplified with the primer sets 799F (5-AACMGGATTAGATACCCKG-3)/1193R (5-ACGTCATCCCCACCTTCC-3) (Li et al., 2023b) and ITS1-F_KYO2 (5-TAGAGGAAGTAAAAGTCGTAA-3)/ITS-86R (5-TTCAAAGATTCGATGATTCAC-3) (Toju et al., 2012), respectively. The obtained PCR samples were subjected to paired-end sequencing on an Illumina MiSeq platform at Gene Denovo Biotechnology Co., Ltd. (Guangzhou, China). The raw sequences of bacteria and fungi were analyzed and processed using the UPARSE pipeline according to standard protocols and quality controlled by USEARCH software to generate clean reads (Edgar, 2013). Chimeras were eliminated via UCHIME, and subsequently, the remaining clean sequences were allocated to operational taxonomic units (OTUs) on the basis of a similarity standard of 97% (Edgar et al., 2011). Ultimately, the sequence of each OTU was compared to the RDP database of bacteria and UNITE database of fungi according to the Naïve Bayesian algorithm of the RDP Classifier for taxonomic annotation at a confidence threshold level of 0.8~1 (Wang et al., 2007; Nilsson et al., 2019). The raw data from the greenhouse experiments are available in the NCBI Sequence Read Archive (SRA) under BioProject No. PRJNA1132778 with the sample names of CK-R, T1-R, and T2-R (R; root) and CK-S, T1-S, and T2-S (S; stem).

2.10 Statistical and bioinformatics analyses

The alpha diversities of diversities (Shannon, Chao, PD-whole-tree, and Chao-1) bacterial and fungal communities alpha were calculated using QIIME 2 (Bolyen et al., 2019). We used principal coordinate analysis (PCoA) based on the Bray–Curtis distance metric to assess the variations in the structure of the bacterial and fungal community compositions. PERMANOVA with Adonis function was employed to determine the overall dissimilarity in the structure of the microbial communities using "vegan" package in R (version 4.0.1) (Oksanen et al., 2013). The relative abundance bar, box, and bubble plots for the bacterial and fungal communities were generated using the "ggplot" package in R (version 4.0.1). The intra-kingdom microbial network analysis was performed at the OTU level by excluding those with a relative abundance < 0.01, $p < 0.05$, and Pearson correlation coefficient > 0.7 using R sparcc package and visualized with Gephi 0.9.2 (Zhang et al., 2024). We employed one-way ANOVA in SPSS v20.0 (SPSS Inc. USA) to evaluate the impact of different treatments on the disease severity index, nematicidal activity, alpha diversity, and microbial community composition and were considered significant if $p < 0.05$ according to Tukey-HSD and Duncan's multiple range tests. The figures were edited, merged, and combined using Adobe Illustrator 2022.

3 Results

3.1 Isolation and characterization of *Luteibacter pinisoli* DP2-30

A total of 63 bacterial strains were preliminarily isolated and purified from the rhizosphere soil of healthy *Pinus massoniana* plants. The nematicidal activity of isolated bacterial strains was investigated against PWN using fermentation filtrates (FFs) by the immersion method, among which 10 bacterial strains showed various degree of nematicidal activity (20.70% to 92.08%) against PWN after 48 h of exposure. The strain DP2-30 displayed the

highest nematicidal activity with a corrected mortality rate (C-M-R) of 92.08% against PWN (Figures 1A, B), followed by strains DP1-4 and DP2-15 with C-M-R of 75.01% and 73.94% (moderate nematicidal activity), respectively. Several strains, including DP2-13, DP2-27, DP1-2, DP1-18, Dp2-2, DP2-24, and DP2-41 exhibited low nematicidal activity against PWN, with C-M-R values less than 40% (Table 1). In light of these findings, we therefore, chose DP2-30 as a possible biocontrol strain for further investigation. Morphological and biochemical analyses were performed for strain DP2-30. On NA media strain DP2-30 produced smooth, opaque, and round to convex yellow color colonies (Figures 1C, D). Scanning electron microscopy revealed that the bacterial cells were rod-shaped with 1.19 ± 0.20 µm in length and 0.37 ± 0.03 µm in diameter, and Gram staining was negative (Figures 1E, F). Molecular identification of strain DP2-30 was performed via PCR amplification of the 16S rDNA gene using primer set 27F/1492R. A 938 bp PCR product was obtained, and NCBI BLASTN analysis showed 98.80% similarity with *Luteibacter pinisoli* MAH-14 (NR_179163.1). Further phylogenetic tree analysis via neighbor-joining method revealed that strain DP2-30 was in the same clade as *L. pinisoli* and was different from other *Luteibacter* species (Figure 1G). Thus, on the basis of morphological, biochemical, and molecular analyses, the isolated strain DP2-30 was determined to be *L. pinisoli* and was named as *L. pinisoli* P2-30.

3.2 Fermentation conditions for maximal nematicidal activity of *Luteibacter pinisoli* DP2-30

The effects of various fermentation conditions, including culture medium time, pH, temperature, and shaker speed on the nematicidal activity of *L. pinisoli* DP2-30 were assessed against pine wood nematode (PWN) using fermentation filtrates (FFs). Results revealed that the nematicidal activity of strain DP2-30 FFs first increased with the increasing in incubation time, temperature, speed, and fermentation medium pH and then gradually decreased (Figures 2A–D). The nematocidal activity of strain DP2-30 FFs was the highest against PWN at 3 d of incubation with a C-M-R of 95.21% (Figure 2A). At pH 7, the nematicidal activity of strain DP2-30 FFs was maximum, with a C-M-R of 94.10% (Figure 2B). When the incubation temperature was 28°C, strain DP2-30 FFs presented the highest killing rate against PWN with a C-M-R of 94.60% (Figure 2C). The FFs of strain DP2-30 exhibited strong nematicidal

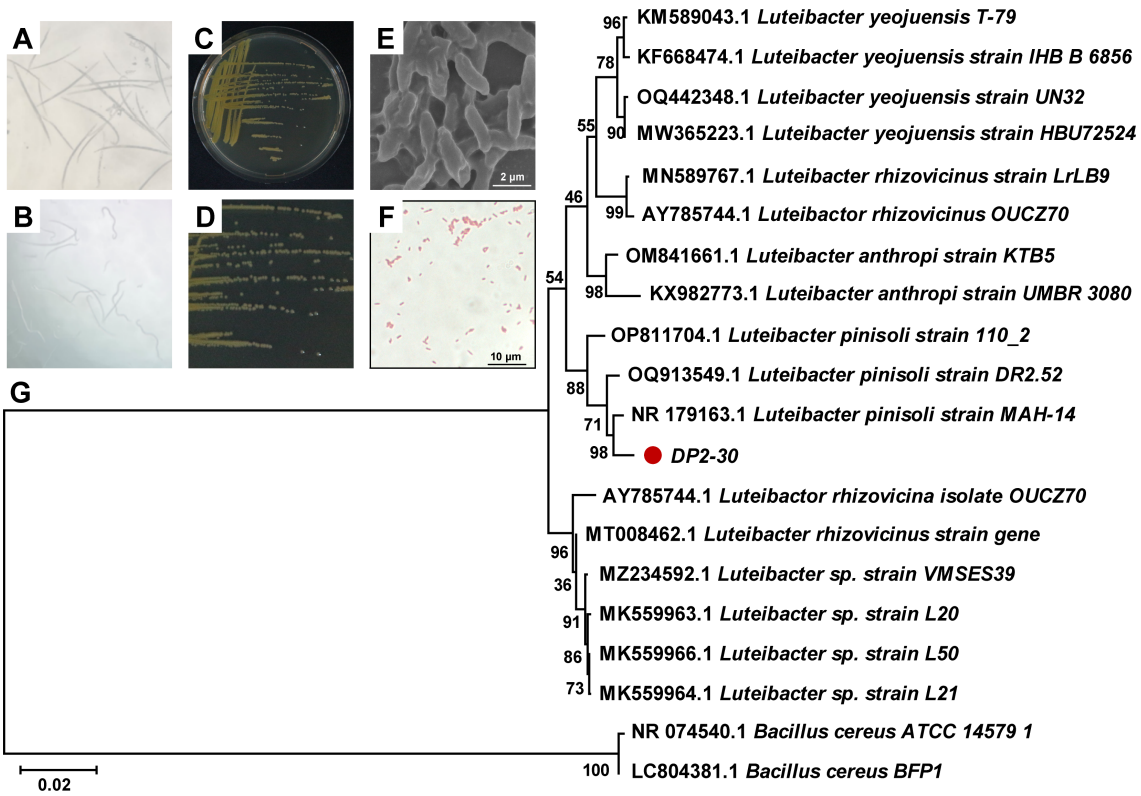

FIGURE 1
Nematicidal activity, morphological, and molecular characterization of *Luteibacter pinisoli* DP2-30. Nematicidal activity of strain DP2-30 against PWN **(A)**, control **(B)**, colony morphology on NA medium **(C, D)**, scanning electron microscope image of bacterial cells **(E)**, Gram staining **(F)**, and phylogenetic tree based on 16S rRNA sequence illustrating the evolutionary position of strain DP2-30 via neighbor-joining method with a bootstrap value of 1000.

10.3389/fpls.2025.1515506

TABLE 1 Nematicidal activity of fermentation filtrates of isolated bacterial strains on pine wood nematode in a co-culture assay.

Strains	48 h mortality rate (%)	48 h corrected mortality rate (%)
DP1-2	38.01 ± 2.16 b	35.70 ± 2.24 b
DP 1-4	75.90 ± 2.52 ab	75.01 ± 2.61 ab
DP1-18	70.33 ± 2.93 b	69.22 ± 2.93 b
DP 2-2	35.19 ± 5.96 b	32.78 ± 6.18 b
DP2-13	57.72 ± 3.81 ab	56.14 ± 3.96 ab
DP2-15	74.87 ± 4.61 ab	73.94 ± 4.78 ab
DP2-24	34.12 ± 2.95 b	31.67 ± 3.06 b
DP2-27	56.21 ± 1.23 b	54.58 ± 1.28 b
DP2-30	92.36 ± 1.26 a	92.08 ± 1.31 a
DP2-41	23.55 ± 1.95 b	20.70 ± 2.02 b
CK-NB	12.66 ± 3.06 bc	—–
CK-sdH_2O	9.14 ± 1.27 c	—–

Different letters within a column indicate significant differences among bacterial strains according to the Duncans multiple range test at $p < 0.5$.

activity against PWN when cultured at 180 rpm/min and 200 rpm/min, having a C-M-R values of 92.43% and 91.71%, respectively (Figure 2D). On the basis of these findings, the optimal fermentation conditions for maximizing the nematicidal activity of *L. pinisoli* DP2-30 against PWN appear to be 3 days of incubation at 28°C, pH 7, and a shaking speed of 180 rpm/min.

3.3 *Luteibacter pinisoli* DP2-30 fermentation broth inhibits PWN egg-hatching

The effects of strain DP2-30 fermentation broth (FB), FFs, and bacterial suspension on PWN egg hatching were calculated after 36 hours of incubation at 28°C. The FB and FFs significantly reduced PWN egg hatching compared to the control group. The hatchability rates were recorded at 41.17% and 46.33% for the FB and FFS, respectively, which were substantially lower than the control. In contrast, the bacterial suspension of strain DP2-30 itself had only a slight inhibitory effect on egg hatching, with a hatchability rate slightly lower than that of the control group. The FB and FFs demonstrated a relatively high inhibition rates of 49.38% and

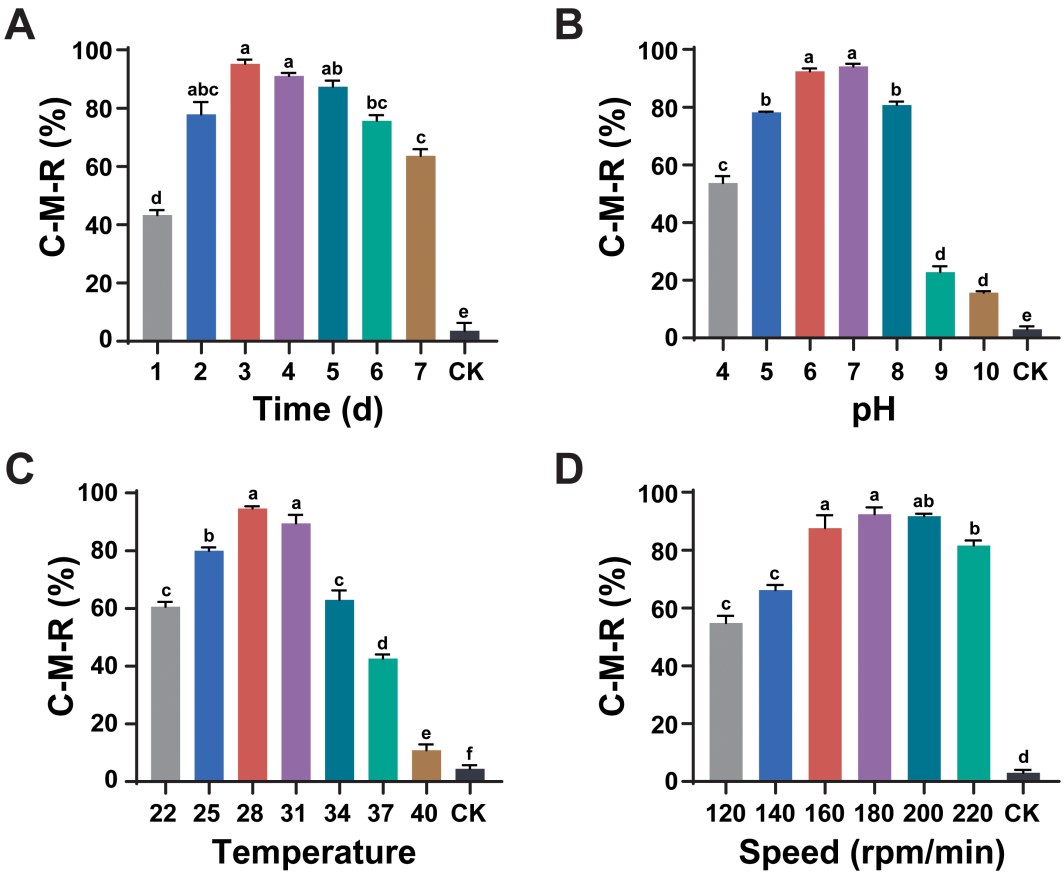

FIGURE 2
Optimization of fermentation conditions for maximal nematicidal activity of *Luteibacter pinisoli* DP2-30. Effects of different fermentation conditions, including incubation time **(A)**, pH **(B)**, temperature °C **(C)**, and rotation speed (rpm/min) **(D)**, on the nematicidal activity of *L. pinisoli* DP2-30 against PWN. Different letters on the error bars (± SD of three biological replicates) indicate significant differences among treatments according to Duncan's test at $p < 0.05$.

43.055%, respectively, on PWN egg hatching compared to the control (Table 2). These results indicate that the metabolites produced during fermentation by strain DP2-30, rather than the bacteria themselves, are responsible for the significant inhibition of PWN egg hatching.

3.4 Growth-promoting effects of *Luteibacter pinisoli* DP2-30 on tobacco as model plant

The effects of strain DP2-30 FB and FFs were evaluated on tobacco seed germination and seedling growth (Supplementary Table S1; Supplementary Figure S1). After the tobacco seeds were soaked in strain DP2-30 FB, FFs, nutrient broth (NB medium) and sdH_2O for 12 h, they germinated normally and no significant effects were observed among treatments. The germination rate reached more than 90.00% in all treatments, and no significant difference was observed among treatments, indicating that strain DP2-30 did not affect the tobacco seed germination rate. After 14 days of tobacco seed growth in the dish, the tobacco seeds in the treatment group had stronger buds, thicker green leaves, longer roots, and greater fresh weight than the control group (Supplementary Figure S1). The root length of tobacco seedlings treated with FB was significantly increased by 75.05% and 74.30% compared with control groups, while the fresh weight was increased by 58.6% and 61.4%, respectively. Similarly, the root length of tobacco seedlings treated with FFs significantly increased by 60.4% and 59.8% compared with control groups, whereas the fresh weight increased by 49.1% and 51.8%, respectively (Supplementary Table S1). The results showed that strain DP2-30 significantly promote the growth of the tobacco seedlings, and could be used as a potential plant growth promoting agent.

3.5 *Luteibacter pinisoli* DP2-30 fermentation broth reduces pine wilt disease incidence in pine seedlings

The biocontrol efficacy of *L. pinisoli* DP2-30 was assessed in mitigating PWD in pine seedlings treated with PWN and strain DP2-30 FB. The disease severity index (%) was calculated from the 9th day after inoculation with PWN till the 45th days, with the interval of 9 days, whereas the control effect (%) was calculated at the end of the experiment (Table 3 and Figure 3). The results indicated that symptom of PWD (fade, yellowing, and wilting of needles) were first observed on the 9th day post-inoculation with PWN in treatment T1 (pine seedlings solely inoculated with PWN). In contrast, the application of DP2-30 FB (T2; combined treatment with DP2-30 FB and PWN) resulted in delayed symptom development in pine seedlings, and PWD symptoms were first observed on the 27th after inoculation with PWN. The disease incidence of PWD gradually increased with the increasing time in treatments T1 and T2, whereas the control plants (CK) treated with sdH2O exhibited normal growth, were healthy, and remained lush green (Figure 3). At 45 days after inoculation with PWN, the highest disease severity index of 100% was observed in treatment T1. However, pine seedlings treated with DP2-30 FB + PWN (T2) displayed a minimum disease severity index of 37.5% and maximum control effect of 62.50% (Table 3). These results showed that the application of DP2-30 FB (T2) significantly delayed the occurrence of PWD in pine seedlings.

TABLE 2 Impact of *Luteibacter pinisoli* DP2-30 on pine wood nematode egg hatching.

Treatments	Egg hatching rate (%)	Relative inhibition rate (%)
Fermentation broth	41.17 ± 1.03b	49.38 ± 1.54b
Fermentation filtrate	46.33 ± 1.71b	43.05 ± 1.54b
Bacterial suspension	77.25 ± 0.94a	5.01 ± 1.81a
Sterile distilled water (CK)	82.00 ± 0.94a	—–

Data are present as mean ± SD of three biological replicates. Different letters within a column indicated significant differences among treatments according to Duncan's test at $p < 0.05$.

3.6 Pine plant microbial community assembly, diversity, and structure analyses

Thirty-six samples (18 roots and 18 stems) of pine plants from different treatments (CK, T1, and T2) were subjected on the Illumina platform for analysis of the host endophytic microbiome (bacteria and fungi). The 16S rRNA and ITS amplicon sequencing of V5-V7 and ITS1 variable regions of bacteria and fungi resulted in a total of 4.547 and 4.523 million raw reads, respectively. After quality control and chimera removal, 3.285 and 4.228 million effective tags of bacteria and fungi were obtained, with an average of 0.091 and 0.117 million effective tags per sample of bacteria and fungi, respectively. These effective tags were then clustered into 29909 bacterial and 16952 fungal OTUs for taxonomic annotation, with an average of 830 bacterial and 470 fungal OTUs per sample (Supplementary Tables S2, S3). The obtained OTUs were used to calculate the alpha diversity indices (Chao-1, Shannon, Simpson, and PD-whole-tree indices) and the beta diversity (changes in the structure) of the bacterial and fungal communities in different samples. A significant difference was observed in the alpha diversity indices of bacterial and fungal communities among the samples under different treatments (Figures 4A, B; Tukey-HSD, $p < 0.05$). The values of alpha diversity indices for bacterial communities under treatment T2 (T2-S) were significantly decreased as compared to other treatments (Figure 4A; Tukey-HSD, $p < 0.05$), while for fungal community values of alpha diversity indices were increased dramatically under treatment T2 (T2-S) than other treatments (Figure 4B; Tukey-HSD, $p < 0.05$). PCoA based on Bray–Curti's dissimilarity matrix and PERMANOVA (Adonis) demonstrated a significant difference in the structure of bacterial and fungal communities under different treatments. The first two components of PCoA explained 77.10% (PERMANOVA, $p = 0.001$ and $R^2 = 0.8259$) and 60.74% (PERMANOVA, $p = 0.001$ and $R^2 = 0.7257$) of the variation in the structure of the bacterial and fungal communities, respectively under different treatments (Figures 4C, D; Supplementary Table S4). First, we generated Upset plots to show the shared and unique bacterial and fungal OTUs among samples (roots and stems) under different treatments (Supplementary Figures S2A–

TABLE 3 Control effect of *Luteibacter pinisoli* DP2-30 fermentation broth on incidence of pine wilt disease.

Treatments	Disease severity index (%)					Control effect %
	9d	18d	27d	36d	45d	
T1	15.63 ± 1.23a	34.38 ± 2.52a	59.38 ± 3.51a	84.37 ± 2.92a	100.00 ± 0.00a	—–
T2	0.00 ± 0.00b	0.00 ± 0.00b	12.50 ± 1.24b	21.86 ± 1.94b	37.50 ± 2.24b	62.50 ± 1.79a
CK	0.00 ± 0.00b	0.00 ± 0.00b	0.00 ± 0.00c	0.00 ± 0.00c	0.00 ± 0.00c	—–

Here: T1; sdH_2O + PWN, T2; *L. pinisoli* DP2-30 fermentation broth + PWN, and CK; sdH_2O. Data are present as mean ± SD of three biological replicates. Lowercase letters in each column show significant differences among treatments according to Duncans's test at $p < 0.05$.

C). The flower Venn diagram also revealed 303 bacterial and 92 fungal shared OTUs among the samples (roots and stems) under the different treatments. Further OTUs analysis revealed that 397, 51, 73, 130, 88, and 13 bacterial and 68, 22, 66, 150, 20, and 158 fungal OTUs were presented as unique OTUs in CK-R, T1-R, T2-R, CK-S, T1-S, and T2-S, respectively (Figures 4E, F). These results suggested that the variations in the diversity and structure of the bacterial and fungal communities might be due to these common and shared OTUs.

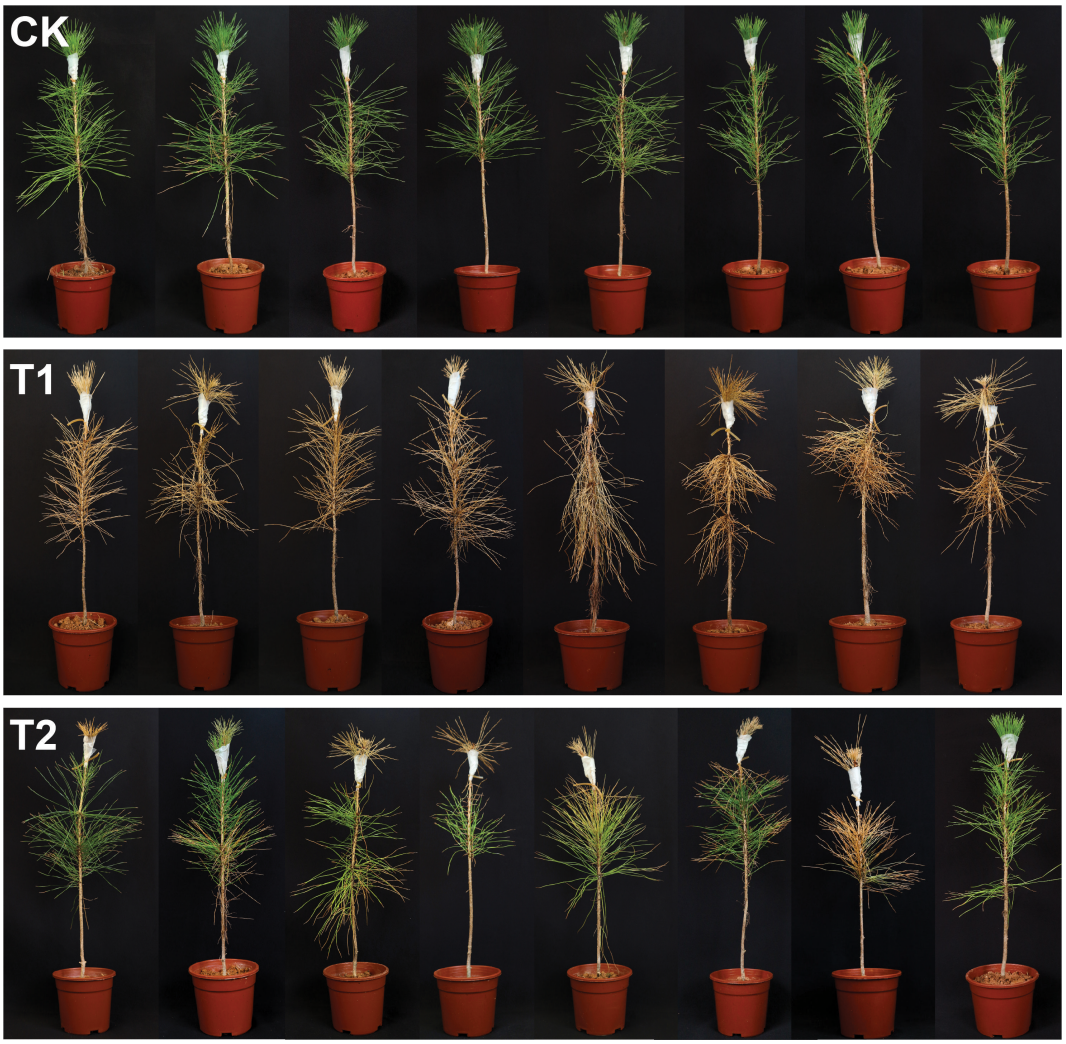

FIGURE 3
Biocontrol potential of *Luteibacter pinisoli* DP2-30 fermentation broth against pine wilt disease in a greenhouse assay. Here: CK; application of sdH2O, T1; application of PWN, and T2; combined application of *L. pinisoli* DP2-30 fermentation broth + PWN. Different letters on the error bars represent significant differences among treatments according to Duncan's test at $p < 0.05$. Data related to the disease severity index (%) and control effect (%) are presented in Table 3.

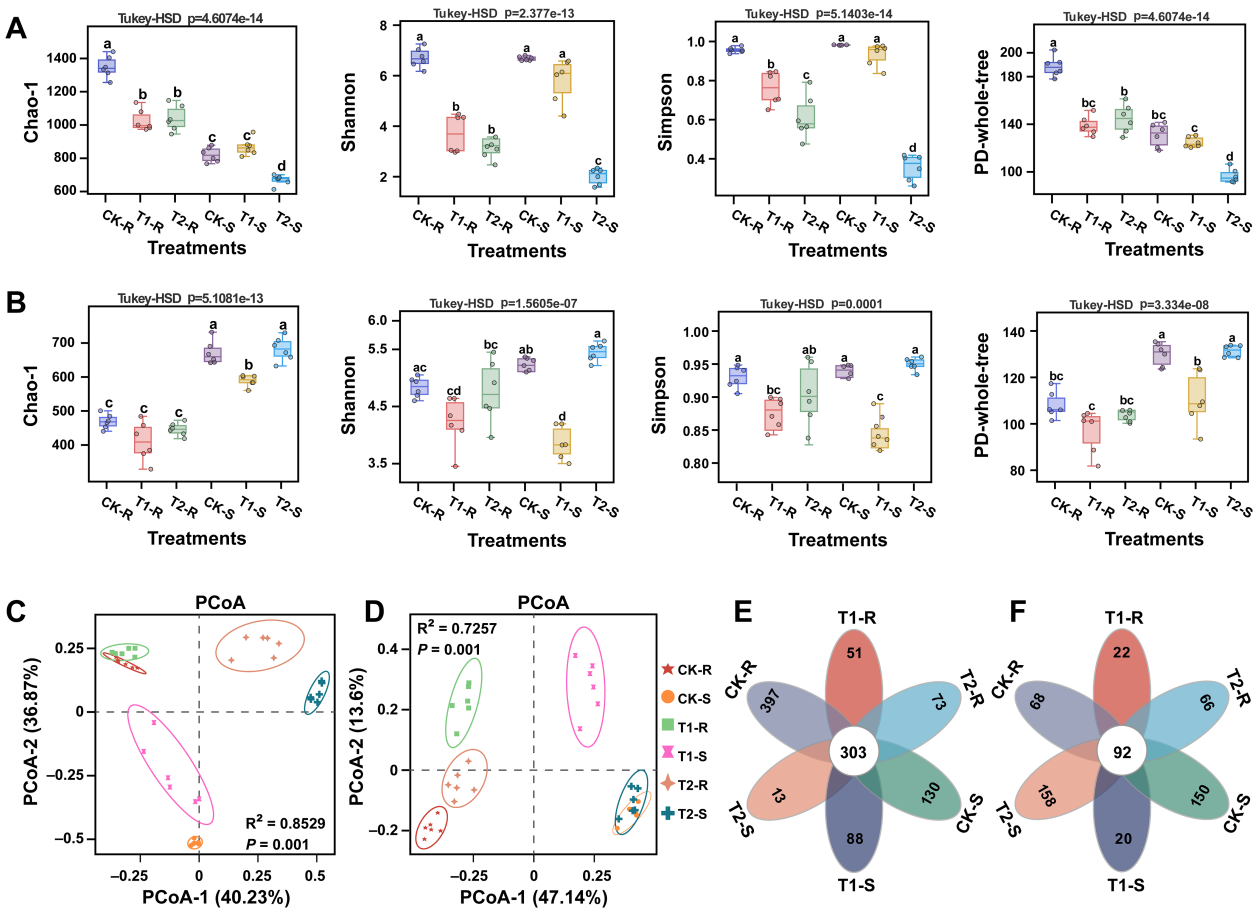

FIGURE 4
Diversity and structure of root and stem-associated microbial communities under different treatments. Alpha diversity metrics of bacterial **(A)** and fungal **(B)** communities under different treatments. Principal coordinate analysis (PCoA) based on Bray-Curtis dissimilarity metrics and permutational multivariate analysis of variance (PERMANOVA) showing the distance in the bacterial **(C)** and fungal **(D)** communities between the treatments. The flower Venn diagram displays the common and unique bacterial **(E)** and fungal **(F)** OTUs under different treatments. Here, CK; application of water as control, T1; application of PWNs, and T2; combined application of PWNs + *L. pinisoli* DP2-30. R, root; S, stem. Different letters on the error bars indicate significant differences among treatments according to the Tukey-HSD test $p < 0.05$.

3.7 Variations in the microbial community composition under different treatments

Analysis of the microbial community composition across different treatments revealed significant variations in the relative abundances of major bacterial and fungal communities at the phylum, class, and family levels in the samples (root and stem) (ANOVA, p-adjusted < 0.0001; Figures 5, 6). We detected the top 10 bacterial and fungal phyla in the samples (root and stem) under different treatments and their average relative abundance (RA) in each sample is shown by taxon bar plots (Figures 5A, B). Bacterial phylum, such as Proteobacteria, Actinobacteriota, Chloroflexi, and Acidobacteriota and fungal phylum, including Ascomycota and Basidiomycota were the dominant microbial phyla in all the samples with an average RA > 1% across the treatments. Phylum Proteobacteria and Actinobacteriota accounted for 81.63% and 11.45% of the host total bacteriome, respectively (Figure 5A), and the phylum Ascomycota and Basidiomycota described 86.38% and 12.82% of host total fungal communities, respectively (Figure 5B). Further box plots were constructed to observe the overall variations in microbial community compositions of the most abundant bacterial and fungal phyla among the treatments. Phylum Proteobacteria was present in significantly high RA in T1-R, T2-R, and T2-S compared to CK-R, CK-S, and T1-S (Tukey-HSD, $p < 0.05$). The RA of phyla Actinobacteriota, Chloroflexi, and Armatimonadota was significantly higher in CK-S, and Acidobacteriota was the dominated bacterial phyla in CK-R and T1-S than other treatments (Tukey-HSD, $p < 0.05$; Figure 5C). In the fungal communities, the RA of phylum Ascomycota varied significantly among treatments ($p < 0.05$) and was present in significantly high RA in T1-R, T1-S, and T2-S samples compared to others CK-R, T2-R, and CK-S. The RA of phylum Basidiomycota was substantially higher in T2-R than others, and phylum Mortierellomycota was present in significantly higher RA in CK-R than others (Tukey-HSD, $p < 0.05$; Figure 5D).

At the class and family levels, the taxonomic distribution patterns of bacterial and fungal communities became more apparent (Tukey-HSD, $p < 0.05$; Figure 6). The RA of the top 10 most abundant bacterial and fungal communities at class and family levels are shown by bubble plots (Figures 6A–D). Among the bacterial communities,

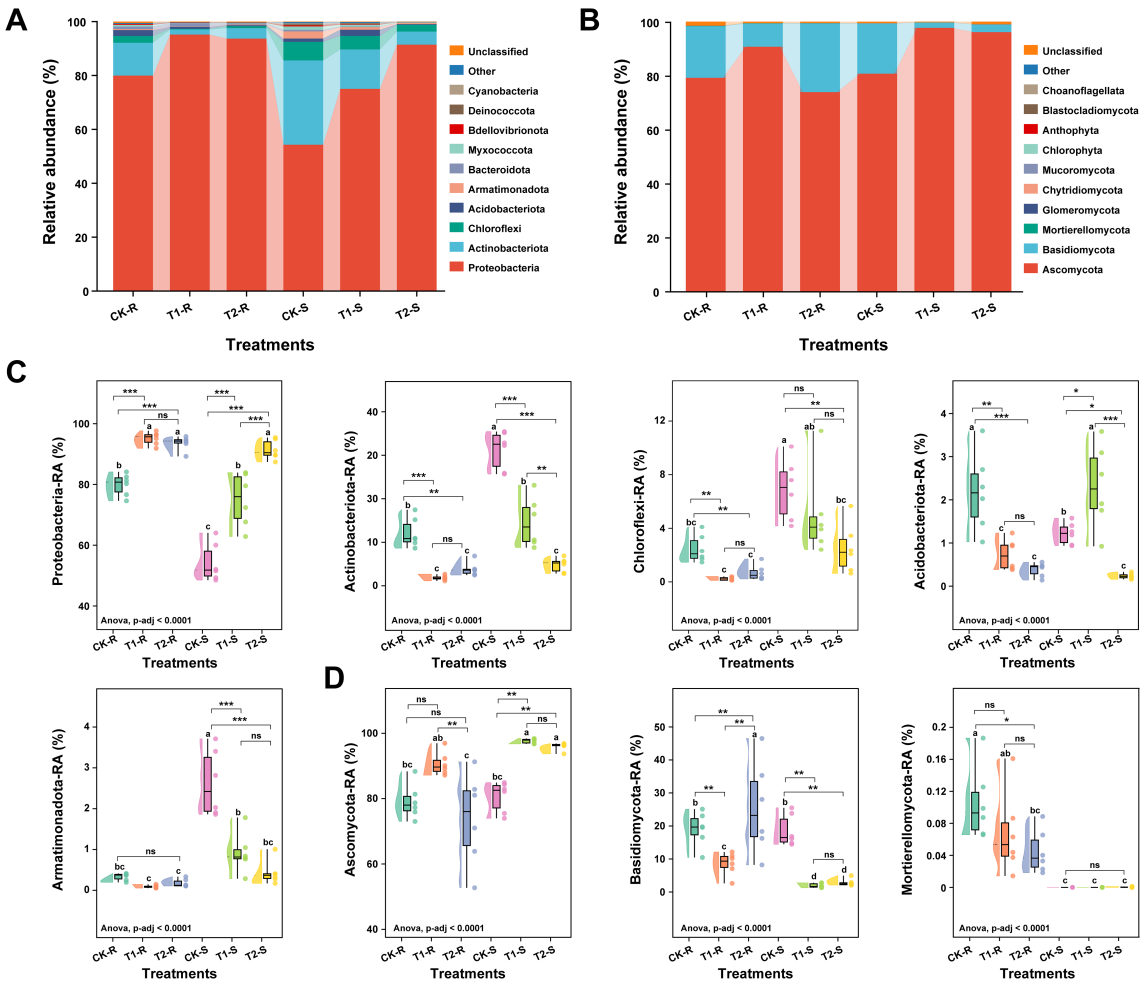

FIGURE 5
Relative abundance of the most abundant bacterial and fungal communities at the phylum level. Stacked bar graphs showing the variations in the relative abundance (average, n=6) of the top 10 bacterial **(A)** and fungal **(B)** phyla under different treatments. Box plots displaying the significant differences in the relative abundance most dominant bacterial **(C)** and fungal **(D)** under different treatments. Here, CK; application of water as control, T1; application of PWNs, and T2; combined application of PWNs + *L. pinisoli* DP2-30. R, root; S, stem. Different letters on the box plots show significant differences among treatments according to the Tukey-HSD test at $p < 0.05$. According to Tukey-HSD, asterisks indicate statistically significant differences at $*p < 0.05$, $**p < 0.001$, and $***p < 0.001$. ns, non significant.

Gammaproteobacteria and Alphaproteobacteria were the highly abundant classes, and Rhodanobacteraceae and Burkholderiaceae were the most abundant families in all samples across the treatments. The class Gammaproteobacteria was present in significantly high RA in T1-R, T2-R, and T2-S as compared to other samples and class Alphaproteobacteria was significantly dominated in CK-S than in the other samples (Tukey-HSD, $p < 0.05$; Figure 6E). The RA of the family Rhodanobacteraceae increased considerably in T2-S followed by T2-R compared with CK-R, CK-S, T1-R, and T1-S, and the family Burkholderiaceae was present at a high RA in T1-R than in the other samples (Tukey-HSD, $p < 0.05$; Figure 6F). Among the fungal community's classes, Sordariomycetes and Dothideomycetes and the families Nectriaceae and Diaporthaceae were present at high RA in all samples among the treatments. The class Sordariomycetes had significantly higher RA in T1-S than in the other samples, and Sordariomycetes exhibited in significantly greater RA in CK-S and T2-S than in the other samples under different treatments. The family Nectriaceae was more dominant in the T1-R sample than other samples, and the family Diaporthaceae was more abundant in the T1-S sample than in the other samples across the treatments (Tukey-HSD, $p < 0.05$; Figures 6G, H). Analysis of the bacterial community composition at the family level revealed that the application of biocontrol agent *L. pinisoli* DP2-30 significantly increased the RA of the family Rhodanobacteraceae in the roots and stems (T2-R and T2-S) of pine seedlings, as *L. pinisoli* belongs to the family Rhodanobacteraceae.

3.8 Intra-kingdom microbial co-occurrence network analysis of pine plants under different treatments

To further explore the impact of different treatments on the host microbiome, we assessed the intra-kingdom co-occurrence patterns of the bacterial and fungal communities in the different components (root and stem) of the host plants (Figures 7, 8). For bacterial

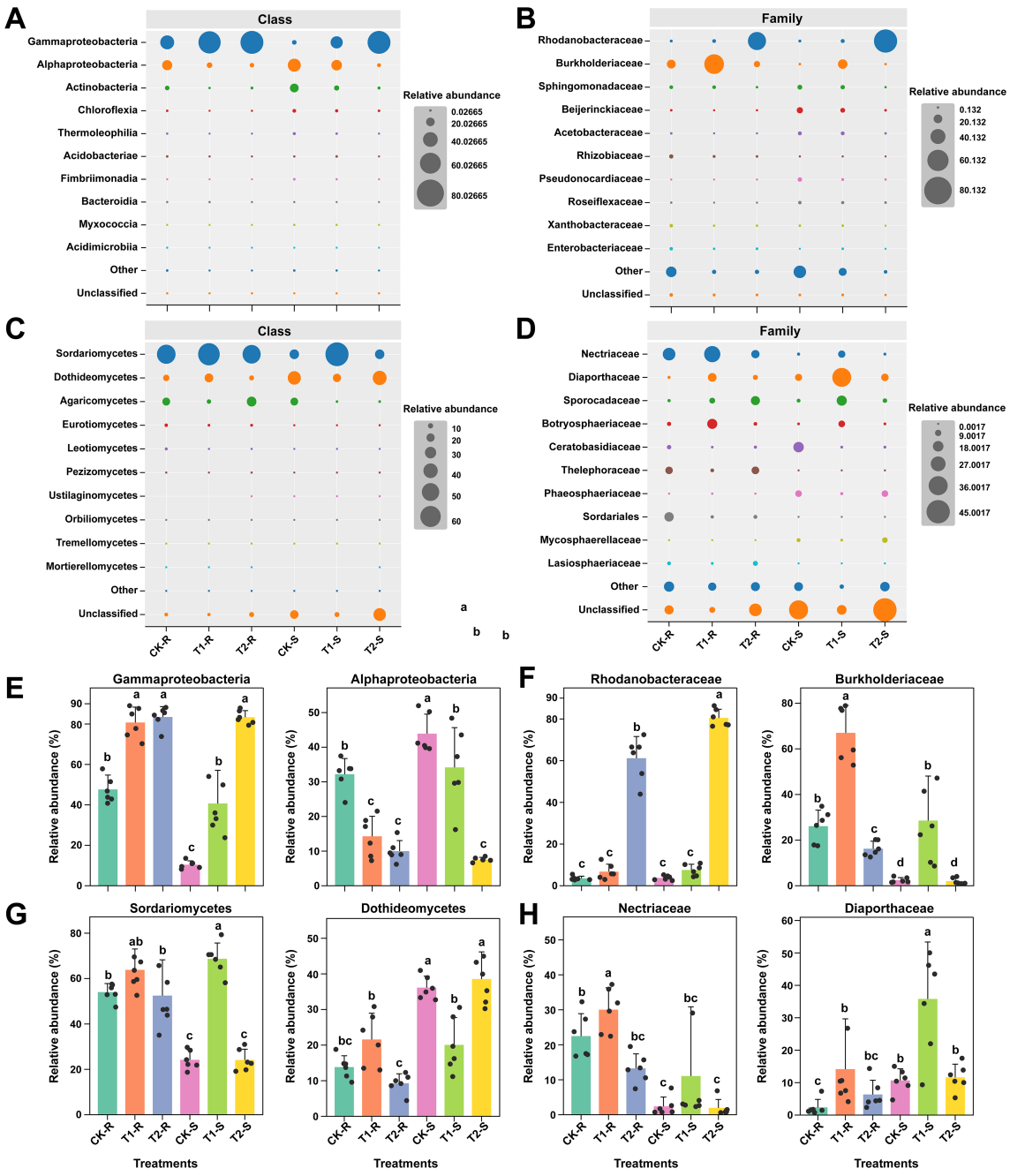

FIGURE 6
Variations in the relative abundance of microbial communities at the class and family levels under different treatments. Bubble plots illustrating the relative abundance (%) of the most abundant bacterial classes and families **(A, B)** and fungal classes and families **(C, D)** across the treatments. Bar plots showing the significant differences in the relative abundance of dominant bacterial classes and families **(E, F)** and fungal classes and families **(G, H)**. Here, CK; application of water as control, T1; application of PWNs, and T2; combined application of PWNs + *L. pinisoli* DP2-30. R, root; S, stem. Different letters on the error bars indicate the significant differences among treatments according to the Tukey-HSD test at $p < 0.05$.

communities, the control group (CK) exhibited a complex co-occurrence network; however, the complexity of the bacterial co-occurrence network was reduced significantly from the root to stem in CK and T2 than in T1, in which the network complexity increased (Figure 7). For fungal communities treatment T2 showed a more complex co-occurrence network as compared to CK and T1, and network complexity increased from the root to stem (Figure 8). The modularity of all networks was calculated to be >0.4, which suggests a modular network structure of bacterial and fungal communities (Figures 7, 8). The bacterial co-occurrence network of CK-R and T1-S was divided into 3 modules, which showed a more complex network with a maximum number of nodes (CK-R; 541, T1-S; 307), edges (CK-R; 9444, T1-S; 3557), and average degree (CK-R; 34.913, T1-S; 23.173). In contrast, the networks of T1-R (nodes; 264, edges; 2719, and average degree; 20.598), T2-R (nodes; 297, edges; 3401, and average degree; 22.902),

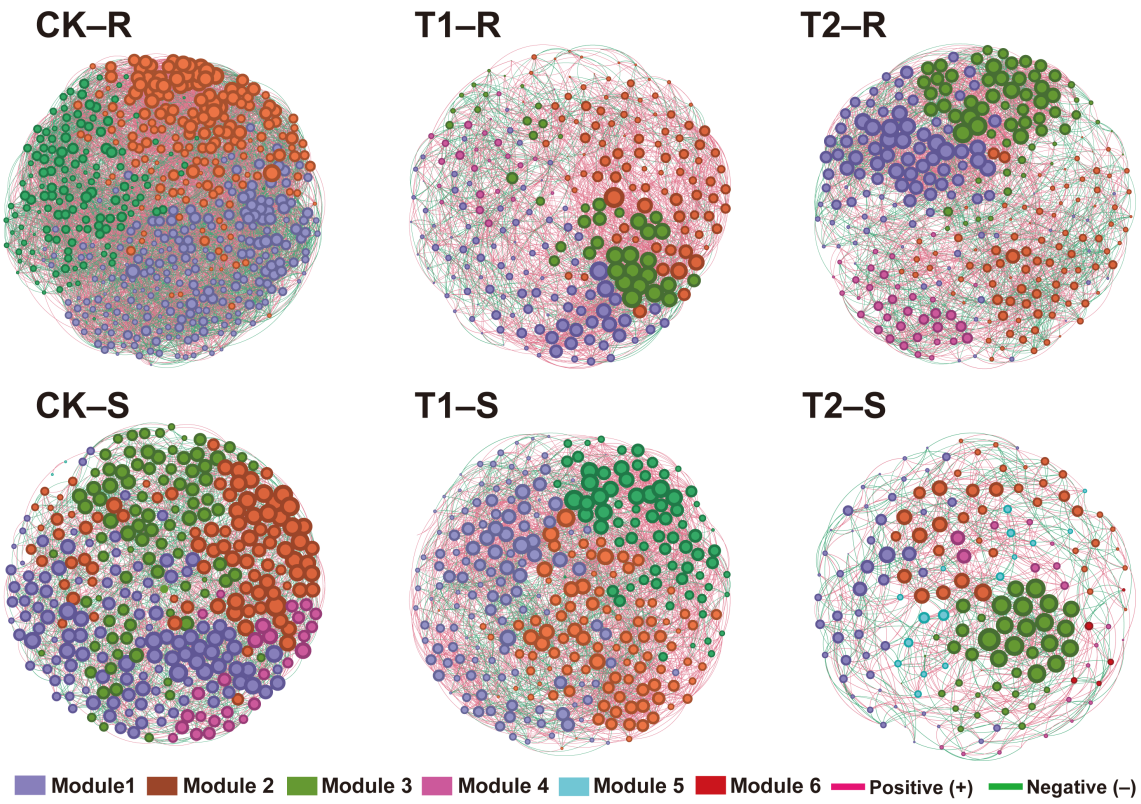

Treatment	Node	Edges	Positive (+)	Negative (−)	Average degree	Average path length	Network diameter	Average clustering coefficient	Modularity	Network modules
CK-R	541	9444	5784	3660	34.913	2.245	3	0.481	0.433	3
T1-R	264	2719	2043	676	20.598	2.336	5	0.498	0.405	4
T2-R	297	3401	2311	1090	22.902	2.351	4	0.532	0.492	4
CK-S	331	3453	1802	1641	20.864	2.379	4	0.486	0.482	5
T1-S	307	3557	2670	887	23.173	2.306	5	0.487	0.437	3
T2-S	181	1081	652	429	11.945	2.581	5	0.501	0.519	6

FIGURE 7
Intra-kingdom (bacteria-bacteria) co-occurrence network analysis under different treatments. The topological characteristics of the co-occurrence network within each compartment niche are listed in the table. Red and green lines in the networks represent the significant positive and negative relationships among bacterial communities (Spearman's correlation, $p < 0.05$). Network analysis was performed at the OTU level by excluding the relative abundance < 0.01 ($p < 0.05$ and correlation coefficient > 0.7). Here, CK; application of water as a control, T1; application of PWNs, and T2; combined application of PWNs + *L. pinisoli* DP2-30. R, root; S, stem.

CK-S (nodes; 331, edges; 3453, and average degree; 20.864), and T2-S (nodes; 181, edges; 1081, and average degree; 11.945) were divided into 4, 4, 5, and 6 modules, respectively which demonstrated a decrease in the network complexity. The number of nodes decreased in CK and T2 from the root to stem but increased in T1 from the root to stem. A higher number of positive edges were observed in T1-S (2670) than in CK-S (1802) and T2-S (652), which increased in the order T1-S > CK-S > T2-S (Figure 7). In contrast, the complexity of the fungal co-occurrence network was increased from root to stem under different treatments. A highly complex microbial co-occurrence network was observed for fungal communities in T2-S S (nodes; 260, edges; 2163, average degree; 16.431, and module; 4) and CK-S (nodes; 243, edges; 1821, average degree; 14.987, and module; 4). In comparison, the networks of CK-R (nodes; 165, edges; 855, average degree; 10.363), T1-R (nodes; 148, edges; 794, average degree; 10.730), T2-R (nodes; 162, edges; 880, average degree; 10.864), and T1-S (nodes; 164, edges; 873, average degree; 10.646) were divided into 5 modules, which showed less complexity in co-occurrence network. In the stem, the number of positive edges decreased from T2-S (1104) to CK-S (1034) to T1-R (525), while in root, the number of positive edges decreased in order CK-R (455) < T1-R (562) < T2-R (578) (Figure 8). These results suggest that the application of *L. pinisoli* DP2-30 significantly reduced the positive correlation between the PWN and bacterial communities, which resulted in low disease development. The decrease in complexity of the T2 bacterial co-occurrence network might be due to the strong colonization *L. pinisoli* DP2-30 ability in the host plant, as it significantly enhances

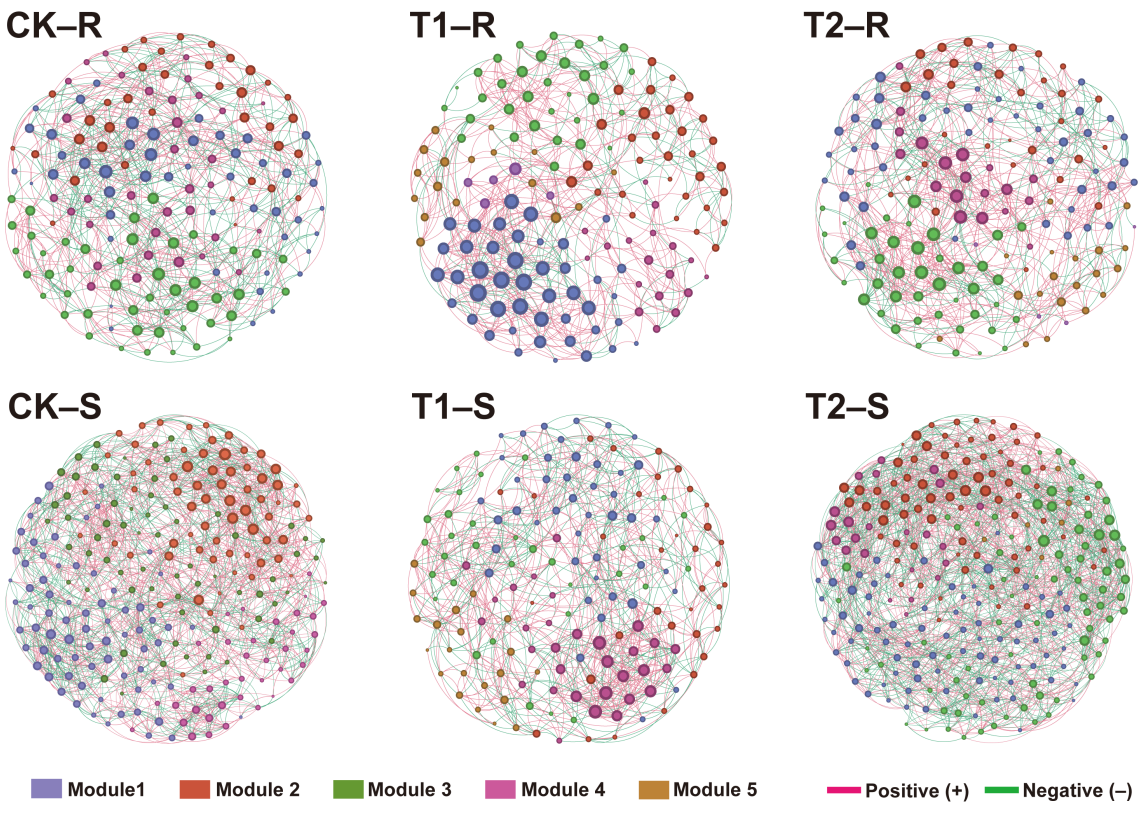

Treatment	Node	Edges	Positive (+)	Negative (−)	Average degree	Average path length	Network diameter	Average clustering coefficient	Modularity	Network modules
CK-R	165	855	455	400	10.363	2.670	3	0.464	0.524	5
T1-R	148	794	562	232	10.730	2.675	5	0.515	0.543	5
T2-R	162	880	578	302	10.864	2.608	4	0.484	0.509	5
CK-S	243	1821	1034	787	14.987	2.543	4	0.488	0.501	4
T1-S	164	873	525	348	10.646	2.643	5	0.484	0.523	5
T2-S	260	2136	1104	1032	16.431	2.416	5	0.459	0.447	4

FIGURE 8
Intra-kingdom (fungi-fungi) co-occurrence network analysis under different treatments. The topological characteristics of the co-occurrence network within each compartment niche are listed in the table. Red and green lines in the networks represent the significant positive and negative relationships among bacterial communities (Spearman's correlation, $p < 0.05$). Network analysis was performed at the OTU level by excluding the relative abundance < 0.01 ($p < 0.05$ and correlation coefficient > 0.7). Here, CK; application of water as control, T1; application of PWNs, and T2; combined application of PWNs + *L. pinisoli* DP2-30. R, root; S, stem.

the RA of Rhodanobacteraceae family in the host plant. Moreover, *L. pinisoli* DP2-30 make the fungal network more complex by recruiting more fungal communities that plays an important role in disease suppression.

4 Discussion

Pine wilt disease (PWD) caused by *B. xylophilus* is a severe threat to pine forests around the globe, affecting forest ecology, natural biodiversity and habitats, climate, and timber production (Pires et al., 2022). Thus, it is necessary to manage the spread of this devastating disease through the application of environmentally friendly management measures to save the natural ecosystem and biodiversity. Pine trees provide habitats for diverse microbial communities, which are crucial for plant health and can suppress by combating pests, thus showing great potential for use as biocontrol agents (Liu et al., 2019b; Kamaruzzaman et al., 2024). This study aimed to explore the potential of *Luteibacter pinisoli* DP2-30 in mitigating PWD via direct antagonism and manipulation of the host microbiome.

Sixty-three bacterial strains were isolated from the rhizosphere soil of healthy *P. massoniana*. Among these strains, DP2-30 showed the highest nematicidal activity against pine wood nematode (PWN), with a C-M-R of 92.08% after 48 hours of treatment. The strain DP2-30 has been identified as *L. pinisoli* through morphological, biochemical, and molecular studies and is identical to a strain previously isolated from the rhizosphere of *P.*

koraiensis (Akter and Huq, 2018). The significant nematicidal activity observed in this study is consistent with earlier research that has shown the potential of bacterial BCAs in effectively managing PPNs in different plants (Liu et al., 2019b; Sun et al., 2022; Ali et al., 2023). To further investigate the biocontrol ability of *L. pinisoli* DP2-30 against PWN, we modified the fermentation conditions to maximize the nematicidal activity of strain DP2-30 fermentation filtrates (FFs) against PWN. The results of optimizing fermentation conditions for *L. pinisoli* DP2-30 showed that the highest level of nematicidal activity (>95%) of FFs was obtained after 3 days of incubation at a temperature of 28°C, a pH of 7, and a shaking speed of 180 rpm. These findings emphasize the importance of improving fermentation conditions to increase the biocontrol efficiency of BCAs against phytopathogens. Many other studies have highlighted the impact of these environmental factors on enhancing the biocontrol potential of BCAs (Spadaro et al., 2010; Liu et al., 2017; Kamaruzzaman et al., 2024).

The application of *L. pinisoli* DP2-30 fermentation broth (FB) and FFs resulted in 49.38% and 43.05% decreases in the hatching of PWN eggs, respectively, compared to the bacterium itself (5.01%) and control. We assumed that this inhibitory effect was mainly due to the metabolites produced during fermentation rather than the bacteria (DP2-30). The substantial suppression of PWN egg hatching by fermentation metabolites indicates that secondary metabolites play an important role in inhibiting nematode growth; a similar phenomenon has also been reported in other rhizobacteria, such as *Lysinimonas* sp. M4. The nematicidal compounds 2-coumaranone and cyclo-(Pro-Phe) produced by *Lysinimonas* sp. M4 significantly inhibited the PWN egg hatching by 59.92% and 50.77%, respectively, at 0.1 mM concentration (Sun et al., 2022). The root drenching of *L. pinisoli* DP2-30 FB substantially mitigated the PWD in pine seedlings treated with PWN with a control effect of 62.50%. The achieved control effect of *L. pinisoli* DP2-30 against PWD might be due to the direct nematicidal activity of *L. pinisoli* DP2-30 on PWN and the induction of host resistance against PWN infestation. Previous studies have demonstrated that beneficial rhizobacteria trigger plant defense against PWN and effectively reduce PWD, supporting our findings (Han et al., 2021; Sun et al., 2022; Li et al., 2023a). Although not the main goal, the growth-promoting effect of *L. pinisoli* DP2-30 on tobacco seedlings indicates its potential as a strong plant growth-promoting rhizobacterium (PGPR). The ability of *L. pinisoli* DP2-30 to serve as both a BCA and PGPR is highly advantageous for sustainable agriculture and forestry management. This finding is in accordance with previous reports that some rhizobacteria can play a dual role, promoting plant growth and providing protection from diseases simultaneously (Ayaz et al., 2021; Han et al., 2021; Ahmed et al., 2022b).

Analysis of the microbiome in *L. pinisoli* DP2-30 treated and untreated pine seedlings revealed notable differences in the proportions of bacterial and fungal communities in the roots and stems of the pine plants. These results align with prior findings that the use of BCAs alters the relative abundance of microbial communities (Han et al., 2021; Dai et al., 2023). The prominent bacterial phyla identified in all samples were Proteobacteria, Actinobacteriota, Chloroflexi, and Acidobacteriota, whereas the dominant fungal phyla were Ascomycota and Basidiomycota, corroborating the findings of previous researchers (Ponpandian et al., 2019; Zhang et al., 2022c). The proportion of Proteobacteria was notably greater in T1-R, T2-R, and T2-S samples than in the other samples, but Actinobacteriota, Chloroflexi, and Armatimonadota were more dominant in the CK-S samples. The Ascomycota phylum of fungi showed substantial variation across treatments and exhibited high relative abundance in the T1-R and T2-S samples. The results indicate a notable change in the microbial community composition in the treated samples compared with the untreated ones. This change involves an increase in the abundance of beneficial bacteria and fungi, specifically Proteobacteria and Ascomycota, which are recognized for their ability to decrease diseases (Mendes et al., 2011). *Lysobacter* and *Trichoderma*, which belong to Proteobacteria and Ascomycota, respectively, are widely used to prevent plants from diseases by producing specific secondary metabolites and volatile organic compounds (VOCs) (Khan et al., 2020; Liu et al., 2022; Dai et al., 2023; Xing et al., 2023). The notable increase in the proportion of Basidiomycota in the treated roots (T2-R) of the fungal communities is worth mentioning. This phylum includes various members, such as *Arbuscular mycorrhizae* and *Ectomycorrhizae*, which are known to establish mycorrhizal associations with plant roots. These associations improve the absorption of nutrients by plants and offer protection against pathogens (Sharma et al., 2014; Tripathi et al., 2017).

At the class and family levels Gammaproteobacteria and Alphaproteobacteria were the predominant bacterial classes and Rhodanobacteraceae and Burkholderiaceae were the most dominant families. The prevalence of Rhodanobacteraceae was notably higher in T2-S and T2-R samples than in the other samples, suggesting successful colonization by *L. pinisoli* DP2-30. Interestingly, the application of *L. pinisoli* DP2-30 (T2) resulted in a decrease in bacterial alpha diversity but an increase in fungal alpha diversity compared to control (CK) and PWN-infected (T1) plants. The reduction in bacterial alpha diversity in T2 might have occurred because the application of DP2-30 increased the relative abundance of Rhodanobacteraceae (to which *L. pinisoli* belongs). This finding is in accordance with the study of Li and colleagues, who reported that *B. subtilis* L1-21 enhanced its diversity in the host by successful colonization (Li et al., 2023b) and also Proteobacteria is fasting growing bacteria that prefers to grow under nutrient-rich conditions and healthy environment (Fierer et al., 2007). The PCoA and PERMANOVA results revealed distinct microbial community structures between the treated and control samples. These findings suggest BCAs may create a hostile environment for pathogens by promoting the abundance of beneficial microbes. Ahmed et al. (2022b) and Zhang et al (Zhang et al., 2022a), reported similar results, demonstrating that the application of beneficial microorganisms can effectively modify the structure of microbial communities, lowering the prevalence of decreases in agricultural crops. Sordariomycetes and Dothideomycetes were the most dominant classes in the fungal communities, whereas the most prevalent families were Nectriaceae and Diaporthaceae. Application of biocontrol strain DP2-30 significantly reduced the RA of family Diaporthaceae in the root and stem of pine seedling combine treated

with PWN+DP2-30. Studies showed that members (*Diaporthe ampelina*, *D. eres*, and *D. foeniculina*) of Diaporthaceae found be pathogenic to grapevines and causes Phomopsis cane and leaf spot diseases (Fedele et al., 2024). This also suggest the antifungal potential of strain DP2-30, however future study is suggested to prove this claim.

Intra-kingdom co-occurrence network analysis revealed that the complexity of bacterial co-occurrence networks was reduced from the root to stem in both control (CK) and *L. pinisoli* DP2-30-treated (T2) plants compared to PWN-infected (T1) plants, where network complexity increased. These findings suggests that the populations of the bacterial ecological network increased following PWN infection. The decrease in bacterial network complexity in T2 plants suggests a more stable and resilient microbial community structure, which could help suppress diseases. Conversely, complexity of fungal co-occurrence network was increased from root to stem in the pine seedlings under different treatments (CK, T1, and T2), with the most complex network was observed in the stem of pine seedlings under treatment T2 (T2-S). This increased complexity in fungal networks may be due to the recruitment of more fungal communities that play a role in disease suppression. Previous studies revealed that bacterial communities nodes or network complexity significantly increased in the phyllosphere and rhizosphere of pine plants after PWN infection (Deng et al., 2021).

5 Conclusions

In summary, we conclude that *Luteibacter pinisoli* DP2-30 isolated from the rhizosphere soil of *P. massoniana* demonstrated solid nematicidal activity against PWN, with a corrected mortality rate of 92.08%, and could be used as a promising biocontrol agent for the management of pine wilt disease. The optimization of fermentation conditions (pH 7 and 3 days of incubation at 28°C and 180 rpm) plays a role in maximizing (>95%) the nematicidal activity of strain DP2-30 against PWN. *L. pinisoli* DP2-30 fermentation broth and filtrates significantly inhibited PWN egg hatching, indicating that the metabolites produced during fermentation play a critical role in nematode suppression. Additionally, the application of *L. pinisoli* DP2-30 fermentation broth significantly reduced PWD severity in pine seedlings, with a control effect of 62.50%, demonstrating its efficacy in mitigating disease symptoms and improving plant health. A key finding of this study is the ability of *L. pinisoli* DP2-30 to reshape the pine seedling microbiome, potentially enhancing disease resistance. Intra-kingdom co-occurrence network analysis revealed reduced complexity in the bacterial networks but increased complexity in the fungal networks of the pine seedling combine treated with PWN+DP2-30, indicate a shift towards a community composition dominated by taxa that can effectively compete against PWN (Figure 9). This study also revealed the plant growth-promoting potential of *L. pinisoli* DP2-

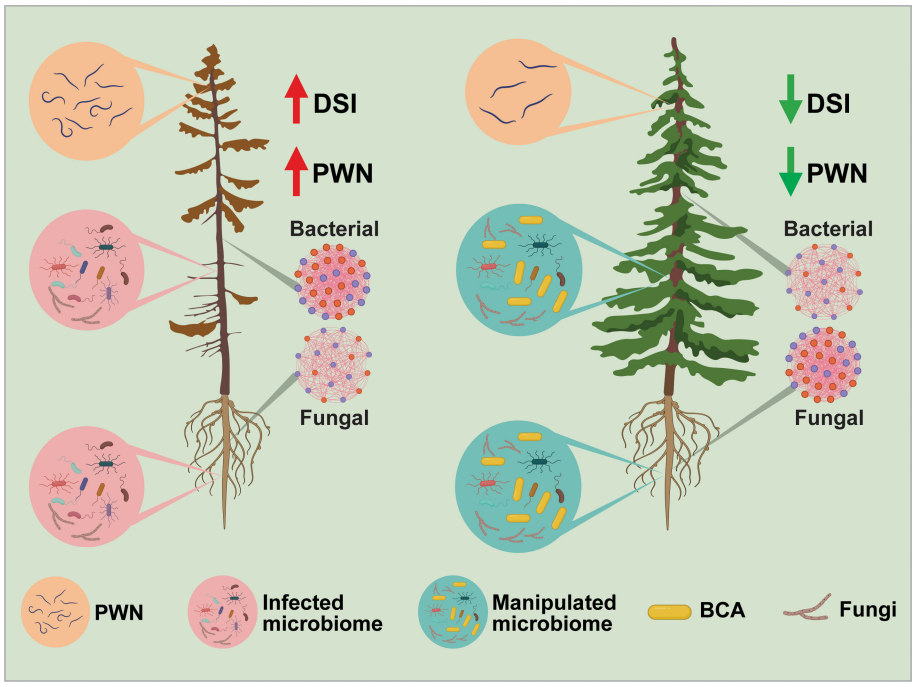

FIGURE 9
The concluding figure illustrates the effects of biocontrol agent (BCA) on the host microbiome and its role in reducing pine wilt disease. *Luteibacter pinisoli* DP2-30 (BCA) altered the composition of the host microbiome, promoting the growth of beneficial microorganisms and increasing microbial diversity, resulting in reduced PWD severity and healthier pine trees. The left side displays the pine tree subjected to the PWN, exhibiting a reduced abundance of beneficial microbes, a higher population of PWN, and higher disease incidence. The right side displays the pine tree treated with PWN +BCA, which showed an increase in beneficial microbes and an elevated microbial diversity, thus resulting in a healthier pine tree. The microbial networks depict the alterations in the diversity and interactions of microbial populations. The bacterial networks in the BCA-treated plants exhibited decreased complexity, whereas the fungal networks showed increased complexity, indicating a more stable and resilient microbial community structure.

30, as it significantly enhanced the growth of tobacco seedlings. Overall, this study demonstrates the dual functionality of *L. pinisoli* DP2-30 as both a biocontrol agent and a plant growth-promoting bacterium, offering a sustainable and environmentally friendly strategy for managing PWD. However, future research will be carried out to optimize BCA formulations, clarify the specific underlying mechanisms of host-microbe interactions, and conduct field trials to validate the biocontrol efficacy of *L. pinisoli* DP2-30 under natural conditions.

Data availability statement

The datasets presented in this study can be found in online repositories. The names of the repository/repositories and accession number(s) can be found below: https://www.ncbi.nlm.nih.gov/genbank/, PRJNA1132778.

Author contributions

WA: Conceptualization, Data curation, Formal analysis, Funding acquisition, Investigation, Methodology, Project administration, Resources, Software, Supervision, Validation, Visualization, Writing – original draft, Writing – review & editing. WY: Data curation, Formal analysis, Investigation, Methodology, Writing – original draft. JP: Data curation, Investigation, Methodology, Writing – original draft. SL: Data curation, Investigation, Methodology, Writing – original draft. WJ: Data curation, Formal analysis, Methodology, Writing – original draft. SZ: Data curation, Formal analysis, Methodology, Writing – original draft. FW: Data curation, Investigation, Methodology, Writing – original draft. ZL: Data curation, Formal analysis, Methodology, Writing – original draft. MM: Data curation, Formal analysis, Writing – original draft, Writing – review & editing. XW: Conceptualization, Funding acquisition, Methodology, Resources, Supervision, Writing – review & editing.

Funding

The author(s) declare that financial support was received for the research, authorship, and/or publication of this article. This work was financially supported by the National Natural Science Foundation of China (No. 32350410423), Guangdong Provincial Key Laboratory Development Fund (GDKL202330), the Key Research and Development Project of the National Forestry and Grassland Administration (GLM[2021]68), the Guangdong Forestry Ecological Restoration Project (GDF2023-245), the South China Agricultural University Undergraduate Innovative Training Project (2024105641197 and 2024105641176), and the Researchers Supporting Project (RSPD2025R758) King Saud University, Riyadh, Saudi Arabia.

Conflict of interest

The authors declare that the research was conducted in the absence of any commercial or financial relationships that could be construed as a potential conflict of interest.

Generative AI statement

The author(s) declare that no Generative AI was used in the creation of this manuscript.

Publisher's note

All claims expressed in this article are solely those of the authors and do not necessarily represent those of their affiliated organizations, or those of the publisher, the editors and the reviewers. Any product that may be evaluated in this article, or claim that may be made by its manufacturer, is not guaranteed or endorsed by the publisher.

Supplementary material

The Supplementary Material for this article can be found online at: https://www.frontiersin.org/articles/10.3389/fpls.2025.1515506/full#supplementary-material

References

Ahmed, W., Dai, Z., Liu, Q., Munir, S., Yang, J., Karunarathna, S. C., et al. (2022a). Microbial cross-talk: dissecting the core microbiota associated with flue-cured tobacco (*Nicotiana tabacum*) plants under healthy and diseased state. *Front. Microbiol.* 13, 845310. doi: 10.3389/fmicb.2022.845310

Ahmed, W., Dai, Z., Zhang, J., Li, S., Ahmed, A., Munir, S., et al. (2022b). Plant-microbe interaction: mining the impact of native *Bacillus amyloliquefaciens* WS-10 on tobacco bacterial wilt disease and rhizosphere microbial communities. *Microbiol. Spectr.* 10, e01471–e01422. doi: 10.1128/spectrum.01471-22

Ahmed, W., Zhou, G., Yang, J., Munir, S., Ahmed, A., Liu, Q., et al. (2022c). *Bacillus amyloliquefaciens* WS-10 as a potential plant growth-promoter and biocontrol agent for bacterial wilt disease of flue-cured tobacco. *Egyptian J. Biol. Pest Control* 32, 25. doi: 10.1186/s41938-022-00527-5

Akbulut, S., and Stamps, W. (2012). Insect vectors of the pinewood nematode: a review of the biology and ecology of *Monochamus* species. *For. Pathol.* 42, 89–99. doi: 10.1111/j.1439-0329.2011.00733.x

Akter, S., and Huq, M. A. (2018). *Luteibacter pinisoli* sp. nov., a casein degrading bacterium isolated from rhizospheric soil of *Pinus koraiensis*. *Arch. Microbiol.* 200, 1017–1023. doi: 10.1007/s00203-018-1515-1

Ali, Q., Yu, C., Wang, Y., Sheng, T., Zhao, X., Wu, X., et al. (2023). High killing rate of nematode and promotion of rice growth by synthetic volatiles from *Bacillus* strains due

to enhanced oxidative stress response. *Physiologia Plantarum* 175, e13868. doi: 10.1111/ppl.v175.1

Ayaz, M., Ali, Q., Farzand, A., Khan, A. R., Ling, H., and Gao, X. (2021). Nematicidal volatiles from *Bacillus atrophaeus* GBSC56 promote growth and stimulate induced systemic resistance in tomato against *Meloidogyne incognita*. *Int. J. Mol. Sci.* 22, 5049. doi: 10.3390/ijms22095049

Bolyen, E., Rideout, J. R., Dillon, M. R., Bokulich, N. A., Abnet, C. C., Al-Ghalith, G. A., et al. (2019). Reproducible, interactive, scalable and extensible microbiome data science using QIIME 2. *Nat. Biotechnol.* 37, 852–857. doi: 10.1038/s41587-019-0209-9

Bonifácio, L. F., Sousa, E., Naves, P., Inacio, M. L., Henriques, J., Mota, M., et al. (2014). Efficacy of sulfuryl fluoride against the pinewood nematode, *Bursaphelenchus xylophilus* (Nematoda: Aphelenchidae), in *Pinus pinaster* boards. *Pest Manage. Sci.* 70, 6–13. doi: 10.1002/ps.2013.70.issue-1

Chen, Y., Yan, E., Jiang, J., Zhang, G., and Mo, D. (2023). An efficient approach to monitoring pine wilt disease severity based on random sampling plots and UAV imagery. *Ecol. Indic.* 156, 111215. doi: 10.1016/j.ecolind.2023.111215

Chu, H., Wang, C., Li, Z., Wang, H., Xiao, Y., Chen, J., et al. (2019). The dark septate endophytes and ectomycorrhizal fungi effect on *Pinus tabulaeformis* Carr. seedling growth and their potential effects to pine wilt disease resistance. *Forests* 10, 140. doi: 10.3390/f10020140

Dai, Z., Ahmed, W., Yang, J., Yao, X., Zhang, J., Wei, L., et al. (2023). Seed coat treatment by plant-growth-promoting rhizobacteria *Lysobacter antibioticus* 13–6 enhances maize yield and changes rhizosphere bacterial communities. *Biol. Fertility Soils* 59, 317–331. doi: 10.1007/s00374-023-01703-x

Deng, J., Yu, D., Zhou, W., Zhou, L., and Zhu, W. (2021). Variations of phyllosphere and rhizosphere microbial communities of *Pinus koraiensis* infected by *Bursaphelenchus xylophilus*. *Microbial Ecol.* 84, 285–301. doi: 10.21203/rs.3.rs-443731/v1

Diyapoglu, A., Chang, T.-H., Chang, P.-F. L., Yen, J.-H., Chiang, H.-I., and Meng, M. (2022). Fumigant Activity of Bacterial Volatile Organic Compounds against the Nematodes *Caenorhabditis elegans* and *Meloidogyne incognita*. *Molecules* 27, 4714. doi: 10.3390/molecules27154714

Dou, G., and Yan, D.-H. (2022). Research progress on biocontrol of pine wilt disease by microorganisms. *Forests* 13, 1047. doi: 10.3390/f13071047

Edgar, R. C. (2013). UPARSE: highly accurate OTU sequences from microbial amplicon reads. *Nat. Methods* 10, 996–998. doi: 10.1038/nmeth.2604

Edgar, R. C., Haas, B. J., Clemente, J. C., Quince, C., and Knight, R. (2011). UCHIME improves sensitivity and speed of chimera detection. *Bioinformatics* 27, 2194–2200. doi: 10.1093/bioinformatics/btr381

Estorninho, M., Chozas, S., Mendes, A., Colwell, F., Abrantes, I., Fonseca, L., et al. (2022). Differential impact of the pinewood nematode on *Pinus* species under drought conditions. *Front. Plant Sci.* 13, 841707. doi: 10.3389/fpls.2022.841707

Fedele, G., Armengol, J., Caffi, T., Languasco, L., Latinovic, N., Latinovic, J., et al. (2024). Diaporthe foeniculina and D. eres, in addition to D. ampelina, may cause Phomopsis cane and leaf spot disease in grapevine. *Front. Plant Sci.* 15, 1446663. doi: 10.3389/fpls.2024.1446663

Fierer, N., Bradford, M. A., and Jackson, R. B. (2007). Toward an ecological classification of soil bacteria. *Ecology* 88, 1354–1364. doi: 10.1890/05-1839

Han, G., Mannaa, M., Kim, N., Jeon, H. W., Jung, H., Lee, H.-H., et al. (2021). Response of pine rhizosphere microbiota to foliar treatment with resistance-inducing bacteria against pine wilt disease. *Microorganisms* 9, 688. doi: 10.3390/microorganisms9040688

He, R., Cui, X., Ying, Y., Qu, L.-J., Wang, R.-Z., and Zhang, Y. (2020). Screening and identification of *Beauveria bassiana* strains for biocontrol of *Monochamus alternatusadults* (Coleoptera: Cerambycidae). *Scientia Silvae Sinicae* 56 (10), 129–134.

Jones, J. T., Haegeman, A., Danchin, E. G., Gaur, H. S., Helder, J., Jones, M. G., et al. (2013). Top 10 plant-parasitic nematodes in molecular plant pathology. *Mol. Plant Pathol.* 14, 946–961. doi: 10.1111/mpp.2013.14.issue-9

Kamaruzzaman, M., Zheng, L., Zhou, S., Ye, W., Yuan, Y., Qi, Q., et al. (2024). Evaluation of the novel endophytic fungus Chaetomium ascotrichoides 1-24-2 from *Pinus massoniana* as a biocontrol agent against pine wilt disease caused by *Bursaphelenchus xylophilus*. *Pest Manage. Sci.* 80 (10), 4924–4940. doi: 10.1002/ps.v80.10

Kamata, N. (2008). "Integrated pest management of pine wilt disease in Japan: tactics and strategies," in *Pine wilt disease* (Tokyo: Springer Japan), 304–322.

Kang, M. K., Kim, M. H., Liu, M. J., Jin, C. Z., Park, S. H., Lee, J. M., et al. (2021). Nematicidal activity of teleocidin B4 isolated from *Streptomyces* sp. against pine wood nematode, *Bursaphelenchus xylophilus*. *Pest Manage. Sci.* 77, 1607–1615. doi: 10.1002/ps.v77.4

Khan, R., Najeeb, S., Hussain, S., Xie, B., and Li, Y. (2020). Bioactive secondary metabolites from *Trichoderma* spp. against phytopathogenic fungi. *Microorganisms* 8, 817. doi: 10.3390/microorganisms8060817

Kim, J. C., Baek, S., Park, S. E., Kim, S., Lee, M. R., Jo, M., et al. (2020b). Colonization of *Metarhizium anisopliae* on the surface of pine tree logs: A promising biocontrol strategy for the Japanese pine sawyer, *Monochamus alternatus*. *Fungal Biol.* 124, 125–134. doi: 10.1016/j.funbio.2019.12.006

Kim, N., Jeon, H. W., Mannaa, M., Jeong, S. I., Kim, J., Kim, J., et al. (2019). Induction of resistance against pine wilt disease caused by *Bursaphelenchus xylophilus* using selected pine endophytic bacteria. *Plant Pathol.* 68, 434–444. doi: 10.1111/ppa.2019.68.issue-3

Kim, B.-N., Kim, J. H., Ahn, J.-Y., Kim, S., Cho, B.-K., Kim, Y.-H., et al. (2020a). A short review of the pine wood nematode, *Bursaphelenchus xylophilus*. *Toxicol. Environ. Health Sci.* 12, 297–304. doi: 10.1007/s13530-020-00068-0

Kwon, T.-S., Song, M.-Y., Shin, S.-C., and Park, Y.-S. (2005). Effects of aerial insecticide sprays on ant communities to control pine wilt disease in Korean pine forests. *Appl. entomology zoology* 40, 563–574. doi: 10.1303/aez.2005.563

Li, Y., He, P., Ahmed, A., Liu, Y., Ahmed, W., Wu, Y., et al. (2023b). Endophyte mediated restoration of citrus microbiome and modulation of host defense genes against Candidatus *Liberibacter asiaticus*. doi: 10.21203/rs.3.rs-2863977/v1

Li, D., Li, Y., Wang, X., Zhang, W., Wen, X., Liu, Z., et al. (2023a). Engineered pine endophytic *Bacillus toyonensis* with nematocidal and colonization abilities for pine wilt disease control. *Front. Microbiol.* 14, 1240984. doi: 10.3389/fmicb.2023.1240984

Li, L., Tan, J., and Chen, F. (2018). *Bacillus pumilus* strain LYMC-3 shows nematicidal activity against *Bursaphelenchus xylophilus* via the production of a guanidine compound. *Biocontrol Sci. Technol.* 28, 1128–1139. doi: 10.1080/09583157.2018.1514587

Li, J., Wang, C., Liang, W., and Liu, S. (2021). Rhizosphere microbiome: The emerging barrier in plant-pathogen interactions. *Front. Microbiol.* 12, 772420. doi: 10.3389/fmicb.2021.772420

Liu, M. J., Hwang, B. S., Jin, C. Z., Li, W. J., Park, D. J., Seo, S. T., et al. (2019a). Screening, isolation and evaluation of a nematicidal compound from actinomycetes against the pine wood nematode, *Bursaphelenchus xylophilus*. *Pest Manage. Sci.* 75, 1585–1593. doi: 10.1002/ps.2019.75.issue-6

Liu, J., Li, G., and Sui, Y. (2017). Optimization of culture medium enhances viable biomass production and biocontrol efficacy of the antagonistic yeast, Candida diversa. *Front. Microbiol.* 8, 2021. doi: 10.3389/fmicb.2017.02021

Liu, Y., Ponpandian, L. N., Kim, H., Jeon, J., Hwang, B. S., Lee, S. K., et al. (2019b). Distribution and diversity of bacterial endophytes from four *Pinus* species and their efficacy as biocontrol agents for devastating pine wood nematodes. *Sci. Rep.* 9, 12461. doi: 10.1038/s41598-019-48739-4

Liu, Q., Yang, J., Ahmed, W., Wan, X., Wei, L., and Ji, G. (2022). Exploiting the antibacterial mechanism of phenazine substances from *Lysobacter antibioticus* 13-6 against Xanthomonas oryzae pv. oryzicola. *J. Microbiol.* 60, 496–510. doi: 10.1007/s12275-022-1542-0

Maehara, N., He, X., and Shimazu, M. (2007). Maturation feeding and transmission of *Bursaphelenchus xylophilus* (Nematoda: Parasitaphelenchidae) by *Monochamus alternatus* (Coleoptera: Cerambycidae) inoculated with Beauveria bassiana (Deuteromycotina: Hyphomycetes). *J. economic entomology* 100, 49–53. doi: 10.1093/jee/100.1.49

Mannaa, M., and Seo, Y.-S. (2023). Improved and simplified method for aseptic isolation of nematodes and nematode-endosymbiotic bacteria from pine seedlings. *MethodsX* 11, 102421. doi: 10.1016/j.mex.2023.102421

Mendes, R., Kruijt, M., De Bruijn, I., Dekkers, E., van der Voort, M., Schneider, J. H., et al. (2011). Deciphering the rhizosphere microbiome for disease-suppressive bacteria. *Science* 332, 1097–1100. doi: 10.1126/science.1203980

Modesto, I., Mendes, A., Carrasquinho, I., and Miguel, C. M. (2022). Molecular defense response of pine trees (*Pinus* spp.) to the parasitic nematode *Bursaphelenchus xylophilus*. *Cells* 11, 3208. doi: 10.3390/cells11203208

Moo-Koh, F. A., Cristóbal-Alejo, J., Andrés, M. F., Martín, J., Reyes, F., Tun-Suárez, J. M., et al. (2022). *In vitro* assessment of organic and residual fractions of nematicidal culture filtrates from thirteen tropical *Trichoderma* strains and metabolic profiles of most-active. *J. Fungi* 8, 82. doi: 10.3390/jof8010082

Nascimento, F. X., Vicente, C. S., Barbosa, P., Espada, M., Glick, B. R., Mota, M., et al. (2013). Evidence for the involvement of ACC deaminase from *Pseudomonas putida* UW4 in the biocontrol of pine wilt disease caused by *Bursaphelenchus xylophilus*. *BioControl* 58, 427–433. doi: 10.1007/s10526-012-9500-0

Nilsson, R. H., Larsson, K.-H., Taylor, A. F. S., Bengtsson-Palme, J., Jeppesen, T. S., Schigel, D., et al. (2019). The UNITE database for molecular identification of fungi: handling dark taxa and parallel taxonomic classifications. *Nucleic Acids Res.* 47, D259–D264. doi: 10.1093/nar/gky1022

Oksanen, J., Blanchet, F. G., Kindt, R., Legendre, P., Minchin, P. R., O'hara, R. B., et al. (2013). Package 'vegan'. *Community ecology package* 2 (9), 1–295.

Pimentel, C. S., and Ayres, M. P. (2018). Latitudinal patterns in temperature-dependent growth rates of a forest pathogen. *J. thermal Biol.* 72, 39–43. doi: 10.1016/j.jtherbio.2017.11.018

Pires, D., Vicente, C. S., Inácio, M. L., and Mota, M. (2022). The Potential of *Esteya* spp. for the Biocontrol of the Pinewood Nematode, *Bursaphelenchus xylophilus*. *Microorganisms* 10, 168. doi: 10.3390/microorganisms10010168

Ponpandian, L. N., Rim, S. O., Shanmugam, G., Jeon, J., Park, Y.-H., Lee, S.-K., et al. (2019). Phylogenetic characterization of bacterial endophytes from four *Pinus* species and their nematicidal activity against the pine wood nematode. *Sci. Rep.* 9, 12457. doi: 10.1038/s41598-019-48745-6

Puttawong, K., Beesa, N., Kasem, S., Jindapunnapat, K., Chinnasri, B., and Sasnarukkit, A. (2024). Potential of *Bacillus* spp. against root-knot nematode, *Meloidogyne enterolobii* parasitizing chili (*Capsicum annuum* L.). *Crop Prot.* 184, 106780. doi: 10.1016/j.cropro.2024.106780

Raaijmakers, J. M. (2014). "The minimal rhizosphere microbiome," in *Principles of plant-microbe interactions: microbes for sustainable agriculture*, ed. B. Lugtenberg (Cham: Springer International Publishing), 411–417.

Rodrigues, A. M., Carrasquinho, I., and António, C. (2021). Primary metabolite adjustments associated with pinewood nematode resistance in *Pinus pinaster*. *Front. Plant Sci.* 12, 777681. doi: 10.3389/fpls.2021.777681

Sharma, Y., Watpade, S., and Thakur, J. (2014). Role of mycorrhizae: a component of integrated disease management strategies. *J. Mycology Plant Pathol.* 44, 12–20.

Sheikh, T. M. M., Zhou, D., Ali, H., Hussain, S., Wang, N., Chen, S., et al. (2023). Volatile organic compounds emitted by the biocontrol agent *Pythium oligandrum* contribute to ginger plant growth and disease resistance. *Microbiol. Spectr.* 11, e01510–e01523. doi: 10.1128/spectrum.01510-23

Shoyeb, M., Kanis Fatema, M., Sarkar, A., Rahman, A., and Rahman, S. (2020). Efficient regeneration of tobacco (*Nicotiana tabacum* L.) plantlets from cotyledon, hypocotyl and leaf explants: an excellent model plant for gene function analysis. *Curr. J. Appl. Sci. Tech* 39, 1–9. doi: 10.9734/cjast/2020/v39i3230996

Spadaro, D., Ciavorella, A., Dianpeng, Z., Garibaldi, A., and Gullino, M. L. (2010). Effect of culture media and pH on the biomass production and biocontrol efficacy of a *Metschnikowia pulcherrima* strain to be used as a biofungicide for postharvest disease control. *Can. J. Microbiol.* 56, 128–137. doi: 10.1139/W09-117

Sun, Y., Wang, C., Du, G., Deng, W., Yang, H., Li, R., et al. (2022). Two nematicidal compounds from *Lysinimonas* M4 against the pine wood nematode, *Bursaphelenchus xylophilus*. *Forests* 13, 1191. doi: 10.3390/f13081191

Taheri, E., Tarighi, S., and Taheri, P. (2023). An endophytic bacterium with biocontrol activity against important wheat pathogens. *Biol. Control* 183, 105243. doi: 10.1016/j.biocontrol.2023.105243

Takai, K., Suzuki, T., and Kawazu, K. (2003). Development and preventative effect against pine wilt disease of a novel liquid formulation of emamectin benzoate. *Pest Manage. Science: formerly Pesticide Sci.* 59, 365–370. doi: 10.1002/ps.651

Tamura, K., Stecher, G., and Kumar, S. (2021). MEGA11: molecular evolutionary genetics analysis version 11. *Mol. Biol. Evol.* 38, 3022–3027. doi: 10.1093/molbev/msab120

Toju, H., Tanabe, A. S., Yamamoto, S., and Sato, H. (2012). High-coverage ITS primers for the DNA-based identification of ascomycetes and basidiomycetes in environmental samples. *PloS One* 7, e40863. doi: 10.1371/journal.pone.0040863

Tripathi, S., Mishra, S. K., and Varma, A. (2017). Mycorrhizal fungi as control agents against plant pathogens. *Mycorrhiza-Nutrient Uptake Biocontrol Ecorestoration*. Springer, Cham. 161–178. doi: 10.1007/978-3-319-68867-1_8

Trivedi, P., Leach, J. E., Tringe, S. G., Sa, T., and Singh, B. K. (2020). Plant–microbiome interactions: from community assembly to plant health. *Nat. Rev. Microbiol.* 18, 607–621. doi: 10.1038/s41579-020-0412-1

Wang, Q., Garrity, G. M., Tiedje, J. M., and Cole, J. R. (2007). Naive Bayesian classifier for rapid assignment of rRNA sequences into the new bacterial taxonomy. *Appl. Environ. Microbiol.* 73, 5261–5267. doi: 10.1128/AEM.00062-07

Wang, C. Y., Yin, C., Fang, Z. M., Wang, Z., Wang, Y. B., Xue, J. J., et al. (2018). Using the nematophagous fungus *Esteya vermicola* to control the disastrous pine wilt disease. *Biocontrol Sci. Technol.* 28, 268–277. doi: 10.1080/09583157.2018.1441369

Xing, M., Zhao, J., Zhang, J., Wu, Y., Khan, R. A. A., Li, X., et al. (2023). 6-Pentyl-2 H-pyran-2-one from *Trichoderma erinaceum* Is Fungicidal against Litchi Downy Blight Pathogen *Peronophythora litchii* and Preservation of Litchi. *J. Agric. Food Chem.* 71, 19488–19500. doi: 10.1021/acs.jafc.3c03872

Yin, C., Wang, Y., Zhang, Y.-A., Wang, H., Duan, B., Tao, R., et al. (2020). Hypothesized mechanism of biocontrol against pine wilt disease by the nematophagous fungus *Esteya vermicola*. *Eur. J. Plant Pathol.* 156, 811–818. doi: 10.1007/s10658-019-01930-9

Zhang, J., Ahmed, W., Dai, Z., Zhou, X., He, Z., Wei, L., et al. (2022a). Microbial consortia: An engineering tool to suppress clubroot of Chinese cabbage by changing the rhizosphere bacterial community composition. *Biology* 11, 918. doi: 10.3390/biology11060918

Zhang, J., He, Y., Ahmed, W., Wan, X., Wei, L., and Ji, G. (2022b). First report of bacterial angular leaf spot of strawberry caused by *Xanthomonas fragariae* in yunnan province, China. *Plant Dis.* 106, 1978. doi: 10.1094/PDIS-12-21-2648-PDN

Zhang, W., Wang, X., Li, Y., Wei, P., Sun, N., Wen, X., et al. (2022c). Differences between microbial communities of *Pinus* species having differing level of resistance to the pine wood nematode. *Microbial Ecol.* 84, 1245–1255. doi: 10.1007/s00248-021-01907-4

Zhang, J., Zhou, X., Zhang, Y., Dai, Z., He, Z., Qiu, Y., et al. (2024). Pre-soil fumigation with ammonium bicarbonate and lime modulates the rhizosphere microbiome to mitigate clubroot disease in Chinese cabbage. *Front. Microbiol.* 15, 1376579. doi: 10.3389/fmicb.2024.1376579

frontiers | Frontiers in Plant Science

TYPE Original Research
PUBLISHED 13 March 2025
DOI 10.3389/fpls.2025.1554992

Check for updates

OPEN ACCESS

EDITED BY
Yasser Nehela,
Tanta University, Egypt

REVIEWED BY
Manoj Choudhary,
University of Florida, United States
Tetiana Kalachova,
Academy of Sciences of the Czech Republic, Czechia
Esraa Halawa,
Cairo University, Egypt
Shanwen Ding,
Guangdong Academy of Agricultural Sciences, China

*CORRESPONDENCE
Ke Yi
yik0113@hngytobacco.com
Tianbo Liu
tianboliu@126.com
Wu Chen
wuchen77@hunau.edu.cn

†These authors have contributed equally to this work

RECEIVED 03 January 2025
ACCEPTED 19 February 2025
PUBLISHED 13 March 2025

CITATION
He H, Yi K, Yang L, Jing Y, Kang L, Gao Z, Xiang D, Tan G, Wang Y, Liu Q, Xie L, Jiang S, Liu T and Chen W (2025) Development of a lytic Ralstonia phage cocktail and evaluation of its control efficacy against tobacco bacterial wilt. *Front. Plant Sci.* 16:1554992. doi: 10.3389/fpls.2025.1554992

COPYRIGHT
© 2025 He, Yi, Yang, Jing, Kang, Gao, Xiang, Tan, Wang, Liu, Xie, Jiang, Liu and Chen. This is an open-access article distributed under the terms of the Creative Commons Attribution License (CC BY). The use, distribution or reproduction in other forums is permitted, provided the original author(s) and the copyright owner(s) are credited and that the original publication in this journal is cited, in accordance with accepted academic practice. No use, distribution or reproduction is permitted which does not comply with these terms.

Development of a lytic Ralstonia phage cocktail and evaluation of its control efficacy against tobacco bacterial wilt

Haoxin He[1†], Ke Yi[2*†], Lei Yang[2], Yongfeng Jing[2], Lifu Kang[2], Zhihao Gao[2], Dong Xiang[2], Ge Tan[2], Yunsheng Wang[1], Qian Liu[1], Lin Xie[1], Shiya Jiang[1], Tianbo Liu[3*] and Wu Chen[1*]

[1]College of Plant Protection, Hunan Agricultural University, Changsha, China, [2]Tobacco Leaf Raw Material Procurement Center, China Tobacco Hunan Industrial Co., Ltd, Changsha, China, [3]Plant Protection Research Center, Hunan Tobacco Science Research Institute, Changsha, China

Introduction: Bacterial wilt (BW) caused by *Ralstonia pseudosolanacearum* is a devastating soil-borne disease. Bacteriophages are important biocontrol resources that rapidly and specifically lyse host bacteria, showing good application potential in agricultural production.

Methods: This study isolated nine phages (YL1–YL9) and, using host range and pot experiments, identified two broader host range phages (YL1 and YL4) and two higher control efficacy phages (YL2 and YL3), which were combined to obtain five cocktails (BPC-1–BPC-5).

Results: Pot experiments showed that BPC-1 (YL3 and YL4) had the highest control efficacy (99.25%). Biological characterization revealed that these four phages had substantial thermal stability and pH tolerance. Whole genome sequencing and analysis showed that YL1, YL2, YL3, and YL4 belonged to the genus *Gervaisevirus*. AlphaFold 3 predictions of tail fiber protein II structures showed that YL1 differed significantly from the other phages. Amino acid sequence alignment revealed that the ORF66 (YL1) "tip domain" of contained a higher proportion of aromatic and positively charged amino acids. However, the surface of the ORF69 (YL4) "tip domain" exhibited more positively charged residues than ORF66 (YL2) and ORF70 (YL3). These characteristics are hypothesized to confer a broader host range to YL1 and YL4.

Discussion: This study demonstrates that phages assembling a broad host range and high control efficacy have better biocontrol potential, providing high-quality resources for the biological control of BW.

KEYWORDS

bacteria wilt (BW), *Ralstonia solanacearum*, Ralstonia phage, phage cocktail, control efficacy, tail fiber

1 Introduction

The *Ralstonia solanacearum* species complex (RSSC) infects over 200 plant species from 50 families, including tobacco, tomato, potato, and pepper, causing typical bacterial wilt (BW) (Denny, 2000; Lowe-Power et al., 2020; Paudel et al., 2020). Surveys have shown that BW is the second most frequent plant disease globally, causing annual economic losses of about USD 1 billion (Mansfield et al., 2012; Elphinstone, 2005). RSSC has high variability and complex genetic diversity (Jiang et al., 2017). Based on its geographical origins and phylogenetic analysis, RSSC can be divided into three species: *R. pseudosolanacearum* (formerly Asian phylotype I and African phylotype III), *R. solanacearum* (formerly American phylotype II), and *R. syzygii* (formerly the Indonesian phylotype) (Paudel et al., 2020; Zhao et al., 2023).

Lytic Ralstonia phages that infect hosts have the following characteristics: fast infection, short lysis time, and high host specificity (Dion et al., 2020; Mushegian, 2020). They reduce the number of host bacteria in the environment in a short time, without causing harm to beneficial microorganisms in the environment, while simultaneously regulating rhizosphere microbial composition and function to collectively resist pathogen invasion. (Trivedi et al., 2020; Ji et al., 2021; Markwitz et al., 2022). Therefore, phage therapy is considered an effective method for BW control (Buttimer et al., 2017). Askora et al. (2017) isolated and purified Ralstonia phage ϕRSY1 from the soil, and root irrigation and stem injection with *R. solanacearum* M4S infected with ϕRSY1 (10^8 cell/mL) significantly reduced the incidence and disease index of tomato BW. Wang X et al. (2019) inoculated soil with Ralstonia phages (10^6 PFU/mL) and found that they significantly reduced the *R. solanacearum* population, with a control efficacy of 83.4% against tomato BW.

Due to the strong host specificity of phages, their application mostly follows the principle of "isolating phages from farm soil and returning them to the farm" (Díaz-Muñoz and Koskella, 2014; Ye et al., 2019). Studies have shown that the combination of multiple phages effectively inhibits resistance development in *R. solanacearum* and improves the control efficacy of BW (Wang et al., 2024). In current reports on phage cocktail applications, most Ralstonia phages used in these combinations belong to the class Caudoviricetes. Wei et al. (2017) screened phage P1 combinations capable of lysing the host within a short period based on lysis kinetics, resulting in a 20% reduction in BW incidence; Magar et al. (2022) utilized a combination of Ralstonia phages RpT1 and RpY2, which exhibit a broad host range, to significantly reduce BW incidence. Therefore, the biological characteristics of phages, such as host range and lysis kinetics, are critical criteria for formulating effective phage cocktails (Gill and Hyman, 2010; Villalpando-Aguilar et al., 2022; Tang et al., 2024).

To construct a phage cocktail with good control efficacy on tobacco BW in different areas of Xiangxi Tujia Zu and Miao Zu Autonomous Prefecture, Hunan Province, China, this study isolated *R. pseudosolanacearum* and its phages from tobacco fields with a high BW incidence in this region. After comparing the host range and single phage control efficacy, four phages were selected to construct a phage cocktail. Pot experiments showed that phage cocktails improved the control efficacy of BW. This study provides high-quality candidate resources for the biological control of BW.

2 Materials and methods

2.1 Isolation, purification, and identification of *R. pseudosolanacearum* and phages

Ralstonia pseudosolanacearum strains were isolated from tobacco plants with BW collected among towns in the Xiangxi Tujia Zu and Miao Zu Autonomous Prefecture (Xiangxi Prefecture), Hunan Province. *Ralstonia pseudosolanacearum* strains were obtained using the plate streaking method on nutrient broth (NB) medium (10 g tryptone, 3 g beef extract, 10 g glucose, and 5 g NaCl, 1000 mL ddH_2O) and identified using 16S rRNA gene sequencing and strain-specific PCR (759/760) (Wicker et al., 2007). Lytic phages were isolated from tobacco rhizosphere soil using the isolated *R. pseudosolanacearum* strains as hosts and employing the modified double-layer agar method, in which 1 g of soil was added to 10 mL of sterile water, vortexed, and centrifuged at 12,000 rpm for 10 min. The supernatant was filtered through a 0.22-μm bacterial filter (Millex, Tullagreen, Carrigtwohill, Co. Cork., Ireland). Equal volumes of NB medium and 0.3% host bacterial suspension (V/V) were added to the filtrate and co-cultured at 30°C for 12 h. The culture was centrifuged and filtered, and the filtrate was diluted 1000-fold with SM buffer (50 mM Tris-CL, pH=7.5, 100 mM NaCl, 10 mM $MgSO_4$, and 0.01% gelatin solution). The diluted solution was mixed with an equal volume of the *R. pseudosolanacearum* suspension (OD_{600} = 1.0), comprising the top layer of the plate, which was incubated at 37°C until plaques appeared. This process was repeated more than five times to complete phage purification (Kropinski et al., 2009).

2.2 Phage host range determination

Host range determination experiments were conducted using 38 *R. pseudosolanacearum* strains, among which 31 were isolated from tobacco (RStab-1 to RStab-31), 2 from peppers (RSpep-1, RSpep-2), 2 from potatoes (RSpot-1, RSpot-2), and 3 from peanuts (RSpea-1, RSpea-2, RSpea-3) (Supplementary Table S1). Each *R. pseudosolanacearum* strain was mixed with NB solid medium (0.2%, V/V) at 45°C and poured into plates. After the medium solidified, 5 μL of phage was added to the plate surface, spread evenly, and incubated overnight at 30°C. Plaque transparency was observed, and the host range was recorded. *Ralstonia pseudosolanacearum* strains with clear plaques were selected for subsequent pot inoculation experiments (Wang et al., 2022).

10.3389/fpls.2025.1554992

2.3 Pot experiments for the control of tobacco BW with phages

Yunyan 87 tobacco plants at the four-leaf stage were transplanted into a seedling substrate (Hunan Xianghui Agricultural Technology Development Co., Ltd., China). The pathogen used to inoculate tobacco was selected from the *R. pseudosolanacearum* strain, which was lysed using all nine phages in section 2.2. The pathogen was adjusted to OD_{600} = 0.1 with phosphate-buffered saline (PBS: 137 mM NaCl, 2.7 mM KCl, 10 mM Na_2HPO_4, and 1000 mL ddH_2O), and the phage titer was adjusted to 10^8 PFU/mL. Each plant was first inoculated with 10 mL of the *R. pseudosolanacearum* suspension (OD_{600} = 0.1), followed by 50 mL of the phage suspension. The experimental design comprised 12 individual tobacco plants per treatment with 3 experimental replicates, the temperature of the greenhouse was kept at 30°C throughout the experiment. The disease incidence was investigated and recorded for each plant at the early and peak stages of disease development. The disease index (DI) and control efficacy (CE) were calculated (Huang et al., 2024) as follows:

$$DI = 100 \times (1 \times n1 + 3 \times n3 + 5 \times n5 + 7 \times n7 + 9 \times n9)/(n \times 9) \quad (1)$$

$$CE = (C - T)/C \times 100\,\% \quad (2)$$

Where DI is the disease index; 1–9 refers to different disease classification levels; n1–n9 is the number of infected plants in each disease classification level; n is the number of plants investigated; CE is the control efficacy (T versus C); C is the disease index of the control group; and T is the disease index of the treatment group.

2.4 Construction and efficacy evaluation of the phage cocktail

Lytic Ralstonia phages were divided into two groups based on the host range and control efficacy. Two phages were selected from each group to construct five phage cocktails following the principle of 'broader host range + higher control efficacy': BPC-1 (YL3, YL4), BPC-2 (YL1, YL2, YL3, YL4), BPC-3 (YL1, YL3, YL4), BPC-4 (YL1, YL4), and BPC-5 (YL2, YL3). Adjust all phage titers to 1×10^8 PFU/mL using PBS buffer, then combine the phages in equal proportions according to the cocktail combination to ensure a consistent final titer of 1×10^8 PFU/mL in each cocktail. To simulate the infection of plants with different *R. pseudosolanacearum* strains under natural conditions (Genin and Denny, 2012), three virulent *R. pseudosolanacearum* strains (RStab-5, RStab-12, and RStab-19) were mixed for inoculation (Supplementary Figure S1). Pot experiments were conducted to evaluate the control efficacy of the five phage cocktails.

2.5 Biological characteristics and lysis curves

For the temperature tolerance experiments, 1 mL of phage culture with an initial phage titer of 1×10^9 PFU/mL was subjected to water bath treatment at different temperatures (30, 37, 50, 60, 70, 80, and 90°C) for 1 h and then cooled to room temperature. The plaques number were determined in the double-layer plate method to compare the phage titers after different temperature treatments. For the pH tolerance experiments, 10 µL of phage culture with an initial phage titer of 1×10^9 PFU/mL was added to 990 µL of SM buffer with different pH values (1.0, 2.0, 3.0, 4.0, 5.0, 6.0, 7.0, 8.0, 9.0, 10.0, 11.0, 12.0, and 13.0) and treated in a water bath at the optimal temperature for 1 h. The pH was monitored using pH test strips (JINLIDA, Tianjin Jinda Chemical Reagent Co., Ltd., China) after the experiment to verify the stability of acid–base conditions throughout the experimental process. Phage titers after different pH treatments were determined using the double-layer plate method. For optimal multiplicity of infection (MOI) determination, phages and host bacteria (0.3%, V/V) were used for inoculation and cultured overnight, and the host bacterial and phage concentrations were determined. They were then mixed at MOI = 10^3, 10^2, 10^1, 1, 10^{-1}, 10^{-2}, and 10^{-3} (Table 1) and incubated at the optimal temperature and pH for 6 h. The phage titers were determined at different ratios using the double-layer plate method (Huang et al., 2022; Tian et al., 2022). Equal proportions of the phage culture and host were added to 48-well plates at the optimal MOI and co-cultured at the optimal temperature for 12 h. The OD_{600} values of the co-culture were measured after 0–12 h using a microplate reader (TECAN spark, Tecan (Shanghai)Trading Co., Ltd., Shanghai) to plot the lysis curves (Wei et al., 2017).

2.6 Electron microscopy observation of phage morphology

Each phage culture (1×10^8 PFU/mL) was concentrated using a 100-kDa ultrafiltration tube (Millipore, Tullagreen, Carrigtwohill, Co. Cork., Ireland), and 20 µL of concentrated phage solution was dropped onto a copper grid and allowed to settle naturally for 15 min. The excess liquid was removed with filter paper, and 20 µL of 2% phosphotungstic acid was added and left for 5 min for staining. After drying, four phages were observed and photographed using a Hitachi transmission electron microscopy (HT7800, Hitachi America Ltd., Japan) (Ahmad et al., 2021).

2.7 Genome sequencing and assembly

Each phage suspension was concentrated using 100-kDa ultrafiltration tubes (Millipore, Tullagreen, Carrigtwohill, Co. Cork., Ireland). DNase I (1 µg/mL, TransGen Biotech, TransGen Biotech

TABLE 1 Phage MOI rationing.

MOI (Phage/Host)	10^{-3}	10^{-2}	10^{-1}	1	10^1	10^2	10^3
Phage (PFU/mL)	10^5	10^5	10^5	10^5	10^5	10^5	10^5
Host bacteria (CFU/mL)	10^8	10^7	10^6	10^5	10^4	10^3	10^2

Co., Ltd., Beijing) and RNase A (1 μg/mL, TransGen Biotech) were used to digest possible host nucleic acids in the suspensions and inactivated using water bath treatment at 75°C for 30 min. Phage genomes were extracted using a Virus DNA/RNA Extraction Kit (Beijing Tiangen DP-315). DNase I, RNase A, and EcoRI (New England Biolabs, Inc) were used to determine the nucleic acid type of the phages (Wilcox et al., 1996).

Whole genome sequencing was performed on the Illumina NovaSeq platform. The original sequencing data were quality controlled using FastQC and quality trimmed using Trimmomatic (Bolger et al., 2014). The A5-MiSeq and SPAdes *de novo* assembly methods were used to obtain complete phage genome sequences (Bankevich et al., 2012; Coil et al., 2015).

2.8 Comparative genomic analysis

GeneMarkS and RAST were used to predict the open reading frames (ORFs) in phage genomes (Besemer and Borodovsky, 2005; Aziz et al., 2008). For functional annotation, Diamond was used to compare the predicted protein sequences with the NCBI Non-Redundant (NR) database (Buchfink et al., 2015). Gene Ontology (GO) term annotation was performed using Blast2GO (Conesa et al., 2005).

Skani was used to calculate the average nucleotide identity (ANI) between phage genomes, and heat maps were generated to visualize genome similarities (Shaw and Yu, 2023). Phylogenetic analysis was performed using the Mashtree method based on Mash distances (Katz et al., 2019). Mash was used to calculate Mash distances between phage genomes (Ondov et al., 2016), and Mashtree was used to construct a phylogenetic tree based on Mash distances, with the kmer set to 21 and sketch set to 1000. iTOL was used to visualize and annotate the phylogenetic tree (Letunic and Bork, 2021). To identify genome structure conservation and variation, Easyfig 2.2.5 was used for collinearity analysis of phage genome sequences (Sullivan et al., 2011).

2.9 Tail fiber protein structure and function analysis

Jalview was used to visualize the alignment results and identify conserved and variable regions (Sievers and Higgins, 2018; Procter et al., 2021). AlphaFold 3 was used for three-dimensional structure prediction of tail fiber protein amino acid sequences (Abramson et al., 2024). To verify the AlphaFold prediction results, SWISS-Model was used for homology modeling (Waterhouse et al., 2018). PyMOL was used for visualization analysis and coloring of the predicted structures, focusing on analysis the tip domain, which may affect host recognition (Rosignoli and Paiardini, 2022).

2.10 Statistical analysis

Analysis of variance (ANOVA) in SPSS was used to identify significant differences in the control efficacies of single phages and phage cocktails ($p<0.05$).

3 Results

3.1 Isolation and identification of *R. pseudosolanacearum* and phages, and construction of phage cocktails

3.1.1 Isolation and identification of *R. pseudosolanacearum* and phages, evaluation of single-phage biocontrol potential, and construction of phage cocktails

This study collected tobacco with BW to screen phages with effective lytic activity against tobacco BW pathogens in Xiangxi Tujia Zu and Miao Zu Autonomous Prefecture, Hunan Province. A total of 26 *R. pseudosolanacearum* strains (RStab1–RStab26) and 9 phages (YL1–YL9) were isolated and purified (Supplementary Figure S2).

Host range analysis (Supplementary Table S1) showed that there were significant differences in the host ranges of nine phages against 38 *R. pseudosolanacearum* strains isolated from tobacco, peanut, pepper, and potato. YL1 and YL4 lysed 84.21 and 81.58% of the tested *R. pseudosolanacearum* strains, respectively, showing higher lysis rates than the other seven phages. Therefore, YL1 and YL4 were defined as broader host range phages. As all nine phages could lyse RStab-12 with obvious plaques, RStab-12 was selected to evaluate the biocontrol potential of individual phages.

Pot experiments were conducted to compare the control efficacies of nine individually inoculated phages against tobacco BW to evaluate their biocontrol potential. The survey showed that at 7 days after inoculation with RStab-12, seedlings in the control treatment (CK) entered the peak period of BW, while only partial wilting was observed in the phage-treated groups at the same time. At 14 days after inoculation, the DI of CK were significantly higher than that of the phage-treated groups. Among them, YL3 had the highest control effect on BW (93.98 ± 3.03%), followed by YL2 (76.39 ± 8.37%), and YL9 had the lowest control efficacy (61.11 ± 1.60%) (Figures 1A, B). This indicates that phage inoculation effectively reduces the occurrence of BW but that there are large differences in efficacy between phages.

The two phages with the highest control efficacy (YL2 and YL3) were selected and combined with YL1 and YL4 to construct five phage cocktails: BPC-1 (YL3, YL4), BPC-2 (YL1, YL2, YL3, YL4), BPC-3 (YL1, YL3, YL4), BPC-4 (YL1, YL4), and BPC-5 (YL2, YL3). Further research on YL1, YL2, YL3, and YL4 was conducted to clarify their biological characteristics and taxonomic relationships.

3.1.2 Control efficacy of phage cocktails against tobacco BW inoculation with three *R. pseudosolanacearium* strains

Using pot experiments, the control efficacy of five cocktails and four single phages was compared against mixed inoculation with three *R. pseudosolanacearum* strains of high virulence (Supplementary Figure S1). At 14 days after inoculation, the survey results showed that the control efficacies of all five phage cocktails against BW were above 87%. BPC-1 exhibited the highest control efficacy (99.25 ± 0.65%), and the control efficacies of BPC-2, BPC-3, BPC-4, and BPC-5 were 95.49 ± 1.95, 95.49 ± 4.06, 94.36 ± 3.90, and 87.22 ± 11.30%, respectively. The control efficacy of each phage was between

62.03 ± 6.60 and 78.57 ± 13.30%. Comparisons between phage cocktails and individual phages showed no significant differences among the five cocktails. However, the control efficacies of BPC-1, BPC-2, BPC-3, and BPC-4 were significantly higher than those of the individual phages; all phage cocktails achieved control efficacies above 94% against BW. The combination of two high control efficacy phages (YL2 and YL3) in a cocktail (BPC-5) exhibited a control efficacy of 87.22 ± 11.30%, which was significantly improved compared to that of phage YL1. BPC-5 had a 10.9% increase in control efficacy compared to YL2 and YL3. The addition of two broader host range phages (YL1 and YL4) to BPC-5 (forming BPC-2) improved the control efficacy against BW by 8.27% (Figures 1C, D). The experimental results indicate that combining phages with a broad host range and high control efficacy enhances their coverage against *R. pseudosolanacearum* strains and improves their control efficacy against BW.

3.2 Biological characteristics

Phage stability is affected by environmental factors, such as temperature and pH. Temperature sensitivity experiments showed that YL1's titer remained stable in the range of 30–50°C but decreased significantly at temperature greater than 60°C. The titers of YL2, YL3, and YL4 remained stable in the range of 30–60°C but decreased significantly after water bath treatment at 70°C for 1 h, with YL2 showing a smaller decrease than YL3 and YL4. No plaques were detected for the four phages at 80 or 90°C (Figure 2A-a), indicating that 80°C was the lethal temperature.

pH stability experiments showed that the titers of all four phages remained stable above 10^7 PFU/mL in the pH range of 4–11 but decreased significantly at pH 11. No plaques were detected at pH 3. At pH 12, YL2 showed no plaque, while the titers of YL1, YL2, and YL3 decreased to 10^4 PFU/mL. No plaques were detected at pH 13 (Figure 2A-b). These results indicate that the four phages have substantial application potential under environmental conditions of 30–50°C and pH 4–11.

The optimal MOI for all four phages was 10^{-2} (Figure 2A-c). The lysis curves of phages against RStab-12 were determined at the optimal MOI. After combining the four phages, the OD_{600} of the co-culture decreased to less than 0.074 within 4 h. Notably, the OD_{600} of YL3 increased to 0.135 at 5 h and decreased again to 0.053 after 1 h. In CK (RStab-12), the OD_{600} of CK continued to increase within 12 h, reaching 1.128 at 12 h (Figure 2A-d). The experimental results showed that an MOI = 10^{-2} enabled all four bacteriophages to produce more progeny and lyse the host within 4 h.

Transmission electron microscopy observation revealed that all four phages had large icosahedral heads (YL1: 72.03 ± 6.50 nm; YL2: 70 ± 0.82 nm; YL3: 71 ± 0.82 nm; YL4: 72.67 ± 1.25 nm) and relatively short tails (YL1: 31.33 ± 1.70 nm; YL2: 32 ± 2.83 nm; YL3: 30 ± 2.45 nm; YL4: 29.67 ± 1.25 nm). (Figure 2B).

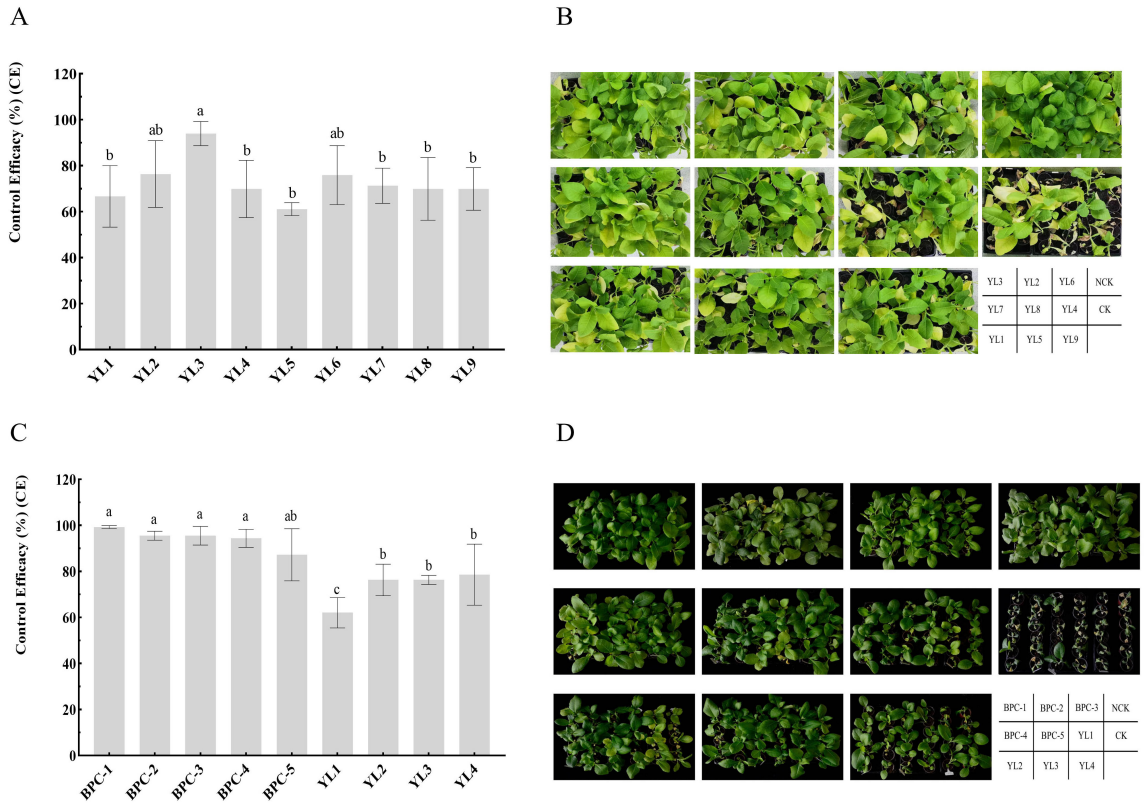

FIGURE 1
Control efficiency of phages and phage cocktails against BW in pots. **(A, B)** show the evaluation of single-phage biocontrol potential; **(C, D)** show the control efficacy of phage cocktails against tobacco BW inoculation with three *R. pseudosolanacearium* strains. Letters in the bar chart indicate significant differences according to Duncan's analysis ($P \leq 0.05$); NCK is the negative control group.

3.3 Genomic analysis

3.3.1 Genome characteristics and phylogenetic analysis

The nucleic acids of YL1, YL2, YL3, and YL4 were not digested by RNase A but were all cleaved into DNA fragments of different sizes by EcoRI (Supplementary Figure S3), indicating that they were all double-stranded DNA phages. Genome sequencing also confirmed that they were all double-stranded circular DNA phages, with genome lengths of 59,600, 60,770, 61,339, and 60,673 bp, respectively, G + C contents of 64.52, 64.86, 64.92, and 65.02%, respectively, and 73, 73, 75, and 74 ORFs, respectively (Supplementary Tables S2-S5). The genome sequences of YL1, YL2, YL3, and YL4 were submitted to GenBank under accession numbers PQ295876, PQ295877, PQ295878, and PQ295879, respectively. BLASTn analysis showed that YL1, YL2, YL3, and YL4 had more than 92% similarity with the genome sequences of previously reported *Gervaisevirus* phages in the Caudoviricetes class, such as QKW1 (GenBank accession no. PP236328), AhaGv (GenBank accession no. OR820515), P2110 (GenBank accession no. OP947226), and GP4 (GenBank accession no. MH638294), indicating that they belong to this genus and class.

The genome sequences of these four phages were compared with 317 Ralstonia phages of the Caudoviricetes class recorded in the NCBI database. These 321 phages were divided into four families and eight genera according to their evolutionary relationships. YL1, YL2, YL3, and YL4 were all located in the *Gervaisevirus* branch (Supplementary Figure S4), showing high similarity with other members of this genus. All four phages were identified as belonging to the *Gervaisevirus* genus of the Caudoviricetes class based on the classification principles of the Bacterial and Archaeal Viruses Subcommittee (BAVS) (Adriaenssens and Brister, 2017). Skani was used to calculate the ANI between phage genomes to further quantify the differences between genomes. The ANI values of YL2, YL3, and YL4 were all above 95%, indicating that they belong to the same species, while the ANI values between YL1 and YL2, YL3, and YL4 ranged from 92 to 94%, indicating that they are not the same species (Figure 3).

3.3.2 Protein function annotation and comparative genome analysis

Annotation results of the four phage genomes showed that the three functional proteins in YL1 and YL3 did not have similar proteins in the NR protein database (BLASTp e-value less than 1e−5), while YL2 and YL4 each had four. YL1, YL2, YL3, and YL4 had 36, 38, 41, and 54 hypothetical proteins, respectively. ORF2 occupied a large proportion of their genomes (YL1: 5.32%, YL2: 7.29%, YL3: 7.29%, YL4: 7.29%), and annotation showed that ORF2 was homologous to *DarB* (defense against restriction), which is required to protect foreign genomic DNA from restriction by host type I R-M systems (Piya et al., 2017).

This study classified the ORFs of the four phages into four functional types: lysis, morphogenesis, replication and regulation, and packaging genes. Among the ORFs related to lysis, all four phages had holin proteins. ORFs related to morphogenesis mainly encoded head proteins, tail fiber proteins, virion structural proteins, and portal proteins. ORFs related to replication and regulation encoded functional proteins, such as RecE-like recombination exonuclease and plasmid-derived single-stranded DNA-binding protein. ORFs related to packaging encoded functional proteins such as terminase small subunit and phage terminase large subunit (Supplementary Tables S2-S5).

Easyfig was used for comparative genome analysis of the four phage genomes, which showed good consistency with GP4 (Wang R et al., 2019). The arrangement positions and transcription directions of most genes with the same functions in the genome were consistent, but there were partial gene deletions and position shifts between phages. Compared to the other three phages, YL1 had nucleic acid sequence deletions in ORF2, significant differences in ORF11, ORF30-31, and ORF67 compared to YL2, and position shifts in ORF55. ORF56 in YL1 showed gene shifts in YL2, and YL2, YL3, and YL4 showed high genome consistency, with ORF54 in YL3 and ORF58 in YL4 having position shifts (Figure 4).

3.3.3 Structure and function prediction of tail fiber proteins

Host range analysis showed that the four phages had significant differences in lysis capacity against 38 *R. pseudosolanacearum* strains. Since phage tail fiber proteins play a key role in host

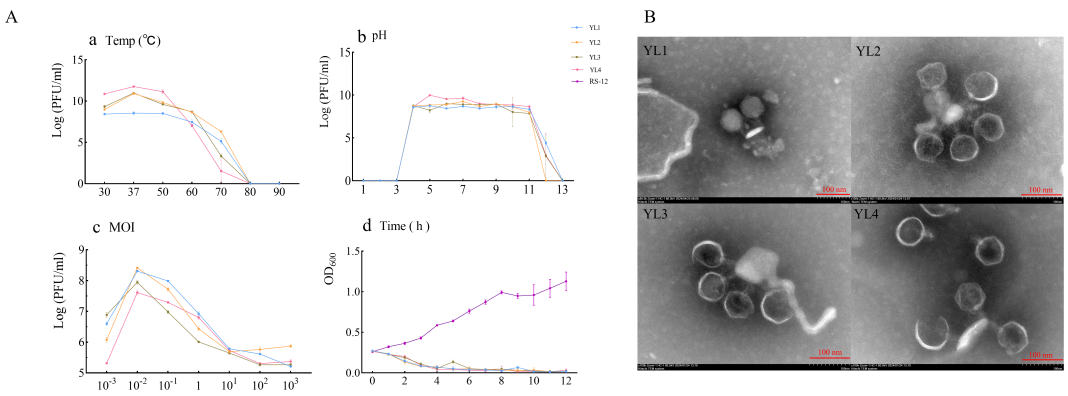

FIGURE 2
Biological characteristics, lysis curves, and transmission electron microscopy showing the morphology of four phages. **(A-a–A-d)** show temperature sensitivity, pH stability, MOI, and lysis curves, respectively of four phages; **(B)** shows the morphology of four phages observed using transmission electron microscopy.

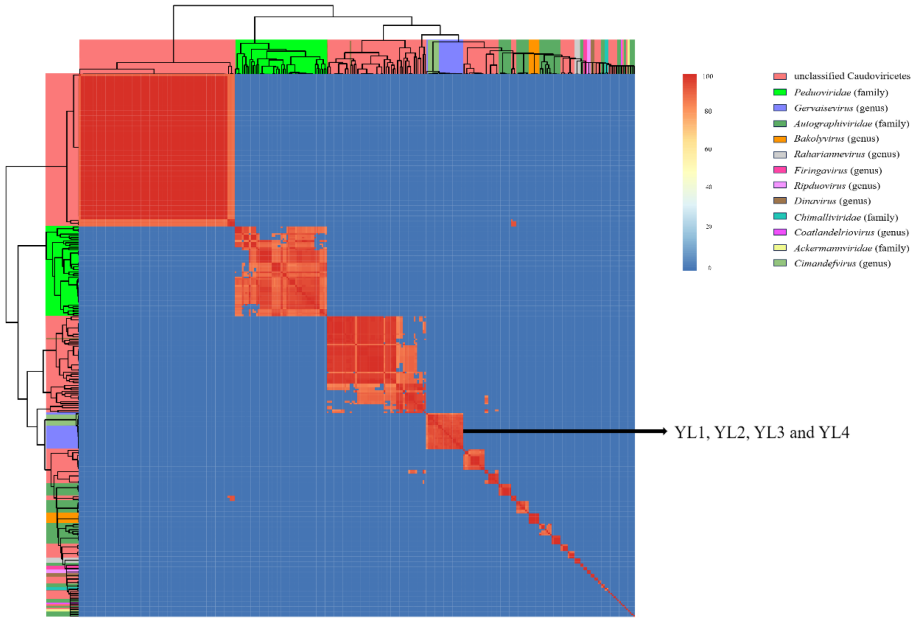

FIGURE 3
Nucleotide similarity heatmap of four phages with 317 Ralstonia phages in the Caudoviricetes class. The ANI between phage genomes was calculated using Skani and visualized as a heatmap. Different colored squares on the top and left sides of the heatmap represent different taxonomic relationships among the phages. The color intensity in the heatmap indicates the degree of nucleotide similarity between phage genomes.

recognition and infection processes, analysis found that all four phages had two types of tail fiber proteins: tail fiber protein I (ORF65 (439 aa, YL1), ORF65 (439 aa, YL2), ORF69 (439 aa, YL3), ORF68 (439 aa, YL4)), and tail fiber protein II (ORF66 (338 aa, YL1), ORF66 (295 aa, YL2), ORF70 (290 aa, YL3), ORF69 (290 aa, YL4)). Based on amino acid sequence alignment using Jalview, the amino acid sequences of tail fiber protein I had high consistency in the four phages, while the C-terminal amino acid sequences of tail fiber protein II showed significant differences (Figure 5A). Therefore, highly conserved tail fiber protein I is expected to have little effect on host recognition, while tail fiber protein II may play an important role in host recognition.

AlphaFold 3 was used to predict the three-dimensional structure of tail fiber protein II from four phages. The visualization of the predicted structure revealed that tail fiber protein II adopts a trimeric structure. Furthermore, the N-terminal structure of tail fiber protein II was highly consistent with that of ORF78 (GP4) (Zheng et al., 2023). However, the "tip domain" (P160-V338) of ORF66 (YL1) was significantly different from the "tip domains" of ORF66 (T207-T242, YL2), ORF70 (T207-T242, YL3), and ORF69 (H207-T237, YL4), with 11 β-sheets and 5 α-helices. However, the "tip domains" of ORF66 (YL2), ORF70 (YL3) and ORF69 (YL4) had similar structures (Figure 5B). In addition, the ORF66 (YL1) "tip domain" region also had more aromatic amino acids, such as phenylalanine (F), tryptophan (W), and tyrosine (Y), and positively charged amino acids, such as arginine (R) and lysine (K), which provide more binding sites for its interaction with hosts (Bartual et al., 2010; Vyas, 1991). The "tip domain" amino acid sequences of ORF66 (YL2), ORF70 (YL3), and ORF78 (GP4) had high consistency, but those of ORF69 (YL4) had a large number of amino acid deletions and mutations, including seven deleted polar amino acids (T207, N208, S209, N210, Y211, Y212, N213) and three polar amino acids mutated to non-polar amino acids (T221A, Q230A, S233A).

To further elucidate the differences in the "tip domains" between ORF66 (YL2), ORF70 (YL3), and ORF69 (YL4), protein surface electrostatic analysis was performed using Adaptive Poisson–Boltzmann Solver in PyMOL (APBS) (Jurrus et al., 2018). Five amino acid residues (G217, G218, S219, G220, and T221) on the "tip domain" surfaces of ORF66 (YL2) and ORF70 (YL3) carried negative charges, while that in ORF69 (YL4) carried more positive charges (G218, G219, G220, A221, and F222) (Supplementary Figure S5). More positive charges in the "tip domain" are believed to enhance the binding ability of YL4 to its host receptor, thereby potentially conferring a broader host range.

4 Discussion

Phage therapy is considered a most promising technology for controlling plant bacterial diseases (Kering et al., 2019; Pandit et al., 2022). *Ralstonia pseudosolanacearum* is a typical "species complex" with diverse genotypic variations. Due to the strong host specificity and narrow host range of most phages, mixing phages with different host ranges in phage cocktails can improve the efficacy of phage therapy or biocontrol (Buttimer et al., 2017; Magar et al., 2022). This study isolated 26 *R. pseudosolanacearum* strains and 9 lytic phages from Xiangxi Tujia Zu and Miao Zu Autonomous Prefecture, Hunan Province. By comparing the host range and pot control efficacy of phages, four were selected to construct five phage cocktails. The control efficacy of combined phages against

mixed inoculation with *R. pseudosolanacearum* was significantly higher than that of individual phages.

In field applications, complex soil environments affect phage lytic activity. Most reported phages are stable in the range of 28–50°C and pH 5–10 (Magar et al., 2022; Wang et al., 2022; Lin et al., 2023; Huang et al., 2024). In this study, YL1, YL2, YL3, and YL4 maintained stable titers at 30–50°C and pH 4–11, enabling better adaptation to problems caused by changes in environmental temperature and soil pH, which may reduce phage activity or infection ability (Figures 2A-a, A-b).YL1, YL2, YL3, and YL4 had high lysis efficiency and rapidly reduced the *R. pseudosolanacearum* population within 4 h, thereby reducing disease occurrence (Figure 2A-d). Wei et al. (2017) summarized four types of phage lysis curves, including a mode that showed immediate growth inhibition of host bacteria, similar to the lysis curves of the four phages in this study. To delay host bacterial resistance to phages, phages with broad lysis spectra, high control efficacy, and short infection cycles should be used when constructing phage cocktails (Jones et al., 2007; Kaur et al., 2021). This study, building on the method established by Wei and Magar, concentrated on screening phages with a broad host range and high control efficacy, which were subsequently combined into a phage cocktail. The results demonstrated that, compared to individual phages, the phage cocktail significantly enhanced the control efficacy against a mixed inoculation of three *R. pseudosolanacearum* strain. BPC-1 exhibited the highest control effect (99.25% ± 0.65%). Subsequent field experiments should further compare the control efficacy of phage cocktails against BW in agricultural and ecological environments. In addition, through whole genome sequencing and AlphaFold 3 prediction, this study discovered the tail fiber II and its three-dimensional structure, hypothesizing that this structure provides the capability to bind with the outer membrane protein receptors of *R. pseudosolanacearum*. These findings provide valuable materials for further research into the interaction mechanisms between phages and their host receptors.

Whole genome sequencing provides critical insights into the taxonomic relationships and genomic characteristics of bacteriophages (Dion et al., 2020). According to genomic analysis and BAVS classification principles (Adriaenssens and Brister, 2017), the four Ralstonia phage strains belonged to the *Gervaisevirus* genus within the Caudovirivetes class, demonstrating high similarity (>92%) with other members of this genus. Functional annotation revealed that the genomes of the four Ralstonia phage strains contained four functional types, namely lysis, morphogenesis, replication and regulation, and packaging genes, consistent with previously reported Gervaisevirus phages GP4 and P2110 (Wang et al., 2019; Chen et al., 2023). Comparative genome analysis revealed variations in gene arrangement, even among genomically similar phages. These variations suggest dynamic genomic rearrangement and gene mutation processes potentially driven by horizontal gene transfer and evolutionary selective pressures, which are critical mechanisms underlying bacteriophage genomic diversity (Brüssow

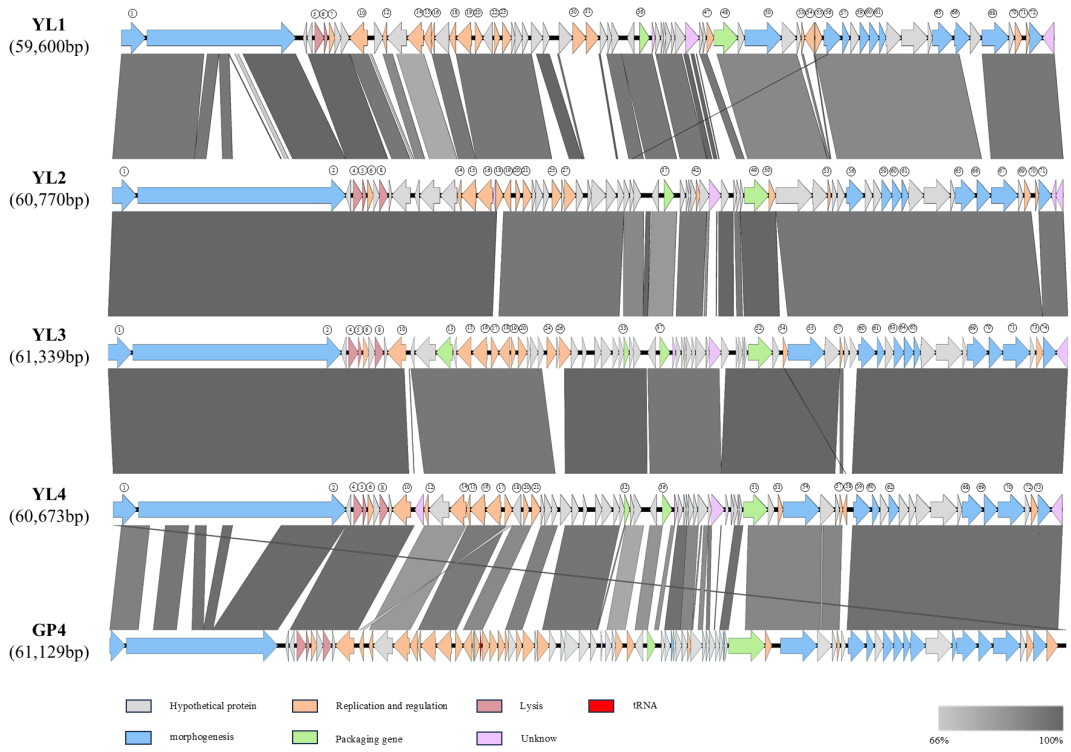

FIGURE 4
Comparative genome of four phages. Comparison of whole genome similarity between YL1, YL2, YL3, and YL4. Arrows represent transcription direction of genes, and genes with consistent functional annotations are represented by the same color. Gray bands between genomes indicate amino acid similarity.

and Hendrix, 2002). Overall, the genetic diversity and functional predictions for these four bacteriophage strains highlight the conserved characteristics and plasticity of bacteriophages in the *Gervaisevirus* genus.

The abundant lipopolysaccharides (LPS) and outer membrane proteins in bacteria are the main binding sites for phages. The interactions between phage tail fiber proteins and bacterial receptors determine the phage's host range. The number of positively charged amino acids and aromatic amino acids in the "tip domain" of tail fiber proteins affects the host range and adsorption ability of phages (Nobrega et al., 2018; Mourosi et al., 2022). The "tip domain" of tail fiber protein II of ORF66 (YL1) had more aromatic amino acids and positively charged amino acids, which interact with rough LPS and negatively charged phospholipids in the host outer membrane, respectively (Vyas, 1991; Raetz and Whitfield, 2002; Bartual et al., 2010; Rakhuba et al., 2010). Phages that bind rough LPS usually have a broader host lysis range, which potentially explains the broader host range of YL1. The amino acid sequences of the "tip domains" of ORF66 (YL2) and ORF70 (YL3) were highly similar, with amino acid mutations (S228G, V237I) in ORF70 (YL3), which reduced its lysis rate by 13.16%. Compared to ORF69 (YL4), the amino acid deletions and mutations in ORF66 (YL2) and ORF70 (YL3) may reduce the binding ability of tail fiber II to the host receptor site (Bolen and Rose, 2008). Further, the "tip domain" of tail fiber protein II of ORF69 (YL4) also contained a positively charged histidine (H207), which enhanced its electrostatic adsorption ability to the host outer membrane (Bartual et al., 2010), increasing the host range of YL4 (Figure 5B). Subsequent studies should verify these speculations by performing amino acid mutations on the "tip domain" of tail fiber protein II.

5 Conclusion

Phage therapy shows promising biocontrol potential for managing BW caused by *R. pseudosolanacearum* in agricultural production. This study isolated nine phages and selected those with a broader host range (YL1 and YL4) and high control efficacy (YL2 and YL3) to construct five cocktails. In pot experiments, BPC-1 (YL3 and YL4) exhibited the highest control efficacy (99.25%). The four phages maintained stable titers at 30–50°C and pH 4–11, demonstrating substantial thermal stability and pH tolerance. Whole genome sequencing revealed that phages YL1, YL2, YL3, and YL4 belonged to the genus *Gervaisevirus*. AlphaFold 3 prediction of the three-dimensional structures of tail fiber protein

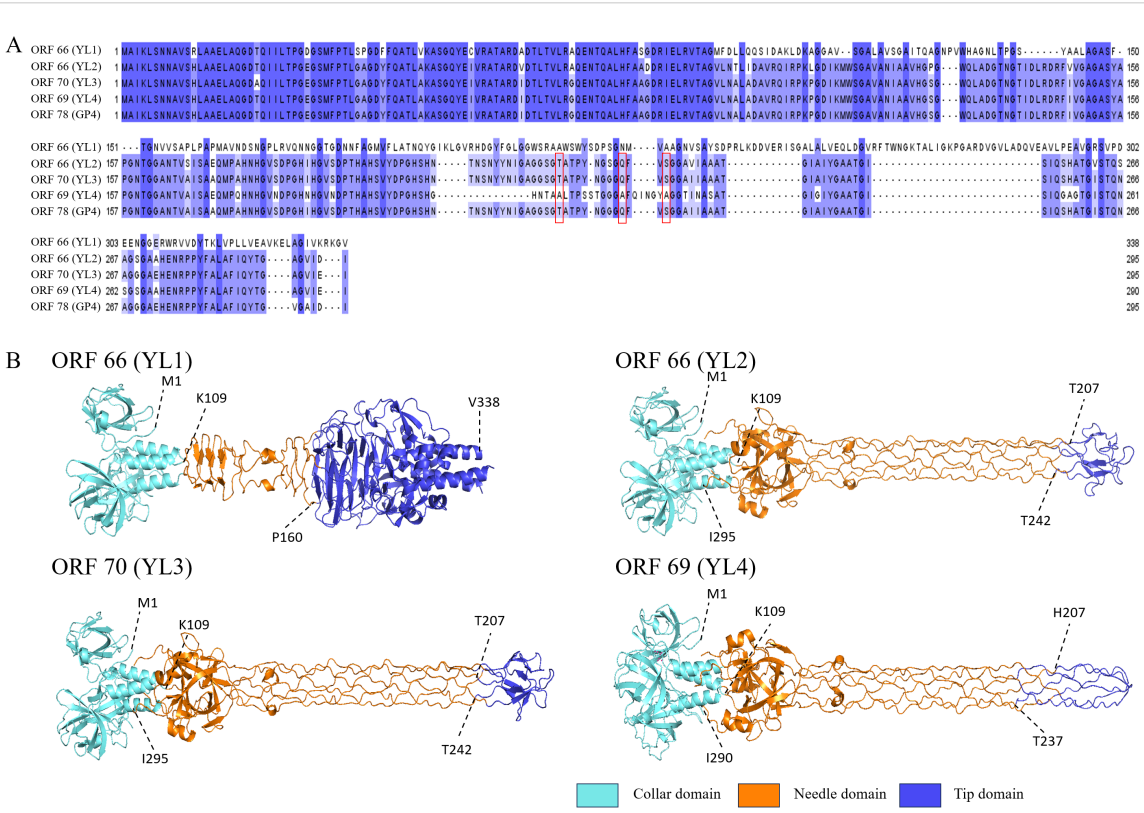

FIGURE 5
Amino acid sequence similarity and three-dimensional structure prediction of tail fiber protein II. **(A)** shows amino acid sequence similarity of tail fiber protein II. Red boxes indicate mutations of polar amino acids in ORF66 (YL2), ORF70 (YL3) and ORF78 (GP4), and deeper blue indicates higher conservation. **(B)** shows predicted structures of tail fiber II proteins of four phages using Alphafold 3. Light blue areas are collar domains located at the base of phage tail fibers; orange areas are needle domains located in the middle long part of tail fibers; dark blue areas are tip domains located at the "tip" part of the end structure of phage tail fiber II; and dotted lines with numbers indicate connections between structural domains.

II in the four phages showed that ORF66 (YL1) had a distinct structure in the "tip domain" compared to the other three phages, with more aromatic amino acids and positively charged amino acids. ORF70 (YL3), ORF66 (YL2), and ORF69 (YL4) had similar structures, but ORF69 (YL4) had more amino acid mutations and deletions and more positive charges in the tip region, potentially explaining their different host ranges.

Data availability statement

The datasets presented in this study can be found in online repositories. The names of the repository/repositories and accession number(s) can be found in the article/Supplementary Material.

Author contributions

HH: Methodology, Writing – original draft, Writing – review & editing. KY: Funding acquisition, Methodology, Supervision, Validation, Writing – original draft. LY: Investigation, Methodology, Resources, Writing – original draft. YJ: Investigation, Methodology, Writing – original draft. LK: Investigation, Methodology, Writing – original draft. ZG: Investigation, Methodology, Writing – original draft. DX: Investigation, Methodology, Writing – original draft. GT: Conceptualization, Methodology, Supervision, Writing – review & editing. YW: Methodology, Writing – review & editing. QL: Data curation, Visualization, Writing – original draft. LX: Methodology, Writing – original draft. SJ: Methodology, Writing – original draft. TL: Funding acquisition, Supervision, Writing – original draft, Writing – review & editing. WC: Methodology, Resources, Supervision, Writing – original draft, Writing – review & editing.

Funding

The author(s) declare that financial support was received for the research and/or publication of this article. This work was supported by funding from the Research and Application of New Green Prevention and Control Technology of Main Root Diseases in the Tobacco Growing District of Northwest Hunan (grant number, KY2023YC0009); Precise Identification, Key Trait Analysis, and Resource Database Construction of Tobacco Biocontrol Bacteria (grant number, 110220001019 (LS-03)); and Integration and Application of Green Control Technologies for Root and Stem Diseases in Xiangxi Mountainous Tobacco Areas Based on Synergistic Enhancement with Food and Oil Crops (grant number, HN2024KJ04).

Conflict of interest

Authors KY, LY, YJ, LK, ZG, DX and GT were employed by the company China Tobacco Hunan Industrial Co., Ltd.

The remaining authors declare that the research was conducted in the absence of any commercial or financial relationships that could be construed as a potential conflict of interest.

Generative AI statement

The author(s) declare that no Generative AI was used in the creation of this manuscript.

Publisher's note

All claims expressed in this article are solely those of the authors and do not necessarily represent those of their affiliated organizations, or those of the publisher, the editors and the reviewers. Any product that may be evaluated in this article, or claim that may be made by its manufacturer, is not guaranteed or endorsed by the publisher.

Supplementary material

The Supplementary Material for this article can be found online at: https://www.frontiersin.org/articles/10.3389/fpls.2025.1554992/full#supplementary-material

References

Abramson, J., Adler, J., Dunger, J., Evans, R., Green, T., Pritzel, A., et al. (2024). Accurate structure prediction of biomolecular interactions with AlphaFold 3. *Nature* 630, 493–500. doi: 10.1038/s41586-024-07487-w

Adriaenssens, E., and Brister, J. R. (2017). How to name and classify your phage: an informal guide. *Viruses* 9 (4), 70. doi: 10.3390/v9040070

Ahmad, A. A., Addy, H. S., and Huang, Q. (2021). Biological and molecular characterization of a jumbo bacteriophage infecting plant pathogenic *Ralstonia solanacearum* species complex strains. *Front. Microbiol.* 12. doi: 10.3389/fmicb.2021.741600

Askora, A., Kawasaki, T., Fujie, M., and Yamada, T. (2017). Lysogenic conversion of the phytopathogen *Ralstonia solanacearum* by the P2virus ϕRSY1. *Front. Microbiol.* 8. doi: 10.3389/fmicb.2017.02212

Aziz, R. K., Bartels, D., Best, A. A., DeJongh, M., Disz, T., Edwards, R. A., et al. (2008). The RAST Server: rapid annotations using subsystems technology. *BMC Genomics* 9, 75. doi: 10.1186/1471-2164-9-75

Bankevich, A., Nurk, S., Antipov, D., Gurevich, A. A., Dvorkin, M., Kulikov, A. S., et al. (2012). SPAdes: a new genome assembly algorithm and its applications to single-cell sequencing. *J. Comput. Biol.* 19, 455–477. doi: 10.1089/cmb.2012.0021

Bartual, S. G., Otero, J. M., Garcia-Doval, C., Llamas-Saiz, A. L., Kahn, R., Fox, G. C., et al. (2010). Structure of the bacteriophage T4 long tail fiber receptor-binding tip. *Proc. Natl. Acad. Sci. U.S.A.* 107, 20287–20292. doi: 10.1073/pnas.1011218107

Besemer, J., and Borodovsky, M. (2005). GeneMark: web software for gene finding in prokaryotes, eukaryotes and viruses. *Nucleic Acids Res.* 33, W451–W454. doi: 10.1093/nar/gki487

Bolen, D. W., and Rose, G. D. (2008). Structure and energetics of the hydrogen-bonded backbone in protein folding. *Annu. Rev. Biochem.* 77, 339–362. doi: 10.1146/annurev.biochem.77.061306.131357

Bolger, A. M., Lohse, M., and Usadel, B. (2014). Trimmomatic: a flexible trimmer for Illumina sequence data. *Bioinformatics* 30, 2114–2120. doi: 10.1093/bioinformatics/btu170

Brüssow, H., and Hendrix, R. W. (2002). Phage genomics: small is beautiful. *Cell* 108, 13–16. doi: 10.1016/s0092-8674(01)00637-7

Buchfink, B., Xie, C., and Huson, D. H. (2015). Fast and sensitive protein alignment using DIAMOND. *Nat. Methods* 12, 59–60. doi: 10.1038/nmeth.3176

Buttimer, C., McAuliffe, O., Ross, R. P., Hill, C., O'Mahony, J., and Coffey, A. (2017). Bacteriophages and bacterial plant diseases. *Front. Microbiol.* 8. doi: 10.3389/fmicb.2017.00034

Chen, K., Guan, Y., Hu, R., Cui, X., and Liu, Q. (2023). Characterization of the lysP2110-HolP2110 lysis system in Ralstonia solanacearum phage P2110. *Int. J. Mol. Sci.* 24 (12), 10375. doi: 10.3390/ijms241210375

Coil, D., Jospin, G., and Darling, A. E. (2015). A5-miseq: an updated pipeline to assemble microbial genomes from Illumina MiSeq data. *Bioinformatics* 31, 587–589. doi: 10.1093/bioinformatics/btu661

Conesa, A., Götz, S., García-Gómez, J. M., Terol, J., Talón, M., and Robles, M. (2005). Blast2GO: a universal tool for annotation, visualization and analysis in functional genomics research. *Bioinformatics* 21, 3674–3676. doi: 10.1093/bioinformatics/bti610

Denny, T. P. (2000). *Ralstonia solanacearum*–a plant pathogen in touch with its host. *Trends Microbiol.* 8, 486–489. doi: 10.1016/s0966-842x(00)01860-6

Díaz-Muñoz, S. L., and Koskella, B. (2014). Bacteria-phage interactions in natural environments. *Adv. Appl. Microbiol.* 89, 135–183. doi: 10.1016/B978-0-12-800259-9.00004-4

Dion, M. B., Oechslin, F., and Moineau, S. (2020). Phage diversity, genomics and phylogeny. *Nat. Rev. Microbiol.* 18, 125–138. doi: 10.1038/s41579-019-0311-5

Elphinstone, J. G., Allen, C., Prior, P., and Hayward, A. C. (2005). The current bacterial wilt situation: a global overview. *Bacterial Wilt the Disease & the Ralstonia Solanacearum Species Complex*. Available online at: https://www.semanticscholar.org/paper/The-current-bacterial-wilt-situation%3A-a-global-Elphinstone-Allen/87ad9037d22c7dc6c6dc288405ac82d6793f9959.

Genin, S., and Denny, T. P. (2012). Pathogenomics of the Ralstonia solanacearum species complex. *Annu. Rev. Phytopathol.* 50, 67–89. doi: 10.1146/annurev-phyto-081211-173000

Gill, J. J., and Hyman, P. (2010). Phage choice, isolation, and preparation for phage therapy. *Curr. Pharm. Biotechnol.* 11, 2–14. doi: 10.2174/138920110790725311

Huang, B., Ge, L., Xiang, D., Tan, G., Liu, L., Yang, L., et al. (2024). Isolation, characterization, and genomic analysis of a lytic bacteriophage, PQ43W, with the potential of controlling bacterial wilt. *Front. Microbiol.* 15. doi: 10.3389/fmicb.2024.1396213

Huang, S., Tian, Y., Wang, Y., García, P., Liu, B., Lu, R., et al. (2022). The broad host range phage vB_CpeS_BG3P Is able to inhibit clostridium perfringens growth. *Viruses* 14 (4), 676. doi: 10.3390/v14040676

Ji, M., Liu, Z., Sun, K., Li, Z., Fan, X., and Li, Q. (2021). Bacteriophages in water pollution control: advantages and limitations. *Front. Environ. Sci. Eng.* 15 (5), 84. doi: 10.1007/s11783-020-1378-y

Jiang, G., Wei, Z., Xu, J., Chen, H., Zhang, Y., She, X., et al. (2017). Bacterial wilt in China: history, current status, and future perspectives. *Front. Plant Sci.* 8. doi: 10.3389/fpls.2017.01549

Jones, J. B., Jackson, L. E., Balogh, B., Obradovic, A., Iriarte, F. B., and Momol, M. T. (2007). Bacteriophages for plant disease control. *Annu. Rev. Phytopathol.* 45, 245–262. doi: 10.1146/annurev.phyto.45.062806.094411

Jurrus, E., Engel, D., Star, K., Monson, K., Brandi, J., Felberg, L. E., et al. (2018). Improvements to the APBS biomolecular solvation software suite. *Protein Sci.* 27, 112–128. doi: 10.1002/pro.3280

Katz, L. S., Griswold, T., Morrison, S. S., Caravas, J. A., Zhang, S., den Bakker, H. C., et al. (2019). Mashtree: a rapid comparison of whole genome sequence files. *J. Open Source Softw* 4 (44), 1762. doi: 10.21105/joss.01762

Kaur, G., Agarwal, R., and Sharma, R. K. (2021). Bacteriophage therapy for critical and high-priority antibiotic-resistant bacteria and phage cocktail-antibiotic formulation perspective. *Food Environ. Virol.* 13, 433–446. doi: 10.1007/s12560-021-09483-z

Kering, K. K., Kibii, B. J., and Wei, H. (2019). Biocontrol of phytobacteria with bacteriophage cocktails. *Pest Manag Sci.* 75, 1775–1781. doi: 10.1002/ps.5324

Kropinski, A. M., Mazzocco, A., Waddell, T. E., Lingohr, E., and Johnson, R. P. (2009). Enumeration of bacteriophages by double agar overlay plaque assay. *Methods Mol. Biol.* 501, 69–76. doi: 10.1007/978-1-60327-164-6_7

Letunic, I., and Bork, P. (2021). Interactive Tree Of Life (iTOL) v5: an online tool for phylogenetic tree display and annotation. *Nucleic Acids Res.* 49, W293–w296. doi: 10.1093/nar/gkab301

Lin, Z., Gu, G., Chen, C., Zhou, T., Hu, F., and Cai, X. (2023). Characterization and complete genome sequence analysis of the novel phage RPZH3 infecting *Ralstonia solanacearum*. *Arch. Virol.* 168, 105. doi: 10.1007/s00705-023-05737-2

Lowe-Power, T., Avalos, J., Bai, Y., Munoz, M. C., Chipman, K., Tom, C. E., et al. (2020). A meta-analysis of the known global distribution and host range of the Ralstonia species complex. *bioRxiv*. doi: 10.1101/2020.07.13.189936

Magar, R., Lee, S. Y., Kim, H. J., and Lee, S. W. (2022). Biocontrol of bacterial wilt in tomato with a cocktail of lytic bacteriophages. *Appl. Microbiol. Biotechnol.* 106, 3837–3848. doi: 10.1007/s00253-022-11962-7

Mansfield, J., Genin, S., Magori, S., Citovsky, V., Sriariyanum, M., Ronald, P., et al. (2012). Top 10 plant pathogenic bacteria in molecular plant pathology. *Mol. Plant Pathol.* 13, 614–629. doi: 10.1111/j.1364-3703.2012.00804.x

Markwitz, P., Lood, C., Olszak, T., van Noort, V., Lavigne, R., and Drulis-Kawa, Z. (2022). Genome-driven elucidation of phage-host interplay and impact of phage resistance evolution on bacterial fitness. *ISME J.* 16, 533–542. doi: 10.1038/s41396-021-01096-5

Mourosi, J., Awe, A., Guo, W., Batra, H., Ganesh, H., Wu, X., et al. (2022). Understanding bacteriophage tail fiber interaction with host surface receptor: the key "blueprint" for reprogramming phage host range. *Int. J. Mol. Sci.* 23 (20), 12146. doi: 10.3390/ijms232012146

Mushegian, A. R. (2020). Are there 10(31) virus particles on earth, or more, or fewer? *J. Bacteriol* 202 (9), 2–20. doi: 10.1128/JB.00052-20

Nobrega, F. L., Vlot, M., de Jonge, P. A., Dreesens, L. L., Beaumont, H. J. E., Lavigne, R., et al. (2018). Targeting mechanisms of tailed bacteriophages. *Nat. Rev. Microbiol.* 16, 760–773. doi: 10.1038/s41579-018-0070-8

Ondov, B. D., Treangen, T. J., Melsted, P., Mallonee, A. B., Bergman, N. H., Koren, S., et al. (2016). Mash: fast genome and metagenome distance estimation using MinHash. *Genome Biol.* 17, 132. doi: 10.1186/s13059-016-0997-x

Pandit, M. A., Kumar, J., Gulati, S., Bhandari, N., Mehta, P., Katyal, R., et al. (2022). Major biological cantrol strategies for plant pathogens. *Pathogens* 11 (2), 273. doi: 10.3390/pathogens11020273

Paudel, S., Dobhal, S., Alvarez, A. M., and Arif, M. (2020). Taxonomy and phylogenetic research on *Ralstonia solanacearum* species complex: A complex pathogen with extraordinary economic consequences. *Pathogens* 9 (11), 886. doi: 10.3390/pathogens9110886

Piya, D., Vara, L., Russell, W. K., Young, R., and Gill, J. J. (2017). The multicomponent antirestriction system of phage P1 is linked to capsid morphogenesis. *Mol. Microbiol.* 105, 399–412. doi: 10.1111/mmi.13705

Procter, J. B., Carstairs, G. M., Soares, B., Mourão, K., Ofoegbu, T. C., Barton, D., et al. (2021). Alignment of biological sequences with jalview. *Methods Mol. Biol.* 2231, 203–224. doi: 10.1007/978-1-0716-1036-7_13

Raetz, C. R., and Whitfield, C. (2002). Lipopolysaccharide endotoxins. *Annu. Rev. Biochem.* 71, 635–700. doi: 10.1016/0167-5699(92)90009-V

Rakhuba, D. V., Kolomiets, E. I., Dey, E. S., and Novik, G. I. (2010). Bacteriophage receptors, mechanisms of phage adsorption and penetration into host cell. *Pol. J. Microbiol.* 59, 145–155. doi: 10.33073/pjm-

Rosignoli, S., and Paiardini, A. (2022). Boosting the full potential of PyMOL with structural biology plugins. *Biomolecules* 12 (12), 1764. doi: 10.3390/biom12121764

Shaw, J., and Yu, Y. W. (2023). Fast and robust metagenomic sequence comparison through sparse chaining with skani. *Nat. Methods* 20, 1661–1665. doi: 10.1038/s41592-023-02018-3

Sievers, F., and Higgins, D. G. (2018). Clustal Omega for making accurate alignments of many protein sequences. *Protein Sci.* 27, 135–145. doi: 10.1002/pro.3290

Sullivan, M. J., Petty, N. K., and Beatson, S. A. (2011). Easyfig: a genome comparison visualizer. *Bioinformatics* 27, 1009–1010. doi: 10.1093/bioinformatics/btr039

Tang, Y., Zhou, M., Yang, C., Liu, R., Du, H., and Ma, M. (2024). Advances in isolated phages that affect *Ralstonia solanacearum* and their application in the biocontrol of bacterial wilt in plants. *Lett. Appl. Microbiol.* 77 (4), 37. doi: 10.1093/lambio/ovae037

Tian, Y., Wu, L., Lu, R., Bao, H., Zhou, Y., Pang, M., et al. (2022). Virulent phage vB_CpeP_HN02 inhibits clostridium perfringens on the surface of the chicken meat. *Int. J. Food Microbiol.* 363, 109514. doi: 10.1016/j.ijfoodmicro.2021.109514

Trivedi, P., Leach, J. E., Tringe, S. G., Sa, T., and Singh, B. K. (2020). Plant-microbiome interactions: from community assembly to plant health. *Nat. Rev. Microbiol.* 18 (11), 607–621. doi: 10.1038/s41579-020-0412-1

Villalpando-Aguilar, J. L., Matos-Pech, G., López-Rosas, I., Castelán-Sánchez, H. G., and Alatorre-Cobos, F. (2022). Phage therapy for crops: concepts, experimental and bioinformatics approaches to direct its application. *Int. J. Mol. Sci.* 24 (1), 325. doi: 10.3390/ijms24010325

Vyas, (1991). Atomic features of protein-carbohydrate interactions. *Curr. Opin. Struct. Biol.* 1, 732–740. doi: 10.1016/0959-440X(91)90172-P

Wang, K., Chen, D., Liu, Q., Zhu, P., Sun, M., and Peng, D. (2022). Isolation and characterization of novel lytic bacteriophage vB_RsoP_BMB50 infecting *Ralstonia solanacearum*. *Curr. Microbiol.* 79, 245. doi: 10.1007/s00284-022-02940-3

Wang, R., Cong, Y., Mi, Z., Fan, H., Shi, T., Liu, H., et al. (2019). Characterization and complete genome sequence analysis of phage GP4, a novel lytic Bcep22-like podovirus. *Arch. Virol.* 164, 2339–2343. doi: 10.1007/s00705-019-04309-7

Wang, X., Wang, S., Huang, M., He, Y., Guo, S., Yang, K., et al. (2024). Phages enhance both phytopathogen density control and rhizosphere microbiome suppressiveness. *mBio* 15, e0301623. doi: 10.1128/mbio.03016-23

Wang, X., Wei, Z., Yang, K., Wang, J., Jousset, A., Xu, Y., et al. (2019). Phage combination therapies for bacterial wilt disease in tomato. *Nat. Biotechnol.* 37, 1513–1520. doi: 10.1038/s41587-019-0328-3

Waterhouse, A., Bertoni, M., Bienert, S., Studer, G., Tauriello, G., Gumienny, R., et al. (2018). SWISS-MODEL: homology modelling of protein structures and complexes. *Nucleic Acids Res.* 46, W296–w303. doi: 10.1093/nar/gky427

Wei, C., Liu, J., Maina, A. N., Mwaura, F. B., Yu, J., Yan, C., et al. (2017). Developing a bacteriophage cocktail for biocontrol of potato bacterial wilt. *Virol. Sin.* 32, 476–484. doi: 10.1007/s12250-017-3987-6

Wicker, E., Grassart, L., Coranson-Beaudu, R., Mian, D., Guilbaud, C., Fegan, M., et al. (2007). *Ralstonia solanacearum* strains from Martinique (French West Indies) exhibiting a new pathogenic potential. *Appl. Environ. Microbiol.* 73, 6790–6801. doi: 10.1128/AEM.00841-07

Wilcox, S. A., Toder, R., and Foster, J. W. (1996). Rapid isolation of recombinant lambda phage DNA for use in fluorescence in *situ* hybridization. *Chromosome Res.* 4, 397–398. doi: 10.1007/BF02257276

Ye, M., Sun, M., Huang, D., Zhang, Z., Zhang, H., Zhang, S., et al. (2019). A review of bacteriophage therapy for pathogenic bacteria inactivation in the soil environment. *Environ. Int.* 129, 488–496. doi: 10.1016/j.envint.2019.05.062

Zhao, Q., Geng, M. Y., Xia, C. J., Lei, T., Wang, J., Cao, C. D., et al. (2023). Identification, genetic diversity, and pathogenicity of *Ralstonia pseudosolanacearum* causing cigar tobacco bacterial wilt in China. *FEMS Microbiol. Ecol.* 99 (3), 18. doi: 10.1093/femsec/fiad018

Zheng, J., Chen, W., Xiao, H., Yang, F., Song, J., Cheng, L., et al. (2023). Asymmetric structure of podophage GP4 reveals a novel architecture of three types of tail fibers. *J. Mol. Biol.* 435, 168258. doi: 10.1016/j.jmb.2023.168258

frontiers | Frontiers in Plant Science

TYPE Original Research
PUBLISHED 23 May 2025
DOI 10.3389/fpls.2025.1554915

Check for updates

OPEN ACCESS

EDITED BY
Temoor Ahmed,
Zhejiang University, China

REVIEWED BY
Munusamy Madhaiyan,
Agency for Science, Technology and Research, Singapore
Gökhan Boyno,
Yüzüncü Yıl University, Türkiye

*CORRESPONDENCE
Xingyuan Men
menxy2000@hotmail.com

RECEIVED 03 January 2025
ACCEPTED 21 April 2025
PUBLISHED 23 May 2025

CITATION
Yang L, Li L, Song Y, Zhang Y, Yang J, Cui H, Guo W, Lv S and Men X (2025) The role of foliar endophytes in modulating southern corn rust severity: implications for biocontrol strategies. *Front. Plant Sci.* 16:1554915. doi: 10.3389/fpls.2025.1554915

COPYRIGHT
© 2025 Yang, Li, Song, Zhang, Yang, Cui, Guo, Lv and Men. This is an open-access article distributed under the terms of the Creative Commons Attribution License (CC BY). The use, distribution or reproduction in other forums is permitted, provided the original author(s) and the copyright owner(s) are credited and that the original publication in this journal is cited, in accordance with accepted academic practice. No use, distribution or reproduction is permitted which does not comply with these terms.

The role of foliar endophytes in modulating southern corn rust severity: implications for biocontrol strategies

Lujia Yang[1], Lili Li[1], Yingying Song[1], Yongsheng Zhang[2], Jie Yang[2], Hongying Cui[1], Wenxiu Guo[1], Suhong Lv[1] and Xingyuan Men[1*]

[1]Shandong Key Laboratory for Green Prevention and Control of Agricultural Pests, Institute of Plant Protection, Shandong Academy of Agricultural Science, Jinan, China, [2]College of Plant Protection, Hunan Agricultural University, Changsha, China

Southern corn rust (SCR), caused by *Puccinia polysora*, is a major foliar disease that threatens global maize production. Current SCR management strategies prioritize genetic resistance and chemical control, but how foliar endophytic fungal communities modulate host susceptibility to *P. polysora* remains poorly understood. In this study, we profiled the endophytic communities in *P. polysora*-infected and non-infected maize leaves across 14 geographically distinct regions in eastern China. Our results revealed that *P. polysora* infection significantly altered the foliar endophytic community, with infected leaves exhibiting higher operational taxonomic unit (OTU) richness (722 vs. 572 OTUs) while reducing community evenness. Diversity metrics were significantly altered, with significant reductions in Shannon diversity and Chao1 index values for non-infected states. Network analysis revealed that infection caused a notable reduction in microbial connectivity and complexity, particularly in low- and medium-susceptibility regions, where positive intertaxon associations declined by 42.6% and 35.3%, respectively. High-susceptibility region networks retained greater stability, suggesting differential microbial resilience under pathogen pressure. Redundancy analysis further demonstrated that temperature was the dominant environmental factor shaping microbial assemblages, especially under infection conditions. Notably, correlation analysis further revealed that *Alternaria* was positively associated with host resistance (r = 0.37, p = 0.05), underscoring its potential role in enhancing resistance to *P. polysora*. Conversely, *Dioszegia* and *Naganishia* were negatively correlated with resistance (r = −0.36, p = 0.056; and r = −0.34, p = 0.074, respectively), implying potential roles in facilitating infection. This study reveals key mechanistic links between foliar endophytic communities and SCR infection, providing a basis for sustainable biocontrol interventions in maize.

KEYWORDS

southern corn rust, *Puccina ploysora*, foliar endophyte fungi, microbial diversity, host-pathogen interactions

1 Introduction

Maize (*Zea mays* L.) is a globally vital crop that is integral to food security and economic stability. In China, the increasing demand for maize has prompted efforts to develop high-yielding and disease-resistant cultivars, contributing to sustained production gains. However, maize cultivation continues to face substantial threats from both biotic and abiotic stressors. Among these is southern corn rust (SCR), caused by the fungal pathogen *Puccinia polysora* Underw. (*P. polysora*), which has emerged as a major constraint, particularly in subtropical and temperate maize-growing regions (Sun et al., 2021a; Sun et al., 2023; Yang et al., 2024). Globally, SCR can cause yield losses ranging from 10% to 50% in susceptible cultivars. In 2024, SCR was responsible for an estimated loss of 244.27 million bushels of corn in the USA alone (Crop Protection Network, 2025). Since its first report in China in 1972, SCR has expanded swiftly across major maize-growing regions, now affecting more than 100 million acres annually, with approximately 19.38 million hectares subjected to chemical control measures (Ma et al., 2022; Ministry of Agriculture and Rural Affairs of the People's Republic of China, 2023). In epidemic years, yield losses can reach 50%, and their widespread distribution threatens national food security (Wang et al., 2020; Meng et al., 2020; Sun et al., 2021a; Ma et al., 2022).

The geographic spread of SCR is coupled with the rapid dissemination and capacity of the pathogen to inflict severe crop damage. While fungicides provide short-term control of SCR, their widespread application poses significant challenges, including environmental contamination, increased production costs, and the emergence of fungicide-resistant *P. polysora* strains (Ma et al., 2022; Yang et al., 2024). These concerns have intensified interest in sustainable alternatives to fungicide control. Among these, microbial-based strategies have gained attention for their ecological compatibility and potential long-term efficacy.

Foliar endophytes play a pivotal role in modulating plant health by influencing host immune responses, outcompeting pathogens for niche occupancy, and altering the leaf microenvironment to suppress disease development (Busby et al., 2013; Hardoim et al., 2015; Busby et al., 2016; Collinge et al., 2022). Community-level shifts in foliar microbiota have been shown to significantly affect disease susceptibility (Johnston-Monje and Raizada, 2011; Raghavendra and Newcombe, 2013; Busby et al., 2016; Collinge et al., 2022). A study revealed that *Exserohilum turcicum*, the causal agent of northern corn leaf blight, is associated with reduced microbial diversity, potentially compromising host resilience. This association underscores the broader role of microbial community composition in modulating plant health (Chao et al., 2025). Studies have also shown that certain *Bacillus* and *Pseudomonas* species isolated from maize leaves have antagonistic effects on *Puccinia sorghi* while simultaneously promoting systemic resistance (Sartori et al., 2017). These findings highlight the potential of harnessing the native microbiome as a sustainable strategy for enhancing crop disease resistance and reducing dependence on chemical control.

While previous studies have largely focused on endophyte–pathogen interactions under controlled conditions (Porras-Alfaro and Bayman, 2011; Liu et al., 2022), the extent to which these relationships are shaped by natural field variability remains unclear. Emerging evidence suggests that geographic variations in disease severity may have a stronger influence on the composition and functional dynamics of foliar endophytic fungal communities than pathogen–host interactions alone (Wheeler et al., 2019; Wagner et al., 2020; Tedersoo et al., 2020a, b; Tay et al., 2023; Wang et al., 2023). However, investigations into how these communities respond to *P. polysora* under natural infection pressure are notably lacking. Moreover, the role of spatial heterogeneity in modulating endophyte assemblages and its correlation with disease outcomes has not been systematically addressed. These gaps constrain the development of microbiome-informed strategies for SCR suppression and limit our capacity to harness beneficial endophytes in field-based disease management.

Given that pathogen-induced shifts in foliar endophytic fungal communities may directly influence disease trajectories, addressing these gaps represents a critical frontier in plant–microbe interaction research. A mechanistic understanding of the assembly, composition, and functional traits, particularly in the context of *P. polysora* infection, is essential for linking microbial diversity to host health and disease resistance in maize. Realizing the potential of such approaches requires detailed insights into the structure and ecological roles of endophytic communities in both infected and non-infected tissues and how these roles are related to gradients of disease severity.

This study aims to elucidate the ecological dynamics of foliar endophytic fungal communities in maize under natural *P. polysora* infection and to determine how shifts in community composition correlate with disease severity. We hypothesize that common endophytic fungi present in both healthy and *P. polysora*-infected maize leaves influence SCR severity through shifts in community composition and functional interactions. To test this hypothesis, we i) characterize the taxonomic composition, richness, and diversity of foliar endophytic communities in healthy versus infected leaves using high-throughput internal transcribed spacer (ITS) amplicon sequencing; ii) examine the relationships between community structure and the relative disease index (RDI) across a gradient of field infection severity; iii) identify keystone taxa and ecological interactions using co-occurrence network analysis and random forest modeling; and iv) assess the role of environmental drivers, such as temperature, humidity, and rainfall, in shaping endophytic community assembly and disease dynamics. By identifying key fungal taxa that potentially suppress or promote SCR, we provide a framework for developing sustainable, microbiome-informed biocontrol strategies.

2 Materials and methods

2.1 Study locations, maize material collection, and disease assessment

Maize plants were sampled and assessed during the 38th to 40th weeks of the year (the grain-filling stage) across 14 geographically

distinct regions in Shandong Province, China (Figures 1A, C) (Yang et al., 2024). At each sampling site, six leaves were collected from healthy maize plants, alongside six leaves from *P. polysora*-infected plants. Infected leaves were selected based on lesion coverage of 40%–60% of the leaf area with *P. polysora* pustules (Figure 1B). All samples were taken and assessed from the fourth leaf up from the base of each plant (Yang et al., 2024). The samples were immediately placed in sterile bags and transported to the laboratory on dry ice to preserve microbial integrity.

2.1.1 Endophyte sample collection

To eliminate epiphytic microorganisms and remove *P. polysora* pustules from the leaf surface, a rigorous sterilization and washing protocol was applied. Approximately 2 g of plant tissue was excised from each sample and initially rinsed with sterile water to remove surface debris. For infected samples, leaf tissues were immersed in 1× phosphate-buffered saline (PBS) and vibrated for 1 h to facilitate the detachment of *P. polysora* uredinia into the solution. All the samples were subsequently surface sterilized by sequential

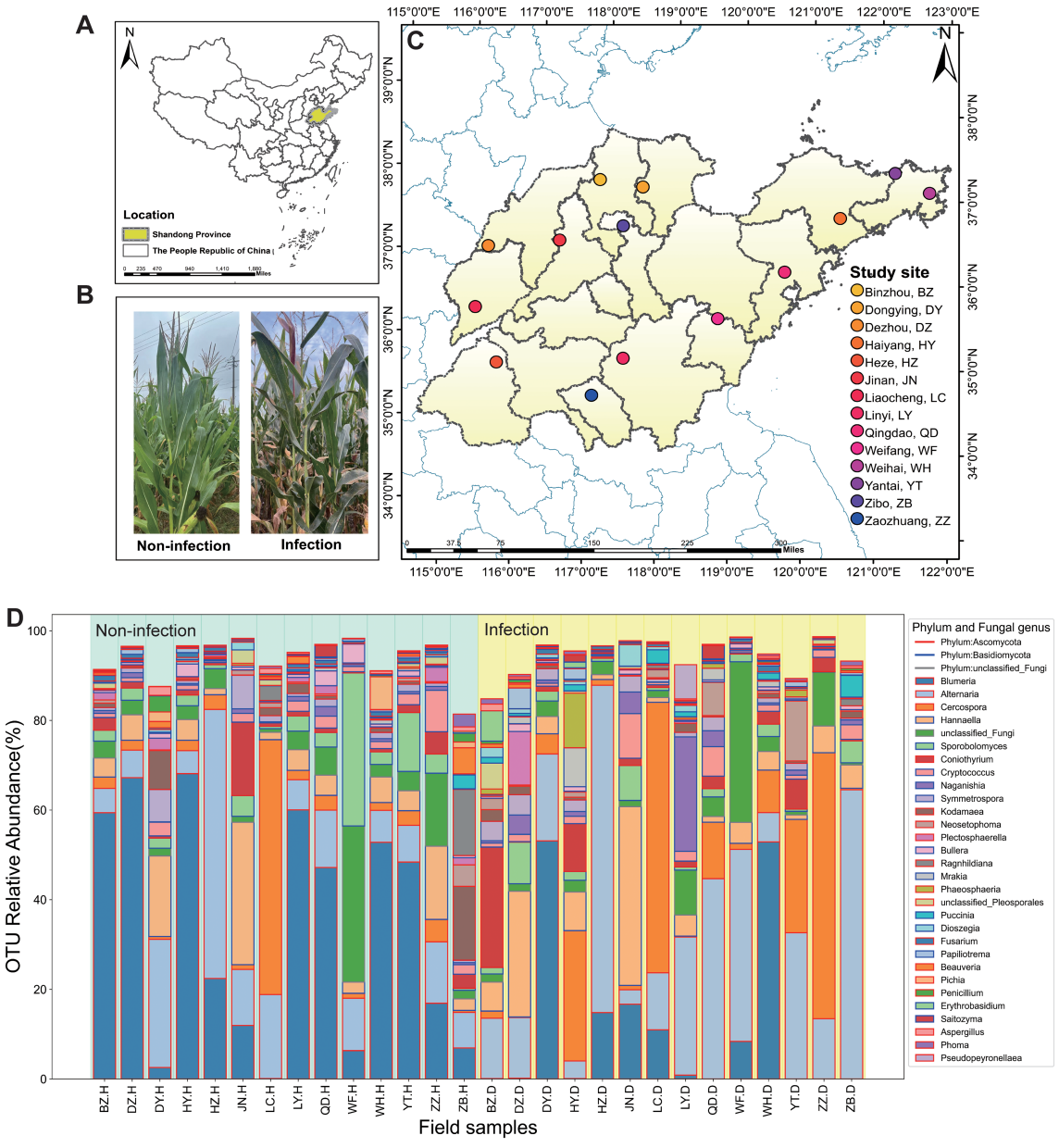

FIGURE 1
Foliar endophytes across the study location are compositionally variable. **(A)** The location of Shandong Province in China. **(B)** Non-infection (H) and infection (D) symptoms of southern corn rust (SCR) of maize in the field. **(C)** Multiple sampling sites in Shandong Province. **(D)** The operational taxonomic unit (OTU) relative abundance within non-infected and *Puccinia polysora*-infected samples at the phylum level and genus level are shown for taxa with >1% mean relative abundance across all sites. Field samples are grouped along the x-axis by study, with color-coded site labels located above the bars. The lines represent different phyla, and the different colored columns represent the taxonomic units of different fungal genera.

immersion in 70% ethanol for 1 min and 2% sodium hypochlorite for 5 min, followed by three rinses in sterile distilled water (Yang et al., 2023). To ensure the complete removal of residual disinfectants, the tissues were additionally washed three times with 1× PBS and then air-dried under sterile conditions. The sterilized leaf tissues were then frozen at −80°C for subsequent DNA extraction.

2.1.2 Disease and regional susceptibility assessment

For disease assessment, *P. polysora*-infected maize leaves were evaluated once at each sampling site during the same collection period. A 5-point survey method was employed, in which 10 maize plants per site were assessed. Evaluations began from the fourth leaf above the base of each plant. The number of infected leaves and the severity of infection were visually recorded. Disease severity was classified on the basis of the percentage of leaf area covered by *P. polysora* pustules, using the following scale: level 0 (0%), level 1 (1%–5%), level 3 (6%–25%), level 5 (26%–50%), level 7 (51%–75%), and level 9 (76%–100%) (Yang et al., 2024). The disease index (DI) (Equation 1) values obtained from each assessed site depict the severity of the SCR (Madden et al., 2017; Yang et al., 2023):

$$\text{Disease index DI\%} = \sum \frac{(\text{No. of diseased leaves} \times \text{disease grade per leaf})}{\text{Total no. of disease leaves} \times \text{highest disease grade}} \times 100 \quad (1)$$

The RDI (Equation 2) was computed to normalize SCR susceptibility across regions (Xu and Hu, 2015):

$$\text{Relative disease index (RDI)} = 1 - \frac{\text{The DI of each study site}}{\text{The highest DI of all study sites}} \quad (2)$$

The regions were categorized on the basis of RDI values (0–1) as follows: high-susceptibility (HS) regions, RDI < 0.20; medium-susceptibility (MS) regions, 0.20 ≤ RDI < 0.50; low-susceptibility (LS) regions, 0.50 ≤ RDI < 0.80; and high-resistance (HR) regions, 0.80 ≤ RDI ≤ 1.00.

2.2 DNA extraction and high-throughput sequencing protocol

Total genomic DNA was extracted from maize leaf tissues via a modified cetyltrimethylammonium bromide (CTAB) protocol (Yang et al., 2023). Leaf samples were transferred into 2-mL microcentrifuge tubes and ground in liquid nitrogen. Preheated 2% CTAB extraction buffer was then added, and the mixture was incubated at 65°C for 1 h with random mixing. Following incubation, an equal volume of phenol to chloroform:isoamyl alcohol (24:1) was added to each tube, and the samples were centrifuged at 10,000 rpm for 10 min. The upper aqueous phase ensuring no visible cloudiness was transferred to new 1.5-mL tubes. DNA was precipitated by adding 0.6 volumes of isopropanol and incubating at −20°C for 1 h (Abeywickrama et al., 2023). The DNA pellet was collected by centrifugation at 12,000 rpm for 10 min, washed twice with 70% ethanol, dried under vacuum, and resuspended in 20–30 μL of Tris-EDTA (TE) buffer containing RNase. DNA concentrations were quantified via a NanoDrop 2000 spectrophotometer (Thermo Fisher Scientific, Waltham, MA, USA), and DNA quality was evaluated via 1% agarose gel electrophoresis.

High-throughput sequencing (HTS) amplicon sequencing was used to identify endophytic fungal taxa within maize leaf tissues following established protocols (Pérez-Jaramillo et al., 2018; Xia et al., 2020). Individual morphotypes were selected for molecular identification based on the amplification of the ITS region of the nuclear ribosomal DNA (rDNA). The ITS region was targeted using the primers ITS1-F and ITS2-R and subsequently used for amplicon library preparation (Smith and Peay, 2014). PCR amplification was performed in a 30-μL reaction volume containing 15 μL of 2×Hieff® Robust PCR master mix (Yeasen, Shanghai, China), 1 μL each of primers (forward and reverse), 20 ng of DNA template, and nuclease-free water to the final volume. The thermal cycling conditions were as follows: initial denaturation at 94°C for 3 min; 25 cycles of denaturation at 94°C for 30 s, annealing at 55°C for 30 s, and extension at 72°C for 30 s; and a final extension at 72°C for 5 min.

Amplicons were purified using AMPure XP magnetic beads and quantified using a Qubit fluorometer, and dual-index barcodes were ligated to each sample following the standard Illumina library preparation protocol (Nilsson et al., 2019). Equimolar amounts of purified amplicons were pooled and sequenced using the Illumina MiSeq platform (Illumina, San Diego, CA, USA) with a 2 × 250 bp paired-end configuration, generating approximately 45,000 raw reads per sample. The raw sequence data were subjected to quality filtering using the QIIME2 (version 2024.2) and USEARCH pipelines. Low-quality reads with a Phred score < Q30, ambiguous bases, or read lengths < 200 bp were discarded. Paired-end reads were merged using a minimum 20-bp overlap and a maximum mismatch rate of 10%. Chimeric sequences were identified and excluded using UCHIME. After sequencing, the raw reads were quality-checked, and regions with a base error probability > 5% were trimmed using GENEIOUS 6.1.7 (Kearse et al., 2012). Paired-end reads were assembled into consensus sequences, and chimeric sequences were removed.

2.3 Data processing and bioinformatics analysis

2.3.1 OTU clustering, taxonomic assignment, and database validation

Cleaned sequences were clustered into operational taxonomic units (OTUs) at a 97% similarity threshold using the URAPE algorithm against the UNITE fungal ITS reference database (Wagner et al., 2020). Taxonomic assignments were performed using QIIME2. OTUs with fewer than 10 reads were excluded to reduce analytical noise and enhance result robustness.

To ensure taxonomic accuracy, OTUs were annotated to the genus level only if they shared ≥95% sequence identity with a reference, whereas species-level assignments required ≥99% identity and ≥90% alignment coverage (Raja et al., 2017). For validation, a subset of high-abundance OTUs was subjected to BLAST searches against the NCBI nucleotide database (https://blast.ncbi.nlm.nih.gov/Blast.cgi). Only OTUs with consistent genus-level classification across both databases were retained for ecological interpretation.

2.3.2 Diversity indices and community analysis

To investigate the influence of *P. polysora* infection on the endophytic community composition, both alpha and beta diversity indices were computed. Differential abundance analysis between non-infected and *P. polysora*-infected samples was conducted using Python (v.3.9.0). OTUs with statistically significant differences ($p < 0.05$) were identified as potential indicators of SCR susceptibility. Alpha diversity indices, including the ACE, Chao1, Shannon, and Simpson indices, were used to evaluate the richness and evenness within samples. Fungal richness and abundance were defined as the average number of OTUs and isolates per sample, respectively, and were calculated using Species Diversity and Richness v4.0 (Martins et al., 2021). Beta diversity was assessed using the Bray–Curtis and weighted UniFrac dissimilarity indices. Community composition differences between the infected and non-infected groups were visualized through principal coordinate analysis (PCoA). These analyses provide insights into how SCR infection influences the composition and diversity of maize foliar fungal endophytes under natural field conditions.

2.4 Statistical analysis

2.4.1 Diversity and community composition

Microbial diversity differences were analyzed using an analysis of variance (ANOVA) in Python (v.3.9.0), with *post-hoc* comparisons using Tukey's honestly significant difference (HSD) test ($p < 0.05$). To quantitatively link shifts in endophytic diversity to *P. polysora* infection, permutational multivariate analysis of variance (PERMANOVA) was employed to assess the effects of infection status and sampling site on community variance. Pearson's correlation analysis was used to explore the relationship between endophytic diversity and SCR severity.

2.4.2 Network analysis

Co-occurrence network analysis was used to identify potential synergistic or antagonistic interactions among fungal genera during *P. polysora* infection. Networks were constructed to compare microbial interactions in infected vs. non-infected samples and to detect keystone taxa that formed ecological hubs. Functional and phylogenetic structural shifts were evaluated to reveal community-level reorganization and adaptation in relation to SCR severity.

2.4.3 Differential abundance and functional analysis

Redundancy analysis (RDA) was performed using the Hellinger-transformed OTU data to evaluate the effects of *P. polysora* infection and abiotic factors [temperature (T), rainfall (R), and relative humidity (RH)] on endophytic fungal communities. RDA was conducted in Python using linear regression followed by principal component analysis (PCA) of the fitted values. The statistical significance of the model and constrained axes was evaluated using permutation tests (n = 999). The relative contribution of each explanatory variable was visualized via ordination plots with fitted environmental vectors.

To identify endophytic taxa and functional pathways associated with infection, a random forest algorithm was used to identify the most critical fungal OTUs for distinguishing infected from non-infected samples, with the mean decrease in Gini impurity quantifying each OTU's importance (Martins et al., 2021). Specific OTUs associated with *P. polysora*-infected and non-infected samples were identified, offering insights into microbial roles in disease suppression or facilitation (Hardoim et al., 2015). Fungal OTUs were categorized as commensal (no host effect), beneficial (promoting growth or protection), or pathogenic (including latent pathogens). After grouping, the changes in fungal abundance and richness of each functional group across different disease susceptibilities were determined among the LS, MS, and HS regions. Regression analysis and ANOVA were then applied to correlate the relative abundance of fungal OTUs identified by the random forest with the RDI.

3 Results

3.1 Differences in fungal community composition between non-infected and *P. polysora*-infected maize leaves

At both the OTU and genus levels, the fungal community composition differed between non-infected and *P. polysora*-infected maize leaves. Compared with non-infected leaves, infected leaves harbored a greater number of OTUs (n = 722; n = 572), reflecting an infection-induced expansion of the foliar endophytic community. The fungal communities in both groups were dominated by members of the phyla Ascomycota (non-infection = 62.76%, infection = 63.02%) and Basidiomycota (non-infection = 29.90%, infection = 32.55%). The Ascomycota phylum is composed of the key genera *Blumeria*, *Alternaria*, and *Cercospora*, whereas Basidiomycota is represented by the genera *Hannaella*, *Sporobolomyces*, and *Cryptococcus*, each displaying distinct distribution patterns under healthy and infected conditions (Figure 1D).

Non-infected samples were characterized by relatively uniform community structures, with dominant genera including *Bullera*

(33.6%), *Alternaria* (14.62%), *Cercospora* (6.13%), *Hannaella* (7.73%), *Sporobolomyces* (5.52%), *Coniothyrium* (2.60%), *Cryptococcus* (2.13%), and *Puccinia* (0.31%) (Figure 1D). In contrast, infection induced a shift in fungal community structure, with increased relative abundances of *Alternaria* (26.76%), *Cercospora* (14.75%), *Hannaella* (8.30%), *Coniothyrium* (4.21%), *Cryptococcus* (2.29%), and *Puccinia* (1.01%).

At the species level, *Blumeria graminis*, *Cercospora coniogrammes*, *Hannaella sinensis*, *Naganishia albida*, and *Kodamaea ohmeri* were consistently present across multiple sites, with higher abundances observed in infected leaves compared to non-infected leaves (Supplementary Figure S1). While most sites presented increased fungal richness in infected leaves, the patterns were site-specific, suggesting that *P. polysora* infection may drive localized shifts in endophytic community composition and diversity.

3.2 Diversity analysis of endophytic fungal communities

Comparative diversity analyses revealed substantial differences in the fungal community between the non-infected and *P. polysora*-infected groups. At the genus level, the non-infected samples contained 49 unique genera, whereas the infected samples contained 86 unique genera, with 222 genera shared between the two groups (Figure 2A). These findings suggest that pathogen infection may facilitate the recruitment or activation of rare or dormant fungal taxa. Analysis of fungal richness across sites revealed that 64% of the regions presented relatively high fungal richness in non-infected samples (Figure 2B). Alpha diversity further highlighted significant differences. Both ACE and Chao1 indices were lower in the infected samples (Figures 2C, D), indicating reduced species richness. In contrast, the Shannon index slightly increased fungal diversity in the infected samples, suggesting that infection increased community heterogeneity (Figure 2E). The Simpson index was marginally greater in non-infected samples (Figure 2F), reflecting greater evenness in the healthy state.

Beta diversity analysis, as visualized by PCoA, revealed distinct clustering between the non-infected and infected groups. Weighted UniFrac distances revealed that PCo1 and PCo2 explained 38.76% and 12.35% of the variance, respectively (Figure 2G), with 71% of the non-infected individuals forming a distinct cluster. Similar clustering patterns were observed via the Bray–Curtis dissimilarity (PCo1 = 26.28%, PCo2 = 13.65%), with 78% of the non-infected samples clustering into a single group (Figure 2H).

3.3 Foliar endophyte abundance across SCR susceptibility regions and environmental correlations

The DI values clearly classified the 14 sites based on their susceptibility to SCR, revealing significant variation across the HS, MS, and LS regions (Figure 3A). The DI values ranged from 48.42 to 58.29 for the HS regions (HY, JN, LY, WF, and ZZ), 31.76 to 45.46 for the MS regions (BZ, DY, DZ, LC, and QD), and 18.86 to 26.98 for the LS regions (HZ, WH, YT, and ZB) (Figure 3A). Across all categories, *P. polysora* infection led to a significant reduction in OTU richness (Figure 3B). In the non-infected state, the HS and MS regions presented greater richness than the LS regions, with a significant difference observed between the MS and LS regions ($p < 0.001$ and $p < 0.05$) (Figure 3B). Under infection, the OTU richness was significantly greater in the HS regions than in the LS regions ($p < 0.001$), whereas no significant differences were detected between the MS regions and either the HS or LS regions (Figure 3B).

Pearson's correlation analysis between the OTUs and DI showed negative correlations in the HS regions ($r = -0.35$) and LS regions ($r = -0.73$), whereas the MS regions displayed a positive correlation ($r = 0.30$). In the infection samples, the HS regions still presented a weak negative correlation ($r = -0.33$), the MS regions presented a moderate positive correlation ($r = 0.42$), and the LS regions presented a weaker negative correlation ($r = -0.38$) (Figure 3C).

The Shannon diversity for both the infection and non-infection states was analyzed in relation to the DI, and the results revealed that, in the non-infection state, the HS regions showed a slight positive correlation ($r = 0.27$), whereas the MS regions exhibited a significantly negative correlation ($r = -0.91$, $p = 0.034$), indicating that greater fungal diversity in the non-infected samples was associated with lower disease severity in the MS regions. The LS regions displayed a weaker positive correlation ($r = 0.40$). In the infection state, the HS regions presented a moderate positive correlation ($r = 0.74$), suggesting that greater diversity in infected samples may correspond to greater disease severity. The MS regions showed a moderate negative correlation ($r = -0.38$), whereas the LS regions demonstrated a weak negative correlation ($r = -0.18$) (Figure 3D).

RDA revealed that under non-infected conditions, T and R were the primary environmental variables influencing community structure, with JN and ZZ showing unique microbial structures (Figure 3E). The overall variance explained by the first two axes (34.3%) suggested moderate environmental filtering of fungal endophytes in non-infected maize leaves (Figure 3E). In the infected group, T emerged as the dominant environmental factor, showing the longest gradient vector and strongest alignment with samples (LC and JN). In contrast, RH and R appeared to decrease, indicating that biotic stress may override the influence of microclimatic factors under pathogen pressure. DI exhibited a strong directional effect, suggesting that disease severity reshaped the endophytic community. The distinct spatial separation of samples along the RDA1 axis highlights the role of temperature and DI in driving microbial reassembly during SCR infection (Figure 3F).

3.4 Network analysis of the foliar endophytic community

Microbial co-occurrence networks were constructed to explore interactions among fungal genera under non-infected and infected conditions. The networks revealed distinct structural differences between the two groups. In non-infected samples, the endophytic fungal community exhibited a dense network with numerous significant positive correlations ($p < 0.05$), suggesting stable and

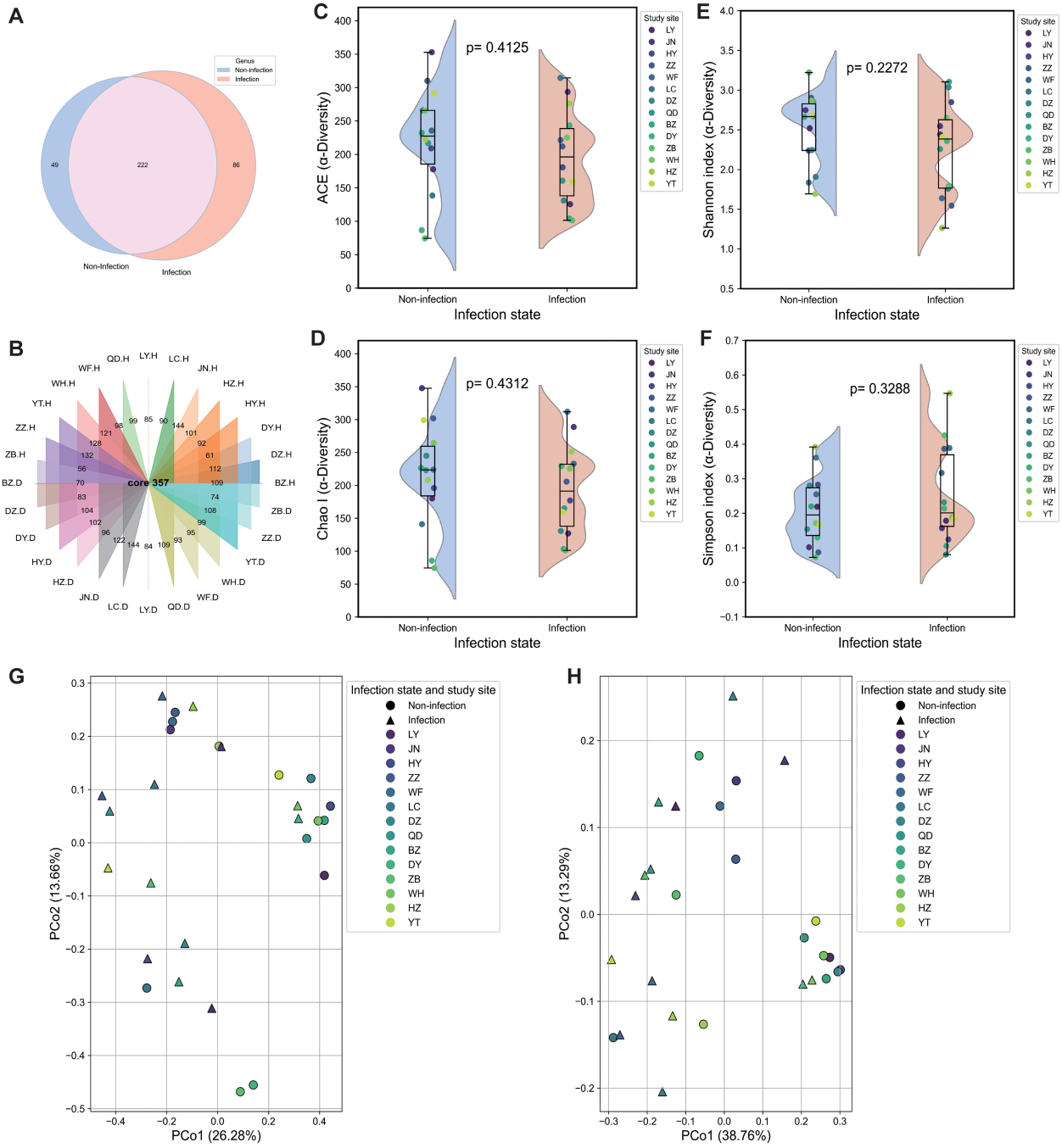

FIGURE 2
Differential analysis of fungal microbial communities and diversity. **(A)** Total analysis of genera in the non-infected and infected groups. **(B)** Analysis of genera associated with non-infected and infected states at each sampling site. **(C)** ACE index. **(D)** Chao index. **(E)** Shannon index. **(F)** Simpson index. Box plots depict medians (central horizontal lines), interquartile ranges (boxes), 95% confidence intervals (whiskers), and outliers (dots). Statistically significant differences between pairs of values are shown over horizontal lines. *p*-Values indicate statistically significant differences between the non-infected and infected samples. **(G, H)** Principal coordinate analysis (PCoA) plots based on weighted UniFrac **(G)** and Bray–Curtis **(H)** dissimilarity of non-infected and infected fungal communities at the study sites.

cooperative interactions among endophytic taxa (Figure 4A). In contrast, the infection network showed a reduction in connectivity, with a higher proportion of non-significant correlations, indicating a disruption of microbial interactions under infection stress (Figure 4B).

Networks from the HS, MS, and LS regions further highlighted site-specific differences. Among the non-infected networks, the HS regions displayed the most highly connected network, followed by the MS and LS regions (Figures 4C–E). Upon infection, these networks exhibited reduced connectivity, with the HS regions maintaining higher connectivity than the MS and LS regions (Figures 4F–H). Some OTUs emerged as hubs-larger nodes with multiple connections, which are

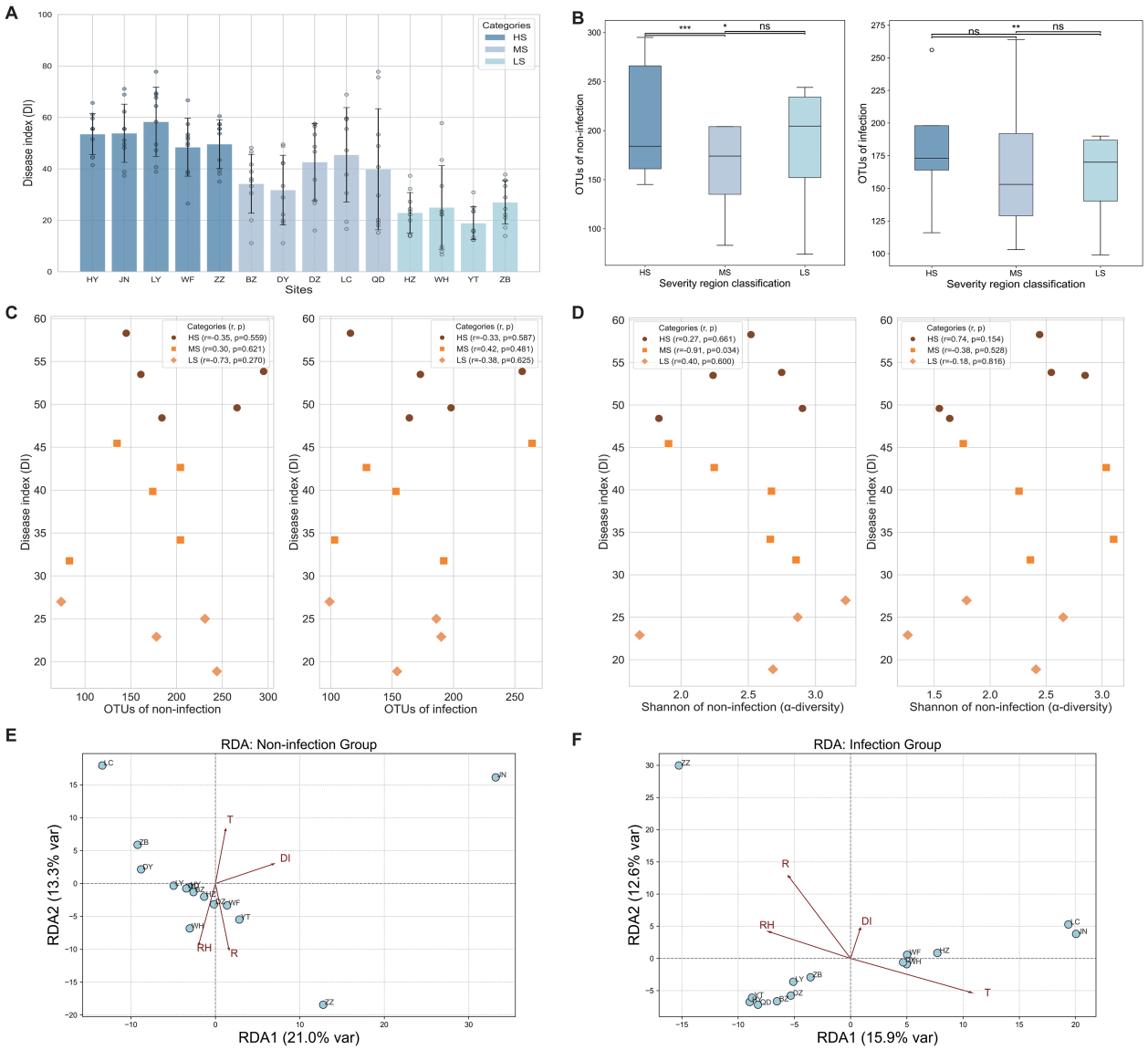

FIGURE 3
Microbial diversity and its relationship with disease severity across regions of varying susceptibility. **(A)** Disease index (DI) of southern corn rust (SCR) as the means of replicates (n = 10), displaying Standard error (SE) values across 14 study sites. **(B)** Number of operational taxonomic units (OTUs) of non-infected and infected samples observed in regions exhibiting different levels of disease severity. Box plots depict medians (central horizontal lines), interquartile ranges (boxes), 95% confidence intervals (whiskers), and outliers (dots). Statistically significant differences between pairs of values are shown over horizontal lines. Statistical significance among high susceptibility (HS), medium susceptibility (MS), and low susceptibility (LS) was evaluated using Tukey's honestly significant difference (HSD) test, with differences deemed significant at $*p < 0.05$, $**p < 0.01$, and $***p < 0.001$. **(C)** Correlations between OTUs and DI in the HS, MS, and LS regions. **(D)** Correlations between alpha diversity (Shannon index) and DI in the HS, MS, and LS regions. **(E, F)** Redundancy analysis (RDA) of foliar endophytic fungal community composition in relation to environmental variables under non-infected and *Puccinia polysora*-infected conditions. The scattered points represent different study regions, and T, RH, and R represent temperature, relative humidity, and rainfall, respectively.

likelyto represent key taxa that underpin network stability and functionality.

3.5 Correlation analysis between specific OTUs and the relative disease index

The random forest model revealed that OTU2 (*Alternaria*) and OTU5 (*Hannaella*) were the most influential taxa shaping community structure in both the non-infected and infected groups (Figures 5A, B). In the non-infected group, OTU15 (*Dioszegia*), OTU16 (*Plectosphaerella*), and OTU17 (*Naganishia*) were the main contributors to the microbial community structure (Figure 5A); in the infected group, OTU26 (*Puccinia*) and OTU39 (*Phaeosphaeria*) also emerged as major contributors (Figure 5B). These relationships, although moderate, were consistent across the sampling sites, suggesting a potentially conserved ecological role of these genera in SCR infection.

10.3389/fpls.2025.1554915

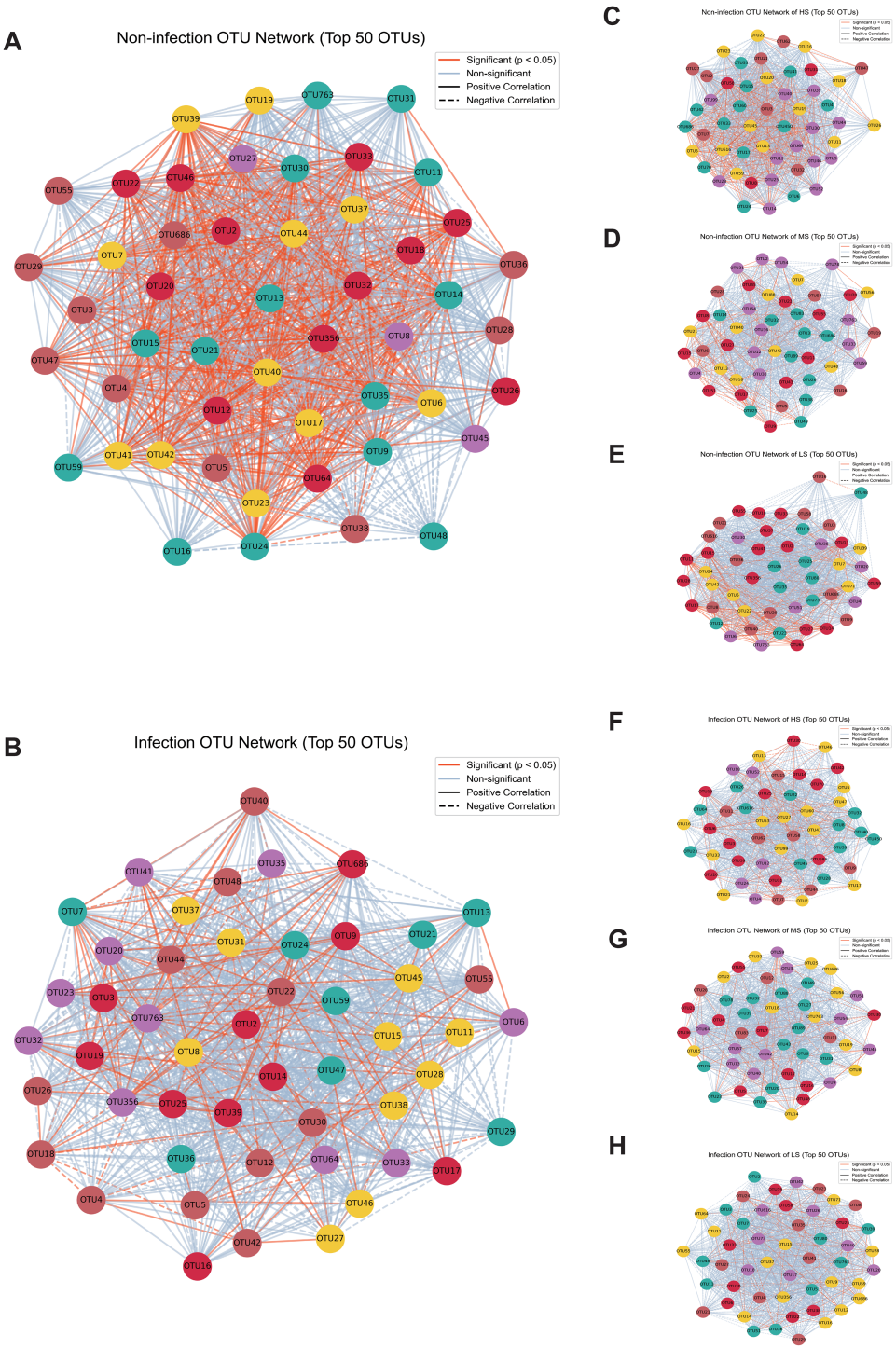

FIGURE 4
Microbial co-occurrence networks in infection and non-infection conditions across regions with high susceptibility (HS), middle susceptibility (MS), and low susceptibility (LS). **(A)** The microbial co-occurrence network under non-infection conditions. **(B)** The microbial co-occurrence network during *Puccinia polysora* infection. **(C, E, G)** The microbial co-occurrence network at the HS, MS, and LS regions under non-infection conditions. **(D, F, H)** The microbial co-occurrence network at the HS, MS, and LS regions under infection conditions. The orange lines indicate statistically significant correlations ($p < 0.05$), and the light blue lines represent non-significant correlations between operational taxonomic units (OTUs). The solid lines indicate positive correlations, and the dashed lines indicate negative correlations between OTUs.

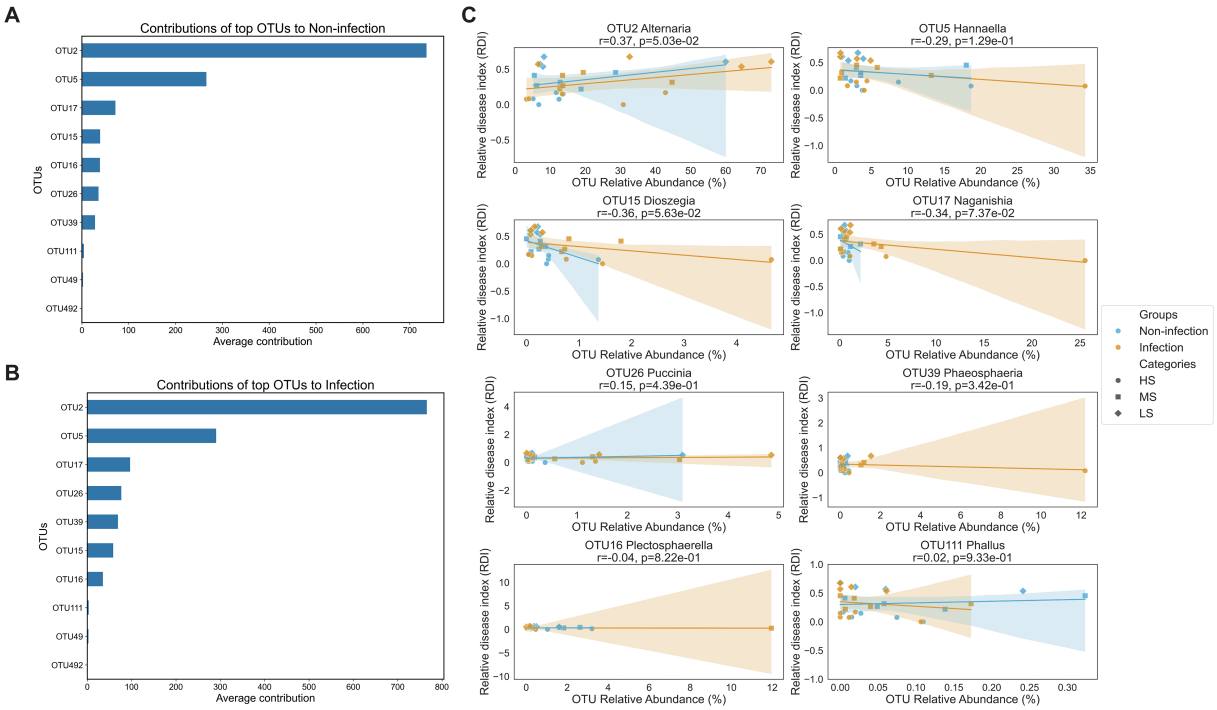

FIGURE 5
Functional prediction of foliar endophyte abundance and southern corn rust (SCR) severity. **(A, B)** Relative importance of the top 10 operational taxonomic units (OTUs) for predicting the severity of SCR as identified by random forest analysis, comparing the mean contribution values between the non-infected and infected groups. **(C)** Correlations between the relative abundances of eight high-prevalence fungal OTUs and the relative disease index (RDI) of the SCR associated with resistance. The symbols are colored according to the sampling site and shaped to indicate the SCR severity region categories (HS, MS, and LS). Each panel displays a linear regression line with a shaded area representing the 95% confidence interval. Pearson's correlation coefficients (r) and corresponding *p*-values are provided for high-prevalence OTUs.

Correlation analyses revealed distinct association patterns between specific OTUs and RDI, where higher RDI values corresponded to increased resistance. Approximately 39% of the OTUs were associated with increased disease severity, whereas 61% were linked to potential roles in disease suppression. OTU2 was significantly positively correlated with RDI (r = 0.37, p = 0.05), suggesting its potential role in promoting host resistance to *P. polysora*. Conversely, OTU15 and OTU17 showed moderate negative correlations with RDI (r = −0.36, p = 0.056; and r = −0.34, p = 0.074, respectively), and the remaining OTUs exhibited weak or no significant associations (Figure 5C). Notably, the correlations tended to be stronger in the infected group than in the non-non-infected group, implying that microbial dynamics are more predictive of disease severity under pathogen pressure.

4 Discussion

4.1 Composition and diversity of foliar endophytes in maize

This study provides a comprehensive characterization of foliar fungal endophytic communities in maize under natural field conditions, comparing healthy (non-infected) and diseased (*P. polysora*-infected) states. Marked differences in community composition and relative abundance were observed between infection states, with variation also evident across geographically distinct sites. Genera such as *Alternaria*, *Blumeria*, *Hannaella*, *Naganishia*, and *Dioszegia* were consistently abundant across multiple sites, suggesting possible roles in disease progression or opportunistic colonization of infected tissues. Diversity analyses revealed that *P. polysora* infection significantly increased fungal richness but reduced community evenness, indicating a skewed proliferation of certain taxa in infected tissues, facilitated by pathogen-induced niche openings or host immune suppression. The PCoA results further supported the infection-driven restructuring of fungal communities, marked by an increased abundance of select genera, potentially contributing to disease progression and host stress responses. These findings emphasize the dual role of endophytic fungi during disease development, which act as mutualistic symbionts under healthy conditions while potentially transitioning into opportunistic pathogens under stress (Raghavendra and Newcombe, 2013; Abeywickrama et al., 2023; Zhang et al., 2018).

The regional patterns of foliar endophytic fungal richness followed a trend of LS < MS < HS, with a 1.3-fold increase observed between the LS and HS regions. This difference suggests that local foliar endophytes change in relation to the severity of the disease. Fungal richness was significantly greater in *P. polysora*-infected samples from the HS regions than in those from the LS

regions, suggesting pathogen-driven community expansion. However, the correlation between OTU richness and DI showed divergent patterns across susceptibility levels, with the LS regions showing a strong negative trend ($r = -0.73$), although the difference was not statistically significant, likely due to the limited sample size. These findings support the hypothesis that fungal diversity increases with disease progression (Wagner et al., 2020; Martins et al., 2021) and highlight the importance of site-specific microbial dynamics in shaping host–pathogen interactions. These results underscore the critical role of foliar endophytes in SCR infections and plant stress responses, providing a foundation for future investigations into their potential applications in disease prevention and management strategies.

4.2 Network analysis of microbial interactions

Co-occurrence network analysis revealed core fungal genera shared among multiple study sites, suggesting that the presence of conserved taxa is critical for maintaining host health and mediating responses to *P. polysora* infection, revealing the profound effects of *P. polysora* infection on community stability and diversity. Under non-infected conditions, microbial networks were dense and cooperative, reflecting the stability and connectivity of endophytic fungal communities in healthy hosts. The microbial networks from the HS regions presented the highest connectivity, followed by those from the MS and LS regions, indicating site-specific differences in network complexity. Upon infection, network connectivity declined significantly, characterized by fewer significant correlations and fragmented networks. This destabilization was particularly evident in the LS and MS regions, whereas the HS regions retained greater connectivity, suggesting that certain endophytic fungal communities exhibit greater resistance to infection. The shifts in endophytic fungal diversity and network stability observed in response to *P. polysora* infection are broadly consistent with previous reports in other pathosystems (Wagner et al., 2020; Ampt et al., 2022), such as corn leaf blight in maize (Chao et al., 2025), *Melampsora* rust in poplar (Raghavendra and Newcombe, 2013), and powdery mildew in pumpkin (Zhang et al., 2018). This shift toward a more heterogeneous and unstable microbial network could compromise the functional resilience of the microbiome, thereby influencing disease progression and plant fitness. This finding suggests that infection-driven perturbations reshape endophytic community dynamics and highlight keystone taxa as potential targets for biocontrol interventions aimed at disease suppression or mitigation.

4.3 Associations of specific fungal genera with SCR susceptibility

Keystone taxa emerged as critical nodes within microbial networks, maintaining community structure and functionality. The infection-induced loss or diminished connectivity of these keystone taxa underscores their importance in sustaining microbial stability (Ampt et al., 2019, 2022). Our findings demonstrate that specific fungal genes are distinctly associated with SCR severity, highlighting the functional divergence of endophytic fungal communities in non-infected and infected states. *Alternaria* emerged as a dominant genus in both healthy and infected tissues, and its positive correlation with disease severity suggests that it may act as a latent pathogen or disease-facilitating endophyte. This dual role aligns with previous observations (Busby et al., 2016), where *Alternaria* enriched under stress may serve as a competitive colonizer or conditionally pathogenic taxon. Furthermore, 60% of the genera were identified as potential protective agents, likely modulating host resistance to *P. polysora*, underscoring their potential as biocontrol agents for targeted disease management. The core genera identified here have been consistently reported in maize studies across diverse environments (Johnston-Monje and Raizada, 2011; Busby et al., 2016; Chao et al., 2025), suggesting a degree of ecological generalizability. These data support the concept of disease-modulating endophytic consortia and emphasize the need for functional validation of candidate taxa. While further validation is needed, the selective enrichment of beneficial endophytes through microbial inoculants or cropping practices could increase maize resilience.

4.4 Environmental and geographic factors shaping endophytic communities

Our results also revealed that shifts in foliar endophytic communities in response to *P. polysora* infection were modulated by environmental and geographic factors. Regional variation in pathogen pressure, along with local microclimatic conditions such as temperature and humidity, contributed to the observed differences in both disease severity and microbial community composition. These results suggest that pathogen stress amplifies the influence of environmental variables on endophyte assembly, driving spatial heterogeneity in community dynamics and disease outcomes. Although sampling was standardized at the grain-filling stage, unaccounted seasonal and weather-related fluctuations may further shape the microbial structure and confound infection effects. These findings emphasize the importance of incorporating site-specific environmental variables into predictive models of SCR risk and microbiome dynamics in future research. Such models could facilitate the disentanglement of the direct effects of endophytic communities on SCR progression from the indirect effects of environmental drivers.

5 Conclusions

This study highlights the critical role of foliar endophytic community restructuring in mediating maize resistance to SCR under natural environmental conditions. By linking changes in SCR severity to shifts in foliar endophytic communities, we provide novel insights into the maize–*P. polysora* pathosystem. Core fungal

genera such as *Alternaria* and *Kodamaea* have emerged as key modulators of disease severity, whereas *Hannaella* and *Naganishia* have been implicated in disease facilitation, offering a nuanced understanding of the dual roles of endophytes in host–pathogen interactions. The identification of fungal taxa with potential biocontrol activity presents opportunities for the development of sustainable disease management strategies. Future studies should incorporate multi-seasonal sampling, controlled inoculation experiments, and detailed microclimatic monitoring to better understand the ecological mechanisms shaping the foliar microbiomes of maize. Functional validation of candidate taxa through culture-dependent methods and *in planta* assays will be critical for confirming their biocontrol potential. Additionally, predictive models incorporating host–microbiome interactions under varying environmental conditions could offer critical insights into endophyte-mediated plant defense mechanisms. Such efforts will facilitate the development of targeted biocontrol strategies that leverage the natural variability in fungal communities to mitigate the severity of SCR and increase crop resilience.

Data availability statement

The original contributions presented in the study are publicly available. This data can be found here: NGDC, PRJCA040135 https://ngdc.cncb.ac.cn/gsa.

Author contributions

LY: Conceptualization, Data curation, Investigation, Methodology, Software, Writing – original draft, Writing – review & editing. LL: Conceptualization, Methodology, Writing – review & editing. YS: Writing – review & editing. YZ: Data curation, Writing – review & editing. JY: Data curation, Writing – original draft. HC: Validation, Visualization, Writing – review & editing. WG: Writing – review & editing. SL: Validation, Visualization, Writing – review & editing. XM: Funding acquisition, Project administration, Supervision, Writing – original draft, Writing – review & editing.

Funding

The author(s) declare that financial support was received for the research and/or publication of this article. This research was funded by the National Key R&D Program of China (2023YFD1400800) and the National Natural Science Foundation of China (32202316).

Conflict of interest

The authors declare that the research was conducted in the absence of any commercial or financial relationships that could be construed as a potential conflict of interest.

Generative AI statement

The author(s) declare that no Generative AI was used in the creation of this manuscript.

Publisher's note

All claims expressed in this article are solely those of the authors and do not necessarily represent those of their affiliated organizations, or those of the publisher, the editors and the reviewers. Any product that may be evaluated in this article, or claim that may be made by its manufacturer, is not guaranteed or endorsed by the publisher.

Supplementary material

The Supplementary Material for this article can be found online at: https://www.frontiersin.org/articles/10.3389/fpls.2025.1554915/full#supplementary-material

SUPPLEMENTARY FIGURE 1
The relative abundance of fungal species across different sampling sites under infection and non-infection states. The size of the bubbles indicates the relative abundance of each species, and the color gradient reflects their abundance levels, with yellow representing higher abundance and blue representing lower abundance.

References

Abeywickrama, P., Qian, N., Jayawardena, R., Li, Y., Zhang, W., Guo, K., et al. (2023). Endophytic fungi in green manure crops; friends or foe? *Mycosphere* 14, 1–106. doi: 10.5943/mycosphere/14/1/1

Ampt, E. A., Francioli, D., van Ruijven, J., Gomes, S. I., Maciá-Vicente, J. G., Termorshuizen, A. J., et al. (2022). Deciphering the interactions between plant species and their main fungal root pathogens in mixed grassland communities. *J. Ecol.* 110, 3039–3052. doi: 10.1111/1365-2745.14012

Ampt, E. A., van Ruijven, J., Raaijmakers, J. M., Termorshuizen, A. J., and Mommer, L. (2019). Linking ecology and plant pathology to unravel the importance of soil-borne fungal pathogens in species-rich grasslands. *Eur. J. Plant Pathol.* 154, 141–156. doi: 10.1007/s10658-018-1573-x

Busby, P. E., Peay, K. G., and Newcombe, G. (2016). Common foliar fungi of Populus trichocarpa modify Melampsora rust disease severity. *New Phytol.* 209, 1681–1692. doi: 10.1111/nph.13742

Busby, P. E., Zimmerman, N., Weston, D. J., Jawdy, S. S., Houbraken, J., and Newcombe, G. (2013). Leaf endophytes and Populus genotype affect severity of damage from the necrotrophic leaf pathogen, *Drepanopeziza populi*. *Ecosphere* 4, 1–12. doi: 10.1890/ES13-00127.1

Chao, S., Chen, Y., Wu, J., Zhang, Y., Song, L., Li, P., et al. (2025). *Exserohilum turcicum* alters Phyllosphere microbiome diversity and functions-implications for plant health management. *Microorganisms* 13, 524. doi: 10.3390/microorganisms13030524

Collinge, D. B., Jensen, B., and Jørgensen, H. J. (2022). Fungal endophytes in plants and their relationship to plant disease. *Curr. Opin. Microbiol.* 69, 102177. doi: 10.1016/j.mib.2022.102177

Crop Protection Network. (2025). Corn Disease Loss Estimates from the United States and Ontario, Canada — 2024. Available online at: https://cropprotection network.org/publications/corn-disease-loss-estimates-from-the-united-states-and-ontario-canada-2024 (Accessed April 8, 2025).

Hardoim, P. R., Van Overbeek, L. S., Berg, G., Pirttilä, A. M., Compant, S., Campisano, A., et al. (2015). The hidden world within plants: ecological and evolutionary considerations for defining functioning of microbial endophytes. *Microbiol. Mol. Biol. R.* 79, 293–320. doi: 10.1128/mmbr.00050-14

Johnston-Monje, D., and Raizada, M. N. (2011). Conservation and diversity of seed associated endophytes in *Zea* across boundaries of evolution, ethnography and ecology. *PLoS One* 6 (6), e20396.

Kearse, M., Moir, R., Wilson, A., Stones-Havas, S., Cheung, M., Sturrock, S., et al. (2012). Geneious Basic: an integrated and extendable desktop software platform for the organization and analysis of sequence data. *Bioinformatics* 28, 1647–1649. doi: 10.1093/bioinformatics/bts199

Liu, B., Ju, Y., Xia, C., Zhong, R., Christensen, M. J., Zhang, X., et al. (2022). The effect of *Epichloë* endophyte on phyllosphere microbes and leaf metabolites in *Achnatherum inebrians*. *iScience* 25 (4).

Ma, Z., Sun, Q., Li, L., Zhang, K., Gao, J., and Dong, J. (2022). Research progresses of southern corn rust in China: a review. *J. Plant protect.* 1, 276–282. doi: 10.13802/j.cnki.zwbhxb.2022.2022814

Madden, L. V., Hughes, G., and van den Bosch, F. (2017). doi: 10.1094/9780890545058

Martins, F., Mina, D., Pereira, J. A., and Baptista, P. (2021). Endophytic fungal community structure in olive orchards with high and low incidence of olive anthracnose. *Sci. Rep.* 11, 689. doi: 10.1038/s41598-020-79962-z

Meng, R., Lv, Z., Yan, J., Chen, G., Zhao, F., Zeng, L., et al. (2020). Development of spectral disease indices for southern corn rust detection and severity classification. *Remote Sens.* 12, 3233. doi: 10.3390/rs12193233

Ministry of Agriculture and Rural Affairs of the People's Republic of China. (2023). Forecast of the trend of major diseases and pest in corn nationwide in 2023 [In Chinese]. Available online at: http://www.moa.gov.cn/ztzl/2023cg/jszd_29356/202302/t20230209_6420231.htm (Accessed April 8, 2025).

Nilsson, R. H., Anslan, S., Bahram, M., Wurzbacher, C., Baldrian, P., and Tedersoo, L. (2019). Mycobiome diversity: high-throughput sequencing and identification of fungi. *Nat. R. Microbiol.* 17, 95–109. doi: 10.1038/s41579-018-0116-y

Pérez-Jaramillo, J. E., Carrión, V. J., de Hollander, M., and Raaijmakers, J. M. (2018). The wild side of plant microbiomes. *Microbiome* 6, 1–6. doi: 10.1186/s40168-018-0519-z

Porras-Alfaro, A., and Bayman, P. (2011). Hidden fungi, emergent properties: endophytes and microbiomes. *Annu. Rev. Phytopathol.* 49, 291–315. doi: 10.1146/annurev-phyto-080508-081831

Raghavendra, A. K., and Newcombe, G. (2013). The contribution of foliar endophytes to quantitative resistance to *Melampsora* rust. *New Phytol.* 197, 909–918. doi: 10.1111/nph.12066

Raja, H. A., Miller, A. N., Pearce, C. J., and Oberlies, N. H. (2017). Fungal identification using molecular tools: a primer for the natural products research community. *J. Nat. Prod.* 80, 756–770. doi: 10.1021/acs.jnatprod.6b01085

Sartori, M. V., Nesci, A. V., Montemarani, A. M., Barros, G. G., García, J., and Etcheverry, M. G. (2017). Preliminary evaluation of biocontrol agents against maize pathogens *Exserohilum turcicum* and *Puccinia sorghi* in field assays. *Agric. Sci.* 8, 1003–1013. doi: 10.4236/as.2017.89073

Smith, D. P., and Peay, K. G. (2014). Sequence depth, not PCR replication, improves ecological inference from next generation DNA sequencing. *PloS One* 9, e90234. doi: 10.1371/journal.pone.0090234

Sun, Q., Li, L., Guo, F., Zhang, K., Dong, J., Luo, Y., et al. (2021a). Southern corn rust caused by *Puccinia polysora* Underw: a review. *Phytopath. Res.* 3, 25. doi: 10.1186/s42483-021-00102-0

Sun, Q., Liu, J., Huang, C., Liu, X., Gao, J., Li, L., et al. (2023). Clonal expansion and dispersal pathways of *Puccinia polysora* in China. *Phytopathol* 113, 21–30. doi: 10.1038/s41598-021-97556-1

Tay, W. T., Meagher, R. L., Czepak, C., and Groot, A. T. (2023). *Spodoptera frugiperda*: ecology, evolution, and management options of an invasive species. *Ann. Rev. Entomol.* 68, 299–317. doi: 10.1146/annurev-ento-120220-102548

Tedersoo, L., Anslan, S., Bahram, M., Drenkhan, R., Pritsch, K., Buegger, F., et al. (2020a). Regional-scale in-depth analysis of soil fungal diversity reveals strong pH and plant species effects in Northern Europe. *Front. Microbiol.* 11. doi: 10.3389/fmicb.2020.01953

Tedersoo, L., Bahram, M., and Zobel, M. (2020b). How mycorrhizal associations drive plant population and community biology. *Science* 367, eaba1223. doi: 10.1126/science.aba1223

Wagner, M. R., Busby, P. E., and Balint-Kurti, P. (2020). Analysis of leaf microbiome composition of near-isogenic maize lines differing in broad-spectrum disease resistance. *New Phytol.* 225, 2152–2165. doi: 10.1111/nph.16284

Wang, Y., Li, Z., and Zhao, Z. H. (2023). Population mixing mediates the intestinal flora composition and facilitates invasiveness in a globally invasive fruit fly. *Microbiome* 11, 213. doi: 10.1186/s40168-023-01664-1

Wang, S., Zhang, R., Shi, Z., Zhao, Y., and Su, A. (2020). Identification and fine mapping of *RppM*, a southern corn rust resistance gene in maize. *Front. Plant Sci.* 11. doi: 10.3389/fpls.2020.01057

Wheeler, D. L., Dung, J. K. S., and Johnson, D. A. (2019). From pathogen to endophyte: an endophytic population of *Verticillium dahliae* evolved from a sympatric pathogenic population. *New Phytol.* 222, 497–510. doi: 10.1111/nph.15567

Xia, E., Tong, W., Hou, Y., An, Y., Chen, L., Wu, Q., et al. (2020). The reference genome of tea plant and resequencing of 81 diverse accessions provide insights into its genome evolution and adaptation. *Mol. Plant* 13, 1013–1026. doi: 10.1016/j.molp.2020.04.010

Xu, X., and Hu, X. (2015). Statistical analysis of data commonly occurred in plant pathology. *Acta Phytopathol. Sin.* 45, 1–6. doi: 10.13926/j.cnki.apps.2015.01.001

Yang, L., Chu, B., Deng, J., Lv, X., Song, S., Zhang, Y., et al. (2023). Exploring the association between latent *Plasmopara viticola* infection and downy mildew epidemic in commercial vineyards: application of qPCR assay. *Plant Pathol.* 73 (2), 378–389. doi: 10.1111/ppa.13808

Yang, L., Li, L., Dong, Z., Zhu, J., Guo, W., Song, Y., et al. (2024). EIRP model driven by machine learning for predicting the occurrence risk of southern corn rust (*Puccinia polysora* Underw.) in northern China. *Agr. For. Meteorol.* 356, 110149. doi: 10.1016/j.agrformet.2024.110149

Zhang, Z., Luo, L., Tan, X., Kong, X., Yang, J., Wang, D., et al. (2018). Pumpkin powdery mildew disease severity influences the fungal diversity of the phyllosphere. *PeerJ* 6, e4559. doi: 10.7717/peerj.4559

Frontiers in
Plant Science

Cultivates the science of plant biology and its applications

The most cited plant science journal, which advances our understanding of plant biology for sustainable food security, functional ecosystems and human health.

Discover the latest Research Topics

See more →

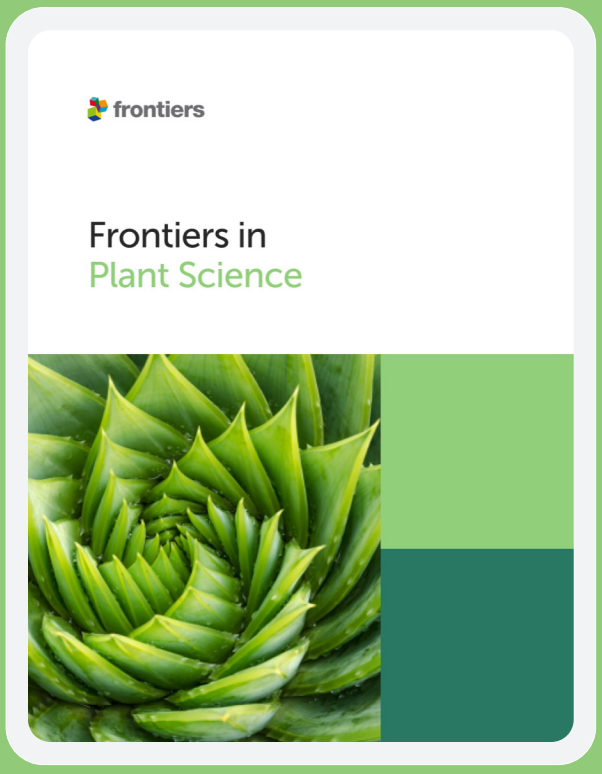

Frontiers

Avenue du Tribunal-Fédéral 34
1005 Lausanne, Switzerland
frontiersin.org

Contact us

+41 (0)21 510 17 00
frontiersin.org/about/contact